

████████████████████  
N65-33539

# NATIONAL ADVISORY COMMITTEE FOR AERONAUTICS

NACA CONFERENCE ON  
TURBOJET ENGINES FOR SUPERSONIC PROPULSION

A COMPILATION OF TECHNICAL MATERIAL PRESENTED

Lewis Flight Propulsion Laboratory  
Cleveland, Ohio

October 8 & 9, 1953

NACA

**CLASSIFICATION CHANGE**

To Unclassified  
By authority of CPN-7  
Changed by M. R. ... Date 9-15-64  
CLASSIFIED DOCUMENT

This material contains information affecting the National Defense of the United States within the meaning of the espionage laws, Title 18, U.S.C., Secs. 793 and 794, the transmission or revelation of which in any manner to unauthorized person is prohibited by law.



NACA CONFERENCE ON  
TURBOJET ENGINES FOR SUPERSONIC PROPULSION

A COMPILATION OF TECHNICAL MATERIAL PRESENTED

Lewis Flight Propulsion Laboratory  
Cleveland, Ohio

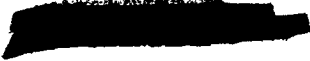
October 8 & 9, 1953

## INTRODUCTION

This document contains papers related to the NACA Conference on "The Turbojet Engine for Supersonic Propulsion" held at the Lewis Flight Propulsion Laboratory October 8 and 9, 1953. Much of the material presented here was presented in the panel-type discussions of the conference. In some cases, in order to supplement those discussions, material not previously presented is included.

A list of the conferees is included.

NATIONAL ADVISORY COMMITTEE  
FOR AERONAUTICS

  
TABLE OF CONTENTS

I - COMPRESSOR AERODYNAMICS PANEL

1. REQUIREMENTS OF COMPRESSORS FOR HIGH-SPEED AIRCRAFT by I. A. Johnsen and R. O. Bullock
2. GENERAL CONSIDERATIONS OF MACH NUMBER EFFECTS ON COMPRESSOR BLADING by J. F. Klapproth
3. FLOW CHARACTERISTICS OF COMPRESSOR BLADE ELEMENTS by S. Lieblein
4. APPLICATION OF BLADE ELEMENT DATA TO STAGE DESIGN by J. E. Hatch and H. B. Finger
5. SINGLE-STAGE RESULTS AIMED AT SATISFYING SUPERSONIC ENGINE REQUIREMENTS by H. B. Finger and W. H. Robbins
6. INVESTIGATION OF A MULTISTAGE COMPRESSOR IMPLYING TRANSONIC INLET STAGES by C. H. Voit and R. P. Geye
7. INVESTIGATION OF MULTISTAGE COMPRESSOR HAVING ALL STAGES OF TRANSONIC TYPE by K. Kovach and D. M. Sandercock

II - TURBINE AERODYNAMICS PANEL

1. INTRODUCTION TO TURBINE AERODYNAMICS by R. E. English and J. J. Rebeske
2. SECONDARY-FLOW LOSSES IN TURBINES by H. Z. Herzig and H. A. Buckner, Jr.
3. STUDY OF TURBINES DESIGNED FOR HIGH-FLOW MACH NUMBERS by W. L. Stewart
4. PERFORMANCE EVALUATION OF A SINGLE-STAGE TURBINE WITH STATOR ADJUSTMENT OVER A WIDE RANGE OF STATOR FLOW AREAS by T. R. Heaton and D. E. Holeski
5. PERFORMANCE PREDICTION OF AN ADJUSTABLE STATOR TURBINE by T. R. Heaton and R. E. Forrette
6. PERFORMANCE OF AN ADJUSTABLE TURBINE STATOR IN A TURBOJET ENGINE by C. L. Walker and J. H. Povolny

III - VIBRATION AND SURGE PANEL

1. SOME PROBLEMS ASSOCIATED WITH OFF-DESIGN PERFORMANCE OF AXIAL-FLOW COMPRESSORS by W. A. Benser
2. ROTATING STALL IN SINGLE-STAGE COMPRESSORS by R. W. Graham
3. ROTATING STALL IN MULTISTAGE AXIAL-FLOW COMPRESSORS by M. C. Huppert and E. L. Costilow
4. BLADE VIBRATION IN AXIAL-FLOW COMPRESSORS by H. F. Calvert and M. C. Huppert
5. COMPLETE COMPRESSOR STALL AND SURGE IN MULTISTAGE AXIAL-FLOW COMPRESSORS by M. C. Huppert and E. L. Costilow
6. ANALYSIS OF THE INTERMEDIATE-SPEED SURGE CHARACTERISTICS OF HIGH-PRESSURE-RATIO AXIAL-FLOW COMPRESSORS by W. A. Benser
7. METHODS FOR INCREASING STALL-FREE OPERATING RANGE OF MULTISTAGE AXIAL-FLOW COMPRESSORS by A. A. Medeiros

IV - TURBINE COOLING PANEL

1. THE ROLE OF TURBINE COOLING IN FUTURE AIRCRAFT ENGINES by J. B. Esgar and R. J. Rossbach
2. INVESTIGATIONS OF AIR-COOLED SHELL-SUPPORTED TURBINE BLADES by R. O. Hickel and J. L. Clure
3. INVESTIGATION OF CONVECTION-COOLED STRUT-SUPPORTED TURBINE BLADES by E. F. Schum and F. S. Stepka
4. DEVELOPMENT OF TRANSPIRATION-COOLED TURBINE BLADES by P. L. Donoughe and A. J. Diaguila
5. LIQUID COOLING OF TURBINE BLADES by J. C. Freche
6. APPLICATION AND OPERATION OF AIR-COOLED TURBINES IN TURBOJET ENGINES by R. R. Ziemer and L. J. Schafer, Jr.
7. TURBINE COOLING SYSTEMS FOR SUPERSONIC FLIGHT by J. E. Hubbartt

[REDACTED]

V - COMBUSTION PANEL

1. CURRENT STATUS AND FUTURE REQUIREMENTS OF TURBOJET COMBUSTORS  
by E. R. Jonash, J. H. Childs, and W. T. Olson
2. RECENT RESEARCH ON HIGH-SPEED COMBUSTION by W. T. Olson and  
E. R. Jonash
3. PERFORMANCE OF EXPERIMENTAL TURBOJET COMBUSTORS by C. T.  
Norgren, E. V. Zettle, and J. H. Childs

VI - MATERIALS AND STRUCTURES PANEL

1. ALLOYS FOR USE AT INCREASED TEMPERATURES by G. M. Ault
2. APPLICABILITY OF CERMETS FOR USE AS TURBINE BLADES by G. C.  
Deutsch, A. J. Meyer, and W. C. Morgan
3. EXPERIMENTAL INVESTIGATION OF SEVERAL METHODS OF REDUCING THE  
WEIGHT OF COMPRESSOR AND TURBINE ROTORS OF TURBOJET ENGINES  
by R. H. Kemp, M. H. Hirschberg, and M. L. Moseson
4. NACA RESEARCH ON LUBRICANTS AND BEARING MATERIALS FOR HIGH-  
TEMPERATURE TURBINE ENGINES by R. L. Johnson and E. E. Bisson

VII - INLETS AND OUTLETS PANEL

1. FACTORS AFFECTING THE PERFORMANCE OF SIDE INLETS AT SUPERSONIC  
SPEEDS by T. G. Piercy
2. INLET-ENGINE MATCHING CONSIDERATIONS FOR HIGH-SPEED SUPERSONIC  
AIRPLANES by L. J. Obery and L. E. Stitt
3. PERFORMANCE OF SEVERAL PLUG-TYPE NOZZLES by G. W. Englert and  
T. B. Shillito
4. THE EJECTOR AS A SUPERSONIC NOZZLE AND COOLING DEVICE by  
W. K. Greathouse, W. K. Koffel, and D. P. Hollister
5. SOME AERODYNAMIC CONSIDERATIONS OF AFTERBODY DESIGN AT SUPER-  
SONIC SPEEDS by E. M. Cortright, Jr.



VIII - ENGINE AND AIRPLANE PERFORMANCE PANEL

1. INTRODUCTION TO ENGINE AND AIRPLANE PERFORMANCE STUDIES by  
B. T. Lundin
2. GENERAL CONSIDERATIONS OF COMPONENT SELECTION AND INTEGRATION  
by R. O. Bullock and H. B. Finger
3. ONE-SPOOL TURBOJET ENGINES FOR PROPULSION OF SUPERSONIC AIR-  
CRAFT by R. E. English, E. C. Wilcox, and H. W. Plohr
4. TWO-SPOOL ENGINES FOR SUPERSONIC FLIGHT by J. F. Dugan and  
D. T. Bernatowitz
5. AIRPLANE PERFORMANCE by R. W. Luidens, H. M. Henneberry, A. V.  
Zimmerman, and P. J. Evans, Jr.
6. SUMMARY OF ENGINE AND AIRPLANE ANALYSIS by D. S. Gabriel and  
E. W. Hall

3078

[REDACTED]

NATIONAL ADVISORY COMMITTEE FOR AERONAUTICS  
LEWIS FLIGHT PROPULSION LABORATORY  
Cleveland, Ohio

LIST OF CONFEREES

The following conferees were registered at the NACA Conference on Turbojet Engines for Supersonic Propulsion, October 8 and 9, 1953.

<u>Name</u>	<u>Affiliation</u>
Abbott, I. H.	NACA - Washington
Alford, J. S.	General Electric
Almassy, G. W.	General Electric
Alpert, S.	Solar Aircraft
Alyanak, E. J.	Goodyear Aircraft
Anderson, J. W.	McDonnell Aircraft
Anderson, Maj. P. B.	Wright Air Development Center
Appold, Col. N. C.	Wright Air Development Center
Arnold, J. E.	Convair
Atkinson, A. S.	Bureau of Aeronautics
Avery, W. H.	Johns Hopkins
Ayres, Lt. Col. L. F.	USAF, Baltimore
Baird, Capt. A. L.	Bureau of Aeronautics
Bartz, M. C.	Bendix Products
Beach, W. C.	North American Aviation
Beckelman, B. F.	Boeing
Bioletti, C.	NACA - Ames
Blanck, A. A.	Office of Naval Research
Blanton, J.	Bell Aircraft
Bodemuller, R.	Bendix Aviation
Bogdonoff, S. M.	Princeton University
Bogert, R. C.	North American Aviation
Bonner, R. W.	Glen L. Martin
Bradley, F. X.	Pratt & Whitney
Brainard, J.	Thompson Products
Brown, A. E.	Bendix Products
Brown, Col. W. G.	Wright Air Development Center
Buck, M. P.	International Nickel
Bunze, Lt. Col. H. F.	USAF, ATIC, Dayton
Burgess, N.	General Electric
Bush, W. R.	Republic Aviation
Butler, E. M.	Redstone Arsenal
Calhoun, Maj. J. D.	USAF, Inst. of Tech., Dayton
Campbell, K.	Wright Aeronautical
Cash, G. M.	Cornell Aero. Lab.

Cesaro, R. S.  
Chatfield, D. S.  
Chenoweth, O.  
Chew, B. B.  
Christensen, R. G.  
Collins, I. K.  
Collins, J. H.  
Collins, W.  
Comberiate, M. B.  
Conlon, E. W.  
Cook, H. A.  
Covington, C.  
Coyle, Cdr. J. C.  
Crites, S. E.  
Crowley, J. W.

Daley, J. A.  
Dearing, Lt. Cdr. H. H.  
DeLosSantos, S. T.  
DeRoze, L. J.  
Diehl, Capt. W. S.  
Dietz, R. O.  
Dillon, A. K.  
DiPiazza, J.  
Doll, W.  
Doolittle, J. H.  
Dougherty, F. G.  
Drell, H.  
Dryden, Dr. H. L.  
Dunholter, Dr. H. F.  
DuBois, Capt. J. M.

Eads, D. K.  
Eckert, Dr. E. R. G.  
Elbel, R.  
Erdmann, J. J.  
Erwin, J. R.  
Evans, Albert J.  
Evard, J. C.

Fedenia, J. N.  
Fejer, A. A.  
Fine, A. W.  
Fox, S. S.  
Fox, W. W.  
Franks, R.  
Fransson, K. E.  
Fremont, H. A.

NACA - Washington  
Reaction Motors  
Wright Air Development Center  
North American Aviation  
Boeing  
Offutt Air Force Base  
NACA - Lewis  
Continental Aviation  
Bureau of Aeronautics  
Fairchild  
Thompson Products  
R&DB  
NAMC, Philadelphia  
General Electric  
NACA - Washington

NAMC, Philadelphia  
Bureau of Aeronautics  
USN, Washington  
USAF, ATIC, Dayton  
USN (Retired), Washington  
Arnold Engineering Development Center  
Wright Air Development Center  
NACA - Washington  
Pratt & Whitney  
Shell Oil  
Allison  
Lockheed Aircraft  
NACA - Washington  
Convair  
USAF - NACA Field Rep., Cleveland

Callery Chemical  
University of Minnesota  
Thompson Products  
Austen Labs.  
NACA - Langley  
NACA - Washington  
NACA - Lewis

Naval Ordnance Lab.  
University of Toledo  
Wright Air Development Center  
Pratt & Whitney  
Convair  
Union Carbide  
Pratt & Whitney  
General Electric

[REDACTED]

Frey, L.	Austen Lab.
Furnas, Dr. C. C.	Cornell Aero. Lab.
Gammon, B.	NACA - Washington
Gangl, A. H.	Wright Air Development Center
Gardner, Capt. A. J.	Wright Air Development Center
Gasich, W. E.	Northrop Aircraft
Gates, C. R.	USAF, Hdqrs., Washington
Gerdan, D.	Allison
Geyer, L. A.	Grumman Aircraft
Gibbons, L. C.	NACA - Lewis
Gibson, E. B.	Lockheed Aircraft
Gibson, J. O.	Goodyear Aircraft
Glick, H.	Cornell Aero. Lab.
Glodeck, E.	R&DB
Glover, L. S.	David Taylor Model Basin
Green, A. W. F.	Allison
Greenwald, R. E.	Bell Aircraft
Grimminger, G.	USAF, Washington
Guarnieri, G.	Cornell Aero. Lab.
Hall, J. H.	NACA - Lewis
Hall, J. R.	Bell Aircraft
Hall, M. J.	Mathieson Chemical
Hand, W. H.	North American Aviation
Hanjian, Capt. J.	Offut Air Force Base
Harrison, W. N.	Nat. Bureau of Standards
Hausmann, G.	United Aircraft
Havenstein, Lt. P.	Bureau of Aeronautics
Hazard, H. R.	Battelle Inst.
Herald, J. M.	Wright Air Development Center
Herman, I.	USAF, ATIC, Dayton
Hesse, W. J.	NATC
Higginbotham, R. R.	Republic Aviation
Hipsh, H. M.	Convair
Holden, Capt. G. M.	Eglin Air Force Base
Holmquist, Lt. Cdr. C. O.	NATC
House, W. C.	Aerojet
Hunter, W. H.	NACA - Lewis
Hurley, W. V.	Air Res. & Dev.
Ivey, H. R.	TAC, Langley Field, Virginia
Jasen, Capt. F.	Wright Air Development Center
Jordan, D. J.	Pratt & Whitney
Jordan, L. R.	Douglas Aircraft
Joyner, T. A.	Callery Chemical

Kamerling, G. J.  
Kappus, P.  
Karanik, J.  
Kasley, J. H.  
Katkov, R. B.  
Kelber, C. C.  
Kemper, C.  
King, J. A.  
Klein, H.  
Knott, J. E.  
Kopplin, C. H.  
Kretsch, H. W.  
Krouse, L. M.

LaRou, L. V.  
Lazar, J.  
Lee, J. G.  
Leslie, W. C.  
Leverette, T. H.  
Lewis, R.  
Linden, J. E.  
Lloyd, R.  
Longstreet, C. S.  
Lundquist, A. G.  
Lush, K. J.  
Luther, J. M.

MacGregor, C. A.  
Maedel, P. H.  
Male, D. W.  
Manganiello, E. J.  
Manildi, J. F.  
Maravell, J.  
Masi, F.  
Matteson, R. C.  
McMurtrey, L. J.  
McVeigh, J. R.  
Mercer, J.  
Mezger, B. J.  
Michaels, C. M.  
Moses, J. J.  
Mullaney, R.  
Multhopp, H.

Nakimura, H.  
Neary, K. J.  
Nesting, I. M.  
Nerad, A. J.

AiResearch  
Wright Air Development Center  
Grumman Aircraft  
Curtiss-Wright  
Northrop Aircraft  
Rand Corp.  
NACA - Lewis  
Fairchild  
Douglas Aircraft  
Allison  
Pratt & Whitney  
Manning, Maxwell & Moore  
Fredric Flader

Wall Colmonoy  
NACA - Washington  
United Aircraft  
Thompson Products  
Eglin Air Force Base  
Wright Aeronautical  
Bureau of Aeronautics  
Cornell Aero. Lab.  
Bendix Products  
Office of Naval Research  
Edwards Air Force Base  
Convair

Propulsion Research Corp.  
Westinghouse  
R&DB  
NACA - Lewis  
Univ. of California  
Republic Aviation  
NAMC, Philadelphia  
Convair  
Boeing  
Kennametal Corp.  
United Aircraft  
Wright Aeronautical  
Wright Air Development Center  
Ryan Aeronautical  
Grumman Aircraft  
Glenn L. Martin Co.

Convair  
Ryan Aeronautical  
Naval Ordnance Lab.  
General Electric

Newton, G. W.	AEDC, Tullahoma, Tenn.
Nichols, J. B.	Hiller Helicopter
Nichols, M. R.	NACA - Langley
Nucci, L. M.	Republic Aviation
O'Donnell, W. J.	Republic Aviation
Olson, G. A.	North American Aviation
O'Mara, Col. J. A.	USAF, ATIC, Dayton
Orton, H. E.	Boeing
Oviatt, S. A.	Kennametal Corp.
Palmer, C.	NACA - Washington
Palsulich, J.	Cleveland Graphite Bronze
Pappas, C. E.	Republic Aviation
Parkins, W. A.	Pratt & Whitney
Patton, J. R.	Office of Naval Research
Pearson, E. O.	NACA - Washington
Peaslee, R. L.	Wall Colmonoy
Pierce, E. F.	Wright Aeronautical
Pinkel, B.	NACA - Lewis
Pinnes, R. W.	Bureau of Aeronautics
Prachar, O. P.	Allison
Pratt, P. W.	Pratt & Whitney
Preston, A. L.	Minneapolis Honeywell
Redmond, J. C.	Kennametal Corp.
Reinhardt, W. J.	Reaction Motors
Rethman, Lt. Col. V. C.	USAF, Washington
Risher, Lt. Cdr. H.	Bureau of Aeronautics
Ritter, A.	Office of Naval Research
Robbins, Maj. H. W.	USAF, NACA Field Rep., Cleveland
Robinson, W. C.	Bureau of Aeronautics
Rock, E. A.	Boeing
Rodert, L. A.	NACA - Lewis
Roddy, V. S.	USAF, Hdqrs., Washington
Rohl, H. T.	Wright Air Development Center
Rolle, S. H.	CAA, Washington
Romanowich, R. R.	Wright Air Development Center
Rosenzweig, S.	Cornell Aero. Lab.
Rothrock, A. M.	NACA - Washington
Russ, D. G.	Bendix Products
Sachs, G.	University of Syracuse
Samaras, D. G.	Wright Air Development Center
Sanders, J. C.	NACA - Lewis
Sanders, J. L.	Redstone Arsenal
Sanders, N. D.	NACA - Lewis
Sarginson, F.	Fredric Flader

Savage, C. A.  
Savage, M.  
Saylor, J. M.  
Scalia, M.  
Schairer, G. S.  
Scherrer, R.  
Schey, O. W.  
Schloesser, V. V.  
Schmidt, Maj. H. R.  
Schoolfield, W. C.  
Schramm, W. B.  
Schwartz, V. D.  
Seaberg, Maj. J. D.  
Sens, W. H.  
Sessions, R. C.  
Sharp, E. R.  
Shayeson, M.  
Shine, W. H.  
Shippen, W. B.  
Siltanen, Lt. Jas. N.  
Silvern, D.  
Silverstein, A.  
Simpson, G. R.  
Slivka, W. R.  
Sloop, J. L.  
Smith, S. W.  
Snodgrass, R. B.  
Sorgen, C. C.  
Spraker, W. A.  
Steen, Maj. C. H.  
Steuernagel, C. A.  
Stoockly, E. E.  
Stranges, P. A.  
Stresen-Reuter, J. H.  
Sulkin, M. A.  
Sweeney, M. Jr.  
  
Tanczos, F. I.  
Tauber, Lt. Col. C. B.  
Taylor, E. B.  
Taylor, J. E. M.  
Tearman, J. O.  
Telerico, J. A.  
Thompson, F. L.  
Thomson, A. R.  
Thoren, T. R.  
Thornton, Capt. L. R.  
Towle, H. C.

Convair  
NACA - Langley  
Lockheed Aircraft  
Glenn L. Martin  
Boeing  
NACA - Ames  
NACA - Lewis  
Westinghouse  
USAF, Hdqrs., Washington  
Chance Vought  
Consultant  
Carrier Corp.  
Wright Air Development Center  
Pratt & Whitney  
NACA - Lewis  
NACA - Lewis  
Wright Air Development Center  
USAF, Inst. of Tech.  
Johns Hopkins Univ.  
Wright Air Development Center  
Continental Aviation  
NACA - Lewis  
NATS, Trenton  
NATS, Trenton  
NACA - Lewis  
Bell Aircraft  
Offut Air Force Base  
Bureau of Aeronautics  
Battelle Inst.  
Wright Air Development Center  
Raytheon Mfg. Co.  
General Electric  
Mathieson Chemical  
Holley Carburetor  
North American Aviation  
MIT, Cambridge

Bureau of Aeronautics  
Wright Air Development Center  
Douglas Aircraft  
Wright Air Development Center  
Ryan Aeronautical  
NAMC, Philadelphia  
NACA - Langley  
Thompson Products  
Thompson Products  
Edwards Air Force Base  
Republic Aviation

CONFIDENTIAL

3078-

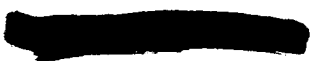
Townsend, S. J.	Chance Vought
Trimble, H. M.	Phillips Petroleum
Ullman, G. N.	NACA - Washington
Underwood, W. J.	NACA - Dayton
Vaiden, J. C.	Eclipse Pioneer
VanDame, F. P.	USAF, ATIC, Dayton
Volkmar, P.	Northrop Aircraft
Von Ohain, H.	Wright Air Development Center
Walker, C. J.	General Electric
Walley, Cdr. D. M.	Office of Naval Research
Walter, D. L.	Marquardt Aircraft
Walters, D. E.	Lockheed Aircraft
Wayman, W. E.	Hughes Aircraft
Weilmuenster, E. A.	Mathieson Chemical
Wetzler, J. M.	Allison
Whitmer, V. W.	Republic Steel
Whitmore, Lt. Cdr. Q. R.	Bureau of Aeronautics
Williams, Lt. Col. F. W.	AEDC, Tullahoma, Tenn.
Williams, H. J.	Bendix Products
Witbeck, N.	R&DB
Withington, H. W.	Boeing
Woershing, T. B.	Goodyear Aircraft
Wolfe, E. A.	Wright Air Development Center
Wood, L. A.	Wright Air Development Center
Woodward, W. H.	NACA - Washington
Worth, W.	Wright Air Development Center
Wosika, L. R.	Solar Aircraft
Wray, Col. R. M.	USAF, Hdqrs., Washington
Wright, F. A.	Wright Air Development Center
Wyatt, D. D.	NACA - Lewis
Young, G. B. W.	Rand Corp.
Zarkowsky, W.	Grumman Aircraft
Zeck, W.	Fredric Flader
Zipkin, M. A.	Goodyear Aircraft
Zucrow, M. J.	Purdue University

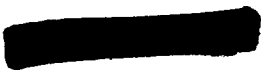
CONFIDENTIAL



I - COMPRESSOR AERODYNAMICS PANEL

- I. A. Johnsen
- H. B. Finger
- J. F. Klapproth
- S. Lieblein





## REQUIREMENTS OF COMPRESSORS FOR HIGH-SPEED AIRCRAFT

By Irving A. Johnsen and Robert O. Bullock

### INTRODUCTION

3078-A

General considerations of the turbojet engine for supersonic-flight application indicate the desirability of minimum weight and maximum efficiency in the engine components. It is apparent, therefore, that compressor research and development should be directed at the attainment of minimum compressor weight for given air-flow and pressure-ratio capacity, while maintaining or increasing, if possible, the efficiency level. This paper considers the general requirements of compressors and indicates an approach optimizing the axial-flow-compressor component of engines for supersonic flight.

### GENERAL REQUIREMENTS OF COMPRESSORS

The desirable features of compressors can be conveniently divided into two categories: (1) mechanical or physical characteristics, and (2) aerodynamic characteristics. Physically, the compressor should be small in size and weight, structurally reliable, and simple and inexpensive to manufacture and maintain. In view of its importance in supersonic propulsion, the size and weight aspect will be considered as the principal objective in this category of mechanical characteristics. Because of the degree to which ingenuity in mechanical design influences weight, however, the aerodynamicist is forced to generalize the weight problem as one of obtaining a compressor of minimum size. That is, if aerodynamic discoveries permit both the diameter and the length of a compressor to be reduced (in the manner indicated in fig. 1), it is likely that a saving in compressor weight can be realized. This viewpoint will be taken in this and succeeding papers.

The aerodynamic characteristics with which the compressor designer is concerned include pressure ratio per stage, air flow per unit frontal area, efficiency, and range. The first two of these form the basis for a reduction in size and weight. That is, compactness can be achieved by increasing stage pressure ratios (reducing the number of stages required for a given over-all pressure ratio), and increasing air-flow-handling capacity (reducing the frontal area for a given air-flow requirement).

A general objective of compressor aerodynamic research can therefore be stated as the desire to improve pressure-ratio and air-flow characteristics of axial-flow compressors without sacrificing efficiency and without penalizing the compressor structurally. Initially, this will be considered as a "design-point" problem. Off-design characteristics,



such as ability to accelerate rapidly and to operate satisfactorily over a wide range of flight conditions, become extremely important in supersonic-propulsion applications. However, this problem is dealt with in succeeding papers and need not be specifically considered at this time.

### CONSIDERATIONS OF HIGH-PERFORMANCE COMPRESSORS

The ability of a compressor to handle high air flows per unit frontal area is basically a function of the axial Mach number (axial component of velocity of entering air flow) and the hub-to-tip radius ratio of the compressor stage. The general relation between these variables is illustrated in figure 2. It is apparent that, in order to minimize the frontal area of the entrance stage of a multistage axial-flow compressor, it is desirable to use a maximum flow area and a maximum axial velocity.

The ability of a compressor to produce a high pressure ratio in a single stage is to a large degree a function of the Mach number relative to the rotor blade and the rotor speed. As shown in figure 3, for a typical design, appreciable increases in pressure ratio can be realized through increases in relative Mach number and rotational speed. Therefore, with respect to both air-flow capacity and pressure ratio per stage it is desirable to utilize high Mach numbers.

A second basic factor that influences stage pressure ratio is "blade loading." Blade loading for the moment may be considered as the lift obtainable from the airfoil that forms the compressor blade. As shown in figure 4 for a rotor (without inlet guide vanes) operating at a rotational speed of 1000 feet per second, substantial gains in pressure ratio can be realized through increased blade loading.

In compressor design, as in most other fields, the optimizing of one feature usually results in a sacrifice in some other feature. Therefore, the parameters that control air-flow capacity and pressure ratio per stage (axial Mach number, hub-to-tip radius ratio, relative Mach number, rotational speed, and blade loading) must be reexamined in terms of their effect on the third important aerodynamic characteristic, efficiency.

The influence of relative Mach number on efficiency is illustrated in figure 5. For conventional subsonic airfoil shapes, efficiency remains at a high level until a relative Mach number of the order of 0.7 to 0.8 is reached, after which there is a sharp reduction in efficiency. This situation is analogous to that encountered in conventional wings and propellers, where serious increases in loss levels occur as sonic conditions are approached. As a result of this fact, the compressor designer has usually been in the position of sacrificing either air flow or pressure ratio in order to stay within reasonable efficiency levels.

Obviously, then, the first problem confronting the aerodynamicist in his attempt to optimize compressors is that of extending the Mach number range over which the blade element can operate efficiently. He must also establish the exact variation of efficiency or loss with Mach number so as to give the designer the "design control" necessary to establish precisely those compromises that he is willing to accept.

The second basic problem in compressor design concerns the factor of blade loading. As previously discussed, high blade loadings are desirable with respect to pressure ratio per stage. However, the effect of loading on efficiency is shown in figure 6. Again, a limit appears to exist above which sacrifices in efficiency must be accepted. It would be desirable, through a fundamental understanding of the problem, to extend the range of loading for high efficiency. This poses difficult problems involving boundary-layer and pressure-gradient phenomena, however, and there is some question as to the magnitude of gains that can be achieved. Therefore, for the moment, the emphasis will be placed on the problem of determining the variation of loss with loading (as required for design control), in order to establish a maximum practicable value of blade loading for design purposes.

Although hub-to-tip radius ratio can be expected to have some effect on aerodynamic performance, it will be shown later that these limits can be essentially avoided by proper aerodynamic design. The radius-ratio problem therefore reduces to one of structural strength. For high-speed, highly loaded compressors such as are being considered here, this structural problem is significant. Therefore, in the design of blading and the selection of rotational speed, the designer must continually be guided by the mechanical aspects of the problem. He must seek blading forms that will minimize centrifugal and vibratory stresses, as well as shapes which are easily machined. These considerations underlie the discussions in the other papers on compressor aerodynamics, even though they are not specifically mentioned.

From the aerodynamic point of view, therefore, the basic problem facing the compressor designer can be restated as that of utilizing high relative Mach numbers and high blade loadings, while maintaining high efficiency levels. Significant strides in this direction have been made through research. For example, as summarized in figure 7, the range of relative Mach number over which high efficiencies can be maintained has been extended to values above Mach number of 1.0. Compressors operating in this Mach number region have been designated as "transonic" compressors. The first transonic compressor investigated by the NACA was designed to operate at a rotor-tip relative inlet Mach number of the order of 1.1; a photograph of this rotor is shown in figure 8. The performance of this compressor, operating as a complete stage, is shown in figure 9 and reported in greater detail in references 1 and 2. As can be seen, the performance characteristics of this initial transonic unit

were very good. A stage pressure ratio of 1.48 was obtained with an air flow per unit frontal area of approximately 30 pounds per second per square foot and a peak efficiency of the order of 0.90. In regard to range, the stage is comparable to subsonic compressors. The transonic compressor, therefore, represents a major advance in the compressor field, in that it enables the designer simultaneously to increase air-flow capacity and stage pressure ratio without sacrificing efficiency or range.

However, the "design control" on this initial transonic compressor was not as precise as desired; as indicated in figure 9, the pressure ratio obtained at the peak efficiency or "design point" was higher than anticipated, and the air flow somewhat less. Obviously, if the transonic compressor is to be utilized in engine applications, the performance of the unit must be predicted rather accurately. Therefore, further research was initiated at the Lewis laboratory to extend the available knowledge on the transonic compressor. In the past  $1\frac{1}{2}$  years, a great deal of this research has been completed. Substantial gains have been made in basic theory and design control, as well as in the extension of the experimental experience to single-stage and multistage units that are well-suited to the needs of the turbojet engine for supersonic propulsion. The following papers of this compressor aerodynamics discussion are devoted to a summarization of the information gained through this research.

#### REFERENCES

1. Lieblein, Seymour, Lewis, George W., Jr., and Sandercock, Donald M.: Experimental Investigation of an Axial-Flow Compressor Inlet Stage Operating at Transonic Relative Inlet Mach Numbers. I - Over-All Performance of Stage with Transonic Rotor and Subsonic Stators up to Relative Inlet Mach Number of 1.1. NACA RM E52A24, 1952.
2. Schwenk, Francis C., Lieblein, Seymour, and Lewis, George W., Jr.: Experimental Investigation of an Axial-Flow Compressor Inlet Stage Operating at Transonic Relative Inlet Mach Numbers. III - Blade-Row Performance of Stage with Transonic Rotor and Subsonic Stator at Corrected Tip Speeds of 800 and 1000 Feet Per Second. NACA RM E53G17, 1953.

3078-A

DESIRED REDUCTION IN COMPRESSOR SIZE

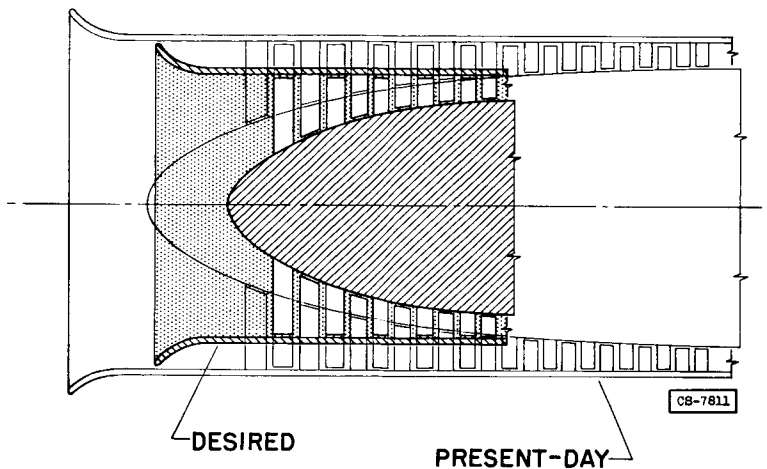


Figure 1

AIR-FLOW CHARACTERISTICS OF AXIAL-FLOW COMPRESSORS

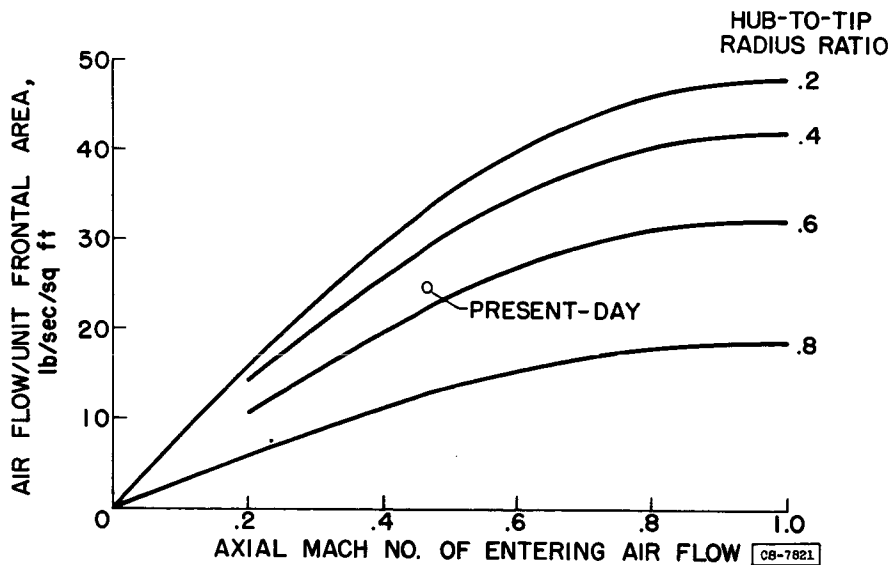
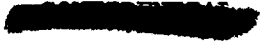
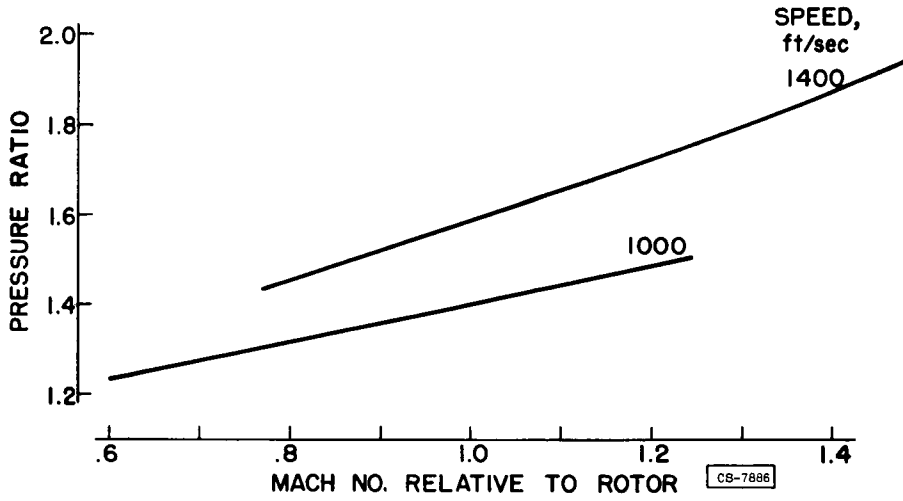


Figure 2



### EFFECT OF RELATIVE MACH NUMBER AND ROTOR SPEED ON PRESSURE RATIO



3078-A

Figure 3

### EFFECT OF BLADE LOADING ON PRESSURE RATIO ROTOR SPEED = 1000 ft/sec

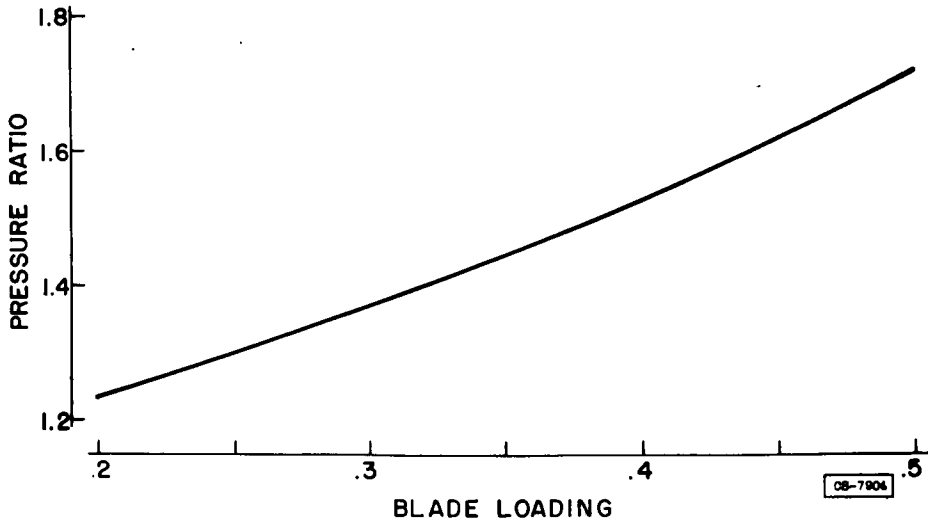


Figure 4



### VARIATION OF EFFICIENCY WITH MACH NUMBER FOR CONVENTIONAL DESIGN

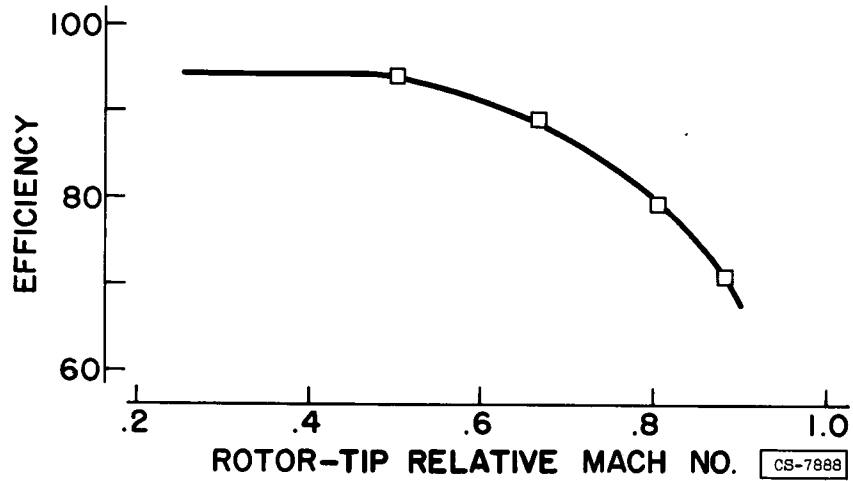


Figure 5

### EFFECT OF BLADE LOADING ON EFFICIENCY OF COMPRESSOR ROTOR

PRESSURE RATIO, 1.4

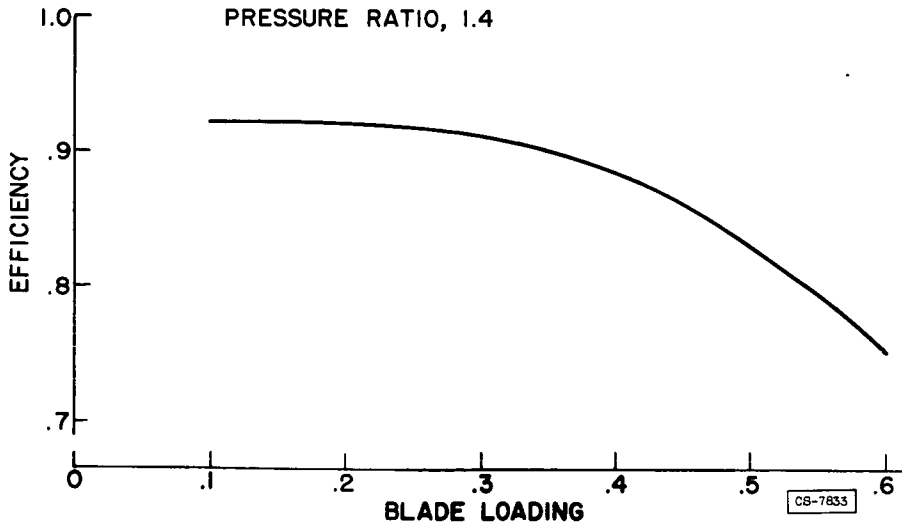
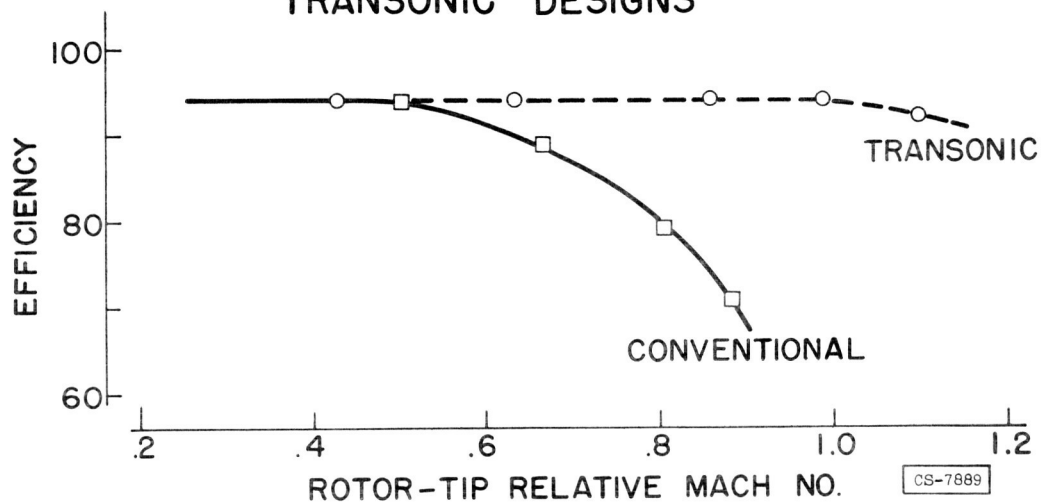


Figure 6

VARIATION OF EFFICIENCY WITH MACH NUMBER FOR CONVENTIONAL AND TRANSONIC DESIGNS



3078-A

Figure 7

FIRST TRANSONIC ROTOR

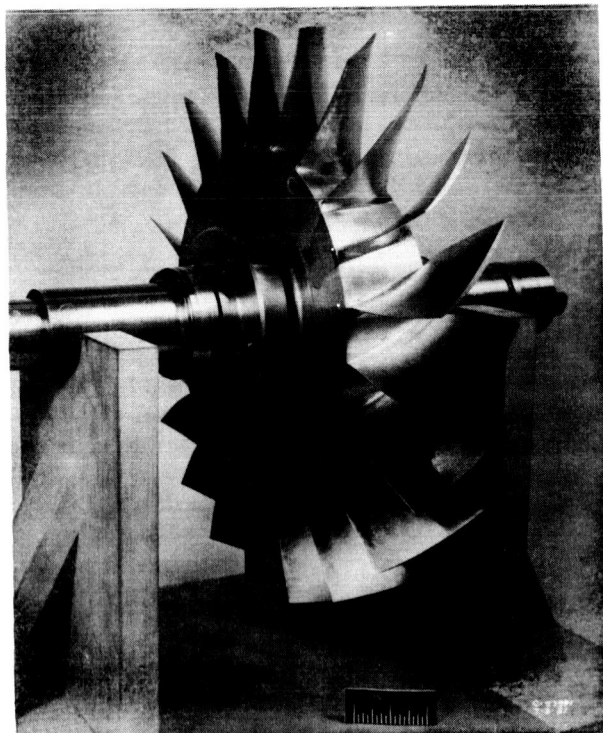


Figure 8

PERFORMANCE OF FIRST TRANSONIC INLET STAGE  
HUB-TIP RADIUS RATIO, 0.52

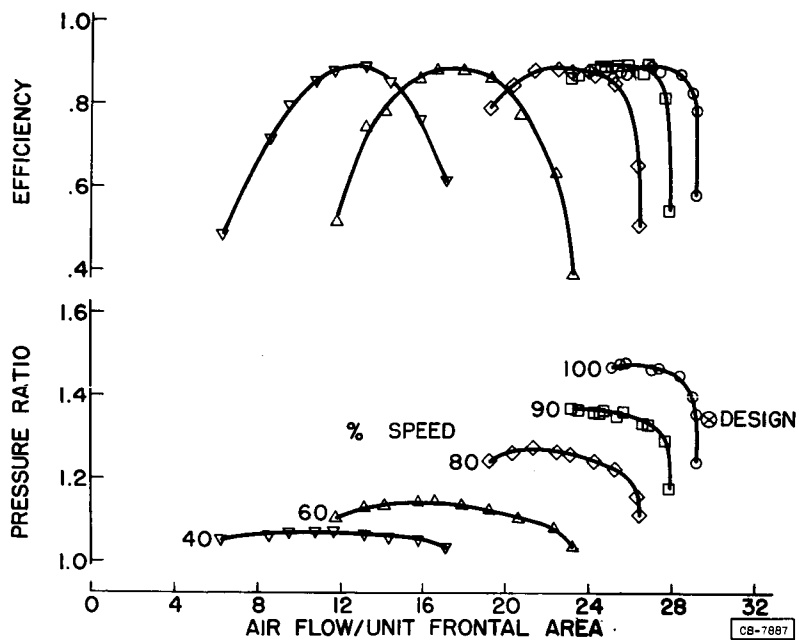


Figure 9

## GENERAL CONSIDERATIONS OF MACH NUMBER EFFECTS

## ON COMPRESSOR BLADING

By John F. Klapproth

## INTRODUCTION

The requirements of high flow capacity and stage pressure ratio, which contribute to the desired compressor performance for supersonic aircraft application, can theoretically be met by increasing both the inlet axial velocity and the rotational speed. However, in order to take advantage of the higher inlet velocity and rotor speed to improve the performance over present levels, Mach numbers above the current limit of approximately 0.8 must be utilized. The principal problem then reduces to that of determining the blade shapes or the stage design characteristics that permit operation in the transonic and low supersonic Mach number range without undue sacrifice in efficiency. The discussion in this paper will describe some of the causes for the loss in efficiency observed with cascades of current blading and the approach that has been used in an effort to reduce or eliminate the usual Mach number restrictions.

## HIGH-SPEED FLOW OVER CONVENTIONAL BLADING

Since conventional compressor blading consists of standard airfoil shapes, the Mach number effects observed with usual subsonic airfoils can be expected to appear in compressor operation. A typical flow pattern observed over an isolated subsonic airfoil is shown in figure 1. For a high subsonic Mach number, the flow accelerates to supersonic velocities near the leading edge. Because of the curvature of the upper surface, the flow expands supersonically, producing a region of supersonic flow which must be decelerated back to the upstream subsonic Mach number. This deceleration generally takes the form of a normal shock with an attendant sudden increase in pressure across the shock. For entrance Mach numbers producing only limited regions of supersonic flow, with maximum surface Mach numbers of 1.1 or 1.15, the occurrence of the normal shock does not usually produce a large loss in lift or increase in drag. However, if the maximum surface Mach number exceeds about 1.25, the normal shock generally is accompanied by a pronounced separation, with an attendant loss in lift and very large increases in drag.

The Mach number effects observed in a cascade of blades are similar to those of an isolated airfoil (fig. 2). The effect of cascading, however, produces a section of minimum area, which limits the maximum mass flow that can be passed through the cascade. This area restriction

forces the cascade to operate at an angle of attack, resulting in a pronounced supersonic expansion near the leading edge of the blade. In addition, the static-pressure rise across the cascade produces a larger change from the minimum pressure to the exit pressure than otherwise occurs on an isolated airfoil. The combination of these factors leads to generally more severe losses at high Mach number for the cascade than for the isolated airfoil. The rapid expansion near the leading edge, as well as the low exit velocity, is illustrated in figure 3, which shows a typical velocity distribution over a subsonic airfoil in cascade at high Mach number.

Schlieren photographs of high-speed flow over a range of Mach number through a cascade of conventional blades are shown in figure 4. The tendency to form a shock is observed at an entrance Mach number of 0.75. Very pronounced shock formations are observed at a Mach number of 0.82, although flow separation is not severe. At Mach numbers of 0.88 and above, a very definite flow separation occurs, increasing markedly with Mach number. These observations are reported for a similar cascade in reference 1.

The observation that both isolated airfoils and cascades operate satisfactorily with local regions of supersonic flow indicates that supersonic Mach numbers in themselves do not constitute an invariable limit. The large static-pressure rise associated with normal shocks at the higher Mach numbers may reasonably be expected to be the cause of flow separation. If it is assumed that the pressure or velocity distribution existing around an airfoil is the principal factor affecting the blade-row performance, then the problems arise as to (1) the proper choice of the velocity distribution and (2) the computation of the blade shape to give the desired distribution. The approximate determination of the blade shapes for a prescribed velocity distribution will be discussed in the following section.

#### BLADE DESIGN

Prescribed velocity distribution. - On the basis of the preceding discussion, the design should control the velocity change that occurs through the shock system. However, the accurate determination of the shock system is questionable; consequently, the control of this velocity change specifically is difficult to achieve. A more convenient approach to the design would be to restrict the over-all velocity change on the suction surface from the peak or maximum velocity to the minimum or exit velocity. The velocity change that occurred through the shock system should then be less than or at most equal to this maximum velocity change.

A dimensionless parameter used to express the velocity change is the ratio

$$\frac{V_{\max} - V_{\min}}{V_{\text{ent}}} = \frac{V_{\max}}{V_{\text{ent}}} - \frac{V_{\text{ex}}}{V_{\text{ent}}}$$

where  $V_{\max}$  is the maximum velocity;  $V_{\text{ent}}$ , the entrance velocity;  $V_{\min}$ , the minimum velocity; and  $V_{\text{ex}}$ , the exit velocity. For isolated airfoils,  $V_{\text{ex}}/V_{\text{ent}} = 1.0$ ; however, for compressor blade rows this term is less than 1.0, and the value of  $V_{\max}/V_{\text{ent}}$  must be reduced to maintain the desired velocity ratio. The velocity ratio and its design use in terms of a diffusion factor will be discussed more completely in the following paper (or ref. 2).

The selection of the ratio between the maximum and exit velocities, as well as the variation of the velocity along the suction surface, should ideally be based on considerations of the boundary layer. However, a much easier starting point is to assume the approximate velocity distribution existing on an airfoil which has good performance characteristics in low-speed cascades. Such a distribution, approximated from the 65-(12)10 airfoil at an angle of attack of  $8^\circ$ , a solidity of 1.00, and an entrance flow angle of  $60^\circ$  (fig. 56, ref. 3), is shown in figure 5 plotted against percent of the axial length of the blade. The ratio of the maximum to exit velocity is held equal to 1.37. Because of the change in mean velocity occurring across the cascade, the maximum surface velocity for the blade in cascade is only 1.12 times the entering velocity.

Computation of blade shapes. - The accurate computation of the blade shape is practically impossible for the Mach number range of interest. The flow field is a mixed supersonic and subsonic field; and, in addition, the passage or stream-tube height decreases through the blade row. However, by applying approximate methods, a qualitative picture may be obtained of the effect of Mach number on blade camber and thickness distribution.

The approach follows that used in channel-flow solutions (ref. 4), where the mean channel velocity is assumed equal to an average of the blade-surface velocities. The pressure difference across the blade is assumed equal to the rate of change in moment of momentum of the average velocity. These assumptions have been found reasonably accurate for high-solidity blade rows, but for solidities below about 1.5, the results must be considered qualitative. Because of the simplicity of the method, mixed-flow regimes may be considered. The computational procedure of reference 4 gives the direction of the mean flow line, the blade-thickness term, and the required solidity. If the blade mean line is assumed to follow the flow mean line, then the blade shapes can be obtained.

The preceding approach is used to compute the approximate blade shape for a given prescribed velocity distribution for several relative entrance Mach numbers. The resulting blade shapes can be used only to obtain general trends that might be expected from high-speed blading. For the example, the prescribed velocity distribution of figure 5 is used with inlet flow angles of  $55^\circ$  and exit angles of  $40^\circ$  and with a constant axial velocity across the blade row. Blade shapes are determined for incompressible flow and for inlet Mach numbers of 0.8, 1.2, and 1.4. Because of the density change across the rotor at the higher Mach numbers, the required stream-tube height at the blade exit becomes appreciably smaller than that at the inlet (for the case of a Mach number of 1.4, the ratio of the exit to inlet stream-tube height is only 0.67).

The blade shapes obtained for the example are shown in figure 6. For incompressible flow, the blade resembles the conventional subsonic airfoil, with the exception that the leading-edge radius is small. Because of the assumption of similar mean velocity and loading distribution, the mean lines for all Mach numbers are very similar. The principal effect of the increased Mach number is the reduction in the maximum blade thickness, as might be expected from single airfoil theory. The position of maximum thickness shifts slightly toward the rear of the blade with increasing Mach number, so that at a relative entrance Mach number of 1.2, the thickness distribution is nearly symmetrical. The mean line of the blade is close to a circular arc; consequently, the blade shape for a Mach number of 1.2 can be approximated closely by the double circular-arc-type airfoil.

The solidity necessary to maintain the prescribed velocity ratios increased very slightly with Mach number, ranging from 1.04 for the incompressible case to 1.08 for a Mach number of 1.4.

#### EXPERIMENTAL RESULTS

Compressor blade shapes similar to those obtained in the example have been experimentally investigated over a range of inlet Mach number as single-stage rotors. Blade shapes very close to the double circular arc were used in a rotor having a design tip speed of 1000 feet per second and a tip relative Mach number of 1.1. The performance for this rotor is shown in figure 7. The rotor gave good performance at design speed and showed no sacrifice in part-speed operation due to the small leading-edge radii (refs. 5 and 6).

Blade shapes similar to that obtained for the inlet Mach number of 1.4 were used in the design of a compressor having a design tip speed of 1400 feet per second. The performance of this rotor is shown in figure 8. Here again, acceptable efficiencies were obtained at the higher tip speeds with no significant sacrifice in part-speed performance. The low values

[REDACTED]

of mass flow per unit frontal area are due to the high inlet hub-tip ratio of 0.7. At maximum-efficiency design-speed operation, the stator-entrance Mach number was less than 0.85 and the stator-entrance angle was about  $45^\circ$ . The exit distribution was similar to that obtained in the usual transonic rotors, and stator design was not considered a serious problem.

The effect of Mach number on over-all performance may be illustrated by figure 9, where the rotor efficiency is plotted as a function of tip relative Mach number. On the basis of the limited data available, the effect of Mach number on efficiency will be small if adequate care is taken in using blade shapes and solidities to limit the maximum velocities occurring on the blade surfaces. The very significant increase in stage pressure ratio available by use of the increased relative Mach numbers and higher rotor speeds is also illustrated.

#### CONCLUSIONS

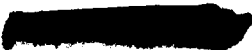
On the basis of limited experimental results, the control of the blade-surface velocity extremes appears to be a more critical factor in the design of high-speed compressor blading than an isolated Mach number effect. Efficient operation of compressors with relative Mach numbers to 1.4 has been obtained.

By use of a very approximate design method to obtain a qualitative picture of the effect of Mach number on blade shapes, the following observations were made:

1. The stream-tube height across the blade row must be appreciably reduced for higher Mach numbers.
2. A double circular-arc airfoil approximates the blade shape obtained for Mach numbers of about 1.2.
3. The principle effects of increasing Mach number were to reduce the blade thickness, shift the position of maximum thickness toward the rear of the blade, and increase the solidity slightly.

#### REFERENCES

1. Bogdonoff, Seymour M.: NACA Cascade Data for the Blade Design of High-Performance Axial-Flow Compressors. Jour. Aero. Sci., vol. 15, no. 2, Feb. 1948, pp. 89-95.
  2. Lieblein, Seymour, Schwenk, Francis C., and Broderick, Robert L.: Diffusion Factor for Estimating Losses and Limiting Blade Loadings in Axial-Flow-Compressor Blade Elements. NACA RM E53D01, 1953.
- [REDACTED]

- 
3. Herrig, L. Joseph, Emery, James C., and Erwin, John R.: Systematic Two-Dimensional Cascade Tests of NACA 65-Series Compressor Blades at Low Speeds. NACA RM L51G31, 1951.
  4. Stanitz, John D.: Approximate Design Method for High-Solidity Blade Elements in Compressors and Turbines. NACA TN 2408, 1951.
  5. Lieblein, Seymour, Lewis, George W., Jr., and Sandercock, Donald M.: Experimental Investigation of an Axial-Flow Compressor Inlet Stage Operating at Transonic Relative Inlet Mach Numbers. I - Over-All Performance of Stage with Transonic Rotor and Subsonic Stators up to Rotor Relative Inlet Mach Number of 1.1. NACA RM E52A24, 1952.
  6. Schwenk, Francis C., Lieblein, Seymour, and Lewis, George W., Jr.: Experimental Investigation of an Axial-Flow Compressor Inlet Stage Operating at Transonic Relative Inlet Mach Numbers. III - Blade-Row Performance of Stage with Transonic Rotor and Subsonic Stator at Corrected Tip Speeds of 800 and 1000 Feet Per Second. NACA RM E53G17, 1953.
- 

HIGH-SPEED FLOW OVER ISOLATED AIRFOIL

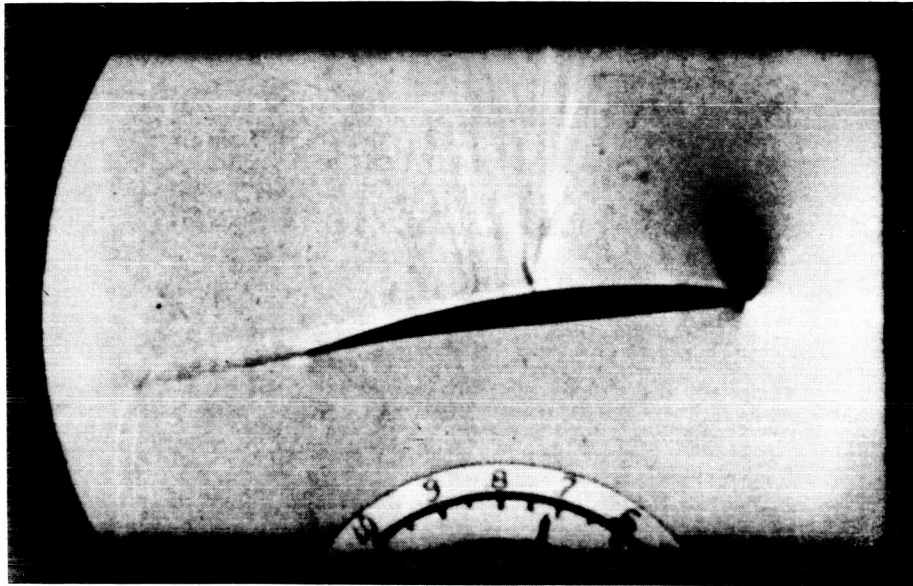


Figure 1

HIGH-SPEED FLOW THROUGH CASCADE

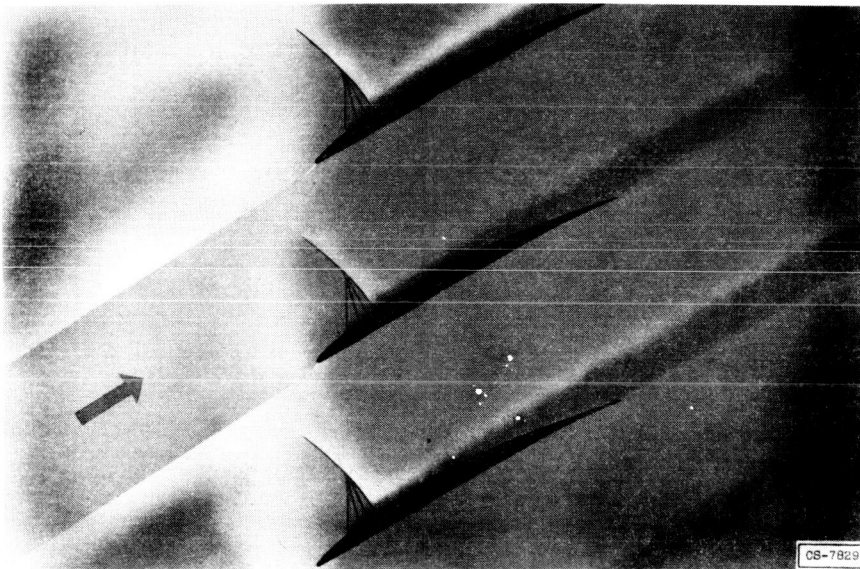


Figure 2



### VELOCITY DISTRIBUTION OVER SUBSONIC AIRFOIL AT HIGH MACH NUMBER

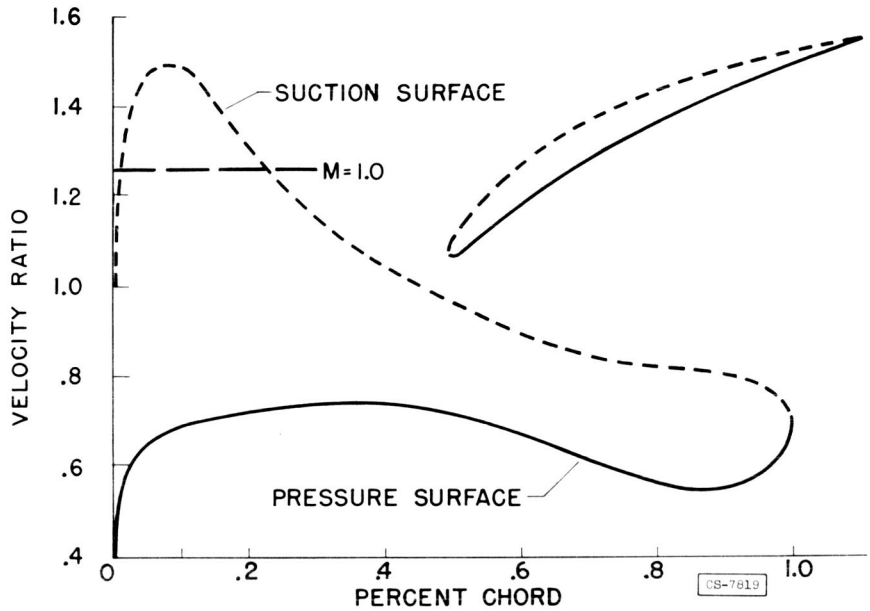


Figure 3

### CASCADE SCHLIEREN PHOTOGRAPHS FOR RANGE OF MACH NUMBER

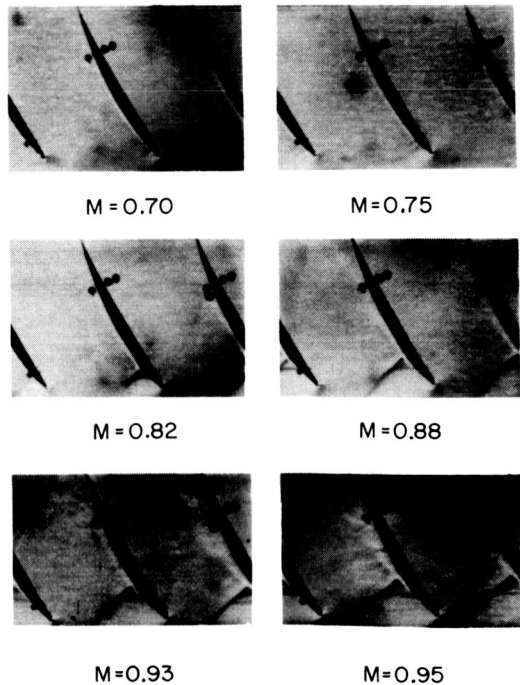
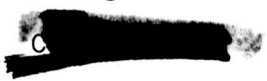


Figure 4



PREScribed VELOCITY DISTRIBUTION  
OVER AN AIRFOIL IN CASCADE

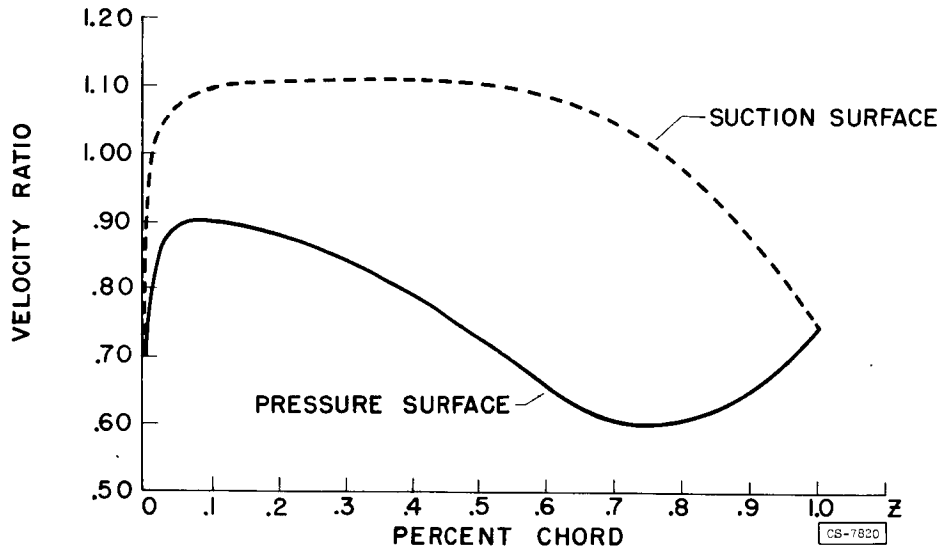


Figure 5

COMPUTED BLADE SHAPES FOR A PRESCRIBED VELOCITY DISTRIBUTION

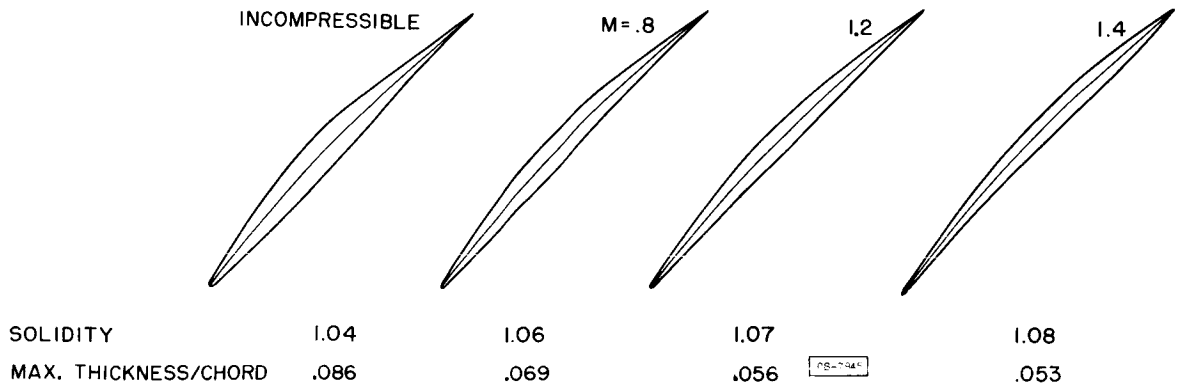
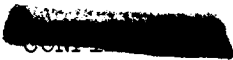


Figure 6



PERFORMANCE OF FIRST TRANSONIC ROTOR

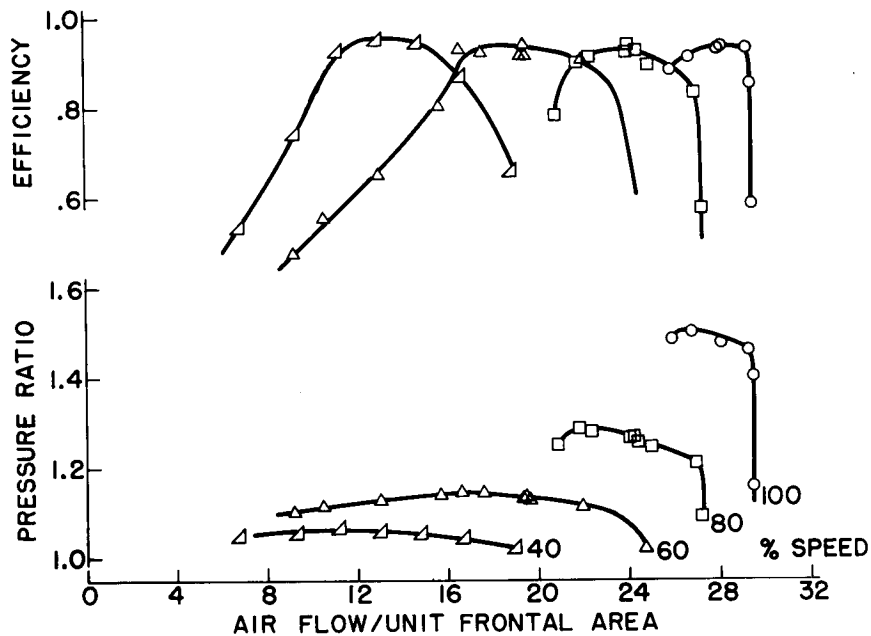


Figure 7

PERFORMANCE OF A 1400 FT/SEC TIP SPEED  
COMPRESSOR ROTOR  
HUB-TIP RADIUS RATIO, 0.7

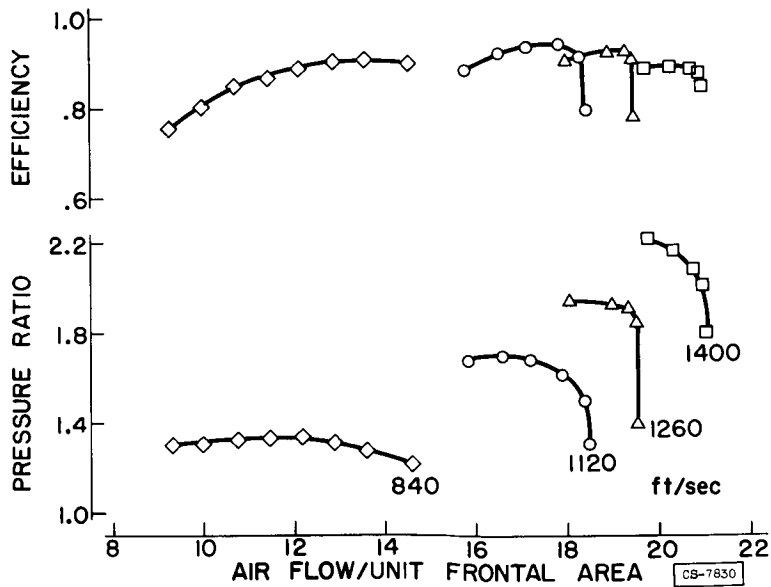
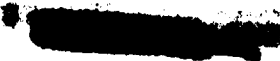


Figure 8



EXPERIMENTAL PERFORMANCE OF TWO COMPRESSOR  
ROTORS HAVING HIGH MACH NUMBERS

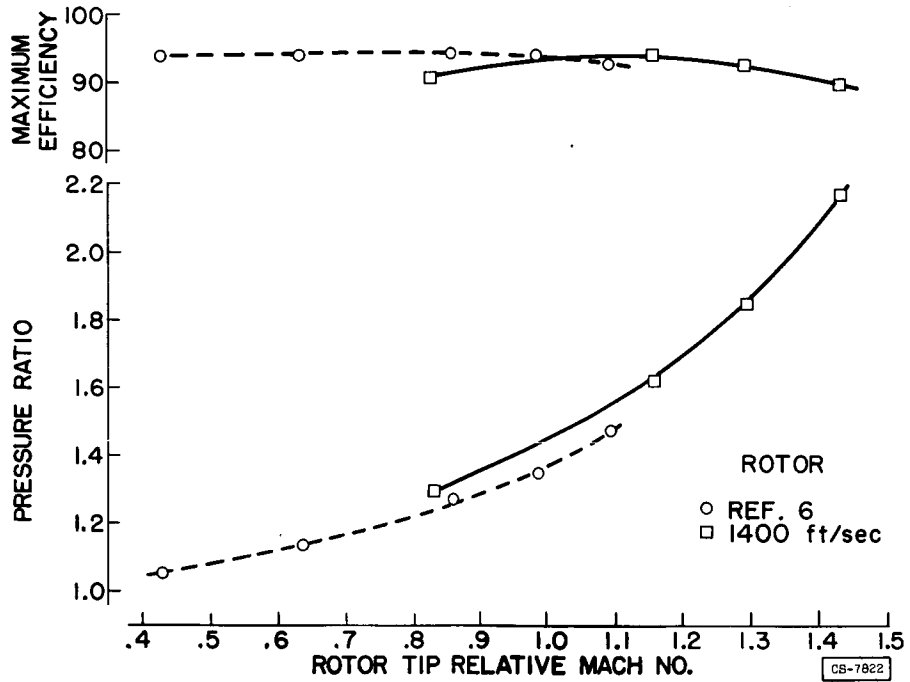


Figure 9

## FLOW CHARACTERISTICS OF COMPRESSOR BLADE ELEMENTS

By Seymour Lieblein

## INTRODUCTION

3078-A

The paper by Klapproth discusses some of the problems and accomplishments associated with the development of compressor blading for rotor operation at transonic relative inlet Mach numbers. The present paper discusses several additional flow characteristics of compressor blade elements and presents some recent results obtained from an analysis of these characteristics. The principal blade-element characteristics discussed are: (1) the design angle of incidence (similar to angle of attack of a wing), (2) the magnitude of the loss in total pressure across the blade, and (3) the blade deviation angle, which determines the direction of the outlet air. The basic parameters defining the flow across blade elements are illustrated in figure 1.

With regard to research, the approach to the problem of obtaining good design control involves a detailed analysis of the basic flow phenomena in compressor blade elements. From this fundamental understanding of the flow can then be evolved a series of empirical correlations and analytical relations that describe the variation of the principal flow characteristics and limitations over a wide range of operating conditions. At the same time, techniques must be developed for incorporating this information into the compressor design procedure in a simple and accurate manner.

## DESIGN INCIDENCE ANGLE

Experiences with compressor blade sections have shown that a considerable reduction in the low-loss range of operation occurs as the inlet Mach number is increased into the transonic range. Typical examples of the variation of total-pressure loss coefficient with air incidence angle in the tip region of a transonic-compressor rotor blade at increasing levels of relative inlet Mach number are shown in figure 2. Each curve represents the range of operation at a given rotor wheel speed. The Mach numbers shown in the figure are the values at the points of minimum loss. Total-pressure loss coefficient is defined as the ratio of the relative drop in total pressure across the blade to the difference between total and static pressure at the inlet to the blade (see ref. 1). It can be readily seen from the figure that in the transonic range of inlet Mach number, the design incidence angle must be known within very close tolerances if minimum loss is to be obtained. (Design incidence angle is defined as the incidence angle at minimum loss coefficient.)

The reduction in range of operation at the higher Mach number levels is a result of compressibility effects on the blade sections. Because of the high values of inlet Mach number, small variations in the inlet flow direction above and below the best approach angle result in very rapid accelerations of the flow around the leading edge of the blade, with the subsequent formation of strong shocks and flow separation. Limited experimental data from transonic rotors indicate a small gradual increase in the magnitude of the minimum loss angle of incidence as the Mach number is increased above values of about 0.75 to 0.85 (fig. 2). However, in the absence of practical theory describing the velocity distributions in the approach and inlet regions of the blade element in the transonic range, these high-speed characteristics cannot be accurately determined. (The calculation methods used in the paper by Klapproth are not sufficiently accurate for this problem.)

Some general observations can be made, however, from an examination of the problem. For blade configurations involving high solidities and low blade-chord angles, as is the case for the hub region of a rotor, the necessity of angles of incidence of several degrees positive becomes apparent from an inspection of the variation of the blade passage area. In figure 3 is shown a typical hub-section blade passage. If the approach direction  $A_1$  is at a negative angle of incidence  $-i$ , as shown by the dashed lines, a minimum area ratio will be formed in the inlet region of the passage which will ultimately result in a premature choking of the flow as the inlet Mach number is increased. At some positive angle of incidence  $+i$ , however, as illustrated by the solid approach lines, the approach area  $A_2$  becomes approximately equal to the passage throat area, and higher values of inlet Mach number can then be tolerated. For the rotor tip region, where the solidity is low and the blade-chord angles are high, however, the previous one-dimensional picture becomes questionable because of the absence of a well-defined blade passage. For example, as shown in figure 3 for a typical tip-section configuration, the minimum flow area may occur outside the blade-passage throat. At the moment, the determination of design incidence angle in the transonic range appears to be primarily an experimental problem.

#### TOTAL-PRESSURE LOSS

The efficiency of a compressor stage at its design condition is determined by the magnitude of the minimum loss of the blade elements in conjunction with the work input level of the rotor. At first thought, it would appear that operation at higher levels of inlet Mach number and pressure ratio would necessarily increase the total-pressure losses across the blade rows, and therefore would result in lower levels of stage efficiency. However, it must be kept in mind that efficiency is a function of both loss and pressure-ratio level; and therefore the success of the high-performance stage will depend on the relative rates of increase of loss and work level with increasing Mach number. In general, the

greater the pressure ratio, the larger the loss may be for the same efficiency. This consideration is demonstrated in figure 4, which shows the variation of rotor relative total-pressure loss coefficient with stage pressure ratio that is allowable in order to maintain a stage efficiency of 0.90 at rotor-inlet Mach numbers of 0.75 (conventional subsonic) and 1.1 (transonic). For example, an increase in stage pressure ratio from 1.2 to 1.4 at either Mach number level can be accomplished without sacrifice in efficiency even if the rotor loss coefficient is approximately doubled.

The curves of figure 4 also provide some insight into a comparative evaluation of the design characteristics of subsonic and transonic stages. At best, the transonic blade element can have a loss coefficient equal to the loss coefficient of the subsonic blade element. Thus, for the same loss coefficient, if a transonic stage operating at a rotor-inlet Mach number of 1.1 is to have the same stage efficiency as a conventional subsonic stage operating at a rotor-inlet Mach number of 0.75 and pressure ratio of 1.25, it must produce a pressure ratio of at least about 1.4.

The accurate prediction or control of efficiency in axial-flow compressors has been very difficult to achieve because of a general lack of specific data concerning the various losses occurring in compressor blade rows. Aside from three-dimensional end effects, the principal factors contributing to the loss across individual compressor blade elements are recognized as (1) the relative inlet Mach number (compressibility and shock losses) and (2) the blade loading (a measure of the strength of the velocity gradients and therefore the boundary-layer growth on the blade surfaces).

Mach number. - As indicated in the previous paper, the principal difficulty with compressibility effects occurs when the surface shock waves become sufficiently strong to result in a separation of the boundary layer behind the shock. Shock separation is generally indicated by a relatively sharp increase in loss as Mach number is increased. An example of a loss against Mach number curve for a conventional 10-percent-thick 65-series blade section in a two-dimensional cascade and in several compressor stators and rotors is shown in figure 5. Each symbol represents a particular tip speed for a particular compressor. A noticeable limitation is indicated for this blade. In the transonic compressor, the picture is somewhat complicated by the close relation between blade loading and inlet Mach number. For example, for an experimentally determined loss value at high rotor relative Mach numbers, it is difficult to ascertain the degree to which the high loss is a result of the shock effects or of the blade loading, since both generally increase with increasing Mach number. Extensive experimental and analytical research will be necessary to establish the relations among inlet Mach number, blade loading, and loss for compressor blade rows.

Blade loading. - In general, at design incidence angle, the velocity along the suction surface of a compressor blade attains some maximum value in the inlet region of the blade and then decreases to the level of the outlet velocity at the trailing edge. Recent studies of boundary-layer theory have indicated that it is primarily the difference between the maximum surface velocity and the outlet velocity that controls the growth of the boundary layer on the blade suction surface. For high values of pressure rise, this velocity difference may become large and may result in a separation of the boundary layer, a condition referred to as blade stall.

As a general design procedure, it is impractical to compute suction-surface velocities for various blade shapes over wide ranges of design conditions. In the interest of simplicity, it was desirable to obtain an approximate blade-loading parameter based on the suction-surface velocity difference but expressed in terms of the over-all velocities and geometry of the element.

In isolated-airfoil theory, the measure of blade loading and stall is given in terms of the well-known lift coefficient. However, the lift coefficient when applied to compressors of high pressure rise has not been universally successful. For the isolated airfoil, since the outlet velocity is always equal to the inlet velocity, the suction-surface velocity difference is generally directly proportional to the lift coefficient. In the compressor blade row, however, because of the over-all pressure rise, the outlet velocity is less than the inlet velocity, and the suction-surface velocity difference is then no longer uniquely proportional to the lift coefficient. It was necessary, therefore, to develop new loading parameters that are more applicable to compressor design. One of these parameters; the diffusion factor, has been very successful in correlating cascade and single-stage compressor losses (ref. 1). The basis of the development of the diffusion factor is shown in figure 6. Specifically, the diffusion factor, by means of several simplifying approximations and assumptions, is an approximate relation that describes the maximum suction-surface velocity difference of a typical compressor blade velocity distribution at design incidence angle with the over-all velocity characteristics and geometry of the blade element. The symbol  $\sigma$  in figure 6 is the solidity of the element defined as ratio of blade chord to spacing (see fig. 1).

Examples of rotor and stator loss correlations are shown in figure 7. Data for the stator loss correlation were obtained from hub-, tip-, and mean-radius regions. At the rotor hub-radius and mean-radius regions, the loss trend is similar to that in the stator. An interesting result of the analysis was the tip-region loss correlation for the rotors. Inasmuch as the tip-region losses are primarily the result of blade end effects (data were obtained at points approximately 12 percent of the radial passage height away from the rotor tip), it appears that the

blade-element loading in this region is related to the strength of the clearance and end effects. At least as far as the inlet stage is concerned, the rotor tip diffusion factor appears to be the principal determinant of the efficiency of the stage.

The development of a satisfactory blade-loading parameter, like the diffusion factor, provides additional uses in the analysis of experimental data and of desirable velocity diagrams. Compressor test data indicate an increase in blade-element loss coefficient as inlet Mach number is increased into the transonic range (see fig. 2). First thought would be to attribute the poorer performance to shock losses. However, this may not necessarily be the case, since the blade loading also becomes greater as Mach number is increased. For example, in figures 8(a), (b), and (c) are shown the variations of relative inlet Mach number, diffusion factor, and loss coefficient with incidence angle for the tip region of a transonic rotor (ref. 2). A plot of loss coefficient against diffusion factor in the minimum loss range is then shown in figure 8(d) in comparison with the limits of data obtained for blades operating below their limiting (high shock loss) Mach numbers shown in figure 7. Thus the increased loss at the higher Mach number level can be explained on the basis of the increased diffusion factor. If strong shock losses had been present, the data points at the higher speed levels in figure 8(d) would be expected to be greater in magnitude than observed.

Velocity diagram analysis. - The use of the blade-element diffusion factor in velocity diagram analysis is illustrated in the following calculation. For a conventional constant-work-input, subsonic inlet stage with inlet guide vanes operating at a specific weight flow of 27 pounds per second per square foot frontal area (0.5 inlet hub-tip ratio) and a maximum rotor-inlet Mach number of 0.75, a maximum stage pressure ratio of 1.20 is indicated for a tip diffusion factor of 0.4. This subsonic stage will then appear as shown on the allowable loss curve of figure 4. For a constant-work-input transonic stage operating at a rotor tip relative inlet Mach number of 1.1 (no inlet guide vanes) at the same tip speed and at a specific weight flow of 31 pounds per second per square foot frontal area (0.5 inlet hub-tip ratio), a maximum stage pressure ratio of 1.38 can be obtained for the same rotor tip diffusion factor of 0.4 and same solidity (also same stator conditions). The transonic stage is also shown in figure 4. Thus, it is seen from figure 4 that, even if the loss coefficient of the transonic stage is increased slightly, it is still possible to achieve the same efficiency as the subsonic stage. Loss coefficients for the transonic rotor not measurably greater than the loss coefficients of the subsonic rotor are entirely reasonable, since, in general, the blade loading losses will be about the same (same diffusion factor) and since recent experimental evidence seems to indicate that, for properly designed blading, shock losses remain small for inlet Mach numbers up to about 1.1.

On the basis of the preceding analysis, a better insight can be gained into the reasons for the initial success of the transonic inlet stage. First, with the elimination of the rotation introduced by the inlet guide vanes, the steep radial gradient of axial velocity at the rotor outlet, which resulted in a large drop in axial velocity across the rotor tip, was eliminated. The absence of this large diffusion in relative velocity across the rotor tip in the transonic rotor then permitted a much higher change in tangential velocity  $\Delta V_\theta$  and therefore pressure ratio to be achieved before the limiting diffusion factor was attained (see equation and velocity diagram of fig. 6). At the same time, the thinner blades kept the shock losses down and maintained a comparable level of total loss. The combination of higher pressure ratio and equivalent loss coefficients then maintained the over-all efficiency level at the higher Mach numbers. Thus, within limits, the transonic configuration presents a compressor stage that is inherently capable of producing at least the same efficiencies as conventional subsonic stages at higher levels of pressure ratio and flow capacity.

#### DEVIATION ANGLE

The third problem involves the accurate control over the direction of the flow leaving the blade element. Flow outlet angles are usually considered in terms of the deviation angle. As shown in figure 1, the deviation angle is defined as the difference between the angle of the air leaving the blade and the angle of the blade trailing edge. Figure 9 illustrates the calculated magnitudes of the differences in pressure ratio and diffusion factor resulting from a misdesign in rotor-outlet (deviation) angle for a typical rotor of an inlet stage. Blade elements that will produce the desired flow conditions must therefore be designed with great care, particularly in the tip region of the rotor.

The importance of the establishment of good design control in high-performance compressors was clearly indicated by the performance of early transonic rotors. For the transonic unit shown in figure 9 of the paper by Johnsen and Bullock, although very good efficiency was obtained, the values of pressure ratio and weight flow at design speed were different from the design values. These differences in performance were the result of a general lack of knowledge of the flow characteristics of transonic blade elements.

The most accurate source of deviation angle data is direct investigations of compressors operating in the transonic range. However, data from rotating units are limited and relatively difficult to obtain. Fortunately, experiences have indicated that Mach number level has a negligible effect on the magnitude of the deviation angle as long as the losses are kept low. Therefore, if attention is restricted to the design incidence-angle setting (condition of minimum loss), it may be possible to utilize low-speed

considerations in predicting deviation angles for transonic application. In view of the fact that deviation angle varies substantially with blade camber, solidity, and air inlet angle, the determination of deviation-angle data at design incidence angle over a wide range of blade configurations is a large undertaking. Accordingly, the possibility of using potential flow theory in establishing the basic trends of variation of the deviation angle was investigated.

The use of a circular-arc mean line as a satisfactory camber shape for transonic application simplifies the problem to a large extent because of the availability of cascade data and potential theory for this blade shape. Low-speed deviation-angle data for circular-arc mean lines can be readily obtained from the theory of reference 3 and, for a more limited range, from Carter's rule (ref. 4). The theory of references 3 and 4 indicates that, at constant solidity, the deviation angle at design incidence angle will vary very nearly linearly with camber angle for given values of air inlet angle.

In investigating the applicability of the theoretical variations of deviation angle, use was made of the extensive low-speed cascade data for the 65-series blade presented in reference 5. The 65-series mean line is very close to a circular arc in shape and can be expressed in terms of an "equivalent" circular arc having the same maximum camber as shown in figure 10. Examples of the variation of deviation angle at midpoint of the loss range with camber angle for the data of reference 5 are shown in figure 11 for a solidity of unity. (The data points for the largest values of camber at an air inlet angle of  $45^\circ$  and  $60^\circ$  were omitted because of excessive boundary-layer separation at these conditions.)

The theoretical curves in figure 11 indicated by the solid line were obtained by applying the theory of reference 3 and displacing the resulting values upward by an amount (constant with camber) necessary to give the best correlation at each inlet angle. The increase in the theoretically derived deviation angles is necessary because the theory of reference 3 considers an airfoil of zero thickness, so that, for the uncambered element, the deviation angle is zero. For blades with finite thickness, however, potential theory indicates that the deviation angle for the uncambered airfoil is generally not zero, but is some finite positive quantity which becomes larger as the solidity and air inlet angle are increased. An upward displacement of the theoretical values should therefore be expected for usual circular-arc profiles. Good correlation is thus obtained when the thickness effect is considered.

These preliminary results suggest the possibility of the use of potential theory in conjunction with experimentally determined deviation-angle characteristics of the uncambered or symmetrical profile as a simple approach to the problem of the establishment of deviation-angle design data for the compressor. However, further work along these lines is required, particularly with respect to experimental verification in the actual compressor, before reliable design data can be presented.

## CONCLUDING REMARKS

The preceding discussion has attempted to demonstrate the importance of accurate and extensive knowledge of the flow characteristics of individual blade elements in the successful development of high performance compressors. A detailed knowledge of blade-element flow is desirable not only for obtaining a better understanding of the actual compressor flow but as a means of developing improved design techniques and basic loss and deviation-angle data. It is hoped that the problems discussed and results presented will be of some help to the compressor designer and also encourage further work in the study of compressor blade-element characteristics.

## REFERENCES

1. Lieblein, Seymour, Schwenk, Francis C., and Broderick, Robert L.: Diffusion Factor for Estimating Losses and Limiting Blade Loadings in Axial-Flow-Compressor Blade Elements. NACA RM E53D01, 1953.
2. Schwenk, Francis C., Lieblein, Seymour, and Lewis, George W., Jr.: Experimental Investigation of an Axial-Flow Compressor Inlet Stage Operating at Transonic Relative Inlet Mach Numbers. III - Blade-Row Performance of Stage with Transonic Rotor and Subsonic Stator at Corrected Tip Speeds of 800 and 1000 Feet Per Second. NACA RM E53G17, 1953.
3. Weinig, Fritz: The Flow Around the Blades of Turbomachines. Johann Ambrosius Barth (Leipzig), 1935.
4. Carter, A. D. S.: The Low Speed Performance of Related Airfoils in Cascade. Rep. No. R.55, British N.G.T.E., Sept. 1949.
5. Herrig, L. Joseph, Emery, James C., and Erwin, John R.: Systematic Two-Dimensional Cascade Tests of NACA 65-Series Compressor Blades at Low Speeds. NACA RM L51G31, 1951.

BLADE ELEMENT PROPERTIES

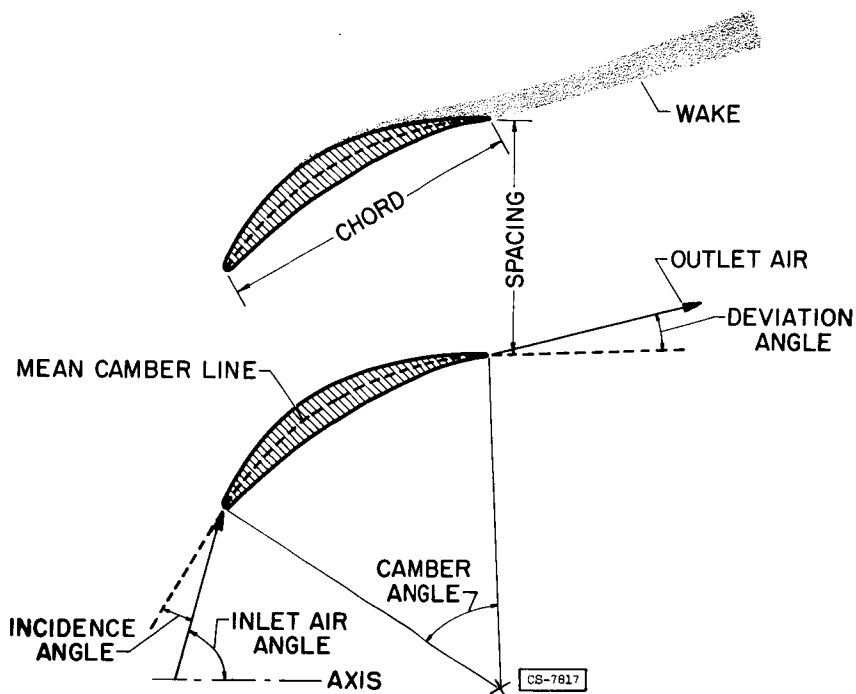


Figure 1

EFFECT OF RELATIVE MACH NUMBER ON ROTOR RANGE OF OPERATION

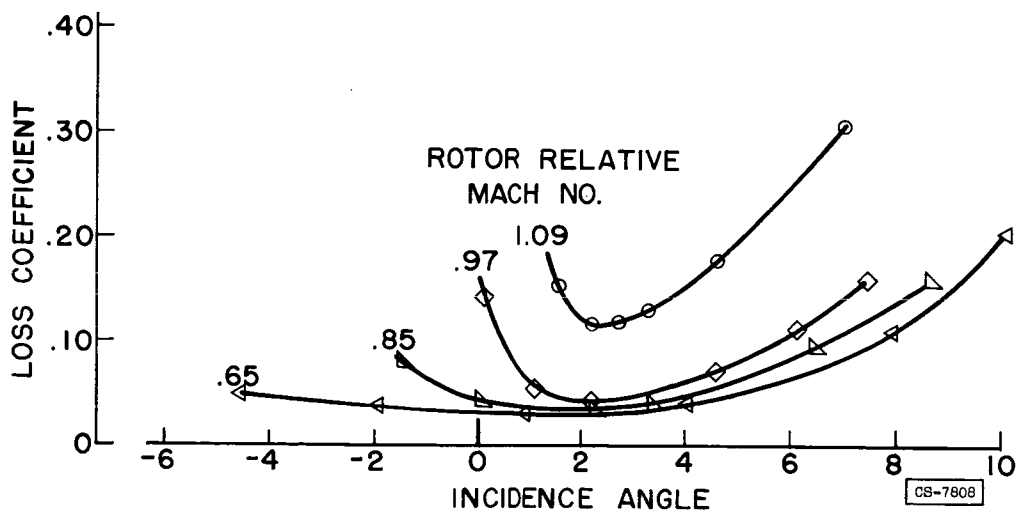
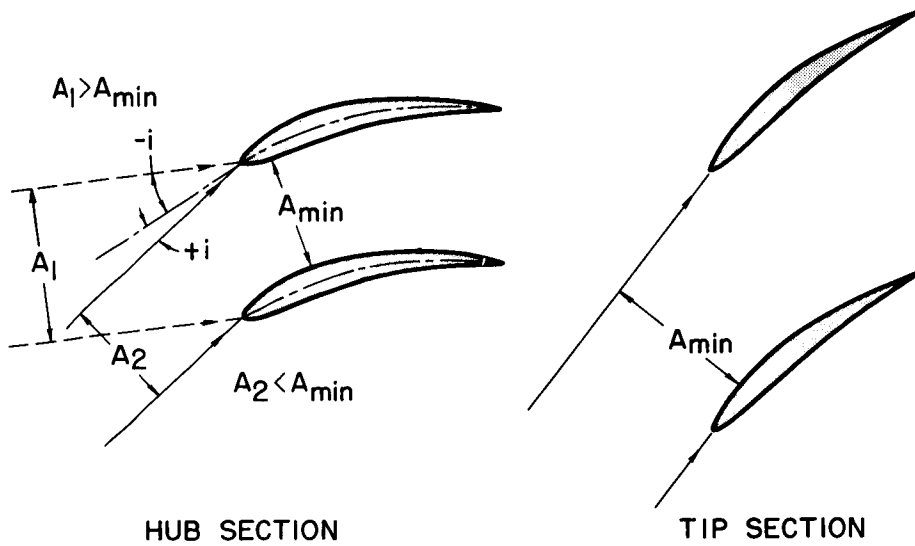


Figure 2

### BLADE PASSAGE AREA



3078-A

Figure 3

### ALLOWABLE ROTOR LOSS FOR STAGE EFFICIENCY OF 0.90

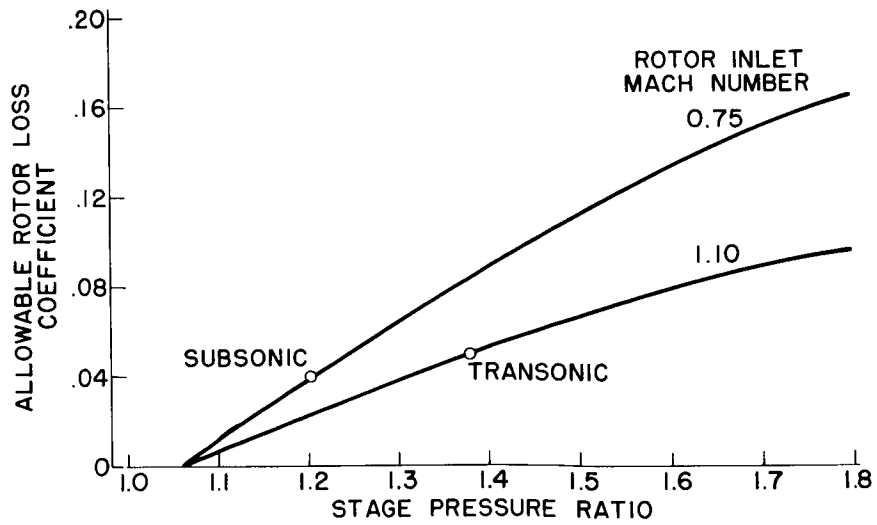


Figure 4

EFFECT OF INLET MACH NUMBER ON CONVENTIONAL BLADE ELEMENT

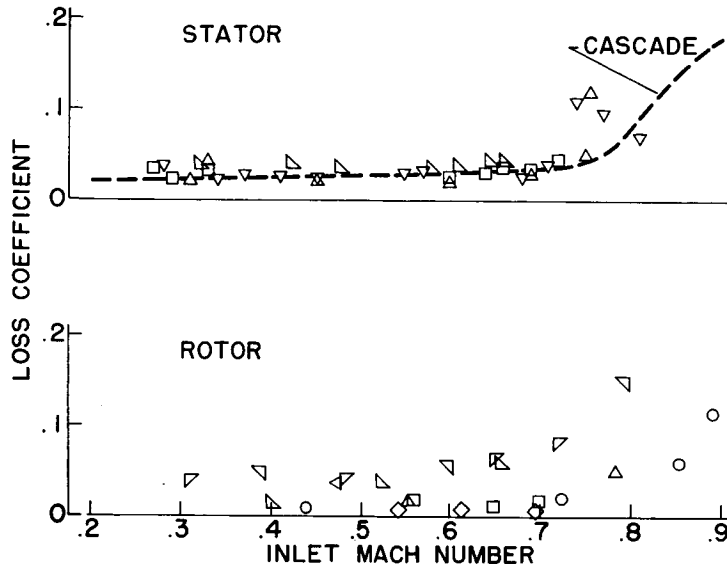
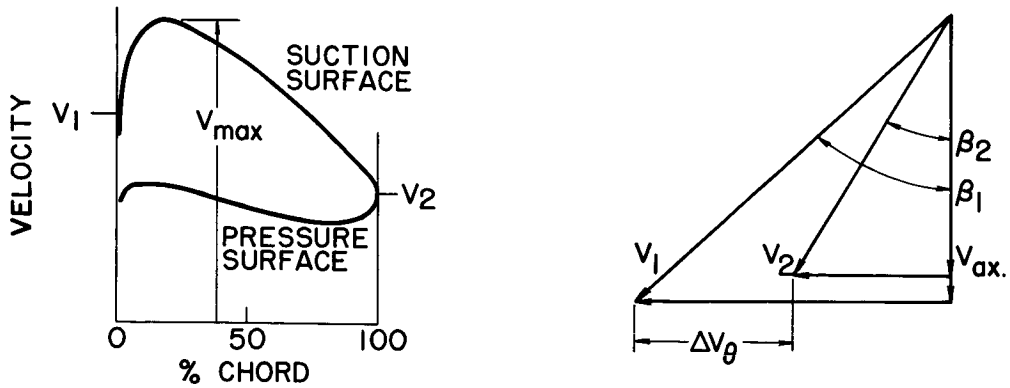


Figure 5

DEVELOPMENT OF DIFFUSION FACTOR



$$\text{DIFFUSION FACTOR} = \frac{v_{\max} - v_2}{v_{\text{av.}}} \approx \frac{v_{\max} - v_2}{v_1} \approx \frac{v_1 + \frac{\Delta V_\theta}{2\sigma} - v_2}{v_1}$$

$$D = 1 - \frac{v_2}{v_1} + \frac{\Delta V_\theta}{2\sigma v_1}$$

Figure 6

DIFFUSION FACTOR CORRELATION FOR COMPRESSOR INLET STAGES

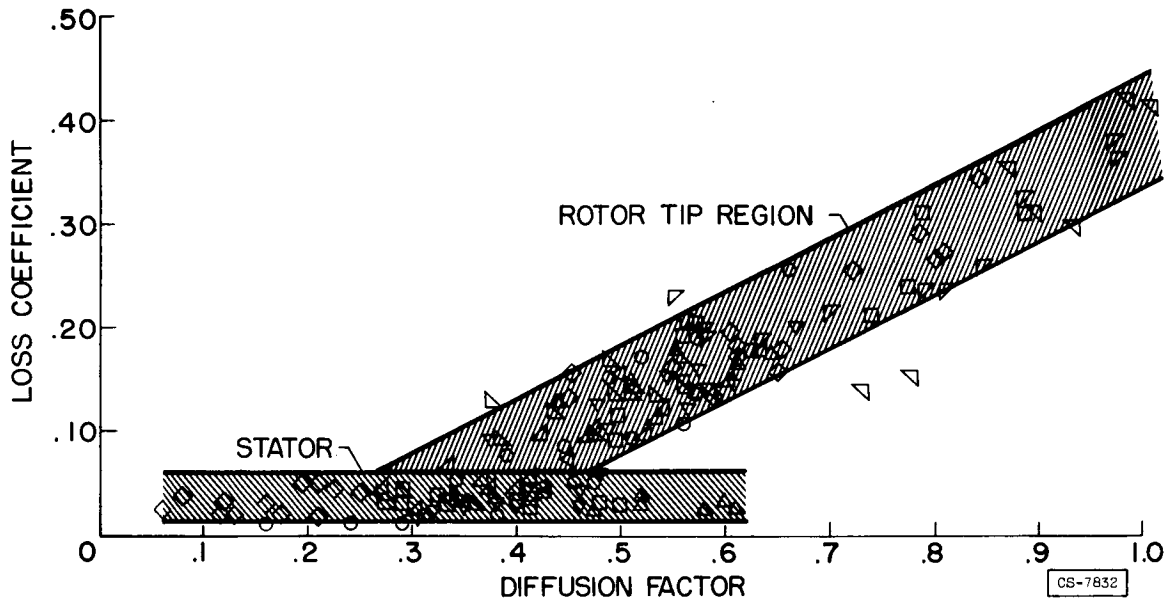


Figure 7

BLADE-ELEMENT LOSS ANALYSIS FOR ROTOR TIP REGION

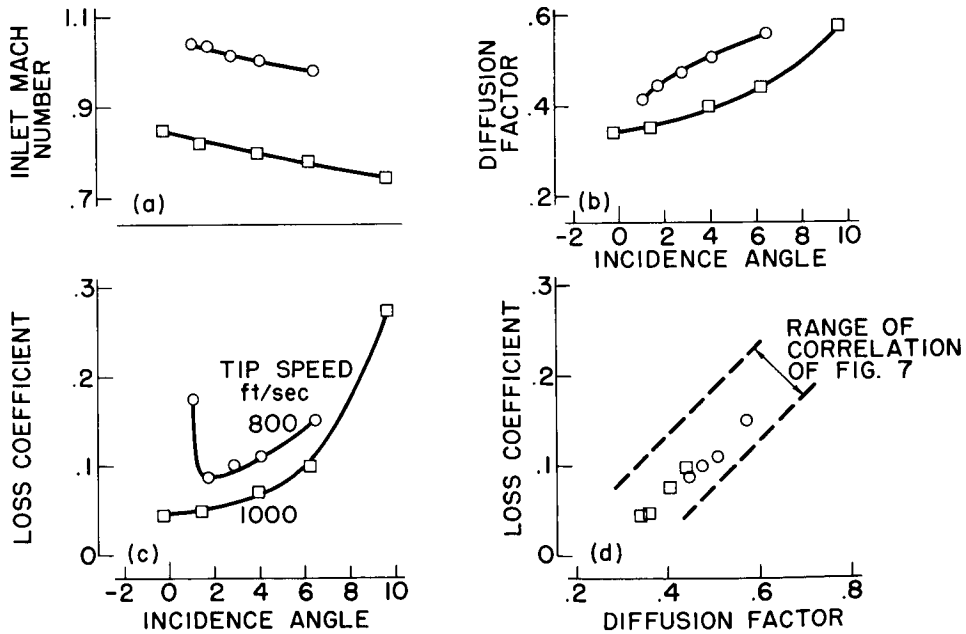


Figure 8

EFFECT OF ERROR IN OUTLET AIR ANGLE FOR TYPICAL TRANSONIC ROTOR

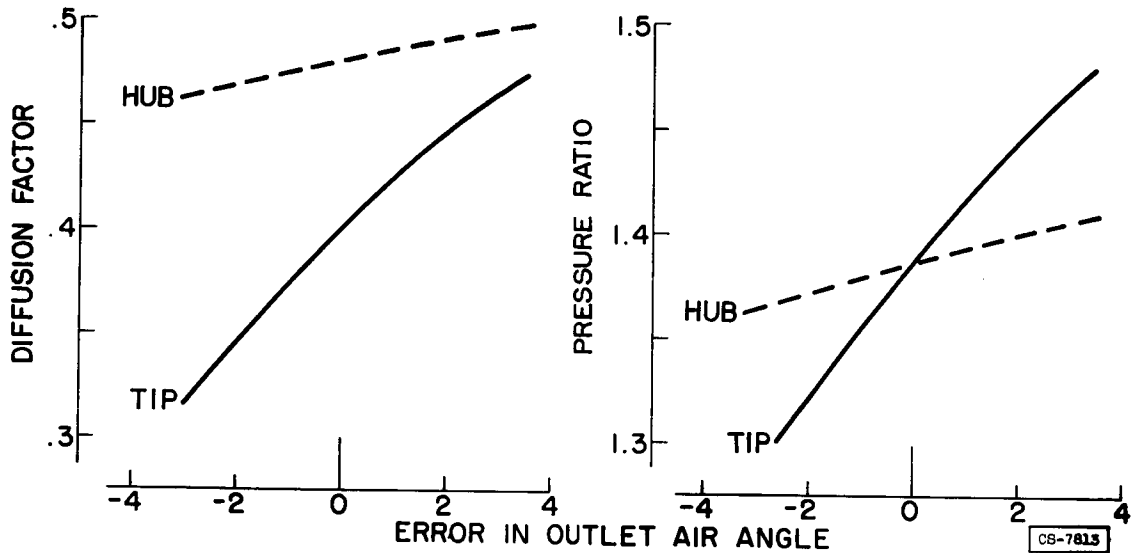


Figure 9

EQUIVALENT CIRCULAR ARC FOR 65-SERIES BLADES

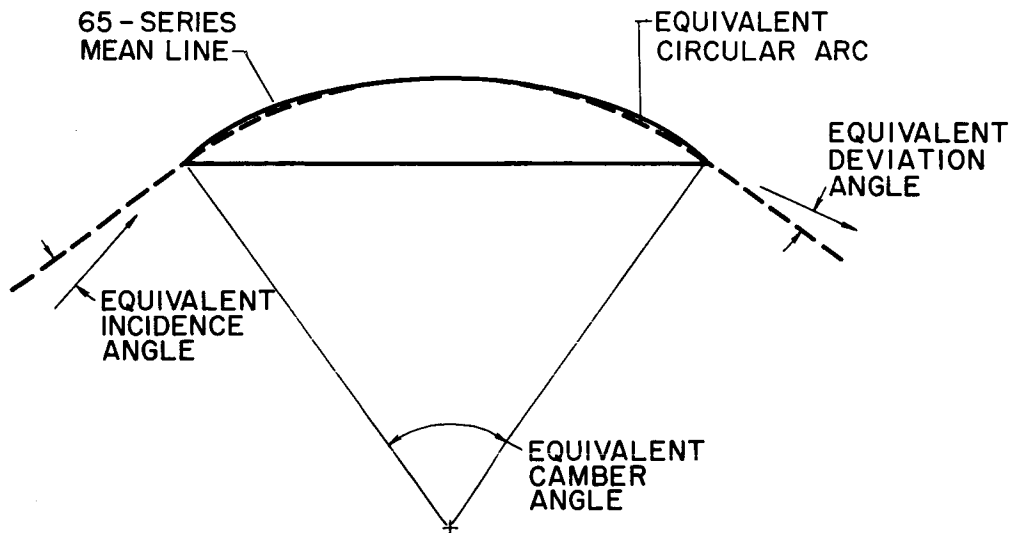


Figure 10

### DEVIATION ANGLE CORRELATION WITH CAMBER ANGLE FOR CIRCULAR ARC BLADES

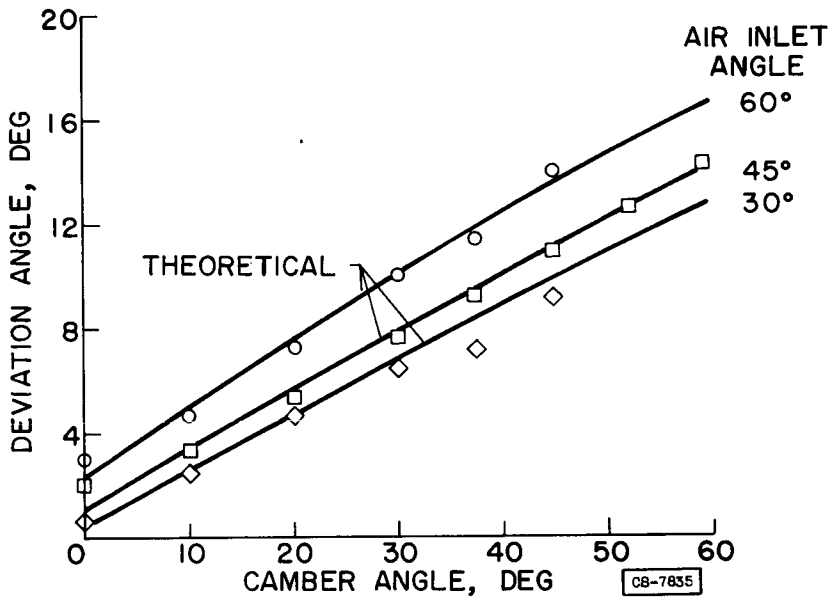


Figure 11

## APPLICATION OF BLADE ELEMENT DATA TO STAGE DESIGN

By James E. Hatch and Harold B. Finger

## INTRODUCTION

Thus far in the discussion of the compressor design and performance analysis, the performance of a blade element has been the principal consideration; that is, the turning and loss characteristics of a row of blades along a given streamline as well as some idea of limits of environment have been studied. A full blade row, however, is made up of an infinite number of these blade element sections stacked one on the other along the radius (fig. 1). Therefore, it becomes necessary to determine the basic flow relations that must be satisfied to stack these blade elements properly so that all the elements together will give the desired blade row performance. The importance of the proper means of stacking the blade elements is demonstrated by the following examples.

To illustrate this problem, in the design procedure (as has been done in some cases), the axial flow in the annulus between the rotor and the casing after the compressor inlet guide vanes is assumed to be similar to the parabolic-shaped flow obtained in a pipe (fig. 2). The blade elements at each radial position are then set to operate at a low loss value of incidence angle. If the velocity distribution behind these guide vanes is then actually measured, the type of axial velocity distribution would be that shown (fig. 2). The actual velocity distribution would depend upon the amount and distribution of turning in the inlet guide vanes. In terms of the angle of incidence on the blade elements, this actual velocity distribution would give the results indicated in figure 3. Obviously, the sections are not operating at the low loss values of incidence angle intended. Poor performance at the design point would result from a lack of understanding of a basic law of nature - that radial distribution of axial velocity depends on the magnitude and distribution of the turning.

A similar case which requires a complete knowledge of the fundamental laws governing the blade element stacking technique is to suppose that this actual measured velocity distribution at the inlet to the rotor row is used and the rotor blade elements are set at the proper angles for this distribution. Then, if the axial velocity distribution after the blade row is assumed to be the same as that at the inlet of the blade row (again, as has been done in some design procedures), with a correction in velocity magnitude determined from the density rise, a condition exists such as shown in figure 4. If the velocity distribution after the rotor row is measured, a condition as shown in the figure actually exists; that is, the axial velocity is lower than the assumed design value at the tip and is higher at the hub. If a streamline is drawn across the rotor row, it is immediately apparent that

there must be a radial displacement of this streamline inward. Therefore, in addition to the static-pressure rise resulting across the blade row from the turning in the given blade element, there is an additional static-pressure rise at the tip region caused by the action of radial equilibrium, as indicated by the decreased axial velocity. If the designer ignored this change in axial velocity distribution, the diffusion factor discussed by Lieblein might be exceeded and losses over and above those expected from the original design assumptions would result. In addition, the following stator row would be poorly matched for the actual velocity distribution. Therefore, when given the radial distribution of turning, it becomes important to know how to predict accurately the resulting velocity distributions before and after each blade row so that the desired performance can be obtained.

#### PREDICTION OF AXIAL VELOCITY DISTRIBUTION

In order to predict the flow distributions between the blade rows of the axial-flow compressor and to determine the streamlines along which the blade sections must be stacked, the fundamental flow laws that govern these flow distributions must be established. The fundamental relation is Newton's law, or expressed more explicitly for the present flow process, the radial component of the Euler equations. It is apparent that stable flow between blade rows requires that all forces be in equilibrium. Consider the radial forces on a particle of fluid in the annular space of an axial-flow compressor (fig. 5). The velocity of the particle can be broken down into radial, tangential, and axial components. Just as for anything moving in a circular path, the tangential velocity of the particle requires that a force be applied in the radial direction to balance the acceleration force required to keep the particle moving on its circular path. In the case of solids, the force is supplied by some internal stress; in the case of the fluid particle, the force is supplied by a pressure gradient in the radial direction; that is, static pressure increases toward the tip and the greater the radius ratio, the greater the pressure difference.

If it is assumed that the centrifugal force due to the tangential velocity is just balanced by the pressure force, then the radial distribution of axial velocity can be computed. For a typical inlet stage of a multistage compressor, the axial velocity distribution outside the boundary layer after the first rotor row might then compare with the measured distribution approximately as shown in figure 6. It is apparent that this means of determining the velocity distribution is fairly accurate for this particular case in the outer portion of the blade height, but deviates near the hub of the blade. The deviation near the hub appears to be the result of an additional centrifugal force term which is indicated in figure 7.

In addition to the centrifugal force resulting from the tangential velocity, there is a centrifugal force resulting from the curvature of the streamlines in the radial-axial plane. It is apparent that there is a "tangential" velocity associated with the streamline curvature in this plane which produces an additional centrifugal force that must be balanced by an additional pressure force in the radial direction. The proper consideration of this additional centrifugal force which appears to exist principally in those stages having long blades, as has been discussed in reference 1, would cause the calculated and measured axial velocities to agree well over the entire blade height.

The preceding discussion has been related to the application of the fundamental flow laws to the radial distribution of axial velocity after a blade row in an inlet stage of the compressor. A marked difference exists, however, in the rear stages of the axial flow unit where radius ratio is low. This marked difference is immediately apparent if the radial distribution of axial velocity in the front stages of the compressor is compared with the distribution in the rear stages (fig. 8). In the front stages, the velocities are determined primarily by the blade design, with only small regions of deviation from the blade design indicated near the annulus walls in the boundary-layer regions. In the rear stages with their short blades, however, the flow becomes more similar to that in a pipe. Here it is apparent that the accumulated effects of secondary flows and wall boundary layer become a more prominent determinant of the flow distribution than the centrifugal force term. Therefore, it is to be expected that the loss gradient associated with these losses may have an appreciable effect on the velocities in the rear stages of a compressor. This has been found to be the case, as illustrated in figure 9, after a stator blade in the last stage of a multistage compressor. Indicated in the figure are the velocity distributions as measured and the velocity distributions as calculated by considering only the balance of pressure and centrifugal forces resulting from the tangential velocity component and assuming that the radial gradient of loss is zero. In figure 10 is shown the velocity distribution as calculated considering the same balance of pressure and centrifugal forces but including the effect of the loss gradient at this section. It is apparent that the inclusion of the loss term in the steady-flow energy equation permits accurate prediction of the velocity distribution in the rear stages of the multistage unit. This has been verified in an unpublished analysis. Therefore, the ability to design a compressor accurately requires a knowledge of the blade element losses and turning angle distribution as well as complete application of the fundamental flow laws.

So far, consideration has been given only to the region of flow in the main stream. For a viscous fluid, the measured velocity in the region near the inner and outer walls decreases rapidly and falls to zero at the wall. This region of rapid change in velocity is known as

the boundary layer. The conventional method of accounting for this phenomenon in the design procedure has been to increase the annulus area by an amount equal to an estimated boundary-layer displacement thickness to assure the attainment of design weight flow and to approximate more nearly design incidence angles on the blade sections in the portion of flow outside the boundary layer. However, if a great amount of accuracy is required, recent investigations have shown that if the change of losses with radius could be evaluated in regions near the walls, an accurate check between design and measured axial velocity distributions would be found. Thus, the need for applying an estimated boundary-layer blockage factor could be eliminated.

#### CONCLUDING REMARKS

It is evident that if good design control is to be achieved, the compressor must be designed by taking into account those of the fundamental factors upon which the axial velocity distribution is dependent at all stations in the compressor where experience has indicated this is required. The radial distribution of axial velocity may be accurately predicted after all blade rows if reliable loss and turning angle information for each blade section is available.

#### REFERENCE

1. Wu, Chung-Hua, and Wolfenstein, Lincoln: Application of Radial-Equilibrium Condition to Axial-Flow Compressor and Turbine Design. NACA Rep. 955, 1950. (Supersedes NACA TN 1795.)

STACKING OF BLADE ELEMENTS TO FORM  
COMPRESSOR BLADE

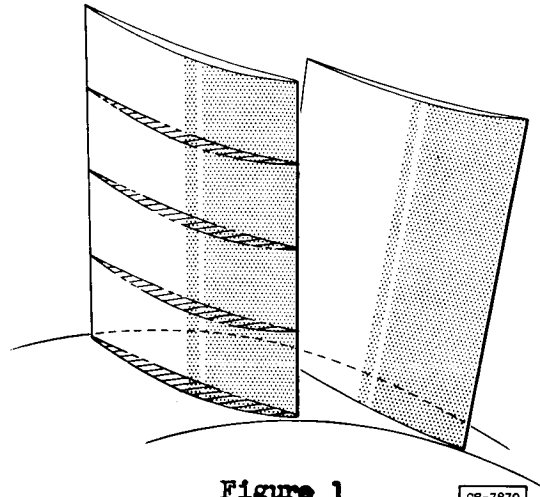


Figure 1

DESIGN AND MEASURED AXIAL VELOCITIES  
AFTER GUIDE VANES

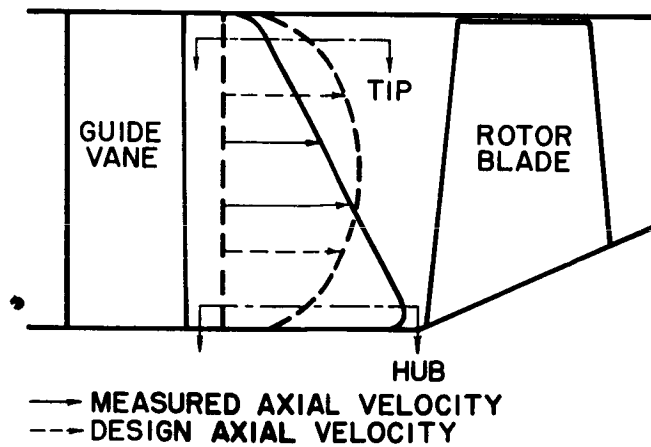
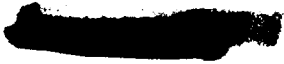
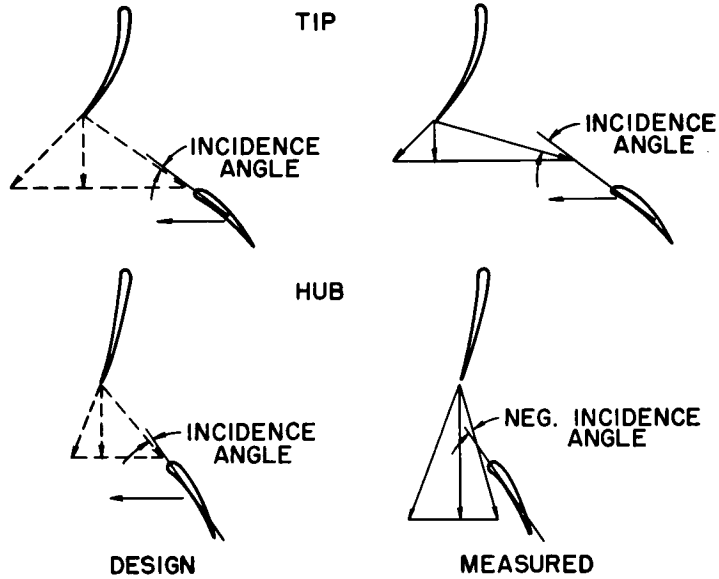


Figure 2



### DESIGN AND MEASURED INCIDENCE ANGLES ON ROTOR BLADE



3078-A

Figure 3

### DESIGN AND MEASURED AXIAL VELOCITIES AFTER ROTOR BLADE ROW

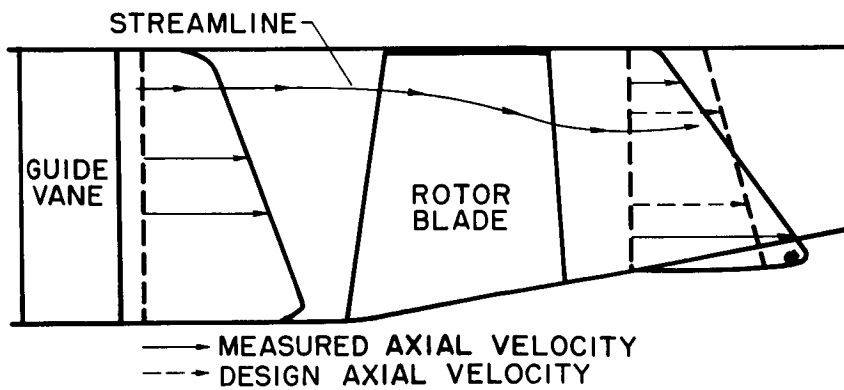
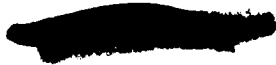
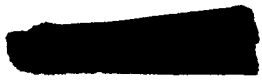


Figure 4





3078-A

### FORCES ON FLUID ELEMENT IN COMPRESSOR ANNULUS

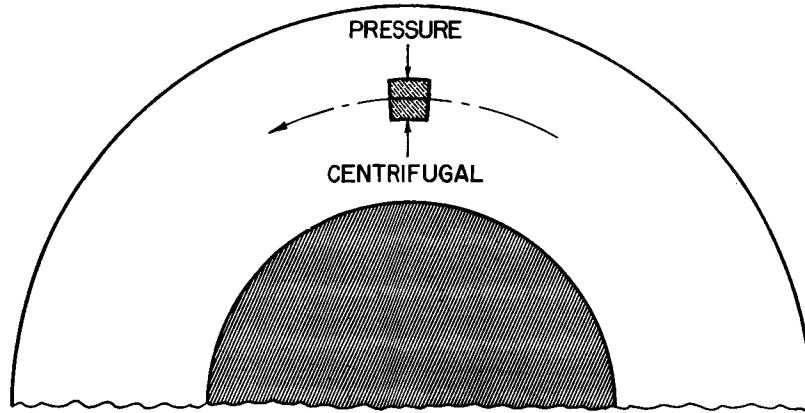


Figure 5

CB-7824

### MEASURED AND CALCULATED AXIAL VELOCITIES AFTER FIRST ROTOR BLADE ROW

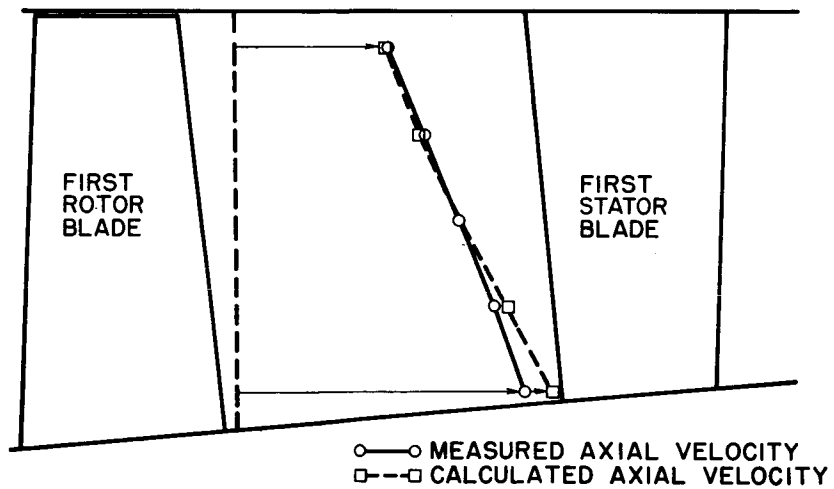


Figure 6





### STREAMLINE PATH OF FLUID ELEMENT

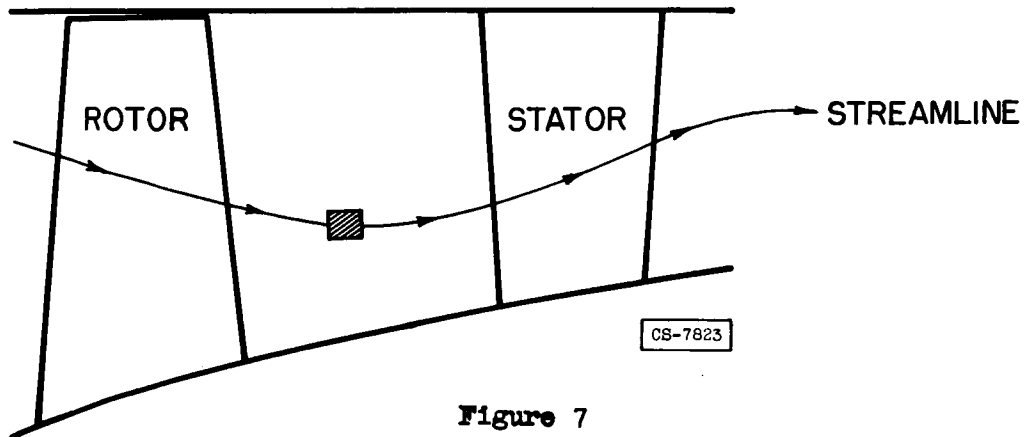


Figure 7

### MEASURED AXIAL VELOCITY PROFILES AFTER INLET AND EXIT ROTOR BLADE ROWS

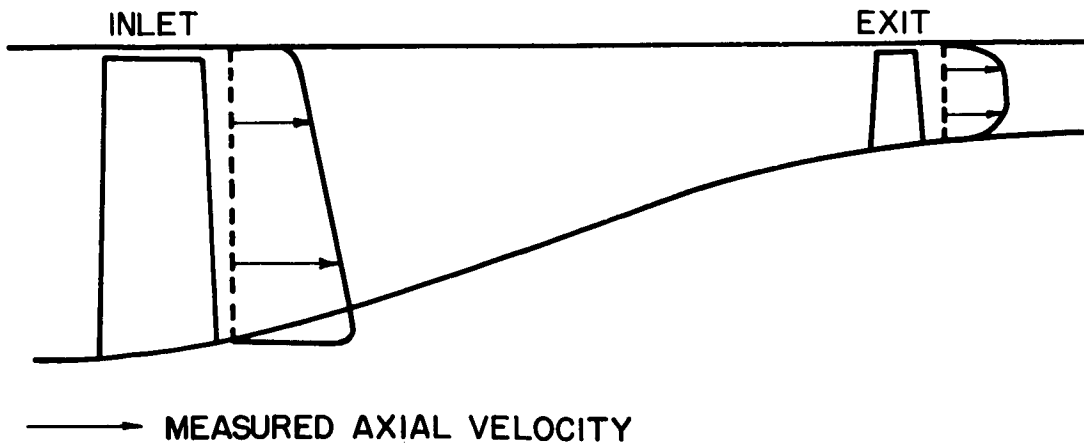
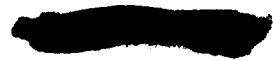


Figure 8



3078-A

### MEASURED AND CALCULATED AXIAL VELOCITIES AFTER NINTH STATOR BLADE ROW

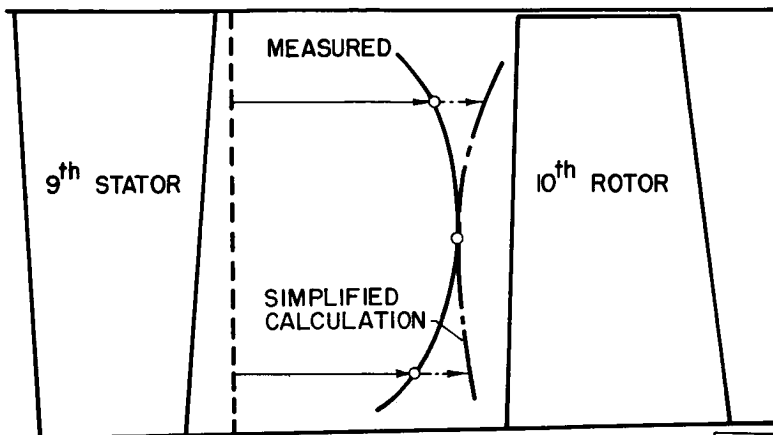


Figure 9

CB-7838

### MEASURED AND CALCULATED AXIAL VELOCITIES AFTER NINTH STATOR BLADE ROW

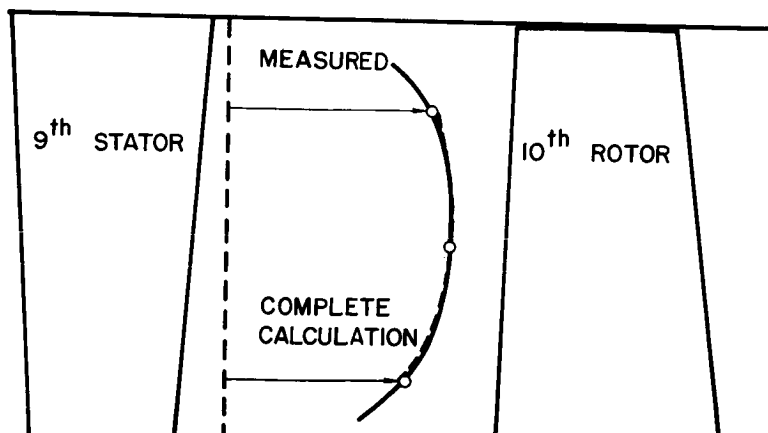


Figure 10

CB-7840

SINGLE-STAGE RESULTS AIMED AT SATISFYING SUPERSONIC  
ENGINE REQUIREMENTS

By Harold B. Finger and William H. Robbins

INTRODUCTION

It has been stated in the introductory paper that the NACA research program is directed toward reduction in diameter and length of compressors, while maintaining good efficiency and range characteristics of the unit. Johnson and Bullock indicated the research approach to be one of increasing air flow per square foot of rotor frontal area and of decreasing the number of stages required to develop a specified over-all pressure ratio. The previous three papers have presented design criteria and design procedures that have been established by research for the transonic compressor.

This paper discusses the results obtained in single-stage compressor investigations in which these principles have been applied in stages satisfying compressor requirements for the supersonic engine. In addition, it will be shown that these compressors exhibit improvements over conventional subsonic compressor designs in air-flow and pressure-ratio characteristics which were attained by the use of transonic stages of reduced hub-tip radius ratios and reduced blade-chord length.

PERFORMANCE OF ROTOR WITH AND WITHOUT INLET GUIDE VANES

The marked advantages of the high Mach number transonic compressor design over conventional subsonic designs is demonstrated by a single-stage investigation conducted at the Lewis laboratory (ref. 1). This investigation demonstrates the "gain all, lose nothing" characteristic of the transonic compressor in achieving the requirements of the supersonic engine. A stage was designed using circular-arc airfoil sections in the rotor with inlet guide vanes to give a prewhirl to the air in the direction of rotor rotation so as to limit the Mach number relative to the rotor tip to 0.8. The hub-tip radius ratio of this rotor was 0.5. Thus, the rotor incidence angles were set for a design condition utilizing essentially "wheel-type rotation" (tangential velocity is proportional to radius) guide vanes, and the turning or camber of the blade was set to give a constant work from root to tip of the blade. The rotor design was flexible in that the rotor-blade-profile shape and rotor-blade setting angles would accommodate operation both with and without guide vanes. This stage was investigated over a wide range

[REDACTED]

of blade speeds and flows both with and without inlet guide vanes installed. A comparison of the performance of the two resulting stages is presented in figure 1 in terms of efficiency, pressure ratio, and air flow per unit frontal area at a blade tip speed of 1000 feet per second. The data show that the pressure ratio, and the flow per unit frontal area are increased simultaneously by the removal of the inlet guide vanes with no loss in peak efficiency.

Removal of the inlet guide vanes caused several of the velocity-diagram characteristics to change. The inlet axial velocity at the peak efficiency point at 1000 feet per second was increased, causing the increase in flow. The Mach number relative to the rotor blade was increased to 1.1 by virtue of the elimination of prerotation of the inlet air and the increase in axial velocity. This increase in Mach number causes the increase in work done by the stage and, therefore, in the pressure ratio of the stage. Although the inlet axial and relative Mach numbers were increased, the tip diffusion factor (which was discussed by Lieblein and is reported in detail in ref. 2) was unchanged. Therefore, the loss coefficient remained constant and the resulting peak efficiencies were essentially unchanged. In addition to these velocity-diagram factors, removal of the inlet guide vanes eliminated the losses encountered in the guide vane wakes and, of course, the weight and space of the guide vanes. These results indicate graphically the considerable advantages to be achieved by elimination of the compressor inlet guide vanes.

#### PERFORMANCE OF 0.4 HUB-TIP-RADIUS-RATIO TRANSONIC ROTOR

By the simple expedient of using circular-arc blade sections with suitable thickness distribution operating without prewhirl at increased Mach numbers, it has been shown how the flow per square foot frontal area can be increased from the conventional values in the range of 25 pounds per second to approximately 31 pounds and, at the same time, appreciably increase stage pressure ratio. Further increases in flow per unit frontal area can be attained by reducing the ratio of hub and tip diameters of the compressor. In order to determine the effect on performance of such a reduction in hub-tip ratio and to determine the validity of the design techniques, a rotor was designed having a 0.4 hub-tip ratio, using circular-arc blade sections (ref. 3). The design rotor tip relative Mach number was 1.1 and the design tip diffusion factor was 0.35, which are within the limiting values indicated by Lieblein. These values are not limits but rather values commensurate with good stage performance.

The over-all performance of this compressor rotor is presented in figure 2 as curves of total-pressure ratio, efficiency, and flow per unit frontal area. In general, the performance was excellent

[REDACTED]

over the entire range of flows and speeds investigated. An efficiency of approximately 90 percent is indicated at the design speed at a flow of approximately 34 pounds per square foot of rotor frontal area and a pressure ratio of 1.36.

The design pressure ratio was limited by imposed restrictions of rotor speed and that the work done be constant radially and with consideration of the performance of the following blade rows. For example, large air turning angles at the rotor hub could require that the hub of the following stator, which is generally critical, operate at higher Mach numbers and possibly higher turnings. An increased pressure ratio would be possible by application of an energy gradient design. This was actually done in the first transonic stage (ref. 4) tested at the Lewis laboratory. Comparison of its performance with the performance shown in figure 2 indicate that the designer has considerable freedom in choosing his design energy input conditions.

Thus, it appears that no new aerodynamic limitations (other than those previously discussed) are encountered in reducing hub-tip radius ratio with a view toward obtaining smaller compressors for a given required mass flow.

#### EFFECT OF REDUCTION IN CHORD LENGTH ON PERFORMANCE

In addition to reducing compressor and, therefore, engine weight by reduction in compressor diameter for a given weight flow, reduction in compressor length by an increase in stage pressure ratio is another means of satisfying the low engine weight requirements of supersonic turbojet engines. The high Mach number designs discussed give stage pressure ratios appreciably higher than those obtained in conventional subsonic designs. However, the first transonic stage built at the Lewis laboratory had a chord length approximately twice as long as would be required of a conventional subsonic design of the same blade length. Thus, even though the pressure ratio of the first transonic stage (ref. 4) may be equivalent to that of two subsonic stages, the weight of the one transonic stage might not be any less than that of the two subsonic stages. Thus reduction in chord length of the transonic compressor is essential.

The effect on aerodynamic performance of reducing chord is indicated by consideration of figure 3. For the same solidity, the short-chord design introduces a more pronounced hub curvature (and thus a greater problem in satisfying the radial equilibrium conditions discussed in the previous paper) and also causes a more severe velocity gradient on the suction surface of the blade, indicating the possibility of a more severe blade stalling and boundary-separation problem. In view of the fact that the diffusion factor, which attempts

[REDACTED]

to evaluate the blade suction-surface velocity difference on the basis of over-all velocity considerations, does not include the chord-length term as such, it is necessary to evaluate the importance of this parameter for the range of chord lengths which might be of practical use in an engine compressor. In addition, of course, the effect of Reynolds number is accentuated by chord reduction.

In an attempt to satisfy the requirements of minimum engine weight by utilizing a high stage pressure ratio rotor and short chord blades, a rotor was designed for a stage pressure ratio of 1.35 with chord length and aspect ratio compatible with those in use in conventional subsonic compressors. A photograph of the rotor is shown in figure 4. The performance of this compressor is presented in figure 5. At an air-flow rate of 30 pounds per second per square foot of frontal area, a pressure ratio of 1.33 was obtained at an efficiency of 0.90. In addition, a wide flow range at good efficiency is obtained at the lower speed of 800 feet per second.

In further emphasizing the effect of reduced chord lengths, the performance of three transonic rotor designs all designed for a pressure ratio of 1.35 can be compared. A diagrammatic sketch of these three designs is presented in figure 6 for the speeds at which a tip relative Mach number of 1.1 was obtained. These designs are not immediately comparable because of differences in hub-tip ratio or flow per unit frontal area, but the performance of these designs serves to emphasize the possible latitude in chord-length selection. The variation in attainable efficiencies is small. In general, it therefore appears that, at least aerodynamically, the chord length of the transonic compressor can be reduced appreciably to values associated with conventional subsonic compressors without encountering any detrimental effects. Any new problems introduced by reduction in chord will probably be mechanical ones, associated with blade stresses and vibrations.

#### CONCLUDING REMARKS

Several important results have been obtained in the transonic compressor research program. Inlet guide vanes can be eliminated from axial-flow compressors and the weight therefore reduced with resultant gains in both air flow per unit frontal area and pressure ratio and no loss in efficiency. In addition, the ratio of hub to tip diameters may be decreased, resulting in increased air flow per unit frontal area with no detrimental effects on pressure ratio and efficiency. It has been further demonstrated that it is possible to reduce transonic blade chords (and thus compressor weight) to those lengths associated with conventional subsonic stages.

[REDACTED]

## REFERENCES

1. Robbins, William H., and Glaser, Frederick W.: Investigation of an Axial-Flow-Compressor Rotor with Circular-Arc Blades Operating up to a Rotor-Inlet Relative Mach Number of 1.22. NACA RM E53D24, 1953.
2. Lieblein, Seymour, Schwenk, Francis C., and Broderick, Robert L.: Diffusion Factor for Estimating Losses and Limiting Blade Loadings in Axial-Flow Compressor Blade Elements. NACA RM E53D01, 1953.
3. Serovy, George K., Robbins, William H., and Glaser, Frederick W.: Experimental Investigation of a 0.4 Hub-Tip Diameter Ratio Axial-Flow Compressor Inlet Stage at Transonic Inlet Relative Mach Numbers. I - Rotor Design and Over-All Performance at Tip Speeds from 60 to 100 Percent of Design. NACA RM E53I11, 1953.
4. Lieblein, Seymour, Lewis, George W., Jr., and Sandercock, Donald M.: Experimental Investigation of an Axial-Flow Compressor Inlet Stage Operating at Transonic Relative Mach Numbers. I - Over-all Performance of Stage with Transonic Rotor and Subsonic Stators up to Rotor Relative Inlet Mach Number of 1.1. NACA RM E52A24, 1952.



### PERFORMANCE OF COMPRESSOR WITH AND WITHOUT INLET GUIDE VANES

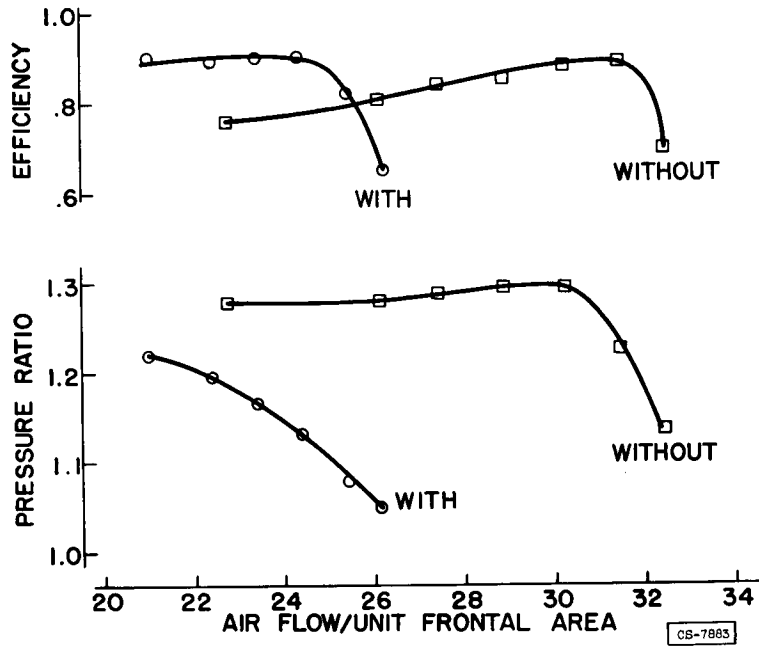


Figure 1

### PERFORMANCE OF 0.4 HUB-TIP-RATIO TRANSONIC ROTOR

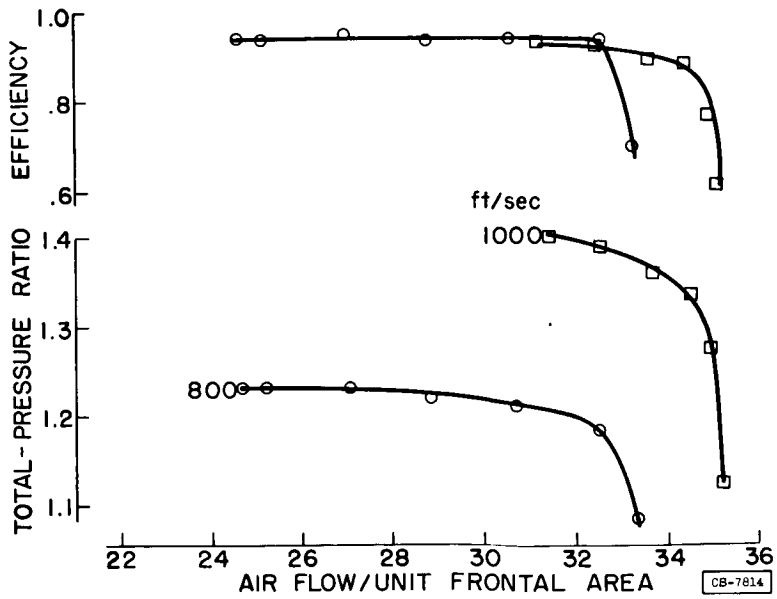
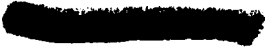


Figure 2



EFFECT OF REDUCED CHORD LENGTH ON HUB PROFILE  
AND BLADE CHARACTERISTICS

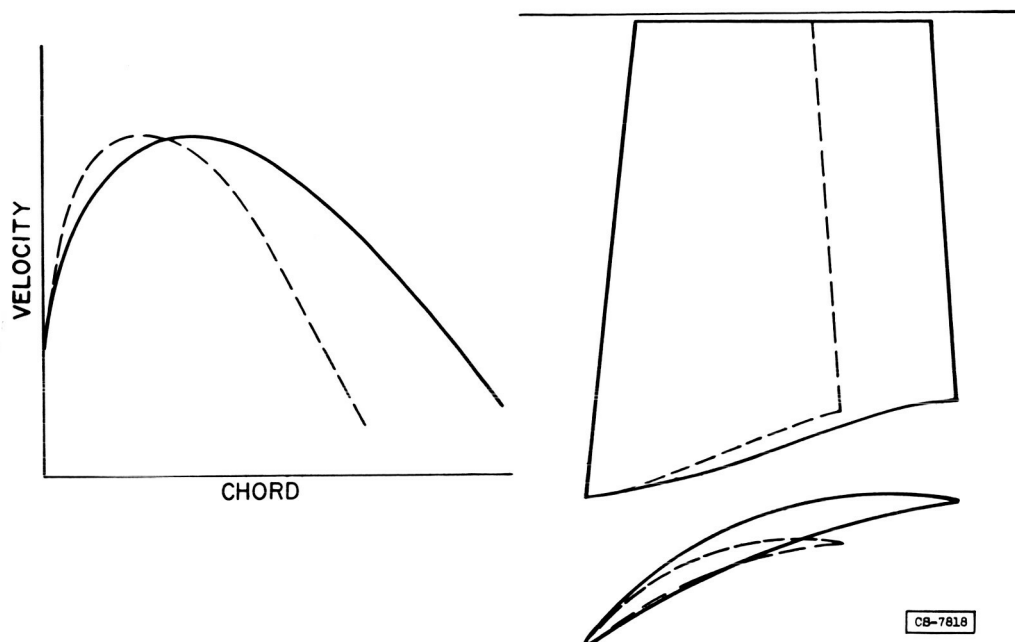


Figure 3

SHORT-CHORD TRANSONIC ROTOR

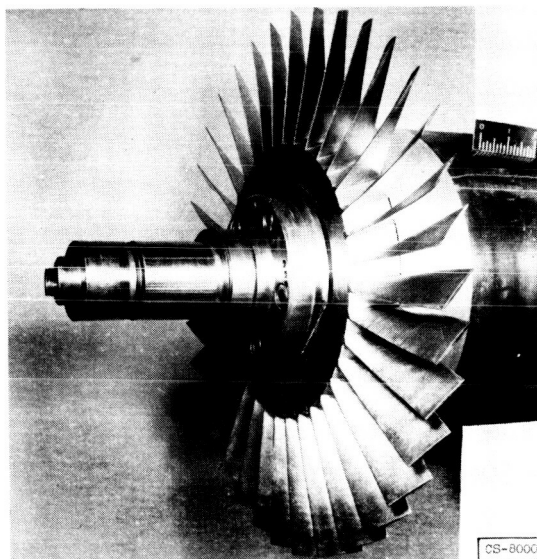


Figure 4

3078-A

PERFORMANCE OF SHORT-CHORD TRANSONIC ROTOR  
HUB-TIP RADIUS RATIO, 0.5

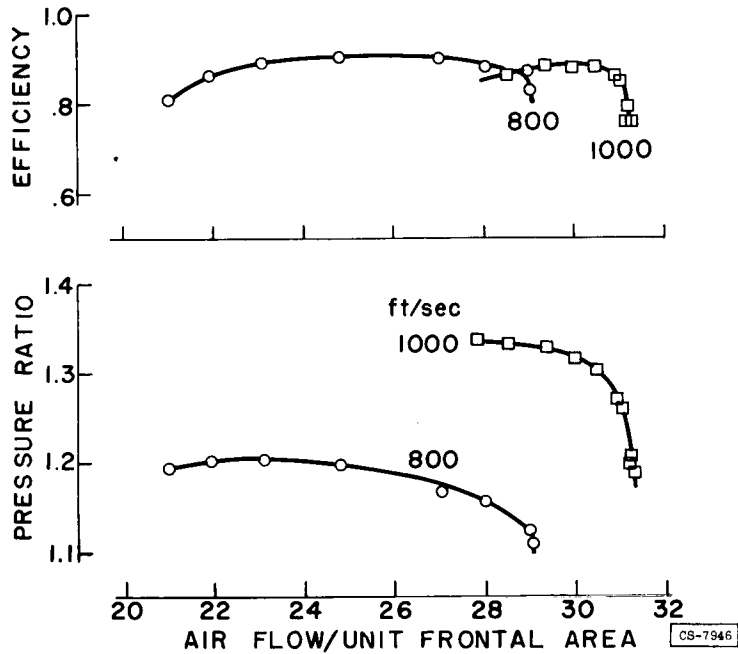


Figure 5

PERFORMANCE OF TRANSONIC ROTORS WITH VARIOUS  
CHORD LENGTHS  
DESIGN PRESSURE RATIO = 1.35  
HUB-TIP RADIUS RATIO

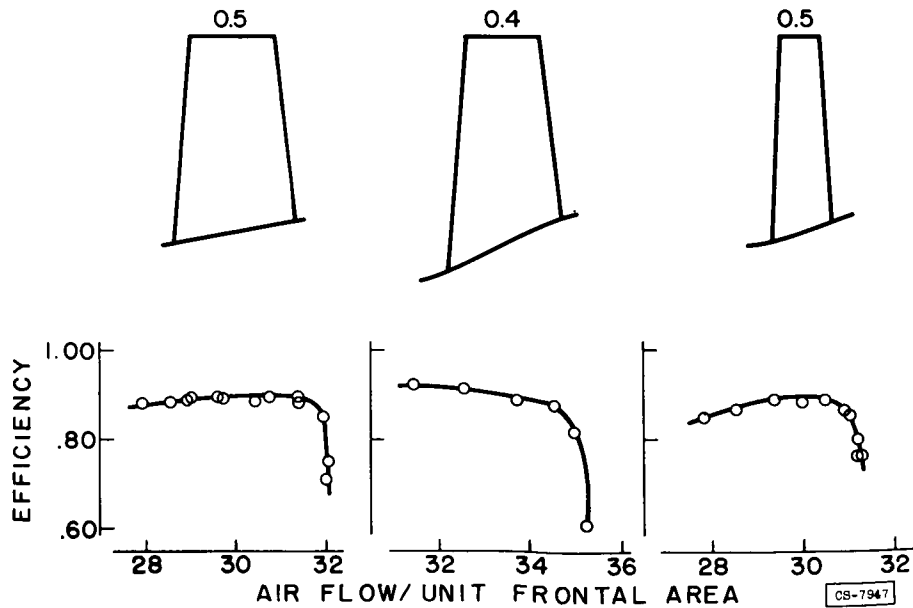


Figure 6

## INVESTIGATION OF A MULTISTAGE COMPRESSOR

## EMPLOYING TRANSONIC INLET STAGES

By Charles H. Voit and Richard P. Geye

## INTRODUCTION

3078-A

Previous papers have discussed the development and performance of single-stage transonic compressors. For a given loading limit, a higher level of pressure ratio can be obtained in a transonic stage than in a subsonic stage, without sacrifice in efficiency or range of operation, particularly at lower speeds. In addition, this type of stage permits higher air-flow-handling capacity, because the axial Mach number (as well as the rotational speed) can be increased above that permitted in subsonic stages. These factors suggest the use of the transonic stage for the inlet stages of a multistage compressor, in order to increase the air-flow-handling capacity and the rotational speed, and thus to permit higher pressure ratios in the entrance as well as in the subsequent stages.

The use of transonic stages in a multistage compressor appeared highly desirable, but it was necessary to discover whether they would maintain good performance when staged or whether some unrecognized characteristic would cause difficulties. In order to obtain an immediate answer to these questions, an existing subsonic multistage design was modified by replacing the first two stages of the subsonic design with transonic stages. A photograph of this compressor is shown in figure 1. In the design of these inlet stages it was necessary that all design equivalent velocities and flow angles leaving the second transonic stage be identical with those leaving the original second subsonic stage. Because the pressure and temperature rises across the transonic stages were higher than for the subsonic stages, it was possible to increase the equivalent weight flow and equivalent tip speed of the modified compressor. High blade loadings were used in the subsonic stages as well as in the transonic stages, which, combined with the high rotational speed, resulted in a compressor design having a high average stage pressure ratio.

The blade sections used for the transonic rotor blades were double circular arc, which varied in camber and maximum thickness from hub to tip. All blading for the subsonic stages and the stators of the transonic stages used conventional sections. Additional design details of this compressor are given in reference 1.

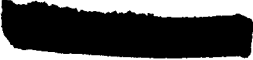
## OVER-ALL PERFORMANCE

The performance of this eight-stage compressor is shown in figures 2 and 3. Figure 2 presents curves of over-all total-pressure ratio against air flow per unit frontal area for rotational speeds from 30 to 100 percent of design speed. Figure 3 presents the corresponding adiabatic-efficiency curves. This compressor achieved a relatively high weight flow, approximately 30 pounds per square foot of frontal area, and a high over-all pressure ratio of approximately 10. This pressure ratio corresponds to an average stage pressure ratio of 1.332. The peak efficiency obtained (fig. 3) was approximately 0.88, which was obtained between 80 and 90 percent of design speed. The peak efficiency at part speed did not drop off sharply but remained at a reasonably high level as contrasted with the sharp reduction in efficiency of a conventional subsonic compressor at these low speeds. The region of high efficiency at a given speed, as shown by the efficiency contours of figure 4, covered a wide range of pressure ratio and extended into the low-speed operating range.

Also shown on figure 4 is a calculated engine operating line which indicates that there is some range between the operating line and the peak pressure ratio at all speeds and that acceleration problems could therefore be expected to be reduced. The operating line passes through the regions of high efficiency, and efficient operation could be expected even at part speed.

As previously mentioned, good efficiency at part speed is especially desirable in compressors for supersonic-flight application, because the compressor equivalent speed at supersonic flight is some fraction of the sea-level compressor speed. This compressor, which has high efficiency over a wide range of speeds, appears to be well-adapted to supersonic-flight application.

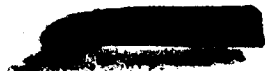
A comparison between a conventional engine and an advanced jet engine using a compressor employing transonic stages is presented in figure 5. These engines were designed for the same air flow and compressor pressure ratio. The conventional engine requires a 16-stage compressor to produce the required pressure ratio as compared with the eight-stages necessary for the transonic compressor. Also, the compressor diameter of the conventional engine is larger than the advanced engine because of the higher air-flow-handling capacity of the transonic compressor. The conventional engine requires bleed over some part of its operating range in order to accelerate satisfactorily, while the engine with the transonic compressor would require little, if any, bleed. The higher rotational speed of the transonic compressor permits the power required to drive the compressor to be obtained with a two-stage turbine as compared with three stages in the conventional engine. Because of the decrease in diameter and length of the advanced engine, compared with the conventional engine, it is likely a reduction in weight could be achieved.

  
CONCLUSION

The performance of this research compressor indicates that transonic stages can successfully be incorporated into multistage compressors and that they maintain the desirable characteristics indicated by single-stage test. By the use of transonic stages in multistage machines, the level of air-flow-handling capacity and stage pressure ratio can be raised while good efficiency is maintained over an increased operating range. Thus, the development of transonic stages and the use of high blade loadings can be expected to result in a significant decrease in compressor size and weight.

## REFERENCE

1. Voit, Charles H.: Investigation of a High-Pressure-Ratio Eight-Stage Research Compressor with Two Transonic Inlet Stages. I - Aerodynamic Design. NACA RM E53I24, 1953.

3078-A  


EIGHT-STAGE COMPRESSOR

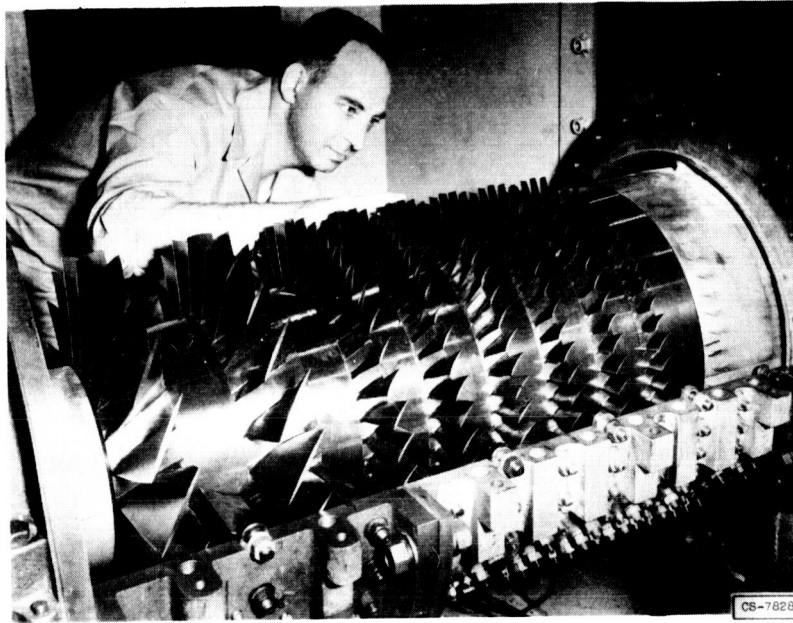


Figure 1

PRESSURE-RATIO CHARACTERISTICS OF  
8-STAGE COMPRESSOR  
INLET HUB-TIP RADIUS RATIO, 0.48

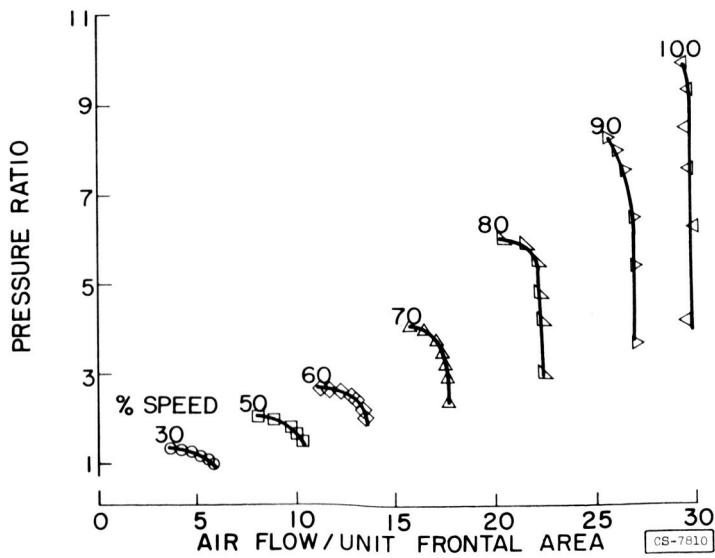


Figure 2

### EFFICIENCY CHARACTERISTICS OF 8-STAGE COMPRESSOR

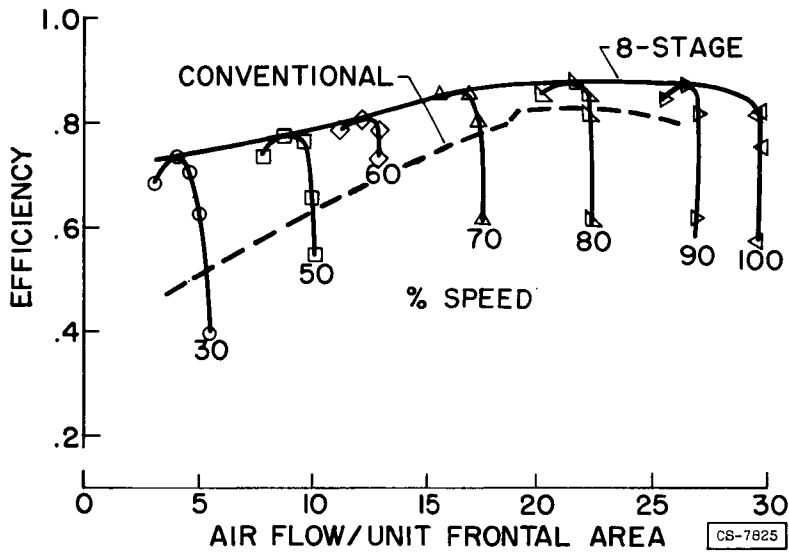


Figure 3

### PRESSURE-RATIO CHARACTERISTICS OF 8-STAGE COMPRESSOR

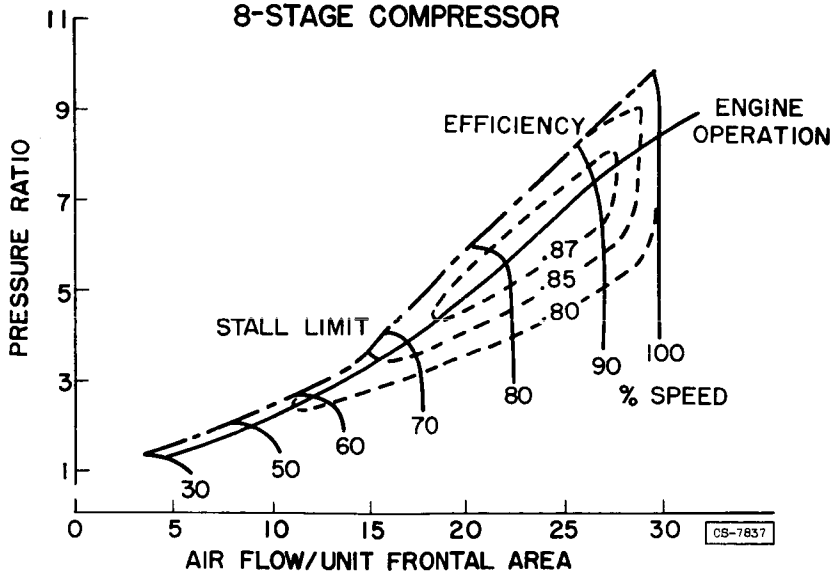
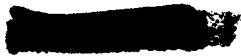


Figure 4



### ENGINE IMPROVEMENTS RESULTING FROM USE OF TRANSONIC COMPRESSOR

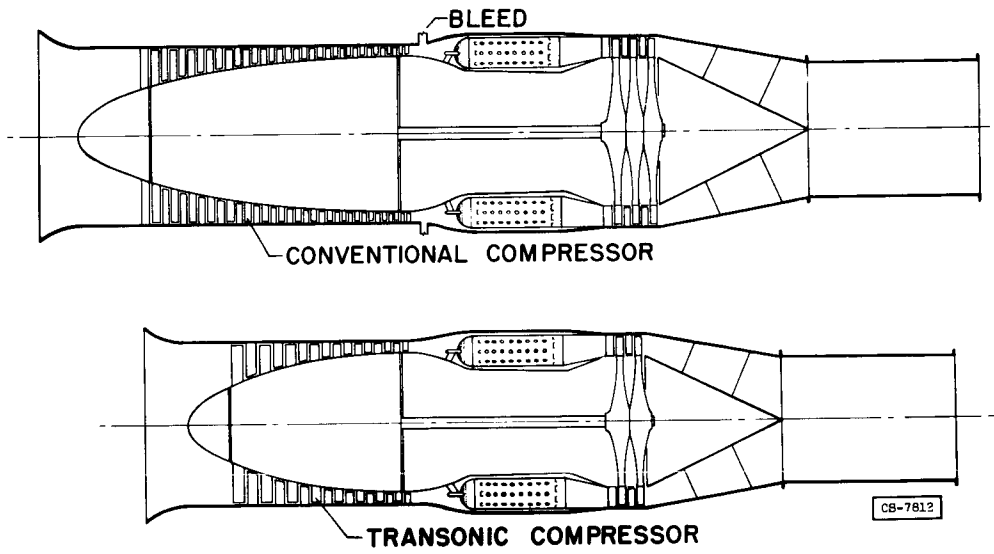
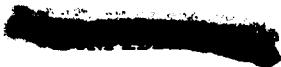


Figure 5



## INVESTIGATION OF MULTISTAGE COMPRESSOR

HAVING ALL STAGES OF TRANSONIC TYPE

BY Karl Kovach and Donald M. Sandercock

## INTRODUCTION

As stated in the paper by Johnsen and Bullock, the requirements of efficient aircraft propulsion indicate the desirability of operating lightweight, compact turbojet engines that are highly efficient over wide ranges of operation. For current turbojet engines incorporating the multistage axial-flow compressor, reductions in compressor size and weight can be effected by increasing stage pressure ratio (reducing the number of stages required to produce the desired pressure ratio) and increasing mass flow per unit frontal area.

Previous papers have shown that axial-flow compressor rotors and stages of high efficiency, high pressure ratio, and high specific mass flow can be obtained by designing for operation in the transonic region of rotor relative inlet Mach numbers. Stator-outlet conditions and general stage performance appeared satisfactory for purposes of multistaging with current stage designs. The paper by Voit and Geye showed that excellent results can be obtained when the transonic rotors are used in inlet stages of a multistage compressor. It was also speculated that transonic operation need not be restricted to the inlet stages. Further increases in average stage pressure ratio might be obtained if all of the stages of a multistage compressor were designed to operate at higher levels of relative inlet Mach number. In order to maintain high relative inlet Mach numbers in succeeding rotor rows without markedly increasing the axial velocity across the stage, it is necessary to establish substantially axial flow at the entrance to each of the transonic rotors. For high-pressure-ratio rotors, this would require stators that turn the air through much greater angles than those of compressors previously discussed. An investigation was therefore conducted to determine the feasibility of using turning in stators that is sufficiently high to turn the flow leaving high-pressure transonic rotors to the axial direction.

## SINGLE-STAGE TRANSONIC COMPRESSOR WITH HIGH STATOR TURNING

It was believed that high air-turning in stator blades could be satisfactorily accomplished if the limits of blading-design criteria previously discussed were respected. On this basis, a set of simple blades with circular-arc pressure and suction surfaces and no radial twist were designed and tested.

Figure 1(a) shows the over-all performance characteristics of a stage consisting of the transonic rotor of reference 1 and the high-turning stator blades. The stator blades for this configuration were required to turn the air through an angle of approximately  $40^\circ$ . The corresponding relative inlet Mach number at the tip of a succeeding rotor would be approximately unity. Shown for comparison in figure 1(b) are the over-all performance characteristics of the transonic stage of reference 1 shown as plots of pressure ratio and efficiency against air flow per unit frontal area. A comparison of these figures indicates that there was a slight efficiency loss for the high-turning stator stage as a result of improper blade-setting angles. Calculations indicate that no loss in efficiency would have occurred if proper design control had been exercised.

### MULTISTAGE COMPRESSOR

The results of the investigation of high stator turning indicate that a transonic inlet stage could be successfully designed for operation with succeeding stages of high Mach number level without any sacrifice in performance. On the basis of these results, a five-stage axial-flow compressor was designed and constructed with all stages operating in the transonic region of rotor relative inlet Mach number. The compressor was designed and operated as a component of an existing turbojet engine, and, therefore, some of the geometry was already specified. The compressor had a hub-tip radius ratio of 0.5 and was designed to produce an over-all total-pressure ratio of 5.0 (corresponding to an average total-pressure ratio of 1.38 per stage). It was pointed out in the paper by Johnsen and Bullock that the ability of a compressor to produce a high pressure ratio in a single stage is a function of the rotational speed and the blade loading and that its ability to handle high air flows per unit frontal area is a function of axial Mach number and hub-tip radius ratio. For this compressor design, the tip speed of 1100 feet per second, which was essentially fixed by the mechanical limits imposed by the existing turbine, was sufficient to produce a tip relative inlet Mach number of 1.18 without guide vanes for an inlet axial Mach number of 0.60. The design values of tip relative inlet Mach number for the succeeding rotors are 1.12, 1.03, 0.96, and 0.90.

The blade sections used for each blade row had a circular-arc mean line. Each rotor row also had circular-arc pressure and suction surfaces, as did the first two stator blade rows; but the last three stators deviated from these surfaces slightly. The blade thickness distribution was chosen from considerations of both strength and Mach number. In general, all the design ideas and limits previously discussed (diffusion factor and incidence and deviation angles) were incorporated in this design.

Figure 2 is a photograph of the five-stage transonic compressor installed as a component of the turbojet engine. The pressure-ratio characteristics of the five-stage compressor are shown in figure 3. This figure is the conventional plot of over-all total-pressure ratio against specific air flow in pounds per second per square foot of frontal area. Performance is shown for a range of equivalent speeds from 40 to 100 percent of design speed. The maximum total-pressure ratio obtained at design speed was 5.07, obtained at a specific air flow of approximately 32 pounds per second per square foot of frontal area.

Figure 4 is a plot of the efficiency characteristics of the compressor against specific mass flow for the same range of equivalent speeds. The peak-efficiency line shows a wide speed range of high efficiency. A maximum peak efficiency of approximately 0.88 was obtained at an equivalent speed of about 90 percent of design.

#### CONCLUSIONS

From the material presented, the following conclusions can be made:

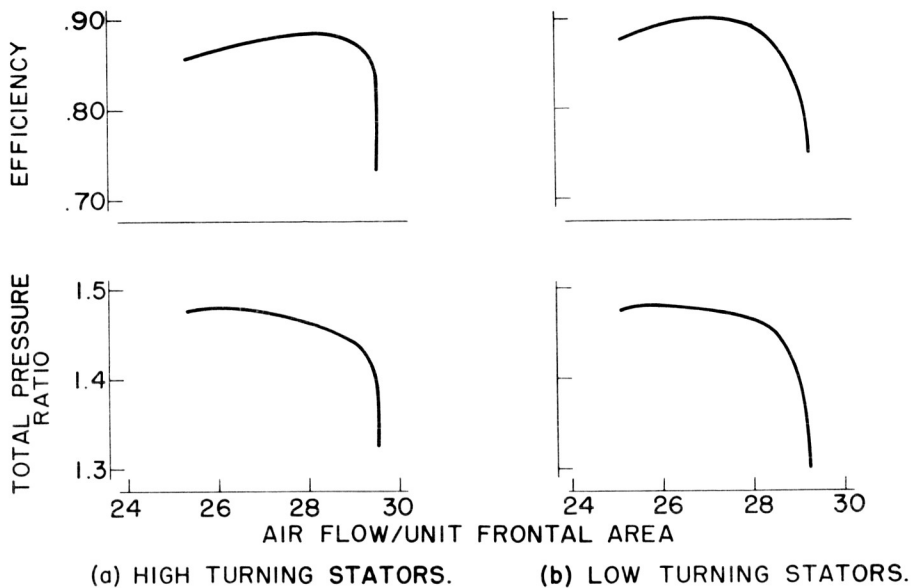
1. By proper design control, a stage can be designed to provide high Mach numbers in succeeding stages without any sacrifice in performance.
2. This type of compressor can be successfully staged to give good over-all performance characteristics.

#### REFERENCES

1. Lieblein, Seymour, Lewis, George W., Jr., and Sandercock, Donald M.: Experimental Investigation of an Axial-Flow Compressor Inlet Stage Operating at Transonic Relative Inlet Mach Numbers. I - Over-All Performance of Stage with Transonic Rotor and Subsonic Stators up to Rotor Relative Inlet Mach Number of 1.1. NACA RM E52A24, 1952.



### EFFECT OF STATOR TURNING ON STAGE PERFORMANCE



3078-A

Figure 1

### FIVE-STAGE TRANSONIC COMPRESSOR

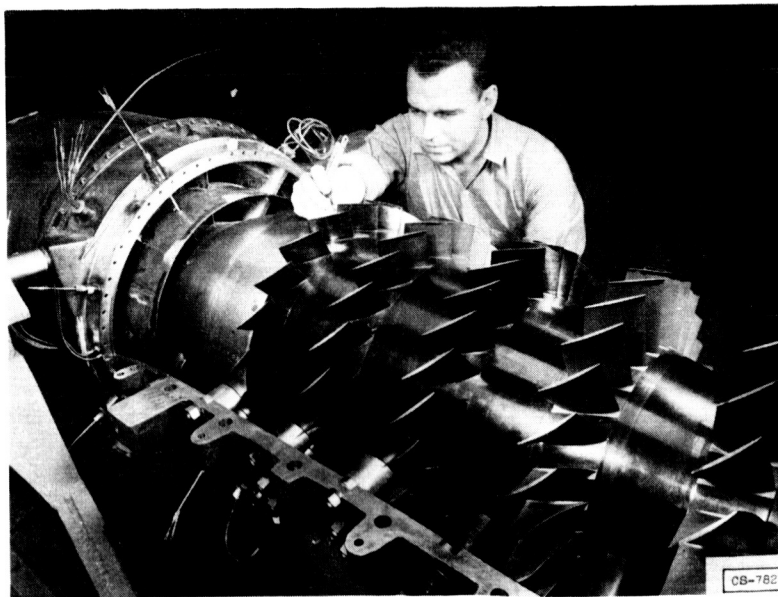


Figure 2



PRESSURE-RATIO CHARACTERISTICS OF FIVE-STAGE TRANSONIC COMPRESSOR  
INLET HUB-TIP RADIUS RATIO, 0.5

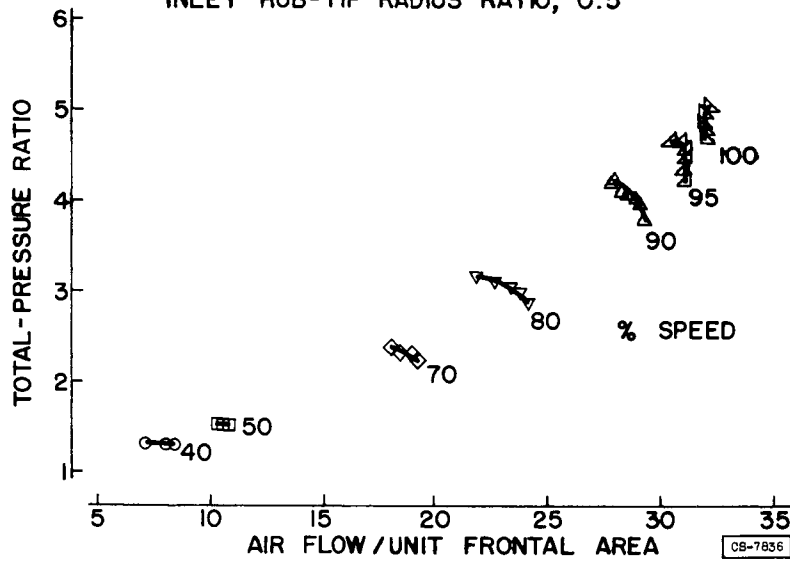


Figure 3

EFFICIENCY CHARACTERISTICS OF FIVE-STAGE TRANSONIC COMPRESSOR

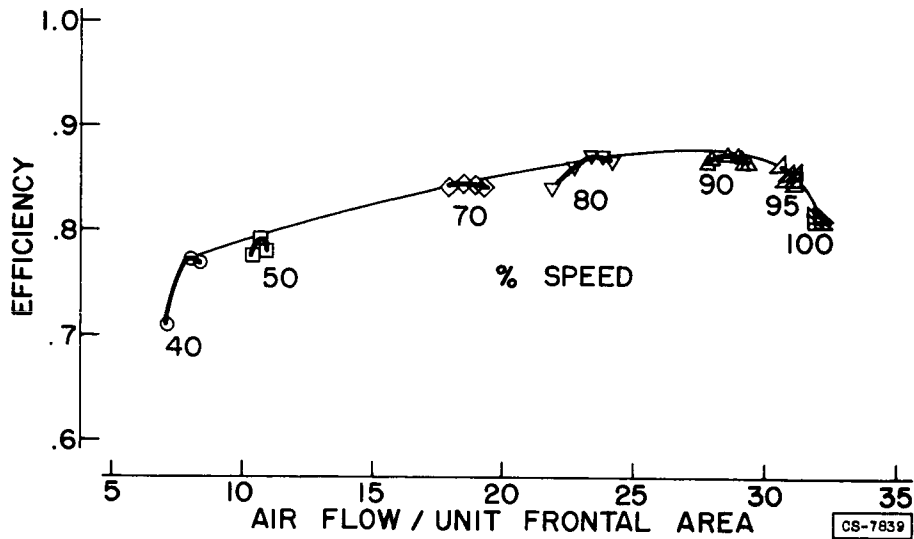
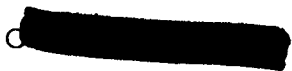


Figure 4

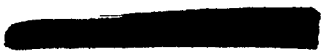


3078-B

II - TURBINE AERODYNAMICS PANEL

- A. Ginsburg
- R. E. English
- W. L. Stewart
- T. R. Heaton
- H. L. Herzig
- C. L. Walker

II - TURBINE  
AERODYNAMICS





## INTRODUCTION TO TURBINE AERODYNAMICS

By Robert E. English and John J. Rebeske

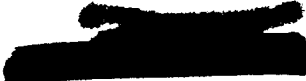
### INTRODUCTION

3078-B

The aerodynamic design of a turbine should be such that the turbine has both high design-point efficiency and operational flexibility (ability to operate over a required range of operating conditions with good efficiency) in combination with geometrical proportions that permit designing for certain other desirable characteristics; examples of these other characteristics are low weight, small size, and low centrifugal stress. One turbine design obviously cannot excel in all of these characteristics. For example, low weight and small size are frequently obtained at the expense of turbine efficiency or operational flexibility; whereas, in another application, high efficiency and operational flexibility are emphasized at the expense of weight and size. A design of a turbine for use in a turbojet engine is a good one if these characteristics are so compromised that a good engine is obtained. A particular combination of these characteristics that results in a good turbine design for one class of turbojet engine will very likely not be best for another.

Turbine aerodynamics includes the study of flow processes and loss mechanisms within turbines in order to improve turbine aerodynamic performance and to establish limits for good turbine design. Two topics in this field, secondary flow and Mach number limits on design, will be treated in subsequent papers.

On the other hand, an adequate study of turbine aerodynamics must extend beyond an investigation of flow phenomena within turbines. It must also relate turbine aerodynamic design to the principal factors affecting engine performance. Examples of such factors are compressor pressure ratio, air flow per unit frontal area, blade-tip speed, and centrifugal stress in the turbine rotor blades. One purpose of this paper is, therefore, to describe those factors that limit turbine aerodynamic design and then to relate those design limits to the principal factors affecting engine design-point performance. A second purpose is to illustrate how turbine stator adjustment can provide engine operational flexibility and to show how the use of turbine stator adjustment affects the turbine design requirements. Two subsequent papers treat how turbine stator adjustment affects turbine and engine performance.



## TURBINE DESIGN CHARACTERISTICS

### Aerodynamic Factors Limiting Turbine Design

The principal factors limiting turbine aerodynamic design can be explained in terms of the turbine velocity diagrams. By velocity diagrams is meant the radial distribution of velocity in the interblade-row spaces such as the axial clearance space between the stator and rotor blade rows in a turbine (see fig. 1).

Turbine work  $E$  is expressed in terms of velocity-diagram variables in the Euler work equation as

$$E = \frac{U(V_{u,4} - V_{u,5})}{gJ}$$

For a given blade speed  $U$ , high turbine work is obtained by having a high value of rotor-inlet tangential velocity  $V_{u,4}$  and a large negative value of rotor-outlet tangential velocity  $V_{u,5}$ .

Increasing rotor-inlet tangential velocity  $V_{u,4}$  corresponds to rising rotor-inlet relative Mach number. By placing a limit on rotor-inlet relative Mach number, the value of rotor-inlet tangential velocity is thereby limited also. Within a specified limit on rotor-inlet Mach number, larger values of tangential velocity  $V_{u,4}$  are obtained if the axial velocity is decreased. Decreased axial velocity and increased tangential velocity correspond to higher turning angle in the rotor, a factor that is limited in turbine design. Another condition that limits the rotor-inlet tangential velocity is that the velocity relative to the rotor is not ordinarily permitted to decrease across the rotor. The rotor-inlet tangential velocity is thus restricted by limits placed on rotor-inlet Mach number, rotor turning angle, and change in relative velocity across the rotor.

The rotor-inlet relative velocity  $W_4$  can be expressed as

$$W_4 = \sqrt{V_{x,4}^2 + (V_{u,4} - U)^2}$$

The centrifugal force caused by the gas rotating about the turbine axis results in a low static pressure at the rotor-hub radius and thus a high gas velocity at the rotor hub. For conventional turbine design, the axial velocity  $V_{x,4}$  is constant along the radius. The tangential velocity  $V_{u,4}$  is thus highest at the hub radius. On the other hand, the blade speed  $U$  is lowest at the hub radius. The result of these trends is that the rotor-inlet relative velocity  $W_4$  is highest at the hub radius. For this reason, the rotor hub is most critical with respect to rotor-inlet Mach number, turning angle, and change in relative velocity across the rotor.

At the exit from a turbine, the tangential velocity  $V_{u,5}$  is limited in order to avoid large losses in kinetic energy  $V_{u,5}^2/2gJ$ , an energy which is usually not recovered. The kinetic energy  $V_{x,5}^2/2gJ$  does not limit the exit axial velocity, because this energy is usually considered to be useful in propelling the aircraft and is therefore not charged against the turbine as a loss. The desirable range of exit axial velocity is limited, instead, by a condition called "limiting blade loading." The effect of limiting blade loading on turbine operation is illustrated in figure 2. For a turbine operated at constant rotational speed, the turbine torque rose as the pressure ratio was increased, and then reached a maximum, limiting value. A further rise in pressure ratio resulted in no further rise in turbine torque, because the loading, or lift, on the rotor blades had reached the maximum value obtainable; hence the name "limiting blade loading."

The blade loading has been shown to reach the limiting value if the turbine-exit axial Mach number is approximately 0.70. The reason for this limiting value of 0.70 can be explained by considering the flow conditions at the trailing edges of the blade profiles in figure 2. The dashed lines represent the shock pattern at the exit from a blade row operating at limiting blade loading. Along the solid line joining the trailing edges, the axial component of velocity is equal to local sonic speed, and thus the annulus is choked at this station. Because at this station a portion of the annulus is blocked by trailing edges and boundary layer on the blade surfaces, a somewhat lower value of axial Mach number is obtained downstream of the blade row where the whole annulus is available as flow area.

#### Conservative and High-Output Turbine Characteristics

For conservative turbine design, the rotor-inlet relative Mach number is usually limited to 0.6 and the exit axial Mach number to 0.5. Such a turbine stage will have a design-point efficiency of about 0.89. A study of several turbine designs has shown that the work factor  $gJE/U_h^2$  of such a conservatively designed one-stage turbine is about 2.1.

A high-output turbine exceeds these design limits. The rotor-inlet Mach number is limited to 0.8. The exit axial Mach number is permitted to rise to 0.7, the value for limiting blade loading. A turbine efficiency of 0.86 is typical, although 0.87 has been obtained from such a turbine design. The work factor  $gJE/U_h^2$  for such a one-stage turbine is about 2.5.

The work output of a two-stage turbine can generally be higher than twice the work that can be obtained from a one-stage turbine. The reason for this is that at the exit from the first stage, the rotor-outlet

[REDACTED]

tangential velocity can be made a large negative number without seriously increasing turbine losses. The kinetic energy contained in the tangential component of velocity is not discarded in this case but is part of the energy supplied to the second stage. For this reason, the work capacity of a two-stage turbine is about three times that of a one-stage turbine. Mach number and rotor turning angle limit the work output of the first stage of such a turbine. Only very small increases in turbine-work capacity result from raising the turning angle above the typical limit of  $120^\circ$ .

Increases in turbine efficiency above the values mentioned here will require an improved knowledge of the nature of turbine losses. Flow measurements within a particular turbine have shown that, of the losses occurring within the rotor blade row, the profile losses account for about 30 percent. The remaining 70 percent of the rotor loss occurs near the blade ends. Because the principal turbine losses are associated with the blade ends, significant gains in turbine efficiency are dependent upon the understanding and subsequent reduction of the losses associated with these blade ends.

In addition to turbine efficiency, turbine aerodynamic characteristics can be classified grossly into work capacity and flow capacity. Factors other than aerodynamic variables affect the work and flow capacity. An examination of Euler's work equation shows that high work capacity can be obtained by means of high blade speed. This high capacity for work from a turbine stage is desirable, because the number of turbine stages is thereby kept low. High blade speed has the undesirable effect of raising centrifugal stresses in the rotor blades and thereby affecting turbine weight as well.

High flow capacity results from use of high values of exit axial Mach number and low values of hub-tip radius ratio. On the other hand, use of high values of exit axial Mach number restricts the turbine operational flexibility, and low values of hub-tip radius ratio correspond to high values of centrifugal stress in the turbine rotor blades. It is thus apparent that the efficiency, size, weight, centrifugal stress, and operational flexibility of a turbine are interrelated factors. There is, thus, a need to relate turbine design variables to attainable engine characteristics such as compressor pressure ratio, engine air flow per unit frontal area, blade-tip speed, and centrifugal stress in the turbine rotor blades.

## ATTAINABLE ENGINE DESIGN-POINT CHARACTERISTICS

### High-Output One-Stage Turbines At Sea Level

For engines that have high-output one-stage turbines, the design-point performance attainable during static operation at sea level is

[REDACTED]

shown on the left in figure 3. The turbine rotor-inlet Mach number was limited to 0.8 and the exit axial Mach number to 0.7. The turbine-inlet temperature was considered to be four times the compressor-inlet temperature, or  $2074^{\circ}$  R ( $1614^{\circ}$  F). Figure 3 shows that at a compressor pressure ratio of 4.5 and with a turbine-tip speed of 1100 feet per second, the maximum compressor air flow the turbine can pass is 19 pounds per second for each square foot of turbine-tip frontal area; the corresponding turbine hub-tip radius ratio is about 0.78. Use of lower hub-tip radius ratio and higher blade-tip speed increases the air-handling capacity and tolerable compressor pressure ratio. Unless very high values of compressor blade-tip speed can be obtained or the turbine diameter increased over that of the compressor, the one-stage turbine limits air flow and compressor pressure ratio to values too low for satisfactory operation of low Mach number airplanes.

#### Conservative Two-Stage Turbines at Sea Level

For engines that have conservative two-stage turbines, the engine design-point performance attainable during static sea-level operation is presented on the right in figure 3. The blade-row inlet Mach number was limited to 0.6 and the turbine-exit axial Mach number to 0.5. Again, the turbine-inlet temperature is  $2074^{\circ}$  R ( $1614^{\circ}$  F). For a turbine-tip speed of 1100 feet per second and a hub-tip radius ratio of 0.5 at the exit from the second turbine stage, such a conservatively designed turbine is capable of driving a compressor having a pressure ratio of 7.0 and passing an air flow 34.5 pounds per second for each square foot of turbine-tip frontal area. For an air flow of 30.0 pounds per second per square foot and a turbine blade-tip speed of 1100 feet per second, a conservative turbine is capable of driving a compressor having a pressure ratio of 10.8. It appears from these numbers that, for subsonic flight, two-stage turbines of comparatively conservative design are capable of driving one-spool compressors having both high air flow per unit frontal area and high pressure ratio.

#### Flow Capacity of Turbines at Flight Mach Number of 2.8

For flight at a Mach number of 2.8 in the stratosphere, the ram temperature is  $1008^{\circ}$  R ( $548^{\circ}$  F). The turbine-inlet temperature is assumed to be three times the compressor-inlet temperature, or  $3024^{\circ}$  R ( $2564^{\circ}$  F). For this engine temperature ratio of 3 and a hub-tip radius ratio of 0.5 at the turbine exit, figure 4 presents the variation in compressor weight flow per unit of turbine-tip frontal area with compressor pressure ratio for exit axial Mach numbers of 0.5 and 0.7. The weight-flow variation depends on the turbine-exit axial Mach number, hub-tip radius ratio at the turbine exit, and the thermodynamic cycle calculation, and is independent of the turbine blade-tip speed, number

of turbine stages, or blade-row entrance Mach number. These curves show that air flows comparable to those of the best compressors are obtainable with a hub-tip radius ratio of 0.5, if the turbine-exit axial Mach number is increased to a value near 0.7.

#### High-Output Two-Stage Turbine at Flight Mach Number of 2.8

If two-stage turbines have exit axial Mach numbers of 0.7 and rotor-inlet Mach numbers of 0.8, the engine performance presented on the right in figure 5 can then be obtained. If the turbine-tip speed is 1400 feet per second, an air flow per unit of turbine-tip frontal area of 34.7 pounds per second per square foot and a compressor pressure ratio of 7.2 are tolerable design conditions. The mass-flow capabilities of a two-stage turbine thus seem to be very good, and the corresponding compressor pressure ratios appear to be even higher than required. However, a two-stage turbine operating with an inlet temperature of  $3024^{\circ}$  R ( $2564^{\circ}$  F) will undoubtedly have blade cooling, and the mechanical aspects of cooling the two stages may be quite complicated.

#### High-Output One-Stage Turbines at Flight Mach Number of 2.8

Because the compressor pressure ratio attainable with two-stage turbines is higher than required and because of the blade-cooling complication, it appears that one-stage turbines may prove more satisfactory for use at high flight speeds. The performance attainable with high-output one-stage turbines is shown on the left of figure 5 for a turbine-inlet temperature of  $3024^{\circ}$  R ( $2564^{\circ}$  F) at a flight Mach number of 2.8. At a turbine blade-tip speed of 1600 feet per second and a compressor pressure ratio of 3, the turbine can pass an air flow of 26 pounds per second for each square foot of turbine-tip frontal area.

One question that arises concerning operation at such high blade-tip speed is whether or not the centrifugal stress is within tolerable limits. As an aid in judging the stress level, lines of constant centrifugal stress in the turbine rotor blades are superimposed on the plot of figure 5 and presented in figure 6. The value of stress of 60,000 pounds per square inch is near the maximum value of stress that it currently appears cooled turbine blades might be developed to withstand. Attainment of an air flow of 26 pounds per second for each square foot of turbine-tip frontal area and a compressor pressure ratio of 3 requires a centrifugal stress slightly greater than even 60,000 pounds per square inch. If the centrifugal stress is reduced to 50,000 pounds per square inch, the air flow is also reduced to 23.7 pounds per second per square foot of turbine-tip frontal area at a compressor pressure ratio of 3.

## Effect of Raising Turbine Design Limits on Attainable Engine Performance

3078-6

The effect of changing turbine design limits is illustrated in figure 7. The two curves have the same centrifugal stress of 50,000 pounds per square inch. The lower curve, for a conventional high-output turbine, is reproduced from figure 6. The higher curve shows the change in engine performance to be obtained by raising the turbine rotor-inlet Mach number from 0.8 to 1.0 and removing the limit of no deceleration across the rotor hub. The rise in air flow per unit turbine-tip frontal area is approximately 10 percent. At the low-pressure-ratio, high-flow end of the Mach 1.0 curve, the flow decelerates across the hub of the rotor. At a compressor pressure ratio of 2.3, the velocity relative to the rotor decreases 18 percent from entrance to exit, the decrease being less at higher values of compressor pressure ratio.

In general, turbines operating at rotor-inlet Mach numbers as high as 1.0 and, in particular, in combination with a static-pressure rise across the rotor, have had low turbine efficiency. On the other hand, the gains to be realized by being able to design for efficient operation in this range are considerable. Impellers of centrifugal compressors have for some time been operated efficiently with inlet conditions such as these, and, more recently, the same is true of transonic compressors. The sensitivity of turbine losses to variations in angle of attack at high rotor-inlet Mach number requires more careful design than is usually necessary. Rather than using only interblade-row velocity diagrams based on simplified radial equilibrium, the first step in refinement of design techniques appears to be the assumption of axial symmetry; in this way, the axial variations in radial position of the streamlines will be determined in a rational manner. For most effective design, such potential-flow techniques must also be combined with knowledge of viscous effects at the blade ends.

### TURBINE STATOR ADJUSTMENT

As has been pointed out previously, turbine stator adjustments may be used to add flexibility to engine operation. For example, consider an engine designed for the following conditions: flight Mach number in stratosphere, 2.8; compressor pressure ratio, 4.0; engine temperature ratio, 3.0. This engine temperature ratio of 3 corresponds to a turbine-inlet temperature of  $3024^{\circ}\text{R}$  ( $2564^{\circ}\text{F}$ ) during flight at a Mach number of 2.8. If an engine having a fixed turbine stator is operated during take-off at sea level in such a way that the compressor operating point is the same as for flight (constant equivalent rotational speed and constant compressor pressure ratio), a constant engine temperature ratio is required, and the compressor and turbine operating conditions are essentially the same as the altitude design values. However, an

[REDACTED]

engine temperature ratio of 3 during take-off at sea level results in a turbine-inlet temperature of only 1555° R (1095° F). The take-off thrust obtainable with this low value of turbine-inlet temperature would be correspondingly low.

One way in which this take-off thrust might be increased is by employing turbine stator adjustment and raising the turbine-inlet temperature to the rated value of 3024° R (2564° F). Turbine stator adjustment might conceivably be employed to keep the compressor operating at its design values of equivalent rotational speed and pressure ratio; in this way, the compressor would continue to operate efficiently. Simultaneously the take-off thrust would be increased, as shown in figure 8, by 98 percent. On the other hand, the range of operating conditions imposed on the turbine must be examined in order to determine whether the turbine is capable of fulfilling the requirements imposed by this range of turbine stator adjustment.

#### Turbine-Inlet Equivalent Weight Flow

The required increase in turbine-inlet equivalent flow ratio with rising turbine-inlet temperature is presented in figure 9. With a turbine-inlet temperature for take-off at 1555° R (1095° F) the turbine-inlet equivalent weight flow is the design value. Raising the turbine-inlet temperature increases the turbine-inlet equivalent flow until, at a temperature of 3024° R (2564° F), the turbine-inlet equivalent flow is 39 percent greater than the design value. Achieving a variation in turbine-inlet equivalent flow of this magnitude is a serious problem in turbines designed to operate with adjustable stators.

Experimental results from operation of a two-stage turbine with an adjustable first-stage stator are presented in figure 10 (ref. 1). In this investigation, the actual turbine stator area was increased by 45 percent. The observed variation in equivalent weight flow at the turbine inlet is shown to be only 10 percent for this 45-percent rise in turbine stator area. This limitation on turbine equivalent flow has previously been attributed to choking downstream of the turbine stator.

The problem of variation in turbine-inlet equivalent weight flow by means of stator adjustment has been investigated analytically by assuming constant loss in the turbine (ref. 2). For an adjustable turbine stator followed by a choked turbine rotor, the turbine-inlet equivalent weight flow was found to be capable of wide variations. In one case, the turbine-inlet equivalent weight flow was increased by 70 percent, of which 20 percent was in the region of stator choking and the remaining 50 percent with the stator unchoked. The limit on turbine equivalent weight flow therefore appears to depend more on the manner in which the

turbine losses vary than on choking downstream of the turbine stator. An analysis of the variation in the rotor-entrance flow direction has shown that this variation in rotor-entrance flow with stator adjustment produces wide variations in angle of attack on the rotor blade row and may well be a source of considerable loss. Analytical investigations have also shown that, for a given change in turbine-inlet equivalent flow, the change in the angle of incidence on the first rotor blade row is considerably greater for two-stage than for one-stage turbines. This indicates that the use of stator adjustment in a one-stage turbine will provide more flexibility in engine operation than is possible with stator adjustment in a two-stage turbine.

### Turbine-Exit Equivalent Flow

The variation in turbine-exit equivalent flow with turbine stator adjustment is important, because it reflects the proximity to limiting blade loading. For the particular engine design conditions under consideration, the variation in turbine-exit equivalent flow with turbine-inlet temperature is presented in figure 11. As the turbine-inlet temperature is increased for take-off, the turbine-exit equivalent weight-flow ratio first decreases and then increases. At a turbine-inlet temperature of  $3024^{\circ}\text{R}$  ( $2564^{\circ}\text{F}$ ) the value of turbine-exit equivalent weight flow is 93 percent of design value, so that in terms of limiting blade loading the turbine-exit conditions have become less critical than the design conditions.

If the engine is designed for a different set of conditions, the trend of turbine-exit equivalent weight flow will be different from that shown in figure 11. Figure 12 shows, for example, that, for another set of engine design conditions, the turbine-exit equivalent weight flow rises above the design value. This trend of turbine-exit equivalent weight flow requires that the turbine be designed conservatively for design-point operation. This redesigning is required in order to avoid limiting blade loading during take-off operation and results in a reduction in the air-flow-handling capacity of the turbine during high-speed flight. The difference between the two changes shown for turbine-exit equivalent weight flow emphasizes the importance of investigating the variation in this quantity when turbine stator adjustment is contemplated.

In general, the use of turbine stator adjustment to obtain increased thrust for take-off requires an increase in the turbine-inlet equivalent flow; the turbine-exit equivalent weight flow may increase or decrease, depending upon the particular engine design conditions and the range of engine temperature ratio over which the engine is required to operate. Whether or not turbine stator adjustment can be employed to provide a satisfactorily wide range of engine operation depends principally on the amount by which the turbine efficiency varies during such operation.

[REDACTED]

### CONCLUDING REMARKS

For flight at high Mach numbers, the centrifugal stress in the turbine rotor blade has a large effect on turbine design. For turbines having either one or two stages, operation at the rotor blade-loading limit during high-speed flight results in considerable improvement in turbine air-flow capacity. Use of high rotor-inlet Mach numbers improves the competitive position of one-stage turbines for high Mach number flight. The variation in turbine efficiency with turbine stator adjustment is the factor controlling whether or not turbine stator adjustment can be used to provide high engine thrust over a wide range of engine operating conditions.

### APPENDIX - SYMBOLS

The following symbols are used in this paper:

$A_T$	turbine-tip frontal area, sq ft
$E$	turbine work, Btu/lb
$g$	standard acceleration due to gravity, 32.17 ft/sec <sup>2</sup>
$J$	mechanical equivalent of heat, 778.2 Btu/lb
$M$	Mach number
$P$	total, or stagnation, pressure lb/sq ft
$T$	total, or stagnation, temperature, °R
$U$	blade speed, ft/sec
$V$	absolute velocity, ft/sec
$W$	relative velocity, ft/sec
$w$	weight flow, lb/sec
$w\sqrt{\theta_1}/\delta_1 A_T$	specific weight flow, lb/(sec)(sq ft)
$\frac{w\sqrt{\theta_3}/\delta_3}{(w\sqrt{\theta_3}/\delta_3)_d}$	turbine-inlet equivalent weight-flow ratio
$\frac{w\sqrt{\theta_5}/\delta_5}{(w\sqrt{\theta_5}/\delta_5)_d}$	turbine-exit equivalent weight-flow ratio

[REDACTED]

$\delta$  pressure reduction ratio,  $\frac{P}{2116}$

$\theta$  temperature reduction ratio,  $\frac{T}{518.4}$

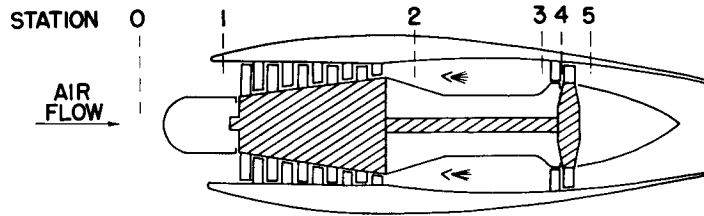
Subscripts:

- d design condition
- h hub
- u tangential component
- x axial component
- 1 compressor inlet
- 2 compressor exit
- 3 turbine inlet
- 4 turbine rotor inlet
- 5 turbine exit

REFERENCES

1. Campbell, Carl E., and Welna, Henry J.: Preliminary Evaluation of Turbine Performance with Variable-Area Turbine Nozzles in a Turbojet Engine. NACA RM E52J20, 1953.
2. English, Robert E., and Cavicchi, Richard H.: One-Dimensional Analysis of Choked-Flow Turbines. NACA Rep. 1127, 1953. (Supersedes NACA TN 2810.)

# TURBOJET ENGINE



## TYPICAL VELOCITY DIAGRAM

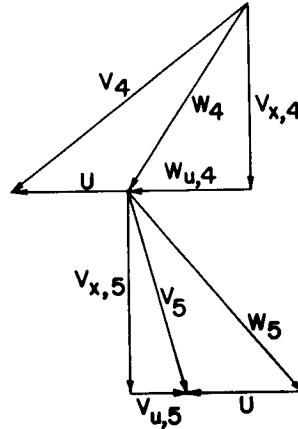


Figure 1

## TURBINE LIMITING BLADE LOADING

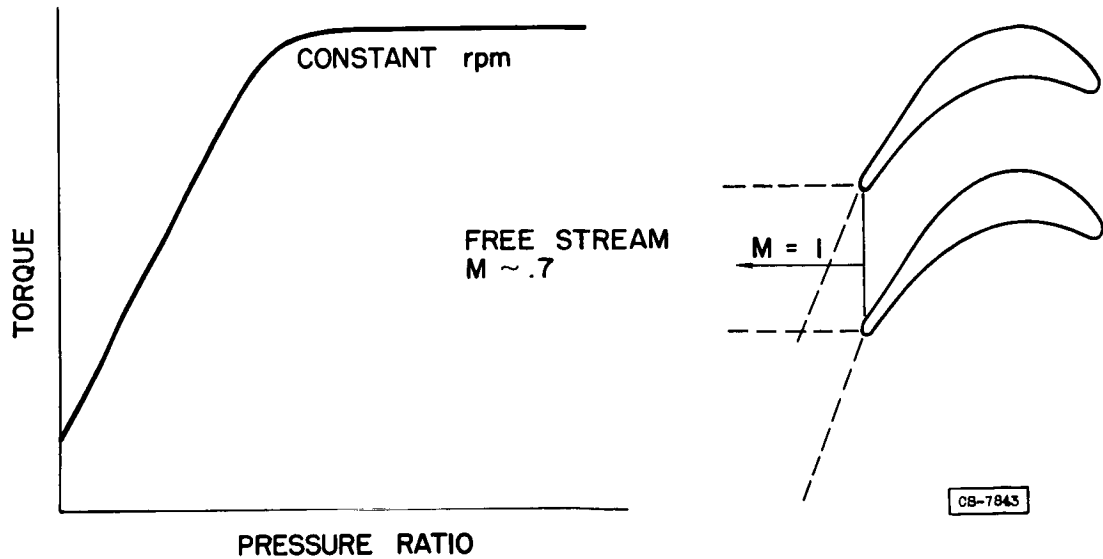


Figure 2

SEA-LEVEL ENGINE WEIGHT FLOW  
TURBINE-INLET TEMPERATURE, 1614° F

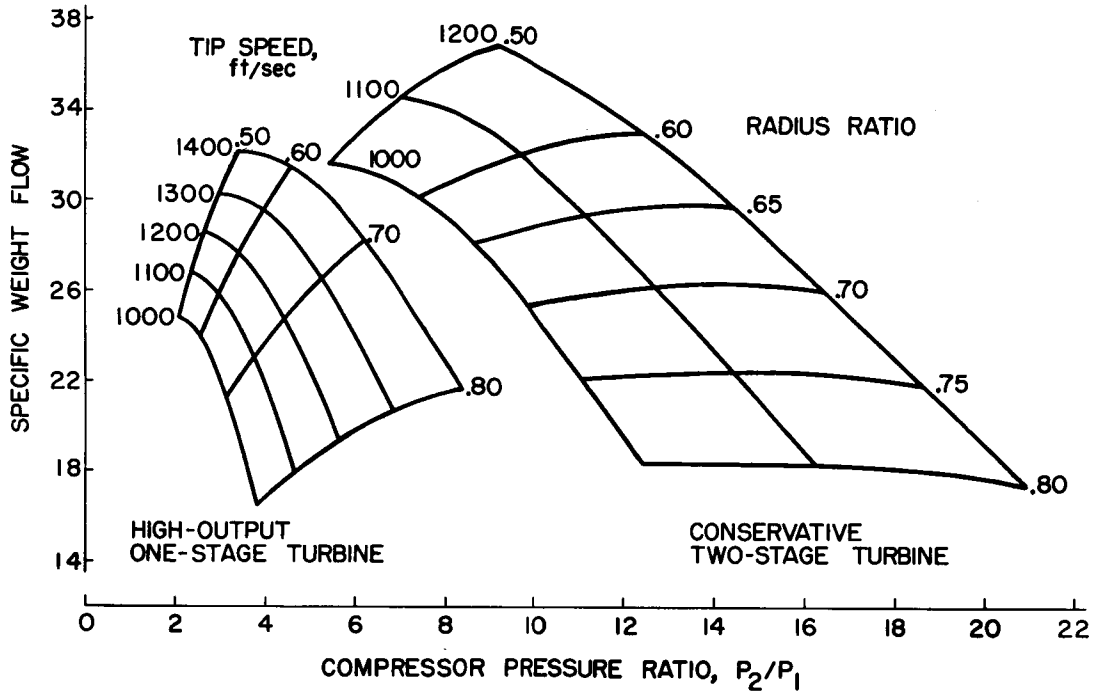


Figure 3

EXIT AXIAL MACH NO. AND FLOW CAPACITY  
TURBINE-INLET TEMP., 2564° F  
RADIUS RATIO, 0.5

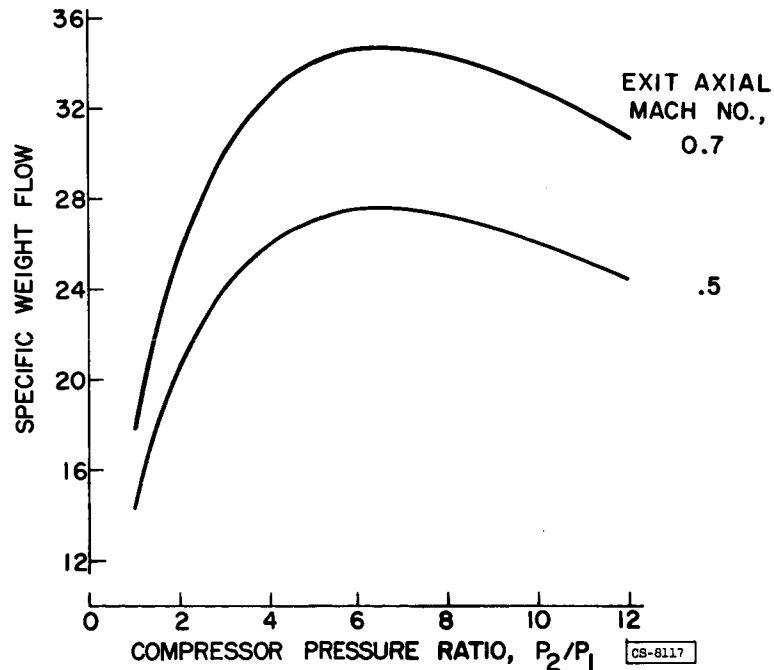


Figure 4

TURBINE LIMITED ALTITUDE ENGINE WEIGHT FLOW  
 TURBINE-INLET TEMPERATURE, 2564° F

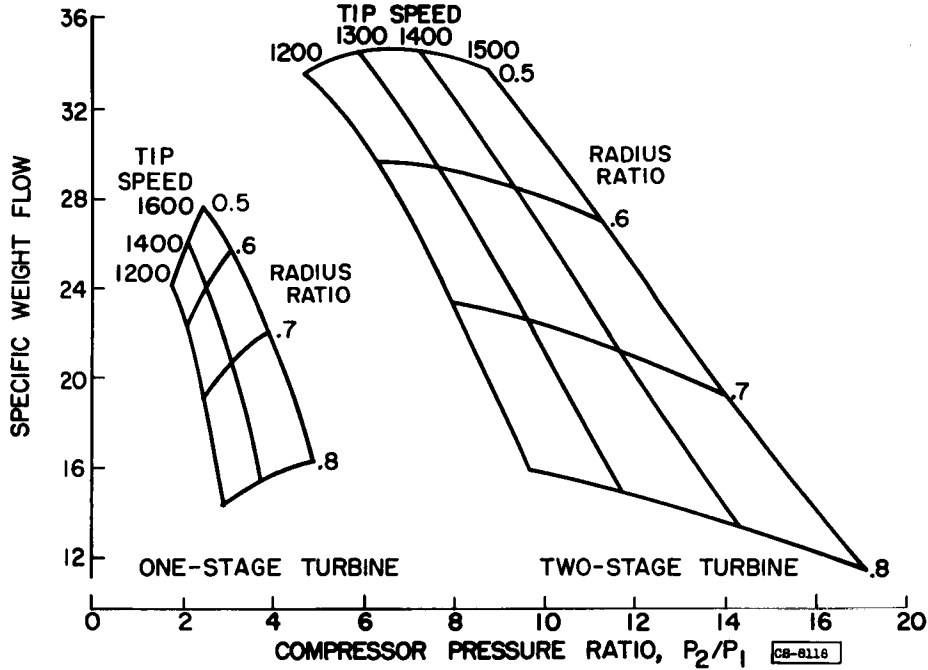


Figure 5

TURBINE LIMITED ALTITUDE ENGINE WEIGHT FLOW  
 TURBINE - INLET TEMPERATURE, 2564° F

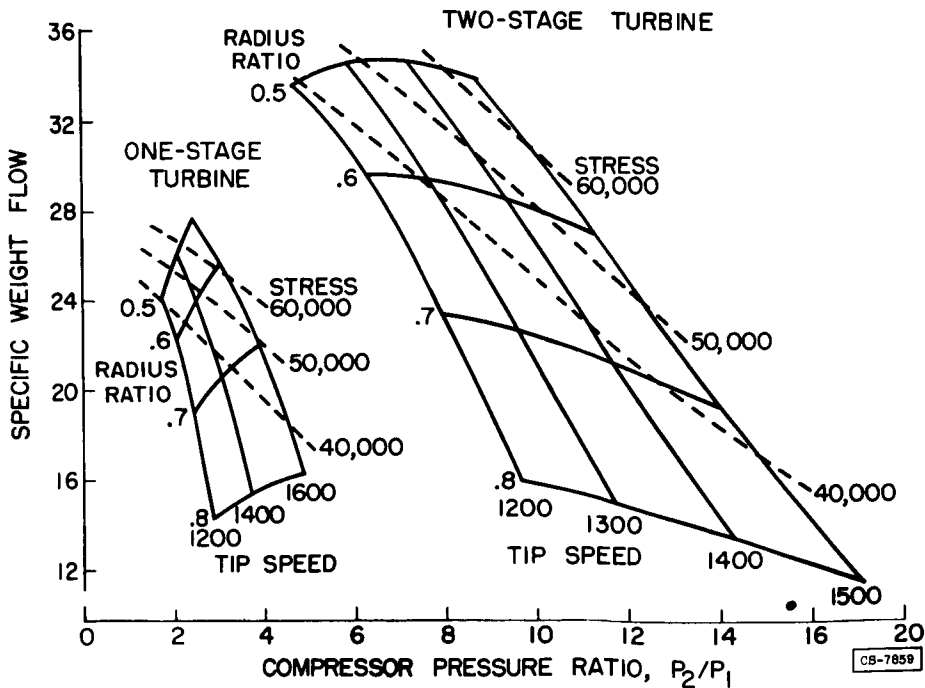


Figure 6

EFFECT OF ROTOR-INLET MACH NUMBER  
STRESS, 50,000 psi

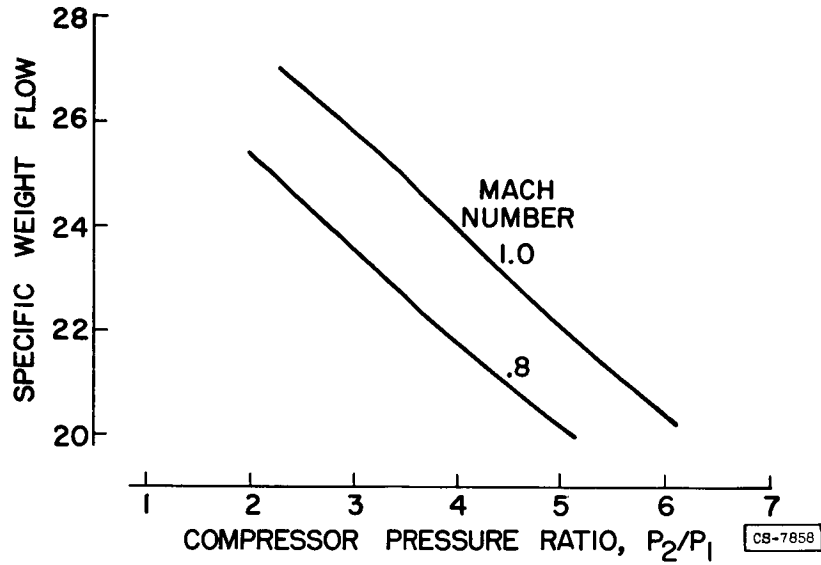


Figure 7

TAKE-OFF THRUST  
DESIGN TEMP. RATIO,  $T_3/T_1$ , 3.0  
COMPRESSOR PRESSURE RATIO,  $P_2/P_1$ , 4.0

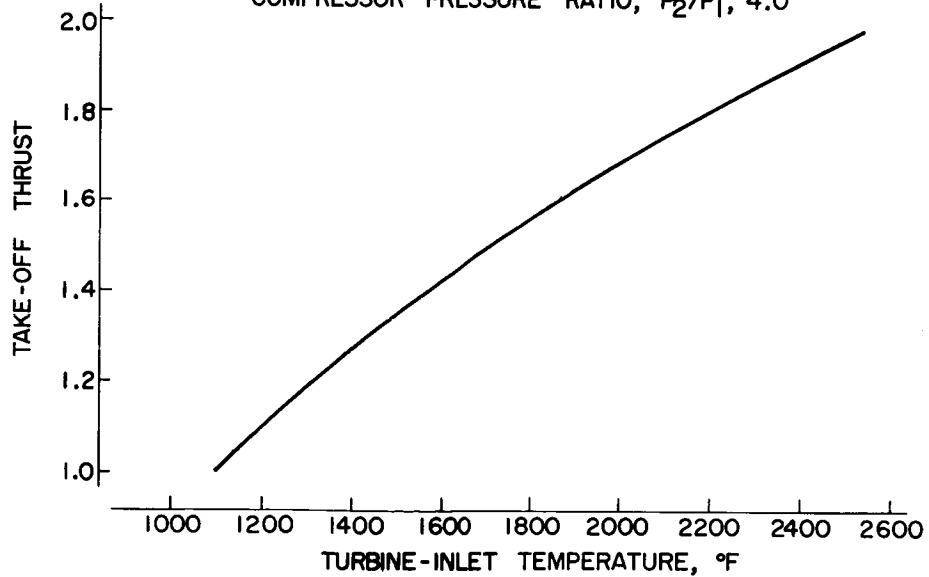
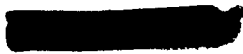
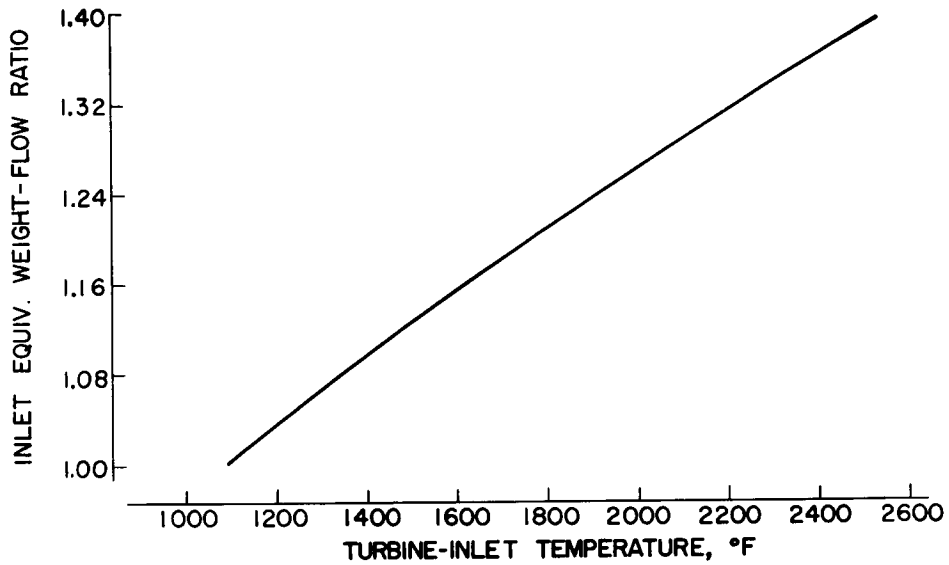


Figure 8



TAKE-OFF TURBINE-INLET EQUIVALENT WEIGHT FLOW  
DESIGN TEMP. RATIO,  $T_3/T_1$ , 3.0



3078-B

Figure 9

OBSERVED EFFECT OF STATOR AREA ON WEIGHT FLOW

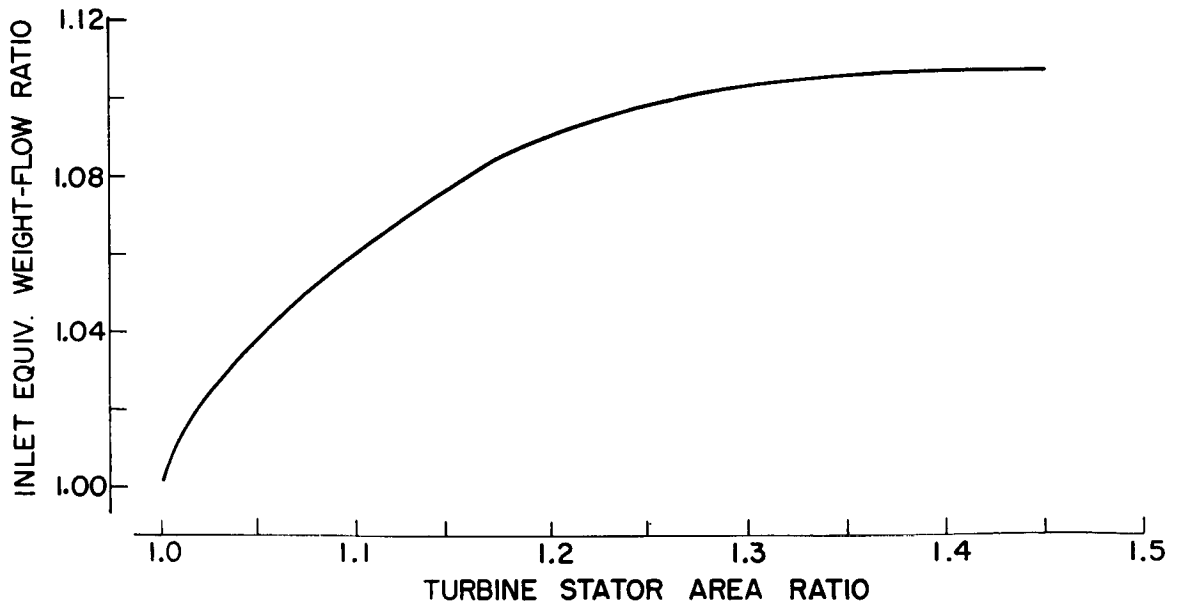
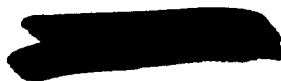


Figure 10



3078-B

TAKE-OFF TURBINE-EXIT EQUIVALENT WEIGHT FLOW

DESIGN TEMP. RATIO,  $T_3/T_1$ , 3.0  
COMPRESSOR PRESSURE RATIO,  $P_2/P_1$ , 4.0

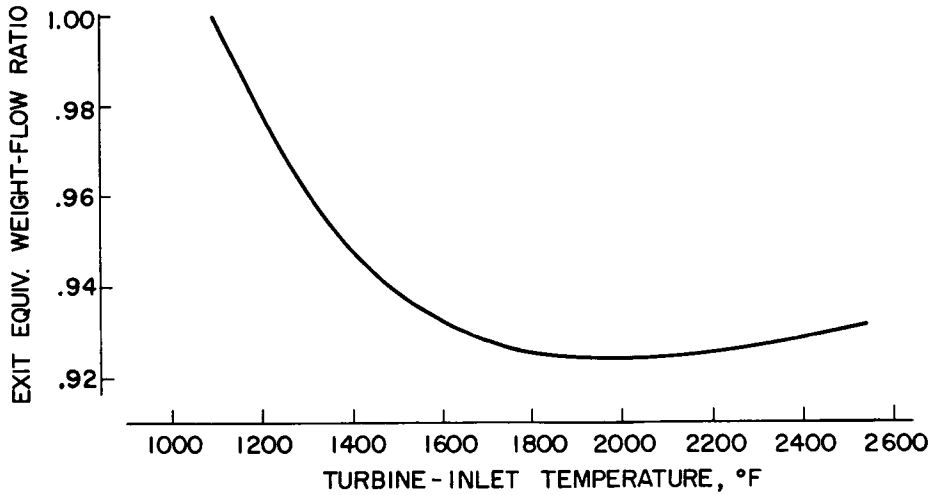


Figure 11

TAKE-OFF TURBINE-EXIT EQUIVALENT WEIGHT FLOW

DESIGN TEMP. RATIO,  $T_3/T_1$ , 3.0  
COMPRESSOR PRESSURE RATIO,  $P_2/P_1$ , 2.0

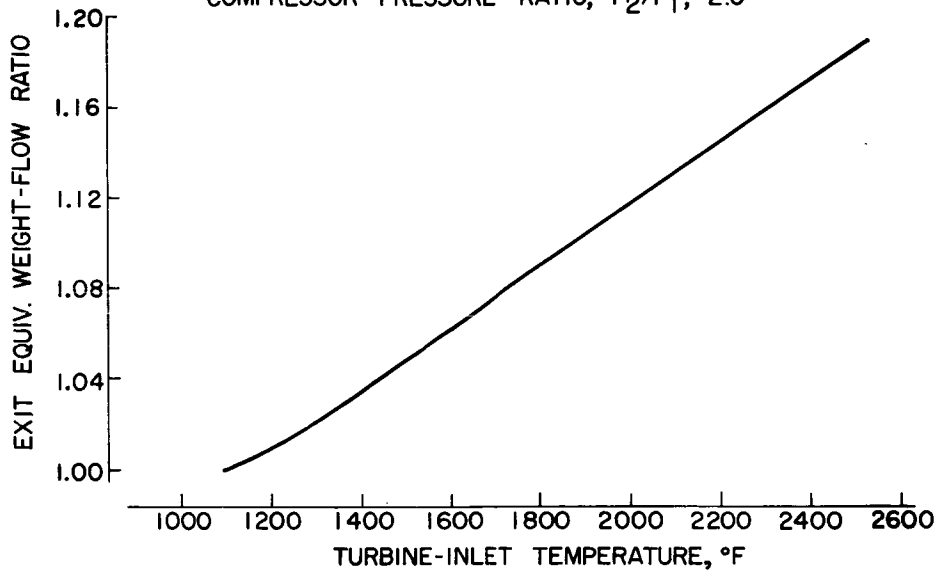


Figure 12

[REDACTED]  
SECONDARY-FLOW LOSSES IN TURBINES

By Howard Z. Herzig and Howard A. Buckner, Jr.

## INTRODUCTION

3078 -B

As pointed out in a preceding paper by English and Rebeske, two of the important design objectives of turbine components for high-speed aircraft are high efficiency and small weight. Reductions in the weight of the turbine as well as of components following the turbine can be obtained by increasing turbine efficiency while maintaining an otherwise fixed set of aerodynamic conditions. Savings in the weight of fuel to be carried by the aircraft can be achieved through increasing the turbine efficiency as a result of the consequent increase in engine or cycle efficiency. In order to be in a position to increase turbine efficiencies, which is in effect reducing the losses, it is necessary to determine the locations, sources, and relative magnitudes of the various losses that may occur in the turbine. This paper presents a study of turbine losses and a discussion of the phenomena involved.

## LOCATION OF SOURCES OF MAJOR LOSSES

Flow measurements made just downstream of a conservatively designed turbine indicate that the major losses are located near the blade ends (ref. 1). Figure 1 compares the relative magnitudes of blade profile losses and flow losses measured in the blade end region. A large portion of these losses is associated with secondary flows. (Secondary flows are defined as any motions of boundary-layer fluid having components normal to the main stream direction.) For example, the secondary flow for the turbine of figure 1 is thus associated with approximately 70 percent of the total loss. The largest loss measured in the case of this turbine appears near the outer wall or tip region, while a somewhat lower loss appears near the inner wall or hub. Between the two blade end regions where the secondary flows are small, the losses are very low. Because the major sources of loss appear to be secondary flows, it is of interest to examine these losses in more detail.

Two general types of loss patterns have been observed. These loss patterns were found by measurements taken downstream of turbine rotors in the measuring plane shown in figure 2. In figure 3, contours of local efficiency for turbines are plotted over a segment of the turbine-rotor discharge annulus of slightly more than one nozzle-passage width. For turbine I (fig. 3), extremely large gradients in efficiency exist downstream of this turbine; the total variation in this case amounts to 14 points. Furthermore, the regions of low efficiency, or

[REDACTED]

high loss, are highly localized and occur at regular circumferential intervals around the annulus. Losses originating in the moving rotor-blade row would necessarily appear evenly distributed around the annulus rather than in regular localized intervals varying with circumferential position. Therefore, the circumferential gradients are evidently the result of some stationary-flow maldistribution upstream of the turbine I rotor. Because the efficiency pattern is approximately repetitive circumferentially at very nearly the value of stator pitch, it appears that these gradients originate in the stator blades. It seems likely from this plot that the efficiency of turbine I, which is 0.87, could be improved considerably by improving the flow issuing from the stator blades. It is important then that an understanding of the phenomena contributing to these flow conditions be obtained; this will be discussed in a later section of the paper.

The second type of loss pattern obtained over a segment of the rotor discharge annulus of a second turbine is shown in figure 3. This pattern is similar to the previous one in the region near the hub in that large circumferential gradients are present. Near the outer wall or tip region, however, the loss pattern in the main takes the form of circumferential bands of low efficiency rather than large circumferential gradients. By the reasoning advanced previously, these losses in the tip region appear to be primarily the result of unfavorable flow conditions in the rotor-blade passages. This is in addition, of course, to the unfavorable flow issuing from the stators of turbine II, similar to that in turbine I, as shown by the small island of low efficiency in this region. These results indicate, then, that the efficiency of turbine II, which is 0.89, could be improved considerably by improving the flow through the rotor-blade passages in the tip region.

From the examination of these two general types of loss pattern, it appears that there are two main causes of these losses: (1) unfavorable flow near both the inner and outer walls in the form of large flow gradients or secondary flows issuing from the stator blades, and (2) unfavorable flow conditions in the rotor-blade passages near the tip region. The remainder of this paper is devoted to a discussion of the phenomena causing these unfavorable flow conditions, of what has been learned regarding the control of these phenomena, and of the current work being done on this problem.

#### STATOR SECONDARY FLOWS

A typical loss pattern obtained from flow surveys just downstream of turbine stator blades is shown in figure 4. Over a large part of the passage, the losses are practically negligible. At the junction of the blade wakes with the inner and outer walls, however, regions of high loss are observed; the loss measured at the inner wall is much higher than that at the outer wall. These losses appear in the form of cores, called passage vortices (ref. 2), which apparently issue from the corner region formed by the blade suction surface and the end wall.

The basic cause of this core formation can be explained as follows: Whenever a gas flows through any kind of a channel, there develops, because of frictional effects, a layer of relatively slow-moving gas on the walls of the channel. This layer of lower-momentum fluid is called the boundary layer. The formation of a boundary layer represents an aerodynamic loss due to the frictional effects.

Whenever the channel is curved and the main gas flow is turned, as, for example, in turbine stators (fig. 5), a balance is established between the centrifugal forces and the local stream (static) pressure gradients.

According to boundary-layer theory (confirmed by experiment), these main-stream pressure gradients are imposed upon the boundary layers. Because of the lower velocities and comparatively lower centrifugal forces in the boundary layer, the imposed free-stream pressure gradients result in more than free-stream turning in the boundary-layer fluid. The result of this process is that the shroud boundary-layer material completely crosses the channel until it reaches the blade suction surface, where it rolls up into a vortex. The photograph in figure 6 (looking upstream toward a cascade exit) shows such a vortex formation as a result of this cross-channel effect in a two-dimensional cascade. The boundary-layer roll-up was traced out by use of smoke. The insert in the picture shows schematically the overturning in the boundary layer leading to the vortex formation. This formation of such a loss core takes place at both the inner and outer shrouds.

In annular cascades, such as shown in figure 7, another factor plays a prominent role in establishing the secondary-flow patterns. Because the fluid possesses tangential components of velocity when turned from an axial direction, a radial pressure gradient must exist to balance the centrifugal forces resulting from the flow around the annulus for the same reasons as discussed previously. As a result, the pressure at the outer wall is greater than that at the inner wall, which causes the loss material at the outer wall to drain partly away to the inner wall through the low-momentum and thickened boundary regions on the blade surface and in the wakes downstream of the trailing edge, as shown by the arrows in figure 7 (refs. 3 to 5).

The photograph in figure 8 shows the location of such thickened boundary-layer regions (caused by existence of shocks across the passages at supersonic flow conditions, refs. 3 and 4) on the suction surfaces of the blades of a set of typical turbine stators. For this photograph, the suction surfaces of blades 1, 2, and 3 were given narrow bands of free-flowing paint at the inner-shroud, midspan, and outer-shroud radial positions, respectively. The paint, dragged by the radial components of secondary flow throughout the thickened boundary-layer regions, flows radially and thus traces out the radial secondary-flow paths. This

explains in part why the loss cores near the inner wall of the stators are generally considerably larger than those at the outer wall.

This radial flow of loss material into the hub region is considered very undesirable, because the rotor in this region is usually operated at more critical conditions, that is, higher Mach number, less reaction, and greater turning.

Studies have been made of a number of blade configurations (ref. 5), and the loss patterns in all are generally similar to the one described. That is, cores tend to form at the junction of the blade suction surface and the end walls, and part of the loss material drains radially from the outer wall to the inner wall. It has been found that carefully designed blades with properly chosen surface velocity distributions tend to minimize, although not completely eliminate, the loss cores. It has also been found that the flow of the loss material to the critical inner-wall region can be blocked (causing it to appear elsewhere in the passage), and the inner-wall loss core can thus be decreased considerably by properly placed flow fences. The energy actually involved in these secondary flows in the stator blades is quite small, as indicated by stator efficiencies of the order of 0.98; the major effects are thus evidently flow blockage and the losses caused by the cores in passing through the rotor blades, as evidenced by the results shown in figure 3. Although the results at present are by far too meager to disclose the mechanism by which the stator secondary flows induce these large losses in the rotor, several effects may be suggested as contributors. First, the through-flow velocities of the fluid in secondary-flow core regions issuing from the stators are known to be considerably lower than free-stream velocity; this difference results in large negative angles of attack at the rotor inlet each time a rotor blade passes through a stator core. Another possible source of loss could be the mixing of fluids of varying energy levels. Still another effect is that caused by the observed failure of the loss cores to be turned with the main stream. This may displace the main-stream fluid and upset blade surface velocity distributions where the cores strike blades and thereby induce consequent losses.

Research is at present being directed toward determining methods of control of these secondary flows in order to obtain the indicated possible gains in turbine performance.

#### ROTOR TIP-REGION SECONDARY FLOWS

The secondary-flow behavior in the rotor tip region is somewhat more complicated than it is in the stators (ref. 2). In the rotor, in addition to the overturning and the roll-up of the boundary layer into a passage vortex that accumulates on the rotor-blade suction surface, there are losses arising (1) because of the clearance space between the

rotor-blade ends and the outer wall (tip-clearance effect), (2) because of the relative motion between the rotor-blade ends and the outer wall (scraping effect), and (3) radial movement of the boundary layer on the rotor blades.

Tip-clearance effect. - Because of the pressure difference that exists across the rotor-blade tip, there is a flow of blade boundary layer from the pressure side of the blade through the tip-clearance space to the suction side of the blade. The flow resulting from the tip-clearance effect is seen in figure 9 to roll up into the so-called tip-clearance vortex on the suction side of the blade. The tip-clearance flow is traced out by smoke introduced at the leading edge of a blade near the blade tip. As in the case of passage vortex formation, the strength of the tip-clearance flow is influenced by the circulation (i.e., main-flow turning and airspeed) about the blade ends. However, the passage vortex and the tip-clearance vortex are opposite in direction and rotate side-by-side without cancelling each other.

The tip-clearance flow causes boundary-layer fluids to accumulate on the blade suction surface and increases the tendency there to flow separation. It likewise serves to unload the turbine-rotor blade at the tip, that is, to reduce the pressure differential across the blade and thereby to reduce the blade work output.

Scraping effect. - Because of the relative motion between the rotor-blade tips and the outer shroud, the blades exert a scraping effect upon the shroud boundary layer. The scraping effect causes the boundary layer to roll up into the so-called "scraping vortex." This effect of relative motion is illustrated in figure 10, in which the scraping effect of a blade on the boundary layer of a moving end wall is visualized by the use of smoke. A schematic diagram of the apparatus used for these tests is presented in figure 11. The scraping effect in a rotor depends upon the blade speed and upon the blade-tip stagger (i.e., orientation of the blade-tip profile relative to the direction of motion). If the rotor-blade-tip stagger is positive (fig. 12), the blade will tend to slice through the boundary layer and thus diminish the scraping effect. Blades oriented more nearly perpendicular to the direction of rotation have a more pronounced scraping effect.

The scraping effect in a turbine rotor acts in the same direction as the passage vortex effect, helps accumulate boundary-layer fluids on the blade suction surface, and abets losses, as described previously. (It may be noted that the scraping effect appears actually to be beneficial in compressors.)

Radial movement of rotor-blade boundary layer. - As the fluid passes through the rotor blades, the radial pressure gradient of the mass flow is decreased as the absolute tangential component of velocity is reduced until, at the exit where the tangential component is usually

close to zero (in the case of a single stage), no radial static-pressure gradient in the main stream exists. The boundary-layer material that has formed on the rotor-blade surface, however, is continually moving with a tangential component of velocity approaching the blade speed. Because the centrifugal forces in the blade boundary layer now exceed the radial pressure gradient of the main flow as the exit of the passage is approached, this boundary-layer material is centrifuged to the tip section. Although no experimental results regarding this flow have been obtained, it is presumed that the radially centrifuged boundary-layer flow in the rotor blades will add to the low-momentum material along the blade-tip suction surface.

Balancing secondary flows. - The breakdown of the turbine-rotor tip region losses into the kinds of flow disturbances described earlier, together with an understanding of their origins, suggests possible methods for reducing the turbine-rotor tip losses. The fact that the tip-clearance effect is opposed in direction to the scraping and cross-channel effects suggests the possibility of balancing off the resultant flow disturbances against each other. The main variables to be controlled in order to do this have been shown to be the circulation (main-flow turning and airspeed) at the blade tip, the blade-tip stagger, and the rotor speed. When this balance was fairly well approximated experimentally in a two-dimensional cascade, the flow in the tip region was considerably smoother. Figure 11 is a schematic diagram of the apparatus used and shows the two-dimensional cascade with the belt sander used to visualize the effects of relative motion between the end wall and the blades. With the end wall stationary, smoke was introduced on the pressure surface near the tip of one of the cascade blades; and, as shown in figure 13(a), the flow in the blade tip region was seen to be disturbed by a large tip-clearance flow. The tip-clearance flow is reduced (fig. 13(b)) when the end wall is set into motion. As the wall speed is increased, the scraping action likewise increases and further reduces the tip-clearance flow until (fig. 13(c)) a balance is established and the flow in the blade tip region along the blade suction surface is relatively smooth and undisturbed.

No such visual proof of establishing this balance in a turbine-rotor configuration has as yet been obtained. It has been possible, however, to vary the relative magnitudes of the scraping and tip-clearance effects in a rotor and to show, in part, how they oppose each other. This was done by varying the rotor speed of a low-speed turbine, as shown in figure 14. The photographs of smoke traces were taken (looking upstream into the discharge section of the turbine built for just such smoke studies). The smoke was introduced through a static tap in the outer shroud at the rotor-blade midchord position, axially.

In figure 14, at low rotor speed, the tip-clearance flow dominates the flow picture. With the rotor speed somewhat increased, the scraping

effect has increased greatly and now masks the tip-clearance effect almost completely. Somewhere between these last two speeds is a balance point for these effects, and at this balance point the flow disturbances in the tip region are reduced to a minimum. These photographs show how the secondary-flow patterns can be varied by varying rotor speed alone. For some turbines in which stress considerations do not rule out the use of shrouding, shrouding turbine rotors has been suggested as a means of eliminating or reducing the turbine-rotor tip-region flow disturbances. In particular, shrouding such turbine rotors might well reduce or eliminate the scraping effect and the tip-clearance effect and could result, for some cases, in better flow conditions in the turbine-rotor tip regions. It should be noted carefully that shrouding a turbine rotor which operates near the balance point of the flow disturbances without the shroud could upset that balance and might actually lead to increased tip-region losses. This probably accounts for the apparently conflicting experimental evidence concerning turbine-rotor shrouding obtained by various investigators.

Further studies are now in progress to evaluate the effects of varying the pertinent rotor parameters in order that the fundamental information concerning rotor-tip-region losses can be put to practical use in the design of more efficient turbines (and compressors).

#### CONCLUDING REMARKS

From these investigations it appears that in well-designed contemporary turbines, the major sources of remaining aerodynamic losses are (a) secondary flows in the stator blades and (b) secondary flows in the rotor-blade tip region. Any further appreciable improvements in performance then must originate from reduction of these losses. Experience has shown that careful design of stator blades to provide favorable blade surface velocity distributions helps to minimize those secondary flows. It has also been established that these secondary flows can be diverted from critical regions by such simple devices as flow fences. Current research is being directed toward determining other means of controlling these stator secondary flows as well as toward the evaluation of the effectiveness of their control in improving over-all turbine performance.

The rotor-tip secondary flow is the result of the interaction of several types of secondary flow. Visualization studies of the interaction of these secondary flows have shown that the secondary flows obtained in this region can be varied considerably by different combinations of rotor speed, blade tip stagger, main-flow turning, circulation about the blade tip, tip-clearance, and so forth. Current work is aimed at determining which type of secondary-flow interaction results in the best turbine performance and what combinations of blade-tip-section variables set up these conditions.

## REFERENCES

1. Whitney, Rose L., Heller, Jack A., and Hauser, Cavour H.: Investigation of Distribution of Losses in a Conservatively Designed Turbine. NACA RM E53A16, 1953.
2. Hansen, Arthur G., Herzig, Howard Z., and Costello, George R.: A Visualization Study of Secondary Flows in Cascades. NACA TN 2947, 1953.
3. Allen, Hubert W., Kofskey, Milton G., and Chamness, Richard E.: Experimental Investigation of Loss in an Annular Cascade of Turbine-Nozzle Blades of Free Vortex Design. NACA TN 2871, 1953.
4. Rohlik, Harold E., Allen, Hubert W., and Herzig, Howard Z.: Study of Secondary-Flow Patterns in an Annular Cascade of Turbine Nozzle Blades with Vortex Design. NACA TN 2909, 1953.
5. Kofskey, Milton G., Allen, Hubert W., and Herzig, Howard Z.: Comparison of Secondary Flows and Boundary-Layer Accumulations in Several Turbine Nozzles. NACA TN 2989, 1953.

PROFILE AND SECONDARY-FLOW LOSSES

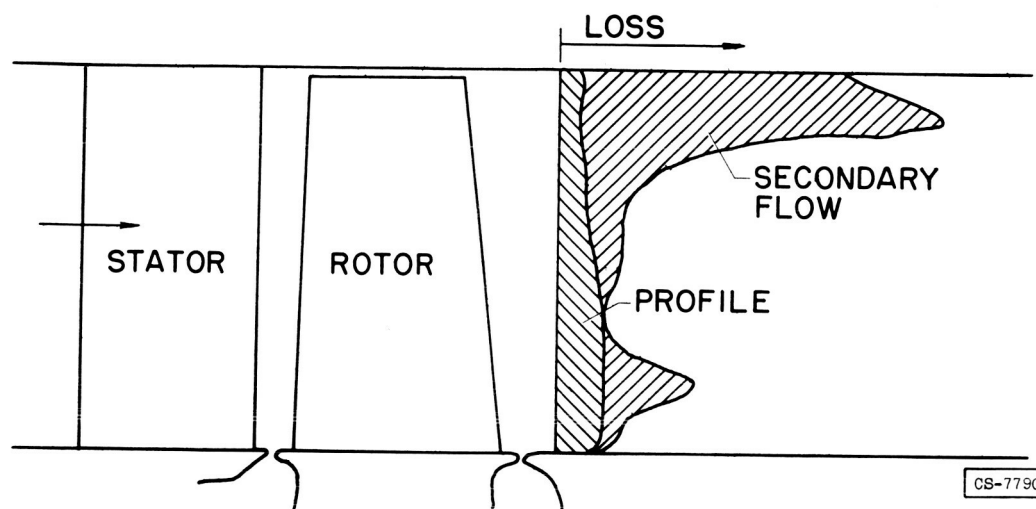


Figure 1

VIEW OF TURBINE AND MEASURING PLANE

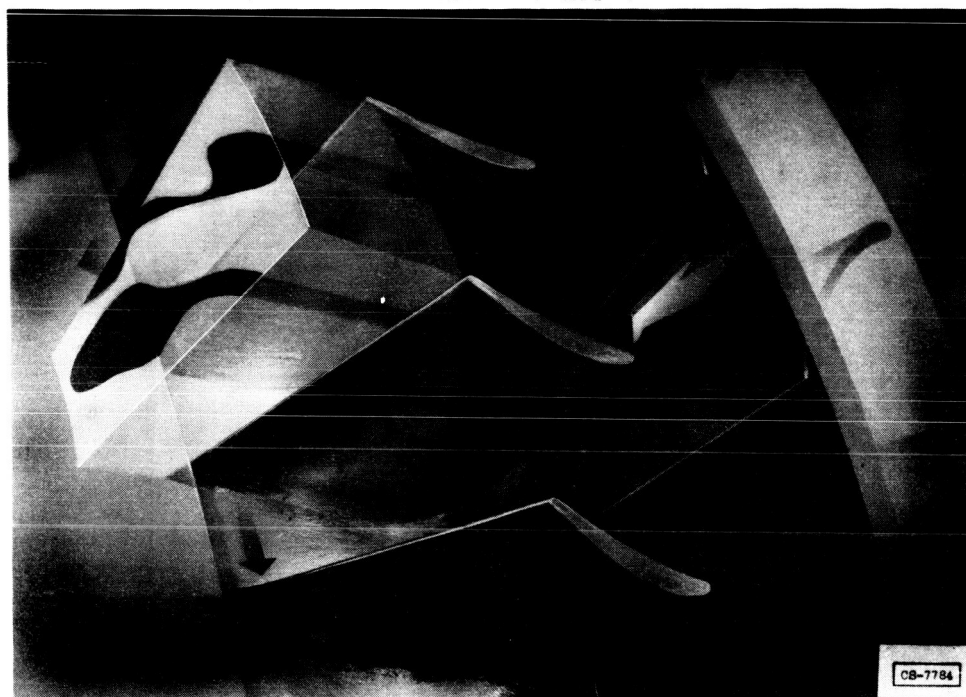


Figure 2



### TURBINE EFFICIENCY CONTOURS

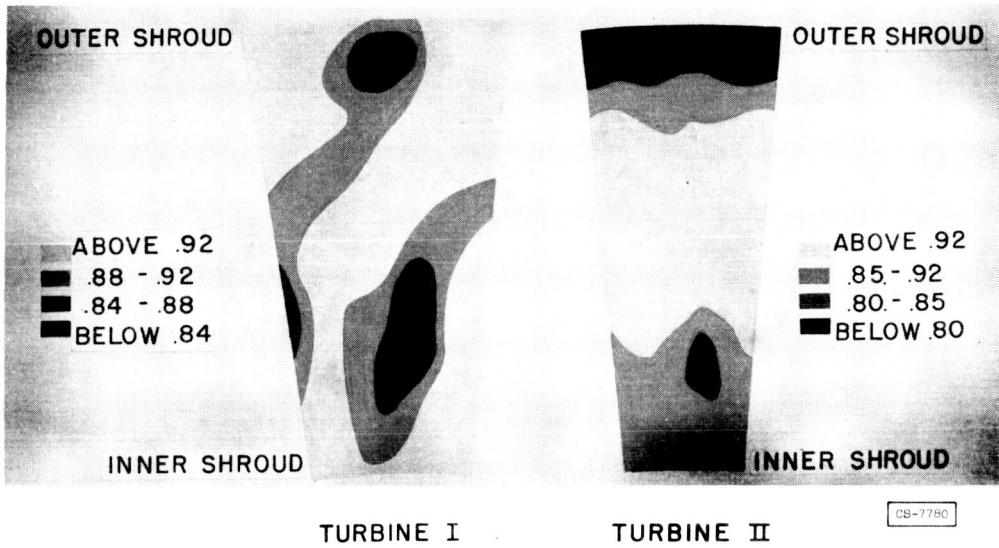


Figure 3

### STATOR EFFICIENCY CONTOURS

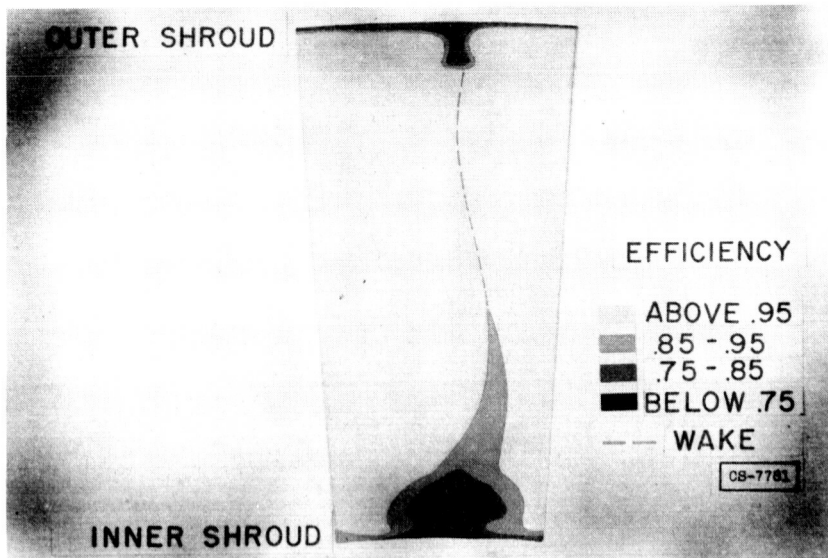
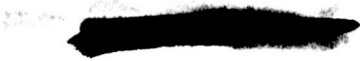


Figure 4



3078-B

OVERTURNING IN BOUNDARY LAYERS

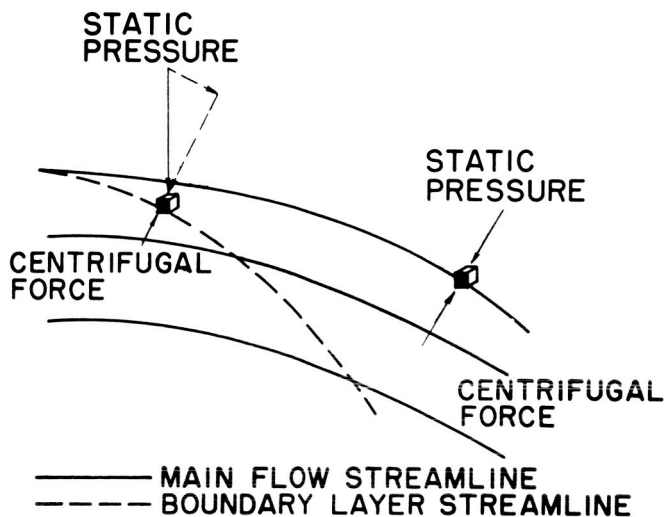


Figure 5

PASSAGE VORTEX FORMATION

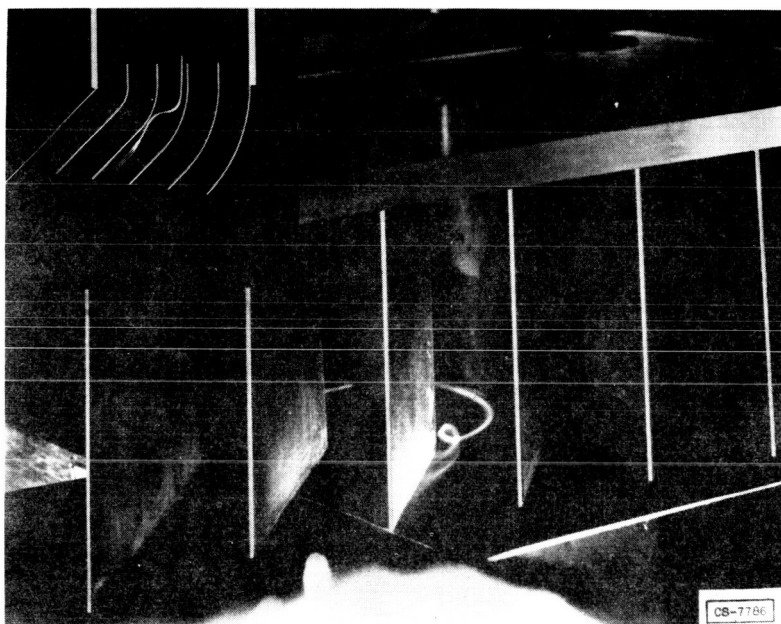
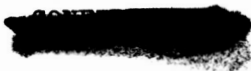


Figure 6



### STATOR SECONDARY-FLOW COMPONENTS

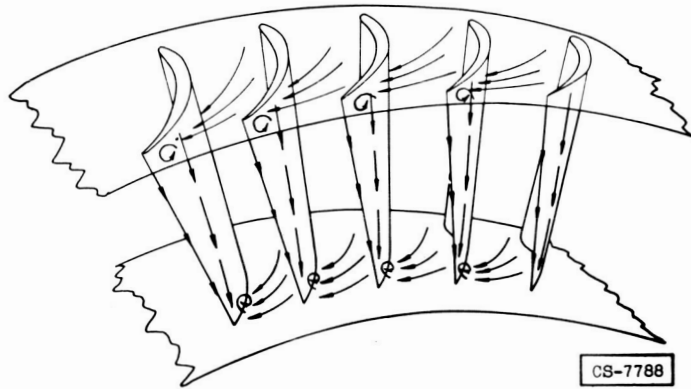


Figure 7

3078-B

### RADIAL FLOW OF LOW-ENERGY FLUID ON SUCTION SURFACES

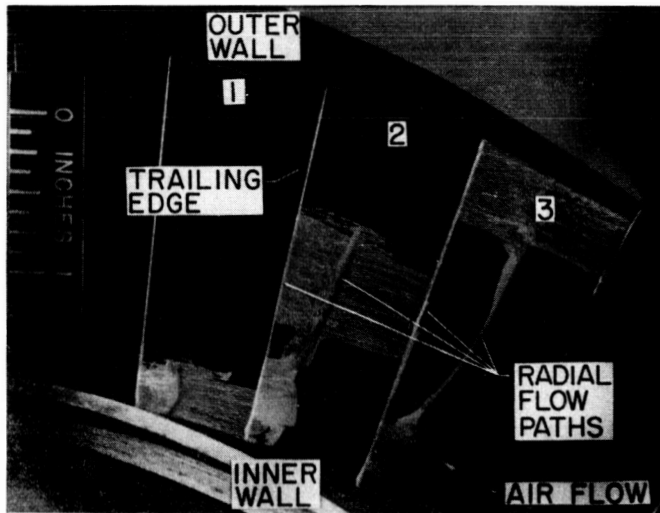
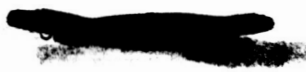
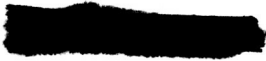


Figure 8





TIP-CLEARANCE VORTEX EFFECT



Figure 9

CS-7787

SCRAPING VORTEX EFFECT

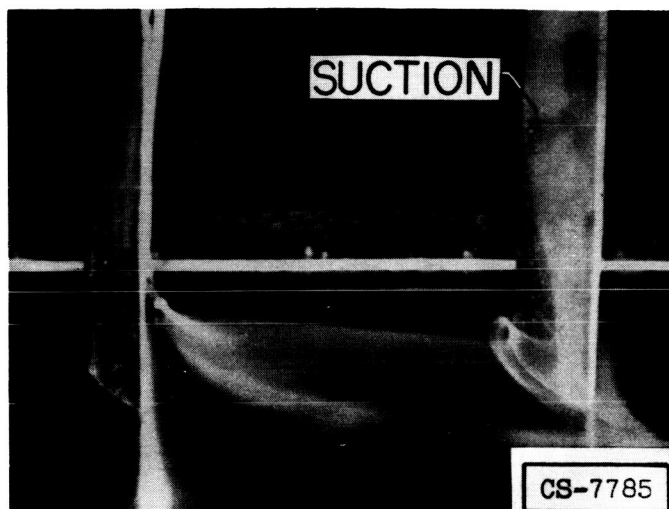


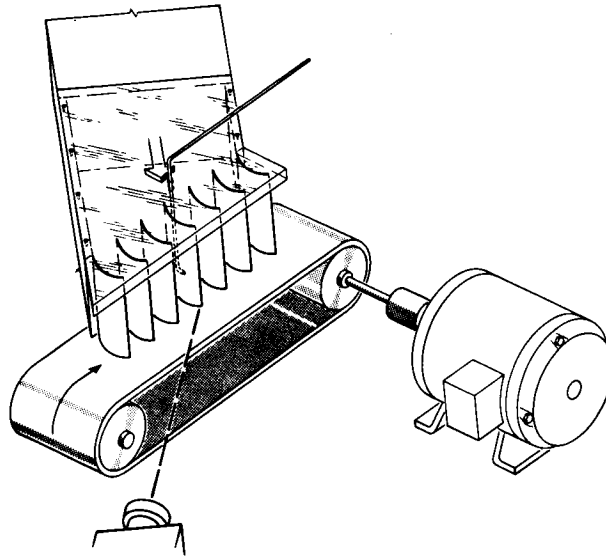
Figure 10



3078-B



### APPARATUS FOR STUDYING CASCADE TIP-CLEARANCE EFFECTS



3078-B

Figure 11

### BLADE TIP STAGGER

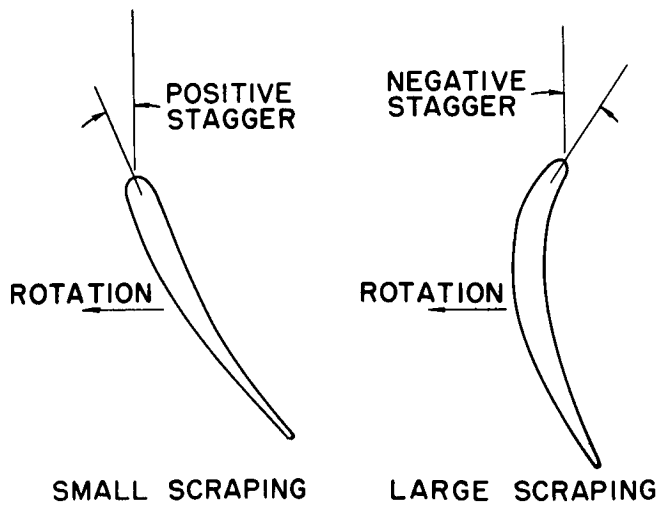


Figure 12



EFFECT OF WALL SPEED ON CASCADE SECONDARY FLOWS IN CLEARANCE REGIONS

(a) STATIONARY WALL

(b) LOW SPEED

(c) HIGHER SPEED

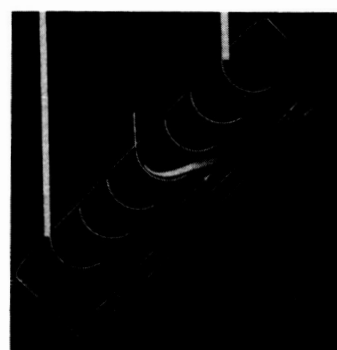
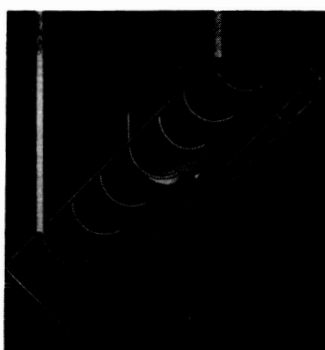
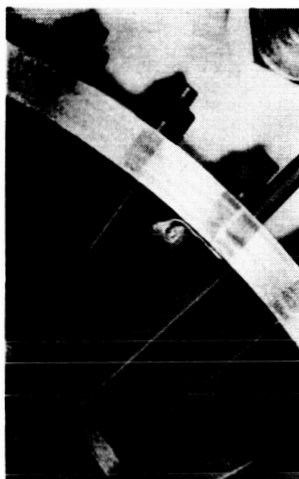
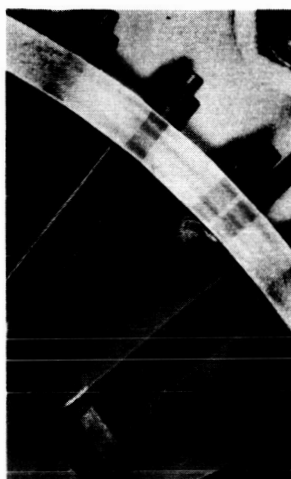


Figure 13

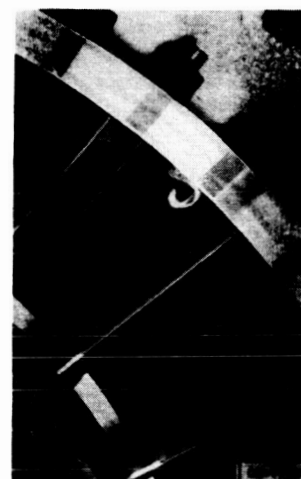
TIP-CLEARANCE AND SCRAPING EFFECTS IN LOW-SPEED TURBINE



LOW SPEED ROTOR



HIGHER SPEED ROTOR



HIGHEST SPEED ROTOR

Figure 14

3078-B

## STUDY OF TURBINES DESIGNED FOR HIGH-FLOW MACH NUMBERS

By Warner L. Stewart

## INTRODUCTION

3078-8

The first of this series of papers pointed out that the utilization of high-flow Mach numbers in turbine designs can result in lighter, more compact turbojet engines through reduction in turbine size and weight. If the entering Mach numbers relative to the rotor could be increased above present limitations, a considerable increase in the turbine specific work output per stage could be obtained. Increases in the turbine exit Mach number above present limitations would result in an increased turbine weight-flow capacity. If these increases could be obtained without serious loss in efficiency, the turbine as a component of the jet engine could be improved considerably through reduction in weight and frontal area. It is therefore essential that these so-called high Mach number turbines be investigated thoroughly to determine if the increases in work output and weight flow can be realized without serious loss in efficiency.

High Mach number turbines are the subject of a research program at the NACA Lewis laboratory. As part of this program, the design and experimental investigation of a transonic turbine has been conducted to study the problems associated with high Mach number turbines. A transonic turbine is defined as one designed to utilize rotor-hub entering Mach numbers of approximately unity. This paper presents the results of the transonic turbine investigation to indicate some of the design concepts needed to obtain satisfactory high Mach number turbine performance and some of the loss characteristics to be found in this type of turbine.

## DESIGN CONSIDERATIONS

The design Mach numbers at the entrance and exit of the transonic-turbine rotor are shown in figure 1 for the rotor hub and tip. The relative Mach number at the rotor entrance is seen to vary from 1.00 at the hub to 0.60 at the tip. In order that these high relative Mach numbers be obtained, the absolute Mach number out of the stator must be considerably higher; this results in choked stator operation. The relative Mach number out of the rotor is seen to vary from 1.00 at the hub to 1.09 at the tip, indicating that the rotor must also be choked. These high design rotor-exit Mach numbers result in turbine-exit absolute Mach numbers exceeding 0.70. As indicated in the first of this series of papers, these high values of Mach number force the turbine design very close to the turbine limiting-work-output point. The design relative

[REDACTED]

Mach number at the hub is also noted in figure 1 to be constant at a value of 1.00 at both entrance and exit, indicating that very little static-pressure drop is designed to occur across the rotor hub. The conditions of choked blade rows, proximity to the turbine limiting-work-output point and adverse static-pressure conditions across the rotor hub, occur, in general, as a result of the increased level of the flow Mach numbers and can be considered important characteristics of high Mach number turbines.

It is, at present, common practice in the design of axial-flow compressors and turbines to specify simple radial equilibrium at the entrance and exit of the blade row and assume a radial streamline variation through the blade. Because of the conservative Mach number level, the flow is relatively insensitive to small area changes, and the Mach number distribution through these turbomachines can be predicted with a fair degree of accuracy. However, as the Mach number level through turbines is increased into the transonic region, the flow becomes very sensitive to small area changes. The radial streamline variation through the turbine rotor cannot then be arbitrarily assumed but must be governed by continuity and radial equilibrium considerations within the blade. A design procedure that considers these three-dimensional effects must therefore be used in the design of the high Mach number turbines and must be sufficiently rigorous that the flow Mach numbers are predicted with sufficient accuracy. One such design procedure has been developed at the Lewis laboratory and used in the design of the transonic turbine. The procedure, which is quasi-three-dimensional in nature, utilizes simple radial equilibrium and continuity throughout the rotor. Although more complex than standard two-dimensional design procedures, the final transonic-turbine design was evolved in approximately 300 man-hours.

The transonic-turbine rotor midchannel and surface Mach number distribution at the hub and tip sections are also shown in figure 1. In the turbine design, the blade solidity was adjusted such that the maximum surface Mach number was limited to a value of 1.33. As indicated by figure 1, this limiting Mach number occurred at the blade tip section. At the hub, although the midchannel Mach number through the blade was unity, the maximum surface Mach number was only 1.24. Thus, the design decrease in Mach number from maximum to that at the outlet, or diffusion, was found to be equally severe at both hub and tip, the Mach numbers decreasing from 1.33 to 1.09 at the tip and from 1.24 to 1.00 at the hub.

It is of interest to examine the transonic-turbine rotor design obtained by using the three-dimensional design procedure to determine how much different the Mach number distribution would have been if conventional two-dimensional design procedures had been used. One such procedure assumes that a linear variation in streamline height occurs across the turbine rotor from entrance to exit. The result of the analysis of the rotor hub design made on this basis is shown in figure 2. The

[REDACTED]

midchannel Mach number distribution specified in the three-dimensional design was constant at a value of unity. It was found in the analysis that the assumption of linear variation in streamline height resulted in premature choking at the rotor inlet, and yielded no solution over the first half of the blade chord. Over the second half of the blade chord a solution was obtained. However, as indicated by figure 2, there is little similarity between the midchannel Mach number distributions obtained in the two- and the three-dimensional solutions. These findings further indicate that high Mach number turbines must be designed on a three-dimensional basis in order that the Mach number distribution be accurately predicted.

A photograph of the transonic-turbine rotor is shown in figure 3. A high solidity (ratio of blade chord to pitch) can be noted and can be attributed to the limitation imposed on the rotor surface Mach number. A fairly sharp leading edge is also indicated. A leading edge thickness of 0.030 inch was used in combination with an incidence angle of  $4^\circ$  in order to avoid premature choking in the rotor. The effect of increased leading edge thickness with corresponding increased incidence angles on the turbine performance must be evaluated in future investigations.

#### RESULTS OF INVESTIGATIONS

The transonic turbine was experimentally investigated over a range of speeds and pressure ratios to obtain its over-all performance characteristics. The resultant performance map based on total-pressure ratio across the turbine is shown in figure 4. The equivalent specific work output is shown as a function of a weight flow - speed parameter. Lines of constant speed, total-pressure ratio, and adiabatic efficiency are included. At design speed and equivalent specific work output, an adiabatic efficiency of approximately 0.85 was obtained. The peak efficiency of slightly over 0.85 was found to occur at speeds slightly above design. The design work output was also found to be 0.97 of the turbine limiting work output. From these results, it can be concluded that the three-dimensional procedure used in the design of the transonic turbine was sufficiently rigorous that the design conditions were met even though the design operating point was deliberately located in a critical region. The results also indicate that turbines designed to operate with rotor-hub entrance Mach numbers as high as unity can be obtained with efficiencies of 0.85 or better.

In many turbine applications, it is important that favorable off-design turbine operating characteristics be obtained. Because of the sharp leading edge used in the transonic-turbine design, it might seem that, although satisfactory design-point operation was obtained, the off-design characteristics might be detrimental because of high relative Mach numbers and poor incidence angles. However, efficiencies of over

0.80 were found to occur over a considerable range of performance (fig. 4), the decrease in efficiency at low speeds being comparable with the decrease for more conservative turbines. Hence, the off-design characteristics of the transonic turbine would not limit its usefulness.

In order to obtain an insight into the loss characteristics of the transonic turbine, the variation in total pressure at the stator exit and the variation in efficiency behind the rotor were determined at the design point. The results of these surveys are shown in figure 5. Cores of high pressure loss are seen to be emanating from the hub of the transonic turbine stator. As indicated by the preceding paper these cores are caused by secondary flow within the stator. The cores are large at the design point because of the high design Mach numbers at the stator exit. Results of the rotor-exit surveys indicate that these cores cause a low-efficiency region to occur near the hub as indicated in figure 5. However, the absence of a band of low efficiency in this region indicates that the high design Mach numbers at the rotor inlet did not appreciably affect the turbine efficiency. At the rotor tip, a region of low efficiency is seen to occur and is apparently attributable to a combination of stator and rotor effects. A large percentage of the losses in this region is probably caused by a boundary layer build-up in the region of the rotor-blade exit, resulting from the blade diffusion, being forced out to the tip by centrifugal force and combining with the losses due to the tip clearance, passage, and scraping vortices to contribute to this region of low efficiency. From these results it appears that the decrease in efficiency as compared with the efficiency obtained for well-designed lower Mach number turbines is mainly due to increased losses caused by large stator cores and large secondary-flow losses at the rotor-tip exit. If these losses can be substantially reduced, a considerable improvement in efficiency can be realized.

One of the important factors affecting the boundary layer build-up across the rotor blade is felt to be the diffusion near the blade exit. In order that the effect of this diffusion on the transonic-turbine performance be established, another transonic turbine designed for much greater diffusion was also investigated. The tip Mach number was designed to decrease from a peak value of 1.33 to only 0.84 as compared with a decrease from 1.33 to 1.00 for the first transonic turbine. The over-all performance of this turbine indicated efficiencies 3 points less than those for the first turbine. Since both turbines were designed for the same stator-exit conditions, the decrease in efficiency must be attributable to rotor losses. The results of the rotor-exit surveys of these two turbines are shown in figure 6. The effect of the cores emanating from the stators can again be noted. The region of low efficiency at the rotor tip is considerably larger for the second turbine than for the first turbine. This low efficiency near the tip is evidently caused by the combination of increased boundary-layer flow to the tip, occurring as a result of the higher diffusion across the rotor

blade, and by possible increased passage and tip-clearance vortex losses. Because the tip section is designed for a very high diffusion, the low-momentum air associated with these losses probably introduces separation resulting in even higher losses in the tip region. These results indicate that the diffusion near the rotor-blade exit is a very important factor to be considered in attaining efficient high Mach number turbines.

#### SUMMARY OF RESULTS

Following is a summary of the important results and conclusions obtained thus far in the investigation of high Mach number turbines:

1. High Mach number turbines designed to operate with rotor-hub Mach numbers as high as unity can be obtained with efficiencies of at least 0.85.
2. The three-dimensional design procedure used in the design of the transonic turbines was found to be sufficiently rigorous that the design conditions, although extremely critical, could be met satisfactorily.
3. The off-design performance of high Mach number turbines is comparable with that of lower Mach number turbines.
4. The main sources of losses in high Mach number turbines appear to be large core losses out of the stator and diffusion losses out of the rotor that show up as a tip loss. Reduction in these losses can mean considerable improvement in the turbine efficiency.

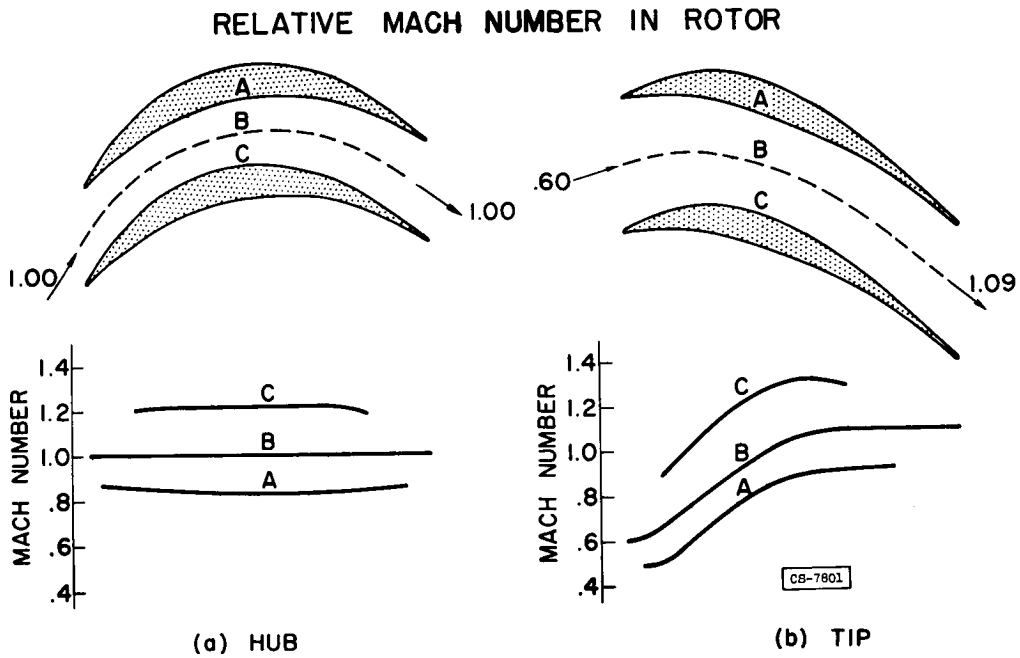


Figure 1

### TWO-AND THREE-DIMENSIONAL DESIGN COMPARISON

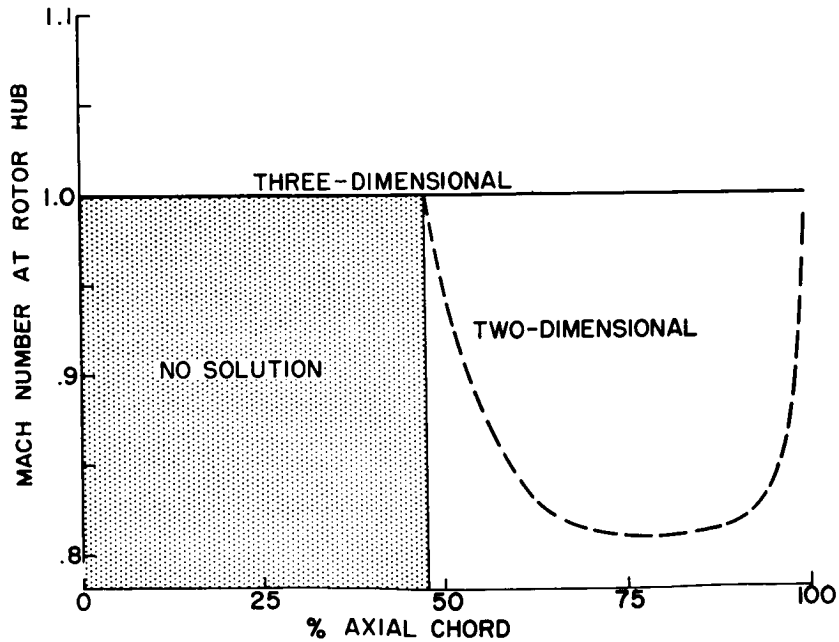
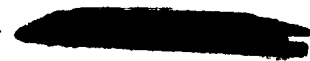


Figure 2



### TRANSONIC TURBINE ROTOR

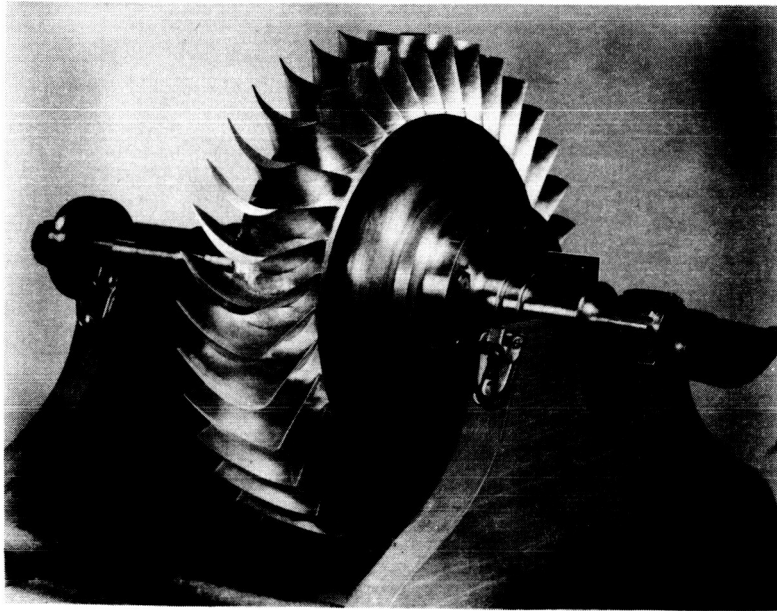


Figure 3

### PERFORMANCE MAP BASED ON ACTUAL TOTAL-PRESSURE RATIO ACROSS TURBINE

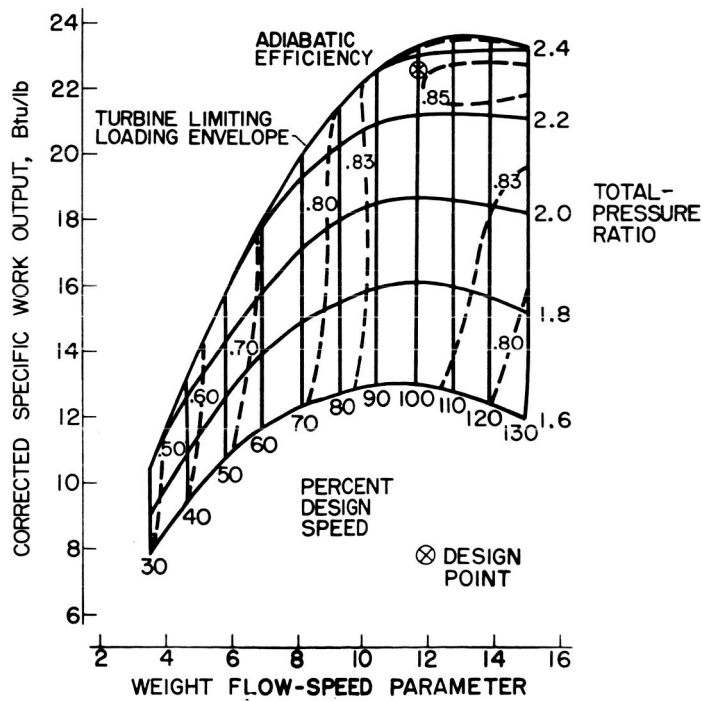


Figure 4

### TRANSONIC TURBINE LOSS PATTERNS

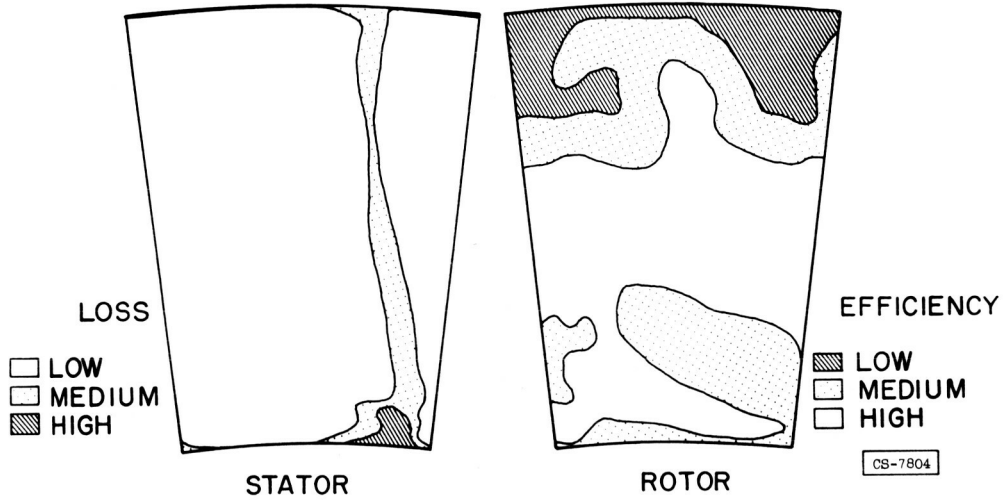


Figure 5

### EFFECT OF INCREASED DIFFUSION ON LOSSES

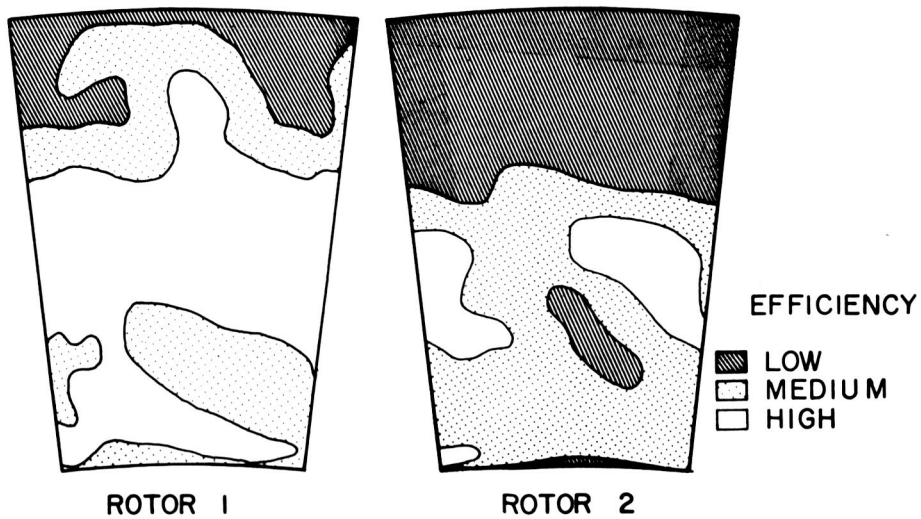


Figure 6

PERFORMANCE EVALUATION OF A SINGLE-STAGE TURBINE WITH STATOR  
ADJUSTMENT OVER A WIDE RANGE OF STATOR FLOW AREAS

By Thomas R. Heaton and Donald E. Holeski

INTRODUCTION

Turbojet engines for the supersonic airplane will be required to operate over a wide range of temperatures at the compressor inlet. This range of inlet temperatures may impose severe problems in engine operation if high thrust and good fuel economy are to be achieved over the range of flight conditions. As suggested in the paper by English and Rebeske, turbine stator adjustment may be one means of satisfying these severe operational problems.

The purpose of this paper is first, to investigate the change in the flow conditions that occurs within the turbine as the stator flow area is adjusted to keep the compressor operating point fixed as the engine is operated over a range of flight conditions, and second, to present the design and experimental performance of a single-stage turbine capable of operation over a wide range of stator adjustment.

ENGINE OPERATION PROBLEM

Consider an airplane flying at a Mach number of 2.8 in the stratosphere, with the compressor operating at its design equivalent speed, a pressure ratio of 3.7, and a turbine-inlet temperature of 2000° F. This compressor operating point is designated as point A on the compressor map in figure 1. If the rotational speed and the turbine-inlet temperature are held fixed as the flight condition changes from the supersonic condition to the take-off condition, a 39-percent increase in compressor equivalent speed is required as a result of the change in compressor-inlet temperature with change in flight condition. At this speed, compressor stall would most likely be encountered and operation could not be achieved. Another mode of engine operation would be to use a variable-area exhaust nozzle to keep the compressor equivalent speed and the turbine-inlet temperature fixed. If the supersonic flight condition were still at point A, the compressor would attempt to operate at point B, but it would reach the stall limit before the take-off condition could be achieved. To avoid this stall condition, the compressor operating point at the supersonic flight condition would have to be at point C in figure 1, and this is in a region of lower compressor efficiency.

One means of avoiding the compressor-surge problem that developed for these two modes of engine operation is to keep the compressor operating point fixed for all flight conditions. One means of accomplishing this is to keep the compressor equivalent speed and the engine temperature ratio fixed for all flight conditions. The engine temperature ratio is defined as the ratio of the absolute turbine-inlet temperature to the absolute compressor-inlet temperature. For engine operation with a specified maximum turbine-inlet temperature, this mode of operation would result in a low thrust for take-off and flight at subsonic speeds. Operation at a Mach number of 2.8 in the stratosphere with a turbine-inlet temperature of 2000° F would require a turbine-inlet temperature of 806° F at the take-off condition. Raising the turbine-inlet temperature to 2000° F for take-off would result in a substantial gain in thrust. This variation in take-off thrust with turbine-inlet temperature or engine temperature ratio is shown in figure 2. The thrust for take-off increases 159 percent as the turbine-inlet temperature changes from 806° to 2000° F. It is possible to increase the turbine-inlet temperature and maintain a fixed compressor operating point by adjusting the turbine-stator flow area and exhaust-nozzle area. Consequently, adjustable-stator turbines can give the freedom of engine operation over a wide range of engine temperature ratios with a fixed compressor operating point. The range of engine temperature ratio that must be considered is summarized in figure 3, which shows the variation in engine temperature ratio with flight Mach number for a constant turbine-inlet temperature of 2000° F. If a plane must fly at a Mach number of 2.8 as well as at a Mach number of 0.9 in the stratosphere, then the engine temperature ratio varies from 2.44 to 5.39, an increase of 121 percent. These conditions require the turbine to operate over a wide range of turbine equivalent weight flow and equivalent speed. The turbine must therefore be flexible in its operation in that it operate over these conditions and maintain a high efficiency.

From the preceding discussion of some different modes of engine operation for supersonic flight, it was shown that the mode that uses turbine stator and exhaust-nozzle adjustment to keep the compressor operating point fixed as the engine temperature ratio varies does not have the disadvantages associated with compressor surge, compressor off-design-point operation, or low turbine-inlet temperatures at take-off. However, the turbine must be capable of satisfactory operation over a wide range of flow conditions, and therefore the problem of turbine stator adjustment requires study.

#### TURBINE ANALYSIS AND DESIGN

Engine operation with turbine stator adjustment for a fixed compressor operating point was analyzed over a range of engine temperature ratios. The range of engine temperature ratios considered is shown in figure 3,

in which the flight condition varied from subsonic (Mach number of 0.9) to supersonic (Mach number of 2.8) in the stratosphere with a constant turbine-inlet temperature of 2000° F. This represents the maximum variation in engine temperature ratio over which the engine may be required to operate.

For a fixed compressor operating point, the turbine-inlet equivalent weight flow varies with the engine temperature ratio, fuel-air ratio, engine leakage, and compressor bleed. The variation of the equivalent weight flow at the turbine inlet or the flow capacity of the turbine is shown in figure 4 over a range of engine temperature ratio. As the engine temperature ratio increases, so must the equivalent weight flow at the turbine inlet, and thus an increase in the turbine stator area is required. As the flight condition changes from that at a Mach number of 2.8 in the stratosphere to take-off, the equivalent weight flow at the turbine inlet must increase 32 percent. The variation of the equivalent weight flow at the turbine exit is shown in figure 5. This equivalent weight flow reaches minimum at an engine temperature ratio of 3.96. If the engine temperature ratio increases or decreases from this value, the equivalent weight flow at the turbine exit will increase.

With a turbine-inlet temperature of 2000° F, the engine temperature ratio is 2.44 for a flight Mach number of 2.8 in the stratosphere, 4.75 for sea-level take-off, and 5.39 for a flight Mach number of 0.9 in the stratosphere. The turbine-exit equivalent weight flow is highest at the supersonic flight condition. Since the turbine has a fixed annulus area, the rotor-exit Mach number will be highest at the supersonic flight conditions and the turbine will be operating nearer to limiting blade loading. Thus, the turbine-exit annulus area must be selected so as to avoid limiting blade loading when the engine is operating at the supersonic flight condition. However, with the increasing characteristic of the turbine-exit equivalent weight flow at the high engine temperature ratio, there will also be some subsonic flight condition in the stratosphere, at a Mach number lower than 0.9, at which the turbine-exit equivalent weight flow will be as high as that at the supersonic flight condition. At this engine temperature ratio, operation will again be near blade limiting loading.

#### Velocity Diagrams

The velocity diagrams at any flight condition or engine temperature ratio must be estimated to determine whether any of the turbine aerodynamic limits are exceeded. The flow conditions over the range of engine temperature ratios are based upon continuity, required turbine work, and certain turbine-geometry parameters that were needed to estimate the rotor-exit relative flow angle. In this analysis, it was assumed that the turbine efficiency was constant at each operation condition. The turbine velocity diagrams thus calculated are summarized in figures 6 to 11.

Figure 6 presents the required variation in work and tip speed with engine temperature ratio. As the flight condition changes from a Mach number of 2.8 in the stratosphere to sea-level take-off, the engine temperature ratio increases from 2.44 to 4.75. Operation between these two conditions requires that at the take-off condition the turbine specific work decrease 45 percent and the tip speed decrease 38 percent from that at the supersonic flight condition. Figure 7 shows the variation of an associated leaving loss due to whirl at the turbine rotor exit. This leaving loss is zero at the supersonic flight condition, and at the take-off condition is 1.35 percent of the required turbine work. The blade leaving loss is a measure of the absolute rotor-exit-whirl velocity. The change in the absolute rotor-exit whirl would be important in considering the use of an afterburner, in that, if the exit whirl were too great, it might result in unsatisfactory afterburner operation. The change in the flow conditions at the stator exit, the rotor inlet, and the rotor exit with engine temperature ratio are shown in figures 8 to 10. For the change in engine temperature ratio between the supersonic flight condition and sea-level take-off, the turbine velocity parameters change as follows:

- (1) The stator-exit Mach number at the mean section decreases from 1.11 to 0.73.
- (2) The relative rotor-inlet Mach number at the hub decreases from 0.77 to 0.50.
- (3) The relative rotor-exit Mach number at the tip decreases from 1.13 to 0.82. This indicates that the exit conditions of the turbine are less critical at the take-off condition than at the supersonic flight condition.
- (4) The static-pressure ratio across the rotor hub increases from 1.06 to 1.15. This static-pressure ratio is a minimum of 1.015 at an engine temperature ratio of 2.86.
- (5) The turning across the rotor hub decreases from  $105^{\circ}$  to  $90^{\circ}$ .

In general, these calculations show that the turbine is operating at less critical flow conditions for take-off than for supersonic flight. The only parameter in which the flow change is adverse was the blade leaving loss; and, in this case, this change was not large enough to produce a loss of any appreciable magnitude to the turbine.

The calculation of these estimated velocity diagrams showed that, for operation between Mach numbers of 2.8 and 0.9 in the stratosphere, the rotor-inlet relative flow angle at the mean section varied a total of  $24^{\circ}$ . The rotor blade-inlet camber angle was set so that the possible incidence angles (analogous to the angle of attack) over the range of flight conditions are divided evenly between the positive and negative incidence on the rotor blade. Thus, at a flight Mach number of 2.8 in the stratosphere, an incidence of  $+12.3^{\circ}$  would exist on the rotor at the mean section, while at a Mach number of 0.9 in the stratosphere, the incidence would be  $-11.2^{\circ}$  (fig. 11). It was felt that this would not cause the rotor blade to stall and increase the blade-profile losses greatly.

## Blade-Profile Design

As has been previously stated, this turbine will operate with a maximum inlet temperature of 2000° F, which requires that either the turbine stator and rotor blades be cooled or constructed of some material capable of withstanding the stresses at this elevated temperature. This turbine was designed so that the stator and rotor blades could be air-cooled. The main problem in the aerodynamic design of a cooled turbine blade, whether a stator or rotor blade, is the problem of designing the trailing-edge section so that adequate cooling can be provided. The use of as small a trailing-edge diameter as possible is consistent with the aerodynamic requirements for minimum blade loss, while the use of a relatively large diameter is consistent with the cooling requirements. Thus, the size of the trailing-edge diameter had to be compromised between the cooling requirements for adequate cooling and the aerodynamic requirements for minimum blade loss.

A scale model of this turbine was fabricated. The turbine rotor is shown in figure 12, and it can be noted that the blades are of conventional shape except for the thick trailing edges.

## RESULTS AND DISCUSSION

The scale model of this turbine was tested in a cold-air turbine test facility, and the performance of the scale-model turbine was obtained with the turbine stator set to correspond to the required positions for several assumed operating engine temperature ratios. The engine temperature ratios at which the model turbine performance was obtained are listed in the following table. For the assumed engine temperature ratios, the ratio of the required turbine equivalent work and equivalent tip speeds to those at an engine temperature ratio of 2.44 are listed. Also listed is the corresponding flight condition for a constant turbine-inlet temperature of 2000° F.

Engine temperature ratio	Mach number in stratosphere at turbine-inlet temperature of 2000° F	Ratio of turbine equivalent work to that of an engine temperature ratio of 2.44	Ratio of equivalent tip speed to that at an engine temperature ratio of 2.44
2.16	3.08	1.14	1.06
2.65	2.61	.93	.96
3.21	2.18	.78	.88
3.80	1.80	.66	.81
4.63	1.33	.56	.73
5.25	.98	.51	.69

The estimated velocity diagrams were used to calculate the required stator throat areas at the mean blade section for a given engine temperature ratio. The stator blade was set so that the required area existed in the stator blade passage at its throat. At each stator blade setting and equivalent tip speed, the turbine was operated over a range of pressure ratio. The inlet equivalent weight flow and turbine efficiency were thus determined for the actual equivalent turbine work corresponding to a given engine temperature ratio. Figure 13 shows the variation of the turbine-inlet equivalent weight flow of the model turbine over the range of engine temperature ratio. This turbine-inlet equivalent-weight-flow variation is one of the two parameters that must be satisfied to make turbine stator adjustment feasible. The other parameter is the necessary work output to drive the compressor. In the model test of this turbine, the required variation in the turbine-inlet equivalent weight flow was obtained over the range of engine temperature ratio in which it was required to operate. Both the stator and rotor were choked at engine temperature ratios below 2.8. At engine temperature ratios above 2.8, the stator was unchoked but the rotor remained choked over the entire range of engine temperature ratios. It is not by chance that this equivalent weight flow continued to increase at the high engine temperature ratios even though rotor choking was limiting the equivalent weight flow. If high losses had been increased at the rotor inlet at the high engine temperature ratios, the required increase in the turbine-inlet equivalent weight flow would not have been attained, especially at the high engine temperature ratios.

At an engine temperature ratio of 2.16, the turbine reached limiting blade loading before the required equivalent work was attained. The data from the cold-air tests were interpolated and it was found that the required equivalent work and the blade-limiting-loading equivalent work coincide at an engine temperature ratio of 2.37. If it were desired to operate at an engine temperature less than 2.37, the compressor operating point would have to be changed to a point at which the turbine could produce enough work to drive the compressor. Thus, the calculated operating point (equivalent turbine work and inlet weight flow) for each given engine temperature ratio greater than 2.37 represents the performance of the turbine at the various engine temperature ratios.

The turbine internal efficiency at the operating point corresponding to each engine temperature ratio is plotted against the engine temperature ratio in figure 14. The corresponding flight conditions for a constant turbine-inlet temperature of 2000° F are also shown. For engine temperature ratios between 2.37 and 4.0 the turbine efficiency varies only slightly, ranging between 0.86 and 0.87. As the engine temperature ratio increases above 4.0, the efficiency decreases gradually to a value of 0.83 at an engine temperature ratio of 5.4. This drop in efficiency may be largely due to the increase in the absolute

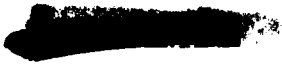
3078 - 3

rotor-exit whirl at these engine temperature ratios. Since the method of evaluating the turbine performance charged the turbine with the energy represented in this whirl, the turbine efficiency may be expected to decrease as shown in figure 7 where the estimated leaving loss is plotted against the engine temperature ratio. At an engine temperature ratio of 5.4, figure 7 shows the magnitude of this leaving loss is 2.6 percent of the turbine work.

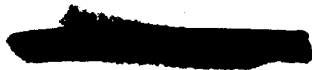
During the process of testing this turbine with the different stator throat areas, it was necessary to remove some metal from the blade ends at either the hub or the tip at each stator-blade setting in order to set the blade at the proper chord angle. After the performance of the turbine at the various stator-blade settings was obtained, the stator blades of the turbine were reset to the position corresponding to an engine temperature ratio of 3.80 and the clearance at the hub and tip measured. The ratio of this clearance to the blade span was 0.008 at the hub and 0.005 at the tip for a blade span of 2.03 inches. The performance of the turbine with this clearance was then determined. This performance is compared with that previously obtained with the blades set in this position, because this position was the first tested and thus was the only position that had no stator-blade clearance. Figure 15 shows the variation of the turbine efficiency with the turbine equivalent work for these two configurations, that is, with and without clearance at the required equivalent tip speed for an engine temperature ratio of 3.80. Over the entire range of turbine equivalent work, the maximum difference in the efficiency is 0.01, and over most of the range, this difference is less than 0.005. Since the probable error in reproducing the turbine efficiency was 0.005 for this scale-model turbine, it must be concluded for this turbine that the stator-blade clearance had little, if any, effect on the turbine performance.

#### CONCLUDING REMARKS

In order that a turbine operate efficiently over a range of engine temperature ratios with stator adjustment, with the compressor operating point fixed, the turbine must be capable of handling a wide range of flow conditions both at the stator inlet and rotor exit. If a turbine were operating near blade limiting loading at the take-off condition (as is the case for several present-day commercial turbojet engines), than it would be impossible to adjust the turbine stator flow area over the wide range of required areas necessary for supersonic flight (with the compressor operating point fixed) and obtained the required work, because a slight decrease in stator area would cause blade limiting loading. The turbine must be analyzed over the entire range of engine temperature ratio over which it must operate. All the flow parameters must be checked to see if any of the turbine aerodynamic limits are exceeded at an operating point. The turbine design presented in this



paper was the result of a careful analysis at all of the possible operating conditions. Because the operation of the turbine over the range of engine temperature ratios was satisfactory, it appears that carefully designed turbines that employ stator adjustment are, therefore, capable of efficient operation over a wide range of stator flow area.



3078-B.

### COMPRESSOR PERFORMANCE

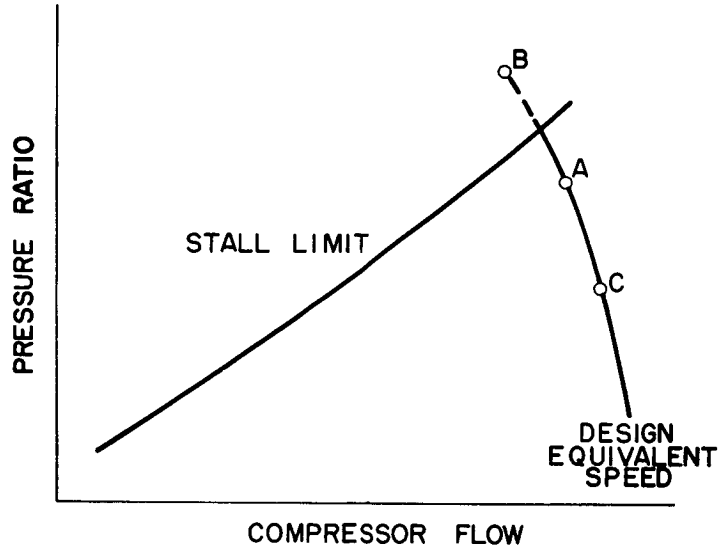


Figure 1

### THRUST GAINS WITH STATOR ADJUSTMENT

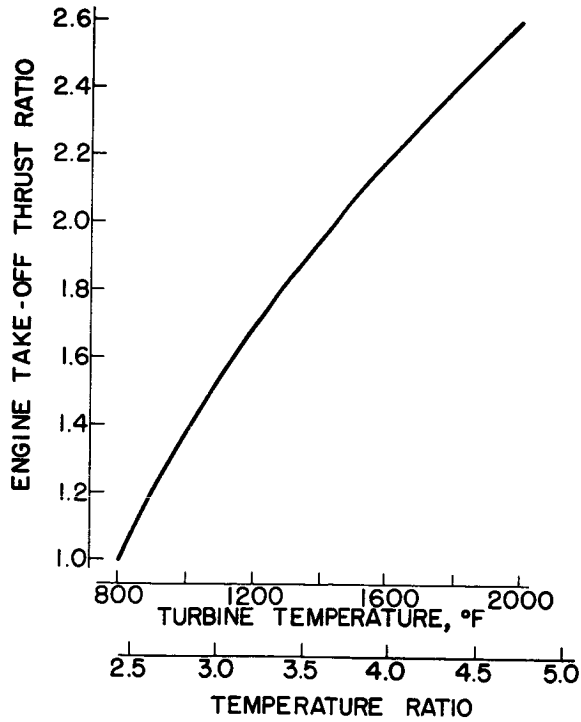
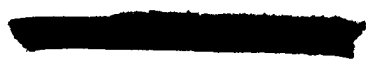


Figure 2



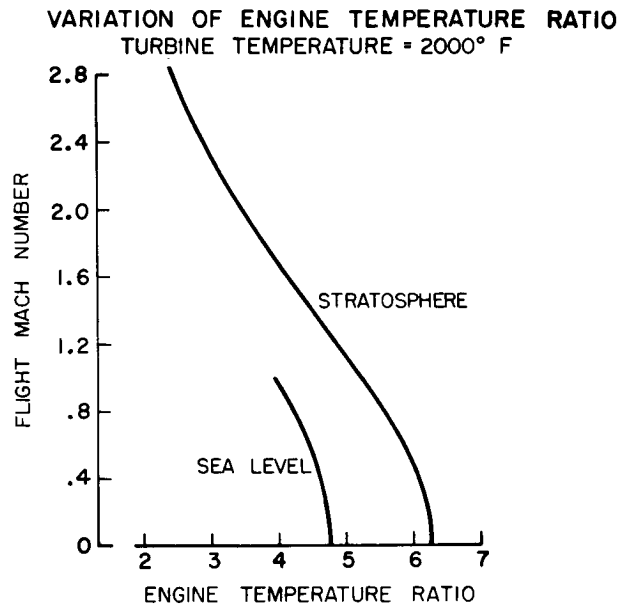


Figure 3

TURBINE-INLET EQUIVALENT WEIGHT FLOW

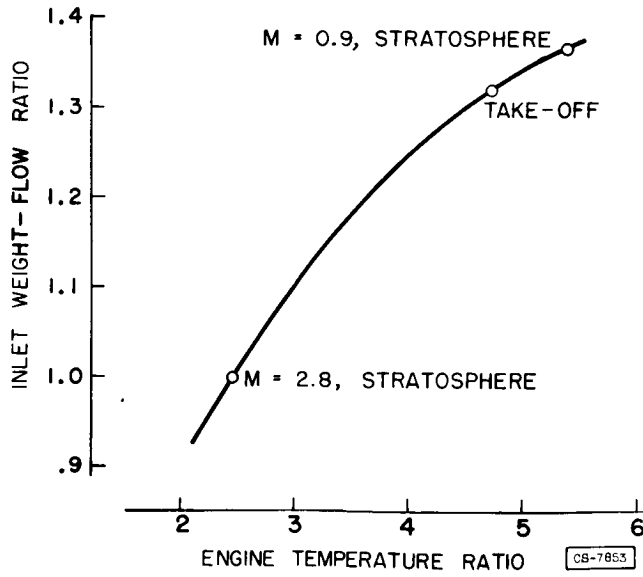
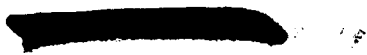


Figure 4



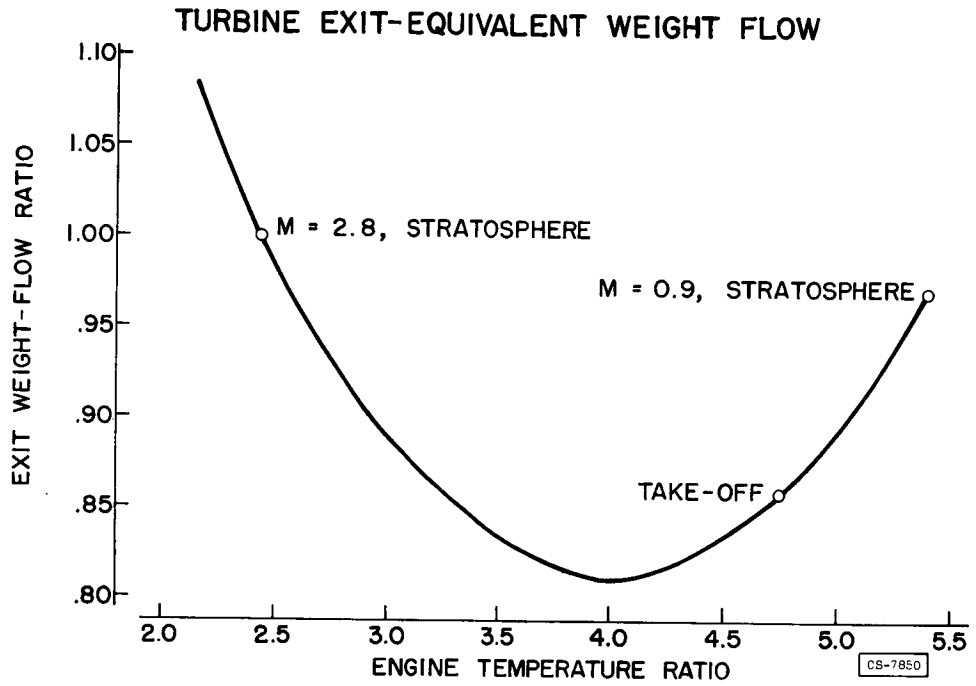


Figure 5

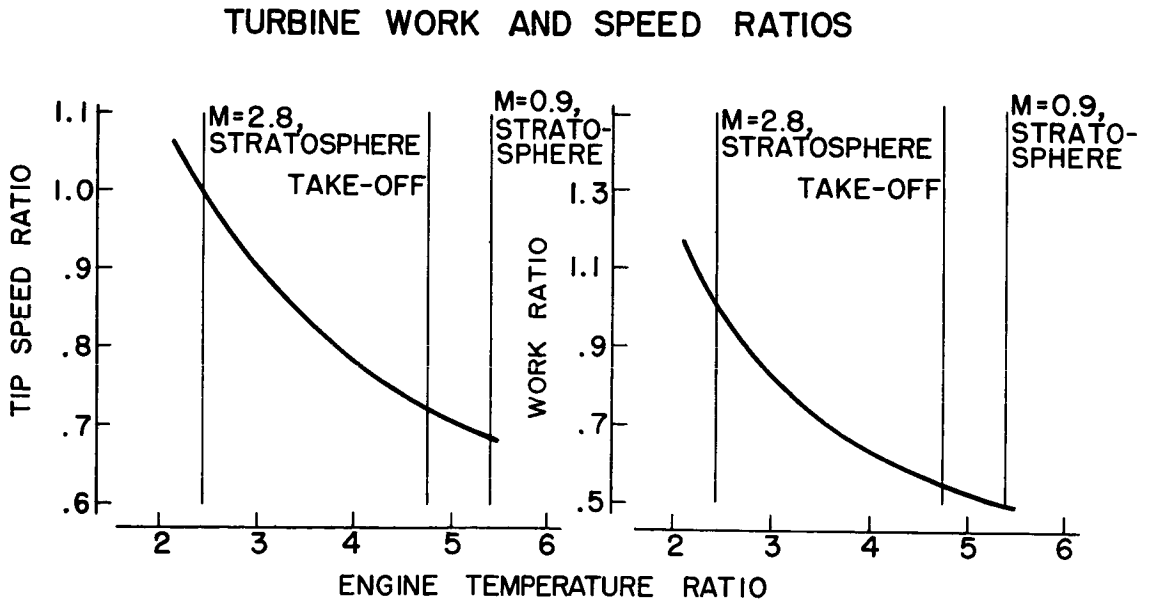


Figure 6

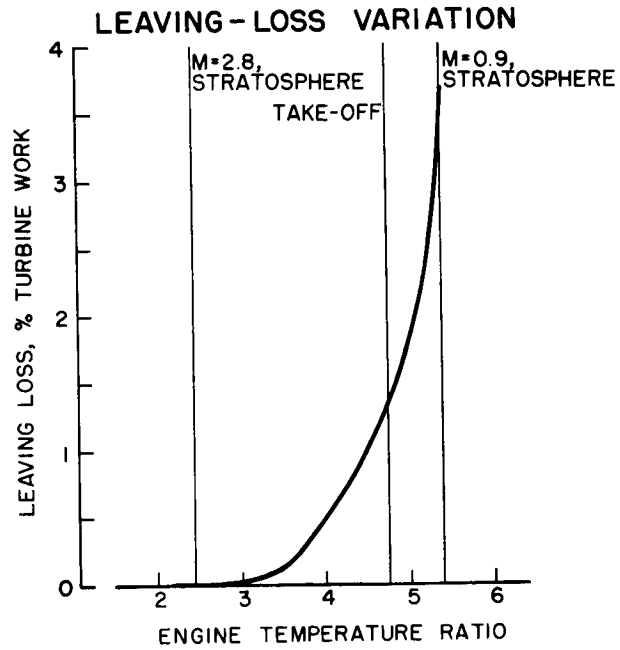
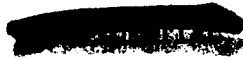


Figure 7

### STATOR EXIT MACH NUMBER VARIATION

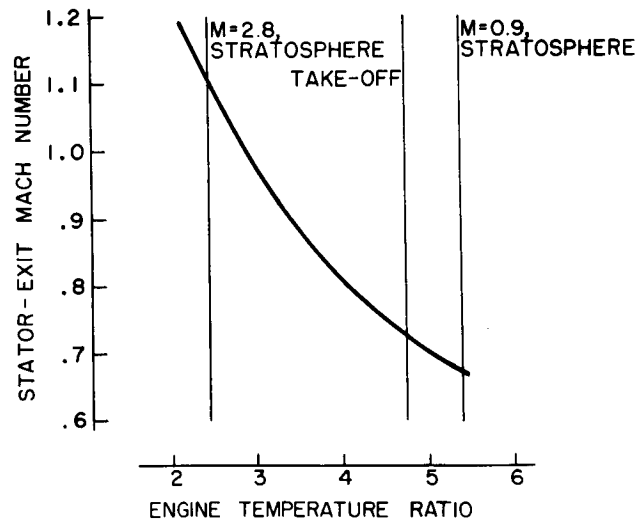
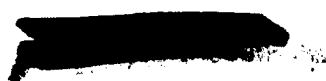


Figure 8



3079-B

TURBINE VELOCITY PARAMETERS

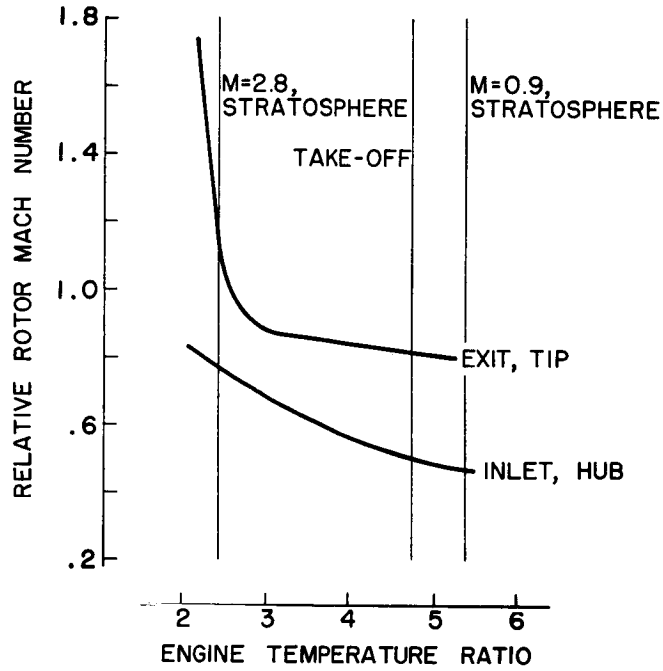


Figure 9

ROTOR TURNING AND STATIC-PRESSURE RATIO

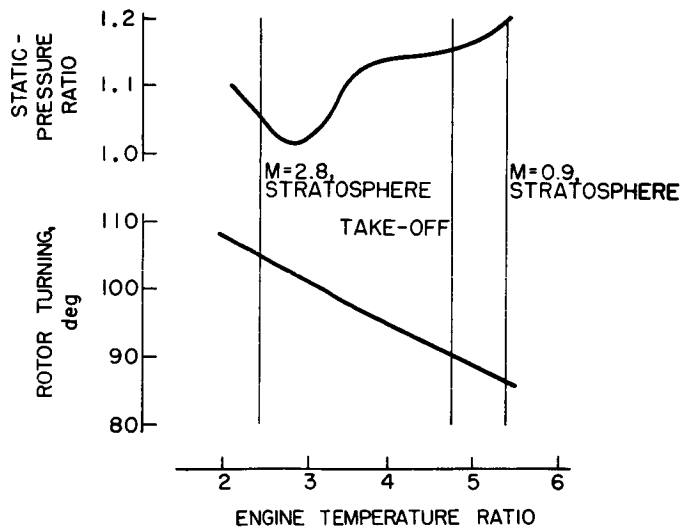
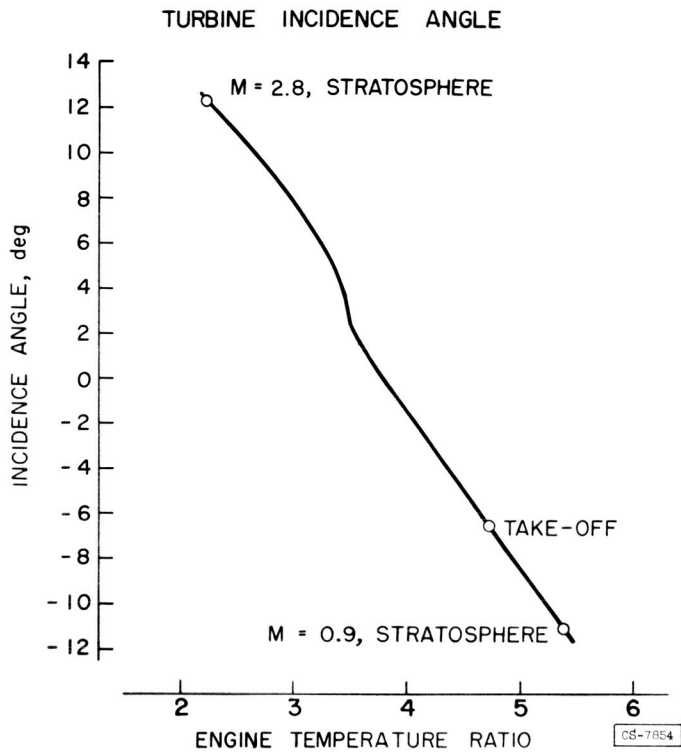


Figure 10

~~CONFIDENTIAL~~



3078-B

Figure 11

### TURBINE ROTOR

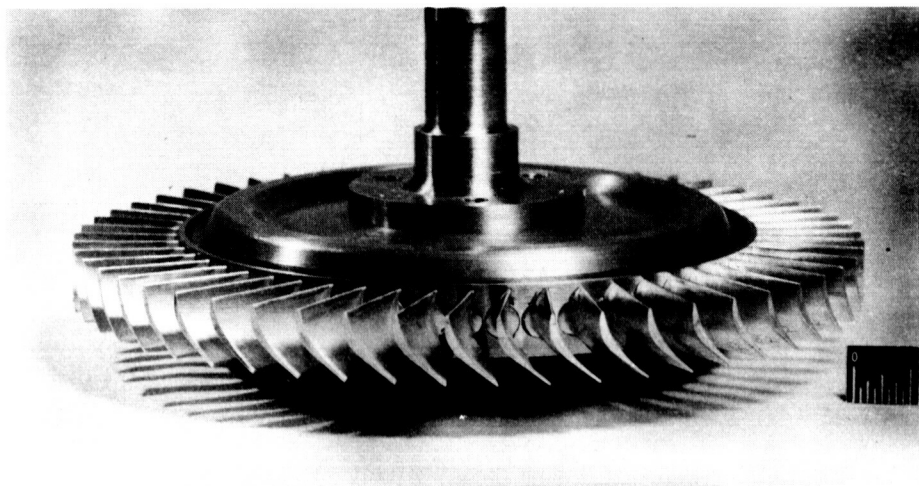


Figure 12

~~CONFIDENTIAL~~

### TURBINE INLET EQUIVALENT WEIGHT FLOW

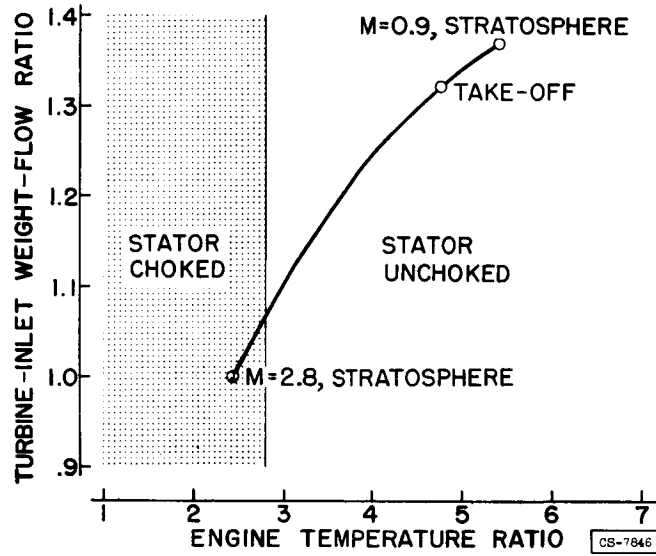


Figure 13

### VARIATION OF TURBINE EFFICIENCY

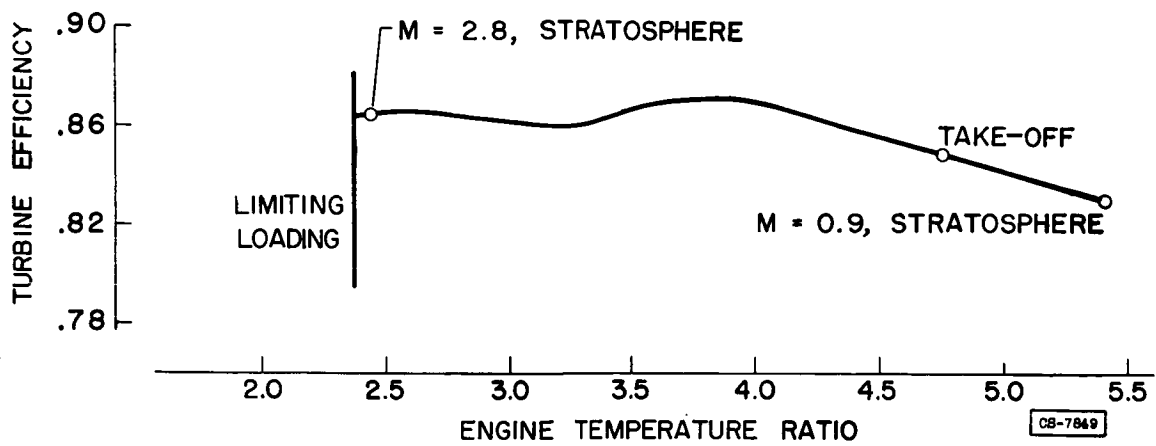


Figure 14

EFFECT OF STATOR CLEARANCE ON PERFORMANCE

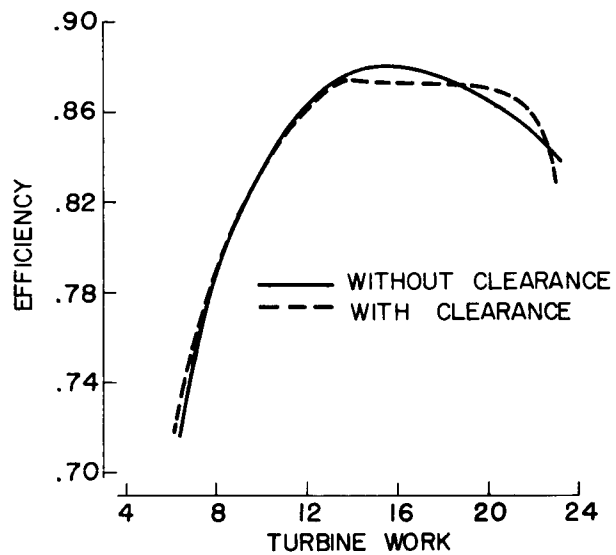


Figure 15

## PERFORMANCE PREDICTION OF AN ADJUSTABLE STATOR TURBINE

By Thomas R. Heaton and Robert E. Forrette

## INTRODUCTION

3078-B

The ability to predict the performance of an adjustable-stator turbine over a wide range of stator flow areas is necessary in order to estimate the engine operating limits. For example, the previous paper by Heaton and Holeski presents the design of a turbine which uses stator adjustment to keep the compressor operating point fixed as the engine operates over a wide range of engine temperature ratios. This mode of operation requires the turbine to operate over a wide range of speed, turbine work, and internal flow conditions. Therefore, it is highly desirable to be able to estimate the turbine performance over the range of operation in order to determine whether the turbine will satisfy the engine requirements.

This paper presents an analytical method to predict the performance of a turbine which uses stator adjustment. The performance of the model turbine described in the previous paper is estimated at several of the required operating points, and this computed turbine performance is compared with the experimental performance of this turbine. Also, a computed loss distribution over the range of engine temperature ratios is presented.

## METHOD AND PROCEDURE

## Turbine Losses

The losses in the turbine are assumed to be as follows:

- (1) Incidence loss at the stator and rotor inlets
- (2) Blade losses through the stator and rotor
- (3) Shock loss at the stator and rotor exits at supersonic flow conditions
- (4) Energy associated with the absolute exit whirl velocity

Incidence loss. - It is assumed that the energy associated with the component of inlet relative velocity normal to the tangent to the blade mean camber line is lost. This assumption results in a parabolic distribution of the pressure loss against the incidence angle, for constant

values of the critical velocity ratio. Actually, it has been shown that the loss for a small positive incidence angle is greater than that for the same negative angle. However, the loss at these incidence angles is small, and thus the error due to this assumption is not large for small incidence angles.

Blade loss. - It is assumed that the blade losses due to friction, secondary flow, and tip clearance of a rotating blade row can be combined into an effective viscous loss. This loss is dependent on the average dynamic head across a blade row and on a blade-loss parameter, which is assumed constant for a particular turbine.

Shock loss. - A shock loss occurs at the exit of the stator or rotor if the exit velocities are supersonic. This loss is assumed to correspond to the loss across a normal shock and represents the maximum shock loss which might occur. Since normal shock losses are small for Mach numbers below 1.25, the error due to this assumption will not be large because in conventional subsonic turbines Mach numbers greater than 1.25 seldom occur.

Exit whirl loss. - It is assumed that the energy represented in the tangential component of absolute velocity at the rotor exit is a loss chargeable to the turbine.

#### Method of Analysis

The method employed herein is a one-dimensional flow analysis at the mean blade section and uses continuity, the loss assumptions, and the basic compressible flow equations to compute the velocity parameters which define the flow conditions at the stator and rotor inlets and exits. These velocity parameters are then used to compute the turbine work, efficiency, and weight flow. In any blade row, with subsonic or sonic flow conditions at the passage throat, the flow angle at a station just upstream of the trailing edge is assumed to be that determined by the ratio of the throat area to the pitch minus the trailing-edge blockage area. The flow conditions downstream of this section (outside the blade passage) are determined through the use of continuity and conservation of momentum between the station just upstream of the trailing edge and the downstream station. For supersonic flow conditions at the blade exit, the weight flow (determined for sonic flow conditions at the blade throat) and the supersonic flow conditions at the blade exit outside the blade passage are used to determine the flow angles.

It is assumed that the turbine work is a maximum, that is, the turbine limiting loading point has been reached, when the axial Mach number at the station just inside the rotor-blade trailing edge is unity, because any increase in pressure ratio will not affect the blade loading.

## Procedure

A value of the blade-loss parameter must first be determined. In the analysis of this turbine, the experimental performance at one stator setting was used to determine the proper value of the blade-loss parameter. The stator setting used corresponds to an engine temperature ratio of 3.80, and the value of the blade-loss parameter was determined such that the calculated efficiency agrees with experimental efficiency at the required equivalent tip speed and equivalent turbine work. This value of the blade-loss parameter was then assumed to be constant and the performance of the turbine at the required equivalent tip speeds for the other stator blade settings was computed.

In the process of calculating the turbine performance over the range of the stator settings, the effect of the various assumed losses on the turbine efficiency can be determined. Thus a breakdown of the computed losses in terms of turbine efficiency was calculated and is included as a part of the estimated turbine performance.

## RESULTS AND DISCUSSION

The results of the performance prediction for the stator set for an engine temperature ratio of 3.80 are presented in figure 1, where the effect of the various turbine losses on turbine efficiency is shown as a function of turbine equivalent work. The experimental performance and the turbine operating point for this engine temperature ratio are also shown. At the turbine operating point (work required to drive the compressor) the total calculated loss consists principally of blade effective viscous losses. The incidence, shock, and exit whirl losses are negligible at this point. The agreement between the predicted and experimental performance is satisfactory except in the region of blade limiting loading. The predicted blade limiting loading work is higher than the experimental value. The disagreement could result from boundary-layer buildup within the turbine which would cause the effective flow areas to be smaller than the geometric areas and thus would cause higher flow Mach numbers than those calculated. In addition, three-dimensional flow effects could cause a greater blade loss at this condition, an effect which is not included in this prediction method.

The results of the performance prediction at stator areas corresponding to several engine temperature ratios for a fixed compressor operating point are shown in figure 2. In general, the predicted turbine efficiency decreases from 0.91 at an engine temperature ratio of 2.16 to 0.82 at an engine temperature ratio of 5.2. The method predicts that the turbine limiting blade loading work and the required turbine work coincide at an engine temperature ratio of 2.12. Figure 2 also shows the loss breakdown through the turbine over the range of engine

temperature ratios considered. Again the stator- and rotor-blade viscous losses contribute the greatest portion of the total loss at all engine temperature ratios. The calculated losses due to stator incidence and normal shocks were negligible over the entire range of engine temperature ratios considered. The calculated loss due to rotor incidence is highest at the low engine temperature ratios where a high positive incidence angle on the rotor blades exists. As the engine temperature ratio increases, the rotor incidence angle decreases until the loss becomes zero for engine temperature ratios between 4.0 and 4.6. For engine temperature ratios greater than 4.6, a negative rotor incidence angle exists. The incidence angle continues to decrease as the engine temperature ratio increases, and thus the loss increases for engine temperature ratios greater than 4.6. The calculated rotor-exit whirl loss is greatest at the high engine temperature ratios. As the engine temperature ratio decreases, the whirl, and thus this loss, decreases to a negligible value for engine temperature ratios less than 3.4.

3078 -G

The comparison of the experimental performance for this turbine, as presented in the previous paper by Heaton and Holeski, and the predicted performance over the range of engine temperature ratios is shown in figure 3. The agreement between the predicted and the experimental performance is satisfactory except at the low values of engine temperature ratios. At the low engine temperature ratios, the turbine is operating near blade limiting loading and figure 1 shows that this method as applied does not predict the performance accurately for this flow condition. There is a difference in the engine temperature ratio at which the required turbine work and the turbine limiting blade-loading work coincide for the predicted and the experimental performance. The discrepancy between predicted and experimental performance at the low engine temperature ratios represents a limitation of this prediction method. Consequently, a further knowledge of losses near turbine limiting blade loading is required.

In addition to the blade limiting-loading condition at the low engine temperature ratios, high rotor-inlet Mach numbers and incidence angles exist, particularly at the hub section. Thus the incidence loss at the hub section is much greater than that at the other blade sections and, consequently, the loss calculated at the mean section may no longer represent the average incidence loss. This may also affect the ability of the method to predict the turbine performance at the low engine temperature ratios.

#### CONCLUDING REMARKS

From the results of this study it appears that the performance of an adjustable-stator turbine may be predicted (with the exception of blade limiting loading) if the proper value of the blade-loss parameter

is known. However, in most instances, performance of the turbine at one stator blade setting would not be available to determine the proper value of the blade-loss parameter. If this is so, then the efficiency could be estimated at one of the stator blade settings, and then the proper value of the blade-loss parameter could be determined such that the calculated efficiency agrees with the estimated efficiency. In a previous paper by English and Rebeske, some attainable efficiencies for certain turbine design limits were listed which might be used as a guide in the first estimation of the turbine efficiency.

3078-13

PERFORMANCE COMPARISON AT ENGINE TEMPERATURE RATIO OF 3.80

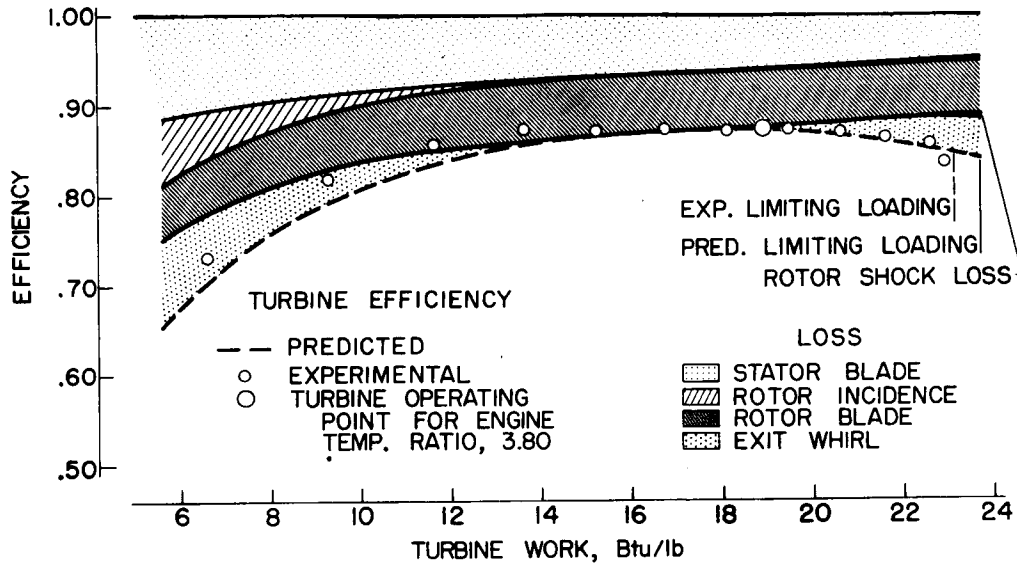


Figure 1

PERFORMANCE PREDICTION

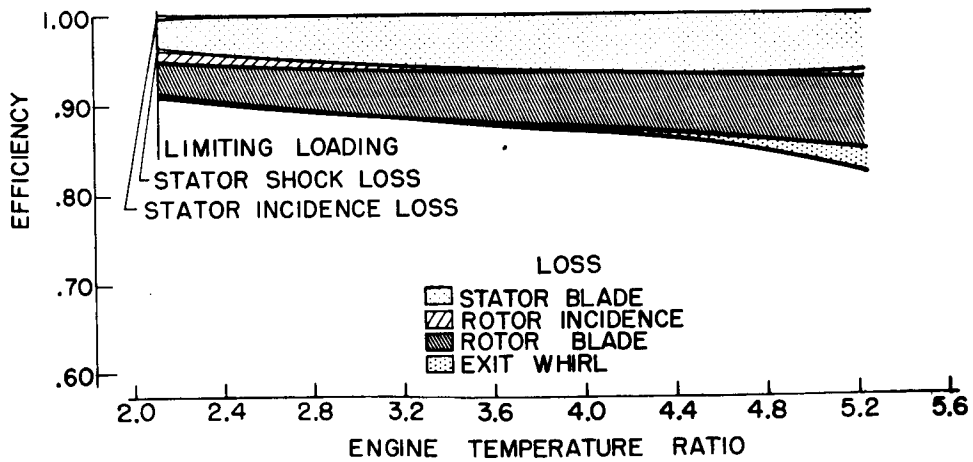


Figure 2

3078-B

### PERFORMANCE COMPARISON

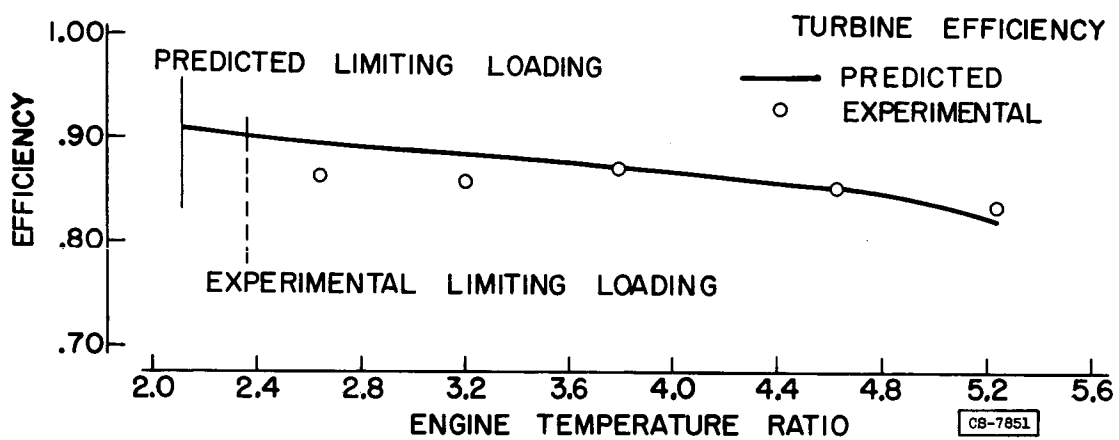


Figure 3

## PERFORMANCE OF AN ADJUSTABLE TURBINE STATOR IN A TURBOJET ENGINE

By Curtis L. Walker and John H. Povolny

## INTRODUCTION

As indicated in the preceding paper by Heaton and Holeski, when a turbojet engine is required to operate over a wide range of flight speeds from sea-level take-off up to some Mach number well in the supersonic range, it may be desirable, in order to alleviate compressor design problems, to operate the compressor at a fixed point on the compressor-performance map and to maintain limiting turbine-inlet temperature by the use of an adjustable turbine stator.

In order to determine the variations in turbine efficiency that would be encountered and to evaluate these effects on engine performance, an experimental adjustable turbine stator was installed on a current production-model turbojet engine and the performance was determined in an NACA Lewis altitude test chamber.

## APPARATUS AND PROCEDURE

A current production-model turbojet engine equipped with an experimental adjustable turbine stator was used for these investigations. The operating mechanism of the adjustable stator used in this investigation is shown in figure 1. Steel balls welded to the blade arm were fitted with slots in the actuating ring. Thus, when the actuating ring was rotated about the engine center line by means of screw-jack actuators, the blades rotated about the axes, changing the stator flow area. The stator was designed to have a total chord-angle variation of  $22^\circ$ , but because of the short actuating arms and the peening of the brass ring by the steel balls, there was a hysteresis of approximately  $5^\circ$  in the indicated chord angle. The stator-blade tip clearance was about 3.5 percent of the blade height.

The performance of the engine was determined in an NACA Lewis altitude test chamber. For the purpose of this investigation, operation was at a constant compressor operating point with a compressor pressure ratio of 3.3 and at a turbine-inlet temperature  $T_3$  of  $1540^\circ$  F. The tests covered a range of flight conditions in the stratosphere from an engine-design Mach number of 2.3 to a Mach number of 0.8.

## TURBINE PERFORMANCE

The range of flow and turbine-stator area variation required to cover a range of flight Mach numbers from 0.8 to 2.3 in the stratosphere is

shown in figure 2. The lower curve represents the flow required as a function of engine temperature ratio and this curve shows that a 37 percent increase in flow is required as the Mach number is reduced from the design value of 2.3 to 0.8. The upper curve represents the turbine-stator area variation required in this investigation to obtain the flow area of the lower curve and it is noted that actual area increase of 63 percent was necessary to obtain the 37 percent increase in flow area. The greater increase in stator area is caused largely by the decreasing turbine-stator pressure ratio accompanying the increase in engine temperature ratio. This variation in area was accomplished by adjusting the stator incidence angle from  $-5^{\circ}$  to  $+7^{\circ}$  and resulted in a variation of rotor incidence angle from  $+10^{\circ}$  to  $-7^{\circ}$ .

The turbine efficiency that was obtained over the operable range for a compressor pressure ratio of 3.3 is presented in figure 3. The maximum efficiency of 0.77 that was obtained is approximately 0.03 lower than the efficiency for this turbine operating at the same point with a fixed stator. It is assumed that this loss in efficiency was due to the large tip clearances previously mentioned and also possibly to nonuniformity of blade settings. Over the range of flight Mach number from 0.8 to 2.3 the variation in turbine efficiency was about 0.06.

A prediction of the turbine efficiency based on loss estimations was made in the same manner as the one presented in the paper by Heaton and Forrette. The results of this prediction are presented in figure 4 which includes a comparison with the experimental results from figure 3. The results are essentially the same as those obtained for the model turbine discussed by Heaton. The agreement of the predicted and experimental curves is good except at the low temperature ratios where the turbine approaches limiting loading and where rotor-incidence angle and rotor-inlet Mach number become high, especially at the hub.

#### ENGINE PERFORMANCE

The variation in net thrust and specific fuel consumption with flight Mach number for an altitude of 60,000 feet was computed from the adjustable-turbine engine data for a constant compressor pressure ratio of 3.3 and is presented in figure 5 for a constant turbine-inlet temperature of  $1540^{\circ}$  F. Included for comparison are the computed performance curves for operation with the standard fixed turbine at a constant compressor pressure ratio of 3.3. As can be seen, the thrust is higher and the specific fuel consumption is lower than those of the fixed-area turbine engine at conditions other than design because of the rapid decrease in turbine-inlet temperature as flight speed is reduced. For instance, at a Mach number of 0.8 the use of the variable turbine stator provides a 370 percent increase in net thrust and at a Mach number of 1.65 a 100-percent increase in thrust although both engines deliver the same thrust at the design Mach number of 2.3.

The take-off thrust for fixed compressor operating point is presented in figure 6 as a function of engine temperature ratio and turbine-inlet temperature. The value of thrust with a fixed turbine stator is taken as 100 percent. By utilizing the adjustable turbine stator to raise the turbine-inlet temperature to 1540° F, a thrust increase of 230 percent for this engine was obtained for the take-off condition.

#### CONCLUDING REMARKS

The data indicated that the turbine efficiency varied about 0.06 over the range of stator adjustment required to cover a range of flight Mach numbers in the stratosphere from 2.3 to 0.8. A comparison of the thrust and specific fuel consumption obtained on an engine equipped with fixed and adjustable turbine stators indicates that turbine stator adjustment provides good off-design engine performance for constant compressor point operation of a turbojet engine over a range of flight speeds from take-off up to a value well in the supersonic region.

# ADJUSTABLE TURBINE STATOR

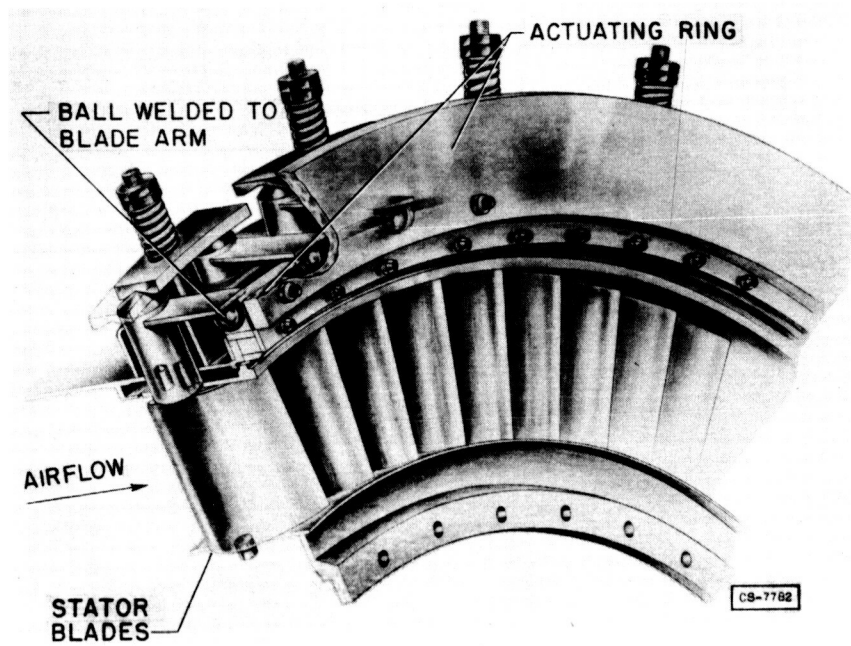


Figure 1

## RELATION OF STATOR AREA AND REQUIRED FLOW $T_3 = 1540^\circ \text{ F}$

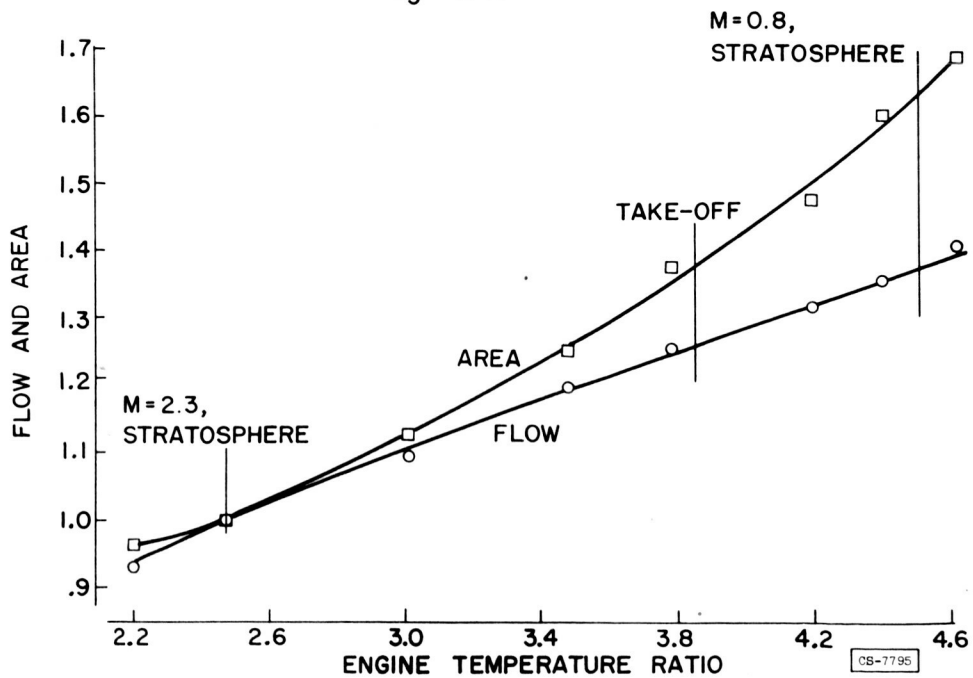


Figure 2

3078-B

TURBINE EFFICIENCY  
 $T_3 = 1540^\circ \text{ F}$

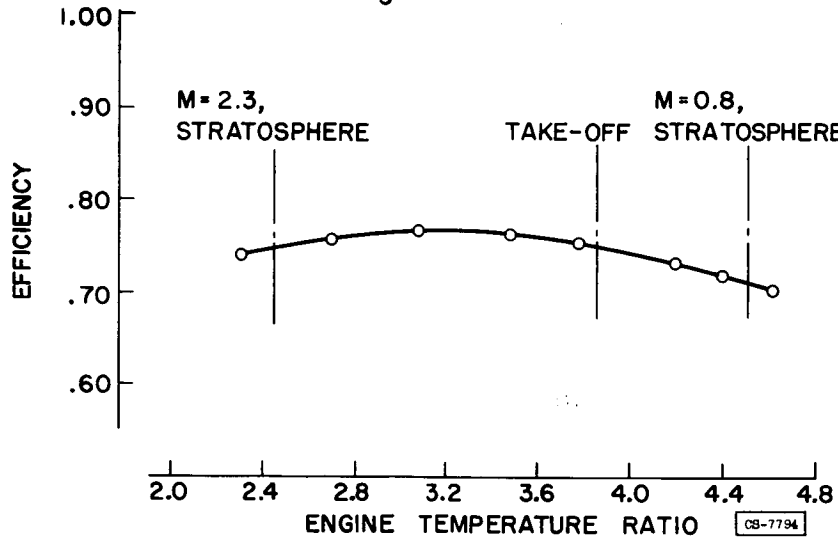


Figure 3

TURBINE EFFICIENCY PREDICTION  
 $T_3 = 1540^\circ \text{ F}$

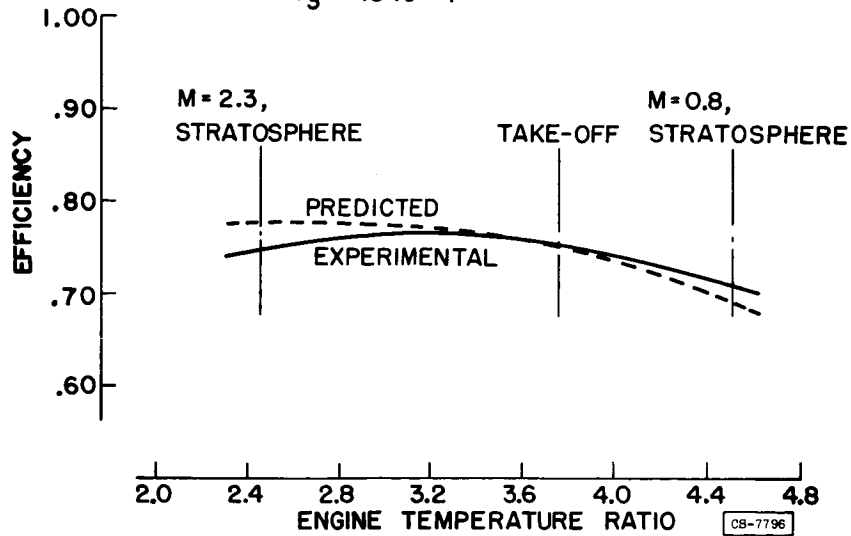
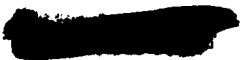


Figure 4



ENGINE THRUST AND SPECIFIC FUEL CONSUMPTION  
ALTITUDE, 60,000 ft

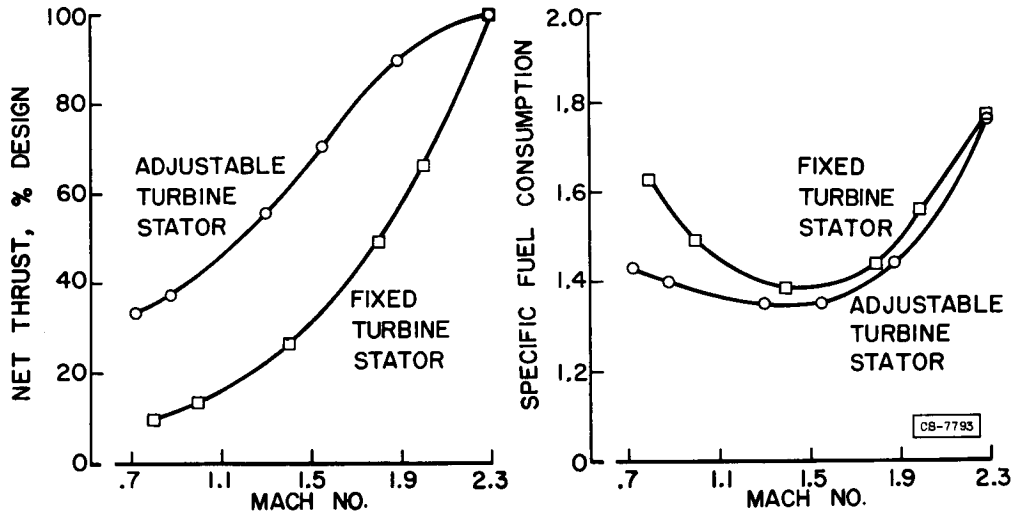


Figure 5

TAKE-OFF THRUST

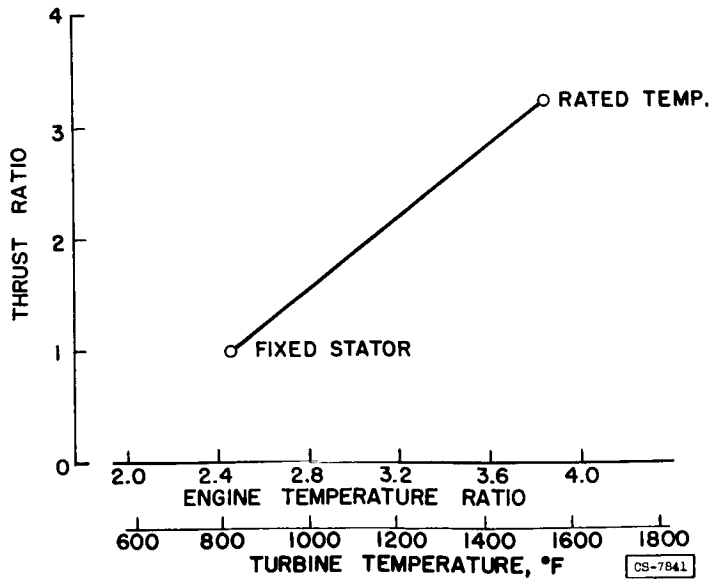
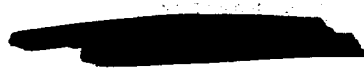


Figure 6





III - COMPRESSOR STALL AND VIBRATION PANEL

W. A. Benser  
M. C. Huppert  
H. F. Calvert  
A. A. Medeiros  
R. W. Graham

III - COMPRESSOR STALL  
& VIBRATION



[REDACTED]

SOME PROBLEMS ASSOCIATED WITH OFF-DESIGN  
PERFORMANCE OF AXIAL-FLOW COMPRESSORS

By William A. Benser

INTRODUCTION

3078-C

In the papers presented in the first section, compressor design problems were discussed. The discussions were devoted primarily to the problems involved in obtaining optimum design-point performance in a compressor of minimum size and weight. Inasmuch as a multistage axial-flow compressor can only operate as designed at a single value of equivalent speed and pressure ratio, off-design compressor operating problems are encountered during engine acceleration and at high flight Mach numbers.

The source of these off-design operating problems will be discussed in this section and, insofar as possible, potential cures. Off-design operation of axial-flow compressors is a relatively new field of research and, therefore, the analysis of sources of these problems will, in general, be qualitative. The discussion of cures will, of necessity, be limited.

TYPICAL COMPRESSOR PERFORMANCE MAP

The problems that may be encountered when an axial-flow compressor is operated at other than its design point can be illustrated by a typical performance map of a compressor designed for a pressure ratio of approximately 8.5 (fig. 1). The total-pressure ratio  $P_2/P_1$  is the ratio of compressor inlet to outlet total pressure. The equivalent speed  $N/\sqrt{\theta}$  is presented in percent of the design value;  $N$  is the absolute compressor rotative speed, and  $\theta$  is the ratio of the compressor-inlet total temperature to standard sea-level temperature.

This compressor map (fig. 1) has been divided into two regions: Region I, surrounding the design point, is shown by the lightly shaded area and represents good performance of the compressor. Some problems may arise at the upper limit of the equivalent speed as a result of excessive Mach numbers relative to the compressor blading. In general, however, these must be considered in the compressor design. Therefore, region I will not be considered with regard to off-design performance of the compressor. The low-speed region, region II, represents operating conditions where aerodynamically excited blade vibrations are prevalent. This region represents an operating area in which relatively poor compressor efficiency is obtained.

[REDACTED]

The compressor stall limit, or compressor surge limit as it is sometimes called, represents the minimum flow obtainable at any speed consistent with usable operation. This off-design compressor limit is defined as item III. The dip in the stall-limit line, item IV, is common to most high-pressure-ratio compressors and represents a definite off-design operating problem of the axial-flow compressor.

### ENGINE ACCELERATION

The effect of these off-design regions and limits of compressor operation can now be considered from the viewpoint of engine acceleration. The engine must be accelerated from the idle speed to the take-off speed and thrust condition. A similar and probably more severe acceleration problem also exists with regard to landing maneuvers of the aircraft. If a pilot finds it necessary to increase thrust because of undershooting or overshooting the landing area, extremely rapid engine accelerations are required because of the high landing speeds of high-speed aircraft. In general, this acceleration will be from an engine speed somewhat higher than idle speed, but the general requirements of acceleration are similar to those first mentioned. For either type of acceleration, the compressor operating condition changes transiently from the idle point or an equilibrium point at some intermediate speed to the take-off point. Figure 2 shows an equilibrium operating line superimposed on a typical compressor map. On this figure, idling speed was assumed to be 50 percent of design speed, and the take-off point was assumed as the design point. The equilibrium operating line represents operation with a jet-nozzle area 20 percent larger than that required for take-off thrust, and the inflection of this line between 95 and 100 percent speed results from closing the jet nozzle to obtain take-off thrust.

For extremely slow accelerations, the transient change in compressor operation would be along the equilibrium operating line. In most cases, however, rapid acceleration is desired. To provide the excess torque required for rapid accelerations, the turbine-inlet temperature must be increased above the value for steady-state operation. This results in lower air flows and higher pressure ratios than those required for steady-state operation at a given speed, and the compressor operation will move closer to the compressor stall limit. In general, the acceleration time decreases for increased displacement of the transient operating line from the equilibrium operating line during acceleration. Inasmuch as the compressor surge or stall limit normally represents the minimum flow consistent with good performance at any speed, the margin between the equilibrium operating line and the surge or stall-limit line is defined as the acceleration margin. Thus for rapid accelerations, it is essential that the compressor have both good efficiency in this intermediate speed range and a large acceleration margin.

As can be seen from figure 2, the idling condition would lie in the darkly shaded region where aerodynamically excited blade vibrations are prevalent. Furthermore, the compressor stall limit minimizes the acceleration margin at low speeds, particularly in the region of the dip in the stall-limit line. Therefore, blade vibrations at low speeds, the compressor stall limit, and the dip in the stall-limit line are all real problems with regard to engine acceleration. Of course, decreased acceleration times can be obtained by the use of jet-nozzle adjustment and the use of "crutches," such as compressor interstage or discharge bleed, or by the use of adjustable blade rows. These crutches, however, add weight and complexity to the engine.

#### HIGH MACH NUMBER FLIGHT AT ALTITUDE

In order to study the effects of variation of flight Mach number at high altitude on the compressor operating conditions, the operating line corresponding to design mechanical speed and design turbine-inlet temperatures has been superimposed on the compressor map. This operating line, which is shown in figure 3, represents the compressor operating condition for maximum thrust as flight Mach number is varied. Operation along this line, of course, requires the use of an adjustable exhaust nozzle. A range of flight Mach numbers from 0.9 to 2.8 was considered. For a flight Mach number of 0.9 in the tropopause, the compressor-inlet temperature will be less than that at sea level. Therefore, the equivalent rotative speed of the compressor will be higher than the design value or 106 percent for this flight condition. As flight Mach number is increased, the compressor-inlet temperature will increase; and for the case of constant mechanical speed, the equivalent rotative speed of the compressor will decrease. At a flight Mach number of 2.8 in the tropopause, the equivalent rotative speed of the compressor will be approximately 71 percent of the design value.

Therefore, figure 3 shows that both the low-speed region where aerodynamically excited blade vibrations exist and the dip in the compressor stall-limit line may present serious problems when such a compressor is operated in an airplane at high supersonic speeds. The equivalent speed of the compressor at high flight Mach numbers can be increased by increasing the mechanical rotative speed of the engine. This may relieve the compressor blade vibration and stall problems, but the resultant increase in material stresses would necessitate increasing the weight of the engine.

Stator-blade adjustment might also be used to relieve these problems, but this technique increases engine weight and complexity.

## OFF-DESIGN COMPRESSOR AERODYNAMICS

Because compressors must be operated at conditions of aerodynamic speed, flow, and pressure ratio other than those for which the compressor was designed, consideration must be given to the aerodynamics of off-design compressor operation. For design inlet conditions, the performance of a compressor stage is principally a function of flow coefficient  $\phi$  or the ratio of axial velocity to wheel speed. The variation of efficiency  $\eta$  with flow coefficient for a typical axial-flow compressor stage is shown at the bottom of figure 4. The flow coefficient is the ratio of average axial velocity to average wheel speed measured at the inlet to a stage and represents a function of the angle of attack for the stage. Also indicated on this typical stage curve are the choke or maximum flow conditions, the maximum efficiency designated as the stage match point, and the flow-coefficient range for stage stall.

For optimum design-point performance of a multistage compressor, it is desirable to have all stages operate at their peak efficiency points. At design rotative speed, the flow coefficient is controlled by variation of the axial velocity. Therefore, the area at the inlet of each stage is determined so as to give the proper axial velocity entering each stage. Of course, compressibility of the air requires that the flow area at the rear of the compressor be much smaller than that at the inlet, as shown by the typical compressor cross section (fig. 4). It should be noted that the efficiency variation with flow coefficient will depend on the particular stage design. For purpose of illustration, however, it will be assumed that the performance of all stages is similar.

If the take-off condition (see fig. 2) is chosen at the design point, the compressor must operate at an equivalent rotative speed appreciably below the design value for idle, acceleration, and supersonic high-altitude flight. For the part-speed operating conditions, the over-all pressure ratio is less than the design value and the desired area variation would be as indicated in figure 5. Thus for the area variation determined for optimum stage matching at the design or take-off condition, the front of the compressor is too big and the rear is too small. Therefore, for part-speed operation, the front stages approach stall, the rear stages approach choking flow, and the over-all efficiency of the compressor must be decreased from that for optimum stage matching.

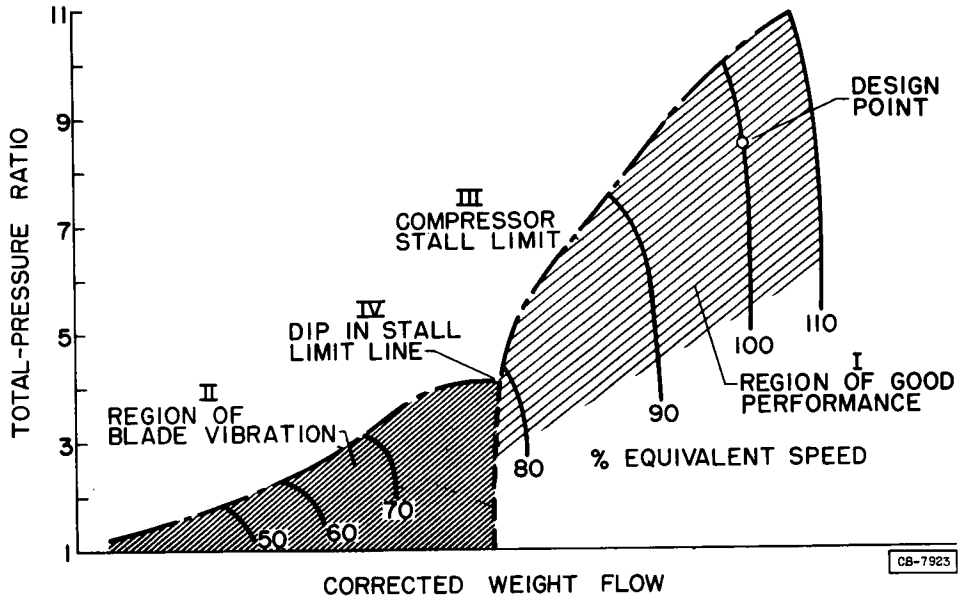
A plot of a typical variation of flow coefficient of the first and last stages against percent of compressor design rotative speed is shown in figure 6. As can be seen from this figure, the rear stages approach their choke limit as speed is decreased. This choking of the exit stages restricts the flow through the compressor and results in stall of the inlet stages. Thus, as indicated, operation of the compressor at equivalent rotative speeds of 50 to 80 percent may result in stall of one or more of the inlet stages of the compressor. Of course, as flow is decreased at any speed, all stages will approach their stall points.

## CONCLUDING REMARKS

From this discussion it can be seen that three of the most important off-design compressor operating problems are (1) blade vibrations at low values of equivalent rotative speed of the compressor, (2) the compressor stall limit, and (3) the dip in the compressor stall limit at intermediate speeds. These are all problems relating to engine acceleration and high flight Mach numbers at altitude. These problems may be avoided by the use of such variable-geometry features as compressor air bleed, adjustable compressor and turbine blades, or compressor over-speeding; but all these techniques add weight and complexity to the engine. Analysis of stage matching characteristics has indicated that these off-design problems may be associated with stall of the individual stages. Therefore, fundamentals of stage stall both with regard to single stages and stages of a multistage compressor must be considered.

3078-C

### TYPICAL AXIAL-FLOW COMPRESSOR PERFORMANCE MAP



3078-C

Figure 1

### ENGINE ACCELERATION REQUIREMENTS

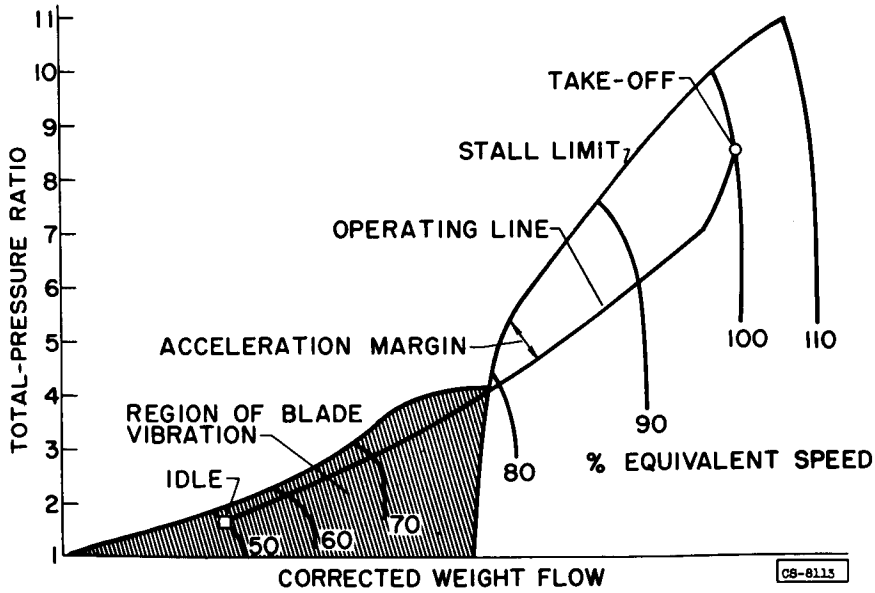


Figure 2

### COMPRESSOR EQUIVALENT SPEED REQUIREMENTS

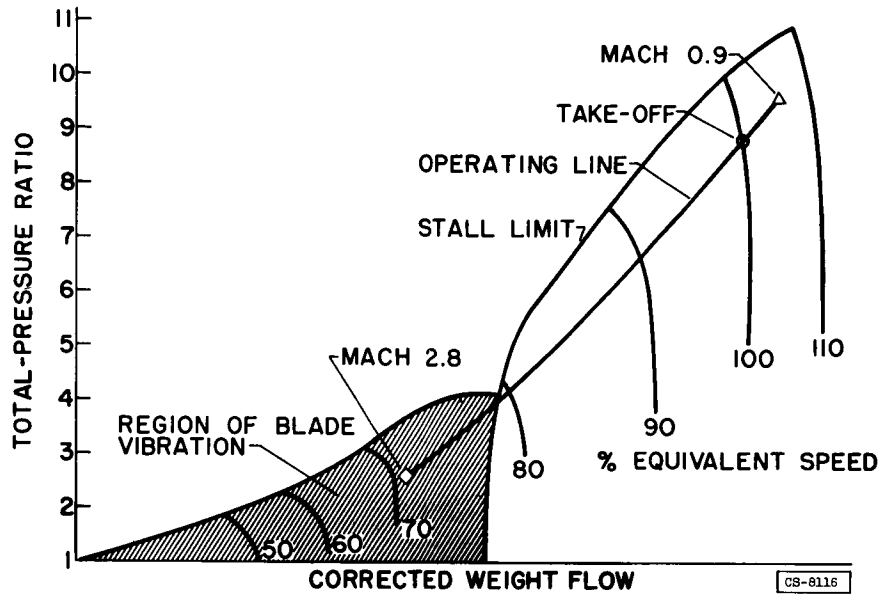


Figure 3

### TYPICAL AXIAL-FLOW COMPRESSOR

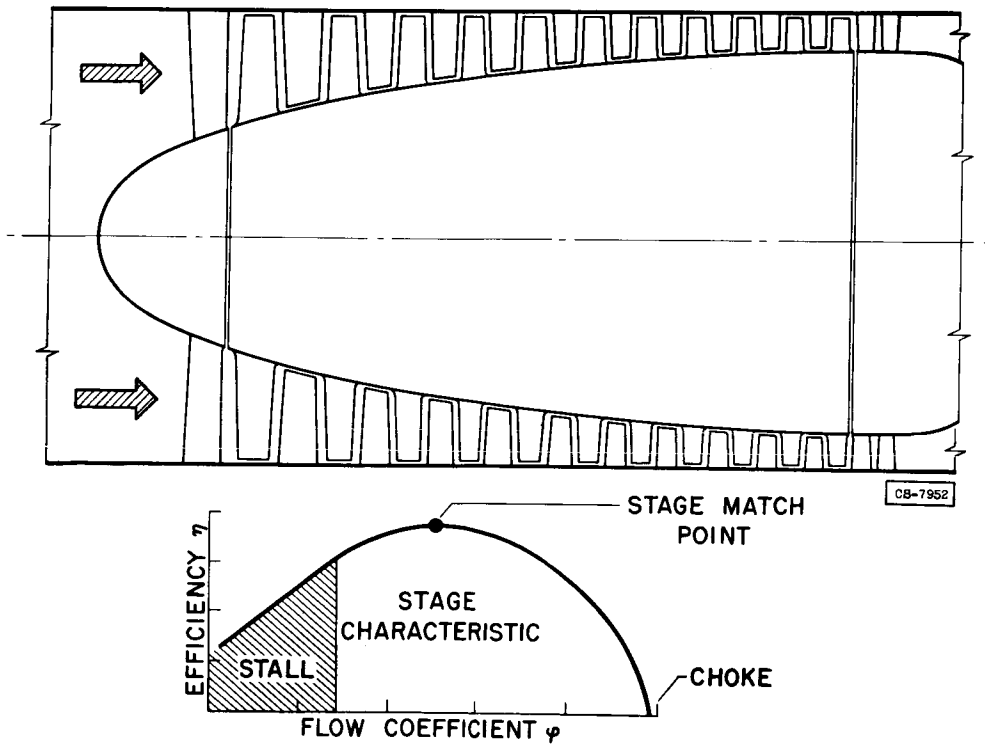


Figure 4

### EFFECT OF PART-SPEED OPERATION ON STAGE MATCHING

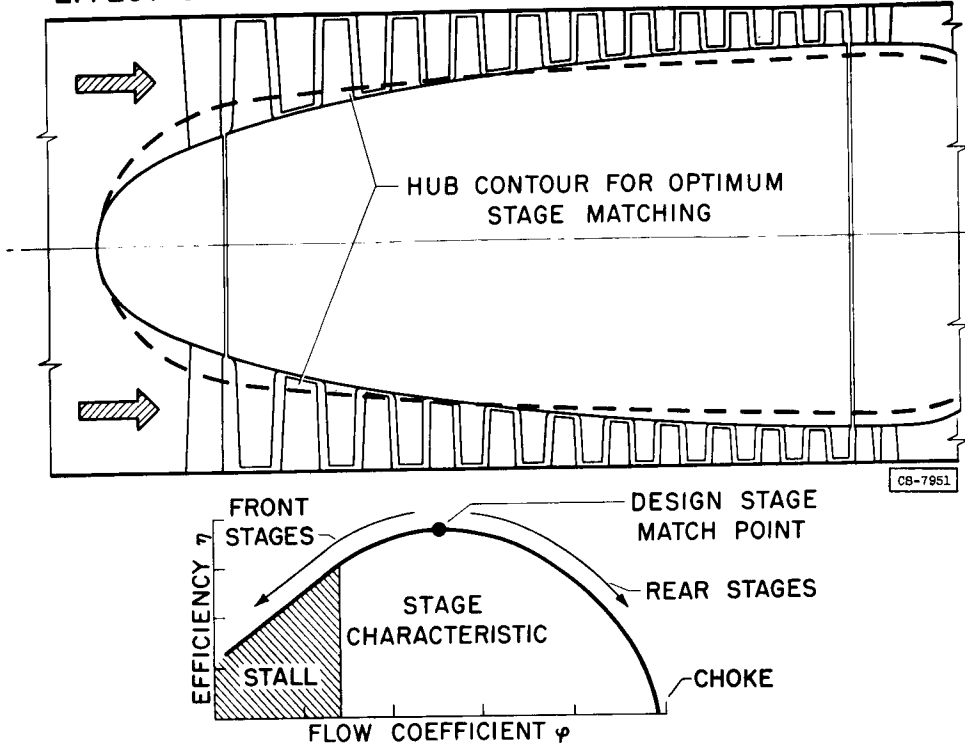


Figure 5

### STAGE OPERATION WITH SPEED

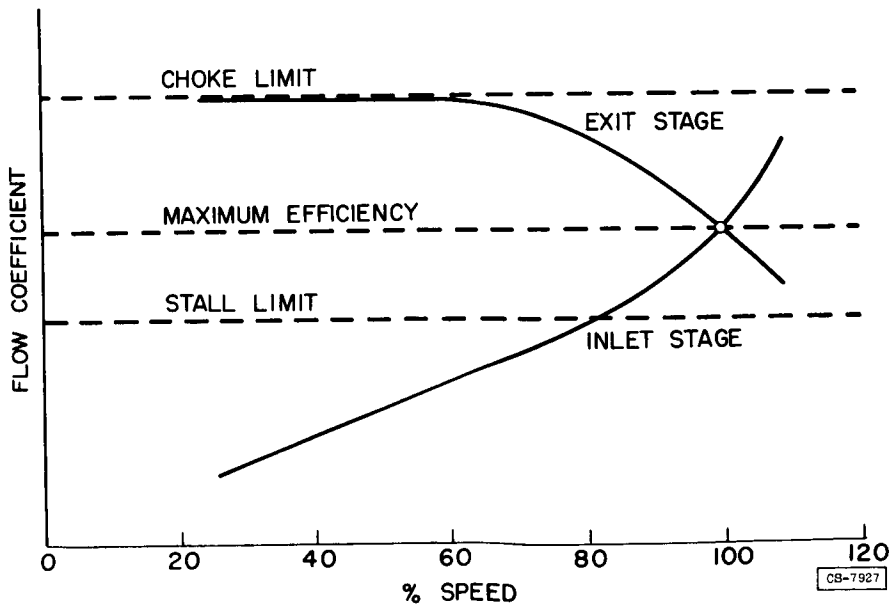


Figure 6

  
ROTATING STALL IN SINGLE-STAGE COMPRESSORS

By Robert W. Graham

## INTRODUCTION

In the preceding paper, it was pointed out that individual stages of a multistage compressor may stall during off-design operation. Therefore, an understanding of the way a compressor stage stalls is necessary for an understanding of the off-design operation of compressors.

The stall of a blade row in an axial-flow compressor usually does not occur uniformly over the entire blade row. Instead, one or more blades or several groups of blades in a blade row stall out first. The resulting stall zones, or zones of low flow, do not remain fixed with respect to the initially stalled blade but propagate around the blade row at a lower speed than the rotor - thus the term "rotating stall." Generally, the stall zone or zones pass a fixed reference in a periodic fashion, although a nonperiodic type of rotating stall does exist.

The phenomenon of rotating stall is generally associated with the performance of the axial-flow compressor, but it is interesting to observe that one of the earliest references to rotating stall appears in a British paper (ref. 1) on centrifugal compressor performance, published in 1947. The phenomenon was not labeled rotating stall at this date, but the description contained in the reference leaves no doubt that it was rotating stall.

Perhaps reference 2 was the first American publication containing a reported observation of rotating stall. Reference 2 is a report of an investigation conducted with an impulse axial-flow compressor. The authors of this paper did not label the phenomenon rotating stall either, but they presented an explanation of the mechanism of stall propagation around the compressor annulus.

In 1951 a technical report (ref. 3) used the term "rotating stall" to describe the phenomenon. In this reference, the experimentally obtained rotating-stall flow patterns were presented as data. High-frequency-response instrumentation was employed to detect the stall patterns; whereas, in references 1 and 2, observation of tufts had been the only means of stall detection.

In the past two years, much effort has been devoted to the experimental and theoretical study of rotating or propagating stall. Much of the research has been done with single-stage compressors. In this paper, some of the important experimental results pertaining to rotating-stall behavior in single-stage compressors will be discussed.



3078 - C

III - 2

## MECHANISM OF PROPAGATING STALL

Theoretically, a row of airfoils that are absolutely identical and are located in a perfectly uniform one-dimensional flow field would stall uniformly as depicted in figure 1. The uniform stall illustrated in figure 1 is an idealized condition in which all the blades have stalled simultaneously.

Obviously, a slightly different profile shape of one of the blades or a small flow perturbation in front of the blade row would cause one of the blades to stall ahead of the others in the blade row. Consequently, the "uniform stall" is an improbable phenomenon that is of academic interest only, since the blade row in a compressor would not stall in this idealized manner.

The way in which a compressor blade row stalls is schematically depicted in figure 2. Blade 2 has reached a stalled condition before the other blades in the row and does not produce sufficient pressure rise to support the flow around it. As is indicated in figure 2, back-flow begins, and the net flow through the blade channel is appreciably diminished. The region of low flow, or the stall zone, that results from the restricted flow is represented by the shaded area. This stall zone may extend over several blade passages. The flow continuity requirements across the blade row will cause spillage around the stall zone. The spilled flow causes the angle of attack on blade 3 to increase, whereas the angle of attack on blade 1 is diminished. The increase in the angle of attack on blade 3 generates a stall, and the stall region progresses downward. The spilled flow resulting from the stall of blade 3 reduces the angle of attack on blade 2, and it is unstalled. In this manner, the stall zone propagates across the blade row and each blade is successively stalled and unstalled.

In figure 3, the blade row is bent into an annular ring to represent a compressor blade row. The propagating-stall zone progresses around the blade row or rotates in the compressor annulus - thus, rotating stall is produced. Experimental investigations show that the number, the geometrical size, and the propagation rate of these stall zones may vary widely. In most cases, the stall patterns are periodic, but nonperiodic rotating stall can and does occur. An explanation of the propagation rate of the stall zones is of interest currently. Emmons, Marble, and Sears, who presented some of the first papers on rotating stall, have proposed theoretical models of rotating-stall propagation. Phase lag or time lags similar to the aerodynamic-lag parameter proposed by Mendelson (ref. 4) of the NACA Lewis laboratory have been introduced into the theoretical explanations of stall-propagation rate. From a limited amount of stall data obtained from single-stage-compressor tests, there appears to be a relation between stall-propagation rate and a phase-lag parameter.

## ROTATING STALL

### Direction of Rotation

Measurements of rotating-stall-propagation rates have been made in several single-stage axial-flow compressors. When measured with respect to an absolute frame of reference, the stall zones propagate in the direction of the rotor rotation and at a lower speed than the rotor. If the rotating-stall pattern is viewed from a frame of reference that is rotating at rotor speed, the stall zones propagate in a direction opposite to the absolute direction of rotor rotation and at a lower speed than the rotor.

### Detection of Rotating Stall

The frequency of rotating stall is far beyond the frequency-response limitations of the pressure-sensing probe and manometer tube employed in the performance-testing of compressors. The hot-wire anemometer, the high-frequency-response thermocouple, and electronic pressure pickups are sensitive to high-frequency flow fluctuations. If the rotating stall is periodic, an average image of the flow-fluctuation pattern can be synchronized on the screen of a cathode-ray oscilloscope. If the stall pattern is nonperiodic, continuous time traces of the stall zones can be recorded on an oscillograph or similar recording instrument. Figure 4(a) shows a representative trace of a periodic rotating stall viewed on a cathode-ray oscilloscope and detected with hot-wire-anemometer probes like those pictured in figure 4(b). The troughs represent the stall zones, the depth of the trough being a measure of the reduced weight flow in the stall zone and the width of the trough an indication of the width of the stall zone. The pitch distance between adjacent troughs measured in units of time is the reciprocal of the frequency of the stall disturbance. The frequency of a rotating-stall disturbance can be determined by a frequency meter or by forming Lissajous figures on the cathode-ray oscilloscope screen.

In order to be able to determine the number of equispaced stall zones in a compressor annulus, two hot-wire-anemometer probes are fixed in the compressor casing. By varying the known circumferential distance between the probes and observing the phase shift between the stall traces of each hot-wire probe, the number of stall zones can be determined. References 3 and 5 include complete descriptions of the analytical method.

## Nonperiodic Rotating Stall

Although rotating stall is generally considered to be a periodic phenomenon, experimental evidence indicates that nonperiodic rotating stalls do exist. Nonperiodic stall zones that cover several blade passages are observed frequently slightly above the flow-coefficient value that marks the beginning of a periodic rotating stall. Within the region of rotating stall, nonperiodic rotating stalls have been observed to occur during the transition from one periodic stall pattern to another. It is hypothesized that nonperiodic rotating stall may result from a nonequidistant distribution of stall zones around the compressor annulus.

### Characteristics of Rotating Stalls Observed in Single-Stage Compressors

Since periodic rotating stalls are more prevalent than the non-periodic variety, more investigations of periodic rotating stalls have been conducted. The investigations reveal that rotating stalls exhibit varied characteristics as to the number of stall zones, the size of the stall zones, and the stall-zone propagation rate. In the current literature, rotating stalls are classified according to the radial extent of the stall zones as compared with the span or length of the blade. Those stall zones that extend over only a part of a blade-span length of the annular flow passage are referred to as "partial-span" rotating stalls, and those that extend over the entire passage are referred to as "total-span" rotating stalls or hub-to-tip stalls. The radial dimension of the stall zones was selected in classifying the rotating stalls because it indicates whether the entire blade or just a part of each blade in the blade row is supporting the rotating-stall phenomenon. For most of the partial-span rotating-stall patterns observed, the stall zones were located at the tip region of the rotor blades. However, if the region near the hub of the stage is critical, that is, at a stalled angle of attack, rotating-stall zones near the hub are possible. A maldistribution of inlet velocity or a blade design incorporating high angles of attack near the hub may make the blade critical at the hub region.

### Characteristics of Observed Rotating Stalls

Table I is a collection of rotating-stall data obtained from references 5 to 8. As is obvious from an inspection of the table, the rotating stalls are characterized by a variety of stall-propagation rates, weight-flow fluctuations, geometry of the stall zones, and number of stall zones. The number of stall zones for the partial-span rotating-stall patterns varied from 1 to 8, and the absolute propagation rates ranged from 0.23 to 0.87 rotor speed. The number of stall zones for the total-span patterns varied from 1 to 6, and the propagation rate from 0.10 to 0.49 rotor speed.

In general, for a given type of rotating stall (partial or total span), the stall-propagation rate is a fixed ratio of the compressor speed. Thus, the stall-propagation rate is a linear function of compressor speed.

For the NACA data presented in table I, the flow-fluctuation parameter  $\Delta pV/\rho\bar{V}$  was calculated by the method described in reference 5. The magnitude of  $\Delta pV/\rho\bar{V}$  varied from 0.76 to 2.24 for the stall patterns observed in several compressors. No correlation between the type of rotating stall and the magnitude of  $\Delta pV/\rho\bar{V}$  is evident. The authors of reference 6 use a different parameter  $\Delta V/V$  to express the flow fluctuation. However, the Mach number level of the flow is approximately the same for all the investigations referred to in table I; thus, the parameters  $\Delta V/V$  and  $\Delta pV/\rho\bar{V}$  can be used interchangeably.

#### Experimental Observation

One of the testing procedures used in observing the rotating-stall patterns peculiar to a specific compressor is to operate the compressor at constant speed and gradually diminish the weight flow until the rotating-stall patterns are observed. If hot-wire anemometers are used in conjunction with an oscilloscope, the form of the flow traces on the scope will follow a definite evolutionary process as the flow coefficient is diminished. It is assumed that the hot wires are located at the "critical" radial station where the blade elements will stall out ahead of other portions of the blade span. If the procedure starts at a flow coefficient near the best operating point of the compressor for the operating speed, the observer will see sharply defined blade wakes similar to those shown in figure 5. Region A marks the flow-coefficient range over which sharp blade wakes will be observed.

After the flow coefficient is reduced below the peak-pressure-ratio flow coefficient, the sharply defined blade wake becomes less well defined on the suction side of each blade. This is the first indication of the flow separation that accompanies blade stall. This stalled region is labeled B in figure 5. The fuzzy appearing areas on the oscilloscope, which represent the stalled condition, appear to grow larger as the flow coefficient is further diminished. The nonuniform manner in which the blade row stalls makes it difficult to obtain a stationary pattern on the oscilloscope screen. At the low-flow end of region B, the blade wakes cannot be distinguished amid the erratic separating flow traces of the stalled blades. Sometimes a momentarily occurring stall zone that covers several blade passages will appear on the screen. This sporadic stall zone is often the herald of a periodic rotating-stall pattern that develops at a still lower flow coefficient.

Region C is the region of rotating stall in which the periodic low flow or stall zones are observed. The shape of the rotating-stall traces has been discussed previously. Further throttling of the flow may promote changes in the rotating-stall patterns with respect to the number and size of the stall zones (radial and circumferential extent). If the flow-control valve is opened gradually, the same rotating-stall patterns will appear that appeared when the flow was throttled. However, the rotating-stall patterns accompanying increasing flow will occur at higher values of flow coefficient than during decreasing flow.

### Effect of Rotating Stall on Performance

The compressor designer is interested in rotating stall because of its effect on compressor performance and the way in which the periodic flow fluctuations affect blade life. For several single-stage compressors investigated in the stall region, the compressor performance maps obtained can be classified into two types. The first type has a smooth, continuous performance characteristic in the rotating-stall region; the second has an appreciable discontinuity in the characteristic at the stall point.

Figure 6 shows a typical stall pattern associated with a smooth continuous characteristic. The performance characteristic is shown at the left of the figure. The numbers above the performance curve represent the number of stall zones present in the stall pattern. The first stall pattern observed in the stall region comprised three stall zones that extended over a part of the blade span. With further reductions in weight flow, the pattern changed to four and then to five stall zones. The radial extent of the stall zones increased until the five zones extended over the entire blade span. It is important to note that no discontinuities in the performance characteristic occurred as the stall patterns developed. Stalls that exhibit gradual growth of the stall zones and do not effect discontinuities in the performance characteristic are called "progressive" stalls.

Single-stage-compressor performance without discontinuities in the characteristic has been observed for many compressors that operated within the rotating-stall region. As described in references 6 to 8, partial-span rotating stalls were observed in which no discontinuities in compressor performance took place. The number of stall zones varied with the weight flow, but no discontinuities accompanied the changes in the stall patterns.

In contrast to the progressive stalls, some stalls have been observed to develop abruptly, with a resulting discontinuity in the performance characteristic. A schematic representation of an abrupt stall and the resulting discontinuous characteristic are shown in figure 7.

3078-C

This single-zone abrupt stall that extends across the entire blade span is typical of the type of stall observed in several single-stage compressors with high hub-tip ratios. The severity of the drop-off in performance from the upper branch of the performance characteristic to the lower branch differs among those compressors which exhibited this kind of characteristic. According to reference 5, the drop-off in total-pressure ratio for a symmetrical design compressor with 0.8 hub-tip ratio amounted to approximately 33 percent; whereas, in reference 6, the drop-off in pressure ratio for a wheel-type and a vortex-type design amounted to approximately 5 percent.

Hysteresis. - As has been discussed in a previous section, the flow-coefficient values that mark the location of a rotating-stall region or a particular rotating-stall pattern within the stall region on the compressor performance map are different for increasing and decreasing weight-flow operation. This difference in the flow-coefficient values is attributed to a hysteresis effect. Generally, it has been observed that rotating-stall patterns are quite stable, and to eliminate a specific stall pattern by increasing the weight flow, the flow must be increased beyond the value where the stall pattern began originally. Apparently, the aerodynamic conditions that sponsor the establishment of a rotating-stall pattern lag the changes in weight flow.

Hysteresis effects have been observed for all types of rotating-stall patterns. The hysteresis effect is most marked for the case where the single-zone total-span stall causes a discontinuity in the performance characteristic. The hysteresis effect is observable also in the case where no performance discontinuity is present. Hysteresis has been observed wherever the stall pattern changed within the stall region, or at the boundary between the periodic rotating-stall region and the region of blade stall (fig. 5).

#### CONCLUDING REMARKS

Rotating stall consists of one or more low-flow or stall zones that rotate around the compressor annulus at a fraction of rotor speed. The phenomenon is thought to be initiated by a flow instability that causes one or more stall regions to develop in the blade row. Predominantly, the stall patterns have periodicity, although nonperiodic rotating stall does exist.

The periodic rotating stalls investigated in single-stage compressors show different effects on the compressor performance characteristic. If a rotating stall occurs in which an appreciable portion of the compressor annulus area is stalled abruptly, a discontinuous performance characteristic at the stall point may occur. Smooth performance characteristics are associated with a gradual stalling of the compressor annulus area.

The region of flow coefficient over which a definite rotating-stall region prevails moves to higher values of flow coefficient for increasing weight flow than the values of flow coefficient corresponding to compressor operation for a decreasing weight flow. This effect is attributed to hysteresis.

The flow fluctuations accompanying rotating stall are appreciable. The increment of flow velocity fluctuation may range from one-half to twice the magnitude of the mean flow velocity.

#### REFERENCES

1. Chesire, L. J.: The Design and Development of Centrifugal Compressors for Aircraft Gas Turbines. War Emergency Issue No. 12 pub. by Inst. Mech. Eng. (London), 1945. (Reprinted in U.S. by A.S.M.E., Jan. 1947, p. 438.)
2. Schulze, Wallace M., Erwin, John R., and Westphal, Willard R.: Investigation of an Impulse Axial-Flow Compressor Rotor over a Range of Blade Angles. NACA RM L50F27a, 1950.
3. Grant, Howard P.: Hot Wire Measurements of Stall Propagation and Pulsating Flow in an Axial Flow Inducer-Centrifugal Impeller System. Pratt and Whitney Res. Rep. No. 133, June 1951.
4. Mendelson, Alexander: Effect of Aerodynamic Hysteresis on Critical Flutter Speed at Stall. NACA RM E8B04, 1948.
5. Huppert, Merle C.: Preliminary Investigation of Flow Fluctuations During Surge and Blade Row Stall in Axial-Flow Compressors. NACA RM E52E28, 1952.
6. Iura, T., and Rannie, W. D.: Observations of Propagating Stall in Axial-Flow Compressors. Rep. No. 4, Mech. Eng. Lab., C.I.T., Apr. 1953. (Navy Contract N6-ORI-102, Task Order 4.)
7. Graham, Robert W., and Prian, Vasily D.: Experimental and Theoretical Investigation of Rotating-Stall Characteristics of Single-Stage Axial-Flow Compressor with Hub-Tip Ratio of 0.76. NACA RM E53I09, 1953.
8. Huppert, Merle C., Johnson, Donald F., and Costilow, Eleanor L.: Preliminary Investigation of Compressor Blade Vibration Excited by Rotating Stall. NACA RM E52J15, 1952.

TABLE I. - SURVEY OF SINGLE-STAGE ROTOR STALLS

Compressor design	Hub-tip ratio	Type of stall	Number of stall zones	Stall speed, abs rps	Weight-flow fluctuation	Discontinuity in performance characteristics
Symmetrical	0.50	Partial	3	0.420	1.39	---
			4	.475	2.14	---
			5	.523	1.66	---
	0.90	Total	1	0.305	1.2	Yes
			8	0.87	0.76	No
	0.80	Total	1	.36	1.30	Yes
			7	0.25	2.24	No
	0.76	Partial	8	.25	1.10	No
			5	.25	1.00	No
			3	.23	2.02	No
Total		4	.48	1.47	No	
		3	.48	2.02	No	
		2	.49	1.71	No	
		1	0.48	0.60	No	
Free vortex	0.60	Total	2	.36	.60	No
			1	.10	.68	Yes
			1	0.45	0.60	No
Solid body	0.60	Total	1	.12	.65	Yes
			1			No



### UNIFORM STALL

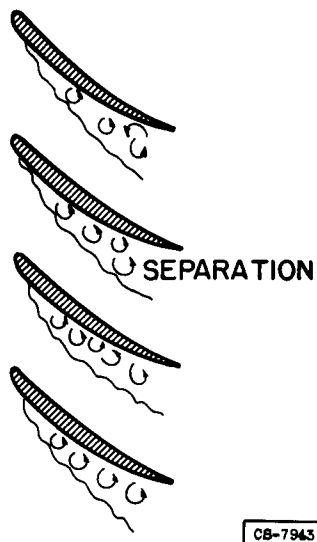


Figure 1

### PROPAGATING STALL

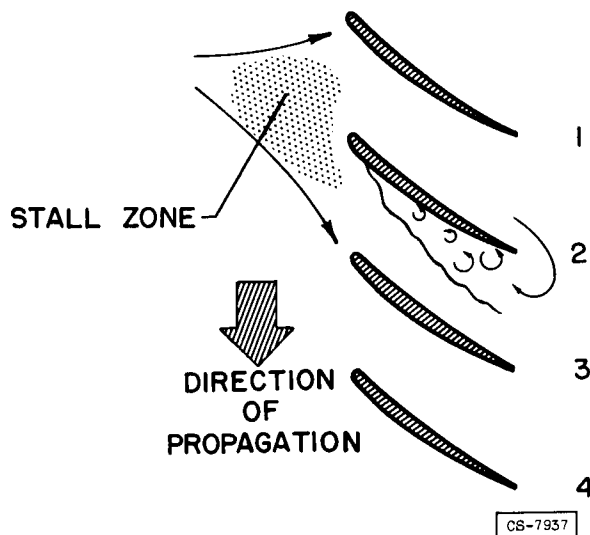


Figure 2



### STALL PROPAGATION IN ROTOR

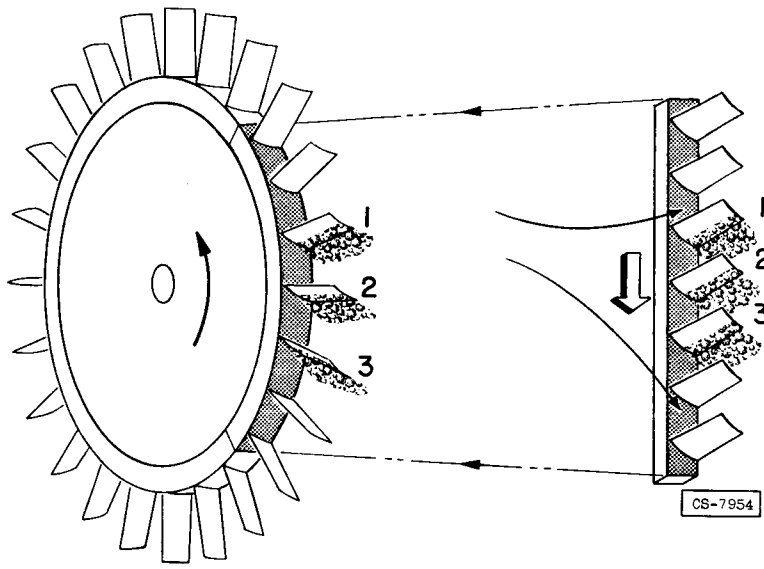
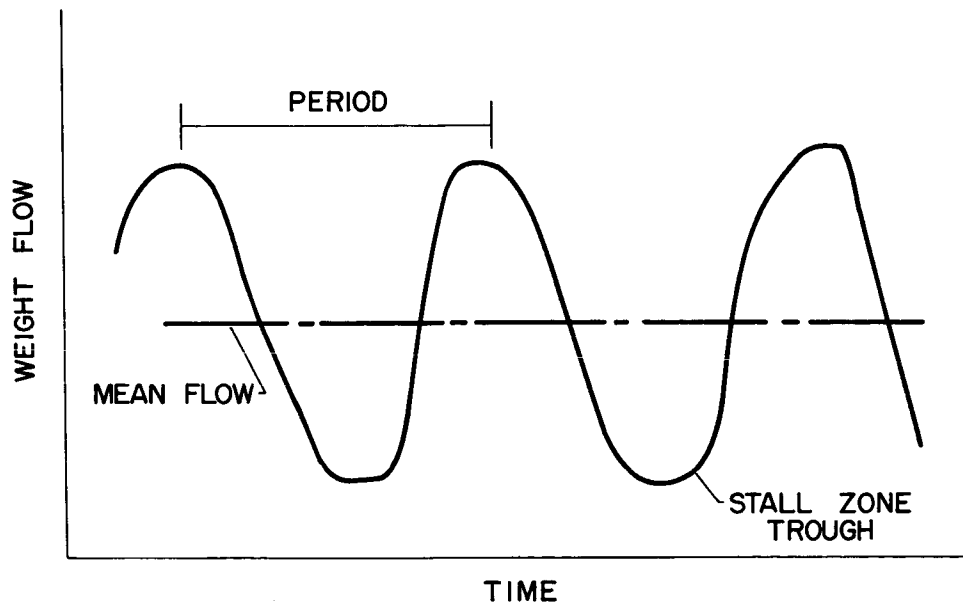


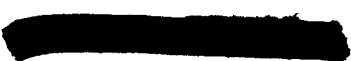
Figure 3

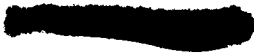
### ROTATING-STALL OSCILLOSCOPE TRACE



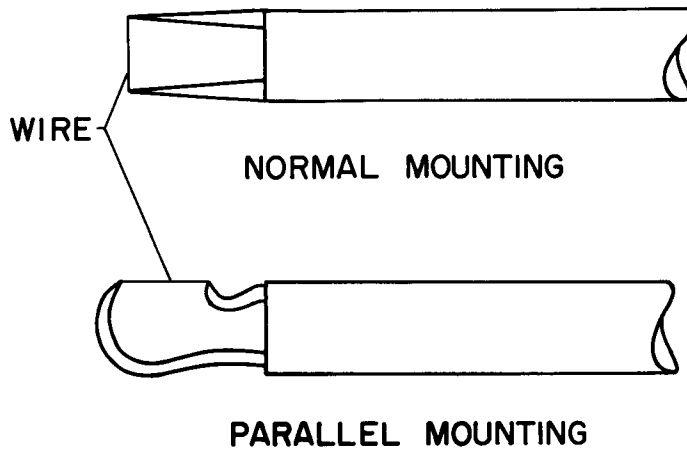
(A)

Figure 4





# HOT-WIRE-ANEMOMETER PROBES



(B)

Figure 4

3078-C

# OSCILLOSCOPE TRACES IN THREE REGIONS OF COMPRESSOR OPERATION

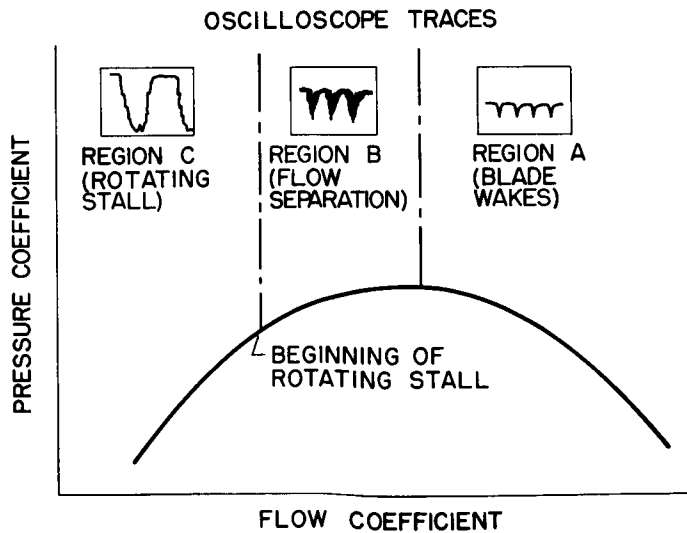
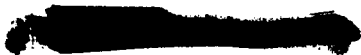


Figure 5



### PROGRESSIVE STALL

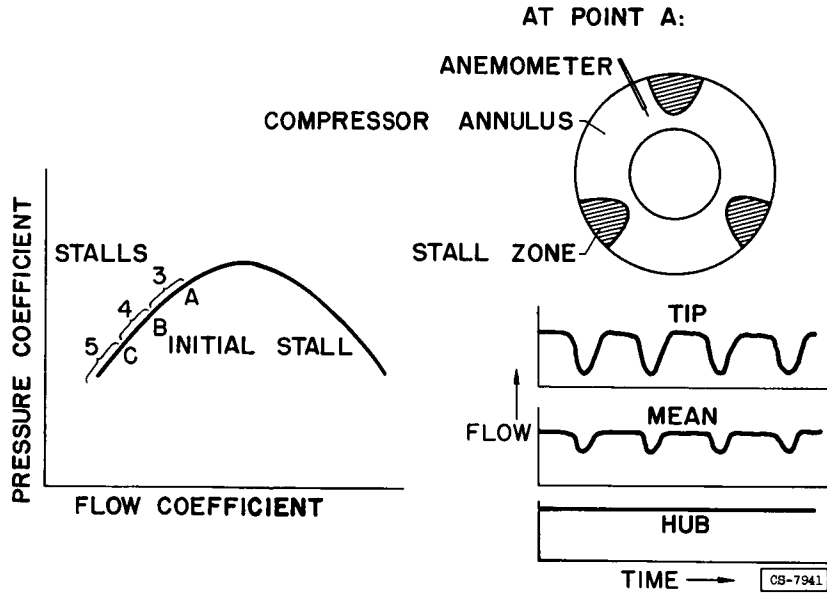


Figure 6

### ABRUPT STALL

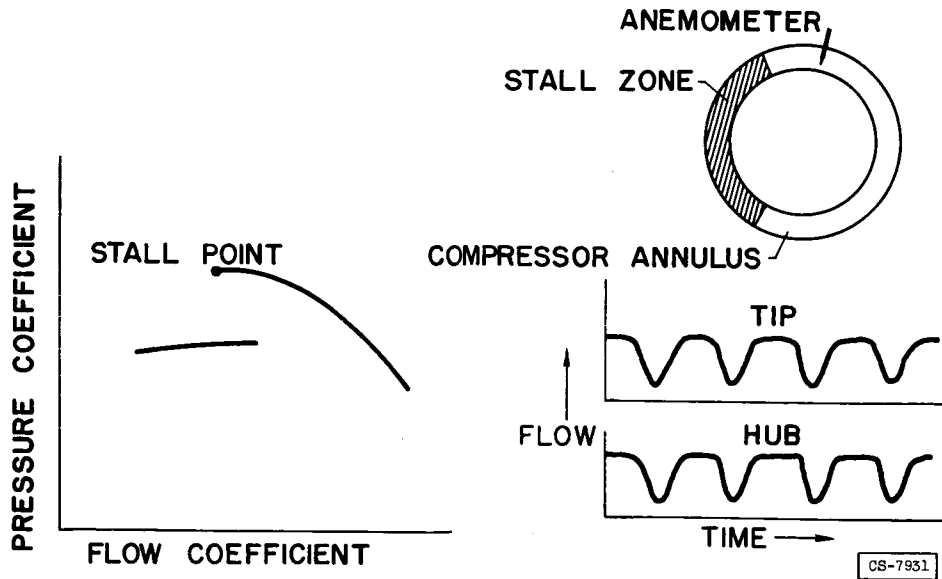


Figure 7

## ROTATING STALL IN MULTISTAGE AXIAL-FLOW COMPRESSORS

By Merle C. Huppert and Eleanor L. Costilow

## INTRODUCTION

Rotating-stall patterns similar to those observed in single-stage compressors (refs. 1 to 3) have been detected in multistage compressors. This paper discusses the experimental studies of rotating stall in multistage axial-flow compressors.

## STALL IN INLET STAGES OF MULTISTAGE COMPRESSORS

The discussion of rotating stall in the inlet stages is introduced by summarizing the results of a study on rotating stall of the NACA 20-inch-diameter ten-stage axial-flow compressor reported in the first paper of this panel. The rotating-stall patterns found at low and intermediate speeds are indicated in figure 1. For this compressor, the number of stalls in the stall pattern increased from three to seven as the flow was reduced at 50 percent of design speed; whereas, at 70 percent of design speed, only the stall pattern with three stall zones was obtained. The operating region of the performance map where each stall pattern existed could be separated as shown and is called region II in the first paper of this panel. The rotating-stall patterns obtained were of the partial-span type associated with a gradual decrease in stage pressure coefficient with flow coefficient. As defined in the preceding paper, this type of stall is called progressive stall. The rotating stalls probably were instigated by rotor-tip stall in one of the first three or four stages. The absolute rotational speed of the stall zones was approximately 57 percent of rotor speed for all stall patterns obtained.

Hot-wire-anemometer measurements were made of the flow variation behind the first, second, third, fourth, fifth, seventh, and tenth stages at the tip, mean, and hub stations. A typical variation in amplitude of the weight-flow fluctuation divided by the average flow rate along the compressor length at the three radial stations is shown in figure 2. The largest fluctuations occurred at the tip of the second, third, and fourth stages and were reduced considerably in the exit stages. It was not possible to determine which stage initiated the stall. In general, if a stall pattern could be detected in one stage of the compressor, it would also be found in any other stage. The comparatively large flow fluctuations in the first four stages indicate that the stall was probably initiated by one of these stages, as would be expected on the basis of stage matching.

The extent to which the stall regions spiraled as they extended through the compressor was determined and found to be negligible; that is, the stall zones extended axially through the compressor.

Rotating-stall patterns instigated by stall of the inlet stages have been observed in several other high-pressure-ratio multistage axial-flow compressors, the number of stall patterns and the variation in number of stall zones with weight flow at a given speed varying somewhat among the compressors investigated. In some compressors, the number of stall patterns changed intermittently among as many as three different patterns at a given operating point (see Calvert and Huppert); and, in other cases, the same stall pattern existed at all weight flows from choked flow to surge at a given speed. The rotational speed of the stall zones for these high-pressure-ratio compressors was between 50 and 60 percent of the rotor speed. This result is contrasted to the rather wide range of stall rotational speed in percentage of rotor speed observed in single-stage compressors (see refs. 1 to 3). In all compressors investigated, the stall zones propagated in the direction of rotor rotation.

As discussed in references 4 and 5, rotating stalls caused by stall of the inlet stages are a source of vibration excitation that may lead to compressor blade failure.

#### EFFECTS OF MULTISTAGING ON STAGE PERFORMANCE

While the rotating-stall phenomenon in multistage compressors appears to be somewhat the same as that occurring in single-stage units, the rotating-stall characteristics are not necessarily predictable from single-stage tests. In the multistage compressor, the number of stall zones and the propagation rate are the same throughout the entire compressor at a given operating point; whereas, if each stage were tested as a single-stage unit, it would probably exhibit stall characteristics different from every other stage. Two obvious sources that combine to cause this difference in rotating-stall characteristics between single-stage and multistage compressors are: (1) unsteady flow effects introduced by the rotating stalls emanating from adjacent stages, and (2) the action of preceding stages, which affect the radial distribution of inlet flow conditions to the stage. These stage-interaction effects caused by multistaging are known to alter the rotating-stall characteristics.

The data presented in reference 3 illustrate the multistaging effect. The multistage compressor used in this investigation consisted of three identical stages. This compressor had an initial hub partial-span rotating stall and then a total-span rotating stall as the flow was further reduced. Accompanying the total-span rotating stall was an abrupt drop in pressure coefficient, which indicated an abrupt stalling of the stages similar to that described for single-stage units in

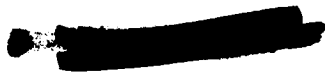
reference 2 and in the preceding paper. However, one stage of the multistage compressor when run as a single-stage unit showed an initial tip rotating stall; and as the flow was reduced it became a full-span stall with a gradual decrease in pressure coefficient, which indicated that the total-span stall was developed by the gradual spreading of the stall at the tip to the hub of the rotor. While no generalizations can be drawn from this one example, it does illustrate the stage-interaction (multistaging) effects, and it shows that the stall characteristics of the multistage compressor cannot generally be predicted from the single-stage results.

#### CONCLUDING REMARKS

Rotating stall is likely to be present in the useful operating range of the multistage axial-flow compressor at speeds below 70 or 80 percent of design speed where the inlet stages operate stalled. Although rotating stalls have been found in all compressors investigated to date, neither the rotational speed of the stall zones, the number of zones formed in the stall pattern, nor the radial extent of the stall zones is necessarily predictable from single-stage data because of stage-interaction effects.

#### REFERENCES

1. Graham, Robert W., and Prian, Vasily D.: Experimental and Theoretical Investigation of Rotating-Stall Characteristics of Single-Stage Axial-Flow Compressor with Hub-Tip Ratio of 0.76. NACA RM E53I09, 1953.
2. Huppert, Merle C.: Preliminary Investigation of Flow Fluctuations During Surge and Blade Row Stall in Axial-Flow Compressors. NACA RM E52E28, 1952.
3. Iura, T., and Rannie, W. D.: Observations of Propagating Stall in Axial-Flow Compressors. Rep. No. 4, Mech. Eng. Lab., C.I.T., Apr. 1953.
4. Huppert, Merle C., Costilow, Eleanor L., and Budinger, Ray E.: Investigation of a 10-Stage Subsonic Axial-Flow Research Compressor. III - Investigation of Rotating Stall, Blade Vibration, and Surge at Low and Intermediate Compressor Speeds. NACA RM E53C19, 1953.
5. Huppert, Merle C., Johnson, Donald F., and Costilow, Eleanor L.: Preliminary Investigation of Compressor Blade Vibration Excited by Rotating Stall. NACA RM E52J15, 1952.



### ROTATING-STALL REGIONS SUPERPOSED ON OVER-ALL COMPRESSOR PERFORMANCE

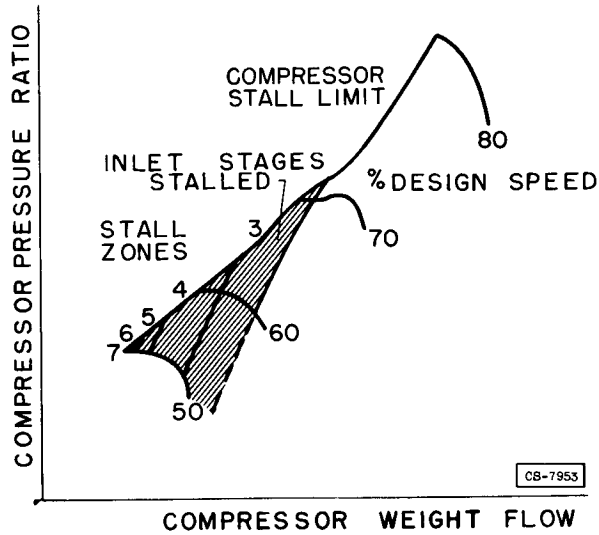


Figure 1

### VARIATION IN WEIGHT-FLOW FLUCTUATION THROUGHOUT A MULTISTAGE COMPRESSOR

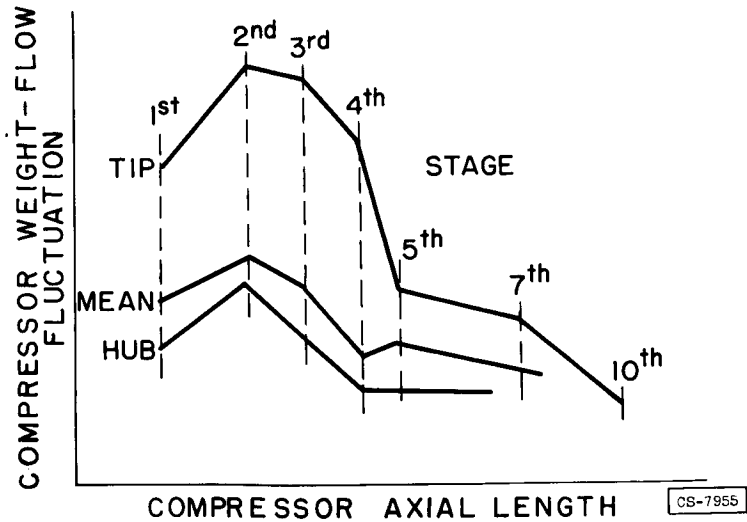
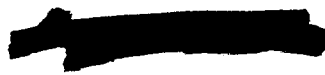


Figure 2



3078-C

## BLADE VIBRATION IN AXIAL-FLOW COMPRESSORS

By Howard F. Calvert and Merle C. Huppert

### INTRODUCTION

Experimental data indicate that the inlet stages of an axial-flow compressor are operating stalled below approximately 70 to 80 percent of design speed, and that this stall results in a series of stalled regions spaced around the compressor annulus and rotating at a speed slower than the rotor. Inasmuch as rotating stall produces alternate high- and low-flow zones that rotate about the compressor axis and extend throughout the total length of the compressor, it may be the potential source of forced vibrations of the compressor blading.

This paper presents a discussion of rotating stall as a potential source of compressor-blade vibration and presents data recently obtained at the NACA Lewis laboratory that associates blade failures with excitation due to rotating stall.

### BLADE VIBRATIONS IN SINGLE-STAGE AXIAL-FLOW COMPRESSORS

In order to determine the variation in blade force normal to the chord line associated with rotating stall, a preliminary investigation was conducted in a single-stage compressor. The stator blades of this compressor were instrumented with strain gages to measure the blade force, and hot-wire anemometers were used to detect the flow fluctuations of rotating stall. This investigation showed that, as a stator blade was passed by one of these low- or no-flow zones, the blade lift approached zero; therefore, the variation of the blade lift due to the passing of the stall zones was approximately equal to the maximum value of the lift when the blade was in the unstalled region. Inasmuch as stall consists of a number of low-flow zones equally spaced around the annulus, the force is periodic and can therefore be a source of resonant blade vibrations. The stator blades are excited by this force at the absolute frequency of the stall zones, as defined by the following formula:

$$f_s = N_s \lambda$$

$f_s$  absolute stall frequency

$N_s$  rotational speed of stall pattern, rps

$\lambda$  number of stall zones in stall pattern

The rotor blades are excited by the relative frequency, which is determined by the following formula:

$$f'_s = (N_r - N_s) \lambda$$

$f'_s$  rotor-blade excitation frequency or relative stall frequency

$N_r$  rotational speed of compressor, rps

$\lambda$  number of zones in stall pattern

The stall frequency is generally measured by a hot-wire anemometer installed in the compressor case, and the number of zones in the stall pattern may be determined by the method discussed in reference 1.

Since the wave form of the force variation resulting from rotating stall is not simply sinusoidal but contains strong harmonics, resonant vibration may be excited when the excitation frequency of rotating stall is a fraction (e.g., 1/2, 1/3, 1/4, etc.) of the natural frequency of the blades.

Several rotor and stator blade failures were experienced while research was being conducted on single-stage axial-flow compressors. In an attempt to determine whether rotating stall could excite blade vibration, an investigation was conducted on a single-stage compressor and reported in reference 2. The compressor had a hub-tip ratio of 0.5 at the rotor inlet, which is representative of the inlet stages of a multistage compressor. This compressor stage had aluminum cantilever-type stator blades. Strain gages mounted on the airfoil section near the blade base measured blade bending stresses, and hot-wire anemometers mounted in the compressor case measured the stall frequency. The compressor pressure-ratio characteristic curve is shown in figure 1, which also indicates the stall patterns obtained. At each rotational speed, the first stall pattern encountered on reducing weight flow contained three stall zones; the next, four; and, at the lowest weight flow investigated, five stall zones were obtained. Figure 2 is a plot of the stall frequency divided by the natural frequency of the stator blade in bending (420 cps) against percent of design speed. The compressor speeds where resonant vibrations would be expected are noted at the intersection of the stall-frequency lines with the horizontal lines corresponding to resonance with the fundamental stall frequency and the first two harmonics. Vibrations were observed at points A and B. The vibratory stress at point A,  $\pm 16,000$  pounds per square inch, was excited by the first harmonic of the stall frequency. Excitation by the second harmonic was also obtained, and the resultant vibratory stresses were  $\pm 7500$  pounds per square inch. These aluminum blades cracked while operating at point A, and no further data could be obtained on this particular stage; however, the results of this investigation showed that rotating stall could excite blade vibration.

## BLADE VIBRATIONS IN MULTISTAGE AXIAL-FLOW COMPRESSORS

As discussed in the preceding paper, rotating stall caused by stall of the inlet stages may exist in multistage axial-flow compressors up to 70 or 80 percent of design speed. The area of the typical multistage compressor performance map where rotating stalls may exist during normal operation is shown in figure 3 along with the equilibrium line for jet-engine operation. The number of stall zones in the stall patterns obtained during operation of multistage axial-flow compressors differs somewhat among the various compressors investigated, but the rotational speed of the stall patterns was between 50 and 60 percent of rotor speed for all high-pressure-ratio axial-flow compressors investigated.

Several multistage-compressor failures believed to have been caused by rotating stall have occurred at the NACA Lewis laboratory, but in only a few cases was sufficient information available to attribute the failures directly to rotating stall. One such case was a current production jet engine with a history of blade failures in the inlet stage at speeds between 60 and 70 percent of rated engine speed. This engine was instrumented with strain gages and hot-wire anemometers in order to determine whether a correlation existed between this vibration problem and rotating stall.

Hot-wire-anemometer data indicated the presence of rotating stall in the compressor inlet stages in this critical speed range. Figure 4 shows a plot of stall frequency against percent of rated engine speed for the stall patterns obtained. In the critical speed range between 60 and 70 percent, stall patterns were observed with four, five, and six zones. The stall zones in these patterns were very unstable; that is, the number of zones was rapidly and intermittently changing among the four, five, and six zones. At all engine speeds and for all stall patterns obtained, the rotational speed of the stall pattern was between 53 and 58 percent of compressor speed.

The speeds at which resonant vibrations would occur in the first-stage rotor were determined from a plot of the stall frequency relative to the rotor and the natural bending frequency of the rotor blade against engine speed, as shown in figure 5. The natural bending frequency of the rotor blade increases with engine speed because of the stiffening effect of centrifugal force, as discussed in reference 3. Resonant excitation is indicated at 62 percent of design speed with the stall pattern with six zones (point A, fig. 5), and at 70 percent of design speed with the stall pattern with five zones (point B, fig. 5). The strain-gage data indicated vibratory stresses of 28,000 pounds per square inch at point A and 34,000 pounds per square inch at point B. Vibrations were observed only at 62-percent speed when the six-zone pattern was present, and only at 70-percent speed when the five-zone pattern was present. Since the

number of zones in the stall pattern was rapidly and intermittently changing among four, five, and six, the vibration patterns or signals were spasmodic.

Since these compressor blades had been fabricated from aluminum, the vibratory stresses observed at points A and B (fig. 5) were sufficient to cause a fatigue failure in a relatively low number of stress cycles. Therefore, the cause of this serious off-design-speed vibration problem has been proved to be resonance between the rotor blades and rotating stall. Thus, the importance of rotating stall as a potential source of destructive compressor-blade vibration is demonstrated.

#### CONCLUDING REMARKS

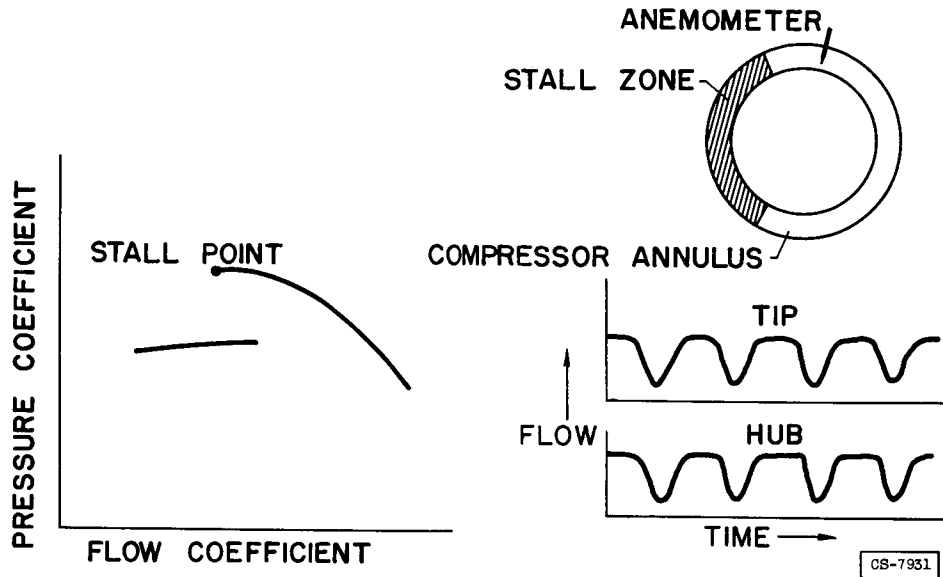
Rotating stall has been shown to be a serious source of blade vibration in compressors and may be the source of many heretofore unexplained vibration problems. At present, insufficient knowledge of rotating stall prevents the prediction of the rotating-stall characteristic of a compressor in the design stage.

Recent trends toward the development of high-pressure-ratio compressors will create more serious rotating-stall problems, since inlet-stage stall will extend over a wider range of engine operation. High-mass-flow, high-pressure-ratio, light-weight compressors of engines for supersonic aircraft will require increased blade lengths and shorter blade chords. This type of blade is extremely susceptible to blade vibration; therefore, rotating stall will become an even more important source of compressor blade vibration.

#### REFERENCES

1. Huppert, Merle C.: Preliminary Investigation of Flow Fluctuations During Surge and Blade Row Stall in Axial-Flow Compressors. NACA RM E52E28, 1952.
2. Huppert, Merle C., Johnson, Donald F., and Costilow, Eleanor L.: Preliminary Investigation of Compressor Blade Vibration Excited by Rotating Stall. NACA RM E52J15, 1952.
3. Hanson, M. P., Meyer, André J., Jr., and Manson, S. S.: A Method of Evaluating Loose-Blade Mounting as a Means of Suppressing Turbine and Compressor Blade Vibration. Proc. Soc. Exp. Stress Analysis, vol. X, no. 2, 1952, pp. 103-116.

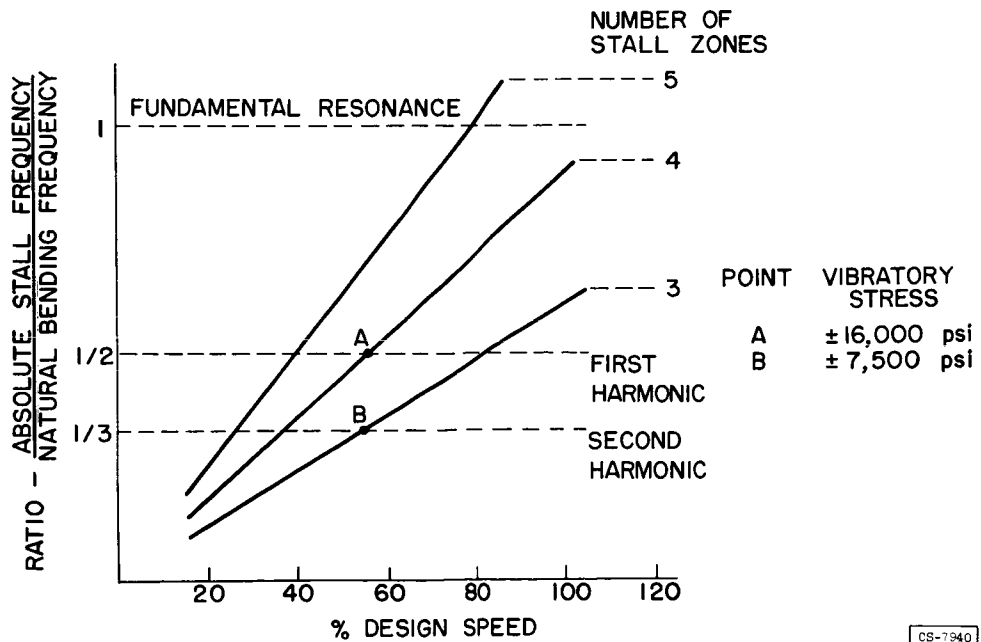
### ABRUPT STALL



CS-7931

Figure 1

### SINGLE-STAGE CRITICAL SPEED DIAGRAM

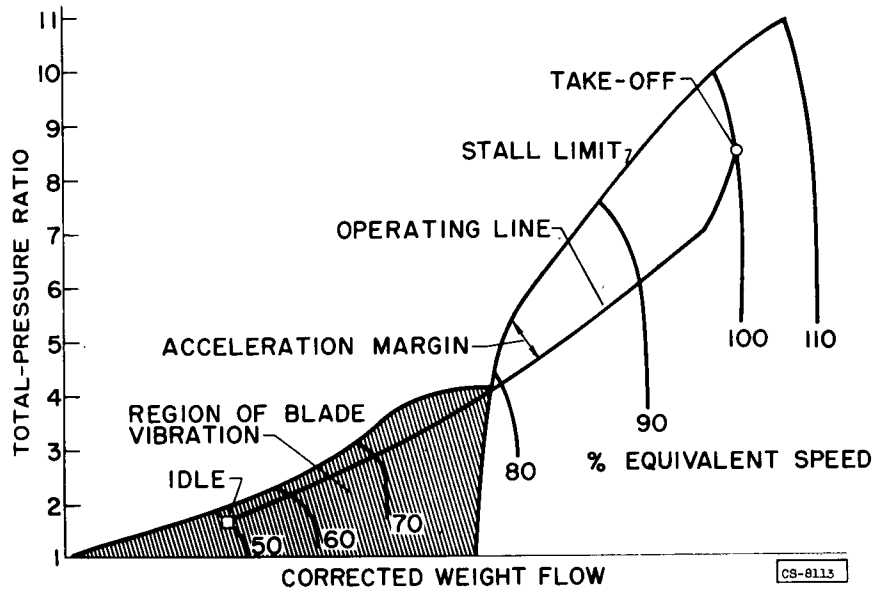


CS-7940

Figure 2



### ENGINE ACCELERATION REQUIREMENTS



3078-C

Figure 3

### MULTISTAGE ROTATING-STALL CHARACTERISTICS

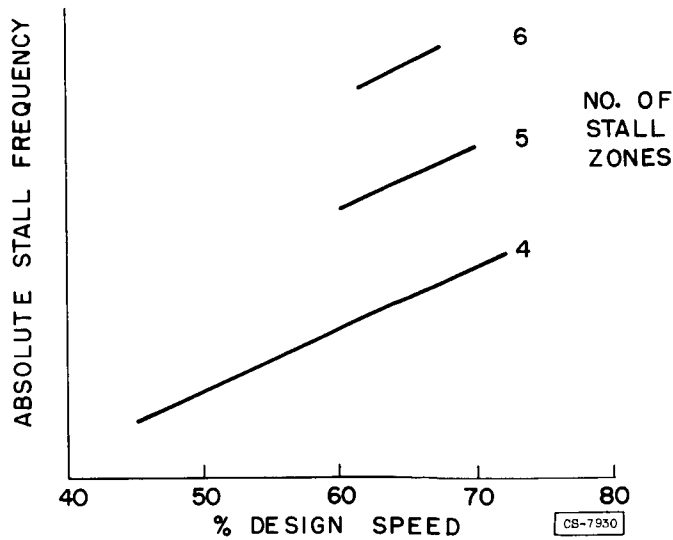
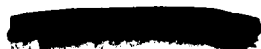


Figure 4



### MULTISTAGE CRITICAL SPEED-DIAGRAM

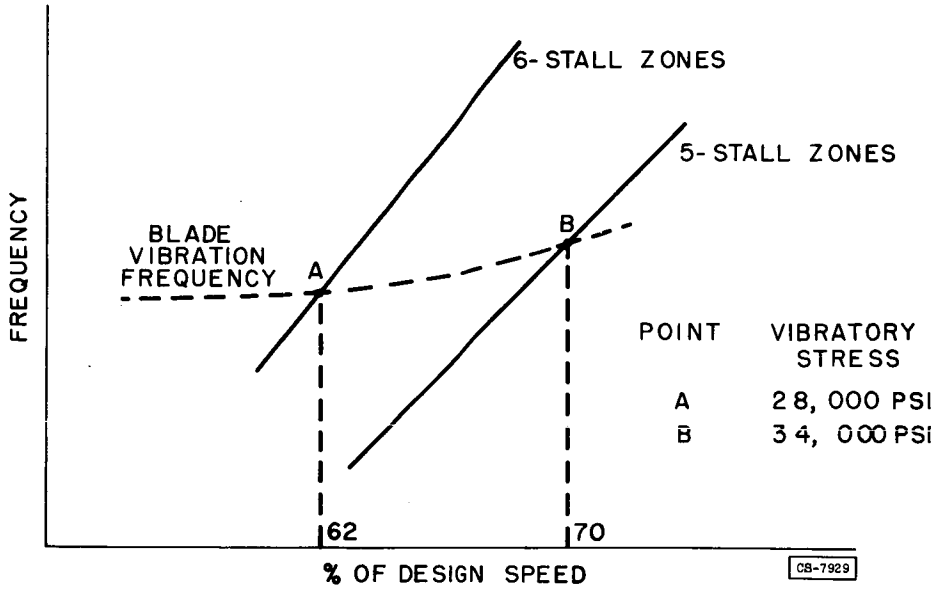


Figure 5

[REDACTED]

COMPLETE COMPRESSOR STALL AND SURGE IN MULTISTAGE  
AXIAL-FLOW COMPRESSORS

By Merle C. Huppert and Eleanor L. Costilow

INTRODUCTION

3078-C

As discussed in the first paper, blade vibrations encountered at low speeds and now attributable to the flow fluctuations of rotating stall represent only one off-design operating problem. Another limitation imposed upon the compressor is the termination of the useful operating range at each speed by the complete compressor stall. The line joining the complete stall points known as the stall-limit line, may exhibit a dip in the intermediate-speed range. In some cases, particularly in compressor test facilities, complete compressor stall can result in surge.

This paper presents a discussion of complete stall and compressor surge in multistage axial-flow compressors.

COMPLETE COMPRESSOR STALL

Complete compressor stall, characterized by the performance shown in figure 1, is generally considered the limit of useful operation of the compressor. As shown in references 1 and 2, the occurrence of surge as a result of operation at the stall point depends largely on the size of receiver into which the compressor is discharging. For the discussion herein, available information for cases where stall occurred without surge will be used to illustrate the effects of complete compressor stall on compressor performance.

The jet-engine data of references 3 and 4 indicate that there is considerable reduction in compressor-discharge pressure due to complete compressor stall. Figure 2 shows a plot of the pressure drop due to stall divided by the compressor pressure rise immediately previous to the stall point plotted against compressor pressure ratio. The compressor component data obtained in compressor test facilities and reported in references 1 and 5 are also included. The data correlation is considered fairly good, but additional data are needed. The pressure drop at stall varies from about 25 percent of the pressure rise at the stall point at low pressure ratios to about 50 percent of the pressure rise at a pressure ratio of 6.

[REDACTED]

Reference 6 reports results similar to those shown in figure 1 and suggests the existence of more than one stalled branch on the performance curve. Though the flow fluctuations associated with stall were described as a surge, it is felt that they were similar to the rotating stall previously described.

In cases where hot-wire-anemometer data have been obtained with complete compressor stall, the stall pattern extended from the compressor casing to the compressor hub and from the compressor inlet to compressor discharge. The amplitude of the fluctuations was about the same in all stages. In cases where sufficient anemometer data were obtained to determine the number of stall zones in the stall pattern, there was a single stall zone covering at least half the annular area. This single zone is directly analogous to the abrupt stall encountered in single-stage compressors, as discussed in the first paper of this panel.

In all likelihood, a hysteresis loop exists at the stall point of the performance curve for a high-pressure-ratio axial-flow compressor. This condition is analogous to the same effect brought about by abrupt rotating stall in the single-stage compressor reported in reference 1 and also observed in the three-stage compressor reported in reference 5. Stall recovery occurs at a higher weight flow than that at which abrupt stall first occurred. Because of the similarity between abrupt stall in single-stage compressors and complete compressor stall in multistage compressors, it seems reasonable to assume that the complete compressor stall can be caused by an abrupt stall of some stage or stages in the multistage compressors. Little information exists as to the nature of the high-pressure-ratio axial-flow-compressor characteristics after complete compressor stall has occurred, not only because of the apparent deleterious effects of the stall on the compressor but also because of the surge frequently encountered in testing these components.

Inasmuch as acceleration margin is needed at all compressor speeds, the shape of the stall line connecting the stall points at each compressor speed is of importance. As discussed in the introductory panel paper, the smallest acceleration margin for the engine is generally obtained in the region of the dip in the stall line.

#### COMPRESSOR SURGE

Compressor surge has been defined as an axisymmetric flow pulsation instability in the compressor and the system in which it is operating. The torque required to drive the compressor during surge will vary as the flow varies during the surge fluctuation; whereas with rotating stall the torque requirement is a constant for a given operating point. The amplitude of the flow fluctuations that occur during surge varies considerably among compressors.

General analyses of surge (see refs. 7 and 8) indicate that surge will occur when the slope of the compressor characteristic curve of pressure ratio against weight flow becomes slightly positive. This condition results in negative damping in the system, so that any slight disturbance in the flow will increase in amplitude until limited by some nonlinearity of the system. Published surge analyses do not attempt to compute the amplitude of the limit cycle of the nonlinear oscillation, so that the consequences of a computed instability are not given.

The agreement of the published criteria for surge and surge data has not been satisfactory in general. Many compressors have been operated with a positive slope of the characteristic curve without encountering audible surge (see refs. 5 and 9), and in many cases surge has occurred when the slope of the compressor characteristic was apparently quite negative.

The surge investigations conducted by the NACA suggests that surge may be classified into one of two types:

- (1) Surge occurring with a continuous compressor characteristic
- (2) Surge associated with a discontinuous drop in pressure ratio due to complete compressor stall (fig. 1)

#### Surge with Continuous Compressor Characteristic

Part of the difficulty encountered with checking surge criteria is probably due to the fact that low-amplitude surge is not always detectable by the criterion of audibility. In many cases where compressors were operated in the positive-slope region of the characteristic, surge may have occurred, but was undetected because of its low amplitude.

In order to check the idea that many cases of surge may be undetected, a single-stage compressor (declared to be surge-free by several experienced operators using the criterion of audibility was instrumented with hot-wire anemometers and pressure transducers. A plot of the receiver pressure rather than the compressor-discharge stagnation pressure is shown in figure 3(a).

Small fluctuations in weight-flow rate were detected when the slope of the compressor characteristic curve became slightly positive (point A, fig. 3(a)). An oscillogram of the hot-wire-anemometer output and the pressure transducers that recorded instantaneous stage static-pressure rise is shown in figure 3(b). The fluctuations were inaudible and of small amplitude, as indicated on the figure. The flow fluctuations of surge were detectable as the flow was reduced until rotating stall was encountered at point B (fig. 3(a)). At this point, the flow fluctuations

[REDACTED]

of rotating stall were quite large and obscured in the compressor annulus any small fluctuations of surge. Pressure transducers installed in the receiver, however, indicated that surge existed also from the point of stall to the lowest weight flow obtained. The surge frequency (23 cps) over the range marked C in figure 3(a) was the same at all weight flows, that is, at weight flows greater and less than that for rotating stall, which occurred at point B.

Similar low-amplitude surges were noted at operating points where the compressor characteristics were continuous in the investigation reported in reference 1. However, stall patterns had already been formed at the flow conditions where surge occurred, so that instrumentation in the compressor indicated a periodic change in stall pattern.

These surge data are evidently explainable on the basis of system stability. The amplitude of the fluctuations of surge was, however, too small to have any significant effect on compressor performance or life expectancy.

#### Surge Associated with Discontinuous Pressure Drop

##### Due to Complete Compressor Stall

Surge associated with complete compressor stall characterized by the abrupt loss in pressure ratio is generally quite violent, and its inception is apparently dependent largely on the size of the receiver into which the compressor is discharging, as discussed in reference 2. This effect is illustrated by the data obtained with the compressor used in the investigation reported in reference 3. When operated in a compressor test facility with a large receiver, the compressor surged violently; whereas, when the compressor was operated as a jet-engine component, surge was not obtained. Complete compressor stall was obtained, instead, with the accompanying decrease in compressor-discharge pressure shown in figure 2. The multistage-compressor investigation reported in reference 1 similarly indicated that surge would not occur if a small receiver was used. Additional jet-engine data indicating compressor stall rather than surge are given in reference 4.

Although too little information is available to give a satisfactory complete explanation of surge associated with complete compressor stall, the data presented in reference 10 and the explanations in references 2 and 10 suggest that whether or not surge occurs as a result of complete compressor stall is determined by the flow transient following the stall. The flow transient following stall may be discussed by use of figure 4. The pressure drop due to stall is designated as  $\Delta P_S$ , and the weight-flow increase above that at the stall point required for stall recovery is called  $\Delta W$ . The characteristic of the compressor-discharge throttle used for controlling the flow through the compressor

[REDACTED]

passes through the stall point. If a small disturbance caused the compressor to stall, or if the throttle were closed slightly, the compressor would stall and be incapable of producing a discharge pressure equal to that in the receiver. Consequently, the flow rate through the compressor would be sharply reduced. However, because the receiver is being emptied through the throttle, its pressure would fall quickly. This reduction in receiver pressure permits an increase in flow rate through the compressor. If the flow rate through the compressor exceeds the value at the stall point by the value  $\Delta W$ , stall recovery occurs and the compressor operates unstalled and comes to equilibrium with the throttle at the stall point; thus the surge pulse is completed. Unless the throttle is opened, the compressor will stall again and the cycle would repeat.

The data of reference 10 reproduced in figure 5, show the flow transient during a surge pulse for the multistage compressor used in that investigation. The hot-wire-anemometer data shown were obtained during surge at 50 percent of design speed for the compressor.

These data (fig. 5) show the flow fluctuations caused by the seven-stall-zone pattern just prior to the single-stall-zone fluctuation produced by complete compressor stall. As shown in reference 10, this same stall pattern was obtained during steady-state operation near the stall point. As the flow rate decreases and then increases to exceed its value prior to complete compressor stall, stall recovery occurs and results in a sharp increase in flow rate. As the flow rate is reduced following stall recovery, the stall pattern with three stall zones is shown; as discussed in reference 10, the stall pattern with three stall zones was obtained at the highest flow rate at 50 percent of design speed. As the flow rate was further reduced (not shown in figure 5), the number of stall zones in the stall pattern increased from three to seven, just as during steady-state operation.

It seems clear that the surge pulse would not have been completed had the system damping been greater. Increased damping would have reduced the weight-flow overshoot during the transient flow following stall. A reduction in receiver volume is one way of increasing the system damping and preventing surge, as demonstrated in reference 1. Presumably, the system damping need not be negative in order for this type of surge to occur, as is required for surge with a continuous compressor characteristic. In addition, the slope of the compressor characteristic prior to stall does not influence the transient following stall.

#### CONCLUDING REMARKS

Complete compressor stall results in a drop in compressor-discharge pressure between 25 and 50 percent of the pressure rise at the stall point for the components investigated thus far. The stall pattern obtained with complete compressor stall has been observed to contain one stall zone extending over the entire annulus height in all stages.

Surge associated with continuous compressor characteristics is believed due to system instabilities caused by a positive slope of the compressor characteristic. Surge of this type may be very low in amplitude and difficult to detect.

Surge associated with complete compressor stall is likely to be quite violent; although this type surge may be eliminated by use of a small receiver, it is not clear whether stall or surge is the more destructive to the compressor.

#### REFERENCES

1. Huppert, Merle C.: Preliminary Investigation of Flow Fluctuations During Surge and Blade Row Stall in Axial-Flow Compressors. NACA RM E52E28, 1952.
2. Huppert, Merle C., and Benser, William A.: Some Stall and Surge Phenomena in Axial-Flow Compressors. Paper Represented at Twenty-First Inst. Aero. Sci. meeting, New York (N.Y.), Jan. 26-29, 1953.
3. Goldstein, Arthur W., Alpert, Sumner, Beede, William, and Kovach, Karl: Analysis of Performance of Jet Engine from Characteristics of Components. II - Interaction of Components as Determined from Engine Operation. NACA Rep. 928, 1949. (Supersedes NACA TN 1701.)
4. Conrad, E. William, Bloomer, Harry E., and Sobolewski, Adam E.: Altitude Operational Characteristics of Prototype Model of the J47D (RX1-1 and RX1-3) Turbojet Engines with Integrated Electronic Control. NACA RM E51E08, 1952.
5. Iura, T., and Rannie, W. D.: Observations of Propagating Stall in Axial-Flow Compressors. Rep. No. 4, Mech. Eng. Lab., C.I.T., Apr. 1953. (Navy Contract N6-ORI-102, Task Order 4.)
6. Foster, D. V.: The Performance of the 108 Compressor Fitted with Low Stagger Free Vortex Blading. Rep. No. R.116, British N.G.T.E., June 1952.
7. Bullock, Robert O., Wilcox, Ward W., and Moses, Jason J.: Experimental and Theoretical Studies of Surging in Continuous-Flow Compressors. NACA Rep. 861, 1946. (Supersedes NACA TN 1213.)
8. Pearson, H., and Bower, T.: Surging of Axial Compressors. The Aero. Quarterly, vol. 1, pt. III, Nov. 1949. (Pub. by Roy. Aero. Soc. (London).)

9. Huppert, Merle C., Johnson, Donald F., and Costilow, Eleanor L.: Preliminary Investigation of Compressor Blade Vibration Excited by Rotating Stall. NACA RM E52J15, 1952.
10. Huppert, Merle C., Costilow, Eleanor L., and Budinger, Ray E.: Investigation of a 10-Stage Supersonic Axial-Flow Research Compressor. III - Investigation of Rotating Stall, Blade Vibration, and Surge at Low and Intermediate Compressor Speeds. NACA RM E53C19, 1953.

3078-C

### ABRUPT DROP IN PRESSURE RATIO AT COMPLETE COMPRESSOR STALL FOR CONSTANT ENGINE SPEED

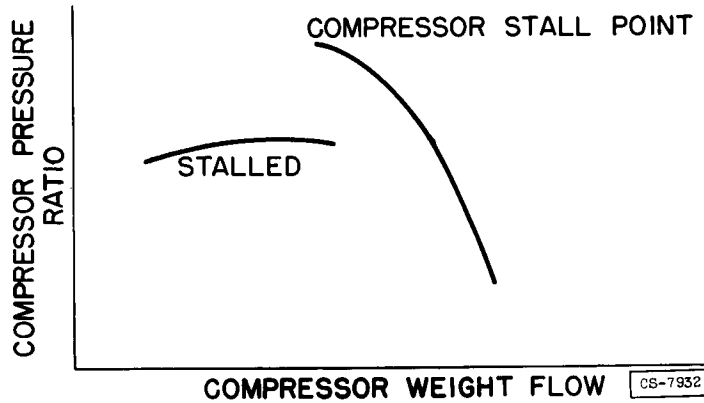


Figure 1

### CORRELATION OF PRESSURE DROP AT STALL WITH COMPRESSOR PRESSURE RATIO AT STALL

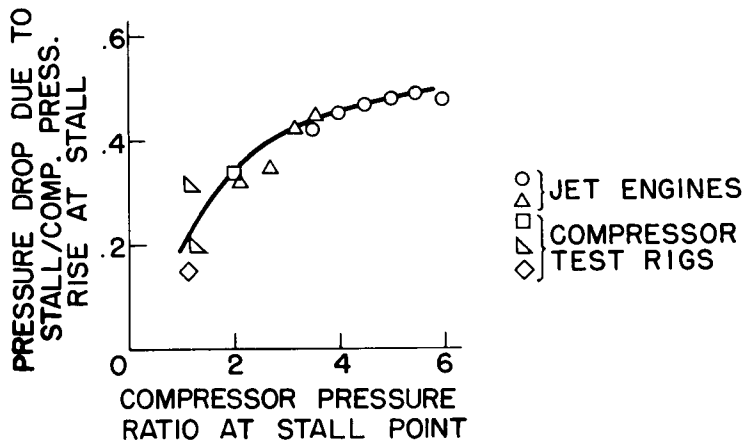
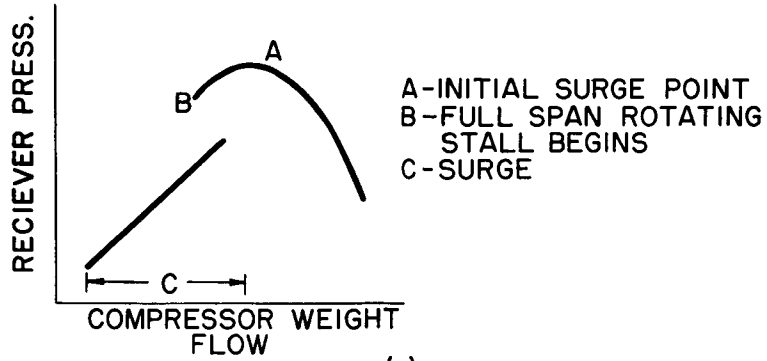
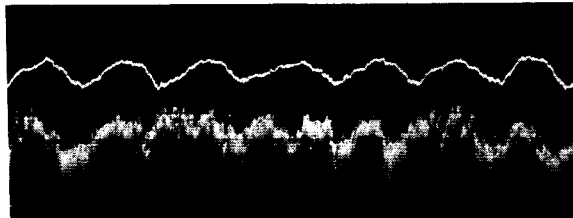


Figure 2

### COMPRESSOR PERFORMANCE MAP SHOWING SURGE AND STALL POINTS



(a)



(b)

Figure 3  
SURGE

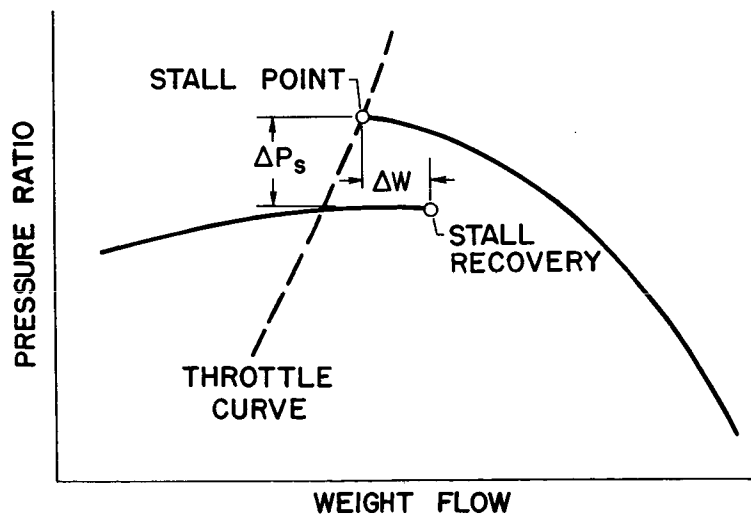


Figure 4

### SURGE OSCILLOGRAMS

SURGE FREQUENCY, 0.57 cps COMPLETE COMPRESSOR STALL, S  
UPPER TRACES BEHIND FIRST ROTOR STALL RECOVERY, R

NO. STALLS



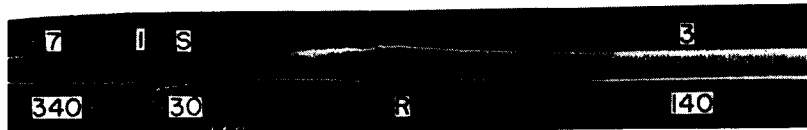
FREQUENCY, cps

(a) LOWER TRACE BEHIND THIRD STATOR.

MASS-FLOW RATE



(b) LOWER TRACE BEHIND SEVENTH STATOR.



TIME

(c) LOWER TRACE BEHIND TENTH STATOR.

Figure 5

ANALYSIS OF THE INTERMEDIATE-SPEED SURGE CHARACTERISTICS OF  
HIGH-PRESSURE-RATIO AXIAL-FLOW COMPRESSORS

By William A. Benser

INTRODUCTION

The dip in the surge or compressor-stall limit of high-pressure-ratio multistage axial-flow compressors presents a serious problem in regard to engine acceleration and high flight Mach number operation, as pointed out in the first paper. Attempts have been made to determine the source of this dip experimentally by means of individual stage data. These experimental approaches show that the dip in the surge-limit line is coincident with stall of the inlet stage, but the occurrence of compressor surge has prevented an evaluation of the effects which led to surge. Therefore, the problem was studied analytically by means of a one-dimensional stage-stacking analysis, in which two variations of stage characteristics were used. The first was based on what would be expected in a multistage compressor, and the second was based on what would be required to eliminate the dip in the surge limit at intermediate speeds.

COMPRESSOR PARAMETERS

For this analysis, a hypothetical 12-stage compressor of constant tip diameter was considered. This compressor, which is representative of current commercial designs, has a design pressure ratio of 7.75 and a flow per unit of frontal area of 26.25. The computed design-point efficiency was slightly over 0.85. The nondimensional performance of all stages was assumed to be identical, except for the stalling characteristics. Stage performance was represented in terms of pressure coefficient and adiabatic efficiency as functions of flow coefficient. These parameters were chosen for simplicity of calculation in the stacking procedure. The pressure coefficient is the ratio of ideal or isentropic work required to produce the stage pressure ratio to the average wheel speed squared. The adiabatic efficiency is the ratio of ideal work input to actual work input, and the flow coefficient is the ratio of average axial velocity to average or mean-radius wheel speed. This method of representing stage performance is a basic one-dimensional approach that neglects the effects of Mach number, Reynolds number, radial maldistribution of flow, and unsteady flow on stage pressure coefficient and efficiency. For this qualitative investigation, the effects of Mach number and Reynolds number are considered unimportant.

## CASE I

For this analysis (case I), the 12-stage compressor was divided into three groups of four stages each with performance characteristics assigned to each group. The assumed stage characteristics for the first group of four stages are given in figure 1. As noted in a previous paper (Huppert and Costilow), interaction effects due to unsteady flows resulting from rotating stall in the first stage may detrimentally affect the performance of several succeeding stages. Therefore, for this analysis a slight discontinuity in the performance of stage 1 was assumed at the stall point (fig. 1). Furthermore, it was assumed that stall of the inlet stage would detrimentally affect the performance of stages 2 to 4. Thus, the performance of stages 2 to 4 was dependent on both the flow coefficient entering these stages and on the operating condition of stage 1. Whenever stage 1 was unstalled, stages 2 to 4 were assumed to operate on the solid or unstalled branch of their performance curve. When stage 1 was stalled, however, stages 2 to 4 were assumed to operate on the stalled or dashed branch of their performance curve. The area variation through these four stages was determined so as to match these stages at the point indicated in figure 1.

The performance characteristics of the second and third groups of stages are given in figure 2. The second group of stages, 5 to 8, was assumed to have first a progressive stall with a continuous decrease in performance as the flow was decreased below the initial stall point. Further reductions in flow were assumed to result in an abrupt stall with the associated discontinuity of performance as indicated. The final group of stages was assumed to have only an abrupt stall with the discontinuity shown in figure 2. These stalling characteristics are consistent with experience on single-stage compressors of comparable hub-tip ratios (see previous paper by Graham and ref. 1). The area ratio was again determined so as to match stages 5 to 12 at the point indicated. The performance of all stages was assumed to be identical, except for the stalling characteristics. No interaction effects were considered for stages 5 to 12.

With these assumed stage characteristics, the reference or match-point total-pressure ratio of the hypothetical compressor was 7.75. The computed performance map is shown in figure 3. These calculations were made for a range of speeds of 50 to 110 percent of the reference value. The maximum flow considered at each speed was that for an assumed choked condition of the exit vanes. At any speed, decreases in pressure ratio below this limit would only increase the exit losses and would not increase the flow through the compressor nor change the operating condition of any stage. The minimum flow considered at each speed was that at which a discontinuity of over-all compressor pressure ratio was encountered. As indicated in the preceding paper, this discontinuity in performance would probably lead to compressor surge. Therefore, this lower limit of flow is designated as the surge limit.

As indicated on the inset performance curve for the first stage, the solid lines on this performance map (fig. 3) represent operation with the first stage unstalled, and the dashed lines represent operation with the first stage stalled and interaction effects in stages 2 to 4. The first-stage stall-limit line is also shown on the over-all performance map, and the shaded area represents operation with the front stages stalled. Thus, the shaded area is a region of potential blade vibration (see papers by Benser and by Calvert and Huppert).

At speeds of 50, 60, and 70 percent, the first stage is stalled at all flows, and stages 2 to 4 also operate on their stall branch as a result of stage interactions (multistaging). Abrupt stall of stage 5 results in a discontinuity of over-all performance which is assumed to precipitate compressor surge. At 80-percent speed, the conditions are identical, except that surge is instigated by abrupt stall of stage 9. For speeds of 85 and 90 percent, the first stage is unstalled at the maximum-flow points. As flow is decreased, the first stage stalls, and this results in a small discontinuity of over-all performance. This discontinuity is amplified by the interaction effects in stages 2 to 4, and the resultant drop in over-all pressure ratio is assumed to precipitate surge. For speeds above 90 percent, the first stage is always unstalled, and surge results from abrupt stall of the last stage of the compressor.

The surge limit faired through the individual surge points at each speed indicates the sharp dip in the surge limit at the intersection of the first-stage stall limit and the high-speed surge limit. Even though this analysis is qualitative, it correlates with experimental results and indicates that the dip in the surge-limit line at intermediate speeds is a result of discontinuities in the performance characteristics of the inlet stages. Since inlet stages do not normally exhibit these discontinuities when tested individually, the sudden deterioration of performance of the inlet stages must be due to interaction effects resulting from rotating stall emanating from the first stage of the compressor. It is possible, however, that certain types of stage design may exhibit discontinuities of performance at their stall points even when tested as single stages.

As can be seen from figure 3, the dip in the surge-limit line is actually a discontinuity. That is, it represents a change from the surge-limit line for speeds where the first stages are stalled at maximum flow to the surge-limit line at speeds where no stages are stalled at maximum flow.

## CASE II

Inasmuch as the analysis of case I indicated the source of the dips in the surge limit at intermediate speeds to be discontinuities in the

performance of the inlet stages, a second case was considered in which continuous characteristics for stages 1 to 4 were used. The characteristics used for these stages are given in figure 4. Unstalled operation of these stages is the same as for the previous case. However, continuous performance at the stall point was considered, and it was assumed that there were no interaction effects for stages 2 to 4. The performance of stages 5 to 12 was assumed to be the same as in the previous case (fig. 2).

The computed performance map for this hypothetical compressor (case II) is given in figure 5. As in case I, performance was computed for a range of speed from 50 to 110 percent of the reference value. The maximum flow considered at each speed was that for the assumed exit-vane choked condition, and the minimum flow at each speed was that at which abrupt stall was encountered in some stage. The point at which this discontinuity occurred was again considered the surge point. Unstalled operation of the inlet stage is represented by the solid curves (see inset of first-stage curve, fig. 5). Stalled operation of the inlet stage is represented by the dashed curves. The shaded portion to the left of the inlet-stage stall limit represents operation with stall in one or more of the inlet stages; whereas, operation to the right of the inlet-stage stall limit represents the condition of no stall in any stage.

As can be seen from the curve for 85-percent speed, there is no discontinuity of over-all performance at the point of first-stage stall. This is to be expected from the shape of the first-stage curve shown in the inset.

The surge-limit line for this case (case II) is relatively smooth, and there is no dip or discontinuity at the intersection of the first-stage stall limit and the high-speed surge limit. Surge at speeds of 50 to 70 percent results from abrupt stall of the fifth stage; at speeds of 80 to 90 percent, from abrupt stall of the ninth stage; and at higher speeds, from abrupt stall of the last or twelfth stage. Comparison of figures 3 and 5 shows that the main gain in surge limit is that the portion of the performance map between 80- and 90-percent speed, which was unavailable for case I because of surge along the inlet-stage stall limit, is now available.

#### CONCLUDING REMARKS

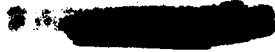
This qualitative analysis indicates that the dip in the compressor surge-limit line at intermediate speeds results from discontinuities in the performance of the inlet stages. This discontinuity can be a result of either the type of stage design or stage interaction resulting from rotating stall emanating from the first stage.

It was also shown that the use of first stages having continuous characteristics at their stall points will result in smooth surge limits at intermediate speeds. Thus, if stages can be designed that are not affected by interactions or that have continuous characteristics even when affected by interactions, the dip in the surge-limit line can be eliminated. Attainment of this goal, however, requires further fundamental research on the problem of stage interactions.

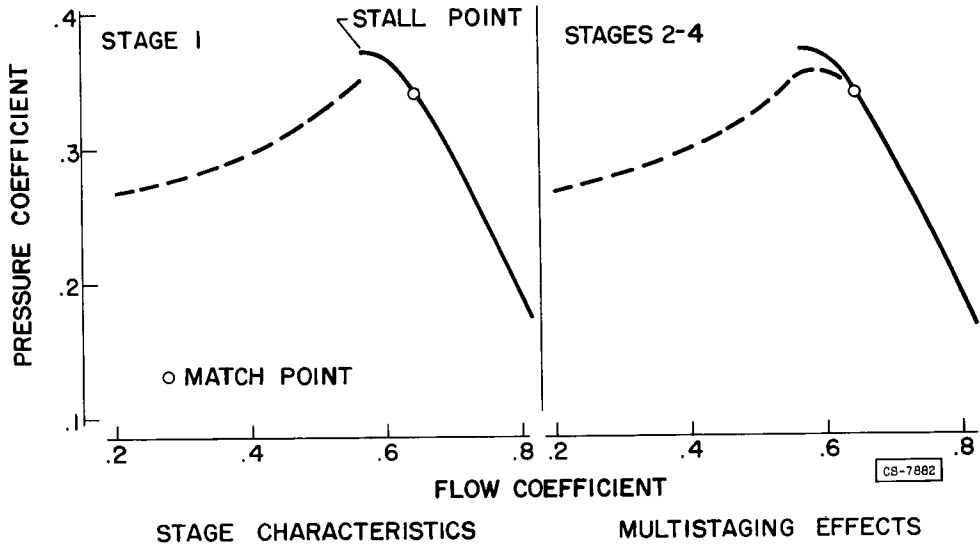
#### REFERENCE

1. Huppert, Merle C.: Preliminary Investigation of Flow Fluctuations During Surge and Blade Row Stall in Axial-Flow Compressors. NACA RM E52E28, 1952.

3078-C



### STAGE PERFORMANCE CHARACTERISTICS



3078-C

Figure 1

### STAGE PERFORMANCE CHARACTERISTICS

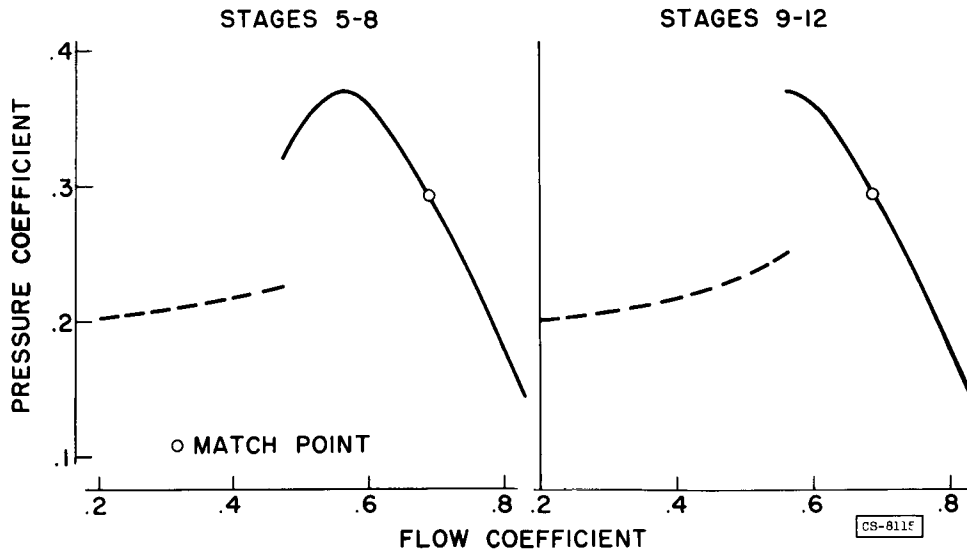
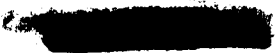


Figure 2



COMPUTED OVER-ALL PERFORMANCE  
CASE I

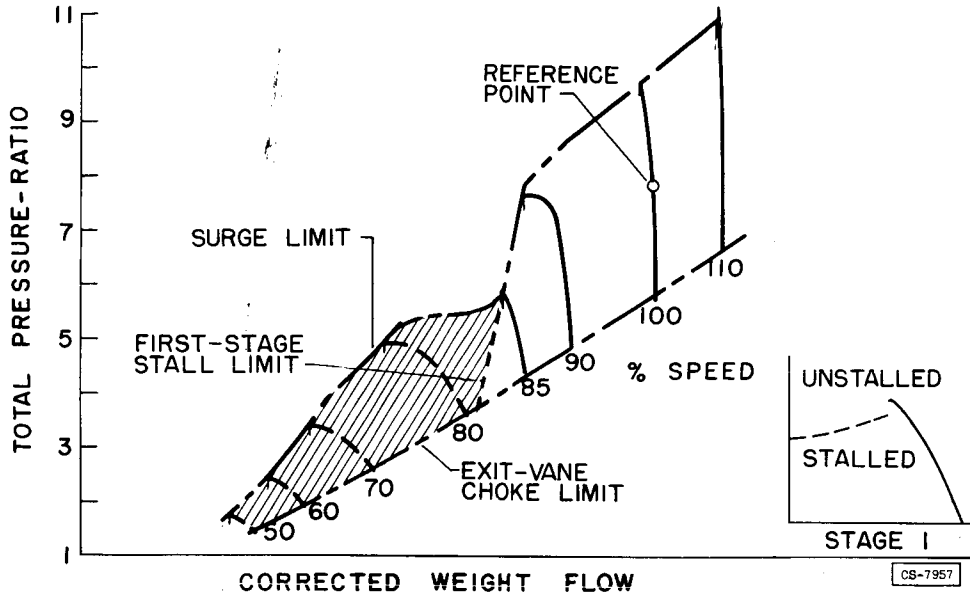


Figure 3

STAGE PERFORMANCE CHARACTERISTICS  
CASE II STAGES 1-4

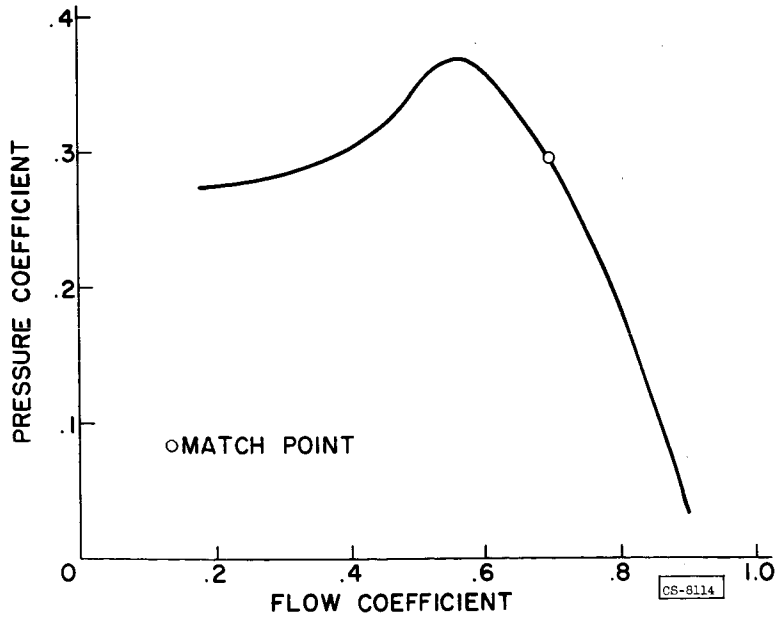


Figure 4

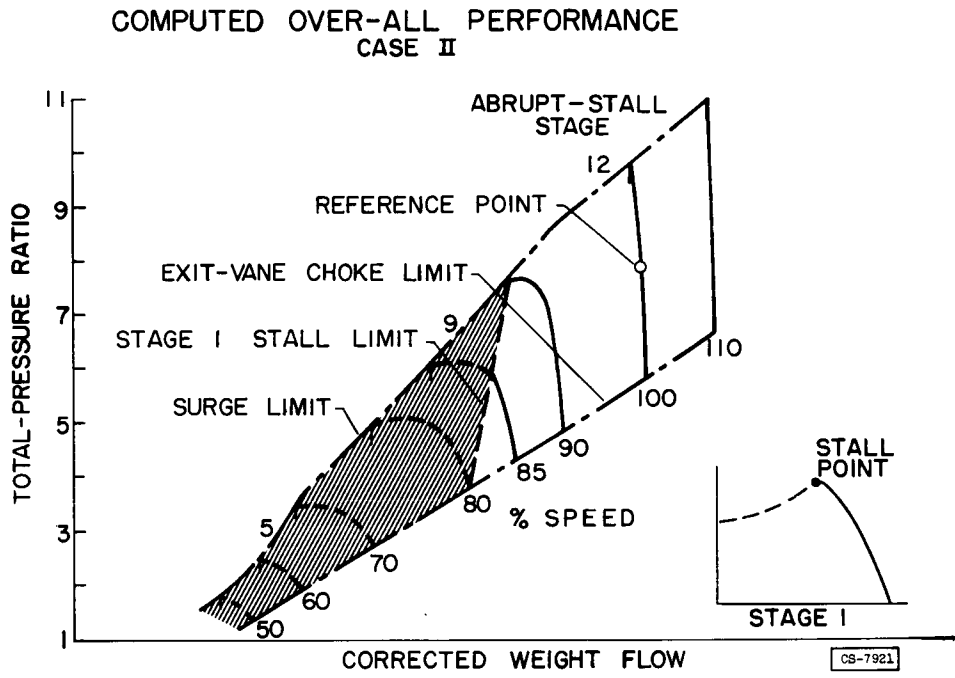
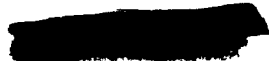


Figure 5



METHODS FOR INCREASING STALL-FREE OPERATING RANGE  
OF MULTISTAGE AXIAL-FLOW COMPRESSORS

By Arthur A. Medeiros

INTRODUCTION

3078 - C

It has been shown in the previous papers that poor low-speed performance, the dip in the stall-limit line at intermediate speeds, and blade vibrations at low speeds can all be associated with rotating stall. Any method for increasing the speed and flow range over which none of the stages are operating stalled will therefore improve the part-speed performance, result in an improved intermediate-speed stall-limit line, and minimize blade vibrations incited by rotating stall. The part-speed performance is important for two reasons: first, the compressor must have a satisfactory surge-limit characteristic to permit rapid acceleration from the idle to take-off condition; second, if the compressor is to be a part of an engine used for supersonic flight at 2.8 Mach number, the compressor may be required to operate efficiently at speeds as low as 71 percent of design take-off speed.

The preceding paper indicates that stall of the inlet stage with its attendant interaction effects results in a severe surge limit at the intermediate speeds. Further, the range of flows and speeds covered by inlet-stage stall is greater than that covered by stall of any other stage. Therefore, the problem can be reduced to finding methods that will delay stall of the inlet stage to lower speeds.

This paper presents some methods available for improving the part-speed performance of axial-flow compressors for good accelerating characteristics and efficient supersonic flight. The methods considered are discussed with relation to single-spool compressors. They could also be applied to twin-spool compressors with the added advantage of a variable ratio of first-spool to second-spool speed, which would permit rematching of the two spools by control of this speed ratio.

GENERAL CONSIDERATIONS

The first paper of this panel showed that, as compressor speed is decreased, the accompanying decrease in pressure ratio across the compressor results in choking of the exit stages. This limits the compressor weight flow that can be handled at speeds below design and forces the inlet stage to operate at decreasing flow coefficients with decreasing speed. At some speed below design, then, the inlet stage will stall.

Further decreases in speed would result in stall of the second stage, then the third, and so forth. However, because of interaction effects, stall of the inlet stage can also result in stall of several inlet stages simultaneously (ref. 1).

In the light of these facts, then, any method that will relieve the choking condition in the exit stages at low speeds will allow a higher inlet weight flow through the compressor and thereby permit the inlet stages to operate stall-free over a wider speed range. Also, any method that allows the inlet stage to operate at a lower angle of attack for any given speed and flow will allow the inlet stage to operate stall-free over a wider speed range. Most of the methods to be discussed are based on one or both of these techniques.

Some of the methods considered are primarily intended to improve the acceleration characteristics of the engine; others to improve the part-speed performance of the compressor for efficient and reliable operation at supersonic flight speeds. The difference in the requirements of these two part-speed problems is in the part-speed weight flow. For supersonic flight, the part weight flow must be high to provide the high thrust required; whereas, for good engine acceleration, it is desirable to keep the weight flow low at speeds below design, in order to permit engine operation at a low pressure ratio or away from the stall-limit line at any given speed.

#### ENGINE ACCELERATION

In order to obtain an engine capable of rapid acceleration during flight maneuvers and take-offs, a large margin between the engine equilibrium operating line and the compressor surge limit is necessary. Therefore, if a severe dip or discontinuity exists in the surge-limit line at intermediate speeds, a severe limit in engine acceleration will be imposed.

The analysis presented in the preceding paper and the experimental results of reference 1 indicate that the dip in the stall-limit line at intermediate speeds and the low compressor efficiencies at low speeds are a result of interaction effects of inlet-stage stall that detrimentally affect the performance of several stages. If the interaction effects of inlet-stage stall can be minimized, it is expected that the dip in the stall limit line can be minimized and higher low-speed efficiencies attained. Figure 1 presents the performance of a ten-stage research compressor with only a slight dip in the stall-limit line at about 72-percent speed. The part-speed efficiencies for this compressor were also quite high (ref. 2). In correlation with the analysis, the stage interaction effects of inlet-stage stall were slight, as indicated by the fact that surge was not instigated when the inlet-stage stall point was encountered at 60 and 70 percent of design speed (fig. 1).

3078-C

Another compressor exhibiting good part-speed performance and only a slight dip in the stall-limit line at intermediate speeds is the eight-stage research compressor, the performance of which is shown in figure 2 and discussed more completely in reference 3. Again the compressor was run through the inlet-stage stall line at 60-percent speed without encountering surge coincident with inlet-stage stall. This fact indicates that the discontinuity in performance of the inlet stages due to inlet-stage stall and interaction effects was insufficient to cause surge.

The performance of these two compressors indicates that some control over the interaction effects of inlet-stage stall can be achieved. However, with present knowledge, this control cannot be predicted from the usual compressor design criteria. Further, even without the dip in the stall-limit line, acceleration at low speeds would probably be sluggish, so that some method of shifting the stall-limit line and the engine equilibrium operating line away from each other is necessary to obtain good acceleration characteristics.

Compressor-discharge air bleed. - If air is bled from the discharge of the compressor, the weight flow through the turbine nozzles is decreased. The decrease in weight flow can be accompanied by a decrease in turbine-inlet (or compressor-outlet) pressure. Therefore, as air is bled from the compressor discharge, the equilibrium operating line moves to a lower compressor pressure ratio or away from the surge limit, and the acceleration margin is improved. Reference 4 presents an analytical evaluation of the effect of compressor-discharge air bleed on engine acceleration.

Interstage air bleed. - Inasmuch as the exit stages of the compressor limit the flow at part-speed and force the inlet stage to operate in a stall condition, air could be bled from the exit stages that are limiting the flow. This would permit a higher weight flow through the inlet stages before choking of the exit stages occurs and thereby allow the inlet stages to operate at lower speeds before the stall point of these stages is reached. The stall-free operating range of the compressor would therefore be increased, which would decrease the range of speeds over which stall-incited blade vibrations would be encountered. The engine acceleration characteristics would be improved because of the rematching of compressor and turbine accomplished by the air bleed, and the improved compressor stall-limit line achieved by rematching the stages of the compressor by the interstage air bleed. The potentialities of interstage air bleed are discussed in reference 5, which presents the results of an analysis of air bleed in various stages of a 16-stage compressor.

Adjustable guide vanes. - Perhaps a more direct approach to delaying inlet-stage stall would be the use of adjustable guide vanes. In this case, as the speed of the compressor is decreased, the turning through the guide vanes is increased by increasing the setting angle of the vane so that for any given flow the average angle of attack on the first rotor is decreased, and thus the inlet flow and hence the speed at which the inlet stage will stall are decreased. An example of the effectiveness of resetting inlet guide vanes on compressor performance is given in reference 1 where it is shown that the speed at which inlet-stage stall and the dip in the stall-limit line occur can be decreased by increasing the guide-vane turning angle.

Compressor-discharge air bleed, interstage air bleed, and adjustable guide vanes can all be used to improve engine acceleration characteristics, and interstage air bleed and adjustable guide vanes can be used to increase the stall-free operating range of the compressor. The use of any of these methods introduces a control problem, since the air bleed must be cut off at high speeds, and, in the case of adjustable guide vanes, the vane must be returned to its design setting at higher speeds in order to attain design weight flow and engine thrust at design conditions. Further, these methods are not desirable in an engine for supersonic flight, because the weight flow at the intermediate compressor speeds at which the engine would operate would probably be decreased, and, therefore, maximum thrust for these speeds would not be attained.

#### SUPERSONIC FLIGHT

The compressor for an engine to be used in supersonic flight must have a high efficiency and a high weight flow at the intermediate speeds at which it must operate (71-percent speed at a flight Mach number of 2.8). Further, it must have a favorable intermediate-speed surge line so that compressor surge is not encountered as flight Mach number is increased, and it must be stall-free at the intermediate speeds so as to avoid stall-incited blade vibrations in the normal engine operating range.

Stage-matching compromise. - The case II compressor of the preceding paper was calculated with smooth continuous performance curves in the first four stages. The result was a compressor having a smooth continuous surge line; however, the inlet-stage stall line in this compressor intersected the surge line at 91-percent speed, so that inlet-stage stall would be encountered over a large part of the operating map. If some sacrifice in low-speed surge margin can be tolerated, it may be possible to decrease the speed at which inlet-stage stall occurs and increase the part-speed weight flow and compressor efficiency by compromising the match points of the individual stages at the design condition. Inasmuch

as the flow coefficient for the inlet stages decreases and the flow coefficient for the exit stages increases with decreasing compressor speed, the inlet stages could be set at a flow coefficient greater than that for maximum efficiency at the design condition and the exit stages could be set at a flow coefficient less than that for maximum efficiency at design conditions. The middle stages remain at essentially the design flow coefficient over the entire speed range of the compressor and could, therefore, be set at their maximum efficiency point. In general, this technique would be expected to reduce design-point efficiency somewhat.

The effectiveness of this method was investigated analytically by utilizing a one-dimensional stage-stacking technique. Figure 3 presents the flow-coefficient - pressure-coefficient stage curves used in the calculation. They are identical to those used for the case II compressor of the preceding paper. The stages in the case II compressor were all set to operate at a flow coefficient of 0.69 at design speed and flow. The operating points for the various stages in the compromise design are shown in figure 3. This compromise can be considered as matching the stages so that they all operate at approximately the reference flow coefficient of 0.69 at some speed below design. An additional stage was required in the compromise design so that the surge margin at high speeds could be maintained. This would, of course, add to engine weight and hence is an undesirable feature of this method.

The pressure-ratio - weight-flow characteristics of the compromise configuration are compared with those of the case II compressor in figure 4. The surge lines for both configurations are about the same at high speeds; but at low speeds, the calculated surge limit for the case II compressor is slightly more favorable. However, the first-stage stall line for the compromise design intersects the surge line at 87-percent speed as compared with 91-percent speed for the case II compressor, so that if stage interaction effects attending inlet-stage stall had been assumed, it is probable that the intermediate-speed surge limit would be more favorable for the compromise design. Staging or interaction effects cannot be quantitatively evaluated; therefore, not much can be said about the surge line below the speed for inlet-stage stall. The weight flow at the intermediate speeds is slightly higher for the compromise design that would be favorable for supersonic flight.

By compromising the stage-matching points, it may be possible to increase the stall-free operating range and increase the flow and efficiency at the compressor speeds encountered in supersonic flight, with possibly only a small penalty in surge margin at low speeds. However, at least one additional stage would be required to maintain the high-speed surge margin.

Adjustable exit stators. - Another possibility for improving the intermediate-speed performance and increasing the part-speed weight flow would be to reset the stator blades in the exit stages. Inasmuch as these stages limit the weight flow at intermediate and low compressor speeds, the stator blades could be reset at these speeds so that they may pass a higher weight flow, which would allow a higher weight flow through the inlet stages and a lower compressor speed before inlet-stage stall is reached. The choke flow for the exit stages can be increased by decreasing the setting angle (with respect to the axis of the compressor) of the stator blades in these stages. For any given flow coefficient, therefore, the angle of attack would be increased into the following rotor row. To avoid compressor surge at high speed, the blade angles would be returned to design setting; therefore, this method would require some control to adjust the exit-stage stator blade angles with speed. This would add to the complexity and weight of the engine, and, therefore, the method would not be wholly satisfactory for supersonic-flight application.

Reference 1 presents the effect on compressor performance of a small resetting ( $6^\circ$ ) for the stator blade angles in the twelfth to fifteenth stages of a 16-stage compressor. These blades could, of course, be reset a greater amount to obtain even larger increases in part-speed weight flows and efficiencies than those indicated in reference 1.

#### CONCLUDING REMARKS

Good part-speed performance and smooth continuous surge lines can be attained by the use of inlet stages that are not susceptible to interaction effects. Since this goal is not always achieved, some other methods of improving part-speed performance must be employed.

If the only purpose is to improve the acceleration margin of the engine in which the compressor is used, compressor discharge air bleed, interstage air bleed, or adjustable guide vanes may be used. These methods usually result in decreased weight flow available for thrust at the intermediate compressor speeds encountered in supersonic flight.

In order to improve the part-speed weight flows and efficiencies and increase the stall-free operating range for supersonic flight, proper compromising of the stage-matching points can be used to obtain slight improvements in part-speed performance. Some penalty in high-speed performance would, of course, be expected from such a compromise.

If the complexity of a variable-geometry engine is warranted or necessary, the use of adjustable exit-stage stator blades could be used to increase the part-speed weight flow and improve the part-speed performance for supersonic flight.

## REFERENCES

1. Medeiros, Arthur A., Benser, William A., and Hatch, James E.: Analysis of Off-Design Performance of a 16-Stage Axial-Flow Compressor with Various Blade Modifications. NACA RM E52L03, 1953.
2. Budinger, Ray E., and Thomson, Arthur R.: Investigation of a 10-Stage Subsonic Axial-Flow Research Compressor. II - Preliminary Analysis of Over-All Performance. NACA RM E52C04, 1952.
3. Geye, Richard P., Budinger, Ray E., and Voit, Charles H.: Investigation of High-Pressure-Ratio Eight-Stage Axial-Flow Research Compressor with Two Transonic Inlet Stages. II - Preliminary Analysis of Over-All Performance. NACA RM E53J06, 1953.
4. Rebeske, John J., Jr., and Rohlik, Harold E.: Acceleration of High-Pressure Ratio Single-Spool Turbojet Engine as Determined from Component Performance Characteristics. I - Effect of Air Bleed at Compressor Outlet. NACA RM E53A09, 1953.
5. Rebeske, John J., Jr., and Dugan, James F., Jr.: Acceleration of High-Pressure-Ratio Single-Spool Turbojet Engine as Determined from Component Performance Characteristics. II - Effect of Compressor Interstage Air Bleed. NACA RM E53E06, 1953.

3078-2

### OVER-ALL PERFORMANCE 10-STAGE RESEARCH COMPRESSOR

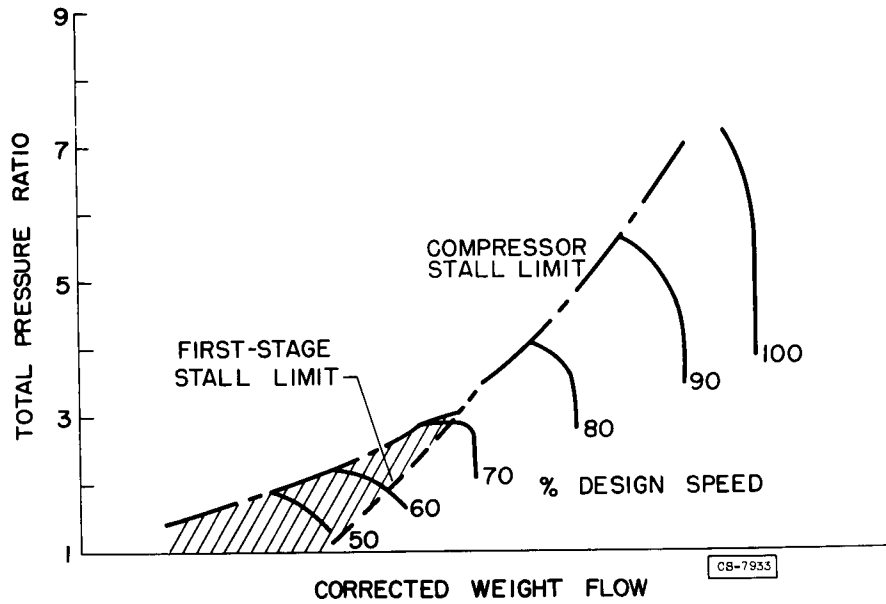


Figure 1

### OVER-ALL PERFORMANCE 8-STAGE RESEARCH COMPRESSOR

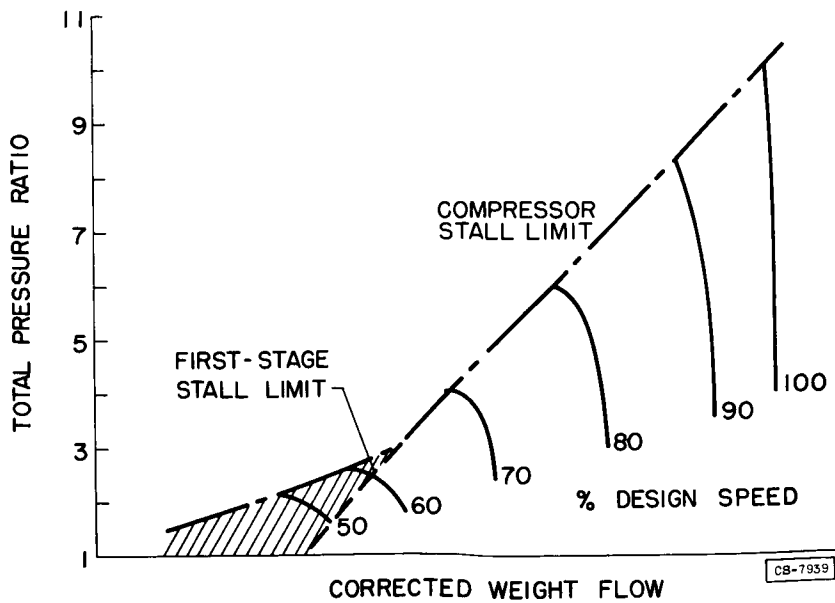


Figure 2

3078-C

### STAGE MATCHING POINTS FOR COMPROMISE DESIGN

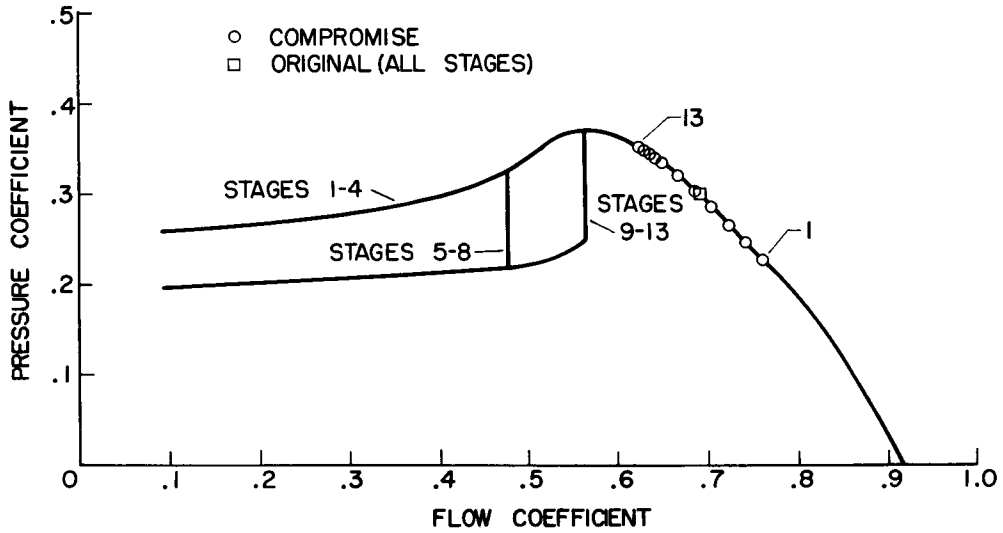


Figure 3

### COMPARISON OF PERFORMANCE

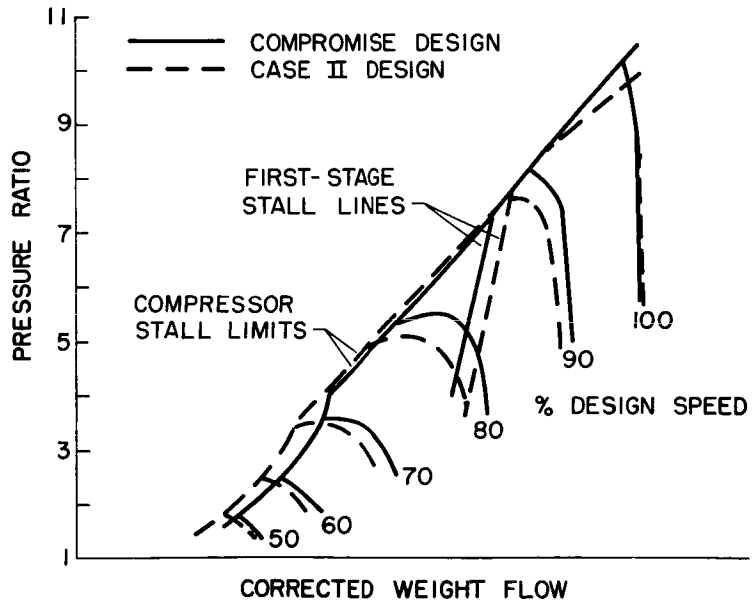
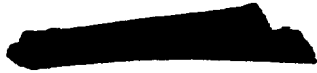


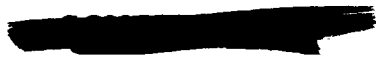
Figure 4

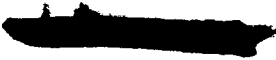
3078-C



IV - TURBINE COOLING PANEL

H. H. Ellerbrock  
J. B. Esgar  
R. O. Hickel  
R. R. Ziemer  
P. L. Donoughe





## THE ROLE OF TURBINE COOLING IN FUTURE AIRCRAFT ENGINES

By Jack B. Esgar and Richard J. Rossbach

### INTRODUCTION

3078-D

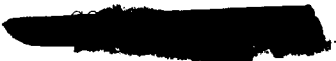
Research has been conducted on cooled turbines at the NACA Lewis laboratory for several years because it was recognized that the cooling of turbines will become more and more necessary as flight speeds increase. In previous conferences, results of NACA research in this field have been presented showing how application of turbine cooling would permit use of noncritical materials and high turbine-inlet temperatures. The papers on turbine cooling for this conference present the results of research conducted within the last year, and an indication is given about how cooling will also permit flexibility in the turbine design so that the requirements for supersonic flight other than high turbine-inlet temperature can be obtained. Such requirements result in high turbine stresses. This aspect of turbine-cooling research has not been presented before.

In previous papers dealing with the objectives of future compressor design, it was shown that the over-all goals are reduced size and weight of the component, with a result that research is being directed towards high pressure ratios per stage to reduce length, and high mass flows per unit of compressor frontal area to decrease diameter. The high pressure ratios per stage will be obtained by increasing the compressor tip speeds, which generally results in increased rotative speeds. Increasing mass flows per unit frontal area together with increasing rotative speeds will cause a considerable modification in present concepts of turbine design.

### DISCUSSION

#### Factors Affecting Turbine-Blade Stress

Many turbines at the present time are operating with a nearly axially choked rotor. This condition precludes the possibility of increasing the mass flow per unit frontal area of a turbine driving a fixed-pressure-ratio compressor at a constant value of the ratio of the turbine-inlet to compressor-inlet temperature unless the turbine-annulus area is increased. It can be shown that the centrifugal stress in a turbine blade is proportional to the turbine-annulus area and the square of the rotative speed; therefore, it is apparent that compressors of the future with high mass flow per unit frontal area and high tip speed can be realized only if the stress levels in the turbine can be increased.



An illustration of how increased turbine-blade stress level can affect engine performance is shown in figure 1, where for a constant value of thrust specific fuel consumption and a turbine-inlet temperature of 1540° F, the percent increase in engine thrust per unit of turbine frontal area is shown plotted against turbine-blade-root stress. The engine-performance results shown on this and other curves to be presented were obtained from a theoretical analysis in which the effects were determined of stress level, air cooling, and turbine-inlet temperature on the performance of turbojet engines driven by single-stage turbines, which were assumed to operate at realistic (but somewhat futuristic) aerodynamic limits. In the analysis, the specification of the aerodynamic limits on the turbine and the commensurate aero-thermodynamic limits on the remainder of the engine components, namely the compressor, the primary burner, and the afterburner, made it possible to relate the engine air-handling capacity and the compressor pressure ratio to the turbine-inlet temperature, the turbine-blade-tip speed, the blade hub-tip radius ratio, and the coolant-flow ratio (ratio of cooling-air flow to compressor air flow). The calculations were made for an engine operating at a flight Mach number of 2 and an altitude of 50,000 feet.

From the results of a portion of this analysis (fig. 1) it can be seen that for a single-stage turbine, over 60-percent increase in thrust per unit frontal area is possible by increasing the turbine-blade stress level in order to permit the higher rotative speeds and larger annulus areas that were previously discussed as being necessary for compressors with high mass flow and high pressure ratio per stage. Multistage turbines will allow further increases in thrust as stress is increased.

The permissible turbine-blade stress level is fixed by the stress-to-rupture characteristics of the blade material. Curves of stress to rupture for a range of temperature and for a range of rupture time from 10 to 1000 hours are shown in figure 2 for a good high-temperature alloy (S-816) commonly used in gas-turbine blades. At a stress level of approximately 60,000 pounds per square inch, the material exhibits a 0.2-percent yield, which is also considered a limiting criterion in blade strength; consequently, the stress-to-rupture curves are not extended above the stress for 0.2-percent yield. For the material shown, the yield stress is essentially independent of temperature. Also superimposed on figure 2 are the ranges of turbine-blade-root stresses for current turbojet engines and for future proposed engines having compressors with mass flows of 35 pounds per second per square foot of compressor frontal area and compressor tip speeds of 1400 feet per second.

In order to illustrate the problem associated with high turbine-blade stresses, a present-day turbine, designed for a 1000-hour life and a root stress of 20,000 pounds per square inch, is considered. It can be seen that the maximum blade operating temperature will be on the

order of 1450° F. If a new engine is designed that utilizes a high-mass-flow compressor resulting in a turbine-blade-root stress of 40,000 pounds per square inch (the minimum stress shown on fig. 2 for future engines), there are two ways of designing the turbine blades to withstand the required stress level. The first method is to design for only a 10-hour life instead of for a 1000-hour life and to leave the blade metal temperature unchanged. This type of design may possibly be satisfactory for a missile, but it would be highly dangerous for a piloted aircraft. The second method is to design for a long life, such as 1000 hours, and to reduce the metal operating temperature from 1450° to about 1250° F. As will be discussed in subsequent papers, however, high turbine-inlet temperatures on the order of 2000° to 2500° F are highly desirable in order to obtain satisfactory performance of flight speeds on the order of Mach 2 and above. It is apparent, therefore, that new turbine materials must be developed that can withstand high stresses at much higher temperatures than presently encountered, or else some means is required to make the turbine-blade-metal temperature independent of the gas temperature. An obvious solution, of course, is to provide some means of cooling the gas-turbine blades.

#### Effects of Cooling Gas-Turbine Blades

Increased cooling above that required for materials such as S-816 in order to further reduce the blade-metal temperature will provide an opportunity to use materials exhibiting strength properties at lower operating temperatures that are superior to the properties obtained from high-temperature materials. The use of cooling, therefore, permits a wider selection of turbine-blade materials, which often results in higher permissible stress levels as shown in figure 3. The 100-hour stress-to-rupture and the 0.2-percent yield curves from figure 2 are again shown in figure 3. In addition, the 100-hour stress-to-rupture and 0.2-percent yield curves are shown for A-286, a material that is considerably less critical than the high-temperature alloy S-816. Materials such as A-286 are not used in turbine blades at the present time because they have relatively poor strength properties in the range of temperature required for uncooled turbines. If such materials are cooled to temperatures less than about 1200° F, however, they exhibit strength properties that are considerably superior to the properties of the high-temperature alloys currently in use. The importance of the possibility of using such materials in cooled turbines is apparent from figure 2, where it is shown that the range of required blade stresses for future engines exceeds the maximum permissible stress for a material such as S-816.

At the present stage of development of turbine cooling, it is not possible to operate turbine blades at the stress levels that are indicated in figure 3 by substituting different materials and cooling them

to a low operating temperature, since completely uniform cooling of the blades has not as yet been obtained and the use of brazed, thin-sheet construction introduces unknowns in permissible stress levels. Experience has shown the necessity of applying a higher factor of safety to the design stresses for air-cooled turbine blades than has been required for uncooled blades. As yet the magnitude of this factor has not been adequately determined, nor have all the fundamental causes of the increased factor of safety been isolated. There are indications, however, that the required factor of safety is small enough to make it profitable to cool blades to the temperature required to utilize higher-strength materials.

### Air-Cooled Engine Configuration

The use of cooling to permit increased stress levels and increased turbine-inlet temperatures has been shown to be desirable. The next question is how to incorporate cooling into the turbojet engine. In figure 4 is shown a cross-sectional view of a turbojet engine with modifications to permit air cooling of the turbine. There are many possible arrangements for ducting cooling air to the turbine and many types of cooled turbine disks and blades that appear practical. Shown on figure 4 is one arrangement that appears promising. High-pressure air is bled from the compressor discharge (or possibly from one of the last stages) and is ducted out through the disk to the turbine blades. In the arrangement shown, the cooling air is discharged at the blade tips and mixes with the gas stream. The possibility exists that by special construction the cooling air would not be discharged in a high-pressure area of the gas stream; in this case, ram air could be used for cooling both rotor and stator blades at high flight speeds. At lower speeds, however, compressor bleed air will be required for both rotor and stator-blade cooling in a manner similar to that shown in the figure. The stator-cooling air does not necessarily have to be ducted back into the gas stream; however, cooling losses are minimized if the cooling air is ducted to obtain increased thrust.

In figure 5, the details of an air-cooled turbine rotor are presented. The rotor shown is similar to a conventional uncooled turbine rotor except that the turbine shaft is made hollow to provide a path for the cooling air and a shroud is attached to the downstream face of the disk to duct the cooling air out to the blades. Vanes are used to form a centrifugal pump for the cooling air and to insure satisfactory distribution of the cooling air to each of the cooled blades. At the turbine-blade base, the cooling air is ducted under the blade to supply cooling air around the complete periphery of the blade. Many types of cooled-blade configurations can be used in the turbine. Various turbine-rotor and blade configurations are discussed in subsequent papers.

## Use of Liquid-Cooled Turbines

Liquid cooling could also be utilized in gas-turbine engines, and there are certain advantages to be gained in performance over that obtained by air cooling, as is discussed in a subsequent paper by J. C. Freche. On the other hand, liquid cooling may not be practical at high flight Mach numbers because, as is discussed in a subsequent paper by J. E. Hubbartt, ram air temperatures become so high that the coolant boiling point is exceeded and it is not possible to reject heat from the coolant to ram air by means of a radiator. Bleeding air from the compressor and using it for turbine cooling appears to be a more practical solution; consequently, most of the discussion in this and subsequent papers on turbine cooling will be concerned with air cooling only. Some of the performance gains that can be expected by use of air cooling to permit increases in turbine-inlet temperature will now be discussed.

## Potential Engine Performance with Air-Cooled Turbines

One of the goals in engine research is to obtain high thrust per unit engine frontal area at low engine weight and low specific fuel consumption. One of the methods of obtaining the greatest amount of thrust for the lowest engine weight is to increase the gas temperature level in the engine. The turbojet-engine thrust increases that can be obtained and the resulting effect on specific fuel consumption by increasing the turbine-inlet or afterburner temperature from 1540° to 3000° F were obtained from the analysis previously discussed and are shown in figure 6. At the present time, the usual method of augmenting thrust is to use an afterburner. In figure 6, it is shown that an increase in thrust per unit frontal area of almost 150 percent ( $2\frac{1}{2}$  times the unaugmented thrust) can be obtained by using an afterburner, at a cost of approximately 60-percent increase in thrust specific fuel consumption. This thrust increase would be obtained at an afterburner temperature of about 3000° F and a turbine-inlet temperature of 1540° F for the conditions of these calculations. The same thrust per unit frontal area can be obtained for a nonafterburning engine by increasing the turbine-inlet temperature to approximately 2500° F at a cost of only 14-percent increase in thrust specific fuel consumption.

Operation at a turbine-inlet temperature of 2500° F is not feasible unless some means of cooling the turbine is utilized. Cooling will result in some loss in engine performance, but using 15 percent of the compressor air for turbine cooling and boosting the turbine-inlet temperature to something less than 3000° F without afterburning will result in a 150-percent increase in thrust per unit frontal area at a cost of about 21-percent increase in thrust specific fuel consumption.

In other words, by using turbine cooling to permit increased turbine-inlet temperature levels and by accounting for air-cooling losses, the same thrust addition can be obtained as was obtained with an afterburner with only 1/3 as much extra fuel being required. In many cases, the air-cooled engine also will be considerably lighter than the afterburner engine, so that the same thrust is obtained with savings in both fuel and engine weight.

The comparison made in figure 6 does not mean that the afterburner will no longer be useful when high turbine-inlet temperatures are obtained. For many applications it will be desirable to combine both high turbine-inlet temperatures and afterburning because of the thrust augmentation that is possible through use of the afterburner. For a constant afterburner temperature, the thrust specific fuel consumption will decrease as the turbine-inlet temperature is increased with the result that there will be smaller differences between the fuel consumptions for afterburning and nonafterburning engines. In addition, higher thrust levels per unit frontal area will be possible than can be obtained by either the high turbine-inlet-temperature nonafterburning engines or low turbine-inlet-temperature afterburning engines. For this case where high turbine-inlet temperatures and afterburning are combined, the thrust specific engine weight will probably be less than for high-temperature nonafterburning engines. As a result, it can be concluded that high turbine-inlet temperatures made possible through use of turbine cooling will be desirable for either afterburning or nonafterburning engines in order to obtain very high values of thrust per unit frontal area from turbojet engines.

Although the results shown in figure 6 indicate that very large gains in thrust can be made through the use of turbine cooling to permit higher turbine-inlet temperatures, the gain is made at the cost of increased thrust specific fuel consumption. The results shown are for a constant turbine tip speed and a constant turbine-annulus area. If, however, the turbine tip speed and annulus area are permitted to vary, it is possible to design engines so that significant gains in engine thrust per unit frontal area are possible without increasing the thrust specific fuel consumption or the turbine-blade stress, as shown in figure 7. The results shown are for a series of engines, all of which require the maximum output obtainable from a single-stage turbine. Because the thrust specific fuel consumption was not allowed to increase, the gains in thrust per unit frontal area, although appreciable, are less than shown in figure 6 for equivalent increases in turbine-inlet temperature. It is shown in figure 7 that by including the effects of using up to 15 percent of the compressor air flow for cooling, an increase in thrust of up to 65 percent is possible without increasing thrust specific fuel consumption or blade-stress level. By combining the effects of increased gas temperature and increased blade stress, even greater increases in thrust than shown in figure 7 are possible at no cost in thrust specific fuel consumption.

Figures 1, 6, and 7 show how turbojet engine performance can be improved through the use of turbine cooling to permit increases in both turbine-inlet temperatures and turbine-blade stress level. The final criterion, however, as to whether the use of cooling is advantageous is to consider the performance of aircraft in which a comparison is made with the performance of both low gas-temperature uncooled engines and high gas-temperature cooled engines. The results of such comparisons will be given in a subsequent paper by Luidens, Henneberry, Zimmerman, and Evans. It is possible to conclude from the results of the present paper, however, that the gains shown in engine thrust per unit frontal area at little or no sacrifice in thrust specific fuel consumption will always result in improved aircraft performance so long as engine weight is not adversely affected. In general, for the type of operation considered, the thrust increases obtained by the use of high-temperature and high-stress cooled engines, far outweigh any increases in engine weight, so that the thrust specific engine weight actually decreases. Consequently, the use of high temperatures or turbine stresses, as permitted by turbine cooling, will be beneficial.

#### CONCLUDING REMARKS

Much research is required in order to obtain a fundamental understanding of effective means of cooling turbines before gas-turbine engines can actually be operated at the high-temperature, high-stress conditions shown to be beneficial in this paper. Fortunately, much of this type of research can be conducted in engines operating at current gas-temperature levels; consequently, nearly all the research that has been conducted by the NACA to date has been at turbine-inlet temperatures on the order of 1650° F or lower. In addition, considerable research effort has been expended to investigate the use of noncritical materials in cooled turbines. Some of this research on turbine cooling will be discussed in subsequent papers.

3078-D

THRUST INCREASE PERMITTED BY INCREASED BLADE STRESS

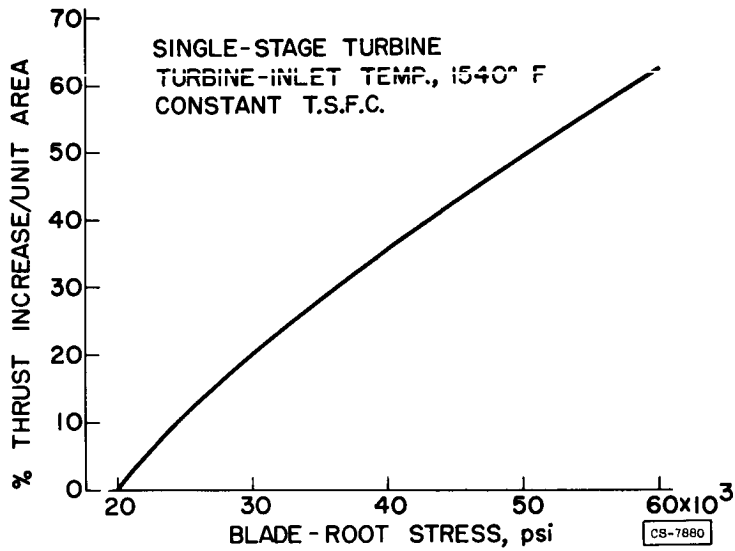


Figure 1

STRESS-TO-RUPTURE FOR S-816 ALLOY

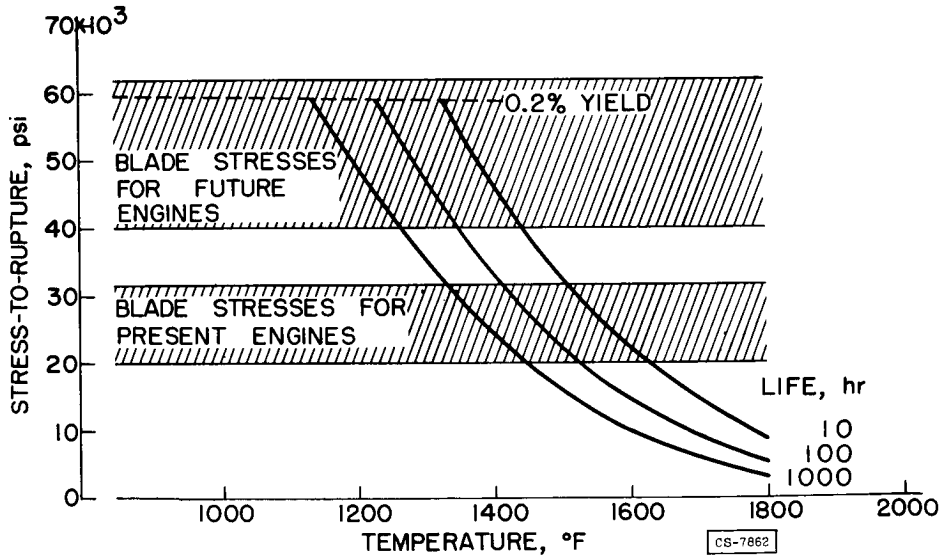


Figure 2

3078-D

### INCREASED STRESSES ALLOWABLE BY MATERIAL SELECTION AIR-COOLED BLADES

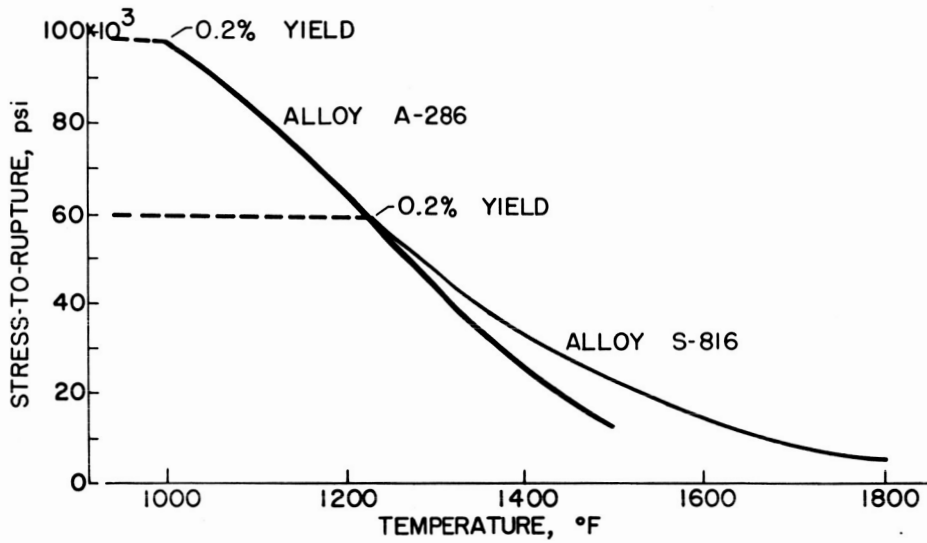


Figure 3

### CROSS SECTION OF AIR-COOLED TURBOJET ENGINE

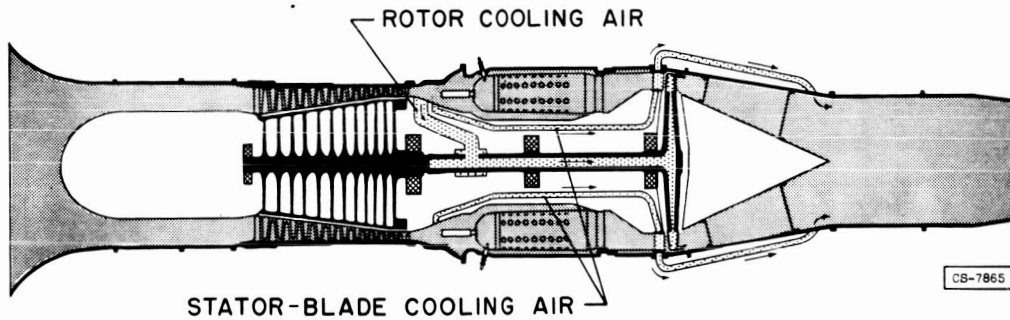


Figure 4



### AIR-COOLED TURBINE ROTOR

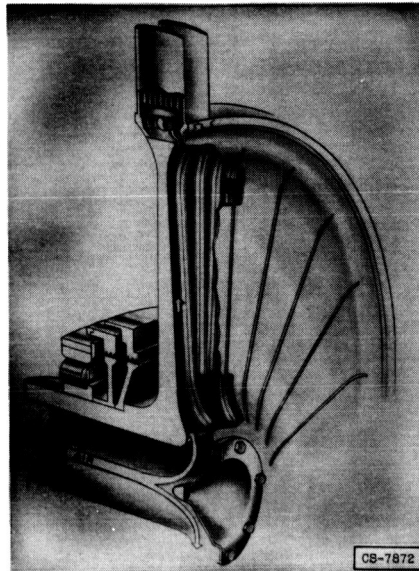


Figure 5

3078-D

### EFFECT OF INCREASED TEMPERATURE ON THRUST AND FUEL CONSUMPTION FLIGHT MACH NO., 2.0

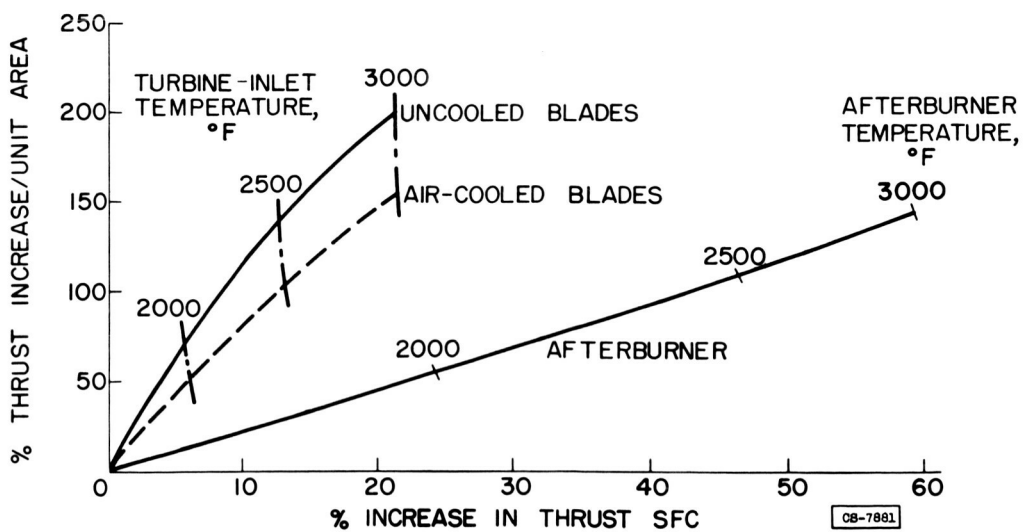


Figure 6



INCREASED THRUST OBTAINABLE AT CONSTANT BLADE  
STRESS AND SPECIFIC FUEL CONSUMPTION

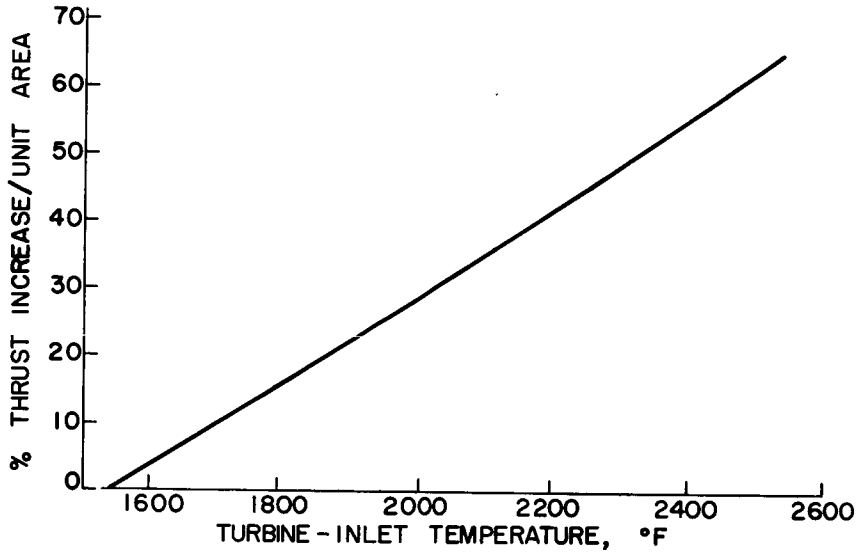


Figure 7

## INVESTIGATIONS OF AIR-COOLED SHELL-SUPPORTED TURBINE BLADES

By Robert O. Hickel and John L. Clure

## INTRODUCTION

In view of the performance gains that may be achieved through the medium of turbine cooling, as indicated in the paper by Esgar and Rossbach, the NACA has done considerable analytical and experimental turbine-cooling research since the end of World War II. The first phase of the research has been applied to forced-convection air-cooled turbine blades. This paper reviews briefly some of the past research in this field and summarizes the progress made in the last year or so toward obtaining satisfactory forced-convection air-cooled shell-supported turbine blades.

An air-cooled shell-supported turbine blade is one in which the airfoil section itself is the main load-carrying member. Two views of a typical shell-supported blade are shown in figure 1. The shell is hollow so that cooling air may flow through the interior of the blade from root to tip (fig. 1(a)). The shell may be made in a number of ways, such as casting, press-forming from a round tube, or press-forming the shell in two halves from sheet steel and then welding the two halves together along the leading and trailing edges. The base can be cast or forged in one or two pieces or machined from a single steel blank in such a manner that cooling air can be introduced into the blade shell. The shell can be attached to the base by welding or brazing methods. It is also feasible to fabricate the shell and base as an integral unit by machining or casting processes.

The general fabrication procedure applied to the blades discussed herein is that in which the base is cast in one piece with an airfoil-shaped hole in the central portion. The blade is formed by pressing a tapered tube to the desired airfoil shape, inserting this shell in the base and brazing the two together. On final machining operations, the blade is cut to proper length and the base serrations are ground.

In order to increase the cooling effectiveness of air-cooled turbine blades and thus reduce the cooling-air mass-flow requirements to a minimum, some method of increasing the internal heat-transfer surface area above that of a plain hollow blade is necessary. The blades discussed herein had their internal heat-transfer surface area increased by the use of tubes or fins, which were placed in the core of the blade. A view of a completed tube-filled blade is shown in figure 1(b). The various blade configurations, fabrication procedures, and experimental results obtained with shell-supported air-cooled blades are discussed in greater detail in the following sections.

[REDACTED]

PROBLEMS ENCOUNTERED IN DEVELOPMENT OF CONVECTION-AIR-COOLED  
SHELL-SUPPORTED BLADES

Considerable research has been and is continuing to be done in order to obtain air-cooled blades that are satisfactory with respect to cooling effectiveness, cooling-air pressure losses, and life. For present-day turbojet engines, the cooling effectiveness should be such that the turbine blades can be adequately cooled with cooling-air-flow rates on the order of about 2 to 4 percent of the combustion-gas-flow rate. (Hereinafter, the ratio of cooling-air to combustion-gas flow rate will be called coolant-flow ratio.) Cooling-air pressure losses should be low enough that the cooling air can be bled from the engine compressor at low pressure levels. Blade life should be such that a minimum of 100 hours at rated engine conditions can be expected without blade failure.

In the past several years, considerable emphasis has been directed toward the reduction of critical materials used in turbine blades, and the greater portion of NACA Lewis research on shell-supported blades has been with noncritical steels containing about 95- to 96-percent iron. These materials generally are somewhat easier to form and machine than critical materials. When brazing processes are used, the problems may be somewhat less difficult with noncritical materials, because the quality of the brazing atmosphere need not be as closely controlled. The heat treatment of noncritical materials, in order to develop desired physical properties, is more important than for critical materials. Noncritical materials would be expected to corrode much easier than critical materials, and a method of inhibiting corrosion during engine operation would be required. The use of noncritical blade materials, however, results in many of the same problems that would be encountered if critical materials were employed. All the problems encountered in research on air-cooled shell-supported blades cannot be discussed in this paper; therefore, only the major problems will be reviewed. The goal sought in the turbine-cooling program is the reduction of blade-metal temperature with a minimum flow of cooling air. In order to obtain this goal, it was first necessary to investigate various forced-convection air-cooled turbine-blade configurations and fabrication techniques that would result in satisfactory cooling and blade life. Furthermore, when noncritical materials were used, methods for preventing corrosion were required.

CONVECTION-COOLED BLADE RESEARCH

Before the major problems encountered in obtaining suitable air-cooled turbine blades are discussed, a brief review of the principles of forced-convection cooling will be made. Figure 2(a) shows the basic

[REDACTED]

3078-D

method by which a material may be air-cooled by forced convection, and the example is analogous to the problem of cooling a turbine blade. Hot combustion gases flow over the upper surface of the metal, and cooling air flows over the lower surface. Heat is transferred from the hot gases to the metal and is, in turn, rejected to the cooling air. The amount of heat rejected to the cooling air can be increased by increasing the coolant velocity, decreasing the coolant temperature, or both, and a reduction in metal temperature results. A further reduction in the metal temperature can be realized for a given coolant flow if the area to which the coolant is exposed is increased. Such a method is shown in figure 2(b), where fins have been added to the coolant side of the material. For a given set of combustion-gas and cooling-air flow conditions, the metal having the augmented cooling surface will be cooler than the metal with a plain cooling surface.

### Blade Configurations

The manner in which these basic heat-transfer principles have been applied to turbine blades is shown in figure 3.

Hollow blade. - Figure 3(a) shows an end view of a cooled turbine blade having a hollow core through which the cooling air flows. For a given coolant flow through the blade, the air velocity is relatively low, because the flow area is large. Furthermore, there is no augmentation of the internal heat-transfer surface area of the blade, and the metal area exposed to the coolant is relatively small. This type of blade, which was used by Germany during World War II in some of their jet engines, was investigated under static conditions at the NACA Lewis laboratory in 1946. It was found to be unsatisfactory for present-day turbojet engines because of the large amount of cooling air required to effect the desired reductions in blade-metal temperature.

Hollow blade with insert. - For a given cooling-air mass flow, the coolant velocity in the hollow blade of figure 3(a) can be greatly increased if an insert such as that shown in figure 3(b) is placed in the core of the blade. The increased air velocity results in an increase in the heat transferred from the blade metal to the cooling air; consequently, the hollow blade with an insert (fig. 3(b)) operates cooler than the hollow blade of figure 3(a) for a given set of combustion-gas and cooling-air conditions. Hollow blades with inserts were investigated analytically in 1948 and were also found to lack sufficient cooling effectiveness to permit engine operation at low coolant flows.

Tube-filled blade. - From the investigations of the hollow blade and hollow blade with an insert, it was apparent that some method of increasing the internal heat-transfer surface area was required in order to operate air-cooled blades successfully at low coolant-flow ratios. A way in which the interior heat-transfer surface area may be increased is

shown in figure 3(c). Small tubes are brazed into the core of the blade, and the cooling air flows through the tubes and the irregular spaces between the tubes and the blade wall. The increase in heat-transfer surface area exposed to the cooling air as compared with that of the hollow blade and hollow blade with insert results in much more effective cooling in the tube-filled blade. Research on the heat-transfer characteristics of this type of blade in full-scale turbojet engines was started in 1950; and, because it had adequate cooling effectiveness for present-day turbine-inlet temperatures of about 1650° F and was relatively easy to fabricate from noncritical materials, the tube-filled air-cooled turbine blade has been used extensively in other phases of turbine-cooling research.

Corrugated-insert blade. - A blade that combines the heat-transfer features of the hollow blade with an insert and the tube-filled blade (figs. 3(b) and (c)) is shown in figure 3(d). This blade incorporates a corrugated-fin insert that increases the internal heat-transfer surface area. An "island" is placed in the central portion of the blade that reduces the flow area of the coolant passage and restricts the air to the spaces between the blade wall and the corrugations or the wall of the island and the corrugations. In this manner, a large heat-transfer surface area and relatively high coolant velocities are achieved that result in a very effectively cooled blade. Investigation of this type blade was first made in a full-scale turbojet engine in 1952. For the relatively thick blade profile discussed here, the corrugated-fin-insert blade cools better than those previously described and is the type of blade being used most widely at the Lewis laboratory in engine performance investigations of completely air-cooled engines. It is also the blade being considered for use in a high-temperature engine designed at this laboratory. For other blade profiles, similar corrugated-fin inserts provide effective cooling, as discussed in greater detail in reference 1.

In the development of various forced-convection air-cooled shell-supported blade configurations, many cooling arrangements were investigated, the most successful of which are discussed herein. More detailed accounts of the configurations investigated in full-scale engines and the results obtained are given in references 2 to 9. A considerable amount of research required with regard to fabrication procedures is discussed in reference 10.

Some of the results obtained on the two most promising configurations, that is, the tube-filled blade and corrugated-insert blade, are discussed in the next section, including the effects of coolant-flow ratio and cooling-air temperature on average blade-metal temperature at about the one-third-span position. This position was selected because it can be considered the critical section of the blade with respect to temperature and centrifugal stress. The ability to calculate the average

blade-metal temperature from theory and the significance of observed nonuniformities in blade-metal temperature are discussed.

### Blade-Metal Temperature

Effect of coolant-flow ratio on average blade temperature. - The effect of coolant-flow ratio on the average blade temperature is shown in figure 4 for tube-filled and corrugated-insert blades. (Views of the tip ends of these blades are shown in figs. 3(c) and (d), respectively.) The data for the blades were obtained on a centrifugal-compressor engine in which the turbine was modified to accommodate several air-cooled blades. The experimental data presented for the tube-filled blade are for an engine speed of 11,500 rpm (rated engine speed) and an effective gas temperature of 1470° F. The cooling-air temperature ranged from 150° to 210° F. The temperatures of the corrugated-insert blade were referred to the engine conditions existing for the tube-filled blade data through the use of correlation procedures such as those discussed in reference 3. As shown in figure 4, the corrugated-insert blade is about 125° F cooler than the tube-filled blade throughout the entire coolant-flow range.

Effect of cooling-air temperature on average blade temperature. - The importance of using the lowest attainable cooling-air temperature is seen in figure 5, which shows the effect of two different cooling-air temperature levels on average blade-metal temperature for a range of coolant-flow ratio. The data, which are for a corrugated-insert blade similar to that shown in figure 3(d), were obtained in an axial-flow compressor turbojet engine modified to accommodate a completely air-cooled turbine rotor. The performance of this particular air-cooled engine is discussed in the paper by Ziemer and Schafer. The low-temperature-level cooling air (temperature range of 190° to about 295° F) was obtained by cooling the blades with air supplied from a laboratory air system. The high-temperature-level cooling air (temperature of about 510° F) was obtained by bleeding the cooling air from the engine compressor. It can be seen that increasing the temperature level of the cooling air about 200° to 300° F resulted in increasing the temperature level of the blade about 100° F (from 965° to 1065° F) at a coolant-flow ratio of 0.025. For a coolant-flow ratio of 0.05, the blade-temperature level was increased about 180° F, from 865° to 1045° F. It should be noted that the effective gas temperature level was about the same for both the low- and high-temperature-level cooling-air investigations. Thus, the differences in temperature of the cooled blades for a given coolant-flow ratio were caused entirely by the difference in cooling-air-temperature level.

It can also be seen in figure 5 that, for the case where high-temperature cooling-air was used, the reduction in average blade temperature with an increase in coolant-flow ratio was very small compared

with the case where low-temperature cooling air was used. For example, when high-temperature cooling air was used, an increase in coolant-flow ratio from 0.025 to 0.05 resulted in a decrease in blade temperature of about 20° F (from about 1065° to 1045° F). When low-temperature cooling air was used, a change in coolant-flow ratio from 0.025 to 0.05 resulted in a reduction in blade temperature of about 100° F (from 965° to 865° F). Part of the reason for the relatively small change in blade temperature with an increase in coolant flow for the case of high-temperature cooling air was that the cooling-air temperature remained essentially constant as the coolant flow changed. In the case of the low-temperature-level cooling air, there was a considerable change in temperature of the cooling air as the coolant-flow ratio changed, the temperature varying from about 280° to 198° F for coolant-flow ratios of 0.025 and 0.05, respectively. Another reason for small changes in blade temperature with changes in coolant-flow ratio for the high-temperature cooling air is that, as the cooling-air temperature becomes higher, it has less effect on blade temperature. If the cooling-air temperature were equal to the effective gas temperature, there would be no change in blade temperature regardless of the coolant-flow ratio.

The increase in average blade temperature that accompanies increases in cooling-air temperature and the relative insensitivity of the blade temperature to changes in coolant-flow ratio for high cooling-air temperatures indicate the need for maintaining the cooling-air temperature at a low level. It is generally assumed that the cooling air is to be bled from the engine compressor. It is thus desirable to maintain the cooling-air pressure losses in the turbine blades and throughout the coolant-system ducting to a minimum. In order to minimize the compressor work required for the cooling air and to keep the cooling-air temperature at a minimum value, it is desirable to bleed the compressor at a point at which the pressure level is no higher than the required coolant-supply pressure. The factors affecting the required coolant-supply pressure and therefore the compressor-bleed point are: (1) duct losses from the compressor to the turbine, (2) pressure ratio of the cooling air as it passes through the turbine disk, (3) pressure losses as the cooling air leaves the turbine disk and enters the base of the turbine blades, and (4) the pressure loss through the turbine blades. All these factors are functions of the cooling-air mass flow, and generally the losses decrease with a decrease in coolant flow. Pressure losses in the tail-cone ducting system are discussed in reference 11; the pressure ratio in one type of cooled-turbine rotor is presented in reference 12; and methods for determining the pressure loss in turbine blades are presented in references 1, 3, and 13. Reference 12 also presents data providing an insight into the amount of heat transferred to the cooling air as it passes through the tail-cone and rotor disk of one type of air-cooled engine.

Calculated blade temperatures. - One of the goals of turbine-cooling research is to be able to calculate theoretically the cooled turbine-blade temperature for a given set of engine conditions for design purposes. References 1 and 14 present methods for predicting air-cooled turbine-blade temperatures. The agreement between calculated and experimental blade temperatures for a corrugated-insert blade is shown in figure 6. It can be seen that satisfactory agreement between the experimental and calculated blade temperatures was achieved, the calculated temperatures being about 25° F higher than the experimental. This blade was designed for operation in a future engine at a turbine-inlet temperature of about 2000° F. The experimental blade temperatures in figure 6 were obtained, however, for a present-day turbojet engine operating at a turbine-inlet temperature of about 1640° F. Because of the good agreement between experimental and calculated blade temperatures for a turbine-inlet temperature of 1640° F, it would be expected that calculated values of blade temperatures for a turbine-inlet temperature of 2000° F would be representative of the experimental temperatures that might be obtained at the higher gas temperatures.

A theoretical analysis was made for a turbine-inlet temperature of 2000° F to determine the effects of the corrugated-fin configuration on the cooling-air flow required to maintain a certain safety factor in the blade. Two blade configurations were analyzed. In making this analysis, the heat-transfer characteristics, cooling-air pressure losses, and present-day fabrication techniques were considered so that the blade configurations investigated were considered to be practical. The blades were assumed to be made from S-816 alloy, and stress-to-rupture data for 100-hour life were employed in the analysis. The results are shown in figure 7. An enlarged representative section of the corrugation configuration of each blade is also shown in figure 7, and it can be seen that the corrugation spacing, height, and thickness were varied for the two configurations considered. Configuration A is the same as shown in figure 6. Variations in the corrugation spacing, height, and thickness of the blades resulted in changes in cooling-air-flow area, cooling-air velocity, and heat-transfer surface area. These changes in turn affected the cooling characteristics and pressure losses within the turbine blade. Figure 7 shows that blade A required a coolant-flow ratio of 0.025 to maintain the design safety factor. Blade B required a coolant-flow ratio of 0.013, which was about 50-percent less than that required by configuration A. From these analyses, it can be seen that significant reductions in the required coolant-flow ratio can be effected by relatively slight alteration of the corrugated insert. The results presented here do not constitute a complete analysis of the coolant requirements of the two blades, because for convenience of presentation, the analyses were made for the same spanwise position as the experimental temperatures shown in figure 6, that is, at about one-third span. Actually, the critical section of the blades will vary somewhat with the different configurations, and the final selection of

the best blade configuration should be based upon the coolant flow required to maintain the design safety factor at the critical section of the blade.

Chordwise temperature distribution. - So far, only average blade-metal temperatures of cooled turbine blades have been discussed. Also of considerable importance is the variation of local temperature within the blade, particularly in a chordwise direction. Figure 8 shows the chordwise temperature distribution at about the one-third-span position for a forced-convection air-cooled shell-supported tube-filled blade. This distribution is typical of all shell-supported convection-cooled blades; that is, the leading- and trailing-edge regions of the blade operate relatively hot, while the midchord region operates quite cool. A major portion of the blade is slightly below the average blade temperature. A temperature distribution such as shown in figure 8 will produce thermal stresses within the blade as a result of the tendency of the hot leading- and trailing-edge regions to expand spanwise to a greater degree than the cooler midchord region. Expansion of the leading and trailing edges is restrained by the midchord section and results in compressive and shear thermal stresses in the leading and trailing edges and tensile stresses in the midchord region. During operation in an engine, a cooled turbine blade is also subject to centrifugal, bending, and vibratory forces and a complex load transfer from the internal blade components to the shell. It is quite difficult to analyze completely and accurately the resultant stresses that occur in a blade, and it is consequently impossible at this time to predict theoretically with any degree of accuracy the life of the blade. In order to determine the life of an air-cooled turbine-blade configuration, it was, therefore, necessary to test the blade for endurance in a turbojet engine or under conditions that simulate engine operation. It was recognized, however, that before extended endurance investigation of air-cooled blades made from noncritical materials could be undertaken, some method of preventing corrosion of the blades would probably be required. Various methods of inhibiting corrosion through the use of various corrosion-resistant coatings were investigated.

#### Methods of Preventing Corrosion

In order to determine the severity of the corrosion problem on blades made of noncritical materials, the first endurance investigations of air-cooled turbine blades in turbojet engines were made on blades that had no special protection from the corrosive effects of the combustion gases. It would be expected that the leading- and trailing-edge regions of the blade, which operate hotter than the midchord region (fig. 8) would corrode more readily than other portions of the blade. The investigation of blade corrosion was started in 1951, and the blades were operated at maximum rated engine speed of 11,500 rpm (1300 ft/sec tip

speed) in a centrifugal-compressor turbojet engine that had the turbine modified to accommodate two or four air-cooled blades. The turbine-inlet temperature was maintained at about 1670° F; and the coolant-flow ratio for the cooled blades was maintained constant, usually at about 0.05, although in a few cases coolant-flow ratios as low as 0.030 were used.

The goal of the endurance tests was arbitrarily set at 100 hours at maximum rated engine conditions, in view of the lack of any standard endurance test for air-cooled turbine blades. In normal flight service, the engine may not be subjected continuously to maximum rated engine conditions for more than 30 minutes at a time; consequently, operation at rated engine conditions for a total of 100 hours subjected the blade to conditions much more severe than would be encountered in normal flight service.

Investigation of noncritical-material blades indicated that corrosion of the blade shell started within the first 5 hours of rated engine speed operation. Typical damage to an unprotected blade having a shell made of SAE 4130 steel is shown in figure 9(a) after 38 hours of rated engine speed operation. Corrosion of the blade started in the hot leading- and trailing-edge regions and spread rapidly in a chordwise direction. From the results shown in figure 9(a), it was obvious that some method of protecting the blade surface of noncritical materials was necessary to obtain the goal of 100-hour blade life.

The use of protective coatings for noncritical blades posed a number of severe requirements for the coating because of the environment in which it must operate. The coating must (1) be able to withstand the corrosive and erosive action of the high-temperature, high-velocity combustion-gas stream, (2) adhere well to the blade when operating at high temperature under the influence of high centrifugal force, (3) withstand the thermal shocks incident to engine operation, (4) have a coefficient of thermal expansion sufficiently close to that of the blade metal over a range of temperatures to prevent spalling and flaking of the coating, (5) have sufficient ductility to withstand the vibration and elongation of the blade that occurs during operation, and (6) be capable of withstanding normal handling. Furthermore, the presence of the coating on the blade surface should not seriously affect the tensile or fatigue strength of the blade shell, and the use of the coating should not adversely affect or restrict the heat-treatment procedures necessary to develop the desired physical properties of the blade shell.

Nickel, nickel-Nicrobraz, Microbraz, ceramic, and aluminized coatings were applied to 20 blades having Timken 17-22A(S) or SAE 4130 steel shells. Acknowledgement is made of the cooperation received from the California Metal Enameling Company, the Calorizing Company, the Ferro Corporation, the Research Laboratories Division of General Motors Corporation, and the Solar Aircraft Company in the application of various types of coatings to the air-cooled turbine blades.

The results of the experimental investigations to determine the durability of these protective coatings were as follows:

(1) Satisfactory protection of the blades was provided by nickel-Nicrobraz, Nicrobraz, ceramic, and aluminized coatings. Each of these coatings gave satisfactory corrosion and erosion protection to the turbine blades for 100 hours of maximum rated engine speed operation with coolant-flow ratios in the range of 0.03 to 0.05.

(2) Blades aluminized by the pack and by the dip processes gave excellent protection against corrosion. Of the six blades that were aluminized, all (except one that failed mechanically) operated for at least 100 hours. Two blades were operated for 124 hours and were in excellent condition when the tests were terminated. Figure 9(b) shows an aluminized blade that was operated for 100 hours which is in very good condition.

(3) A modified National Bureau of Standards A-19 type ceramic coating also provided excellent service. A photograph of this blade after completing 100 hours of operation is shown in figure 9(c).

(4) Nickel coatings required an undercoating of some type at the leading edge of the blade in order to prevent flaking and failure of the nickel in this region. A Nicrobraz undercoat provided a satisfactory base for the nickel at the leading edge. A blade having a combination coating of Nicrobraz undercoat at the leading edge followed by a complete nickel coating over the entire blade surface gave adequate protection for 100 hours of rated speed operation. Since the original coating investigations were made, blades having a nickel-Nicrobraz coating have been operated 135 hours at rated engine speed with no corrosion of the blade surface; such a blade is shown in figure 9(d).

(5) Nicrobraz coatings applied to the entire surface of the blade exhibited very satisfactory corrosion-resistant properties. It is known that Nicrobraz alloys very easily with the parent metal, and it undoubtedly affects to some extent the fatigue strength and stress-to-rupture properties of the metals to which it is applied. Aluminum also alloys with the blade parent metal in the aluminizing process. The effects of the alloying action of Nicrobraz and aluminum on fatigue strength and stress-to-rupture properties of the blade-shell material is not known at the present time, but they should be more clearly understood before either of these protective coatings is considered for service use.

A more complete discussion of the various coatings applied to the noncritical-material turbine blades and of the results obtained is given in reference 15.

## Blade Life

Air-cooled turbine blades must, of course, have adequate and uniform life so that reasonable dependability can be attained. In the preceding section, a goal of 100 hours of blade life at rated engine conditions was arbitrarily considered as satisfactory blade life. When endurance investigations of noncritical blades were started with a group of blades made from Timken 17-22A(S) steel, it was found many blades had short life and that there was considerable variation in blade life. Blades generally failed in the first 5 or 10 hours of engine operation for coolant-flow ratios of 0.05. Also, blades that were of the same configuration and fabricated in the same manner failed at times varying from 1 to 100 hours or more under the same operating conditions. There are many factors affecting blade life for a given blade material. Three of the major factors encountered during endurance investigations that are discussed herein are:

- (1) Changes in root fillets
- (2) Variations in heat treatment
- (3) Changes in brazing techniques

Each of these factors is important in itself; however, it should be noted that in a completed blade, the problems are interrelated and any one problem can very well affect the other. For convenience, each of the problems is discussed separately in the following paragraphs.

Most of the blade failures experienced occurred in the root region of the blade, as shown in figure 10. Figure 10(a) shows a blade that has a crack extending from the leading edge to the trailing edge along the suction surface. Figure 10(b) shows a blade that ruptured completely. Both of these failures occurred after only 1 hour of rated speed operation at a coolant-flow ratio of about 0.05.

Root fillets. - It is, of course, well-known that adequate fillets must be employed to avoid undesirable stress concentrations where rapid changes in cross-sectional area occur in highly stressed parts. In the case of turbine blades, adequate fillets must be provided at the point where the shell joins the base (see fig. 11). Furthermore, the non-critical metals used in the endurance investigations are relatively notch-sensitive, and therefore considerable care must be exercised in avoiding stress concentrations in the already highly stressed root sections of the blade. In the fabrication procedures first used, a root fillet was "puddled-in" after the blade was completely fabricated and heat-treated. A sketch of a puddled-in fillet is shown in figure 11(a). The fillet material used was a low-melting-point silver solder (about 1250° F). This type of fillet could not be applied before the heat treatment, because the heat-treatment temperatures are above the melting

[REDACTED]

point of the fillet material. Welding material or so-called high-temperature silver solders could not be used to puddle-in the fillet, because melting of the braze material (copper or Microbraz) in the blade base would be likely, with resulting weakening of the mechanical bond between mating parts of the blade. Use of puddled-in root fillets was not desirable when large numbers of blades were being fabricated because of the time required to puddle-in each fillet. Furthermore, even when extreme care was exercised in applying the fillet, the blade heat treatment was affected.

It was thought that a root fillet cast integrally with the blade base might be satisfactory. A sketch of a "cast-in" fillet is shown in figure 11(b). Such a fillet results in a slight ledge at the top of the fillet, which is essentially an external notch and results because the fillet cannot be cast infinitely thin at the upper edge. The external notch results in undesirable stress concentrations at the top of the cast-in fillet. It was found that, if the cast-in fillet was carefully faired into the blade shell after the blade was completely fabricated, a satisfactory fillet was obtained and failures caused by stress concentrations were eliminated.

Heat treatment. - Metallurgical examination of the blade fractures indicated excessively large grain structure, which would reduce the stress-to-rupture properties of the steel. It was reasoned that the first heat treatment (see table I) overheated the steel from a metallurgical standpoint and caused excessive grain growth. Inasmuch as the braze materials required in the fabrication process were copper or Microbraz, or both, which require brazing temperatures of about 2050° F, no reduction in brazing temperature could be effected. A refinement in grain size, effected by additional heat treatment, was required. Heat treatment number 2 (table I) was evolved, which resulted in smaller grain size and developed higher stress-to-rupture properties in the steel. Although heat treatment number 2 increased the stress-to-rupture strength, the ductility was decreased and blade failures caused by insufficient fatigue strength were encountered. A third heat treatment (table I) was then employed, which increased the ductility of the steel at a slight sacrifice in stress-to-rupture strength. This heat treatment resulted in excessive creep of the blade, and failures due to excessive elongation of the blade resulted. Finally, a combination heat treatment (number 4, table I) was used that consisted of one type of heat treatment for the root region and another type for the rest of the blade shell. This heat treatment achieved a balance between adequate ductility and stress-to-rupture strength.

Brazing. - Several factors are involved in successfully brazing air-cooled blades made up of several major components. Clearance between the parts brazed together is an important factor; it was found that a clearance of 0.005-inch was the maximum allowable for good braze strength

[REDACTED]

between mating parts. The brazing atmosphere is an important factor, particularly where even small amounts of chromium are present such as in SAE 4130 and Timken 17-22A(S) steels. The brazing must be done in an atmosphere that prevents formation of chromium oxides. Most of the blades discussed in this paper were brazed by a commercial brazing company in a dry hydrogen atmosphere having a dew point of  $-40^{\circ}$  F or lower. In the past several months, this laboratory has vacuum-brazed blades with excellent brazing results on a limited number of blades. Brazing temperature is also an important factor, particularly where high-temperature brazing compounds such as Microbraz are used. A variation of only  $25^{\circ}$  to  $50^{\circ}$  F may result in a successful or unsuccessful brazing job. Other factors, such as the effect of the braze material on the strength properties of the parent material, the alloying action of the braze material with the parent metal, and the effect of brazing temperature on the physical properties of the parent metal should be considered. At the present time, the effects of all of these variables are not completely known, but investigations that are under way will provide a better understanding.

General considerations. - The progress achieved in improved air-cooled turbine-blade life by applying various modifications in blade-fabrication procedures is demonstrated in figure 12. As said previously, a minimum blade life of 100 hours at rated engine conditions has been considered as satisfactory performance. The lower part of figure 12 shows that the average time to failure for 15 original air-cooled blades made from noncritical materials was 10 hours at a coolant-flow ratio of 0.05.

Modifications in heat treatment, root fillets, and brazing techniques were then applied; and the results shown in the upper part of figure 12 were obtained for a coolant-flow ratio of 0.05. Several blades were operated for over 100 hours, the maximum time being 133 hours. Some of the blades were operated only about 35 to 45 hours, but the blades are in excellent condition and further testing of all of these blades is continuing as indicated by the arrows. This was a marked improvement over the time to failure for the original blades. Because the endurance results at a coolant-flow ratio of 0.05 were encouraging, endurance tests were started with blades operated at a reduced coolant-flow ratio of 0.03. Figure 12 shows that one of these blades has operated for 140 hours, three blades for 105 hours, three blades for 90 hours, and two blades for 35 hours. One blade failed after 55 hours. Operation of the unfailed blades is being continued as indicated by the arrows. The results of some of the endurance investigations discussed herein are given in greater detail in references 16 and 17.

The problems associated with developing satisfactory air-cooled turbine blades will vary somewhat, depending on the engine in which the blade is to be used, the mission for which the aircraft is designed, the

blade material used, and the general blade-fabrication procedures that are thought most desirable. The blade-fabrication procedures used at this laboratory were chosen particularly because they lent themselves well to relatively quick, flexible, and inexpensive ways of making useful air-cooled turbine blades in small numbers.

#### SUMMARY OF RESULTS

The results of experimental investigations of convection-air-cooled shell-supported turbine blades in full-scale turbojet engines are as follows:

1. Suitable air-cooled turbine blades can be obtained that require low coolant flows if inserts such as tubes or fins are used.

2. Average blade-metal temperature can be calculated with sufficient accuracy by analytical methods that have been developed to permit the designer to evaluate various blade-cooling configurations and to select the best configuration for a given set of design conditions and fabricating techniques.

3. Because of the difficulty in performing complete stress analyses in cooled-turbine blades and the generally unknown effects of various fabrication procedures upon blade life, air-cooled turbine blades must be endurance-tested in order to determine adequately their life under engine operating conditions.

4. Blades made from noncritical steels must be protected from corrosion. Satisfactory protection of noncritical blades was provided by nickel-Nicrobraz, Nicrobraz, ceramic, and aluminized coatings. Each of these coatings indicated that it would give satisfactory corrosion and erosion protection to the blades for at least 100 hours at rated engine conditions.

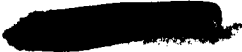
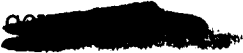
5. In order to obtain satisfactory life in blades made from noncritical steels, particular attention must be given to various fabrication procedures, such as heat treatment, filleting at the blade root, and brazing techniques.

#### REFERENCES

1. Ziemer, Robert R., and Slone, Henry O.: Analytical Procedures for Rapid Selection of Coolant Passage Configurations for Air-Cooled Turbine Rotor Blades and for Evaluation of Heat-Transfer, Strength, and Pressure-Loss Characteristics. NACA RM E52G18, 1952.

2. Ellerbrock, Herman H., Jr., and Stepka, Francis S.: Experimental Investigation of Air-Cooled Turbine Blades in Turbojet Engine. I - Rotor Blades with 10 Tubes in Cooling-Air Passages. NACA RM E50I04, 1950.
3. Hickel, Robert O., and Ellerbrock, Herman H., Jr.: Experimental Investigation of Air-Cooled Turbine Blades in Turbojet Engine. II - Rotor Blades with 15 Fins in Cooling-Air Passages. NACA RM E50I14, 1950.
4. Hickel, Robert O., and Smith, Gordon T.: Experimental Investigation of Air-Cooled Turbine Blades in Turbojet Engine. III - Rotor Blades with 34 Steel Tubes in Cooling-Air Passages. NACA RM E50J06, 1950.
5. Ellerbrock, Herman H., Jr., Zalabak, Charles F., and Smith, Gordon T.: Experimental Investigation of Air-Cooled Turbine Blades in Turbojet Engine. IV - Effects of Special Leading- and Trailing-Edge Modifications on Blade Temperature. NACA RM E51A19, 1951.
6. Smith, Gordon T., and Hickel, Robert O.: Experimental Investigation of Air-Cooled Turbine Blades in Turbojet Engine. V - Rotor Blade with Split Trailing Edges. NACA RM E51A22, 1951.
7. Arne, Vernon L., and Esgar, Jack B.: Experimental Investigation of Air-Cooled Turbine Blades in Turbojet Engine. VI - Conduction and Film Cooling of Leading and Trailing Edges of Rotor Blades. NACA RM E51C29, 1951.
8. Smith, Gordon T., and Hickel, Robert O.: Experimental Investigation of Air-Cooled Turbine Blade in Turbojet Engine. VIII - Rotor Blades with Capped Leading Edges. NACA RM E51H14, 1951.
9. Bartoo, Edward R., and Clure, John L.: Experimental Investigation of Air-Cooled Turbine Blades in Turbojet Engine. XII - Cooling Effectiveness of a Blade With an Insert and With Fins Made of a Continuous Corrugated Sheet. NACA RM E52F24, 1952.
10. Long, Roger A., and Esgar, Jack B.: Experimental Investigation of Air-Cooled Turbine Blades in Turbojet Engine. VII - Fabrication Procedures for Air-Cooled Turbine Blades. NACA RM E51E23, 1951.
11. Smith, Gordon T., and Curren, Arthur N.: Comparison of Pressure-Loss Characteristics of Several Tail-Cone Air-Induction Systems for Air-Cooled Gas-Turbine Rotors. NACA RM E52K07, 1953.

3078-0

- 
12. Nachtigall, Alfred J., Zalabak, Charles F., and Ziemer, Robert R.: Investigations of Air-Cooled Turbine Rotors for Turbojet Engines. III - Experimental Cooling-Air Impeller Performance and Turbine Rotor Temperatures in Modified J33 Split-Disk Rotor up to Speeds of 10,000 RPM. NACA RM E52C12, 1952.
  13. Brown, W. Byron, and Slone, Henry O.: Pressure Drop in Coolant Passages of Two Air-Cooled Turbine-Blade Configurations. NACA RM E52D01, 1952.
  14. Brown, W. Byron, Slone, Henry O., and Richards, Hadley T.: Procedure for Calculating Turbine Blade Temperatures and Comparison of Calculated with Observed Values for Two Stationary Air-Cooled Blades. NACA RM E52H07, 1952.
  15. Bartoo, Edward R., and Clure, John L.: Experimental Investigation of Air-Cooled Turbine Blades in Turbojet Engine. XIII - Endurance Evaluation of Several Protective Coatings Applied to Turbine Blades of Nonstrategic Steels. NACA RM E53E18, 1953.
  16. Stepka, Francis S., and Hickel, Robert O.: Experimental Investigation of Air-Cooled Turbine Blades in Turbojet Engine. IX - Evaluation of the Durability of Noncritical Rotor Blades in Engine Operation. NACA RM E51J10, 1951.
  17. Esgar, Jack B., and Clure, John L.: Experimental Investigation of Air-Cooled Turbine Blades in Turbojet Engine. X - Endurance Evaluation of Several Tube-Filled Rotor Blades. NACA RM E52B13, 1952.
- 

3078-0

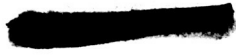
Table I  
HEAT TREATMENTS APPLIED TO BLADES  
OF TIMKEN 17-22A(S) STEEL

HEAT TREATMENT NUMBER	HEAT TREATMENT					
	BRAZE		NORMALIZE		DRAW	
	TEMP., °F	TIME, hr	TEMP., °F	TIME, hr	TEMP., °F	TIME, hr
1	2050	0.25	NONE	NONE	1225	4
2	2050	0.25	1725	1	1225	4
3	2050	0.25	1725	1	1400	1
4	2050	0.25	1725	1	<sup>a</sup> 1225 <sup>b</sup> 1400	4 1

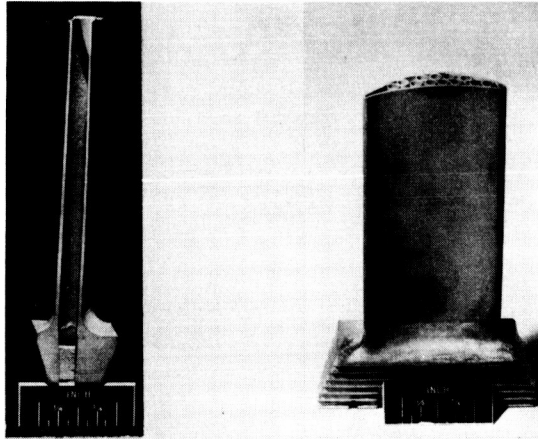
<sup>a</sup>ENTIRE SHELL

<sup>b</sup>ROOT REGION OF BLADE ONLY

(APPROX. 1/2 IN. ABOVE BLADE BASE PLATFORM)



TYPICAL SHELL-SUPPORTED BLADE



(a) HOLLOW BLADE

(b) BLADE WITH TUBE INSERTS

Figure 1

ILLUSTRATION OF CONVECTION COOLING PRINCIPLES

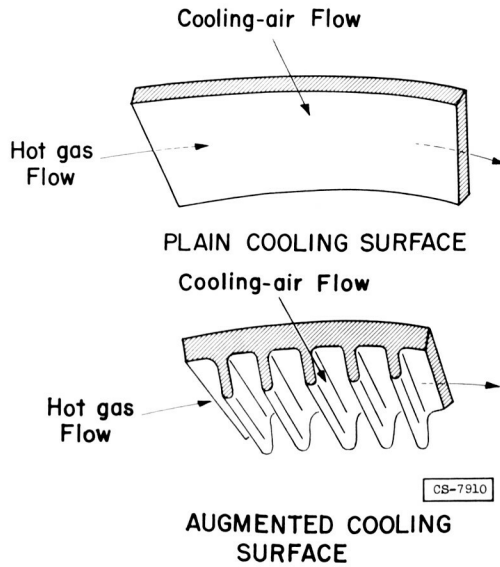


Figure 2



SHELL-SUPPORTED AIR-COOLED BLADES

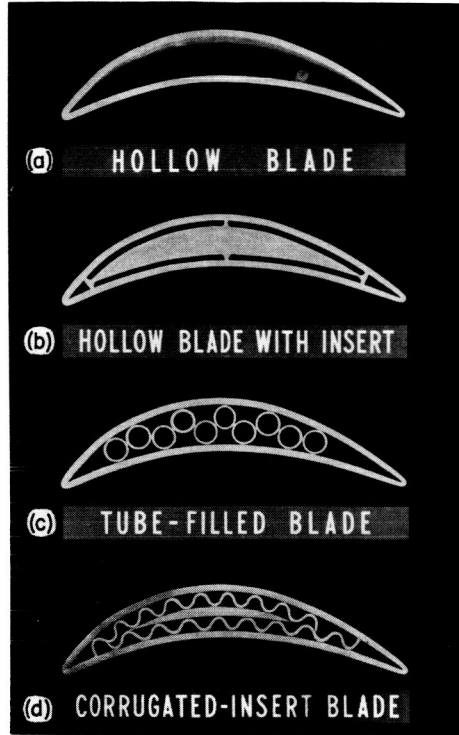


Figure 3

AVERAGE SHELL TEMPERATURES FOR 10-TUBE AND CORRUGATED-INSERT BLADES  
TURBINE-INLET TEMP., 1670° F

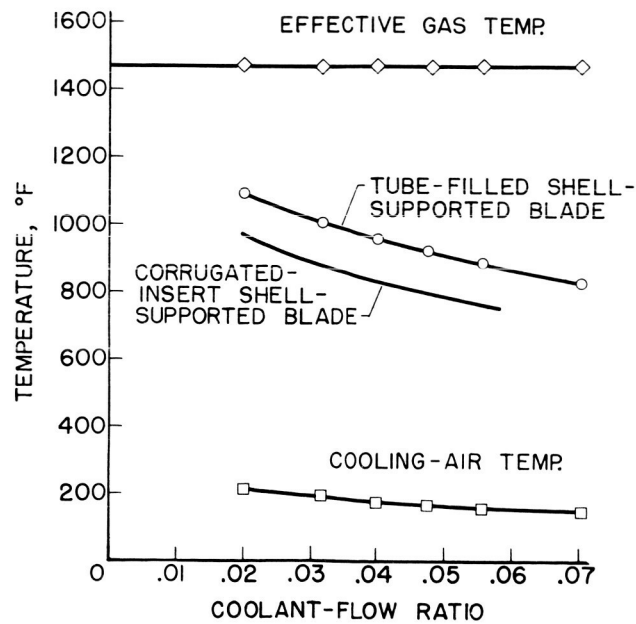


Figure 4

EFFECT OF COOLING-AIR TEMPERATURES ON  
BLADE TEMPERATURE

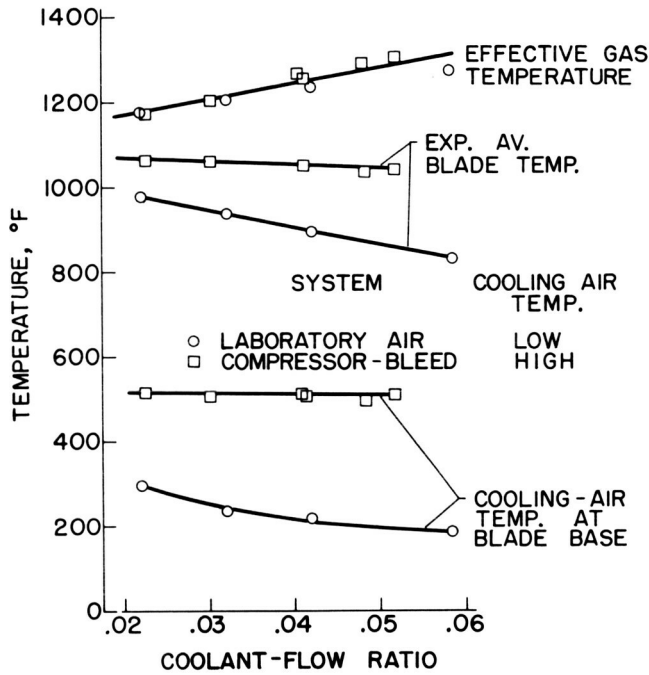


Figure 5

COMPARISON OF EXPERIMENTAL AND ANALYTICAL  
BLADE TEMPERATURES

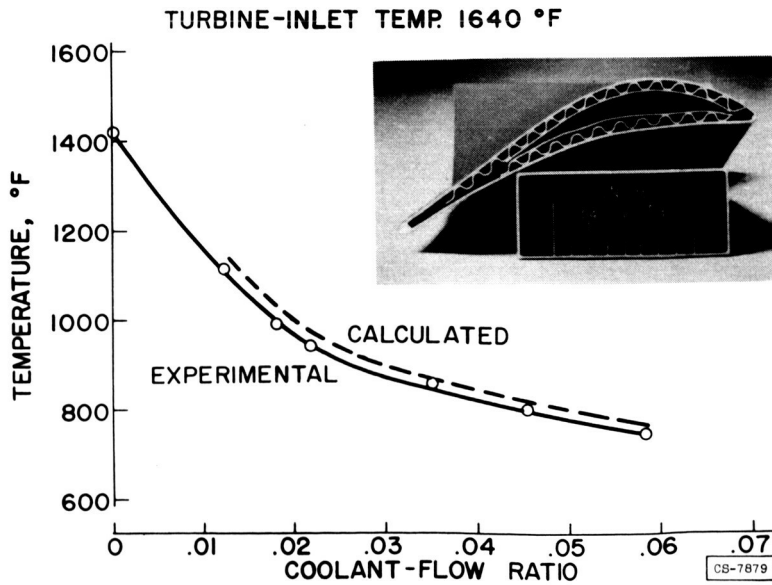


Figure 6

EFFECT OF CONFIGURATION ON COOLANT-FLOW RATIO

TURBINE-INLET TEMP., 2000° F  
 BLADE TEMP., 1250° F

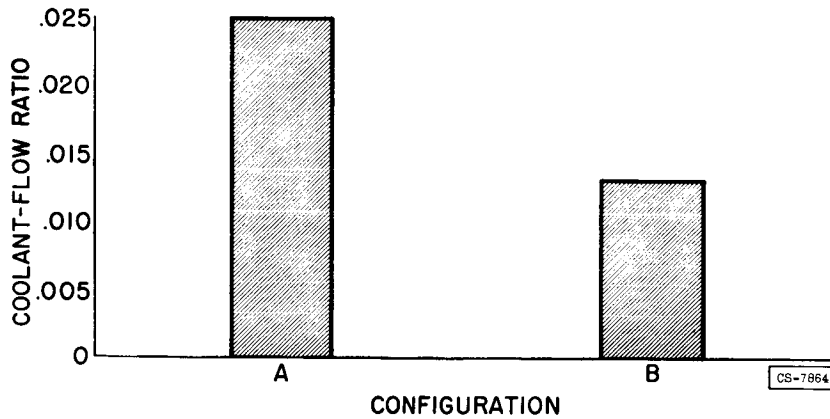


Figure 7

AVERAGE CHORDWISE TEMPERATURE DISTRIBUTION  
 AT 1/3 SPAN OF TUBE-FILLED SHELL-SUPPORTED BLADE

EFFECTIVE GAS TEMPERATURE, 1450°F  
 TURBINE-INLET TEMPERATURE, 1670° F  
 COOLANT-FLOW RATIO, 0.03

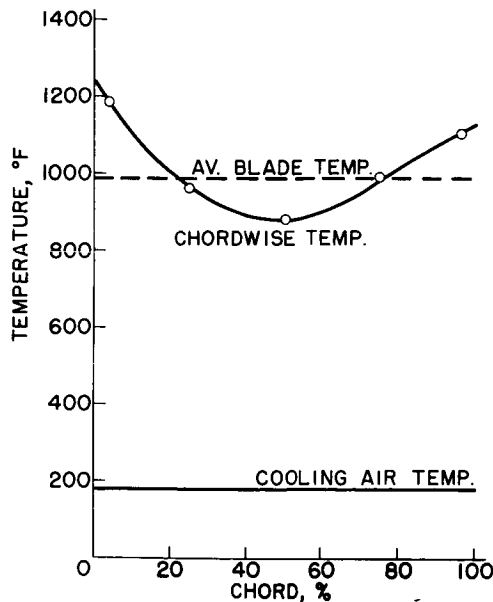
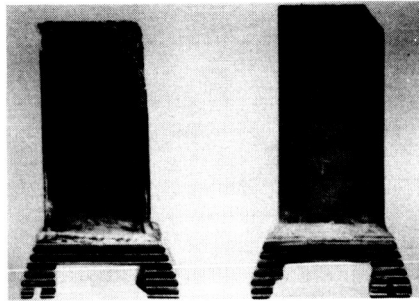


Figure 8

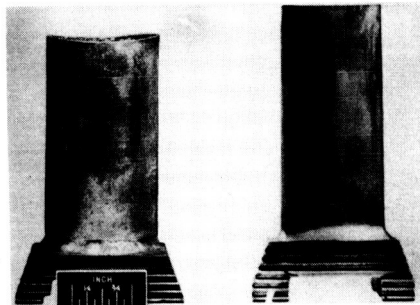
3078-D

CORROSION EFFECTS ON UNCOATED  
AND COATED BLADES



(a) UNCOATED  
BLADE,  
38 hr.

(b) ALUMINIZED  
COATING,  
100 hr.



(c) CERAMIC  
COATING,  
100 hr.

(d) NICKEL  
COATING,  
135 hr.

Figure 9

TYPICAL BLADE FAILURE  
COOLANT-FLOW RATIO, 0.05  
TURBINE-INLET TEMPERATURE, 1670° F

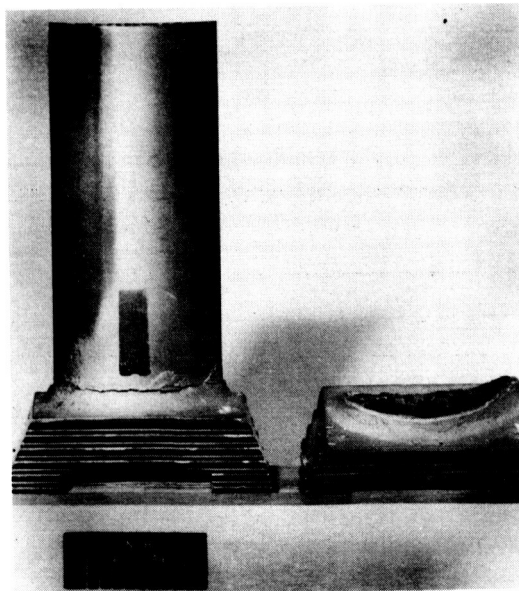


Figure 10

### CROSS-SECTIONAL VIEW OF BLADES WITH PUDDLED-IN AND CAST-IN FILLETS

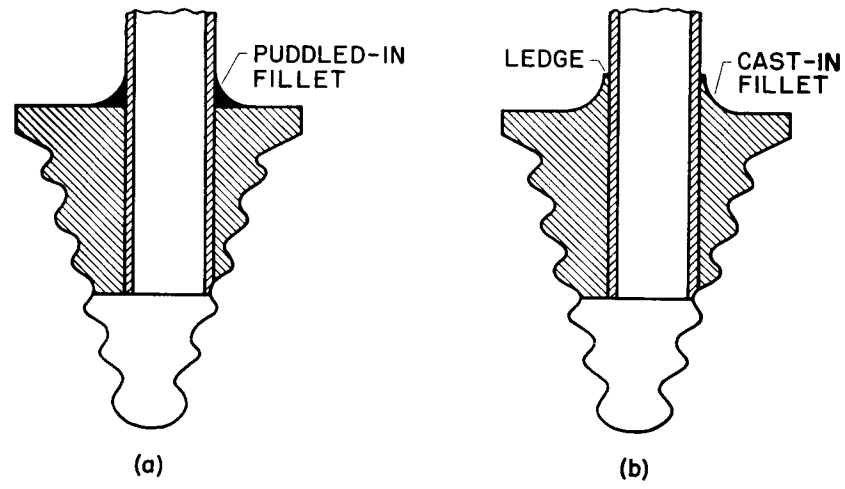


Figure 11

### IMPROVEMENT IN BLADE ENDURANCE WITH VARIOUS TYPES OF HEAT TREATMENTS AND FILLET MODIFICATIONS

TURBINE-INLET TEMP., 1670° F  
ENGINE SPEED, 11,500 rpm

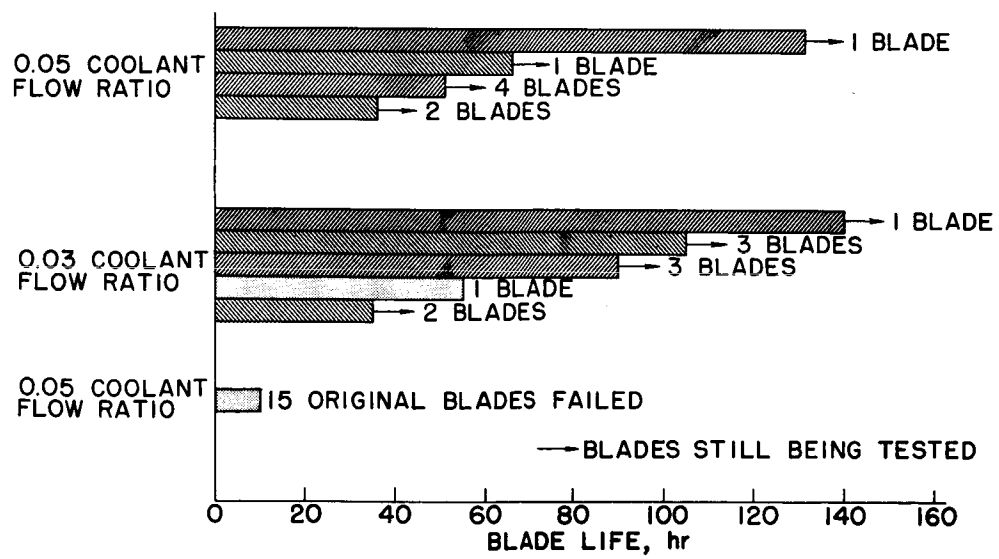


Figure 12

## INVESTIGATIONS OF CONVECTION-COOLED STRUT-SUPPORTED TURBINE BLADES

By Eugene F. Schum and Francis S. Stepka

## INTRODUCTION

The results of investigations conducted by the NACA on a type of convection-cooled turbine blade wherein an internal strut is the primary support member are presented in this paper. The basic principle of this type of blade is the insulation of the load-carrying member from the direct effects of the hot-gas stream. The method in which this insulation is accomplished is illustrated by the use of a segment of a blade of this type, shown in figure 1. The load-carrying member, called the strut, is shielded from the hot-gas stream by a thin airfoil shell and cooled by air which is passed between the shell and the strut. The fins of the strut serve two purposes; the primary fins support the protective airfoil shell and the secondary fins augment the cooling-surface area of the strut.

The insulation of the load-carrying member in this manner apparently not only would result in lower temperatures of the load-carrying member of this type blade as compared with that of the shell-supported blades discussed by Hickel and Clure, but would also provide protection to the load-carrying member from the corrosive action of the hot gases. Consideration of these advantages of the strut-supported blade would indicate that this type blade would eliminate some of the problems encountered with shell-supported blades and that this type of blade has a greater potential for operating at higher turbine inlet temperatures or lower coolant flow ratios than the shell-supported blades, or both.

## ANALYSIS AND DEVELOPMENT

## First Blade Design

Investigations were conducted to determine analytically and to verify experimentally the cooling effectiveness of a blade design utilizing an internal strut as the supporting member. The results of the investigations of the first blade design (refs. 1 and 2) indicated that the strut-supported blades had greater potential for operation at higher turbine-inlet temperatures than the shell-supported blades. This first strut-supported blade design (fig. 2), although satisfactory for use as a test blade for verifying the theoretical analysis as well as for investigating the construction durability, had several deficiencies when considered for service applications. Some of the shortcomings were: (1) The blade was of poor design with respect to production because of the

intricate machine work required; (2) it had a large cooling-air pressure loss at the base because of sudden changes in flow areas and direction as the air entered the blade; and (3) the blade had a dimpled outer shell surface, caused by the attachment method, which may have affected the aerodynamic performance of the blade.

### Improved Blade Design

To improve the first design and to eliminate some of its deficiencies, another blade design was evolved. This blade design, shown in figure 3, is of a five-piece construction: a strut, a two-piece shell, and a two-piece base. The primary advantages of the design are: (1) the straight cooling-air entrance passages at the base to avoid large cooling-air pressure losses, (2) the elimination of intricate machine work by permitting straight-through cutting of the slots in the strut and the base, and (3) the elimination of the dimpled outer shell surface.

In designing the blade, consideration of the strength aspect, the limitations imposed by the aerodynamic characteristics of the blade profile and by current fabrication techniques, was required in conjunction with the analytical investigation of the cooling mechanism of the finned strut. An insight into some of the problems associated with the design of the blade from cooling considerations can be obtained from an explanation of the cooling mechanism of the strut. This mechanism can be illustrated by the use of a segment of the strut shown in figure 1. The heat from the hot gases flowing over the shell is transferred to the shell and then conducted through the shell. A portion of the heat from the shell is transferred directly to the cooling air while the remainder is conducted through the attachment media into the primary fins. Some of the heat entering these fins is then dissipated to the cooling air, while the remainder is conducted to the body of the strut. A portion of the heat entering the body of the strut is then dissipated directly to the cooling air and the remainder is conducted to the secondary fins from which it is dissipated to the cooling air. Thus, from the consideration of the cooling mechanism alone, it is apparent that investigations of the effects of attachment-media area, primary and secondary fin thickness, and number of secondary fins are required in the design of the blade.

An analytical investigation was conducted to determine the effect of these factors on the temperature of the strut with the aerodynamic profile of the improved blade design. Strut temperatures were calculated in the manner described in reference 3. The results of calculations, which were made for an effective gas temperature of 1750° F and a constant cooling-air temperature of 600° F, are shown in figure 4. The temperature data presented are the average of the calculated values at the midchord region of the blade. The results of these calculations, which neglected the small effect of radiation from the shell to the strut, indicate that increasing the number of the secondary fins has the largest

effect in reducing the temperature of the strut. The primary fin thickness has the next largest effect with the attachment contact area and secondary fin thickness having the least effect. At a coolant-flow ratio of 0.03, for example: figure 4(a) shows that providing the strut with three secondary fins of 0.020-inch thickness decreases the temperature of the strut approximately  $110^{\circ}$  F; figure 4(b) shows that decreasing the primary fin thickness from 0.040 to 0.020 inch decreases the strut temperature approximately  $30^{\circ}$  F; figures 4(c) and (d) show that the change in secondary fin thickness and in attachment contact area, respectively, have little effect on strut temperature. Thus, considerable reduction in the temperature of the load-carrying member of this type blade can be achieved by the proper selection of the geometry of the strut.

These results indicate the strut geometry which would be chosen if only the heat-transfer aspect of design were considered. The final design of strut, however, must consider the limitations imposed on the design by strength, fabrication, and cooling-air pressure drop through the blade. The fabrication limitations, for example, govern the minimum spacing of secondary fins, and the strength limitations govern the primary fin thickness and the attachment contact area required to provide sufficient strength in the joint of the shell and the strut. Consideration of these limitations and the modifying of the blade optimum cooling designs to satisfy these limitations resulted in the strut design shown in figure 3.

A photograph of a completed blade of this design (fig. 5(a)) is shown adjacent to a photograph of a blade of the first design (fig. 5(b)) to illustrate by comparison the improved shell surface condition of the present blade design. The strut and the base of the improved blade design were made of Timken 17-22A(s) steel, a material which contains only about 3 percent of critical materials. The airfoil shell was made of 0.020-inch-thick sheet stock of N-155, an alloy containing high percentages of nickel, chromium, and other critical materials. The use of this alloy for the shell was dictated by the need for a material which possessed high strength at the relatively high temperatures at which the shell would operate and the need for good oxidation resistance in order to avoid the coating problems discussed in the preceding paper. The first step in the fabrication of this blade was the milling of the slots in the forged, twisted-airfoil strut and in the cast, split base shown in figure 3. The slots cut in the strut were 0.080 inch wide, and spaced so that the primary fins would be 0.040 inch thick and the secondary fins 0.020 inch thick. The second step in the fabrication was the inserting of the strut into the base and the brazing of these members with Microbraz in a dry hydrogen atmosphere furnace. The halves of the shell were then formed, slipped over the strut, and brazed to it with Microbraz in either a vacuum or a dry hydrogen atmosphere furnace. The final steps were the welding of a small fillet at the base, the grinding of the serrations in the base, and the trimming of the blade to the desired length.

## RESULTS AND DISCUSSION

## Experimental and Analytical Heat-Transfer Results

The cooling characteristics of a pair of strut-supported blades of the design shown in figure 3 were obtained from investigations conducted in a full-scale turbojet engine. The modifications of the engine and the instrumentation used are similar to that described in the preceding paper. The results of the investigation showing the change in the average temperature of the strut over a range of coolant-flow ratios, a blade tip speed of 1300 feet per second, and a turbine-inlet temperature of approximately 1640° F are presented in figure 6(a). The temperature data presented are the arithmetical average of the temperatures indicated by three thermocouples embedded in the strut at about the 1/3 span length from the base at the leading-edge, midchord, and trailing-edge regions. In addition to these data, figure 6(a) also shows curves which were analytically determined for the average strut and the midchord shell temperatures and a curve which was experimentally obtained with a shell-supported, corrugated insert blade which was discussed by Hickel and Clure. Analytical midchord shell and midchord strut temperatures were evaluated according to the method described in reference 3. The analytical average strut temperatures were determined from the calculated midchord strut temperatures and use of a relation of experimental average strut temperatures with experimental midchord strut temperatures. The average strut temperature was evaluated in this manner because of the lack of an existing analytical method to determine temperatures of the leading- and trailing-edge regions of the strut.

The calculated average strut temperature curve is in good agreement over the entire coolant flow range with that experimentally determined. The experimentally obtained curve of the temperature of the support member of the strut-supported blade is considerably lower than that of the shell-supported blade. At low coolant flow ratios, for example, the difference in temperature of the support members of the two blades is approximately 120° F, while at high coolant flow ratios this difference increases to about 230° F. The relatively lower temperatures of the strut, because of the insulation of the strut from the hot-gas stream, result in the shell temperatures being higher than those of the shell-supported blade. The calculated values of the shell temperatures at the midchord region of the strut-supported blade shown in figure 6(a) indicate that the shell in this region would be approximately 60° F higher over a large range of coolant flow ratios than the average shell temperatures of the shell-supported blade. If the error which was obtained in the calculation of the average temperature of the strut is considered, it appears that the difference in the shell temperatures of the two types of blade would be even larger.

## Experimental Investigation of Blade Durability

After the experimental heat-transfer data were obtained, the two strut-supported blades were subjected to an endurance test to determine the durability of the blade construction. The blades were subjected to a cyclic endurance test in order to determine whether the thermal stresses imposed on the blade by sudden changes in gas temperature would cause failure. Each cycle of this test consisted in operating the engine at 4000 rpm and an effective gas temperature of approximately 1050° F for 5 minutes, then accelerating the engine to 11,500 rpm and an effective gas temperature of 1450° F in 15 seconds, maintaining these conditions for 15 minutes, then decelerating the engine to 4000 rpm in 15 seconds. The two blades were subjected to 10 such cycles at a coolant flow ratio of 0.05 and 10 cycles at a coolant flow ratio of 0.03 without a blade failure. A photograph of one of the blades after termination of the 20 cycles is shown in figure.5(a).

## Evaluation of Relative Merit of Blades

In evaluating the merit of the strut-supported blades relative to shell-supported blades, factors such as the stress level of the blades and the blade material properties must be considered in addition to the temperature level of the blades. A method for evaluating the merit of these two types of blade can be illustrated by the use of figure 6(a) and the stress-to-rupture curve of a representative noncritical alloy shown in figure 6(b). The average temperatures of the support members of the blades at a selected coolant flow ratio are obtained from figure 6(a). The metal temperatures thus obtained are then located on the curve of figure 6(b) from which the stress-to-rupture or allowable stress values permitted for a 100-hour life are obtained. The ratio of the allowable stress values of the blades to that of their calculated centrifugal stress levels would thus be an indication of the relative merit of the blades. The values of allowable stress levels for the strut-supported and shell-supported blades, for example, at a coolant flow ratio of 0.015 are approximately 91,000 pounds per square inch and 58,000 pounds per square inch, respectively. The calculated centrifugal stress at the 1/3 span position for the strut-supported and the shell-supported blades is approximately 33,000 and 25,000 pounds per square inch, respectively. Thus the ratio of the allowable stress to the calculated stress for the strut-supported blade is 2.76, while that for the shell-supported blade is 2.32. The larger ratio obtained with the strut-supported blade indicates that it has more merit for operation at the condition shown in figure 6(b) than the shell-supported blade. Furthermore, because of the slope of the stress-rupture curve (fig. 6(b)), small increases in the temperature level of the blades will have a proportionately greater effect on the ratio of the allowable stress to the calculated stress of the shell-supported blade than that

of the strut-supported blade, indicating the greater potential for operating the strut blade at higher turbine-inlet temperature or lower coolant flow ratios than possible with the shell-supported blade or both.

#### CONCLUDING REMARKS

Although the investigations on blades utilizing the principle of insulating the load-carrying member of a blade from the hot gas stream indicated that blades of this type have a greater potential for operating at higher turbine-inlet temperatures or lower coolant flow ratios than the shell-supported blades or both, considerable investigation and development is still required before the strut-supported blade is satisfactory for service application. The cooling-air pressure drop through the blade, for example, must be investigated to determine the magnitude and extent of improvement over the first design; a method for eliminating a portion of the machining operation by casting a strut with fins requires development; and the endurance testing of the blades similar to that described in the preceding paper is required to determine the durability of this type blade.

#### REFERENCES

1. Schramm, Wilson B., and Nachtigall, Alfred J.: Analysis of Coolant-Flow Requirements for an Improved, Internal-Strut-Supported, Air-Cooled Turbine-Rotor Blade. NACA RM E511L13, 1952.
2. Cochran, Reeves P., Stepka, Francis S., and Krasner, Morton, H.: Experimental Investigation of Air-Cooled Turbine Blades in Turbojet Engine. XI - Internal-Strut-Supported Rotor Blade. NACA RM E52C21, 1952.
3. Ellerbrock, Herman H., Jr., Schum, Eugene F., and Nachtigall, Alfred J.: Use of Electric Analogs for Calculations of Temperature Distribution of Cooled Turbine Blades. (NACA TN to be pub.)

3078-D

SEGMENT OF CONVECTION-COOLED  
STRUT-SUPPORTED BLADE

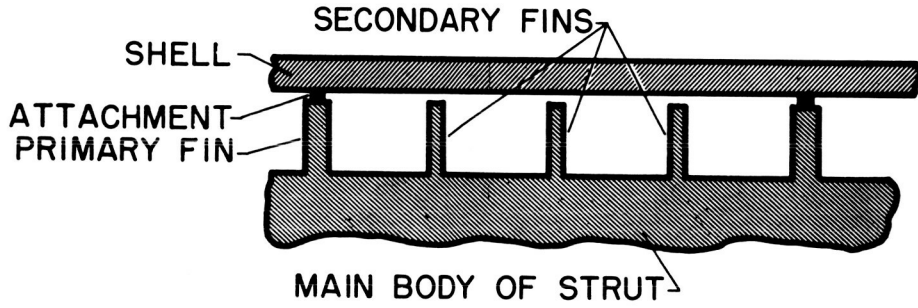


Figure 1

STRUT-SUPPORTED BLADE  
FIRST DESIGN

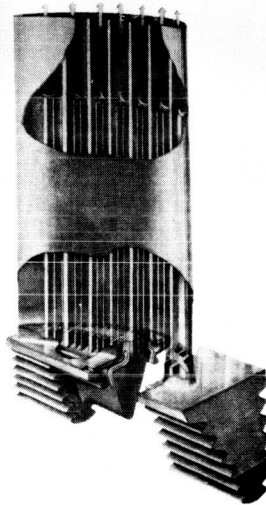


Figure 2

PRESENT DESIGN OF STRUT-SUPPORTED BLADE

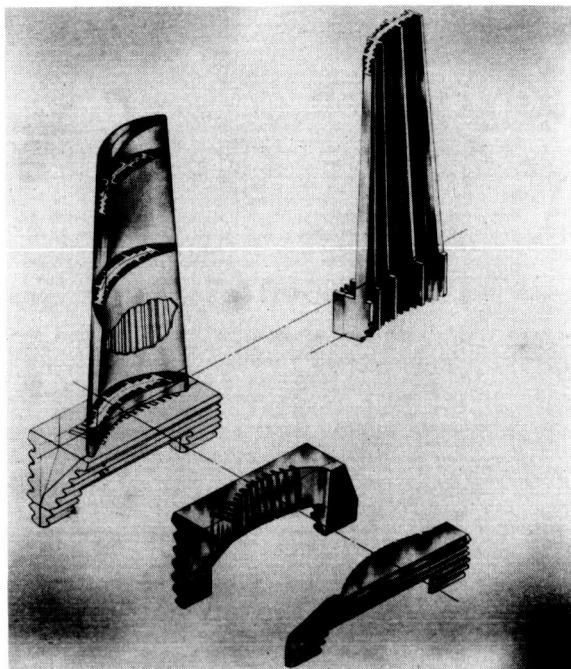


Figure 3

EFFECT OF VARIATIONS IN STRUT GEOMETRY ON AVERAGE TEMPERATURE OF STRUT

MIDCHORD REGION EFFECTIVE GAS TEMP., 1750° F  
 CONSTANT COOLANT TEMP., 600° F

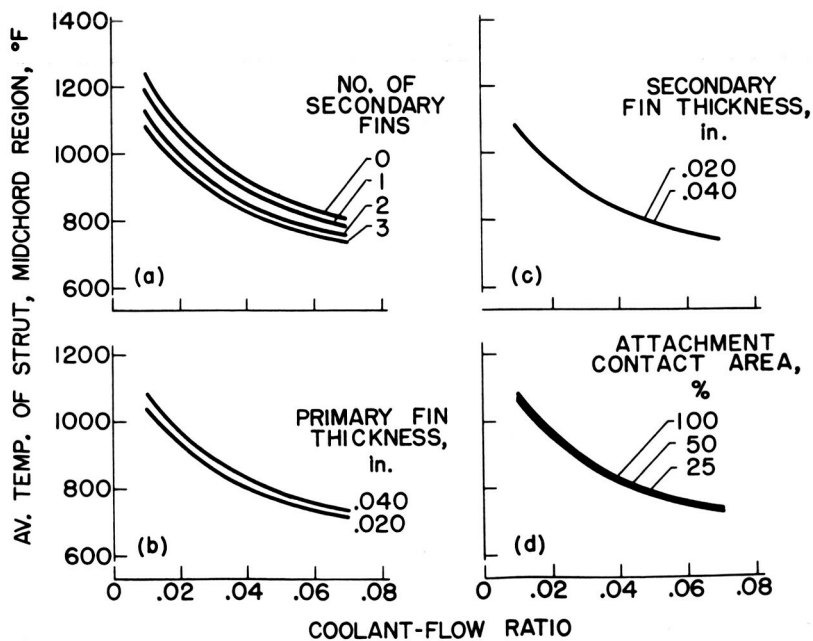


Figure 4

### STRUT-SUPPORTED BLADES

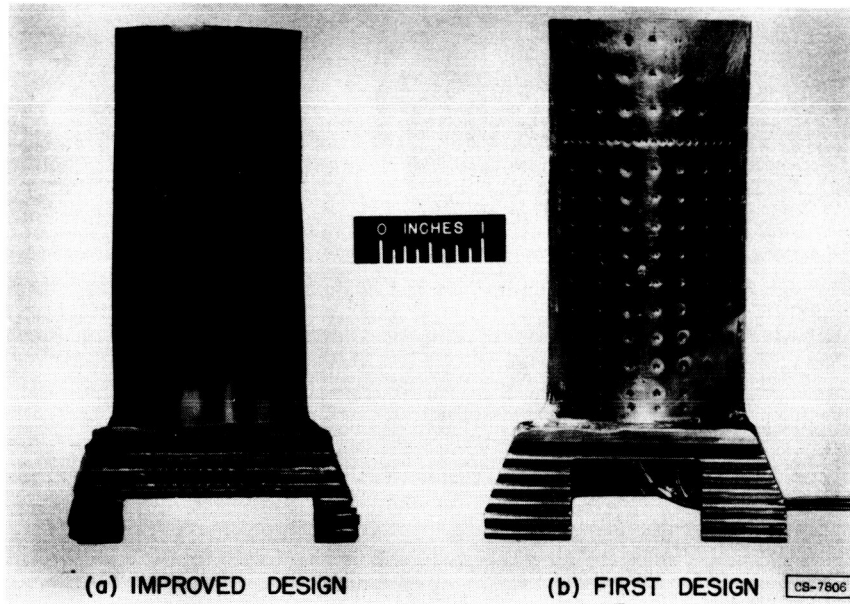


Figure 5

### TEMPERATURE AND STRESS COMPARISONS OF TWO CONVECTION-COOLED TURBINE BLADES

EFFECTIVE GAS TEMP., 1420° F    BLADE TIP SPEED, 1300 ft/sec

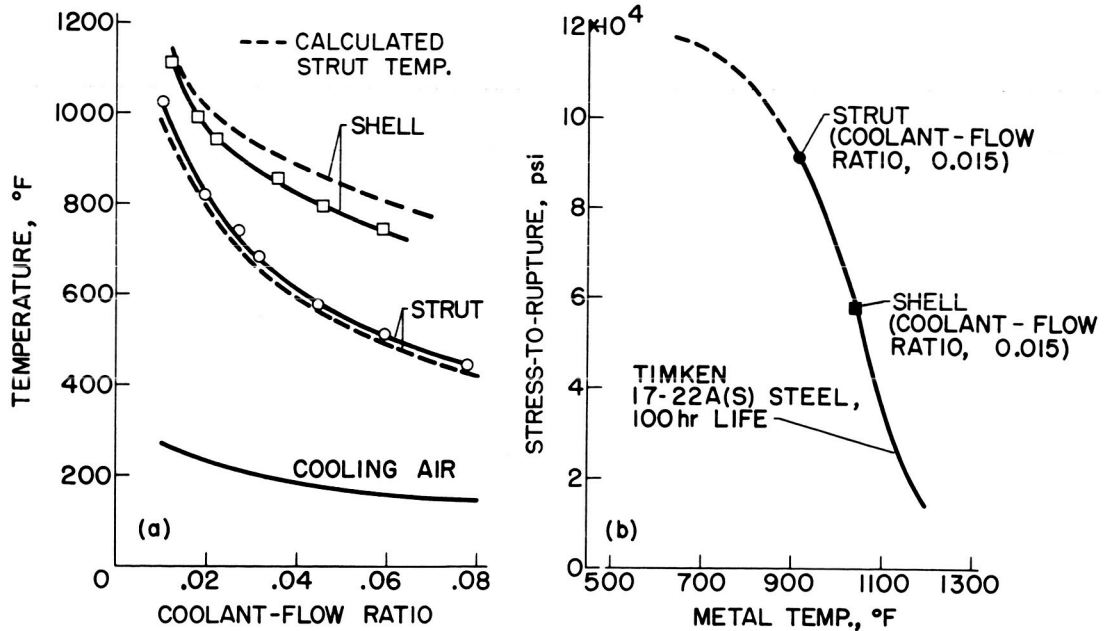


Figure 6

## DEVELOPMENT OF TRANSPIRATION-COOLED TURBINE BLADES

By Patrick L. Donoughe and Anthony J. Diaguila

## INTRODUCTION

In the turbine-cooling research previously described in the papers by Robert O. Hickel and John L. Clure, and by Francis S. Stepka and Eugene F. Schum, the shell and strut of the blade are cooled by convection to the cooling air which passes through the blade in the span-wise direction. Certain restrictions are imposed by this cooling method, since the amount of heat the air can pick up by convection is limited by the inside passage configuration and the cooling-air temperature. A cooling method that relaxes these limitations considerably is transpiration cooling on which research has been conducted at the NACA Lewis laboratory. The purpose of this paper is to give the mechanism of transpiration cooling and to indicate its application to turbine cooling.

## COMPARISON OF CONVECTION AND TRANSPIRATION COOLING

The contrast between the mechanism of convection cooling, described in the paper by Hickel and Clure, and that of transpiration cooling may be seen in figure 1. A convection-cooled, impermeable wall is shown exposed to hot gas flow in figure 1(a). The heat from the gas is conducted through the wall, increases the wall temperature, and is picked up by the cooling air that flows perpendicular to the plane of the paper. A better scheme for reducing the wall temperature is one in which the wall is insulated from the hot gas. Because of its low conductivity and ready availability, air is suggested as an insulating material. The air used for the insulator is forced through a porous material (fig. 1(b)) and reduces the material temperature by convection in its tortuous passage through the wall. This method of temperature reduction is termed transpiration cooling.

An idea of the relative effectiveness of the convection- and transpiration-cooling methods may be obtained from figure 2 where the wall-temperature factor is plotted against mass coolant-flow ratio. The wall-temperature factor is essentially a measure of wall temperature; as this factor decreases, the wall temperature decreases when the gas and coolant temperatures are held constant. The analysis necessary to make a comparison of these cooling methods is given in reference 1.

The results shown in figure 2 are applicable for flow over a flat plate with a turbulent boundary layer for a Reynolds number of  $10^7$ . The efficiency of convection cooling is increased over that indicated in figure 1(a) by augmenting the area exposed to the coolant with the addition of fins on the inner surface. The wall-temperature factor would probably be dictated from a consideration of the required strength of the cooled structure, for example, a turbine blade. If a wall-temperature factor of 0.4 is chosen, the transpiration-cooling method requires only about half as much cooling air as the convection method (fig. 2), even though the convection efficiency has been increased by fin addition. Moreover, it is shown that the difference in coolant requirements between the two methods increases as the temperature reduction increases. It may be deduced, therefore, that the advantages of transpiration cooling are greater in applications where strong cooling is required, for example, for turbine blades subjected to high gas temperatures.

#### DEVELOPMENT

The application of transpiration cooling to a complex structure such as a turbine blade presents many problems. A survey of the advantages and problems resulting from this application was made by the NACA Lewis laboratory in 1949 and 1950 (ref. 2). Experiments were also initiated on transpiration-cooled stator blades fabricated from sintered materials in order to determine proper design methods and validity of existing theories (refs. 3 and 4). References 3 and 4 show that the porous material must be sufficiently thin to allow the cooling air to be brought into the narrow regions near the leading and trailing edges of a turbine blade. For application to turbine rotor blades, the porous shell should also have adequate strength to withstand the imposed forces.

Much research on sintered materials is required to fulfill conditions of sufficient thinness and strength. In view of this urgent need, the U.S. Navy is sponsoring an extensive program for investigating porous sintered materials. At this laboratory, a corduroy wire cloth having the greater portion of wires woven in one direction has been investigated. Enlarged photographs of plan and side views of one of the wire cloths investigated are shown in figure 3. The wires that form the cloth are made of AISI type 304 stainless steel. The mesh of the wire cloth, 20x250, is designated by the number of wires per linear inch in the crosswise direction (20 wires) and lengthwise direction (250 wires). (A greater number of wires in the lengthwise direction might be useful when the lengthwise wires are used in the spanwise direction of a rotor blade where the primary stresses are caused by centrifugal forces.) Cold-rolling the wire cloth improved the tensile strength to values of about 110,000 pounds per square inch at room

temperature and permitted a wide range of permeability to be obtained, so that the cloth was considered satisfactory for turbine blades (refs. 5 and 6).

3078-D

Before a transpiration-cooled turbine blade utilizing wire cloth can be fabricated, many problems must be considered. The permeability required for the wire cloth is dependent on the amount of air passed through the cloth for a given pressure drop across the cloth. The amount of air necessary to obtain sufficient cooling of the porous material is, in turn, determined by the heat transfer through the wall, which is different for laminar and turbulent boundary layers, either one of which may exist adjacent to the turbine blade surface. In addition, there may be some influence on the heat-transfer mechanism by the spanwise flows discussed in the paper by Howard A. Herzig and Howard A. Buckner, Jr. With the assumptions that the spanwise flow is negligible and that the boundary-layer flow is parallel to the chord, the heat transfer to a porous body with a laminar boundary layer was determined in references 7 to 10. Theories for prediction of heat transfer to a porous body with a turbulent boundary layer can be found in references 11 and 12. These laminar and turbulent boundary-layer theories are used in reference 13 to determine the coolant flow necessary to maintain a constant prescribed wall temperature for a transpiration-cooled turbine blade.

For wire cloth (and sintered materials as well), the flow from the inner surface of the cloth to the outer surface is a function of the difference of the squares of the pressures on opposite sides of the wall. Because of this dependency, investigation is required of the pressure distribution around the outside of the blade, which, in conjunction with the coolant pressure inside the blade, will determine the flow through the porous shell and the permeability of the wire cloth. The coolant inside the blade is subjected simultaneously to centrifugal forces, loss of flow, area change, heat addition, compressibility, and friction. A theory for this type flow does not exist at the present time. With the assumption that some of the more influential effects act separately, however, estimates can be obtained for the variation of coolant pressure in the spanwise direction.

The pressure distributions around the outside periphery of a typical turbine blade are given in figure 4. These distributions, obtained with the use of stream-filament theory (ref. 14), were computed for sea-level and 50,000-foot altitude. The coolant supply pressure must always be greater than the total pressure at the leading edge of the blade in order to ensure flow out of the blade. A differential between the coolant supply pressure and the gas pressure at the leading edge (or 0-percent chord) of about 2 pounds per square inch is indicated in figure 4. At the 30-percent-chord location, pressure differences of 375. and 11.5 pounds per square inch are available at the sea-level condition for the

[REDACTED]

suction and pressure surfaces, respectively. These differences at 30-percent chord are reduced to 6 and 3 pounds per square inch at an altitude of 50,000 feet. Because of the different available pressure drops around the periphery of the blade, some parts of a shell with a constant permeability would receive much more coolant than actually required to maintain a constant wall temperature. In addition, the effects of altitude also result in the overcooling at altitude of a blade designed for sea-level conditions (ref. 15).

A means of alleviating the chordwise variation in pressure is to fabricate the blade with different permeabilities at different chordwise locations. Such a method, however, complicates the fabrication of a transpiration-cooled blade. The selection of the permeability, then, is determined by techniques for alleviating the chordwise pressure variation. A method developed at the NACA Lewis laboratory, which not only affords the use of a constant chordwise permeability but also partially compensates for the effects of altitude, is to provide orifices of different sizes in the base of the blade at different chordwise locations (fig. 5). The fins in the spanwise direction of the strut, in conjunction with the porous shell, form compartments for the cooling air fed through the orifices in the blade base. The orifices by their different sizes provide a different pressure inside each compartment. Even though a pressure distribution such as shown in figure 4 may exist around the blade periphery, a constant permeability may be used that simplifies fabrication and yet provides a desired coolant flow and thereby a constant shell temperature (refs. 15 and 16). In addition to forming compartments for the coolant flow, the strut also supports a shell made of wire cloth or a sintered material that does not inherently possess sufficient rigidity or strength.

From the foregoing discussions it may be seen that when the required coolant flow is known from heat-transfer considerations, the permeability of the porous shell of wire cloth can be determined from data given in references 5 and 6. The orifices and the coolant flow are related by the required air flow, the peripheral pressure distribution, and the pressure drop across the orifice.

#### EXPERIMENTS ON COOLING CHARACTERISTICS OF WIRE-CLOTH BLADE

A transpiration-cooled wire blade embodying the strut and orifices was designed for testing in the rotor of a modified jet engine. Although the best range for transpiration cooling is for engines with higher turbine-inlet temperatures than that of this engine, it was believed that by such testing information could be obtained on effects of spanwise flow, wire-cloth forming and fabrication procedures, blockage of pores of the cloth, and the validity of heat-transfer theory used for design. Such experimental work may also indicate further problems to be investigated.

[REDACTED]

Accordingly, a strut was cast of S-816 material (because of its good casting qualities) and orifice and thermocouple holes were located in the cast strut. A 20x200 mesh-wire cloth (unbrazed, to ease forming to a blade shape, ref. 6) was cold-rolled to 0.0205-inch thickness (33.2-percent thickness reduction) for the porous shell. The wire cloth was preformed to the strut shape and attached to it along the fins and at the base by either spot-welding or Microbrazing. (The Microbraze method is thoroughly discussed in the paper by Hickel and Clure.) The tip and trailing-edge sections of the wire-cloth shell were seam-welded, after which serrations were ground in the base to fit the turbine disk. Two such blades were installed in a production turbojet engine that was modified to accommodate the cooled blades similarly to the engines used to test the blades described in the previous papers. Details concerning the necessary engine modifications are given in reference 17.

The experimental heat-transfer results from the engine test of the transpiration-cooled rotor blade are shown in figure 6(b). The temperature data presented are the arithmetical average of the readings of three thermocouples embedded in the strut at about the three-eighths span location from the base at the leading-edge, midchord, and trailing-edge regions. For purposes of comparison, results are also indicated for the corrugated shell-supported blade discussed by Hickel and Clure and for the convection-cooled strut-supported blade discussed by Schum and Stepka. All these results were obtained for a turbine tip speed of 1132 feet per second and a turbine-inlet temperature of 1250° F. The average supporting-member temperature is plotted against the coolant-flow ratio. As would be expected, the shell-supported blade is the hottest, since the shell that supports the blade is exposed directly to the hot gas flow. The temperatures of the transpiration-cooled blade are about the same as the temperatures of the convection-cooled strut which indicates that with respect to heat transfer either cooling scheme is satisfactory at this temperature level. A visual inspection of the transpiration-cooled blade after operation at a tip speed of 1305 feet per second and at a turbine-inlet temperature of 1650° F showed that part of the wire cloth on the trailing edge in the tip region had been severed from the rest of the blade. On other portions of the blade, the wire cloth was not greatly overheated. The severing at the trailing edge indicates that some caution should be exercised in the design of this region; perhaps a shorter span from the trailing edge to the upstream support greatly overheated. The severing at the trailing edge indicates that some caution should be exercised in the design of this region; perhaps a shorter span from the trailing edge to the upstream support would wise flows was not definitely established, it appeared that the wire cloth was cooled sufficiently except in the tip trailing-edge region, regardless of the extent of these flows.

These experiments were considered successful as an initial attempt for a transpiration-cooled rotor blade. There are still many aspects to

be considered, however, before transpiration-cooled blades are at the same state as convection-cooled blades. The attachment techniques should be improved; better estimates of the spanwise flows should be obtained; adequate theories for the flow of coolant inside the compartment should be evolved. These various items should be resolved before studies are carried out on a full-scale engine (all the blades cooled). Such testing is necessary to confirm various analyses which have been and will be made. These problems and others that may arise illustrate the need for continued research in this field of turbine cooling in order that the inherent advantages of transpiration cooling may be utilized to the fullest extent.

#### COMPARISON OF RELATIVE ADVANTAGES OF VARIOUS AIR-COOLED BLADES

In the present and previous papers the relative advantages of different cooled-turbine blades have been compared at a nominal turbine-inlet gas temperature. It has also been shown in the paper by Jack B. Esgar and Richard J. Rossbach that at the present time high turbine-inlet gas temperatures can only be realized by cooling the turbine blades. The particular cooling method to be used at high temperatures is dependent on many items such as ease of blade fabrication, blade weight, and required life. From the results of the various tests and calculations, some fairly definite statements can be made.

At turbine-inlet temperatures of about 2000° F, it appears that the corrugated shell-supported blade and the strut-support blade with impermeable shells will give sufficient cooling. This increase in temperature to 2000° F would yield about a 40-percent increase in thrust over present-day gas temperatures. (See paper by Esgar and Rossbach).

If the turbine-inlet temperature is increased to 2500° F, a thrust increase of the order of 100 percent is obtainable. For this temperature, calculations indicate that reductions in coolant-flow expenditure can be obtained if transpiration cooling is utilized. Before the promise of the gains offered by transpiration cooling can be realized effectively on cooled rotor blades, further research is necessary to resolve the various problems accompanying this cooling method.

The preceding discussion was concerned with turbine rotor blades. For the stator blades, where the strength problems are not as severe, more direct application of transpiration cooling should be possible.

## CONCLUDING REMARKS

The principles and the development of a transpiration-cooled turbine rotor blade have been presented. A comparison of experimental heat-transfer results from a transpiration-cooled blade with a wire-cloth porous shell with those for convection-cooled shell- and strut-supported blades indicated that considerable temperature reductions might be realized. These temperature reductions were accomplished more effectively by the strut-supported blades. The particular cooling method to be used at high turbine-inlet temperatures is dependent on items such as blade fabrication, weight, and life. Convection-cooled blades can be utilized effectively up to turbine-inlet temperatures of 2000° F. At temperatures of about 2500° F, it appears that blade temperature reduction can be accomplished more effectively by transpiration cooling.

## REFERENCES

1. Eckert, E. R. G., and Livingood, John N. B.: Comparison of Effectiveness of Convection-, Transpiration-, and Film-Cooling Methods With Air as Coolant. NACA TN 3010, 1953.
2. Eckert, E. R. G., and Esgar, Jack B.: Survey of Advantages and Problems Associated with Transpiration Cooling and Film Cooling of Gas-Turbine Blades. NACA RM E50K15, 1951.
3. Bartoo, Edward R., Schafer, Louis J., Jr., and Richards, Hadley T.: Experimental Investigation of Coolant-Flow Characteristics of a Sintered Porous Turbine Blade. NACA RM E51K02, 1951.
4. Schafer, Louis J., Jr., Bartoo, Edward R., and Richards, Hadley T.: Experimental Investigation of the Heat-Transfer Characteristics of an Air-Cooled Sintered Porous Turbine Blade. NACA RM E51K08, 1951.
5. Eckert, E. R. G., Kinsler, Martin R., and Cochran, Reeves P.: Wire Cloth as Porous Material for Transpiration-Cooled Walls. NACA RM E51H23, 1951.
6. Donoughe, Patrick L., and McKinnon, Roy A.: Experimental Investigation of Air-Flow Uniformity and Pressure Level on Wire Cloth for Transpiration-Cooling Applications. NACA RM E52E16, 1952.
7. Eckert, E. R. G., and Livingood, John N. B.: Calculations of Laminar Heat Transfer Around Cylinders of Arbitrary Cross Section and Transpiration-Cooled Walls with Application to Turbine Blade Cooling. NACA RM E51F22, 1951.

8. Brown, W. Byron, and Donoughe, Patrick L.: Tables of Exact Laminar-Boundary-Layer Solutions When the Wall is Porous and Fluid Properties are Variable. NACA TN 2479, 1951.
9. Brown, W. Byron, and Livingood, John N. B.: Solutions of Laminar-Boundary-Layer Equations Which Result in Specific-Weight-Flow Profiles Locally Exceeding Free-Stream Values. NACA TN 2800, 1952.
10. Eckert, E. R. G., and Livingood, John N. B.: Method for Calculation of Heat Transfer in Laminar Region of Air Flow Around Cylinders of Arbitrary Cross Section (Including Large Temperature Differences and Transpiration Cooling). NACA TN 2733, 1952.
11. Rannie, W. D.: A Simplified Theory of Porous Wall Cooling. Prog. Rep. No. 4-50, Power Plant Lab. Proj. No. MX801, Jet Prop. Lab., C.I.T., Nov. 24, 1947. (AMC Contract No. W-535-ac-20260, Ord. Dept. Contract No. W-04-200-ORD-455.)
12. Friedman, Joseph: A Theoretical and Experimental Investigation of Rocket-Motor Sweat Cooling. Jour. Am. Rocket Soc., no. 79, Dec. 1949, pp. 147-154.
13. Livingood, J. N. B., and Eckert, E. R. G.: Calculation of Transpiration-Cooled Gas-Turbine Blades. Trans. A.S.M.E., vol. 75, no. 7, Oct. 1953, pp. 1271-1278.
14. Huppert, M. C., and MacGregor, Charles: Comparison Between Predicted and Observed Performance of Gas-Turbine Stator Blade Designed for Free-Vortex Flow. NACA TN 1810, 1949.
15. Esgar, Jack B.: An Analytical Method for Evaluating Factors Affecting Application of Transpiration Cooling to Gas Turbine Blades. NACA RM E52G01, 1952.
16. Esgar, Jack B., and Richards, Hadley T.: Evaluation of Effects of Random Permeability Variations on Transpiration-Cooled Surfaces. NACA RM E53G16, 1953.
17. Ellerbrock, Herman H., Jr., and Stepka, Francis S.: Experimental Investigation of Air-Cooled Turbine Blades in Turbojet Engine. I-Rotor Blades with 10 Tubes in Cooling-Air Passages. NACA RM E50IO4, 1950.
18. Bartoo, Edward R., and Clure, John L.: Experimental Investigation of Air-Cooled Turbine Blades in Turbojet Engine. XIII - Endurance Evaluation of Several Protective Coatings Applied to Turbine Blades of Nonstrategic Steels. NACA RM E53E18, 1953.

ELEMENTS FOR DIFFERENTIATING COOLING METHODS

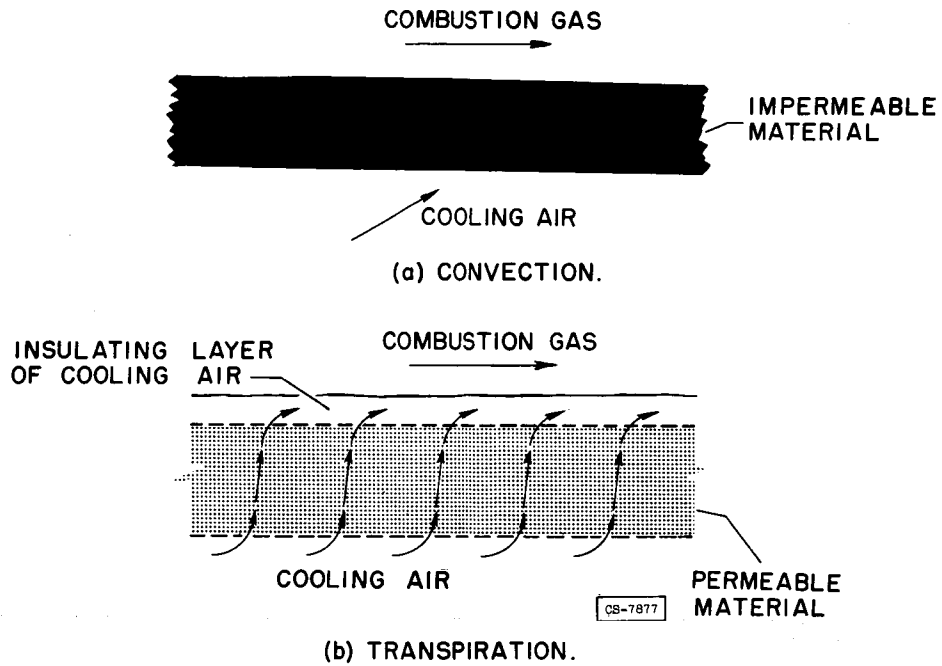


Figure 1

COOLING METHODS FOR TURBULENT FLOW OVER FLAT PLATE

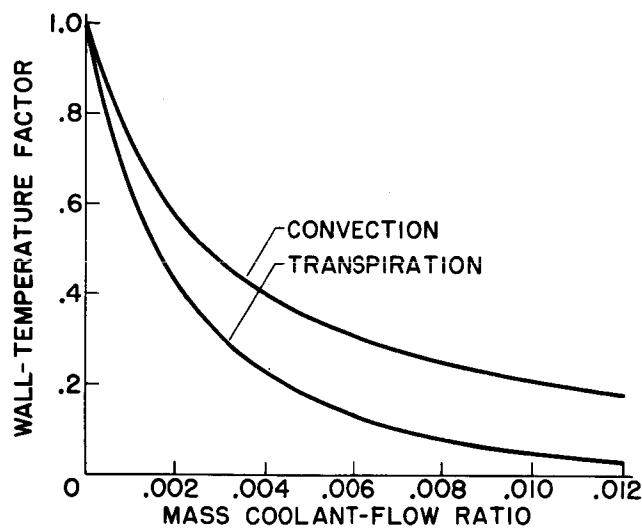


Figure 2



### WOVEN 20x250 MESH CORDUROY WIRE CLOTH

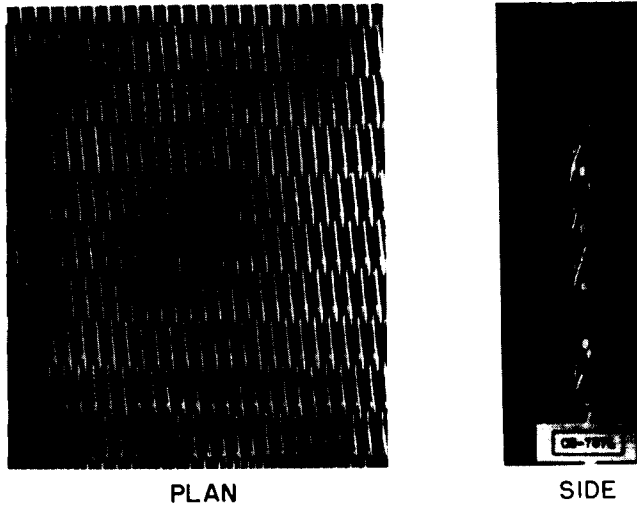


Figure 3

### PRESSURE VARIATIONS AROUND PERIPHERY OF TRANSPIRATION-COOLED ROTOR BLADE

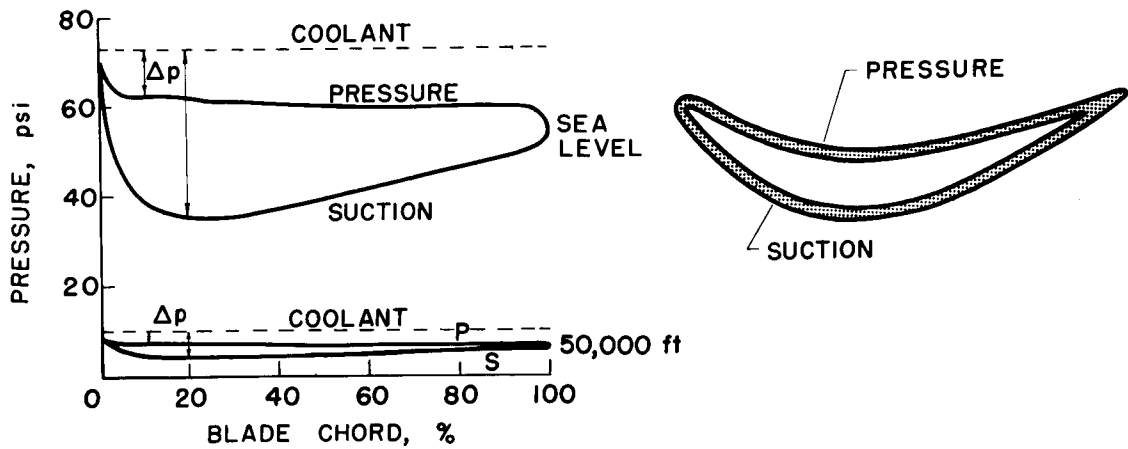
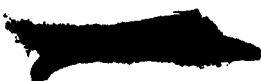


Figure 4



3079-D

### TRANSPIRATION-COOLED BLADE

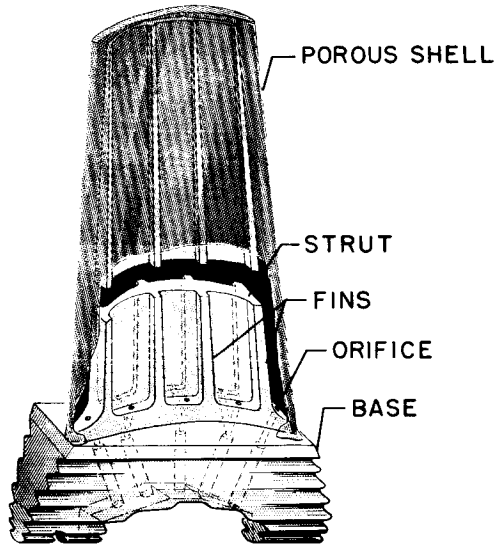
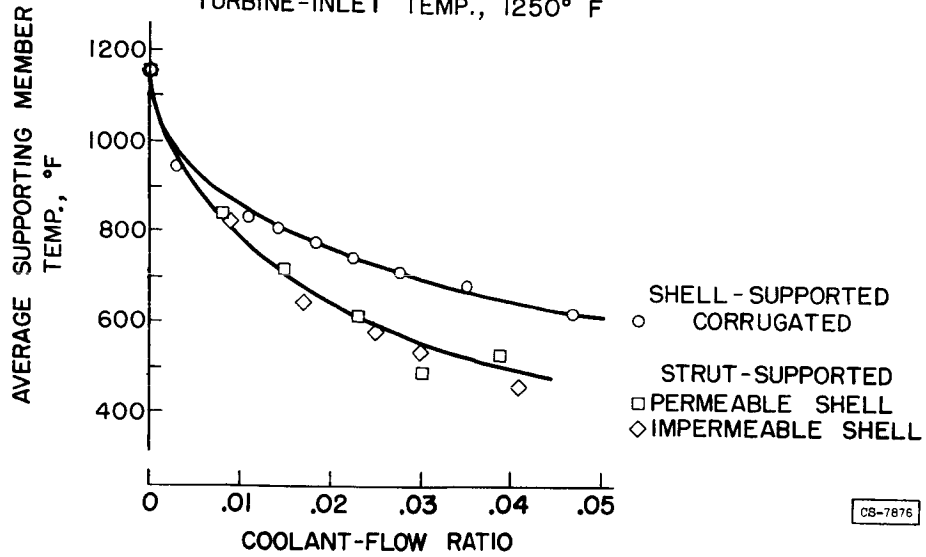


Figure 5

### RESULTS FOR AIR-COOLED BLADES

TURBINE TIP SPEED, 1132 ft/sec  
 TURBINE-INLET TEMP., 1250° F



CS-7876

Figure 6

CONFIDENTIAL

## LIQUID COOLING OF TURBINE BLADES

By John C. Freche

## INTRODUCTION

Despite the wide range of applicability of air cooling, continued turbine-cooling research has shown the desirability of employing liquid cooling in aircraft turbine engines, when very high gas temperatures are encountered and there is a convenient method of dissipating heat from the coolant.

The major objections to liquids as cooling media in aircraft turbines have always been the added weight requirements resulting from the need for a separate cooling supply and the attendant system complexities. In stationary applications where space and weight considerations are generally secondary, this is not a factor and the numerous advantages of liquid cooling make it attractive for such applications. In spite of the weight penalty cited, liquid cooling has sufficient advantages to remain competitive with air cooling in certain aircraft applications and to excel in others. The primary advantages of liquid cooling are the more favorable heat-transfer properties of most liquids in comparison with air and the fact that use of liquid coolants does not necessitate removal of part of the working fluid from the engine thermodynamic cycle as in air cooling. In addition, liquid cooling affords selection from a variety of liquids with widely differing heat-transfer properties as well as the choice of an extremely effective heat-transfer mechanism such as evaporative cooling.

Since it was recognized that liquid cooling may profitably be employed in certain aircraft applications, some liquid cooling research has been conducted at the NACA for the past 6 years. To date, such research has been devoted primarily to defining heat-transfer laws sufficiently to permit their application to liquid-cooled blade design. This paper presents a review of the liquid-cooling investigations conducted to date and indicates the field of applicability of liquid cooling as well as the type and direction of future research on this subject.

## BLADE LIQUID COOLING METHODS

Liquid cooling of turbine blades may be classified as internal and external. A brief description of the heat-transfer processes involved in these classifications follows.



## Internal Blade Cooling

Free convection. - In a free-convection cooling process, coolant circulation depends on buoyant forces arising from differences in density between heated and cooled liquid. This principle has had limited practical applications. When it is considered for application to turbine blade cooling, where circulation is augmented by centrifugal forces as high as 50,000 g's, the potential cooling effectiveness of this process is tremendous. Free-convection circulation within turbine blade coolant passages is illustrated in figure 1(a). The coolant passages provided within the blade need not be interconnected at the blade tip since circulation is effected within the individual passages by the buoyant forces and the large centrifugal forces mentioned. The large arrows in the center of the passages represent the cooler higher-density liquid and the small arrows the heated, lower-density liquid adjacent to the coolant passage walls. In the arrangement shown, analysis of the heat flow is complicated by the fact that a heated boundary layer which may choke coolant circulation is built up along the passage walls.

Forced convection. - In a forced-convection cooling process, the coolant is also forced to flow adjacent to (in the case of a flat plate) or within the heated body. In forced-convection liquid cooling, a continuous path is provided within the blades through which the liquid may be circulated. The process is illustrated in figure 1(b). The main body of flow, indicated by the large arrows in the figure, enters the blade and is forced radially outward, across the blade tip, and radially inward. The smaller arrows indicate free-convection currents which are naturally set up within the passages. When the main body of flow is parallel to these currents, parallel flow results. A condition of counterflow results when these currents oppose the main body of flow.

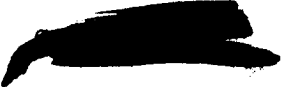
## External Blade Cooling

The mechanism of external or spray cooling is simply one in which the latent heat of vaporization of the liquid is utilized. The cooling liquid is generally injected into the gas stream upstream of the rotor blades. The liquid jet is diffused in the gas stream and the spray particles impinge upon the heated rotor blades. Boiling occurs upon contact and the latent heat of vaporization of the injected liquid is utilized to effect large blade temperature decreases.

## INTERNAL BLADE LIQUID COOLING INVESTIGATIONS

### Free-Convection Heat Transfer

Free-convection heat transfer is discussed in various texts such as reference 1. The process was further examined ideally (ref. 2) and an



[REDACTED]

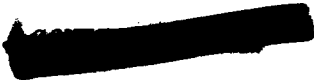
equation describing turbulent-flow free-convection heat transfer along a flat plate was derived. Heat-transfer rates calculated by this equation appeared sufficiently promising to warrant application of free-convection cooling to a turbine. Experimental blade-to-coolant heat-transfer investigations were subsequently conducted with a small-scale free-convection liquid-cooled turbine (ref. 3). Blade coolant passage diameters and locations in this turbine were determined to a great extent by fabrication and stress considerations. The heat-transfer coefficients obtained were found to be less than one-tenth the value that can be calculated from the equation derived in reference 2 for a condition of turbulent free-convection heat transfer along a flat plate. A possible explanation for this failure to achieve the favorable results indicated by theory was circulation blockage within the coolant passages due to the heated boundary layer formed along the passage walls. This possibility was borne out by the analysis of reference 4, which indicated that in blades of 2.5-inch length, the circulation and the cooling effectiveness were considerably decreased in holes with diameters less than 0.146 inch. It therefore appeared that before the principles of free convection could be fully exploited in a turbine application, free-convection flow and boundary-layer formation should be studied experimentally in a suitable apparatus. Consequently, investigations of free-convection flow and mixed free- and forced-convection flow were conducted on a heated stationary tube (refs. 5 and 6). Since free-convection flow is automatically imposed even under conditions of forced-convection circulation (see fig. 1(b)), it was necessary to examine the free-convection component under these conditions as well. A rule for calculation of the heat-transfer coefficients in a mixed-flow regime is cited in reference 1. The investigation of reference 6 indicated that for the case of parallel flow, the actual heat-transfer coefficient was up to 25 percent smaller than the one determined by the rule of reference 1. For the case of counterflow, the measured heat-transfer coefficient was up to 50 percent larger.

Investigations are currently under way with a small-scale turbine in order to establish experimentally the passage diameter limitations which, for a given passage length, will still permit satisfactory free-convection heat transfer.

#### Forced-Convection Heat Transfer

Determination of heat-transfer parameters. - Gas-to-blade and blade-to-coolant heat-transfer investigations were conducted on a small-scale forced-convection liquid-cooled turbine (refs. 7, 8, and 9). An analytically derived method (ref. 10) for calculating the gas-to-blade heat transfer for a given set of conditions and a known blade shape was experimentally verified by the investigation described in reference 8. The investigation of reference 9 indicated that turbine blade-to-coolant heat-transfer data agreed substantially with heat-transfer data for the flow of heated liquids through stationary tubes.

[REDACTED]

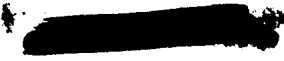


Blade temperature calculations by analytically derived equations. After agreement cited in the previous section had been established, it remained to successfully apply analytical equations for calculation of local liquid-cooled blade temperatures. Similarly derived equations had been applied to air-cooled blades and resulted in reasonable agreement with experimental trailing-edge, leading-edge, and average midchord temperatures both here (refs. 11 and 12) and in England (refs. 13 and 14). The methods of references 10 and 15 were applied to calculating blade temperatures for a small-scale liquid-cooled turbine (ref. 16). Generally good agreement was achieved when the calculated values were compared with those obtained experimentally over a range of gas temperatures from 400° to 1600° F.

Because blades usually have thin trailing edges, it is difficult to locate a coolant passage sufficiently near the trailing edge for adequate cooling. A way of overcoming this difficulty is by use of high-conductivity material inserts as described in reference 17. For accurate calculations of blade trailing-edge temperatures when high-conductivity material inserts were employed, the analytically derived equations had to be adjusted to account for the effect of different thermal conductivities in the blade section under consideration. The calculation procedure was verified experimentally by measured temperatures obtained from an investigation (ref. 16) of a stationary, water-cooled, low-conductivity material blade with a copper insert brazed into the trailing-edge section.

Blade temperature calculations by electric analog. - Numerical methods of calculating blade temperature, although shown to be accurate, are nevertheless time-consuming. Because of the general similarity between heat flow and electrical flow and of the work done by other investigators in reducing the time requirements for certain heat-transfer calculations by use of electrical analogs, the application of electric analogy to blade temperature calculations was considered. It was necessary to determine whether electric analogs could be applied for this purpose without the use of expensive and time-consuming apparatus. A number of electrical resistor network-type analogs were developed at the NACA for specific blade configurations (ref. 18). These are easily fabricated from readily available materials. A network-type analog employing calibrated resistance wire and representing a liquid-cooled blade which was 25 times the size of the actual blade was used to determine blade temperatures for several blade-to-coolant heat-transfer coefficients. The results were considered generally satisfactory for design purposes; it was estimated that for one set of design conditions alone, the time required to obtain blade temperature at a given span position can be reduced from 20 days using numerical methods to one day using an analog.

Cooling effectiveness comparison with air-cooling methods. - In order to provide a more complete picture of where internal blade forced-convection liquid cooling ranks in relation to air-cooling methods



discussed in other papers in this series, a theoretical comparison is presented in figure 2. In this figure a blade temperature reduction factor for a flat plate is plotted against mass coolant flow ratio for the case of convection air cooling, convection liquid cooling, and transpiration air cooling. The blade temperature reduction factor is defined as the ratio of the temperature difference between the blade wall and coolant to the temperature difference between the gas and coolant. This is

expressed in symbol form as  $\frac{T_w - T_c}{T_g - T_c}$ . All symbols are defined in the

appendix. Consideration of the term indicates that the smaller the ratio, the more effective the cooling. The mass coolant flow ratio is defined as the ratio of the coolant mass velocity to gas mass velocity,  $\rho_c V_c / \rho_g V_g$ .

The comparison in figure 2 is based on a flat plate and a constant gas-flow Reynolds number. The calculation procedure is fully described in reference 19. A thermal effectiveness  $\eta_T$  of 0.7 was chosen for the air-cooling methods compared in figure 2 because this value was believed to be representative of that encountered in turbine applications. Thermal effectiveness is defined as the ratio of the coolant temperature rise to the temperature difference between the blade and coolant. A thermal effectiveness of 0.4 was chosen for liquid cooling. In reference 20 a sample calculation was made for an optimum water-cooling circulation system. The liquid-cooling thermal effectivenesses of 0.4 used in figure 2 of this paper was determined from the calculated blade temperature and the assumed gas and coolant temperatures utilized in this sample calculation. Figure 2 indicates forced-convection water cooling to be the most effective of all cooling methods compared up to a mass coolant flow ratio of 0.004. Beyond this point, transpiration cooling is slightly more effective, although forced-convection water cooling remains approximately 10 percent more effective than convection air cooling over the remainder of the coolant flow range likely to be encountered in aircraft turbine applications. The high cooling effectiveness, especially at the higher coolant flows, indicates internal blade liquid water cooling to be desirable for high-gas-temperature applications where larger quantities of coolant flow are required.

#### EXTERNAL BLADE LIQUID-COOLING INVESTIGATIONS

External blade liquid cooling has been investigated both here and abroad. Water sprays were the cooling medium employed. A static cascade and a turbosupercharger were employed in spray cooling investigations conducted in reference 21. The purpose of these investigations was to determine the feasibility of applying spray cooling to turbines fabricated from noncritical materials for marine applications. Water spray cooling was applied to a full-scale turbojet engine in references 22 to 24. In both cases, substantial blade temperature reductions were reported. Because of its apparent effectiveness, spray cooling was considered as a

means of permitting short-time engine operation at elevated engine speeds and gas temperatures in order to achieve thrust increases; an investigation of water spray cooling of standard solid rotor blades was initiated at the NACA Lewis laboratory with a centrifugal-flow turbojet engine. The NACA investigations are fully described in references 25 and 26.

### Methods of Cooling Water Injection

Various methods of cooling water injection were investigated in order to determine the most favorable on the dual basis of cooling effectiveness and general applicability. The general types of injection configuration considered are illustrated in figure 3.

Stator-blade injection configurations. - The stator-blade injection configurations include those designated A and B in figure 3. With configuration A, water is introduced downstream into the gas-flow passage from orifices provided in the stator-blade trailing edge. With configuration B, water is introduced cross stream to the gas-flow passage from orifices provided on the stator-blade suction surface. Configuration A was also employed by the British (refs. 22 to 24).

Stator diaphragm inner- and outer-diameter injection configurations. - The axial location of the injection orifices in the inner ring of the stator diaphragm was varied from the stator-blade trailing edge to slightly upstream of the stator-blade leading edge. Only one orifice in the former location, labeled configuration C, is shown in figure 3. Orifice locations in the outer ring of the stator diaphragm (configuration D) were also varied downstream of the location indicated in figure 3 to a point of injection directly opposite the rotor blade tips.

Spray bar. - The spray-bar-type injection configuration consisted of two Inconel tubes inserted into the gas stream approximately midway between the stator blade leading and trailing edges 180° apart. Each was provided with four orifices directed downstream. The investigation of reference 21 also utilized this general type of configuration.

### Suitability of Spray-Cooling Injection Configurations

Cooling effectiveness. - Since the blade is most highly stressed at the lower spanwise stations (root to midspan), adequate cooling is particularly desirable at these stations. Attempts to cool the blade tip region were ineffective, but this is not considered particularly serious because this region of the blade is lightly stressed. The most satisfactory way of achieving cooling at both the root and midspan simultaneously was by use of different orifice diameters located in the inner ring of the stator diaphragm near the stator-blade trailing edge. Four

orifices were employed; the blade root was adequately cooled by two 0.078-inch-diameter orifices, while the blade surface above the root to the midspan was cooled by two larger orifices, 0.135 or 0.150 inch in diameter, depending upon the maximum flow rates desired.

A comparison of the blade-temperature distribution encountered in the blade root and midspan for a nominal coolant-to-gas flow ratio of 0.022 (approximately 5600 lb/hr of coolant flow) at rated engine speed is presented in figures 4(a) and 4(b), respectively, for the most favorable injection configuration (configuration C, fig. 3), and for one less favorable (combination of configurations A and B, fig. 3). The uncooled midspan blade-temperature distribution is also presented. The tremendous effectiveness of spray cooling is immediately apparent from the approximately 1000° F temperature drop between the uncooled and cooled condition (fig. 4(a)). Although configuration C is more effective, on a quantitative basis of blade temperature reduction, the smaller chordwise temperature differences encountered, particularly at the blade root, are the major factor in labeling it as being more favorable. Elimination of chordwise temperature differences is desirable from a stress standpoint and is discussed in detail in another paper in this series by Hickel and Clure. The effect of these temperature differences on blade life is discussed in references 25 and 26.

The cooling effectiveness demonstrated with configuration C in figure 4 actually represents a degree of overcooling with the blade material (S-816) employed. The degree of overcooling is dependent upon the total blade stress and the type of blade material. The margin between blade stress and allowable material stress increases as the material temperature is decreased. Maximum material strength properties occur at various temperatures depending upon the material under consideration. Cooling below the temperature which results in maximum material strength or below a temperature which provides a desired margin between blade stress and material strength is termed overcooling. Reduction in coolant flow rate will not satisfactorily reduce the degree of overcooling. Operation at the coolant flow rate indicated in figure 4 with the configurations investigated is necessary in order to overcome undesirable blade chordwise temperature differences at rated engine speed. Higher coolant flow rates will be required at overspeed and overtemperature conditions. An approximate indication of the coolant flow requirements for such operation of the engine under investigation was determined by extrapolation from rated speed data (ref. 25). A coolant-to-gas flow ratio of 0.0315 (equivalent to a coolant flow rate of approximately 20 gal/min) appears to be necessary for operation at an overspeed of 10 percent and a turbine-inlet gas temperature of 2000° F. This coolant flow is approximately 30 percent greater than the calculated fuel flow at this operating condition.

General applicability of injection configurations. - Consideration of all the configurations investigated on the basis of practical factors

[REDACTED]

which affect general applicability indicates that the configuration shown to be most favorable on a cooling basis is also most favorable on an overall basis. For example, stator blade injection (configurations A and B) provided considerable difficulty with welding cracks and clogging of the small orifices. The spray bar, besides obstructing gas flow, was badly bent because of the gas temperature and gas forces encountered after only 1 hour of operation, thereby endangering the rotor blades. In addition, the initial installation requirements of these configurations are considerably more complicated than those necessary to provide orifices in the inner ring of the stator diaphragm.

#### Thrust Increases Made Possible by Spray Cooling

In view of its extremely effective cooling potential, spray cooling may be considered as a means of blade cooling under conditions of gas temperature and engine speed higher than the design condition. In order to determine the gains in thrust accruing from engine operation under such conditions, an analysis was conducted with a centrifugal-flow turbojet engine and limited experimental verification obtained with such an engine. These results are considered as follows.

The calculated thrust increases available with a typical centrifugal-flow turbojet engine at overspeed and overtemperature are graphically illustrated in figure 5. The calculated gains available by providing compressor water injection in addition to spray cooling are also presented. A 0.03 coolant-to-gas flow ratio was chosen as being realistic from the standpoint of providing adequate spray cooling to permit engine operation over the range of conditions considered, and a 0.03 compressor water-to-gas flow ratio was considered. The plain bars in the figure are for the spray-cooled condition; the lined bars, for the combination of spray cooling and compressor water injection. Figure 5(a) presents the thrust increase above rated thrust at various turbine-inlet gas temperatures at rated engine speed. When the condition of engine operation with spray cooling alone is considered, the thrust increase at calculated rated gas temperature with a 0.03 spray coolant-to-gas flow ratio is virtually negligible. The engine mass flow is not augmented sufficiently by the amount of water required for spray cooling to provide an appreciable thrust increase. This serves to emphasize the fact that the water spray is not in itself the thrust augmentation medium, but rather the means of permitting engine operation at higher energy levels. As the gas temperature is increased to 1820° F at rated engine speed, analysis indicates that a  $4\frac{1}{2}$ -percent thrust increase occurs. The results of experimental operation at this point, indicated on the figure by the dotted line, show a 3-percent gain in thrust. At the highest gas temperature considered, 2000° F, analysis indicates a 10-percent thrust increase; however, experimental verification is not available at this operating point. In

[REDACTED]

general, thrust increases due to operating the engine at overtemperature and rated speed are not great. This is probably due to losses in overall mass flow at higher gas temperatures which offset in part the gains available from overtemperature operation. When compressor water injection, in addition to spray cooling, is applied at each of the engine operating conditions considered, the thrust increase is more marked in each instance. Again, no experimental data are available to verify the analytical compressor-water-injection results.

Figure 5(b) indicates the thrust increases possible if the engine is permitted to overspeed simultaneously with increases in turbine-inlet gas temperatures. The gains are more appreciable than for the rated-speed condition because of substantial mass-flow increases which occur with increases in engine speed. For a condition of 4-percent overspeed and 1903° F turbine-inlet gas temperature, a 20-percent thrust increase is shown analytically. Experimental results at this condition show a 14.5-percent increase. The compressor component of the engine under investigation limited engine operation to this speed, and burnout of several stator blades due to unsatisfactory burner performance limited the turbine-inlet gas temperature obtainable. However, analysis indicates that a 40-percent thrust increase may be obtained at a 10-percent overspeed condition and 2000° F with spray cooling. When compressor water injection is added, a 50-percent increase occurs at this condition. A total water-to-gas flow ratio of 0.06 is employed in this case. Translated into terms of water requirements for 1-minute operation with the engine considered in the analysis, this is equivalent to approximately 40 gallons.

A complete description of the procedure employed in the foregoing analysis is presented in reference 25. However, it should be noted here that several simplifying assumptions were made. Chief among these were use of a constant turbine efficiency and the use of a compressor map in which the lines of constant corrected speed are somewhat idealized in that they consist of straight segments (fig. 4, ref. 25). In spite of these assumptions, the limited experimental data indicated reasonable agreement with analysis. The differences which exist probably result from the fact that the engine employed in the test did not exactly match the assumed compressor and turbine characteristics used in the calculations, and that the assumptions set forth in the calculations do not account for such factors as the effect of coolant introduction on aerodynamic gas flow. The limited engine operation also indicated that introduction of water spray did not introduce variables of a magnitude sufficient to upset the compressor and turbine matching characteristics. Whether similar agreement exists over the entire range of conditions considered in the analysis cannot be stated with certainty. Substantial thrust increases would still result from overspeed, overtemperature operation, even though experimental values were considerably lower than the analytical values indicate.

It should be emphasized that the thrust increases available by operating the engine at overspeed and overtemperature are dependent upon the compressor and turbine characteristics of the engine under consideration. Although the results presented are for a centrifugal-flow engine, there is no reason to assume that worthwhile gains cannot be similarly achieved with axial-flow engines. In fact, preliminary calculations with a current axial-flow engine indicate the possibility of slightly greater gains than shown here by operation at overtemperature and rated speed with spray cooling.

## APPLICATION OF LIQUID COOLING TO AIRCRAFT TURBINE ENGINES

The preceding discussions have indicated the major features of internal and external blade liquid-cooling methods. Before the discussion of various aircraft applications to which internal or external blade liquid cooling methods may be advantageously applied, a brief survey will be given of several internal blade liquid cooling systems which are described in detail in reference 20 and which utilize the basic heat-transfer mechanisms (free- or forced-convection) described previously.

### Internal Blade Liquid-Cooling Circulation Systems

One-liquid systems. - In order to reduce cooling requirements when gas temperatures are not extreme, it may not be desirable to have extremely high heat-transfer coefficients in the coolant passages. A straight-through flow of the coolant in the rotor blades will result in a minimum heat-transfer rate and as high a level of blade temperature as can be achieved with whatever liquid coolant is used. However, when the coolant is permitted to recirculate through the blades many times prior to discharge from the rotor, a so-called loop circuit is established. By this means, extremely high heat-transfer coefficients and very low blade temperatures may be achieved. This is the type of circulation system employed in the sample calculation in reference 20 which provided the thermal effectiveness factor used to obtain the liquid cooling curve shown in figure 2. Although use of liquids normally provides extremely effective cooling, situations can arise in which further increases in the cooling effectiveness may be desirable. For example, in future turbines driving supersonic compressors, especially with low-strategic-alloy-content metals, stresses may make maintenance of very low blade temperatures desirable. Also, if the less effective liquids, such as fuel, are employed, it may be desirable to utilize the loop circuit.

Two-liquid systems. - Another type of system which may be desirable in some instances is a two-liquid system. For instance, if the turbine blades are to be easily removable, cooling the turbine disk with water or fuel and the blades by means of sodium or some other liquid metal may

be feasible. The liquid metal (the primary fluid) would remove heat from the blades and transport it by free convection to the blade roots, where it would be removed by the secondary fluid which circulates through the rotor adjacent to the blade roots. By this means, the problem of sealing the liquid between the blades and disk is eliminated. However, other disadvantages, a chief one being relatively ineffective heat transfer between primary and secondary coolants, must be carefully considered before this method is adopted. Many additional circulation systems are feasible. However, the foregoing should serve to indicate that if internal blade cooling is utilized, a circulation system can generally be provided which will accommodate specific design requirements such as high heat-transfer coefficients, blade replaceability, and so forth.

#### Aircraft Applications of Internal Blade Liquid Cooling

An insight into the applicability of internal blade liquid cooling to aircraft is given in the analysis of reference 27. This analysis includes the media to which the internal blade coolant rejects its heat as part of the aircraft cooling system. Complete aircraft cooling systems are the subject of another paper in this series by Hubbartt. The analysis indicates that, for interceptor-type aircraft assigned a combat mission at 50,000 feet altitude and a Mach number of 2, most liquid-cooling systems are either inadequate or at best inferior to air cooling. The inadequacy of internal blade liquid cooling in these instances does not stem from inability of the liquid coolant to maintain safe blade operating temperatures, but rather from highly effective blade cooling coupled with relatively ineffective final heat rejection from the system. For example, for interceptor application, an internal blade water-cooling system with final heat rejection to ram air becomes impractical because of high ram air temperatures (425° F at a Mach number of 2.5). At normal pressures water boils well below this temperature. In order to maintain water as a liquid at a sufficiently high temperature to permit heat rejection to ram air under these conditions, extremely high pressures which may be prohibitive from a design standpoint are required. If adequate fuel flow rates are available, use of direct fuel cooling appears feasible. However, heavy demands are currently being made on engine fuel as a heat rejection medium for oil coolers and other auxiliaries, which reduces the quantity available for turbine blade cooling. Possible chemical instability of fuel under extreme pressures which may cause clogging of blade coolant passages is an additional aspect of this application which must also be considered.

In view of the limitations expressed, additional research in several fields is indicated which may serve to make internal blade liquid cooling more readily applicable to the aircraft installations discussed previously. For example, determination of the heat-transfer and vapor-pressure

characteristics of high-boiling-point liquids would be desirable. If suitable liquids can be found, higher coolant-discharge temperatures can be used, which may make an internal blade liquid-cooling system with final heat rejection to ram air feasible. Another likely area of research is the determination of heat-transfer data with fuel under pressure and temperature conditions comparable to those occurring in a turbine engine application to check the cooling effectiveness as well as the chemical stability of fuel.

There are several aircraft applications, however, in which internal blade liquid cooling, even at this stage of the art, may be used advantageously. One application is the guided-missile engine utilizing fuel cooling with final heat rejection to afterburner fuel. If afterburning occurs throughout the flight of the missile, the limitation of periods of nonafterburning operation which made fuel cooling inadequate for interceptor application (see previous discussion) are removed, and fuel may be used as the cooling medium, if centrifuging effects do not result in blade passage clogging or if chemical stability is sufficient to withstand cracking and coking. This provides the most efficient cooling method possible since the heat rejected to the cooling medium is reclaimed by being returned to the engine cycle.

A second application is to subsonic bombers and transports. Here an internal blade water-cooling system with final heat rejection to ram air appears feasible. The limitation of high ram air temperature which occurred with the interceptor (see previous discussion) has been removed. This liquid cooling system may be applied advantageously to both moderately high-gas-temperature engines ( $2000^{\circ}$  F) and high-gas-temperature engines ( $2500^{\circ}$  F). In the former case for nonafterburning engines, small gains in performance can probably be achieved by cooling with water rather than air since liquid cooling does not necessitate removal of part of the working fluid from the cycle. In the latter case, the small loss in thermodynamic efficiency resulting from internally liquid-cooled turbine blades and the large gains in power output available from the large gas temperature increases (ref. 28) also indicate the possibility of profitable application.

#### Aircraft Applications of External Blade Liquid Cooling

Three outstanding facts are apparent from the spray cooling investigations conducted to date which serve to pinpoint the particular fields of applicability of this cooling method. First, the very nature of the spray cooling mechanism (coolant is not recoverable) limits its application to brief periods of time in a turbojet engine since there are definite limitations as to the quantity of coolant which may be provided. Second, simple, easy-to-maintain injection configurations require only minor engine modifications. Finally, the extremely effective cooling made possible by this method warrants its application under engine operating conditions which impose unusually high stresses on the turbine

[REDACTED]

blades. Since such conditions occur at overspeed and overtemperature, and since analysis has indicated that large potential gains in thrust are possible under these conditions, spray cooling may be applied to realize these gains by sufficiently reducing the blade temperature so that the material strength properties can adequately withstand the added stress. The desirability of providing added thrust with a minimum weight penalty is evident. Depending upon the engine size, thrust augmentation may be needed at take-off, passing into the supersonic regime, or for high-speed maneuver. It should be noted that care must be exercised in an application of external blade spray cooling to fabricated air-cooled blades because of the extremely detrimental effect of imposed temperature gradients on life with blades of this type (ref. 25).

#### SUMMARY OF RESULTS

A survey of turbine blade liquid cooling is presented as follows:

1. On the basis of heat-transfer effectiveness, internal blade convection liquid cooling is considerably more effective than convection air cooling over the entire range of coolant flows likely to be encountered in turbines. It is only slightly less favorable than transpiration cooling in the high coolant flow range.

2. Investigations conducted with a small-scale liquid-cooled turbine experimentally verified an analytically derived method for calculating gas-to-blade heat transfer and indicated that blade-to-coolant heat-transfer data agreed substantially with available data for stationary tubes.

3. Liquid-cooled turbine-blade temperatures were calculated by analytical equations and by an electric analog. Satisfactory agreement with experimentally obtained blade temperatures was achieved by both methods and a great saving in time was effected by use of the analog in place of numerical methods.

4. Investigation of external blade liquid cooling by means of water sprays resulted in the determination of the most favorable of several methods of cooling water injection on the dual basis of cooling effectiveness and general applicability. Orifices provided in the inner ring of the stator diaphragm near the stator blade trailing edge were found to be most effective.

5. Internal blade liquid cooling is readily applicable to stationary installations and has a favorable potential as regards certain aircraft installations.

6. Spray cooling affords a means of permitting turbojet engine operation at overspeed and overtemperature in order to achieve large thrust increases for take-off or combat.

[REDACTED]

## APPENDIX - SYMBOLS

The following symbols are used in this report:

T	temperature
V	velocity
W	weight flow
$\eta$	effectiveness
$\rho$	density

## Subscripts:

c	coolant
g	gas
T	thermal
w	wall

## REFERENCES

1. McAdams, William H.: Heat Transmission. Second ed., McGraw-Hill Book Co., Inc., 1942.
2. Eckert, E. R. G., and Jackson, Thomas W.: Analysis of Turbulent Free-Convection Boundary Layer on Flat Plate. NACA TN 2207, 1950.
3. Diaguila, Anthony J., and Freche, John C.: Blade-to-Coolant Heat-Transfer Results and Operating Data from a Natural-Convection Water-Cooled Single-Stage Turbine. NACA RM E51117, 1951.
4. Eckert, E. R. G., and Jackson, Thomas W.: Analytical Investigation of Flow and Heat Transfer in Coolant Passages of Free-Convection Liquid-Cooled Turbines. NACA RM E50D25, 1950.
5. Eckert, E. R. G., and Diaguila, A. J.: Experimental Investigation of Free-Convection Heat Transfer in Vertical Tube at Large Grashof Numbers. NACA RM E52F30, 1952.
6. Eckert, E. R. G., Diaguila, Anthony J., and Curren, Arthur N.: Experiments on Mixed-Free- and Forced-Convective Heat Transfer Connected with Turbulent Flow Through a Short Tube. NACA TN 2974, 1953.

7. Freche, John C., and Diaguila, A. J.: Heat-Transfer and Operating Characteristics of Aluminum Forced-Convection and Stainless-Steel Natural-Convection Water-Cooled Single-Stage Turbines. NACA RM E50D03a, 1950.
8. Freche, John C., and Schum, Eugene F.: Determination of Gas-to-Blade Convection Heat-Transfer Coefficients on a Forced-Convection, Water Cooled Single-Stage Aluminum Turbine. NACA RM E50J23, 1951.
9. Freche, John C., and Schum, Eugene F.: Determination of Blade-to-Coolant Heat-Transfer Coefficients on a Forced-Convection, Water-Cooled, Single-Stage Turbine. NACA RM E51E18, 1951.
10. Brown, W. Byron, and Donoughe, Patrick L.: Extension of Boundary-Layer Heat-Transfer Theory to Cooled Turbine Blades. NACA RM E50F02, 1950.
11. Brown, W. Byron, Slone, Henry O., and Richards, Hadley T.: Procedure for Calculating Turbine Blade Temperatures and Comparison of Calculated with Observed Values for Two Stationary Air-Cooled Blades. NACA RM E52H07, 1952.
12. Ellerbrock, Herman H., Jr.: Some NACA Investigations of Heat-Transfer Characteristics of Cooled Gas-Turbine Blades. Paper presented at the General Discussion on Heat Transfer. Inst. Mech. Eng. (London) and A.S.M.E. (New York) Conference (London), Sept. 11-13, 1951.
13. Andrews, S. J., and Bradley, P. C.: Heat Transfer to Turbine Blades. Memo. No. M.37, British N.G.T.E., Oct. 1948.
14. Smith, A.: Heat Flow in Gas Turbines. War Emergency Issue, No. 41, pub. by Inst. Mech. Eng. (London). (Reprinted in U.S. by A.S.M.E., Apr. 1949, pp. 245-254.)
15. Livingood, John N. B., and Brown, W. Byron: Analysis of Temperature Distribution in Liquid-Cooled Turbine Blades. NACA Rep. 1066, 1952. (Supersedes NACA TN 2321.)
16. Schum, Eugene F., Freche, John C., and Stelpflug, William J.: Comparison of Calculated and Experimental Temperatures of Water-Cooled Turbine Blades. NACA RM E52D21, 1952.
17. Freche, John C.: A Summary of Design Information for Water-Cooled Turbines. NACA RM E51A03, 1951.
18. Ellerbrock, Herman H., Jr., Schum, Eugene F., and Nachtigall, Alfred J.: Use of Electric Analogs for Calculation of Temperature Distribution of Cooled Turbine Blades. (NACA TN to be pub.)

19. Eckert, E. R. G., and Livingood, John N. B.: Comparison of Effectiveness of Convection-, Transpiration-, and Film-Cooling Methods with Air as Coolant. NACA TN 3010, 1953.
20. Jackson, Thomas W., and Livingood, John N. B.: Analytical Investigation of Two Liquid Cooling Systems for Turbine Blades. NACA RM E51F04, 1951.
21. Somers, Edward V., Kemeny, George A., and Burke, Edward B.: Water Spray Cooling of Turbine Blades. Res. Repts. SR-430, May-July 1949; SR-436, Aug.-Oct. 1949; SR-441, Nov.-Dec. 1949-Jan. 1950; SR-454, May-July 1950; SR-460, Nov. 1950; SR-462, Nov. 1, 1950-Jan. 31, 1951; SR-466, Feb. 1 - Apr. 30, 1951; SR-475, May 1 - July 31, 1951; SR-483, Aug. 1 - Oct. 31, 1951; Final Report, SR-521, Dec. 1952. Westinghouse Res. Labs., Westinghouse Electric Corp. (Contract NOBS-47770.)
22. Kenworthy, K. R. F.: Preliminary Tests to Investigate Turbine Blade Cooling by Direct Water Spray. Memo. No. M.75, British N.G.T.E., Mar. 1950.
23. Kenworthy, K. R. F.: Further Tests on a W2/700 Engine with Water Spray Cooling of the Turbine Blades. Memo. No. M.121, British N.G.T.E., Aug. 1951.
24. Kenworthy, K. R. F.: A Test to Ascertain the Turbine Blade Temperature Profiles on a W2/700 Engine Using Direct Water Spray Cooling. Memo. No. M.127, British N.G.T.E., Sept. 1951.
25. Freche, John C., and Stelpflug, William J.: Investigation of Water-Spray Cooling of Turbine Blades in a Turbojet Engine. NACA RM E53A23, 1953.
26. Freche, John C., and McKinnon, Roy A.: Experimental Investigation of Several Water-Injection Configurations for Turbine-Blade Spray Cooling in a Turbojet Engine. NACA RM E53H06, 1953.
27. Schramm, Wilson B., Nachtigall, Alfred J., and Arne, Vernon L.: Analytical Comparison of Turbine-Blade Cooling Systems Designed for a Turbojet Engine Operating at Supersonic Speed and High Altitude. I - Liquid-Cooling Systems. NACA RM E52J29, 1953.
28. Hawthorne, W. R.: A Theoretical Study of the Thermodynamic Conditions in Gas Turbines Due to Blade Cooling by the Use of Liquid - High Temperature Gas Turbines with Cooled Blades - A Preliminary Survey of Two Simple Plants. Tech. Rep. No. 6574-4, Gas Turbine Lab., M.I.T., May 1949. (ONR Contract N5ori-78, Task Order 21, NR-220-010, Proj. DIC 6574.)

3078-D

# METHODS OF INTERNAL BLADE LIQUID COOLING

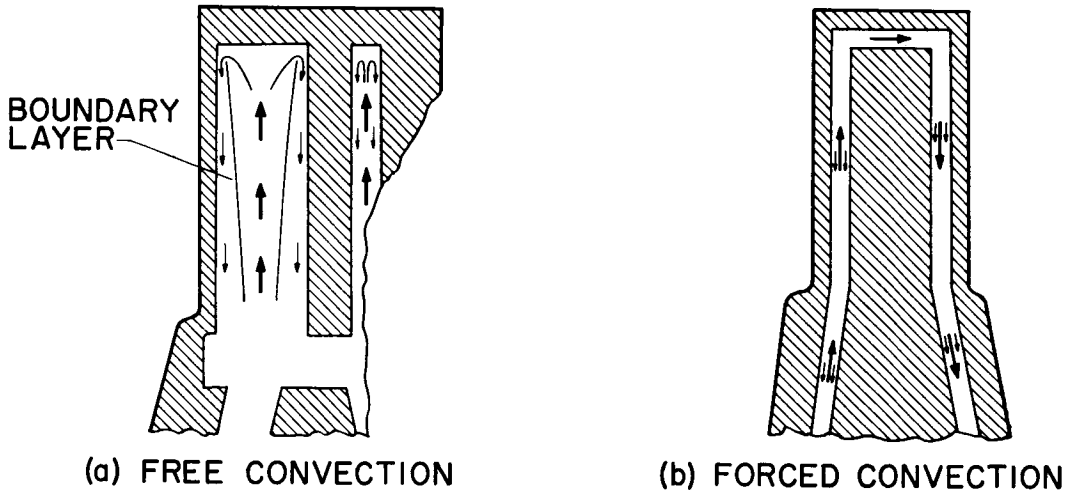


Figure 1

## EFFECTIVENESS OF VARIOUS COOLING METHODS

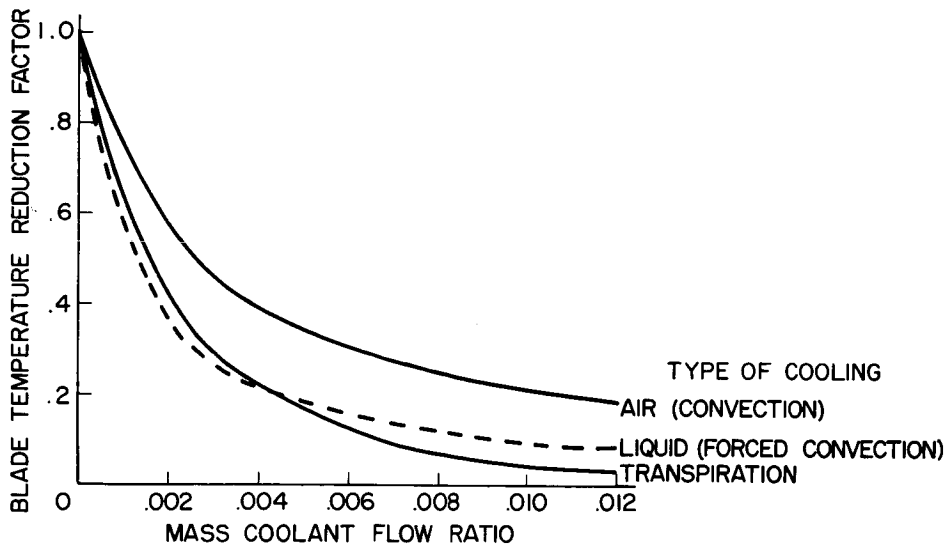


Figure 2

# WATER SPRAY INJECTION CONFIGURATIONS

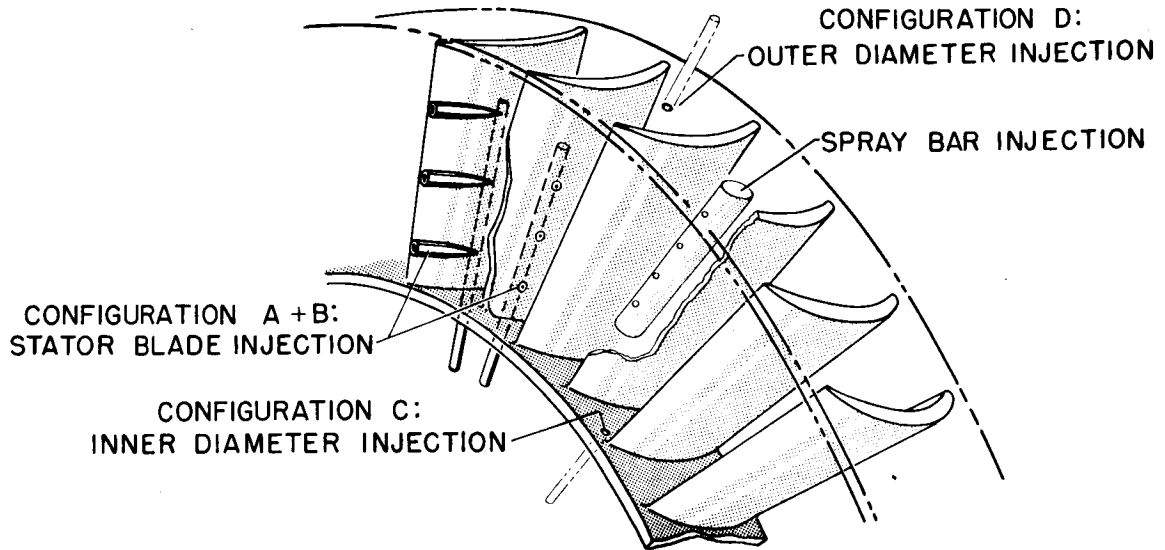


Figure 3

CHORDWISE TEMPERATURE DISTRIBUTIONS WITH TWO WATER-INJECTION CONFIGURATIONS COOLANT-FLOW RATIO, 0.022

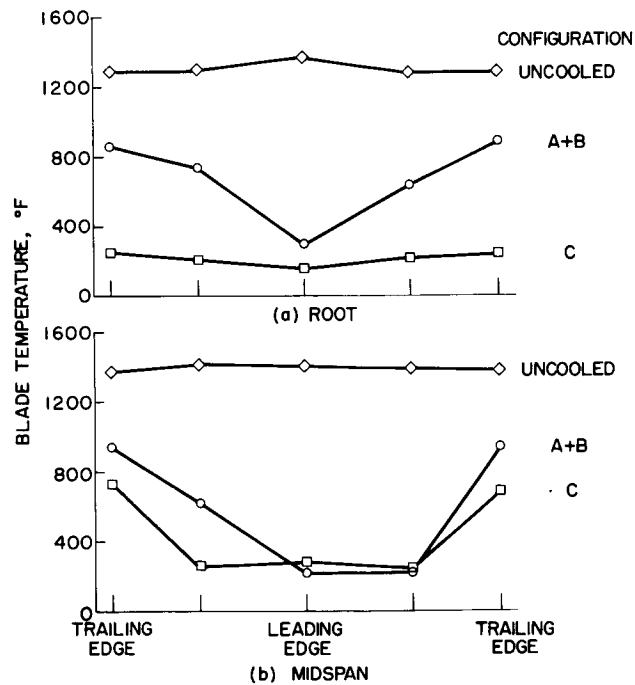
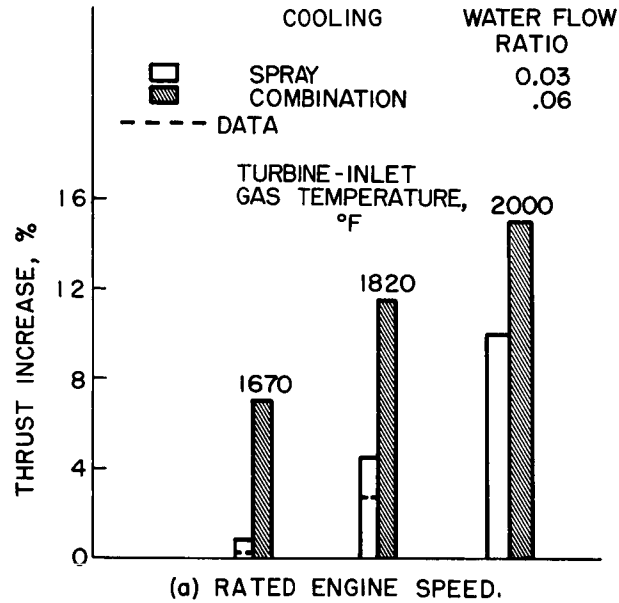


Figure 4

3078-D

### THRUST INCREASE WITH SPRAY COOLING AND COMPRESSOR WATER INJECTION



### THRUST INCREASE WITH SPRAY COOLING AND COMPRESSOR WATER INJECTION

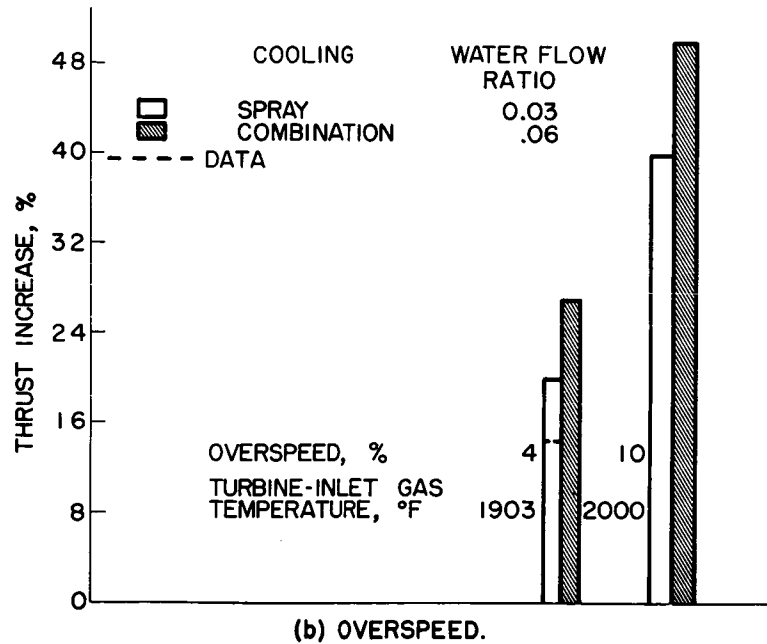


Figure 5



## APPLICATION AND OPERATION OF AIR-COOLED TURBINES IN TURBOJET ENGINES

By Robert R. Ziemer and Louis J. Schafer, Jr.

## INTRODUCTION

It is shown in a previous paper by Esgar and Rossbach that great improvement in supersonic turbojet-engine performance is available when the engine is operated at high tip speeds and at high combustion-gas temperatures. These conditions result in high stresses in the turbine blades and disk at high temperature levels. No materials are presently available that will withstand the stress and gas-temperature levels that would be necessary for future engines (50,000 psi and 2540° F, respectively). The most promising solution to the problem is to cool the turbine disk and blades so that they will operate at temperature levels at which they have sufficient strength to give reasonable turbine life. In addition to the gains in engine and aircraft performance that are made possible through cooling, it is also possible in many applications to reduce the turbine-metal operating temperature such that noncritical materials can be substituted for the critical high-temperature materials presently used in turbines, and at the same time to substantially decrease the turbine weight.

The cooling effectiveness and endurance characteristics of various air-cooled-blade configurations were discussed in the papers by Hickel and Clure, Donoughe and Diaguila, and Schum and Stepka. Some of the design and operational problems associated with turbines having air-cooled blades are considered in the present paper, and experimental turbojet-engine performance data obtained utilizing an air-cooled turbine with corrugated insert-type convection-cooled rotor blades are presented.

The most logical source of air for cooling the turbine disk and blades is some stage of the compressor, preferably at the lowest possible pressure level to minimize the cooling-air temperature. When air is bled from the compressor and ducted to the turbine blades and disk, several new design and operational problems are introduced. The design problems are: (1) the method to be used to introduce the cooling air into the turbine disk and blades, (2) the type of vanes to be used in the turbine disk to distribute the cooling air uniformly to all the turbine blades at a minimum loss in pressure, and (3) the type of turbine-blade cooling-passage configuration to be used. The operational problems include: (1) the effect of bleeding the compressor for cooling air on the performance of the compressor and the turbine, (2) the effect of discharging cooling air from the turbine-blade tips on the aerodynamic performance of the turbine blades, and (3) the over-all effect of cooling the turbine on engine thrust and specific fuel consumption.

[REDACTED]

These problems are discussed in this paper together with the experimental results that have been obtained by the NACA on the performance of engines in which the turbines were air-cooled to permit the substitution of noncritical materials. The effects of cooling on the following items are also discussed:

- (1) Turbine-blade temperatures
- (2) Turbine-disk temperatures and stresses
- (3) Performance of two cooling-air-vane configurations
- (4) Turbine efficiency
- (5) Engine thrust, thrust specific fuel consumption, and engine temperature ratio
- (6) Noncritical material substitution

#### TURBINE-DESIGN CONSIDERATION FOR AIR COOLING

Designing a turbojet engine with a turbine cooled by compressor air involves several design problems that do not exist in an uncooled turbojet engine. Careful consideration must be given to the compressor matching characteristics if discharge air is bled for cooling and to the compressor design if interstage air is used. Some form of ducting must be incorporated to get the cooling air from the compressor into the turbine blades. A representative system cooled by compressor-discharge air is shown in figure 1. In general, particular attention must be given to the design of the cooling-air ducting so that there is a minimum pressure loss between the compressor and turbine. Also, incorporated in the ducting system must be some provision for controlling, at all flight conditions, the amount of cooling air to the turbine blades.

#### Turbine-Disk Configurations

The cooling air can be introduced to the turbine in several ways (see figs. 2 and 3). The types of air induction shown in figure 2 are for split turbine disks in which the cooling air passes between the two disk halves and then into the turbine-blade bases. In figure 2(a), the cooling air is introduced from the upstream side of the turbine disk. Figure 2(b) shows the introduction of cooling air from the downstream side of the turbine; in this case, the air is ducted through the tail cone and is introduced at the hub of the turbine wheel. Figure 2(c) illustrates the case in which the cooling air is passed through the turbine shaft from the compressor and is introduced at the turbine hub.

[REDACTED]

The turbine disk need not be split to allow the cooling air to enter the turbine blades. A cooling-air shroud may be attached to either the upstream or the downstream face of the turbine disk depending on the direction of the cooling-air entry; the cooling air passes between the turbine disk and this shroud through holes drilled from the face of the disk at the rim to the blade bases. This type of disk configuration is shown in figure 3. The types of air inlet to the turbine disk are the same as those that were shown in figure 2; namely, upstream inlet, downstream inlet, and the hollow-shaft inlet.

The first experimental turbine disk investigated (refs. 1 to 3) was of critical material and of the split-disk variety. The cooling air was introduced through the tail cone to the downstream side of the turbine in a manner similar to that shown in figure 2(b). The investigations indicated the feasibility of operating air-cooled disks fabricated from noncritical materials. Photographs of two disks of noncritical materials (Timken 17-22A(S)) are shown in figure 4. A 34-inch-diameter disk with corrugated insert blades that was used in an engine with an axial-flow compressor is shown in figure 4(a); a 26-inch-diameter disk with tube-filled blades that was used in a centrifugal compressor engine is shown in figure 4(b).

All the turbine disks constructed at the NACA Lewis laboratory were designed for downstream entry of the cooling air to the turbine hub, because this method is most easily applied to an engine not originally designed for use with a cooled turbine. Great care should be used in the design of the cooling-air ducts, especially in the tail cone, in order to keep the cooling-air pressure losses to a minimum. (See ref. 4.)

#### Cooling-Air Impeller-Vane Configurations

Impeller vanes were utilized in the cooling-air passage between the halves of the split-type disks. These cooling-air impeller vanes have the dual purpose of distributing the cooling air uniformly to all the turbine blades and of acting as a compressor to accelerate the air to the rotative speed of the turbine at the blade base. Photographs of the inside surfaces of two air-cooled turbine disks are shown in figure 5. In figure 5(a), the impeller vanes have an inducer section in them so that the cooling air will have a zero angle of attack with the vanes at the rated engine speed and designed cooling-air-flow condition. The disk in figure 5(b) has straight vanes which were easier to machine. The vanes in both disks were machined integrally with the disks with one vane for each blade.

## Use of Noncritical Materials

If, through cooling, the turbine disks operate at temperatures not exceeding approximately  $1000^{\circ}$  F, noncritical materials can be substituted for the high-temperature alloys now used for the rim sections of turbine disks. At the lower metal temperatures, noncritical materials possess higher strength than the high-temperature alloys; consequently, for a particular application, reductions in turbine weight can also be accomplished. An example of typical reductions in weight and critical-material content made possible through the use of turbine cooling is shown in table I (data from ref. 5). The weight and critical-material savings shown in the table are for a turbine, the blades of which are attached to the turbine disk by conventional methods. It is possible, however, to fabricate cooled turbine wheels with blades that are brazed or welded to the disk. For such turbines, considerably greater reductions in turbine weight are possible. It is of interest to note in table I that nearly all of the critical material was removed from the turbine. The percentage reduction is greater for the turbine blades than it is for the disk, because there is a considerable amount of iron in the turbine disk of conventional design, but only a negligible amount in the turbine blades. The savings in critical material content in the turbine was thus greater than the actual weight reduction.

## EXPERIMENTAL RESULTS OBTAINED WITH AIR-COOLED TURBINE

## Cooling-Air Impeller Performance

The performance of the two cooling-air impellers that were shown in figure 5 is presented in figure 6. The engine instrumentation used in evaluating these impellers was such that the performance as presented includes the effects of the blades as well as of the vane system. The same type of tube-filled blade was used in both turbines (see insert of fig. 4(b)). The required cooling-air pressure at the turbine hub in percentage of the compressor-discharge static pressure is plotted against the coolant-flow ratio (cooling-air weight flow divided by the compressor-inlet weight flow) for an impeller with the inducer vanes, an impeller without the inducer vanes, and for the case in which the compression efficiency of the vane system was assumed to be 100 percent. The cooling air for the turbine in this experimental investigation was not bled from the compressor but was obtained from the laboratory high-pressure air system. However, the ratio of the measured static pressure at the compressor exit to the total pressure at the impeller inlet could be evaluated from the data that were obtained. This ratio shows the usable range of impeller operation if the cooling air were bled from the compressor exit. Figure 6 shows that, at a coolant-flow ratio of 0.03, which would be required by air-cooled turbine blades with effective coolant-passage configurations

operating at current combustion-gas temperature levels, the cooling-air impeller with the straight vanes required 59 percent of the compressor-discharge static pressure; the impeller with inducer vanes required 54 percent; and the impeller with 100 percent vane efficiency required 46 percent of the compressor-discharge static pressure. These values indicate that, for low coolant-flow ratios, an efficient impeller-vane configuration may be unnecessary. If very high combustion-gas temperatures are used and, as a result, high cooling-air flows are required to keep the turbine blades within safe operating limits, the difference between the performance of the two cooling-air impeller configurations becomes increasingly important. The cooling-air impeller is at its limit of operation when 100 percent of the static pressure at the compressor discharge is needed at the cooling-air impeller inlet. The limiting coolant-flow ratio for the impeller with no inducer vanes is 0.068; the limit for the impeller with inducer vanes is 0.08; and the limit if the impeller had 100 percent efficiency is 0.097. Thus, the impeller with inducer vanes has a coolant-flow-ratio limit that is 17.5 percent less than the 100-percent-efficient impeller, and the impeller without inducer vanes has a coolant-flow-ratio limit that is 30 percent less. This impeller-performance information indicates that an efficient vane configuration may be unnecessary unless high cooling-air weight flows are required.

#### Experimental Air-Cooled-Blade Temperatures

The average blade-metal temperatures obtained with the air-cooled turbine rotor shown in figure 4(a) were presented in a previous paper by Hickel and Clure. According to their data, the noncritical corrugated insert blades (fig. 4(a)) with a nominal factor of safety require a coolant-flow ratio of approximately 0.03 at a turbine-inlet temperature of 1540° F when compressor-discharge air is used for cooling. These conditions of operation represent an average blade temperature of 1050° F. It will be noted that this relatively large required coolant-flow ratio is not representative of the better corrugated insert blades discussed in the paper by Hickel and Clure. The fact that complete air-cooled-turbine investigations must follow the individual-blade studies, which progress much more rapidly than the cooled turbine investigations, accounts for the lag in the use of more effective coolant-passage configurations in the cooled-turbine investigations. The data indicate, however, the feasibility of utilizing noncritical material for air-cooled turbine blades operating at present-day gas temperatures.

#### Experimental Air-Cooled-Disk Temperatures

The radial temperature distribution that was obtained in the two halves of a typical noncritical (17-22A(S)) air-cooled turbine disk (see fig. 4(a)) is shown in figure 7. The temperature distribution was obtained when the engine was operating at a combustion-gas temperature of

approximately 1440° F and a coolant-flow ratio of 0.02. The disk temperature variation from the hub to the turbine rim was 190° to 940° F for the front disk and 510° to 840° F for the rear disk. Also included in this figure is a curve of the allowable temperature distribution for the cooled disks. The curve was obtained using the calculated equivalent stress (see ref. 5) and the stress-to-rupture properties of the non-critical material Timken 17-22A(S). The large temperature difference between the experimental and the allowable disk temperature at all radial stations except at the rim indicates that, at all locations but the rim, the disk was conservatively designed. This margin of safety would permit the use of a much lighter turbine disk (higher stress levels) for this particular engine. The data presented prove that turbine disks made of noncritical materials can be operated safely at the current disk-stress and temperature levels, and it also indicates that satisfactory disk operation at higher temperature and stress levels can probably be attained.

#### Effect of Cooling-Air Discharge on Turbine Efficiency

Another item of concern to the designer is the effect on turbine performance of bleeding cooling air from the compressor and discharging this cooling air from the tips of the turbine blades. The introduction of cooling air into the turbine can alter the turbine performance in two ways. First, bleeding cooling air from the compressor increases the specific turbine work and thereby changes the turbine operating point from what it was for zero cooling-air flow. This shift in the turbine operating point may result in either an increase or a decrease in the turbine efficiency depending on the compressor and turbine matching characteristics at the zero cooling-air-flow condition. Second, the discharge of cooling air from the blade tips may upset the gas flow over the blades and lower the aerodynamic performance of the turbine blades. This loss in blade performance would be reflected in a decrease in the turbine efficiency. The amount by which the turbine efficiency changes because of the shift in the turbine operating point with cooling-air flow can be determined in a matching study based on compressor and turbine component performance for several cooling-air weight flows. The second effect must be experimentally evaluated, and its magnitude may vary for different blade-coolant-passage configurations.

To evaluate these effects, an experimental investigation was conducted over a range of cooling-air flows using an axial-flow-type compressor engine with the turbine cooling-air bled from the compressor discharge. Also, the variation in turbine efficiency resulting from a shift in the turbine operating point was obtained from a cold-air-turbine performance map for the corrected turbine specific work output and the corrected turbine tip speed used in the experimental investigation; the

turbine performance map was obtained from reference 6. The results of this investigation are presented in figure 8 where the ratio of the turbine efficiency with cooling-air flow to the turbine efficiency with no cooling-air flow is plotted against the coolant flow ratio. The solid line on the figure shows the variation in turbine efficiency that resulted from the change of the turbine operating point with the introduction of cooling air to the turbine. For this particular turbine, the efficiency decreased. The data points represent the combined effects of changing the turbine operating point and discharging the cooling air from the blade tips. The data points, which are scattered uniformly around the solid line, indicate that the additive effect of the discharge of cooling air from the blade tips was negligible for this coolant passage configuration. If the discharge of cooling air from the blade tips had a measurable effect on the turbine efficiency, the data points would have fallen below the solid line. Similar results have been obtained on this turbine over a range of engine speeds and on three other turbines with both tube-filled and hollow turbine blades.

#### Engine Performance

The effect of air cooling on the experimentally obtained performance of an engine modified to accommodate an air-cooled turbine for the purpose of eliminating critical materials is shown in figure 9. An axial-flow compressor and the turbine shown in figure 4(a) were used in the investigation; the cooling air was bled from the compressor discharge and introduced into the turbine disk from the downstream side (see fig. 2(b)). The data presented are for an engine speed of approximately 87 percent of rated speed. Data were not obtained at rated speed because of excessive turbine-inlet temperatures which were due to the fact that the turbine had reached limiting loading. Limiting loading occurred sooner than was expected on the basis of cold-air-turbine data, probably because of slight differences in stator-throat area between the engine turbine and the model turbine, and the wide variation in turbine-inlet temperature profile that was evident in the engine investigation.

The experimental results obtained at a constant turbine-inlet temperature of 1550° F are presented in figure 9 where the percentage change in thrust specific fuel consumption and thrust per unit frontal area are plotted against coolant-flow ratio. The solid line represents the experimental data and the broken line shows the results of a compressor and turbine matching study based on component performance. Data points are not shown on the experimental results since the data presented were obtained from a cross plot of data obtained for runs at different jet nozzle areas. As the coolant-flow ratio increased, the thrust specific fuel consumption increased and the thrust per unit frontal area decreased.

The differences between the experimental results and the matching study are probably due to experimental error. The circles represent the lowest coolant flow permissible for safe operation of the noncritical blades used in this investigation. At this coolant-flow ratio, approximately 0.03, there was a 5.3 percent increase in thrust specific fuel consumption and a 2.4 percent decrease in thrust per unit frontal area. Therefore, to minimize these losses, the most effective blade-coolant-passage configuration available should be used.

It should be remembered that the losses shown in figure 9 are those that occur when an existing engine is equipped with a cooled turbine and no basic alterations are made. In the paper by Esgar and Rossbach, it was shown that large increases in specific thrust could be obtained with no increase in specific fuel consumption by allowing the turbine stresses to increase. Therefore, if, in the original design of a cooled engine, the turbine tip speed and the hub-tip radius ratio are so chosen that the turbine operates at stresses above those possible at present with an uncooled turbine, the resulting engine performance with the cooling losses included will be equal to or superior to the performance of current turbojet engines.

#### SUMMARY

The experimental data presented in this paper demonstrate the practicability of building and operating air-cooled turbojet engines. The use of blades and disks of noncritical materials was shown to be feasible, and the effects of two types of cooling-air impeller vanes on cooling-air-flow capacity were indicated. Turbine efficiency data indicated that discharging cooling air from the blade tips had no detrimental effect on turbine efficiency. Small losses in engine performance were obtained when an existing engine was operated at a constant turbine-inlet temperature to permit the substitution of noncritical materials in the turbine. If cooling is considered in the original design of the engine, the turbine can be designed for a higher stress than the uncooled turbine and the resulting engine performance will be equal to or superior to the uncooled engine.

#### REFERENCES

1. Schramm, Wilson B., and Ziemer, Robert R.: Investigations of Air-Cooled Turbine Rotors for Turbojet Engines. I - Experimental Disk Temperature Distribution in Modified J33 Split-Disk Rotor at Speeds up to 6000 RPM. NACA RM E51111, 1952.
2. Kemp, Richard H., and Moseson, Merland L.: Investigations of Air-Cooled Turbine Rotors for Turbojet Engines. II - Mechanical Design, Stress Analysis, and Burst Test of Modified J33 Split-Disk Rotor. NACA RM E51J03, 1952.

3. Nachtigall, Alfred J., Zalabak, Charles F., and Ziemer, Robert R.: Investigations of Air-Cooled Turbine Rotors for Turbojet Engines. III - Experimental Cooling-Air Impeller Performance and Turbine Rotor Temperatures in Modified J33 Split-Disk Rotor up to Speeds of 10,000 RPM. NACA RM E52C12, 1952.
4. Smith, Gordon T., and Curren, Arthur N.: Comparison of Pressure-Loss Characteristics of Several Tail-Cone Air-Induction Systems for Air-Cooled Gas-Turbine Rotors. NACA RM E52K07, 1953.
5. Moseson, Merland L., Krasner, Morton H., and Ziemer, Robert R.: Mechanical Design Analysis of Several Noncritical Air-Cooled Turbine Disks and a Corrugated-Insert Air-Cooled Turbine Rotor Blade. NACA RM E53E21, 1953.
6. Heaton, Thomas R., Slivka, William R., and Westra, Leonard F.: Cold-Air Investigation of a Turbine with Nontwisted Rotor Blades Suitable for Air Cooling. NACA RM E52A25, 1952.

Table I

TYPICAL WEIGHT AND CRITICAL MATERIAL SAVINGS THROUGH  
USE OF TURBINE COOLING

COMPONENT	WEIGHT SAVED WITH COOLED DESIGN COMPARED WITH UNCOOLED PRODUCTION COMPONENTS		SAVING OF CRITICAL MATERIAL	
	PERCENT	POUNDS	PERCENT	POUNDS
TURBINE BLADES	22.4	8.7	98.3	35.9
TURBINE DISKS	25.0	40.0	89.8	23.5
DISK AND BLADES	24.5	48.7	91.6	59.4

### CROSS SECTION OF AIR-COOLED TURBOJET ENGINE

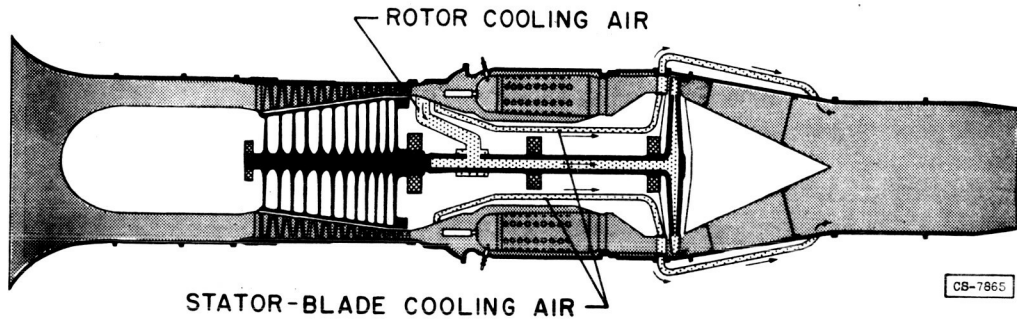


Figure 1

### SPLIT-DISK TYPE AIR-COOLED TURBINE CONFIGURATIONS

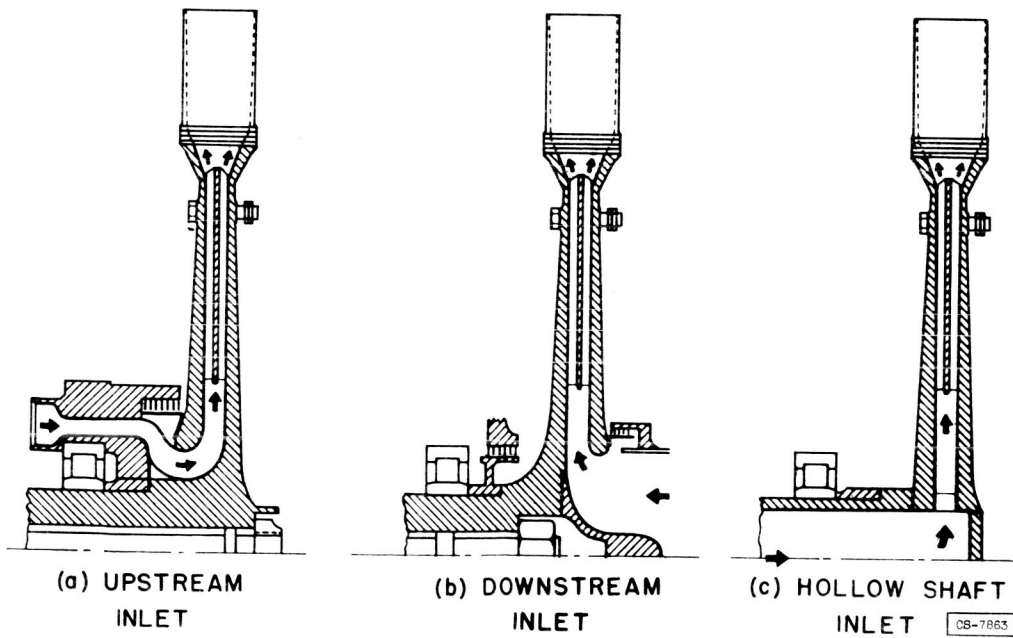


Figure 2

SHROUDED TYPE AIR-COOLED TURBINE DISK CONFIGURATIONS

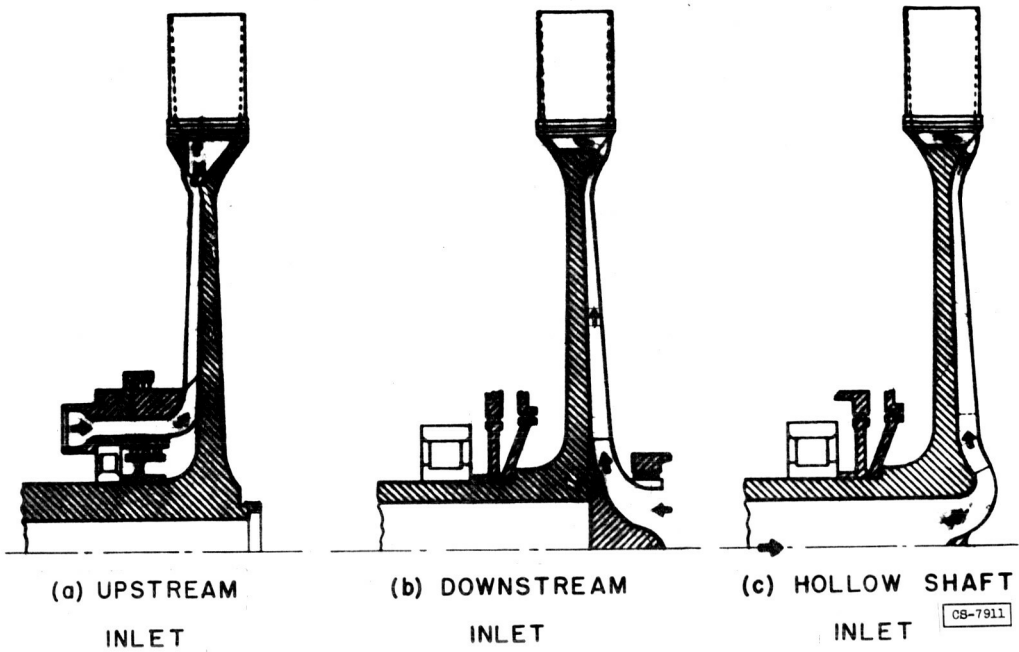


Figure 3

NONCRITICAL AIR-COOLED TURBINE ROTORS

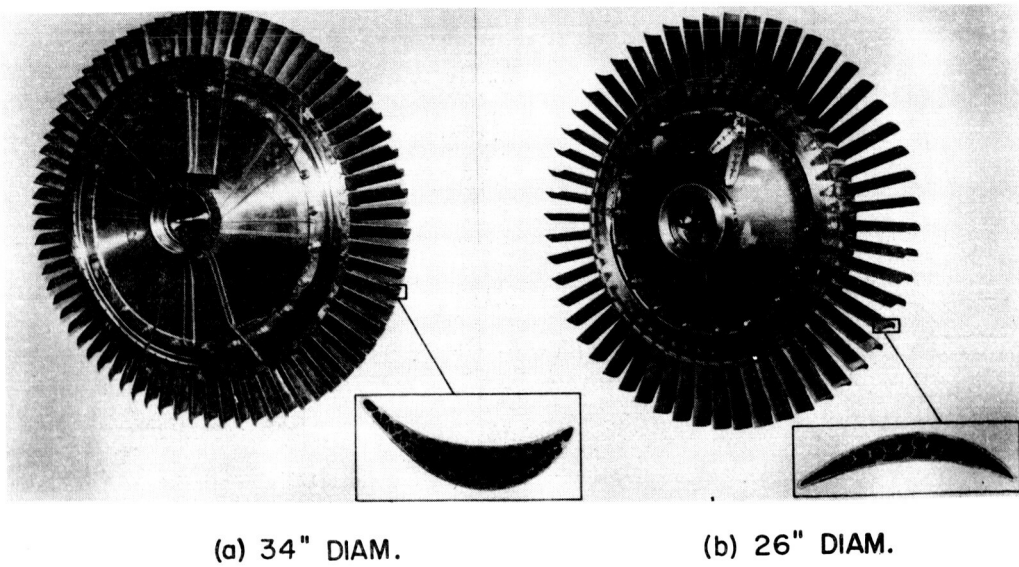
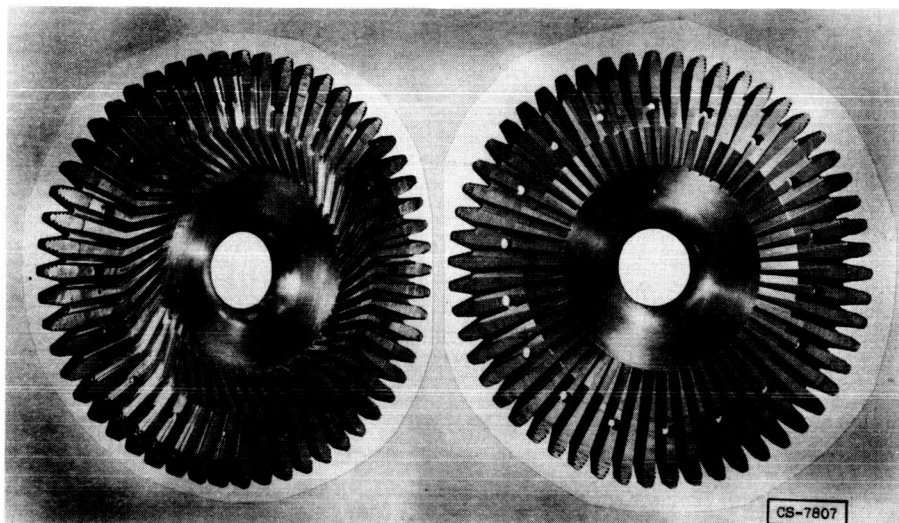


Figure 4

3078-D

### COOLING-AIR VANE CONFIGURATIONS



INDUCER SECTION

STRAIGHT

Figure 5

### PERFORMANCE OF TWO COOLING-AIR IMPELLER-VANE CONFIGURATIONS AT CONSTANT SPEEDS

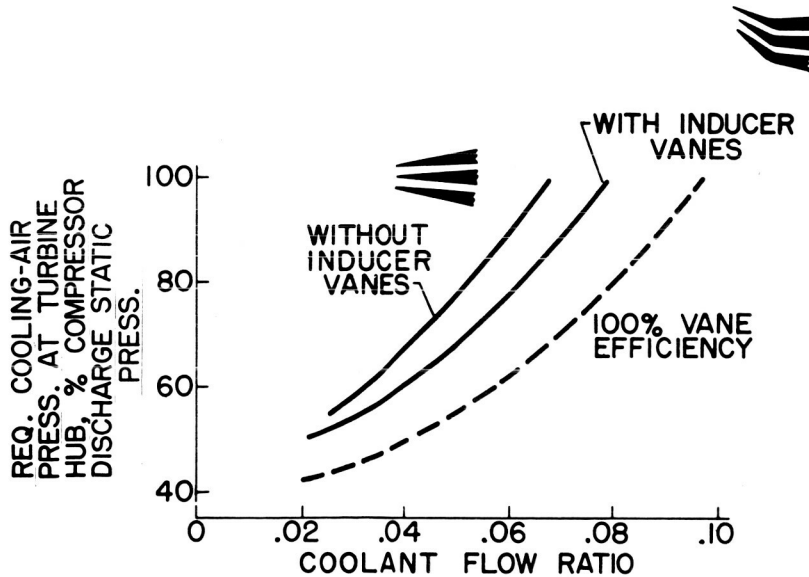


Figure 6

AIR-COOLED DISK TEMPERATURES  
 COOLANT FLOW RATIO, 0.02

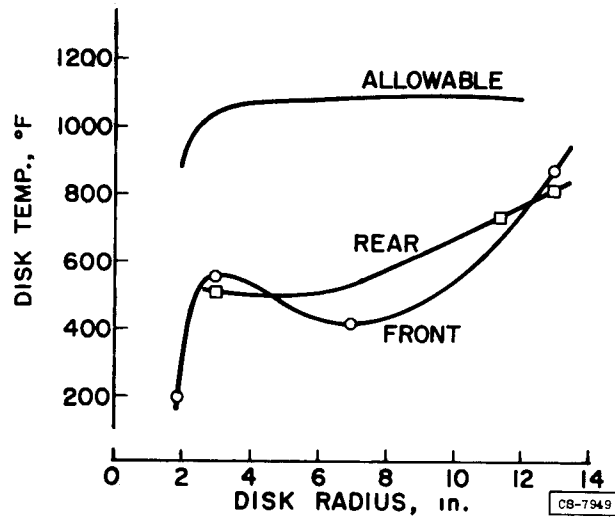


Figure 7

EFFECT OF COOLANT-FLOW RATIO ON  
 TURBINE EFFICIENCY RATIO

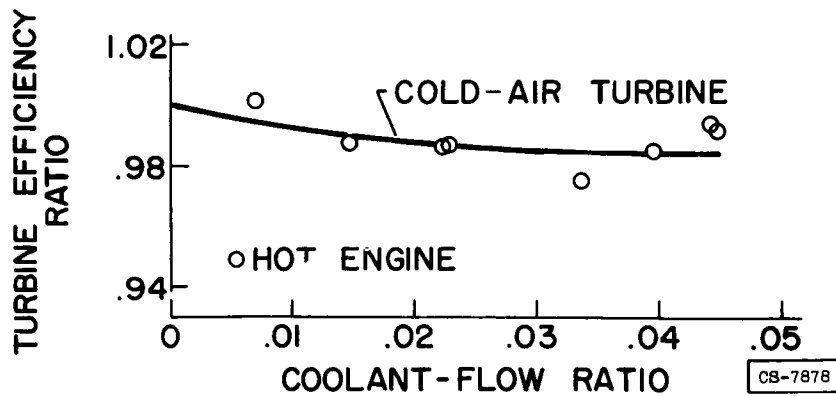


Figure 8

3078-D

EFFECTS OF COOLANT FLOW ON ENGINE PERFORMANCE

TURBINE-INLET TEMPERATURE, 1550° F

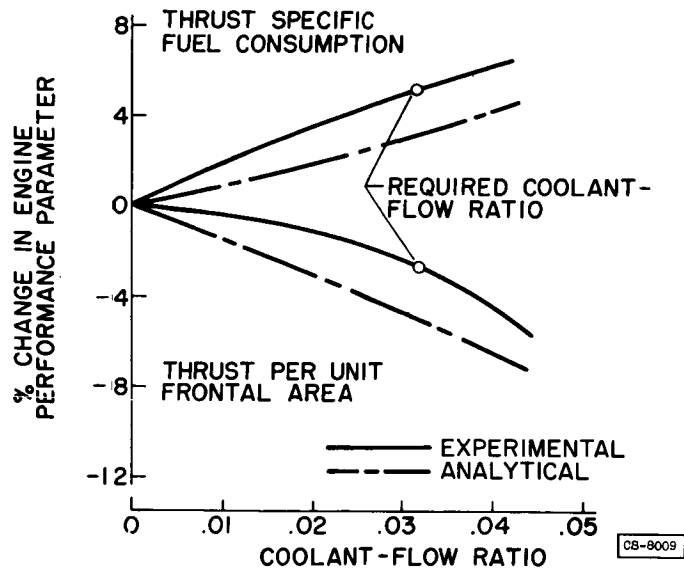


Figure 9

CB-9009

3078-D

## TURBINE COOLING SYSTEMS FOR SUPERSONIC FLIGHT

By James E. Hubbartt

The previous papers on turbine cooling have dealt with the different methods of cooling the turbine and the development of cooled blades and disks. In addition to such work in turbine cooling, the problem of keeping the coolant at a reasonable temperature arises when supersonic flight is encountered. It is the purpose of this paper to illustrate the flight speeds at which this problem arises and to discuss some possible solutions.

## Comparison of Allowable Coolant Temperatures

## with Available Air Temperature

The estimated ranges of the maximum allowable blade-material and coolant temperatures for transpiration and convection cooling with air and for water cooling are shown in figure 1. The ram-air and the compressor-discharge temperatures for compressor pressure ratios of 4 and 10 and for an adiabatic efficiency of 85 percent are also shown on figure 1 for a range of flight Mach numbers in the stratosphere. For flight Mach numbers of 2.2 and below, the ram-air temperature is within or below the range of maximum allowable cooling-water temperature. Therefore, for a simple closed system which uses water for cooling the turbine blades and eventually rejects heat to ram air, only flight Mach numbers below 2.2 are possible. For transpiration cooling, the cooling-air pressure must be approximately equal to the compressor-discharge pressure in order to meter the air through orifices at the blade base and then discharge the air into the main gas stream. As shown on figure 1, for a compressor pressure ratio of 4 the compressor discharge-air temperature is within or below the range of maximum allowable cooling-air temperatures for transpiration cooling for flight Mach numbers below approximately 2.5. As the compressor pressure ratio and, therefore, the bleed pressure ratio is increased, the maximum permissible flight Mach number for turbine cooling with this system is lowered. Since convection cooling is less effective than transpiration cooling, the maximum allowable cooling-air temperature for convection cooling is below that for transpiration cooling. For simple convection cooling with direct use of compressor-discharge bleed air, the maximum permissible flight Mach numbers for pressure ratios of 4 and 10 are approximately 2.1 and 1.5, respectively, as shown on figure 1. However, if convection cooling with ram air is possible, the flight Mach number can be increased to slightly over 3.0. In order to use ram air, however, it is necessary to maintain a low cooling-air discharge pressure.

[REDACTED]

Two possible cooling-air discharge arrangements for convection cooling with air are shown on figure 2. The arrangement illustrated by part (a) of this figure utilizes a cooling-air shroud on the upstream face of the turbine disk similar to the one discussed in the paper by R. R. Ziemer and L. J. Schafer and discharges the air into the main gas stream. This discharge arrangement requires that the cooling air be bled from one of the latter stages of the compressor. The arrangement illustrated by part (b) of figure 2 utilizes a cooling-air shroud on both the upstream and the downstream face of the turbine. In this case, the cooling air enters the upstream shroud, flows radially outward through an insert in the blade, reverses direction at the blade tip and flows radially inward between the insert and outer blade shell, and finally, flows through the downstream shroud from which it is discharged from the turbine. By proper sealing arrangements, the air could be ducted from the turbine to a low pressure such as ambient pressure. This in turn would permit the use of ram air for simple convection cooling.

#### Systems for Removing Heat from Primary Coolant

With convection and transpiration cooling systems which directly use air bled from the compressor and discharge the air into the main gas streams, it may be impossible to fly at Mach numbers above about 2.0 and 2.5, respectively. In addition, a simple water-cooling system is limited to use at flight Mach numbers below approximately 2.0. Therefore, in order to cool with these systems at high flight Mach numbers, it will be necessary to cool the primary blade coolant. A reduction of the primary-coolant temperature always reduces the amount of coolant required. An analysis of various systems devised to remove heat from the primary coolant has been published in references 1 and 2. The analysis was necessarily limited to specific design conditions and must be extended in order to exactly limit the ranges of application of each system. However, the results do serve to illustrate approximate limits and, therefore, are a basis for the following discussion and comparison of systems. The system which uses air as the primary turbine-blade coolant is referred to as an air-cooling system, while, the system which uses a liquid as the primary turbine-blade coolant is referred to as a liquid-cooling system.

Air-cooling systems. - Various systems have been proposed for cooling the air used to cool the turbine. In the simplest system (fig. 3), compressor bleed air is passed through an aftercooler which rejects heat to either the ram air or the fuel. In the case of heat rejection to ram air, adequate temperature differentials must be maintained to provide the necessary heat transfer with reasonable aftercooler size. This system permits very little increase in the flight Mach number except for very high bleed-pressure ratios which correspond to large temperature

[REDACTED]

[REDACTED]

differences between ram and compressor-discharge air. When heat is rejected to the fuel, the amount of cooling is essentially limited by the heat capacity of the fuel, which is interrelated with the flight speed and flight time because frictional heating of the airplane surfaces results in heat being transferred to the fuel in the fuel tanks. The amount of cooling available from fuel used for cooling the air will probably be insufficient, however, since the fuel is already used for oil cooling and has been proposed for cabin and instrument cooling at high flight speeds.

3078-D

An air-cooling system with a refrigeration cycle for increasing temperature differentials, and thus increasing the allowable flight Mach number, is illustrated on figure 4. The cooling air is bled from the compressor and passed through an auxiliary compressor, an after-cooler, an auxiliary turbine which drives the auxiliary compressor, and into the turbine blade which may be cooled either by convection or transpiration. The principle advantage of this system over the simple aftercooling system is that the auxiliary compressor produces higher cooling-air temperatures in the aftercooler permitting the rejection of a larger quantity of heat. The energy supplied by the compressor is removed from the gases in passing through the auxiliary turbine which expands the air to the required turbine cooling-air pressure. This expansion is accompanied by a cooling-air temperature drop that produces cooling-air temperatures below the ram-air temperature. For a given quantity of heat rejection, this refrigeration system is superior to the simple aftercooling system in that it requires a smaller after-cooler. As a result, the refrigeration system provides a substantial improvement at the expense of mechanical complexity, and flight Mach numbers of 3 or higher are possible with either convection or transpiration cooling.

In the case of the convection cooled blade which utilizes ram air and discharges to ambient pressure, a temperature reduction in the ram air before it enters the rotor may be possible by passing the ram air through an auxiliary turbine, which lowers the temperature of the air as a result of the work done by the air on the auxiliary turbine. The work of the auxiliary turbine could be absorbed by engine accessories, or it could be converted into heat and dissipated either to additional ram air or to compressor-discharge air. Although this system has not been analyzed, it appears to be very promising and it is believed that this system will permit flight speeds considerably in excess of a Mach number of 3.

Liquid-cooling systems. - Various systems of cooling turbines by use of liquids have also been proposed; the simplest of these systems is shown in figure 5. This involves a closed liquid system which rejects the heat in a radiator to either ram air or the fuel. In order to have the coolant enter the turbine in the liquid state, a pressurized

[REDACTED]

system is required. For a low-boiling-point liquid such as water, however, practical pressure limits prohibit high primary-coolant temperatures and as a result limit the flight Mach number if the heat is eventually rejected to ram air. For instance, the maximum cooling-water temperatures, as estimated on the basis of seal leakages for present designs, is about 350° R. Accordingly, as illustrated on figure 1, the flight Mach number is limited to approximately 2. However, if the heat is rejected to the fuel in the radiator, the amount of cooling is limited only by the availability and capacity of the fuel.

With the advent of a suitable high-boiling-point liquid, the simple liquid-cooling system will permit essentially the same or slightly higher flight Mach numbers than the simple aftercooling system which uses air as the primary coolant. However, all high-boiling-point liquids which have been investigated possess certain disadvantages.

An improvement in the simple liquid-cooling system, which rejects heat to ram air, is possible if a heat-pump cycle is incorporated to permit discharging the heat at higher temperature levels. However, for this system the need for higher boiling temperatures is more pronounced; and, as a result, the system must depend upon the development of a suitable coolant.

If adequate fuel is available for cooling, it may also be used directly as the primary coolant. In this case, the fuel is pressurized, passed through the cooling passages in the turbine blades (this may further increase the fuel pressure), and then, expanded through fuel nozzles into the combustion chambers. The fuel pressures currently used are adequate to maintain liquid fuel in the systems which have been investigated. Also, within the capacity of the fuel, no flight Mach number limit is imposed. However, local boiling, coking, or instability of the fuel may prove to be troublesome.

#### Summary Remarks

As in the past with internal combustion engines, the application of cooling to the gas-turbine engine may involve complex cooling systems. Because of the increase in ram-air temperature with flight speeds, the maximum flight Mach number with gas-turbine engines using compressor-discharge air for cooling the turbine either by transpiration or convection cooling is estimated to be between 2 and 2.5 for compressor pressure ratios commensurate with those anticipated for interceptor or missile applications. If a suitable aftercooling system is used, the compressor-discharge air can be cooled by ram air and flight Mach numbers of 3 or slightly above are attainable. If convection cooling of the

turbine with ram air is possible by controlling the cooling-air discharge pressure, flight Mach numbers slightly above 3 are permissible. A closed liquid system which rejects heat to ram air will be suitable for flight speeds above approximately 2.0 only if a suitable high-boiling-point liquid is developed. Probably the amount of cooling available from the fuel is insufficient, since it is already used for oil cooling and has been proposed for cabin and instrument cooling at high flight speeds. However, provided efficient cooling is available and local boiling, coking, and instability of the fuel present no formidable problem, no Mach number limitations are imposed if the fuel is used for directly cooling the turbine or for removing heat from the primary coolant.

#### REFERENCES

1. Schramm, Wilson B., Nachtigall, Alfred J., and Arne, Vernon L.: Analytical Comparison of Turbine-Blade Cooling Systems Designed for a Turbojet Engine Operating at Supersonic Speed and High Altitude. I - Liquid-Cooling Systems. NACA RM E52J29, 1953.
2. Schramm, Wilson B., Arne, Vernon L., and Nachtigall, Alfred J.: Analytical Comparison of Turbine-Blade Cooling Systems Designed for a Turbojet Engine Operating at Supersonic Speed and High Altitude. II - Air-Cooling Systems. NACA RM E52J30, 1953.

CONFIDENTIAL

### REQUIRED BLADE, COOLANT, AND AVAILABLE AIR TEMPERATURES

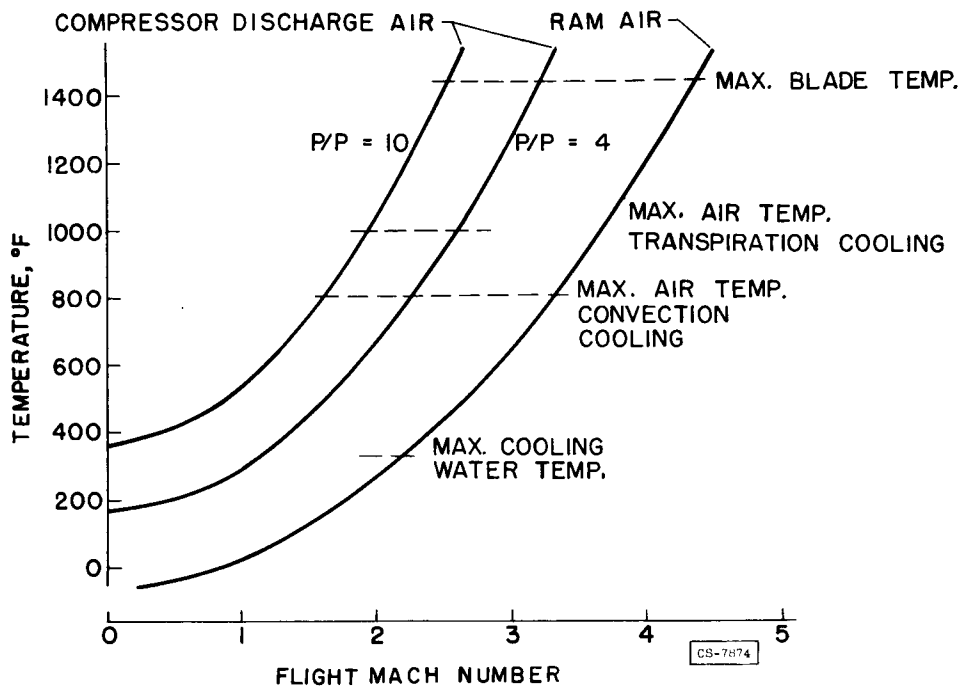


Figure 1

### ILLUSTRATION OF TWO COOLANT DISCHARGE ARRANGEMENTS

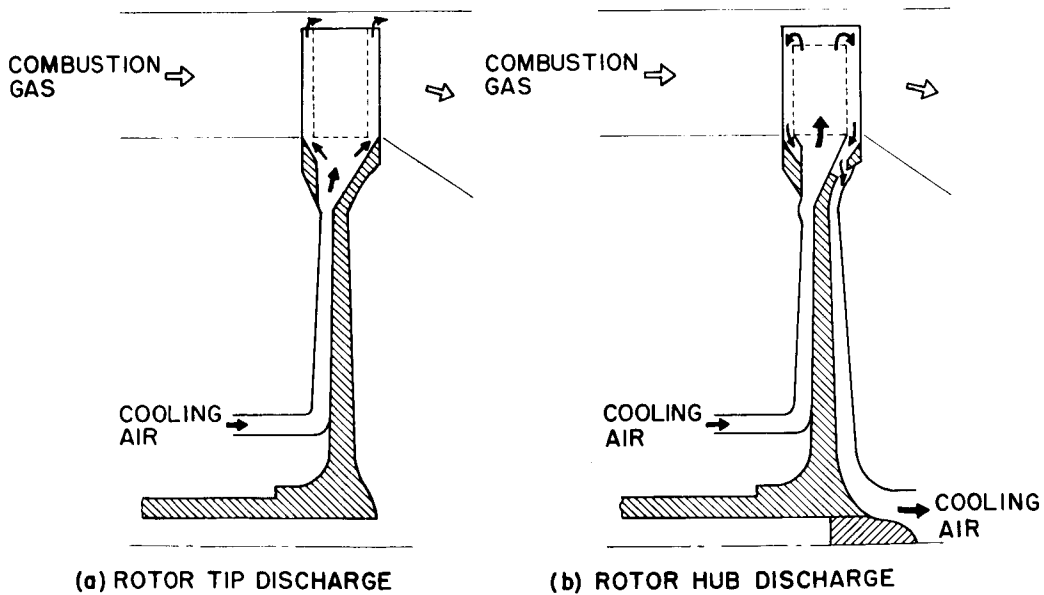


Figure 2

CONFIDENTIAL

3078-D

COOLING-AIR AFTERCOOLING SYSTEM

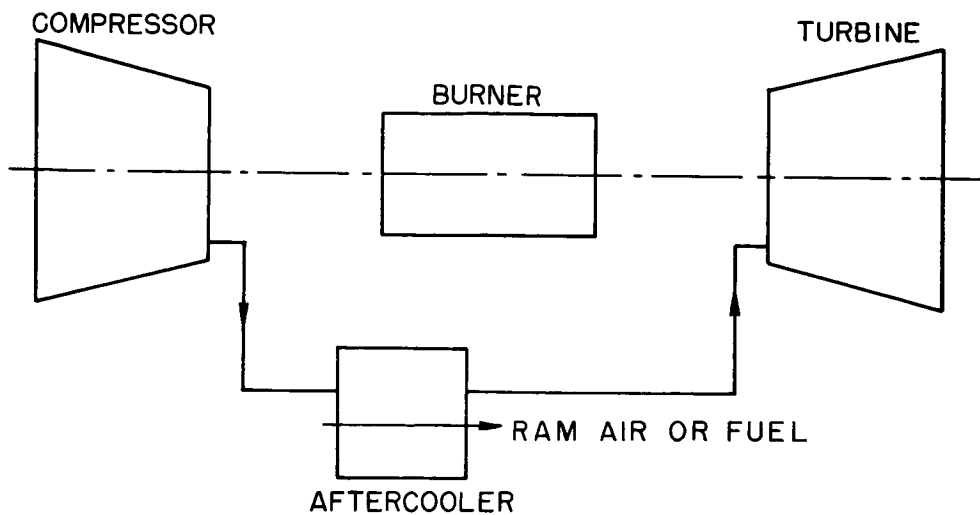


Figure 3

COOLING-AIR REFRIGERATION SYSTEM

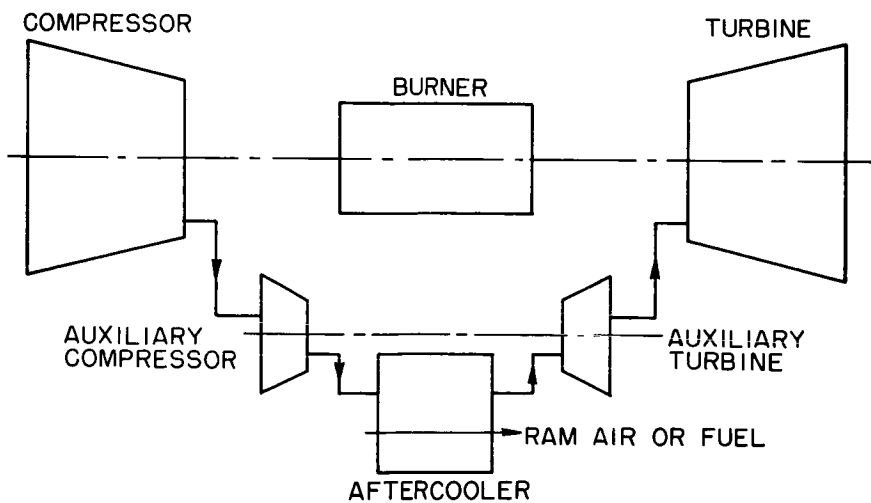


Figure 4

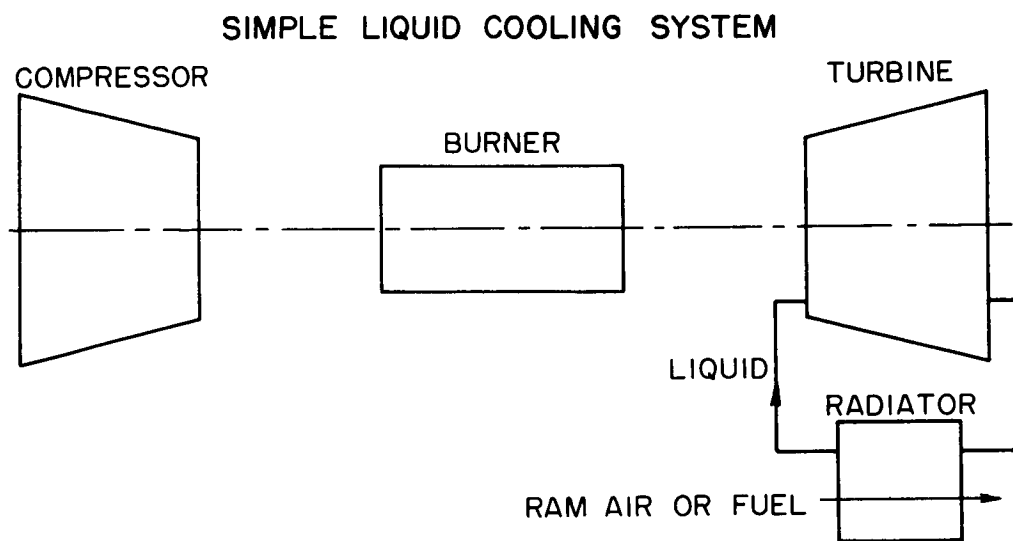
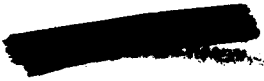
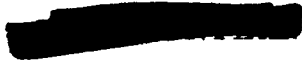


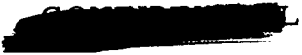
Figure 5





V - COMBUSTION PANEL

- W. T. Olson
- J. H. Childs
- E. R. Jonash
- E. V. Zettle



[REDACTED]

## CURRENT STATUS AND FUTURE REQUIREMENTS OF TURBOJET COMBUSTORS

By Edmund R. Jonash, J. Howard Childs, and Walter T. Olson

### INTRODUCTION

This paper and the subsequent papers on the combustion problem comprise a discussion of the present limitations and future requirements of turbojet combustors, their afterburners, and the research that has been done and is going on to overcome the limitations.

The preceding papers on compressor and turbine aerodynamics indicated that research on these turbojet components has made possible much higher air flows per frontal area for a turbojet engine. In addition, the papers on turbine cooling indicated that much higher operating temperatures may be possible in future turbojet engines. With the higher power resulting from higher air flows and higher temperatures, supersonic flight speeds with turbojet engines can be more easily realized. One is immediately concerned with the question: What do these new possibilities mean in terms of the combustion problem in the turbojet and its afterburner?

Doubtless, the reader is already generally familiar with the problem of obtaining high heat-release rates in the turbojet. It is essentially the difficult problem of keeping a flame burning stably and efficiently in an air stream moving at 100 or more feet per second, with a low pressure drop and with other desirable combustor characteristics. The high air flows possible from aerodynamic research on compressors and turbines require higher velocities through the combustion equipment if its frontal area is not to exceed that of the other engine components; with the higher velocities will go higher fuel flows, or higher heat-release rates. Turbine cooling allows higher temperatures for the combustion systems and thus aggravates the cooling problem. Supersonic flight means higher pressures and temperatures at the inlet of the combustion system than most engines now experience. Essentially, in addition to the already difficult requirements imposed on high-speed combustion systems in the turbojet, a widening of these operating conditions can be expected in the future for both the primary combustor and the afterburner.

The question to be considered, then, is: Can high-speed combustion systems keep up with the increased demands imposed on them? This first paper, which is concerned with the present limitations and future requirements of combustion equipment, discusses performance characteristics of representative current combustion equipment as influenced by various operating conditions. The particular combustion problems that will be examined are: combustion efficiency, outlet temperature profile, pressure drop, and reliability. The following paper will discuss past and present

[REDACTED]

research on present and future combustor problems, both in the main part of the engine and in the afterburner. A third paper will discuss applications of this research to experimental turbojet combustors. In these applications, attempts have been made to integrate ideas found in, or stimulated by, research into experimental hardware.

In the present paper, combustion efficiency is examined with a turbojet combustor from a current production engine in order to see the effect of inlet-air pressure, temperature rise, inlet-air velocity, and pressure drop on the performance of the combustor. An afterburner that is presently used in the production engine is also examined to see the effect of inlet conditions on its performance. Then, a consideration is given to (1) the effect of combustor exhaust-gas temperature profile on turbine blade life, (2) the effect of pressure drop on engine performance, and (3) certain reliability problems for both the principal combustor and the afterburner. The research on which these discussions are based has been conducted over a period of years at the NACA Lewis laboratory with direct-connect ducts in which a combustor is individually evaluated and with full-scale engines both on sea-level test stands and in altitude chambers that can simulate flight under a variety of conditions. The techniques used are discussed in the various reports cited herein. In general, the combustor data presented herein were obtained with MIL-F-5624A, grade JP-4 fuel.

### COMBUSTION EFFICIENCY

The combustion efficiencies obtained in the primary combustor and in the afterburner of the turbojet engine have direct effects on the specific fuel consumption of the engine and, consequently, on the range of the aircraft. It is important, therefore, that these engine components operate with high efficiencies at the conditions that will be encountered. Since combustors in engines designed for supersonic applications will be required to operate over extended ranges of inlet-air pressure, temperature, and velocity, the effects of these variables on efficiency are first considered.

Effect of combustor inlet-air pressure. - Figure 1 illustrates the effect of combustor inlet-air pressure on the combustion efficiency of a current production-model combustor (ref. 1) operating at subsonic flight conditions. This combustor, which is of the tubular type, is designated the reference combustor. The curve shown in figure 1 was estimated from an empirical correlation between efficiency and the combustor inlet-air conditions (ref. 2). This curve shows that combustion efficiencies increased with an increase in inlet-air pressure. As indicated by the altitude scale in the abscissa, combustion efficiency becomes a critical problem as altitude is increased above about 40,000 feet in the reference engine with a pressure ratio of 5. The pressures that may be encountered

[REDACTED]

in an engine with a pressure ratio of 7 at supersonic flight speeds and at altitudes from 60,000 to 80,000 feet are in the range of about 17 to 30 pounds per square inch absolute. These higher pressure conditions would, therefore, result in relatively high combustion efficiencies at the air velocity and temperature conditions encountered in the reference engine. Since combustors for supersonic applications will be required to operate at increased velocities, the effect of velocity on combustion efficiency must next be considered.

Effect of combustor air velocity. - Combustor velocity, as discussed herein, is based on the density of the combustor-inlet air and on the maximum annular cross-sectional area of the combustor. When tubular combustors are considered, the included annular area of the combustor assembly is used, as indicated in figure 2. Use of the included annular area for the computation of velocity penalizes the tubular combustors for the space wasted between the individual tubes (fig. 2). The actual velocities in individual tubes placed tangent to one another would be 30 percent greater than the velocities based on the included annular area.

The effect of combustor inlet-air velocity on the combustion efficiency of the reference combustor at two inlet-air pressures is shown in figure 3. A point on the lower curve (7.4 lb/sq in. abs) at 78 feet per second represents simulated operation in the reference engine at a flight Mach number of 0.6 and an altitude of 60,000 feet. As velocity increases, combustion efficiency decreases; combustor flame blow-out occurs at a velocity of about 88 feet per second. At the higher pressure, which is fairly representative of operation at expected supersonic-flight conditions, the efficiencies are increased about 5 to 8 percent, but are again adversely affected by increases in velocity. The data of figure 3 represent the performance characteristics obtainable with a current production combustor. In combustors designed for supersonic flight, velocities from 120 to 200 feet per second will be required. It is evident, then, that improved combustor designs are needed to obtain high combustion efficiencies at the high velocities required in supersonic-flight applications.

Effect of combustor operating temperatures. - Increases in the combustor inlet-air temperature, resulting from higher pressure-ratio engines and from operation at higher flight speeds, will generally aid the combustion-efficiency problem by promoting more rapid vaporization of the fuel (ref. 3). It has been noted that combustor-outlet temperatures may also be increased through advances in turbine-cooling techniques. Resulting variations in the desired temperature rise across the combustor have very significant effects on combustion efficiency. Figure 4 shows the variation of combustion efficiency with combustor temperature rise for the reference combustor operating at inlet-air conditions corresponding to a flight Mach number of 0.6 and an altitude of 60,000 feet in the reference tubojet engine (data of ref. 1). Maximum combustion efficiency is

[REDACTED]

attained at a temperature rise of 1000° F. Values of temperature rise greater or less than 1000° F result in decreased combustion efficiency. At the flight conditions noted above, the reference engine requires a temperature rise of 1180° F, which is already in the region of decreasing combustion efficiencies. An increase in the required temperature rise beyond this value would result in considerably lower combustion efficiencies, and eventually in flame blow-out.

Afterburner combustion efficiency. - Combustion efficiencies obtained in the turbojet afterburner are affected by operating conditions in a manner similar to that shown for the primary combustor (figs. 1, 3, and 4). The performance of a current production-model afterburner at severe operating conditions is presented in figure 5. Combustion efficiency was adversely affected by decreases in pressure and was markedly affected by variations in the desired exhaust-gas temperature. At the highest pressure condition shown, efficiencies were about 95 percent; however, this value of efficiency was obtained only at a very low value of exhaust-gas temperature. As pressure was decreased, the operable exhaust temperatures increased, but the efficiencies were simultaneously decreased. Afterburners in engines designed for supersonic flight will be required to operate at higher velocities and at higher values of exhaust-gas temperature. Therefore, improvements in the afterburner as well as the primary combustor design are clearly needed to obtain high-combustion-efficiency performance at the extended operating conditions that will be encountered in future turbojet engines.

#### EXHAUST-GAS TEMPERATURE PROFILE

The maximum outlet temperature at which a combustor may operate in the turbojet engine is determined by stress considerations imposed by the turbine. An example of the maximum allowable turbine temperature, as a function of the radial distance from the root to the tip of the blade, is presented in figure 6. The maximum temperature limit is determined by three stress-limit curves, rotor-blade fatigue, rotor-blade creep, and stator-blade stress limits. Erosion at the tip of the rotor may also affect the maximum allowable temperature. The desired combustor-outlet gas profile is obtained from the envelope of the curves, as shown by the solid curve in figure 6. In order to maintain a maximum average outlet temperature, for maximum thrust, the combustor exhaust-gas temperature must fall as closely as possible to the desired profile curve.

The desired temperature profile shown in figure 6 is representative of that required for uncooled turbine blades. If cooled turbine blades are used, then the preferred profile will be different. Preliminary calculations indicate that a flatter temperature profile will be desirable with cooled blades. A major factor affecting the control of the outlet temperature profile is the available pressure drop across the combustor, since the desired profile is obtained by controlled penetration of secondary air into the hot gas stream.

[REDACTED]

## COMBUSTOR PRESSURE LOSS

The combustor configurations necessary to obtain high combustion efficiency and to provide a desired exhaust-gas temperature distribution result in a loss in total pressure across the combustor. Since this pressure loss is reflected in increased engine fuel consumption, it is important to consider (1) the extent to which pressure losses may be increased by the conditions encountered in engines for supersonic applications and (2) the extent to which the fuel consumption of these engines will be affected by the pressure losses.

The variation in pressure loss, expressed as a percentage of the inlet total pressure, with combustor velocity is presented in figure 7. For both the subsonic and the supersonic applications considered, the pressure loss increases approximately with the square of the velocity. The curve for the subsonic-flight conditions represents calculated pressure losses expected in the reference tubular combustor with increased velocities (data from ref. 4). The curve for the supersonic-flight conditions represents the pressure losses expected in an annular combustor having the same pressure-loss coefficient ( $\Delta P/q$ , where  $q$  is the dynamic pressure) as the reference combustor. For the same combustor velocity, based on included annular area, the pressure losses in the annular combustor at supersonic-flight conditions are lower than those in the reference combustor at subsonic-flight conditions. There are two reasons for this: (1) the actual flow velocities in the annular combustor are lower than those in the tubular combustor for the same combustor velocity, as defined herein, and (2) the higher inlet-air temperatures encountered in supersonic flight result in lower pressure losses for equivalent velocities.

The reference combustor operating at the subsonic design conditions requires a combustor velocity of 78 feet per second, resulting in a pressure loss of about 6 percent, as indicated in figure 7. The annular combustor operating at the supersonic design conditions requires a velocity of 200 feet per second, resulting in a pressure loss of about 13 percent. The effects of these pressure losses on engine performance are shown in figure 8. The ratio of the specific fuel consumption, calculated to include the effect of pressure loss, to the specific fuel consumption of an ideal combustor having no pressure losses is plotted against pressure loss. Combustion efficiency was assumed to be 100 percent. The curves were calculated by the method described in reference 5 with the following assumptions:

Pressure ratio	Altitude, ft	Flight Mach number, $M_0$	Compressor efficiency, $\eta_c$ , percent	Turbine temperature, $T_4$ , $^{\circ}F$	Diffuser total-pressure-recovery factor
5 (ref. engine)	60,000	0.6	70	1550	0.95
7	80,000	2.8	80	2040	.65
7	65,000	2.0	85	2040	.88

[REDACTED]

For all three cases, the turbine efficiency  $\eta_T$  was assumed to be 90 percent; the exhaust-nozzle coefficient  $C_V$ , 0.96; and the lower heating value of the fuel  $h_c$ , 18,700 Btu per pound. The upper curve in figure 8 represents the subsonic-flight conditions; the lower curve, two typical supersonic-flight conditions. For comparable combustor pressure losses, smaller penalties in fuel consumption occur at the two representative supersonic-flight conditions in the somewhat higher-pressure-ratio engine. The data points in figure 8 represent the specific-fuel-consumption ratios corresponding to the pressure losses of the reference combustor at subsonic-flight conditions, and of the annular combustor at the flight Mach number of 2.8 and altitude of 80,000 feet. The pressure losses in the reference combustor caused an increase in fuel consumption of about 2.5 percent in the reference engine at subsonic conditions. The pressure losses in the annular combustor, with the much higher velocity (200 ft/sec) at supersonic conditions, caused an increase in fuel consumption only slightly greater, about 3.5 percent. Specific fuel consumption did not increase markedly at the high-velocity supersonic-flight conditions, because (1) at these conditions, pressure loss was reduced by the use of an annular combustor and by the high air temperatures encountered in supersonic flight (see fig. 7), and (2) the effects of pressure loss on fuel consumption are less at the supersonic-flight conditions. Thus, an annular combustor, having a pressure-loss coefficient typical of current combustors, can be used for the high combustor velocities encountered in supersonic-flight applications without suffering appreciably greater losses in fuel consumption than are currently accepted.

## RELIABILITY

The factors that affect combustor reliability include (1) combustion-chamber durability, (2) carbon deposition, and (3) ignition characteristics. Only brief discussions of these factors will be included herein to provide a qualitative evaluation of the problems that may be encountered in current and in future turbojet engines.

Combustion-chamber durability. - High surface temperatures and large temperature gradients result in excessive thermal stresses in the walls of the turbojet combustor that frequently cause cracking and warping of the walls. The problem of adequately cooling combustors would be expected to become more critical as inlet-air and exhaust-gas temperatures are increased at high flight speeds. In addition, increased combustor pressure drop at the higher flow velocities will place greater stress loads on the internal components of the combustor.

One particular problem in chamber durability of the turbojet afterburner is combustion screech. Combustion screech, evidenced by high-intensity, high-frequency noise, can result in the failure of afterburner

3078-E

walls and flame holders within a few seconds after its occurrence. Screech failures occur as a result of increased heat-transfer rates to the walls or flame holders and of vibrational fatigue resulting from the high-frequency high-amplitude oscillations. An example of a failure of an afterburner liner is pictured in figure 9. Sections of the wall of the afterburner are cracked, and in some areas large voids are apparent. It has been possible, in a number of small-scale afterburners, to define screech limits, as for example, those shown in figure 10 (unpublished data). The separate curves of figure 10 denote slightly different screech limits obtained by going into or out of the screech area. The range of fuel-air ratios over which screech was encountered increased somewhat with afterburner pressure. The problem of screech is particularly serious, since it is generally encountered in the range of desired afterburner operating conditions.

Carbon deposition. - Carbon formations frequently occur in the fuel-rich regions of turbojet primary combustors; thus, areas in the vicinity of the fuel injectors are most prone to carbon formation. Operation of both atomizing and prevaporizing injectors may be impaired by clogging of fuel passages or by interruption of spray patterns. Carbon may also harm ignition characteristics of the combustor by fouling the ignition plug. Figure 11 shows the effect of combustor operating conditions - fuel-air ratio, inlet-air pressure, and inlet-air velocity - on carbon deposition obtained in a 7-inch-diameter tubular combustor of current design (unpublished data). Curves are shown for both the total quantity of carbon deposited and for the quantity of carbon deposited per 1000 pounds of fuel burned. The carbon deposits shown in figure 11 were obtained in a 2-hour test period at the indicated operating conditions. The amount of fuel burned during this period was such that a single ordinate scale represents both the total carbon deposited and the carbon deposited per 1000 pounds of fuel burned. Total carbon deposition increased with fuel-air ratio. The quantity of deposits obtained per 1000 pounds of fuel remained substantially constant, however, which indicates that the increased fuel-flow rate caused the increased deposition at high fuel-air ratios. The total carbon deposited increased tenfold with a fivefold increase in pressure. Since these data were obtained at constant velocity and fuel-air ratio, fuel-flow rate increased simultaneously. A part of the increased carbon may, therefore, be attributed to increased fuel-flow rate and a part to the increased pressure. Substantial increases in carbon deposition also resulted from increases in velocity. Again, a part of the increase may be attributed to increased fuel-flow rate and a part to velocity. The effect of velocity on carbon deposition may vary considerably, since such factors as impingement of fuel on the combustor walls and distribution of air entering the combustion chamber are involved. From the data of figure 11, it may be concluded that carbon deposition will become a more serious problem as operating pressures and fuel-flow requirements are increased in future high-capacity engines for supersonic flight.

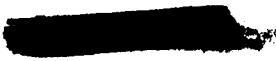


Carbon may also occur in the turbojet combustor in the form of smoke. Smoke exhausted from an engine does not impair engine performance; but it is a nuisance and may be objectionable in tactical operations. The effect of combustor inlet pressure on the concentration of smoke in the exhaust gases is shown in figure 12. The curve for combustor II was obtained from reference 6; the curve for combustor I, from a more recent investigation (unpublished) conducted in a 7-inch-diameter tubular combustor with the experimental techniques described in reference 6. The concentration of smoke, expressed as relative smoke density, increased with pressure in both combustors; however, both the quantity and the rate of increase with pressure were considerably different. The effects of other operating variables, such as velocity and fuel-air ratio, were observed in reference 6 to vary considerably with operating conditions. The largest effect was, however, that of inlet pressure, which indicates that exhaust smoke may become a more serious problem as pressure ratios and flight speeds are increased.

Ignition characteristics. - Ignition must be accomplished in the turbojet combustor over a wide range of ambient sea-level temperatures and may be required at the low pressures and low temperatures encountered in high-altitude flight. Satisfactory ignition characteristics have been obtained in current engines by supplying high spark energies to the combustor ignitor. Since increases in spark energy will increase the weight of the ignition system, it is desirable to provide the minimum energy actually required, in order to minimize total engine weight. Figure 13 presents a relation between the required energy, in joules per spark, and an empirical parameter  $V/\sqrt{P}$ , where  $V$  is the combustor velocity and  $P$ , the combustor-inlet pressure (ref. 7). The relation indicates that the required spark energy increases with an increase in velocity and with a decrease in pressure. These data were obtained at a constant inlet-air and fuel temperature and with an MIL-F-5624A, grade JP-4 fuel; experience has shown that increased energies are also required at decreased temperatures and with fuels of lower volatility. Operation of future engines at higher combustor velocities may increase the energy requirements of the combustor; however, the higher temperatures and pressures encountered at high flight speeds may alleviate the problem of engine relighting during flight.

### CONCLUSIONS

Four basic turbojet combustor problems have been discussed in this paper - combustor efficiency, turbine temperature distribution, pressure loss, and reliability. The combustion-efficiency problem in both the primary combustor and in the afterburner of current engines was observed to be one of maintaining high efficiencies at the low pressure encountered at high altitude, subsonic flight. The problem for the future engines designed for supersonic application is primarily one of obtaining high



combustion efficiencies at the increased combustor velocities that will be encountered in these engines. It was noted that a particular temperature distribution of the gases entering the turbine is required for maximum thrust. The ease with which the desired temperature distribution is obtained is dependent upon the amount of pressure drop that can be tolerated in the combustor. Calculations indicated that pressure-loss coefficients representative of those used in current production-model combustors may be used in annular combustors for supersonic-flight applications without excessive penalties to engine performance.

Three factors affecting combustor reliability were considered: combustion-chamber durability, carbon deposition, and ignition. A critical durability problem in current turbojet engines was observed to be afterburner screech. With respect to future engines operating at supersonic-flight conditions, it is expected that the increased operating temperatures will aggravate both the primary-combustor and the afterburner-wall cooling problems. Increased pressures and fuel-input rates will increase the tendency for the turbojet combustor to deposit carbon and to form excessive quantities of exhaust smoke. Finally, it was noted that satisfactory ignition characteristics can be obtained by supplying adequate ignition energies to the ignitor.

#### REFERENCES

1. Butze, Helmut F., and Jonash, Edmund R.: Turbojet Combustor Efficiency with Ceramic-Coated Liners and with Mechanical Control of Fuel Wash on Walls. NACA RM E52I25, 1952.
2. Childs, J. Howard: Preliminary Correlation of Efficiency of Aircraft Gas-Turbine Combustors for Different Operating Conditions. NACA RM E50F15, 1950.
3. McCafferty, Richard J.: Liquid-Fuel-Distribution and Fuel-State Effects on Combustion Performance of a Single Tubular Combustor. NACA RM E51B21, 1951.
4. Cook, William P., and Butze, Helmut F.: Investigation of Altitude Ignition, Acceleration, and Steady-State Operation with Single Combustor of J47 Turbojet Engine. NACA RM E51A25, 1951.
5. Pinkel, Benjamin, and Karp, Irving M.: A Thermodynamic Study of the Turbojet Engine. NACA Rep. 891, 1947. (Supersedes NACA WR E-241.)
6. Butze, Helmut F.: Effect of Inlet-Air and Fuel Parameters on Smoking Characteristics of a Single Tubular Turbojet-Engine Combustor. NACA RM E52A16, 1952.
7. Foster, Hampton H., and Straight, David M.: Effect of Fuel Volatility Characteristics on Ignition-Energy Requirements in a Turbojet Combustor. NACA RM E52J21, 1953.

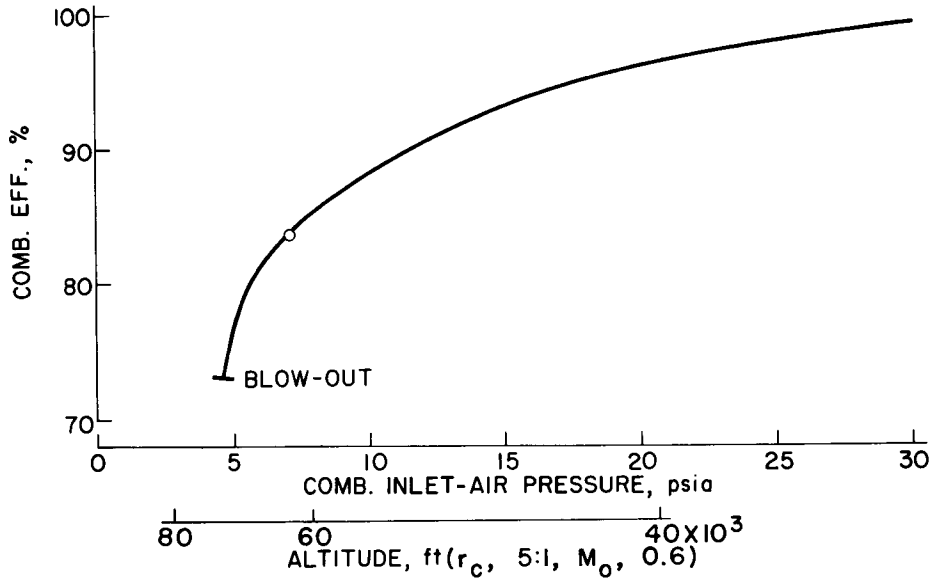


### EFFECT OF PRESSURE ON COMBUSTION EFFICIENCY

$V, 78 \text{ ft/sec}$

$T_i, 268^\circ \text{ F}$

$\Delta T, 1180^\circ \text{ F}$



3078-E

Figure 1

### CROSS SECTION OF COMBUSTOR ASSEMBLY

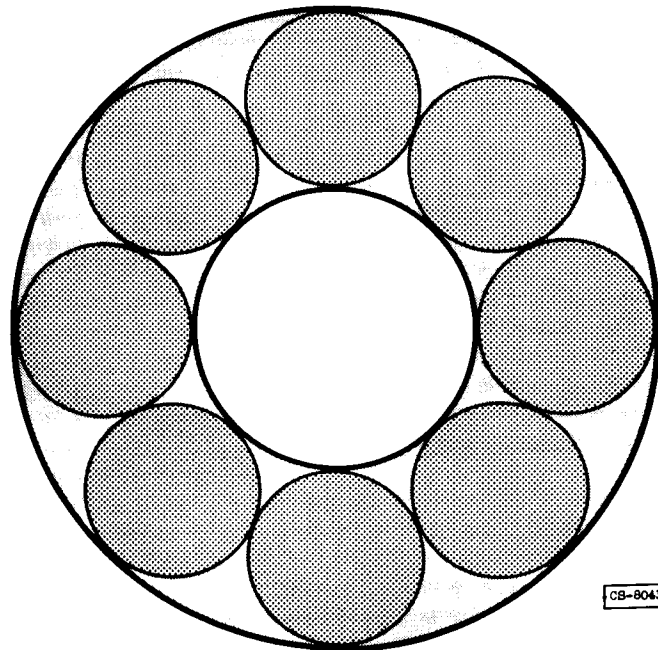
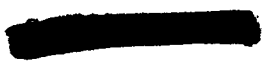


Figure 2



EFFECT OF VELOCITY ON COMBUSTION EFFICIENCY

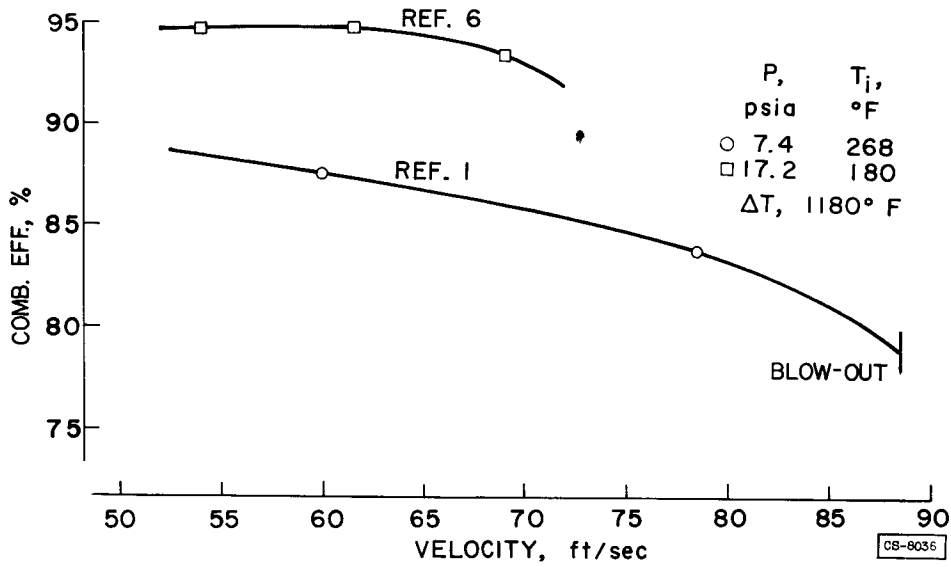


Figure 3

EFFECT OF TEMPERATURE RISE ON COMBUSTION EFFICIENCY

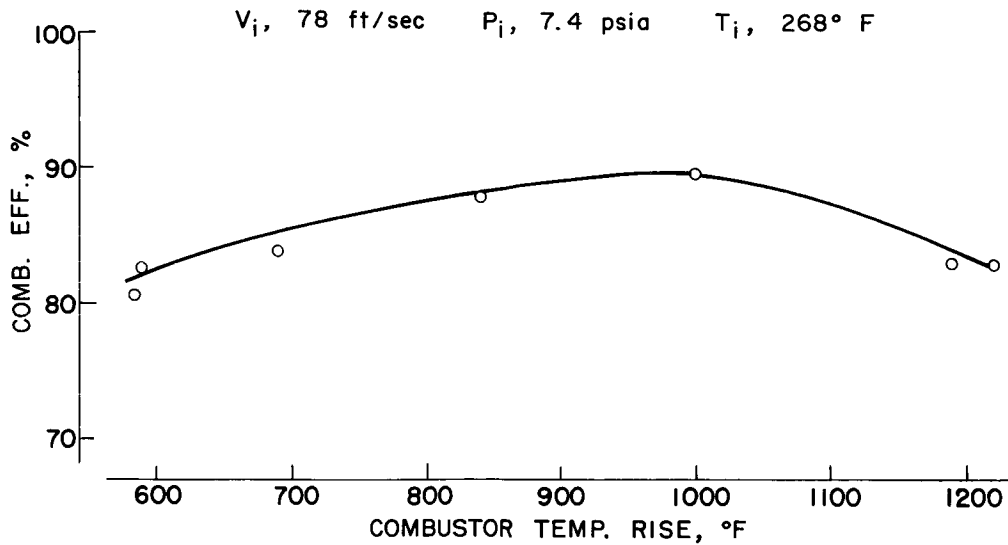
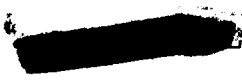


Figure 4



### AFTERBURNER COMBUSTION EFFICIENCY

VELOCITY, 400 ft/sec

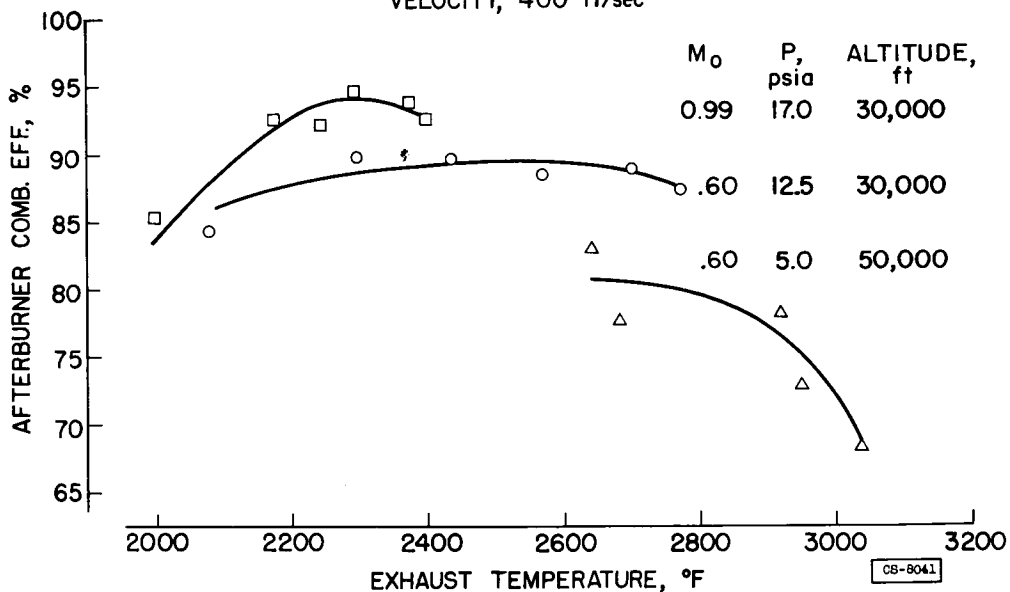


Figure 5

### LIMITING OUTLET TEMPERATURE PROFILE

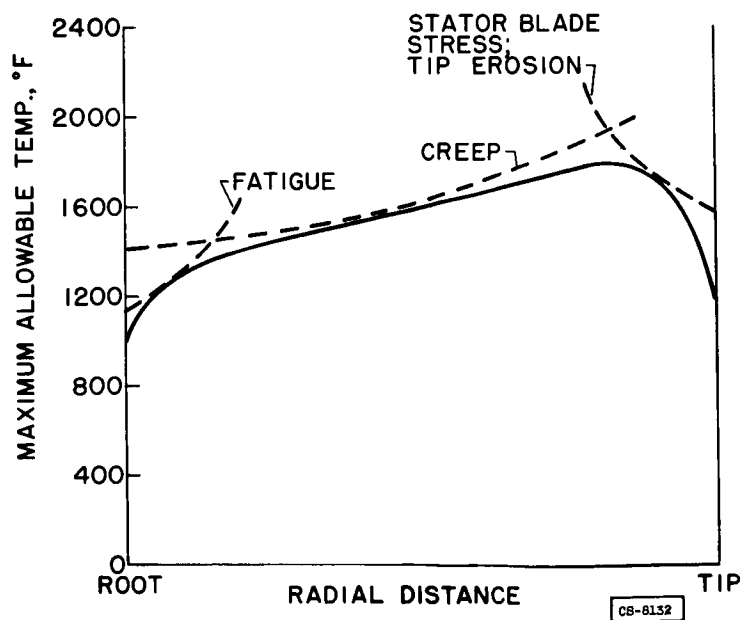


Figure 6



5018-5

EFFECT OF OPERATING CONDITION ON COMBUSTOR PRESSURE LOSS

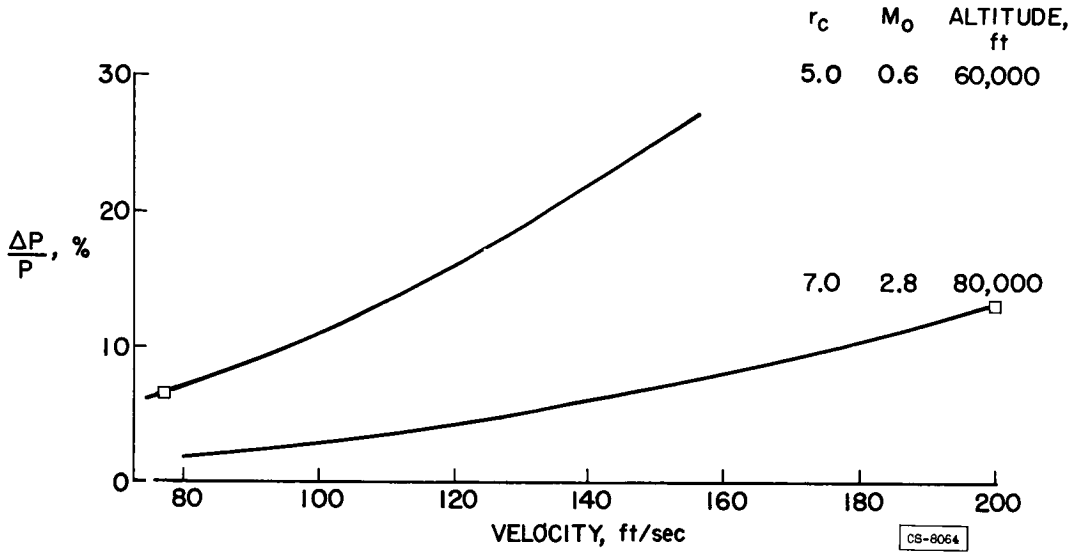


Figure 7

EFFECT OF PRESSURE LOSS ON FUEL CONSUMPTION

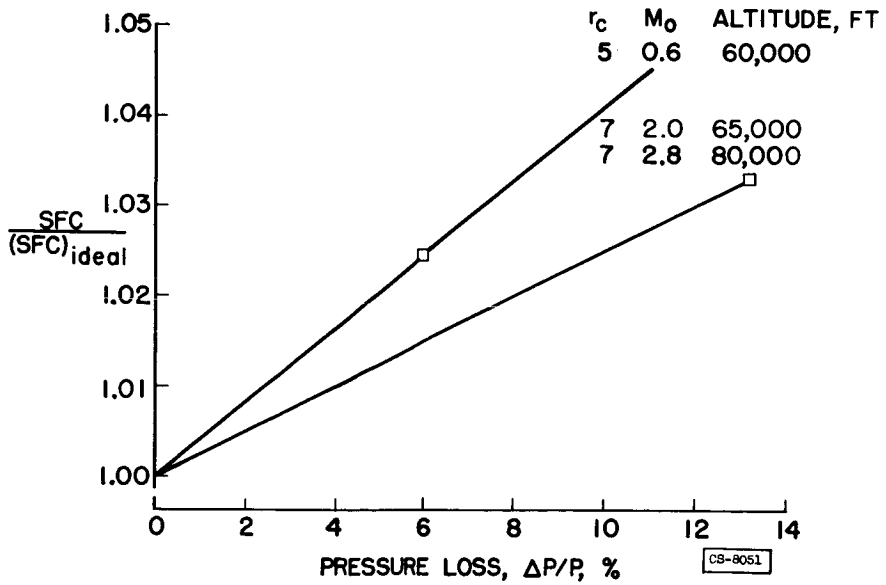


Figure 8

FAILURE DUE TO SCREECH

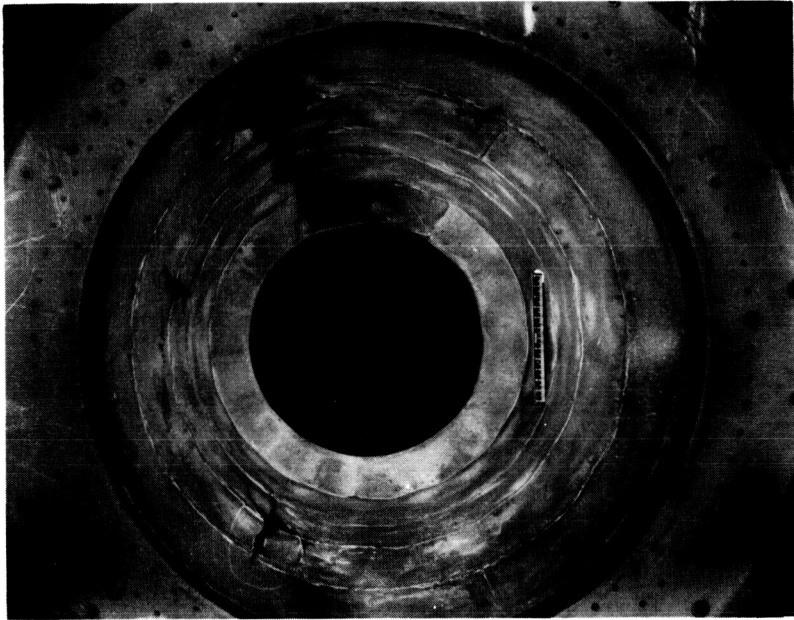


Figure 9

AFTERBURNER SCREECH LIMITS

V, 456 ft/sec

T<sub>i</sub>, 1230° F

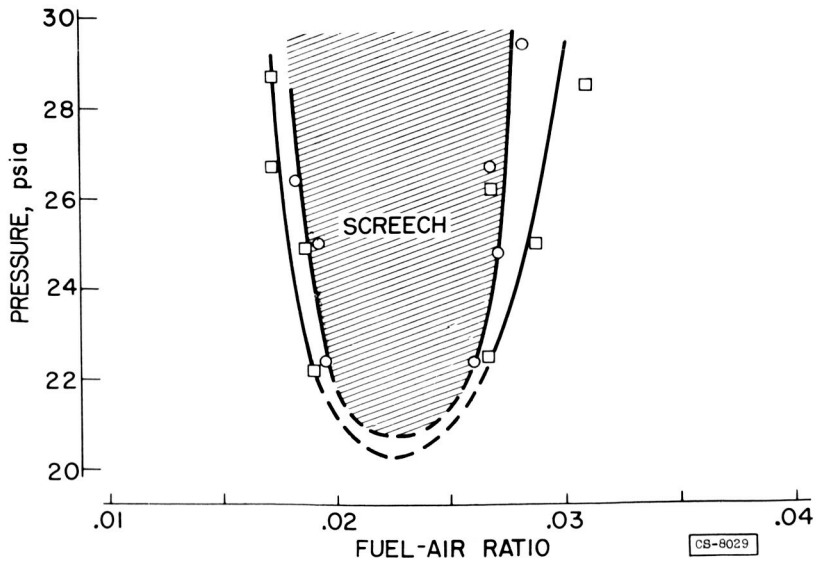


Figure 10

EFFECT OF OPERATING CONDITIONS ON CARBON DEPOSITION

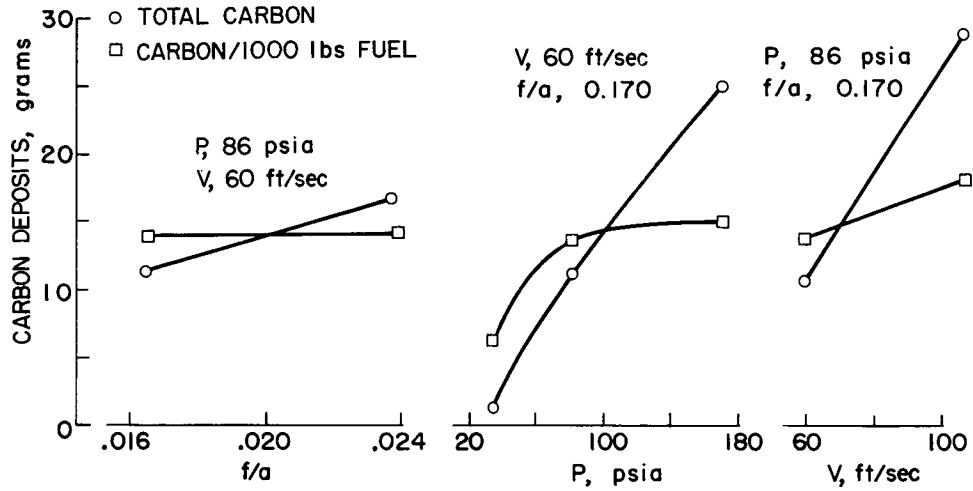


Figure 11

EFFECT OF OPERATING CONDITIONS ON EXHAUST SMOKE FORMATION

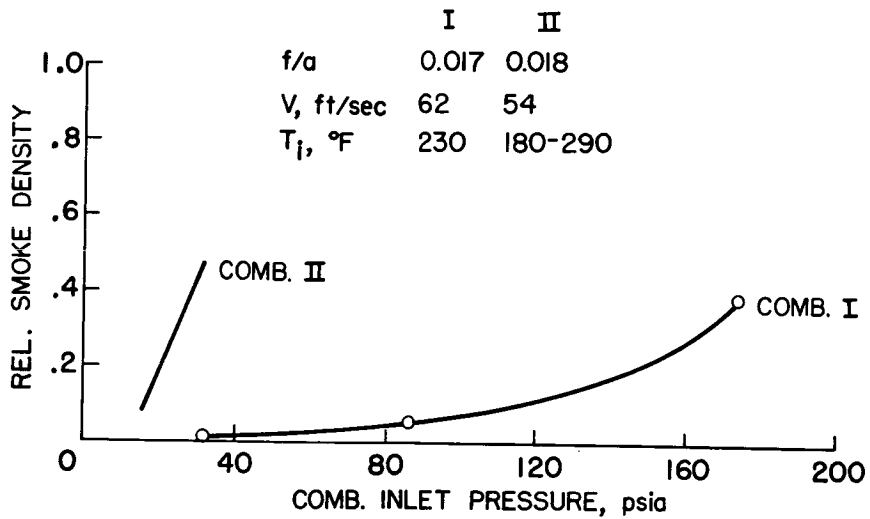


Figure 12

### EFFECT OF OPERATING CONDITIONS ON IGNITION ENERGY REQUIREMENTS

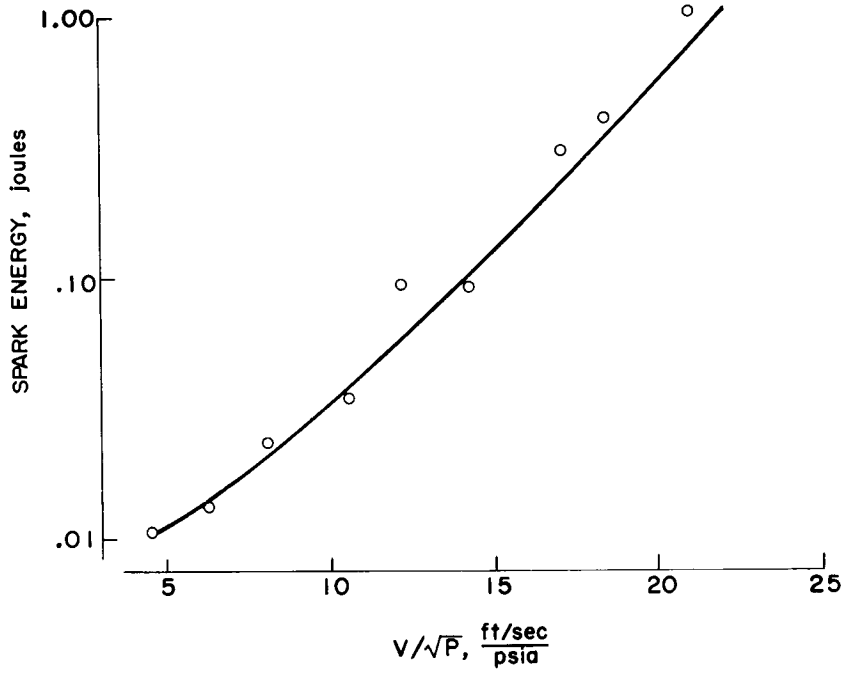


Figure 13

## RECENT RESEARCH ON HIGH-SPEED COMBUSTION

By Walter T. Olson and Edmund R. Jonash

## INTRODUCTION

In the previous paper it was seen that the present science of high-speed combustion for turbojets, as represented by equipment currently in production, has limitations short of some of the present requirements. Further, the future requirements, which, in effect, extend the range of combustor velocities, fuel-air ratios, and inlet pressures and temperatures over which combustors must operate with low internal losses, will make advances in combustor design necessary. The general subject of this paper, then, is the past and current research that aids in overcoming the existing limitations and in meeting the future requirements of high-speed combustion systems. In order to examine this major subject, the same detailed problems reviewed in the previous paper will be considered: combustion efficiency, outlet temperature profile, pressure drop, and reliability. For each of these problems, some background as to the reason for its existence will be discussed, and then some ways to handle the problem will be reviewed. The research covers several years of work at the NACA and at other laboratories and is necessarily a very brief summary of the material.

## COMBUSTION EFFICIENCY

The previous paper showed that combustion efficiency in the main turbojet combustor and in the afterburner is affected adversely by the low pressures encountered at high altitudes. Further, it was seen that the high velocities accompanying high mass flow per frontal area of future high-performance turbojet engines make the attainment of high combustion efficiencies more difficult. Also, some of the present high-speed combustion systems for turbojets do not operate over as wide a fuel-air-ratio range as is desired with high efficiency. Consequently, certain advances in design are needed in order to obtain the desired combustion efficiencies at the operating conditions of interest both in present and future engines. In order to introduce the advances that might be made in design, certain facts about combustion are first discussed. These facts have been found from extensive research on the fundamentals of combustion both at the NACA Lewis laboratory and by others (refs. 1 and 2); and, while they by no means comprise an adequate review of this research, they are nevertheless basic to any engineering approach to the attainment of high combustion efficiencies in turbojet combustors and afterburners.

## Basic Considerations

Flammability limits. - A first principle important in combustor design is that the fuel-air ratios in the burning zone must be confined within narrow composition limits generally near stoichiometric. There are several reasons for this principle. Perhaps the main reason is that the flammability limits of fuel and air mixtures are narrow (refs. 4 and 5), as figure 1 shows (ref. 3). Figure 1, a plot of pressure against fuel-air ratio, shows a flammability-limit curve for a hydrocarbon-air mixture similar to jet fuels. Only at fuel-air ratios and pressures inside this curve can the fuel and air burn. Now the over-all fuel-air ratios for which turbojet combustors are required to operate fall within the shaded region of the figure and clearly are outside the flammability-limit loop. This simply emphasizes the necessity of creating a burning zone somewhere in the combustion chamber where the fuel-air ratios fall within this loop. Also, other combustion properties such as flame speed optimize near stoichiometric or richer.

Flame stabilization. - Once a mixture of correct composition is delivered to the zone in which combustion is to occur, both time and temperature are required to bring the flowing combustible mixture up to flame conditions as it flows through the combustion system, that is, to stabilize a flame by providing for its continuous ignition. Figure 2, based on data in reference 6, is a plot of ignition delay against temperature for kerosene sprayed into a hot gas stream. Ignition requires fractions of milliseconds to several milliseconds, but ignition delays shorten very rapidly as temperatures are increased. The ignition delay is longer at lower pressures; and, although small drop size shortens ignition delay, the effect is not really great over the ranges of drop size that might conventionally be obtained from pressure atomizing nozzles. The important thing about the information in this figure is that high temperatures are required to bring the sprayed fuel to ignition conditions in a short time in the combustion chamber. The time and temperature required to pilot the flame continuously could be provided by recirculating hot gases into the fresh charge.

Although appreciable times are seen to be required for ignition and there is not a large effect of drop size on ignition delay, figure 3 (ref. 7) shows that there is nevertheless an important effect of drop size on the time required for a droplet to evaporate and to burn in a flame. The plot of time against drop size is for data on a single burning drop, but the same general trend may be expected to hold for a spray of a great many drops.

Flame propagation. - Also important to the design idea that a low-velocity recirculating zone be provided in the combustor to provide time and temperature for continuous ignition or stabilization of flame is a consideration of the ability of flame to spread through the combustible

[REDACTED]

mixture once continuous ignition has been reached. Figure 4 shows the velocity of the flame traveling through a combustible mixture perpendicular to itself and with respect to the unburned gas (refs. 8 and 9). This is the fundamental flame speed on which extensive research has been done (refs. 10 and 11), and for ordinary hydrocarbon fuels its value is of the order of only 1 to 2 feet per second. The shaded areas for over-all fuel-air ratios and velocities for turbojet combustors and afterburners indicate that flame propagation must be completed in streams having over-all velocities of hundreds of feet per second. If the flow velocity of the laminar flame is increased for the flame burning above a simple port or tube (fig. 4) while the perpendicular component of the flame velocity remains only about 1 foot per second, the flame assumes a conical shape. An increase of the flame area occurs, and a still greater increase can be achieved by introducing turbulence into the stream to produce a highly wrinkled or greatly extended flame front. These extended or turbulent flames may permit approach stream velocities of the order of 30 feet per second or more, if adequate stabilization of flame is provided (refs. 12 to 15). Blow-out velocities achieved in at least one laboratory investigation with ideal mixtures burning at high combustion efficiencies above the perforated plate were of the order of 100 feet per second and more (ref. 16). Because the over-all operating conditions for both present and future turbojet combustors and for afterburners are actually quite far from the region of good combustion properties, these data on figure 4 serve to emphasize the importance not only of creating a correct mixture composition in the zone where burning will occur, but also of providing for turbulence and recirculation to extend greatly the flame front zones, so that the relatively slow-moving flame fronts can traverse all of the combustible charge within the short times resulting from the high over-all flow velocities of the combustion chamber.

In addition to time for continuous ignition of mixture as it flows through the system and time for the propagation of turbulent flames, space (or volume) is also needed for complete burning if high combustion efficiencies are to be achieved. There are probably several fundamental reasons for the principle. For example, it has been observed that as pressure is reduced on a simple diffusion flame, the flame becomes much thicker and, in effect, requires more volume to release a given quantity of heat. In figure 5 the volume (cu ft) required to release a million Btu per hour is plotted against pressure in pounds per square inch (ref. 17). The data are from direct visual measurements of the volume of a simple diffusion flame at different pressures. Compared with this volume is the volume available in a typical turbojet combustor to effect the design heat-release rate as a function of pressure, or altitude, for an engine with a pressure ratio of 5 at a flight Mach number of 0.6. It is significant that, at the reduced pressures corresponding to high altitudes, a larger and larger fraction of the volume of the turbojet combustor is required for the burning zone alone. A large fraction of the combustor volume is also required for processes such as fuel and air

[REDACTED]

preparation and for mixing of fresh gas with burned gases. The observed thickness of the visible reaction zone in a diffusion flame does not necessarily establish the maximum space-heat-release rate possible in a high-speed combustor, for no account is taken of the space required to bring reactants into and products out of the flame. In one study (ref. 18), the combustion efficiency, and thus the maximum space heat-release rate, of turbojet combustors was related to the inlet-air conditions by means of a chemical kinetic treatment. It was assumed that a second-order reaction controlled the rate of conversion of air and fuel entering the combustor. The point of figure 5 is, however, (1) that there is a fundamental volume required just for a flame that cannot be exceeded in the combustor, (2) that this volume is larger at reduced pressures, and (3) that it is more and more difficult to provide for this volume as higher velocities are imposed on turbojet combustors as, for example, is noted by the dashed line in figure 5.

A second reason for maximizing combustion space is that, if appreciable quantities of fuel are allowed to impinge on the combustor liner walls and flow down the walls out of the combustion zone, combustion inefficiency will result (ref. 19).

A third reason for trying to maximize the combustion space is that combustion reactions are quenched by the cold walls and by cold-air jets. Basic research has shown the relation between quenching distance and pressure, as shown in figure 6 for rectangular slots, tubes, and flat plates (refs. 20 and 21). The quenching distance is simply the slot width, tube diameter, or distance between flat plates that will not propagate the flame. All of the points fall on the same curve after a correction is made for the different geometry. Quenching distances increase as pressures are decreased. These data indicate that certain spaces are unavailable for flame propagation because of wall quenching. And further, it may be surmised that quenching losses will be obtained in the region of any cold-air inlet hole in the combustion zone. Quenching studies thus indicate that a large-diameter combustor, or a combustor having as much volume-to-surface ratio in the combustion zone as possible, is desirable.

#### Application of Basic Considerations to Turbojet Combustor

In the foregoing section it was made evident that in order to obtain high combustion efficiencies in a high-speed combustion system, it would be necessary to achieve three things: (1) preparation of mixtures that fall within a narrow range of composition near stoichiometric, (2) sufficient time and temperature in order to bring the incoming charge to ignition or flame conditions, and (3) adequate time and space or volume for the turbulently burning mixture to burn completely (see also ref. 22).

Mixture compositions. - Localized fuel-air ratios that are at or near stoichiometric in the zone of combustion for all combinations of engine

speed and altitude are customarily achieved in the main combustor of the turbojet by means of a liner or can in the combustion chamber that divides the air and permits only part of it to be admitted to the zone where it will burn with the fuel. The rest of the air is admitted farther downstream and serves to dilute the burned gases and bring them to the temperatures required by the turbine. It is evident, then, that the manner in which the air and fuel are admitted to the upstream end of the combustor where flame will exist is exceedingly important.

First, consider air admission. In early work on turbojet combustor design it was learned that for good altitude performance, the first 20 or 25 percent of the combustion air to be admitted to the combustor liner should be added gradually in as much of the liner length as is reasonably possible. Although this design criterion is based on research on many configurations, both can-type and annular, the point is quickly reviewed in figure 7, which shows the hole distribution along the wall of two turbojet combustors and the efficiencies for each at four different operating conditions. It is seen that configuration O outperforms N. This gradual admission of the so-called primary air ensures that at any fuel flow the combustor will have a favorable mixture in the low-velocity end of the combustor. Because this design criterion is in so much of the literature (e.g., refs. 23 to 26), it will not be reviewed further here.

One further thing that ought to be noted is that the fraction of air passing through the openings in a liner wall is not necessarily directly proportional to the fraction of total open-hole area at the station in question. The over-all combustor pressure drop, the ratio of liner cross section to housing cross section, and the combustor temperature rise all influence air distribution. However, calculations of air distribution can be made as figure 8 illustrates. The plot shows the fraction of total air passing through a combustor liner at a given station  $W_{a,x}/W_{a,total}$  as a function of the fraction of total liner-hole area achieved between the upstream end of the combustor and that station  $A_x/A_{total}$ . The effect of increasing the ratio of liner diameter to housing diameter  $d/D$  is to decrease the fraction of air passing through a station. For diameter ratios of approximately 0.78, which would be typical of those in present use, the kind of air distribution that might be expected for the inlet conditions indicated on the figure is shown by the solid line, as contrasted with the dashed line, which indicates the distribution of air that would occur if air distribution were directly proportional to the fraction of total open-hole area.

Next, consider fuel admission. If it is important to admit the air gradually in the upstream end of a combustor, it may be expected to be equally important to match the distribution of fuel to the admission of air. Essentially, both air admission and fuel admission must be tailored together to achieve correct mixtures in the upstream end of a combustor.

There have been a number of investigations that establish this principle (refs. 27 to 31); one of these is briefly reviewed here. In figure 9, three different methods of introducing vapor (ref. 28), which was propane in this case, and three different methods of introducing liquid fuel (ref. 29), JP-3, to the same tubular turbojet combustor are indicated. With the liquid fuel, the best performance was obtained when the fuel was distributed axially from holes in a tube placed to match the fuel with the air, but almost equally good performance was obtained when the fuel was sprayed directly into the combustion zone and the short distances between the many, many droplets were relied on to achieve mixing by molecular and eddy diffusion processes. The poorest combustion efficiency with liquid fuel occurred when the JP-3 was flowed uniformly across the upstream end; in this case low combustion efficiency probably resulted because the upstream end was overenriched with liquid fuel. It is seen that the combustion efficiency with the vapor fuel was less affected by an increase in altitude. This indicates the importance of eliminating the atomization and vaporization steps, which must be completed in a very short time in the primary zone. It is further noted, however, that even with the vapor fuel, appropriate mixing of the fuel and air must occur, and that, because the air currents spread vapor so much more rapidly than they do liquid, best efficiencies result from distributing the vapor and the poorest efficiencies from a high-velocity axially directed jet of vapor.

The important points of figures 7, 8, and 9 are that it is necessary to control the fuel-air ratio and the quality of the mixture in the combustion zone, and that methods of achieving this control have been demonstrated.

Flame stabilization. - The next obvious point to discuss after correct mixtures have been provided for the turbojet combustor is the problem of obtaining flame stabilization. The manner in which flame stabilization is conventionally achieved in the turbojet combustor is by means of recirculation of the burning gases into the fresh charge that is entering the combustor. This recirculation can be provided by the dome of the liner (or can) that has just been discussed, by swirl vanes, and by impinging air jets, or by combinations of these. Many investigators have used different kinds of tracing techniques, such as probes or particle traces, in order to reveal the air-flow patterns in combustors (refs. 32 to 35). Typical air-flow patterns are shown in figure 10, wherein a high-speed picture was taken of balsa dust flowing through a transparent combustor (ref. 36). The tracing below the photograph shows several regions of recirculation caused both by the obstruction of the upstream end of the combustor in the general stream and by the impingement of the several large air jets entering the combustor. The strong reverse flow down the center of the combustor is noted. The same kind of recirculation for flame stabilization is observed behind a V-gutter, as noted in figure 11 (ref. 37). In the afterburner it is not necessary to separate only a

fraction of the entering gas for combustion, as nearly all of this gas will burn with fuel. Consequently, a bluff object, like a V-gutter, serves for flame stabilization in the afterburner.

A simple mechanism has been described by a number of investigators, including Longwell (ref. 38), DeZubay (ref. 39), and Williams (ref. 40), for flame stabilization behind a bluff object. In this theory, illustrated in figure 12, it is assumed that heat is liberated behind a V-gutter and that this heat, which comes from chemical reaction, kindles fresh charge flowing in behind the gutter. The rate of heat liberation behind the gutter will depend on the size of the shielded zone, or will be proportional to the dimension  $N$ . The rate of heat extraction, that is, the amount of heat given over to heating fresh charge, will be proportional to the rate of inflow of fresh charge, which, in turn, is proportional to the velocity past the bluff object. If the inflow of fresh charge is too great, the flame will be quenched and go out. However, if the velocity past the gutter is low so that the rate of inflow of fresh charge is low, then the reaction rate will provide heat at a greater rate than is required to heat the inflowing fresh charge; flame will persist. Consequently, right at blow-out, the velocity past the gutter will be the blow-out velocity and the rate of heat liberation from reaction will exactly equal the rate of heat extraction to heat fresh charge. Consequently, the velocity at blow-out  $V_{BO}$  divided by the dimension  $N$  will be a constant for any combustible mixture, or as fuel-air ratio  $f$  is varied,  $V_{BO}/N = \varphi(f)$ . In practice,  $V_{BO}/N^a = \varphi(f)$  is found to generalize the data more satisfactorily. This mechanism has been tested by numerous investigators. One such test of the mechanism is shown in figure 13, where flame-stability limits for city gas (ref. 40), which contains a large fraction of carbon monoxide, are plotted as fuel-air ratio against the generalizing parameter  $V_{BO}/N^a$ . The data points are for a variety of shapes and sizes of flame-stabilizing objects, but the generalizing parameter derived from the simple mechanism causes the data to fall in a single curve. This theory of flame stabilization applies in principle to both the turbojet combustor and the afterburner.

Flame propagation. - Considerations of basic fundamental facts about combustion indicate that it is desirable to allow as much space or volume for the flame as reasonably possible in order to avoid wall quenching and excessive fuel impingement. For example, the data on quenching distance indicate that certain spaces are unavailable for flame propagation because of quenching by walls or by cold-air jets. If it be assumed that a narrow annulus near the wall of a tubular combustor exists with a thickness equal to one-half the quenching distance, that this annulus represents a space unavailable for combustion, and that fuel-air mixture in this region will not burn, then the percentage of cross-sectional area that remains available can be computed and plotted, as in figure 14. This percentage of available area is plotted against volume-to-surface ratio

CONFIDENTIAL

for a cylinder for several pressures. The percentage of available area increases as combustor radius increases, and the area increases as pressure increases.

Of course, only wall quenching has been considered. Further quenching losses may be expected in the region of the cold-air inlet holes to the liner. However, a review of research results on various turbojet combustors indicates that the larger combustors produced higher combustion efficiencies at severe operating conditions. This observation is shown in figure 15, a plot of combustion efficiency against volume-to-surface ratio as measured at the upstream end of the combustor liner where the fuel spray would normally impinge if air flow did not disturb it, that is, in the combustion space. Each of the data points in figure 15 shows the combustion efficiency obtained with a different turbojet combustor. All the combustors were tested at operating conditions of equal severity (refs. 41 and 42). It is interesting to note that the curves have the same general shape as those plotted from a consideration of the quenching distance as shown in figure 14, although quantitative agreement does not exist. Of course, one reason for the lack of quantitative agreement is that only quenching at the wall is considered.

Another study of the effect of combustor size on combustion efficiency is reviewed in figure 16 (ref. 43). Four combustor liners that have the same liner hole area, the same fuel nozzle, and the same length were run under identical operating conditions. These liners were as near a scale study of diameter alone as might be expected by a simply empirical approach. In addition to pointing out the fact that the combustion-efficiency problem is less difficult in large combustors or on large engines, these data indicate that, in any given combustor, the combustion zone should be made as large as possible. Of course, making the combustion zone as large as possible must be done with a view to the total-pressure loss that might be entailed, but this problem is discussed later.

#### Application of Basic Considerations to Afterburner

The same principles that apply to the main combustor in the turbojet engine apply to the afterburner as far as the problem of combustion efficiency is concerned. That is, correct mixtures, adequate flame stabilization, and time and space for complete combustion must be ensured.

For the preparation of correct mixtures, it is unnecessary to separate the air as is currently done in turbojet combustors, but it is still quite necessary to match the fuel with it so that combustible mixtures will arrive at the flame-stabilizing part of the combustor. Consequently, the first thing to do in designing the efficient afterburner is to get the air flow into the afterburner under control. There are three things to which particular attention must be paid: (1) Flow separations off the

CONFIDENTIAL

center body of the engine or off the afterburner wall must be eliminated by attention to aerodynamic design; (2) wild velocity distributions must be eliminated, again by attention to aerodynamic design; and (3) swirl of the gases leaving the turbine should be eliminated, even if anti-swirl vanes behind the turbine may be required. It has been found that these distortions in air flow can distort the fuel-air ratios at the flame holder, to the detriment of combustion efficiency. Once the air flow is smooth or at least controlled to give a known velocity distribution that is not too badly distorted or skewed, then it is possible to match the fuel distribution to it (refs. 44 to 47).

Basic research has been done both at the NACA and at other laboratories (ref. 48) on the evaporation and spreading of fuels sprayed into air streams. The kinds of result obtained are illustrated in figure 17 (ref. 47). It is seen that a simple jet of isooctane fuel sprayed upstream into a warm air stream both spreads out and evaporates as it travels downstream. However, even in 10 inches, it is noted that the fuel is rather well concentrated toward the center of the duct. Information like this, together with gas analyses across actual afterburners, was particularly helpful in providing adequate mixture preparation in the afterburner. For example, in figure 18 afterburner combustion efficiency is plotted against exhaust-gas temperature for two different methods of injecting fuel into the afterburners (ref. 49). In one instance, the fuel is rather well concentrated in the center part of the engine; the efficiency is low, and a maximum exhaust-gas temperature of only 2000° F is obtained. For higher efficiencies, and particularly for higher exhaust-gas temperatures, distributing the fuel more uniformly across the duct was beneficial. Of course, the extent to which fuel is distributed in the gas stream depends on the extent to which the air is consumed, or in other words, uniform distribution of fuel and air is desired when nearly stoichiometric combustion is desired; whereas, for lower temperature rise, stratification of the fuel stream would be desired to ensure the arrival of correct compositions at the flame stabilizers (ref. 50).

The V-baffles in an afterburner provide the flame stabilization previously discussed. Research on a wide variety of bluff objects, all with the same blocked area and the same size of bluff end, revealed that combustion efficiency is not strongly dependent on flame-stabilizer shape (ref. 51). V-gutters are used conveniently.

With respect to afterburner combustion volume, the afterburner diameter is generally made as large as possible consistent with the envelope of the engine, in order to reduce the velocity in the afterburner compatibly with good combustion efficiency. The length of the afterburner has been determined in systematic research to be preferably 55 to 60 inches at afterburner velocities of 500 feet per second and subatmospheric pressures with the kind of fuel injection and flame stabilization discussed here (ref. 52 and recent unpublished data).

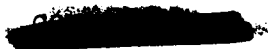


An experimental afterburner that has been under investigation at the NACA Lewis laboratory in a blower duct instead of behind an engine (ref. 51) is illustrated in figure 19. Attention to the aerodynamic shape provides smooth air flow, and the fuel is distributed uniformly in the air stream from 24 bars spraying radially outward from holes along their length. However, distance is allowed for further spreading and evaporation of the fuel. Flame stabilization is with baffles, and 53 inches of combustor length is provided. The performance of this particular afterburner at the rather low pressure of 5 pounds per square inch absolute is shown in figure 20 for 400 and for 625 feet per second. The 400 foot-per-second data show improved performance over the reference afterburner, which is one of the better afterburners presently provided behind a current production engine. Also the temperatures of 3300° F have been reached at this pressure and velocity. Also, this afterburner has been run at 5 pounds per square inch absolute and 625 feet per second with the efficiencies shown. Research is needed to raise these combustion efficiencies. At 0.5 atmospheres, this experimental afterburner has run to 3500° F and at 625 feet per second with efficiencies on the order of 85 percent.

#### OUTLET TEMPERATURE PROFILE

In the previous paper, the important matter of controlling the admission of dilution air to achieve a desired temperature profile at the combustor outlet or into the turbine was discussed.

In order to obtain desired combustor-outlet temperature profiles, penetration and mixing of the dilution air is controlled by the manner in which this air is admitted in the downstream end of the combustor. It has been shown in data such as those of figure 21 (ref. 53) that large slots with the long axis oriented in the line of the general stream afford the best way to achieve maximum penetration of the cold-air jet with the minimum of velocity ratio of that jet to the stream, or with a minimum of the pressure drop required to achieve penetration. The data show that, at a given velocity ratio, the best penetration is obtained with a longitudinal slot. In addition, when a number of slots are used, the spacing between the slots and their size greatly affect their penetrations. For example, in figure 22 two outlet-temperature profiles are shown for an annular combustor (ref. 41). The one for combustor A results when a large number of slots spaced closely together on the inner wall of the combustor are used. The slots push a heavy blanket of air in against the hot burned gases that blow out of the combustor. The corresponding profile shows quite cool gas for some distance in from the root of the blade. Now, when the same total open area in the combustor wall is used so that the over-all pressure drop will be the same, and when the slots in the inner wall are spaced wider apart and made larger, a much greater penetration of the cooling air is achieved and a much flatter temperature



profile results. When the slots are spaced apart, the hot gases can flow between them and the cool gases penetrate and diffuse sideways into the hot gases. It has even been possible with some designs to use air jets that are sufficiently large and well-spaced that cool air penetrates across to the opposite side. In other words, cool gases have been obtained at the root of a blade by using large, widely spaced air jets on the outside wall of the combustor. One further item is that changes to the gas flow in the primary or burning zone also are important to the resulting outlet-temperature profile. A great deal of empirical research has been done to secure reasonable outlet-temperature profiles in experimental combustors, and the preceding kind of information is available (refs. 41, 54, and 55). However, there is still a great deal of artistry connected with this subject.

#### COMBUSTOR TOTAL-PRESSURE LOSS

It was shown in the discussion of combustion efficiency that it is desirable to make the combustion zone as large as possible. However, figure 23 indicates what is entailed in this consideration. Pressure drop, in terms of the fraction of total pressure at the combustor inlet, is plotted as a function of the ratio of the liner diameter to the housing diameter  $d/D$  for three different values of the liner open-hole area to the cross-sectional area of the housing. The data are for the conditions indicated and for a cylindrical liner in a cylindrical housing. As soon as the combustor-liner diameter is increased much beyond about 82 percent, appreciable pressure losses are incurred. Also, liner total open-hole areas greatly in excess of the cross-sectional area of the housing do not help pressure loss much. While it is desirable with respect to combustion efficiency to increase the liner diameter, it is desirable with respect to pressure loss to decrease it, at least as far as about 75 percent, which would provide minimum pressure loss for the conditions of figure 23. The compromise made will, in at least some measure, depend on the application desired. For example, a high-velocity combustor that did not have to run at very low pressures would probably operate with the value of this ratio down around 0.75; whereas a combustor in which high efficiency at very low pressures is required might use a liner much larger. Computations can be made for a variety of combustor situations.

#### RELIABILITY

##### Durability

Cracking and warping of turbojet combustor liners and transition pieces are due to high surface temperatures, high temperature gradients, and buffeting from high-speed air streams (refs. 32 and 56). The problem in future engines is high temperature. For example, in a supersonic engine, the air coming into a combustor may be hot enough to make it glow

[REDACTED]

a dull red even without flame. With high-pressure-ratio engines, or at very high flight speeds, higher pressures will exist in the engine than are presently in general use. These higher pressures and velocities together spell higher convective heat transfer that will heat the walls. On the other hand, if convective cooling is used both on the outside and inside of liner walls, higher convective heat transfer for cooling also results. The higher pressures, however, mean higher radiation heat transfer, for the luminous flames encountered at high pressures radiate many more times than do the nonluminous flames encountered at the lower pressure (ref. 57).

In the afterburner, temperatures as high as  $3500^{\circ}$  may be required for take-off and acceleration, and these temperatures leave only a little over 10 percent of the gas entering the afterburner unburned and available for cooling. Extensive cooling research has been initiated at the NACA Lewis laboratory for the afterburner (refs. 58 to 61). This research involves consideration of porous walls and ceramic linings.

#### Afterburner Screech

The problem of destructive screech in afterburners has been described in the preceding paper. Because of the severity of the screech problem in developing high-efficiency, high-performance afterburners, extensive research has been conducted on the mechanism and on a cure for the problem. Special instrumentation was developed and measurements were made of the amplitude and relative phasing of the pressure oscillations at various locations within the combustion zone of several afterburners that could be made to screech (refs. 62 and 63). Ion gaps were used to detect the presence of chemical reaction and its phasing with the pressure oscillations. These measurements, together with the measurements of screech frequency, revealed a mechanism of afterburner screech. The mechanism essentially is as follows: The acoustic oscillations giving rise to screech are the result of a transverse mode of oscillation of the gases in the combustor as heat is released in them. Pressure oscillations are greatest near the wall of the combustor and are at a minimum near the center of the duct, as indicated by pressure records obtained with special instrumentation. The heat-release rate is greatest in those regions where the pressure is highest. This phasing has been determined by means of both pressure probes and ion gaps. The phasing of the heat-release rate with the pressure results in a time-varying work cycle. The heat-release rate, being in phase with the pressure, provides the energy necessary to overcome such natural damping as exists in the duct and to drive these acoustic oscillations to the high amplitude observed in screeching combustors. This high amplitude is responsible for the mechanical mischief.

One technique for alleviating screech would be to increase the damping of the acoustic oscillations. Since these pressure oscillations are

[REDACTED]

greatest near the combustor wall, it would therefore be expected that some sound-absorbing material in the vicinity of the combustor wall would be quite effective in absorbing the energy from these oscillations and thereby increasing the damping. In order to test this idea, an acoustic damper comprising a perforated inner liner, as shown in figure 24, was installed in a full-scale afterburner behind an engine (ref. 63). The results obtained are shown in figure 25. With no damper, the afterburner screeched over the entire range of fuel-air ratio investigated at the inlet conditions shown on the figure. The arrows at the end of the shaded bar graph indicate that the operating limits of the afterburner were not reached. When a 19-inch-long acoustic damper was installed in the afterburner, the screech limits were narrowed, as shown in the figure, but still occupied an appreciable fraction of the fuel-air-ratio range investigated. When a 29-inch-long damper was installed, no screech was encountered over the entire range of fuel-air ratio investigated. It may be concluded from this research that a mechanism for at least one type of screech has been learned, and a cure both indicated and demonstrated. One note of caution that should be made is that there may be other kinds of afterburner screech encountered.

#### Carbon Deposits

With the higher temperatures, high pressures, and high fuel flows involved in the future requirements for combustors, the problem of carbon deposits becomes increasingly important. Research has shown that carbon deposition is strongly influenced by the quality of the fuel. The higher the boiling point and the lower the hydrogen-carbon ratio, then the greater will be the carbon deposited from that fuel (ref. 64). If a highly volatile fuel is sought in order to alleviate carbon as a problem, then another very serious problem is encountered - evaporative loss of the fuel from the tanks at high flight speeds, because the fuel tank will warm up during high-speed flight (ref. 65). Perhaps the best way of avoiding carbon is to design carefully so that liquid fuel does not hit the combustor wall and accumulate in high-temperature parts of the wall. Detailed attention to providing an air film in the inside of the combustor wall can alleviate carbon deposits. The use of vapor fuel might also eliminate or reduce the problem.

#### Smoke

The higher temperatures, high pressures, and higher fuel flows that promote carbon deposition also promote carbon in the form of smoke (ref. 66). Smoke itself is not particularly harmful to the performance of the turbojet engine; however, it is undesirable to leave great tracks through the sky. Basic research has shown that smoke originates primarily in overrich regions in the burning zone of the combustor (refs. 67 to 69).

This research has also shown that it is possible to burn smoke in rather appreciable quantities by forcing it to pass through a flame front (ref. 70). Unfortunately, those things tried thus far in combustor design for practical application of research principles, while eliminating smoke, lowered combustion efficiency under the severe conditions of low pressure and high velocity in the combustor. It is believed that combustion efficiency should not be sacrificed in order to eliminate smoke.

### Ignition

As noted earlier, the important feature for ignition is high ignition energy. The reasons for this requirement are seen in figure 26. Minimum ignition energy at different pressures is shown for ideal mixtures of hydrocarbon and air, both quiescent (ref. 71) and flowing at 50 feet per second past the ignition source (ref. 72). Minimum ignition energy for a turbojet combustor is also shown for two velocities (ref. 73). Attention should be directed to the strong influence of velocity on ignition energy. It is to be surmised from references 71, 73, and 74 that, in order to minimize the energy required to ignite a turbojet combustor, the energy should be supplied at a region in the combustor where local mixtures are much richer than stoichiometric and where local velocities will be quite low. Barring success in locating the ignition source in such a zone, the only thing that can be done is to provide high enough energy to the system to provide for vaporizing part of the fuel and for initiating a flame large enough to spread in the turbulent heterogeneous mixture (refs. 73 and 75). Chemical ignitors that are spontaneously inflammable have been considered (ref. 76). High-speed motion pictures of the ignition phenomenon have corroborated these contentions. Ignition energy requirements thus can be strongly influenced by combustor design, ignitor location, and ignitor design; plugs with shields to cut down local high velocities are beneficial. The energy is also influenced by fuel volatility, with the more volatile fuels being more easily ignited, although this influence is less than that of design.

### CONCLUSIONS

The problem of combustion efficiency was examined for both the main combustor and for the afterburner of the turbojet engine; and it was indicated that, by applying basic information about mixture preparation, flame stabilization, and flame propagation, certain design principles could be followed that would improve the combustion efficiency at low pressure or at higher velocity for both the main combustor and the afterburner. The design principles used to obtain the desired outlet-temperature profile at low pressure drop in a turbojet combustor were reviewed, as were the design principles for obtaining low pressure drop in the combustor. Among the problems of combustor reliability, it was seen that

additional research attention must be given to the problem of high temperature on combustor walls and on transition-piece walls. The problem of screech was treated; at least one mechanism was examined; and a cure for this screech in an afterburner was both indicated and demonstrated. Carbon and smoke were both examined as reliability problems, but no specific information, other than that the problems can be handled with design, was offered. Ignition can be made much more reliable by careful attention to the design detail of where the ignitor source is located; this location of the ignitor is more important than the fuel volatility.

The value of these research results will only be secured when all the problems discussed are solved together, inasmuch as a number of design compromises must be made in the combustor when these various problems are considered. The task of integrating the ideas and knowledge furnished by the research into completed experimental combustors containing the required design compromises will be the subject of the next paper.

#### REFERENCES

1. Standing Committee on Combustion Symposia: Third Symposium on Combustion and Flame and Explosion Phenomena, The Williams & Wilkins Co., 1949.
2. Standing Committee on Combustion Symposia: Fourth Symposium on Combustion (International), The Williams & Wilkins Co., 1953.
3. DiPiazza, James T.: Limits of Flammability of Pure Hydrocarbon-Air Mixtures at Reduced Pressures and Room Temperature. NACA RM E51C28, 1951.
4. Spakowski, Adolph E., and Belles, Frank E.: Variation of Pressure Limits of Flame Propagation with Tube Diameter for Various Isooctane-Oxygen-Nitrogen Mixtures. NACA RM E52A08, 1952.
5. Spakowski, Adolph E.: Pressure Limits of Flame Propagation of Pure Hydrocarbon-Air Mixtures at Reduced Pressures. NACA RM E52H15, 1952.
6. Mullins, B. P.: Studies on the Spontaneous Ignition of Fuels Injected into a Hot Air Stream. Part III - The Effect of Chemical Factors upon the Ignition Delay of Kerosene-Air Mixtures. Rep. No. R.95, British N.G.T.E., Oct. 1951.
7. Graves, Charles C.: Burning Rates of Single Fuel Drops and Their Application to Turbojet Combustion Process. NACA RM E53E22, 1953.

8. Gerstein, Melvin, Levine, Oscar, and Wong, Edgar L.: Fundamental Flame Velocities of Pure Hydrocarbons. I - Alkanes, Alkenes, Alkynes, Benzene, and Cyclohexane. NACA RM E50G24, 1950.
9. Simon, Dorothy M., and Wong, Edgar L.: Flame Velocities over a Wide Composition Range for Pentane-Air, Ethylene-Air, and Propyne-Air Flames. NACA RM E51H09, 1951.
10. Dugger, Gordon L., and Simon, Dorothy M.: Prediction of Flame Velocities of Hydrocarbon Flames. NACA RM E52J13, 1953.
11. Dugger, Gordon L., and Heimel, Sheldon: Flame Speeds of Methane-Air, Propane-Air, and Ethylene-Air Mixtures at Low Initial Temperatures. NACA TN 2624, 1952.
12. Wohlenberg, W. J.: The Influence of Reaction Interface Extension in the Combustion of Gaseous Fuel Constituents. Trans. A.S.M.E., vol. 70, no. 3, Apr. 1948, pp. 143-156; discussion, pp. 156-160.
13. Bollinger, Lowell M., and Williams, David T.: Effect of Reynolds Number in Turbulent-Flow Range on Flame Speeds of Bunsen Burner Flames. NACA Rep. 932, 1949. (Supersedes NACA TN 1707.)
14. Karlovitz, Béla, Denniston, D. W., Jr., and Wells, F. E.: Investigation of Turbulent Flames. Jour. Chem. Phys., vol. 19, no. 5, May 1951, pp. 541-547.
15. Wohl, Kurt, Shore, L., von Rosenberg, H., and Weil, C. W.: The Burning Velocity of Turbulent Flames. Fourth Symposium (International) on Combustion, The Williams & Wilkins Co., 1953, pp. 620-635.
16. Haddock, Gordon W., and Childs, J. Howard: Preliminary Investigation of Combustion in Flowing Gas with Various Turbulence Promoters. NACA RM E8C02, 1948.
17. Hibbard, Robert R., Drell, Isadore L., Metzler, Allen J., and Spakowski, Adolph E.: Combustion Efficiencies in Hydrocarbon-Air Systems at Reduced Pressures. NACA RM E50G14, 1950.
18. Childs, J. Howard: Preliminary Correlation of Efficiency of Aircraft Gas-Turbine Combustors for Different Operating Conditions. NACA RM E50F15, 1950.
19. Butze, Helmut F., and Jonash, Edmund R.: Turbojet Combustor Efficiency with Ceramic-Coated Liners and with Mechanical Control of Fuel Wash on Walls. NACA RM E52I25, 1952.

20. Belles, Frank E., and Simon, Dorothy M.: Variation of the Pressure Limits of Flame Propagation with Tube Diameter for Propane-Air Mixtures. NACA RM E51J09, 1951.
21. Simon, Dorothy M., and Belles, Frank E.: An Active Particle Diffusion Theory of Flame Quenching for Laminar Flames. NACA RM E51L18, 1952.
22. Olson, Walter T., Childs, J. Howard, and Jonash, Edmund R.: Turbojet Combustor Efficiency at High Altitudes. NACA RM E50I07, 1950.
23. Hill, Francis U., and Mark, Herman: Effect of Air-Flow Distribution and Total-Pressure Loss on Performance of One-Sixth Segment of Turbojet Combustor. NACA RM SE7K16, Bur. Aero., 1947.
24. Olson, Walter T., and Schroeter, Thomas T.: Effect of Distribution of Basket-Hole Area on Simulated Altitude Performance of  $25\frac{1}{2}$ -Inch-Diameter Annular-Type Turbojet Combustor. NACA RM E8A02, 1948.
25. Zettle, Eugene V., and Mark, Herman: Simulated Altitude Performance of Two Annular Combustors with Continuous Axial Openings for Admission of Primary Air. NACA RM E50E18a, 1950.
26. Dittrich, Ralph T.: Investigation of Low-Pressure Performance of Experimental Tubular Combustors Differing in Air-Entry-Hole Geometry. NACA RM E53G01, 1953.
27. McCafferty, Richard J.: Effect of Fuels and Fuel-Nozzle Characteristics on Performance of an Annular Combustor at Simulated Altitude Conditions. NACA RM E8C02a, 1948.
28. McCafferty, Richard J.: Vapor-Fuel-Distribution Effects on Combustion Performance of a Single Tubular Combustor. NACA RM E50J03, 1950.
29. McCafferty, Richard J.: Liquid-Fuel-Distribution and Fuel-State Effects on Combustion Performance of a Single Tubular Combustor. NACA RM E51B21, 1951.
30. Zettle, Eugene V., and Mark, Herman: Effect of Axially Staged Fuel Introduction on Performance of One-Quarter Sector of Annular Turbojet Combustor. NACA RM E53A28, 1953.
31. Norgren, Carl T., and Childs, J. Howard: Effect of Fuel Injectors and Liner Design on Performance of an Annular Turbojet Combustor with Vapor Fuel. NACA RM E53B04, 1953.

32. Watson, E. A., and Clarke, J. S.: Combustion and Combustion Equipment for Aero Gas Turbines. Jour. Inst. Fuel, vol. XXI, no. 116, Oct. 1947, pp. 2-34.
33. Nicholson, H. M., and Field, J. P.: Some Experimental Techniques for the Investigation of the Mechanism of Flame Stabilization in the Wakes of Bluff Bodies. Third Symposium on Combustion and Flame and Explosion Phenomena, The Williams & Wilkins Co., 1949, pp. 44-68.
34. Way, Stewart: Problems in the Development of Turbo-Jet Combustion Chambers. Scientific Paper No. 1421, Westinghouse Res. Labs., Mar. 8, 1949.
35. Nerad, A. J.: Some Aspects of Turbojet Combustion. Aero. Eng. Rev., vol. 8, no. 12, Dec. 1949, pp. 24-26;88.
36. Straight, David M., and Gernon, J. Dean: Photographic Studies of Preignition Environment and Flame Initiation in Turbojet-Engine Combustors. NACA RM E52111, 1953.
37. Younger, George G., Gabriel, David S., and Mickelsen, William R.: Experimental Study of Isothermal Wake-Flow Characteristics of Various Flame-Holder Shapes. NACA RM E51K07, 1952.
38. Longwell, J. P., Chenevey, J. E., Clark, W. W., and Frost, E. E.: Flame Stabilization by Baffles in a High Velocity Gas Stream. Third Symposium on Combustion and Flame and Explosion Phenomena, The Williams & Wilkins Co., 1949, pp. 40-44.
39. DeZubay, E. A.: Characteristics of Disk-Controlled Flame. Aero Digest, vol. 61, no. 1, July 1950, pp. 54-56; 102-104.
40. Williams, G. C., Hottel, H. C., and Scurlock, A. C.: Flame Stabilization and Propagation in High Velocity Gas Streams. Third Symposium on Combustion and Flame and Explosion Phenomena, The Williams & Wilkins Co., 1949, pp. 21-40.
41. Norgren, Carl T., and Childs, J. Howard: Effect of Liner Air-Entry Holes, Fuel State, and Combustor Size on Performance of an Annular Turbojet Combustor at Low Pressures and High Air-Flow Rates. NACA RM E52J09, 1953.
42. Olson, Walter T., Childs, J. Howard, and Scull, Wilfred E.: Method for Estimating Combustion Efficiency at Altitude Flight Conditions from Combustor Tests at Low Pressures. NACA RM E53F17, 1953.

43. Dittrich, Ralph T.: Investigation of Low-Pressure Performance of Experimental Tubular Combustor Liners of  $4\frac{3}{4}$ - to 8-Inch Diameter. (NACA RM to be pub.)
44. Huntley, S. C., and Wilsted, H. D.: Altitude Performance Investigation of Two Flame-Holder and Fuel-System Configurations in Short Afterburner. NACA RM E52B25, 1952.
45. Braithwaite, Willis M., Renas, Paul E., and Jansen, Emmert T.: Altitude Investigation of Three Flame-Holder and Fuel-Systems Configurations in a Short Converging Afterburner on a Turbojet Engine. NACA RM E52G29, 1952.
46. Conrad, E. William, Schulze, Frederick W., and Usow, Karl H.: Effect of Diffuser Design, Diffuser-Exit Velocity Profile, and Fuel Distribution on Altitude Performance of Several Afterburner Configurations. NACA RM E53A30, 1953.
47. Bahr, Donald W.: Evaporation and Spreading of Isooctane Sprays in High-Velocity Air Streams. NACA RM E53I14, 1953.
48. Longwell, J. P., Van Sweringen, R. A., Jr., Weiss, M. A., and Hatt, F. G.: Preparation of Air-Fuel Mixtures for Ramjet Combustors. Bumblebee Series Rep. No. 168, Esso Labs., Standard Oil Dev. Co., Nov. 1951. (Contract NOrd 9233, with Bur. Ord., U.S. Navy.)
49. Thorman, H. Carl, and Campbell, Carl E.: Altitude-Wind-Tunnel Investigation of Tail-Pipe Burner with Converging Conical Burner Section on J35-A-5 Turbojet Engine. NACA RM E9I16, 1950.
50. Cervenka, A. J., Perchonok, Eugene, and Dangle, E. E.: Effect of Fuel Injector Location and Mixture Control on Performance of a 16-Inch Ram-Jet Can-Type Combustor. NACA RM E53F15, 1953.
51. Nakanishi, S., Velie, W. W., and Bryant, L.: An Investigation of Effects of Flame-Holder Gutter Shape on Afterburner Performance. NACA RM E53J14, 1953.
52. Fleming, W. A., Conrad, E. William, and Young, A. W.: Experimental Investigation of Tail-Pipe-Burner Design Variables. NACA RM E50K22, 1951.
53. Hawthorne, W. R., Rogers, G. F. C., and Zacek, B. Y.: Mixing of Gas Streams - The Penetration of a Jet of Cold Air Into a Hot Stream. Tech. Note No. Eng. 271, British R.A.E., Mar. 1944.

54. Mark, Herman, and Zettle, Eugene V.: Effect of Air Distribution on Radial Temperature Distribution in One-Sixth Sector of Annular Turbojet Combustor. NACA RM E9I22, 1950.
55. Mark, Herman, and Zettle, Eugene V.: Axial-Slot Air Admission for Controlling Performance of a One-Quarter-Annulus Turbojet Combustor and Comparison with Complete Engine. NACA RM E52A21, 1952.
56. Weeton, John W.: Mechanisms of Failure of High Nickel-Alloy Turbojet Combustion Liners. NACA TN 1938, 1949.
57. Topper, Leonard: Radiant Heat Transfer from Flames in a Single Tubular Turbojet Combustor. NACA RM E52F23, 1952.
58. Conrad, E. William, and Jansen, Emmert T.: Effects of Internal Configuration on Afterburner Shell Temperatures. NACA RM E51I07, 1952.
59. Wallner, Lewis E., and Jansen, Emmert T.: Full-Scale Investigation of Cooling Shroud and Ejector Nozzle for a Turbojet Engine-Afterburner Installation. NACA RM E51J04, 1951.
60. Koffel, William K., and Kaufman, Harold R.: Empirical Cooling Correlation for an Experimental Afterburner with an Annular Cooling Passage. NACA RM E52C13, 1952.
61. Koffel, William K.: Preliminary Experimental Investigation of Transpiration Cooling for an Afterburner with a Sintered, Porous Stainless-Steel Combustion-Chamber Wall. NACA RM E53D08, 1953.
62. Blackshear, Perry L., Rayle, Warren D., and Tower, Leonard K.: Experimental Determination of Gas Motion Accompanying Screeching Combustion in a 6-Inch Simulated Afterburner. NACA RM E53I28, 1953.
63. Lewis Laboratory Staff: Experimental and Analytical Investigation of the Combustion Screech Problem. (NACA RM to be pub.)
64. Jonash, Edmund R., Wear, Jerrold D., and Hibbard, Robert L.: Relations Between Fuel Properties and Combustion Carbon Deposition. NACA RM E52B14, 1952.
65. McCafferty, Richard J.: Analytical Investigation of Fuel Temperatures and Fuel-Evaporation Losses Encountered in Long-Range High-Altitude Supersonic Flight. NACA RM E53E25, 1953.
66. Butze, Helmut F.: Effect of Inlet-Air and Fuel Parameters on Smoking Characteristics of a Single Tubular Turbojet-Engine Combustor. NACA RM E52A18, 1952.

67. Clark, Thomas P.: Influence of External Variables on Smoking of Benzene Flames. NACA RM E52G24, 1952.
68. Clark, Thomas P.: Examination of Smoke and Carbon from Turbojet-Engine Combustors. NACA RM E52I26, 1952.
69. Schalla, Rose L., and McDonald, Glen E.: Effect of Pressure on the Smoking Tendency of Diffusion Flames. NACA RM E53E05, 1953.
70. Clark, Thomas P.: Combustion of Smoke in Diffusion and Bunsen Flames. NACA RM E51E15, 1951.
71. Lewis, Bernard, and von Elbe, Guenther: Combustion, Flames and Explosions of Gases. Academic Press, Inc., 1951.
72. Swett, Clyde C., Jr.: Spark Ignition of Flowing Gases. I - Energies to Ignite Propane - Air Mixtures in Pressure Range of 2 to 4 Inches Mercury Absolute. NACA RM E9E17, 1949.
73. Foster, Hampton H., and Straight, David M.: Effect of Fuel Volatility Characteristics on Ignition-Energy Requirements in a Turbojet Combustor. NACA RM E52J21, 1953.
74. Metzler, Allen J.: Minimum Ignition Energies of Six Pure Hydrocarbon Fuels on the C<sub>2</sub> and C<sub>6</sub> Series. NACA RM E52F27, 1952.
75. Armstrong, John C., and Wilsted, H. D.: Investigation of Several Techniques for Improving Altitude-Starting Limits of Turbojet Engines. NACA RM E52IO3, 1952.
76. Straight, David M., Fletcher, Edward A., and Foster, Hampton H.: Aluminum Borohydride as an Ignition Source for Turbojet Combustors. NACA RM E53G15, 1953.

### FLAMMABILITY LIMITS

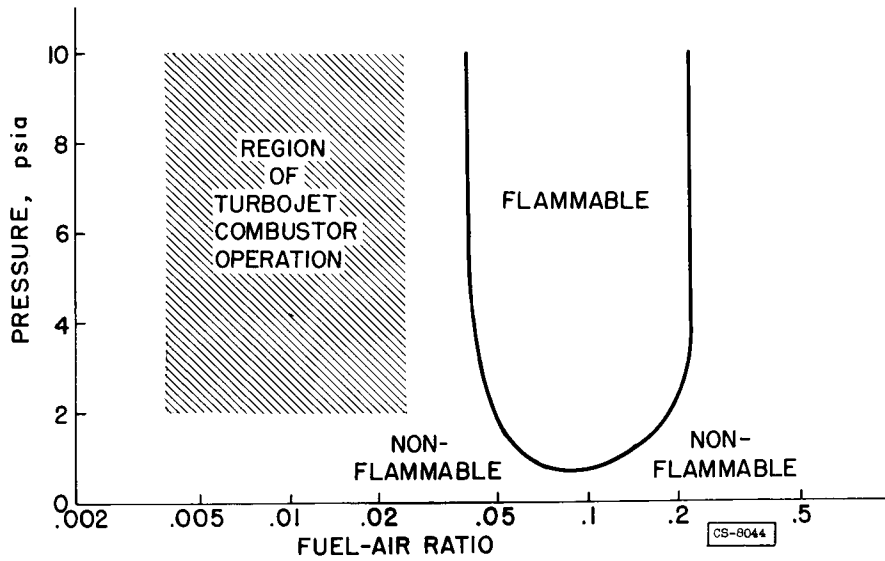


Figure 1

### IGNITION DELAY OF KEROSENE SPRAY

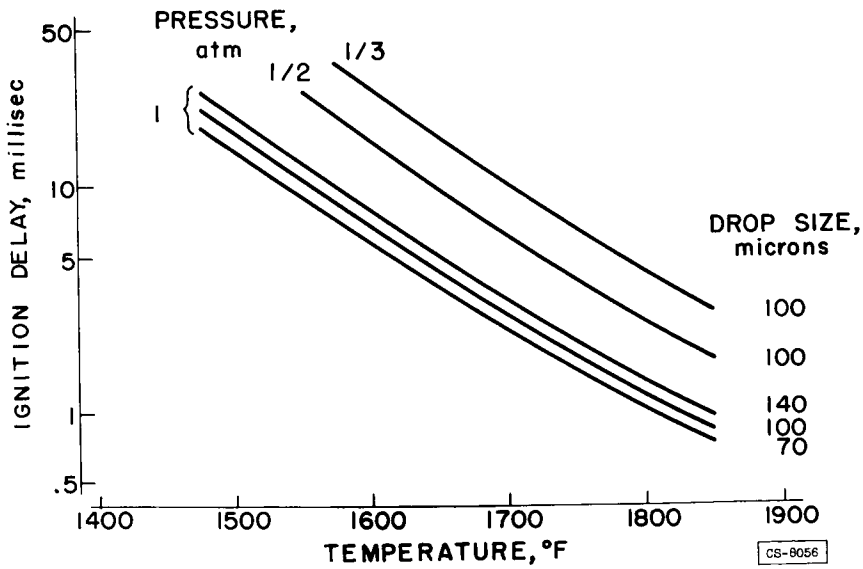


Figure 2

3078-E

### EVAPORATION OF DROP IN FLAME

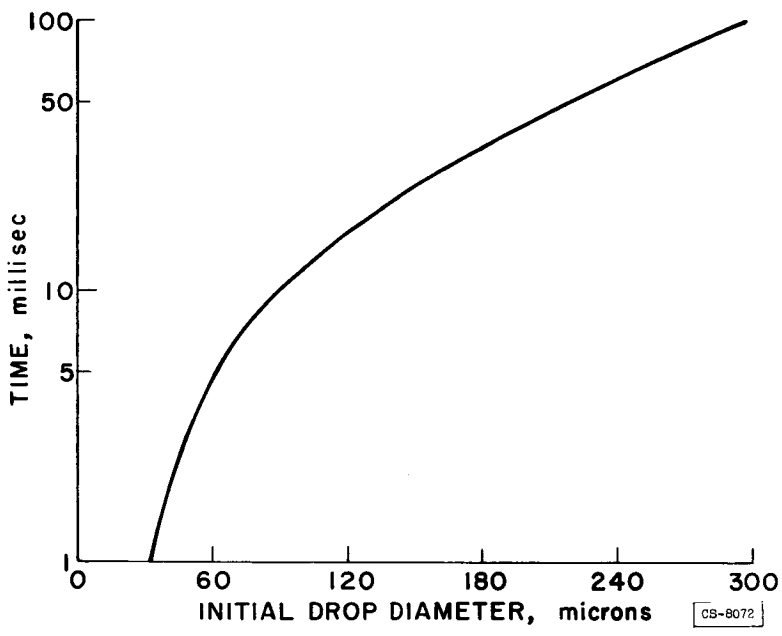


Figure 3

### VELOCITY COMPARISON

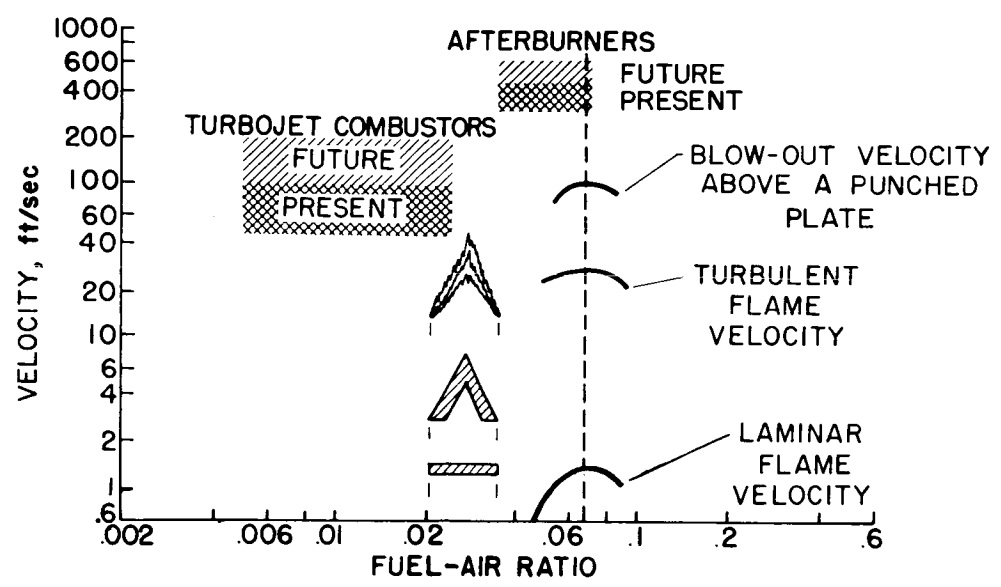


Figure 4

HEAT RELEASE IN DIFFUSION FLAME

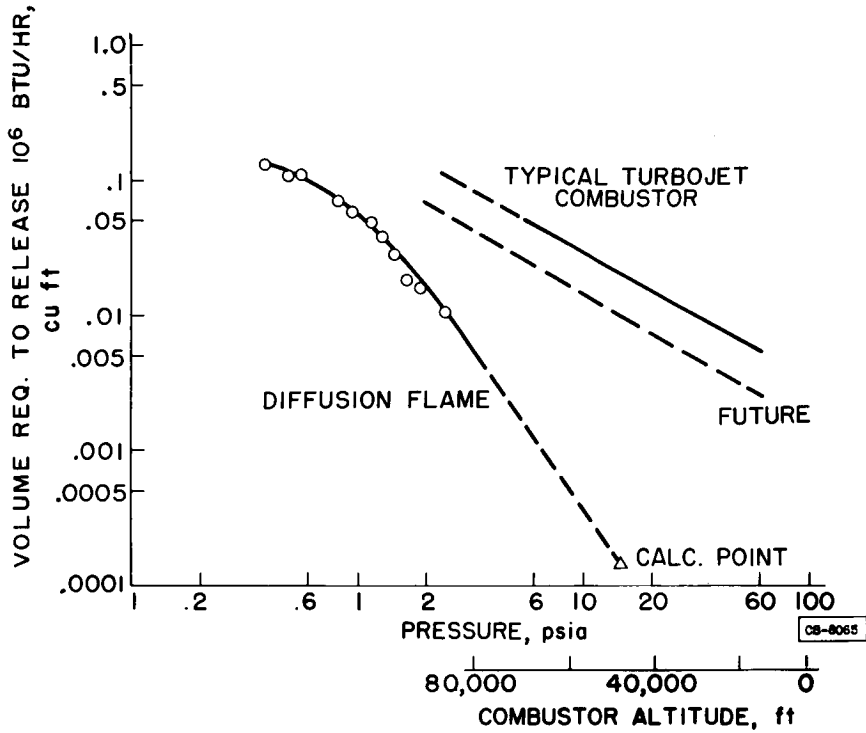


Figure 5

RELATION OF QUENCHING DISTANCE AND PRESSURE

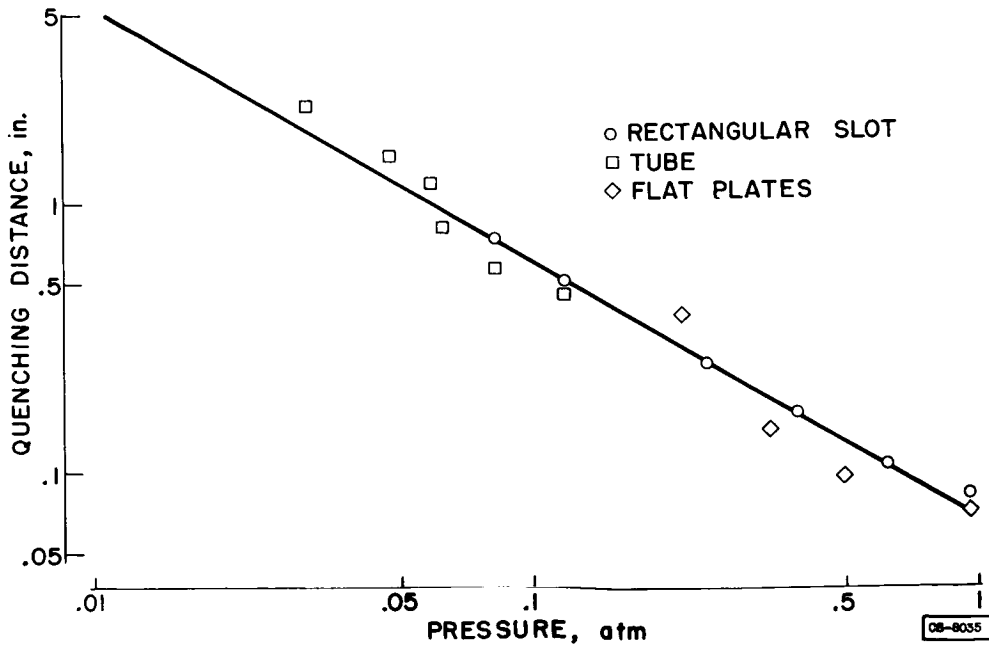


Figure 6

EFFECT OF LINER HOLE DISTRIBUTION

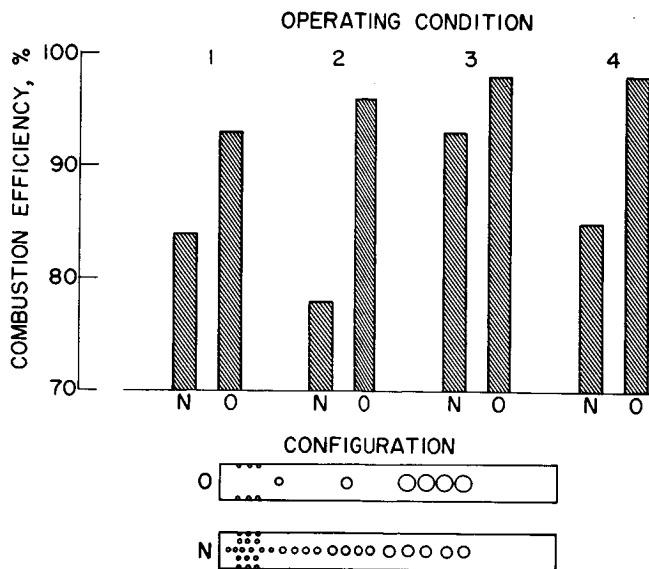


Figure 7

COMBUSTOR AIR DISTRIBUTION

$T_0/T_i, 2$      $V, 100 \text{ ft/sec}$      $T_i, 270^\circ \text{ F}$

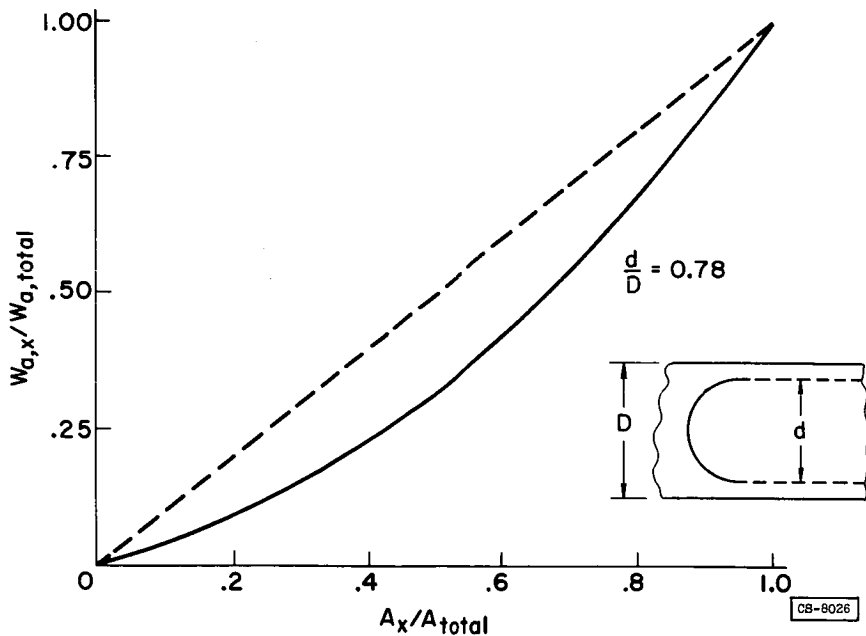


Figure 8

MIXTURE PREPARATION IN TURBOJET

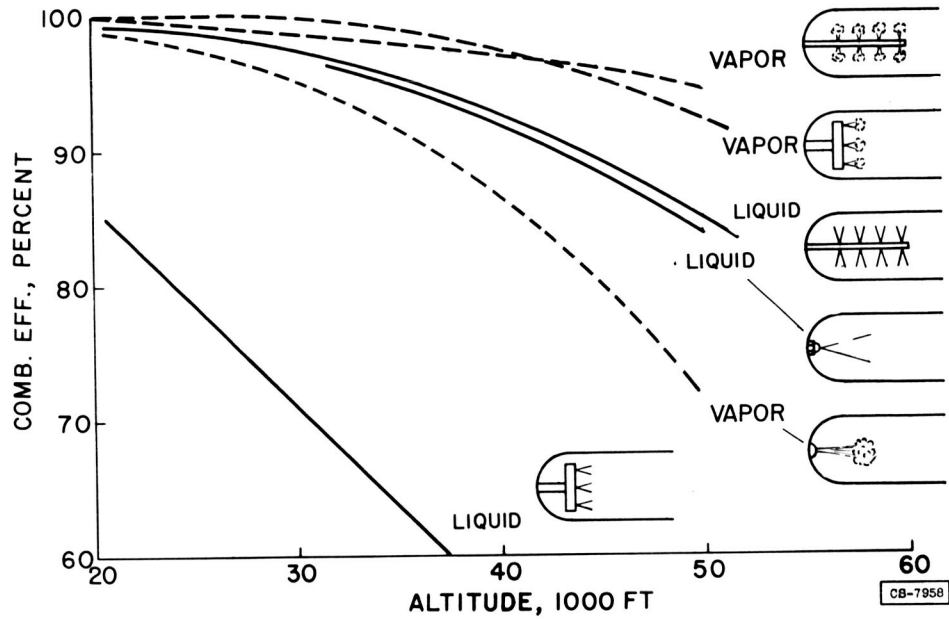


Figure 9

AIR-FLOW PATTERN IN A TUBULAR COMBUSTOR UNDER NON-BURNING CONDITIONS

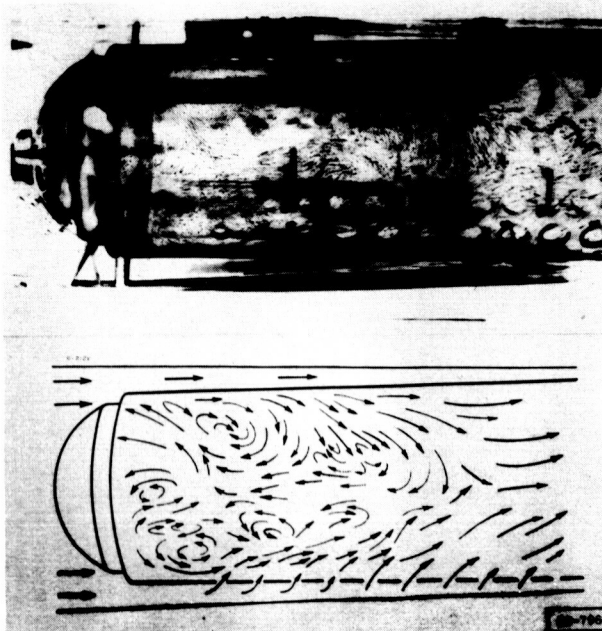


Figure 10

3078-E

## FLOW PATTERN BEHIND V-GUTTER

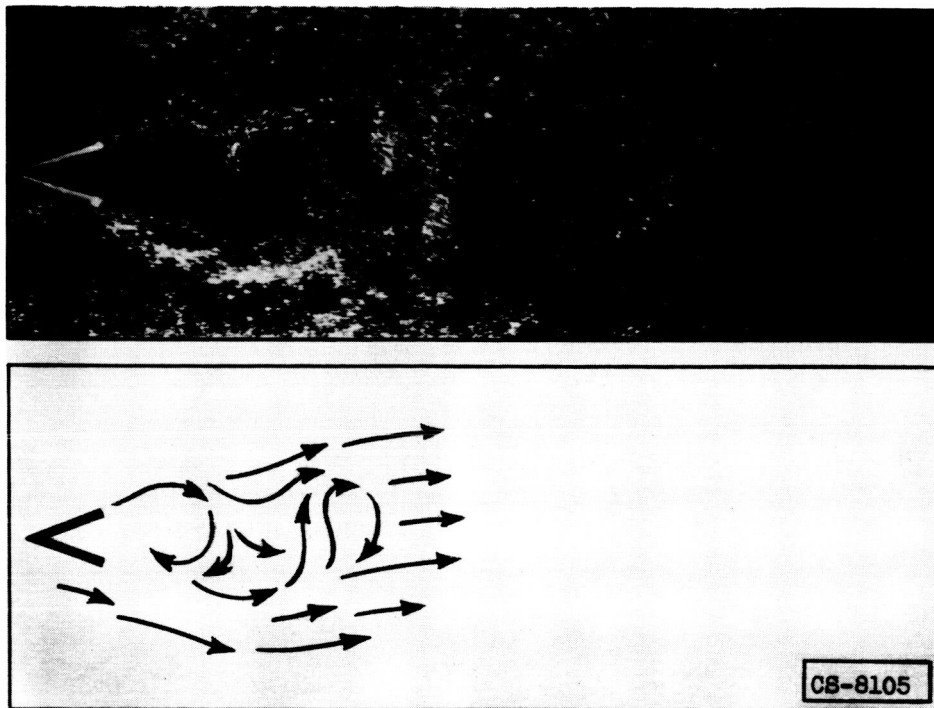
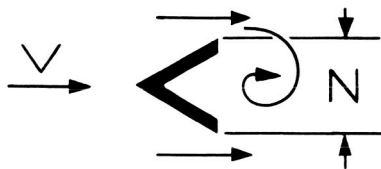


Figure 11

## FLAME-STABILIZATION MECHANISM



$R_1$  = RATE OF LIBERATION  $\propto$  SIZE OF SHIELDED ZONE  $\propto N$

$R_2$  = RATE OF EXTRACTION  $\propto$  RATE OF INFLOW OF FRESH CHARGE  $\propto V$

AT BLOWOUT,  $V = V_{BO}$ , AND  $R_1 = R_2$

$\frac{V_{BO}}{N}$  = CONSTANT FOR ANY COMBUSTIBLE MIXTURE

OR, AS FUEL-AIR RATIO VARIED,

$\frac{V_{BO}}{N} = \phi(f)$

CS-8045

Figure 12

FLAME-STABILITY LIMITS (M.I.T. DATA)

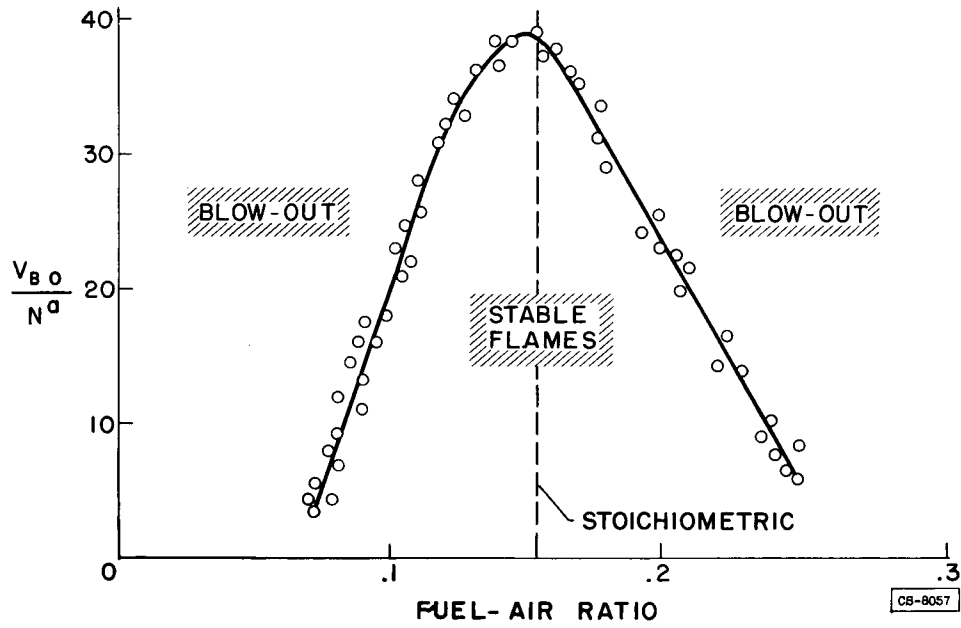


Figure 13

PERCENT OF TOTAL AREA AVAILABLE FOR COMBUSTION

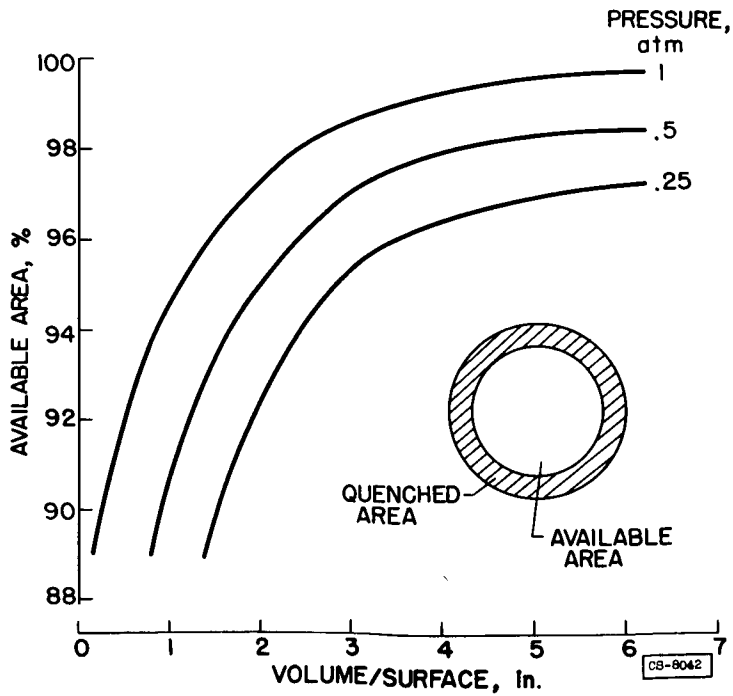


Figure 14

EFFECT OF COMBUSTOR SIZE

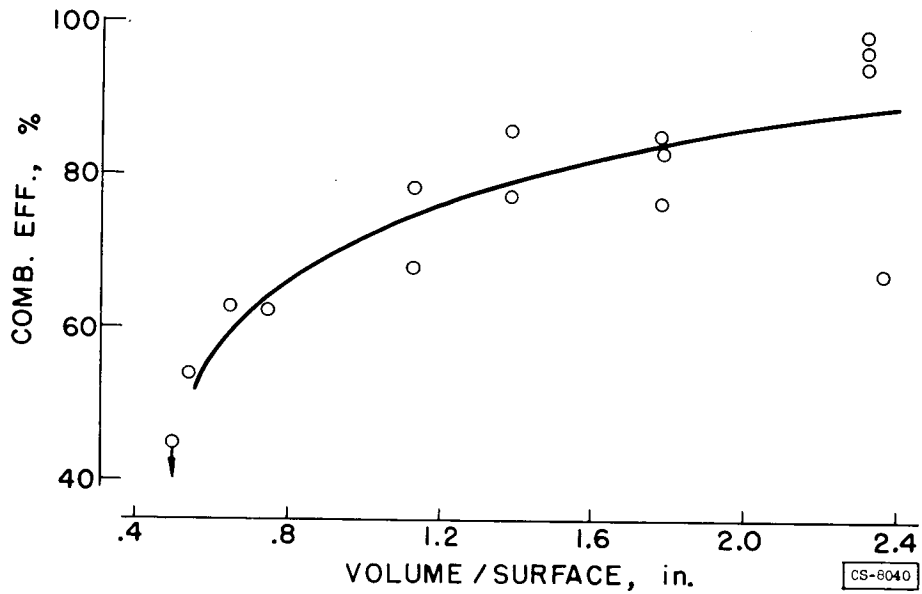


Figure 15

EFFECT OF COMBUSTOR DIAMETER ON COMBUSTION EFFICIENCY

P, 7.4 psia V, 100 ft/sec  $\Delta T$ , 1180° F

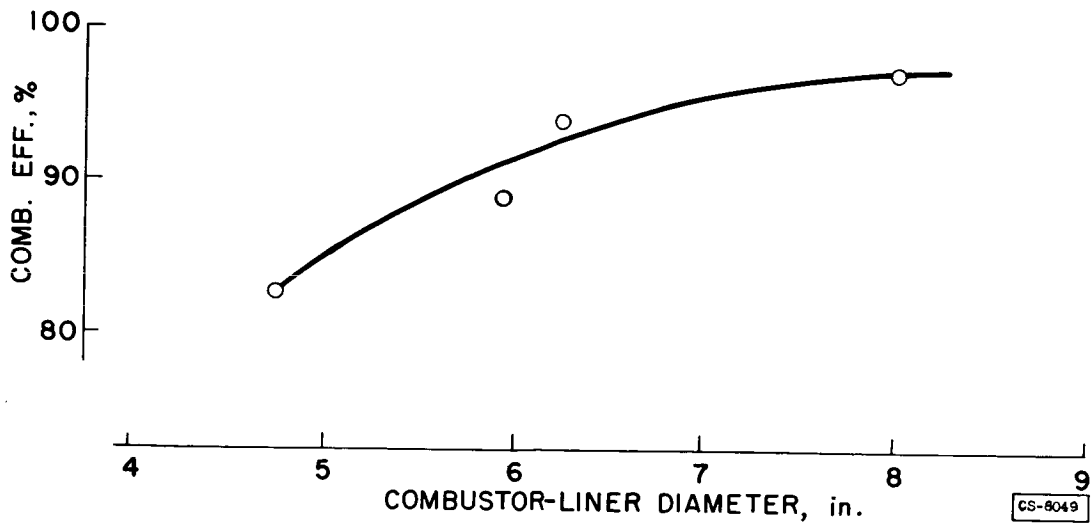


Figure 16

EVAPORATION AND SPREADING OF A FUEL SPRAY

T, 320° F V, 287 ft/sec P, 12.3 psia

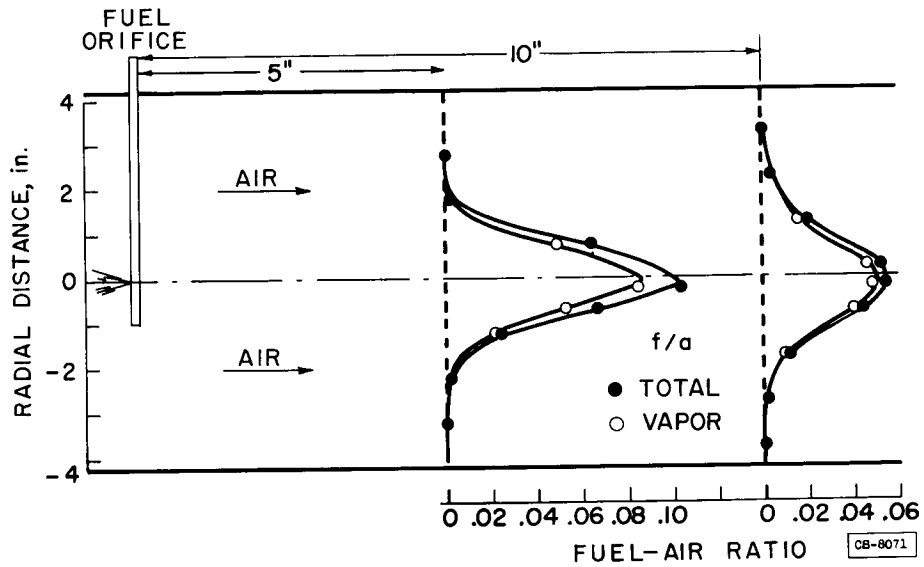


Figure 17

EFFECT OF FUEL DISTRIBUTION ON AFTERBURNER EFFICIENCY

V, 450-500 ft/sec P, 5.7-7.4 psia

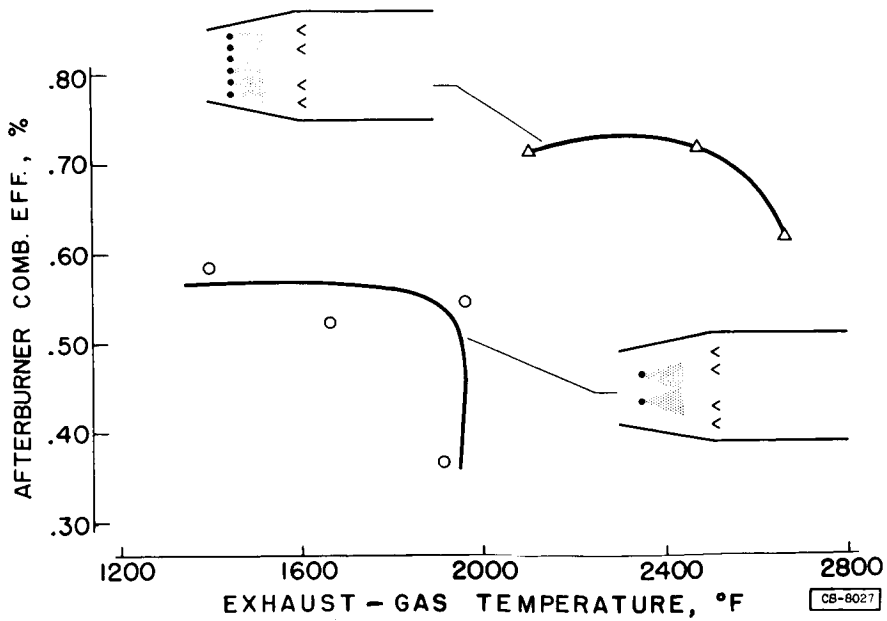


Figure 18

3078-E

### EXPERIMENTAL AFTERBURNER

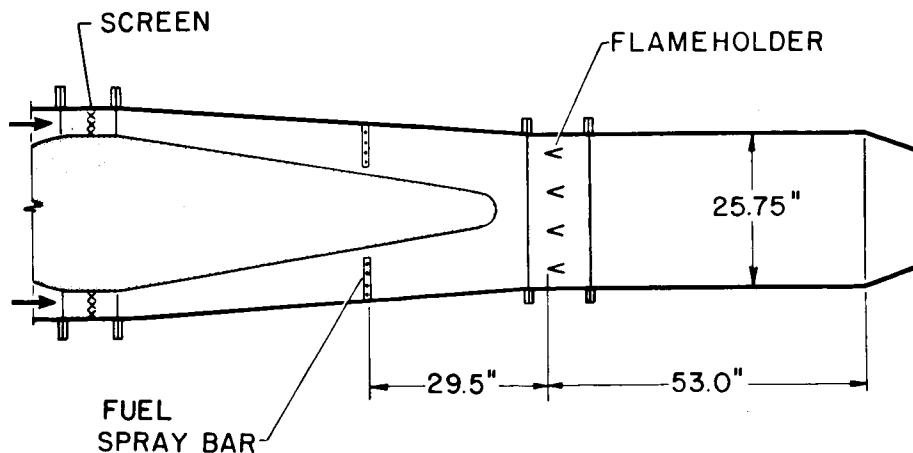


Figure 19

### RESEARCH AFTERBURNER COMBUSTION EFFICIENCY

P, 5 psia

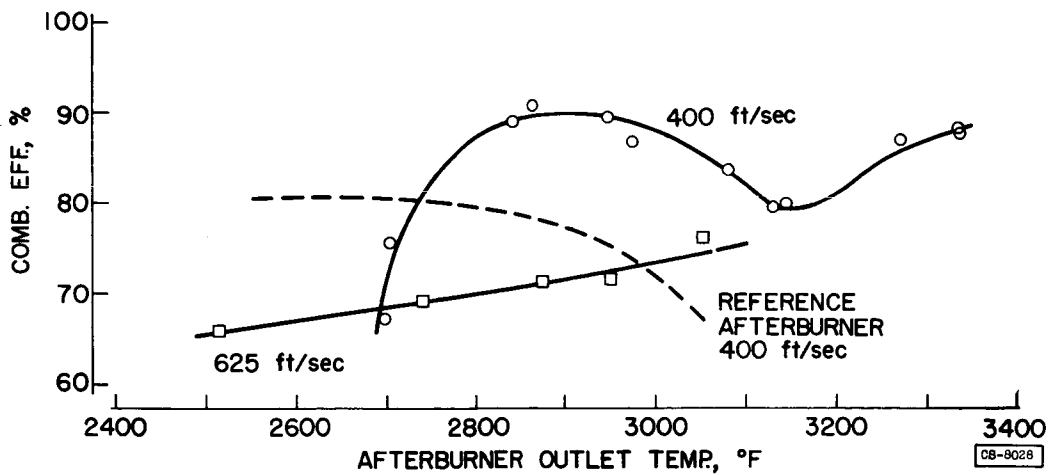
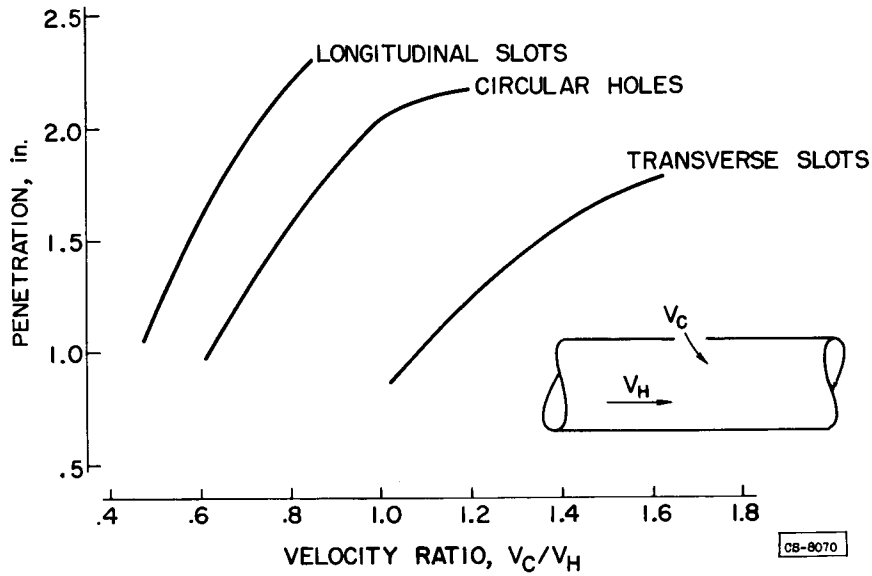


Figure 20

CB-8028



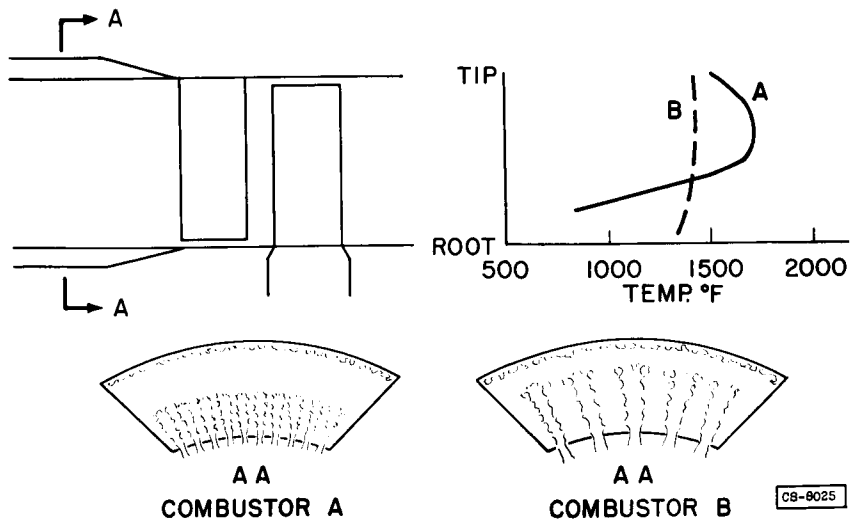
### JET PENETRATION (R.A.E. DATA)



CS-8070

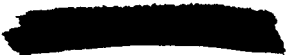
Figure 21

### COMBUSTOR-OUTLET TEMPERATURE PROFILES



CS-8025

Figure 22



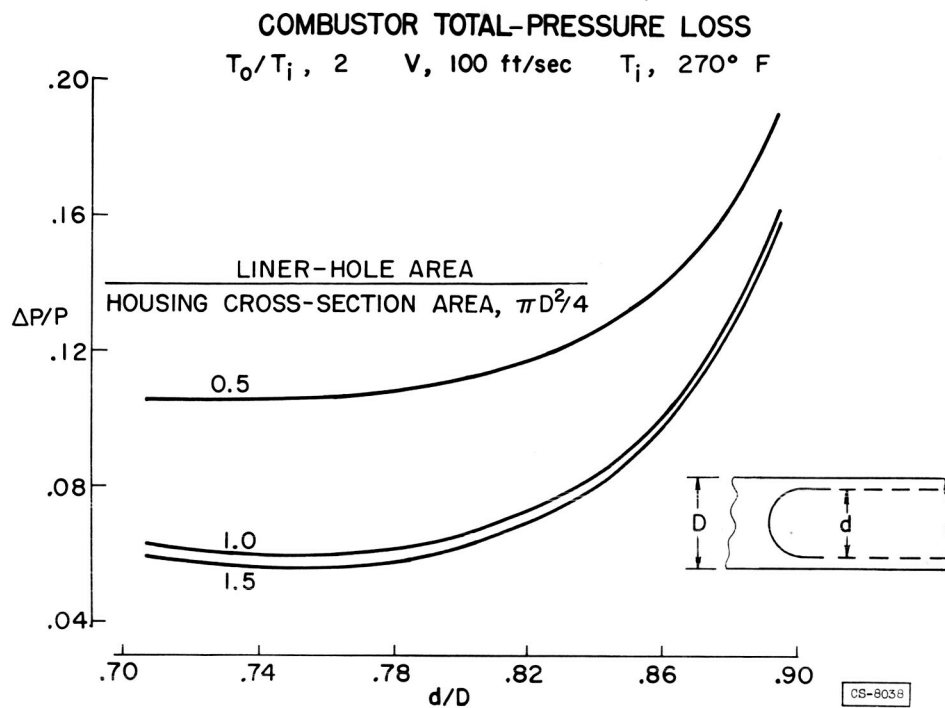


Figure 23

**ACOUSTIC DAMPER**

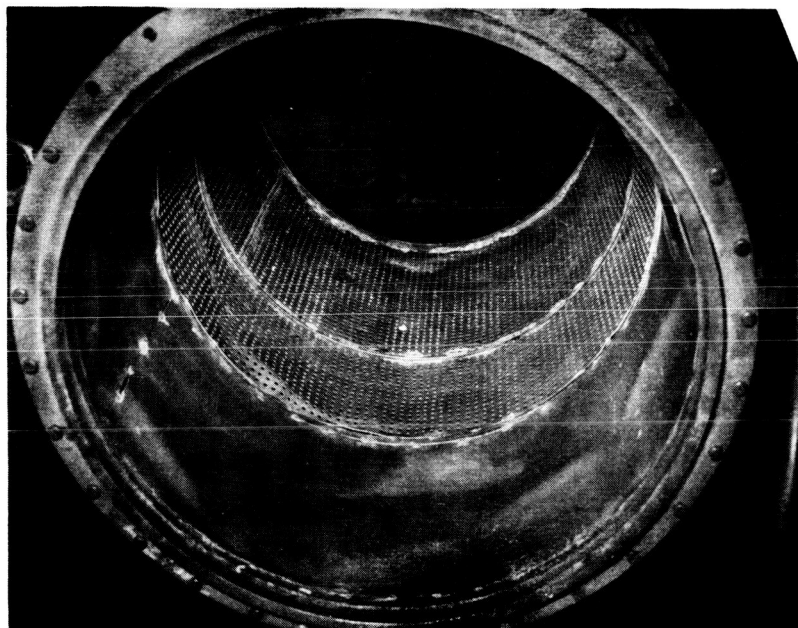
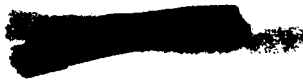


Figure 24



EFFECT OF ACOUSTIC DAMPER ON SCREECH

P, 12.2 psia T<sub>1</sub>, 1250° F V, 300 ft/sec

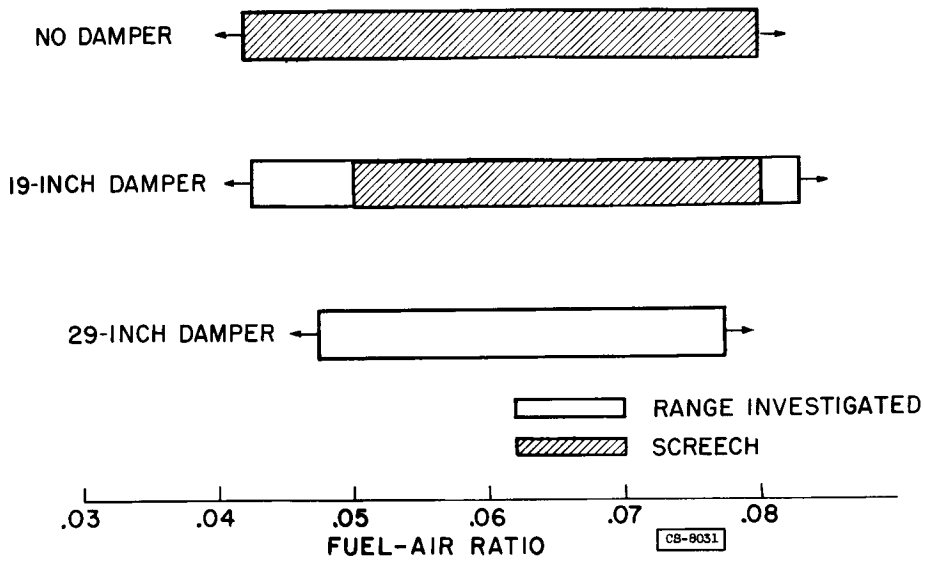


Figure 25

EFFECT OF PRESSURE AND VELOCITY ON IGNITION ENERGY

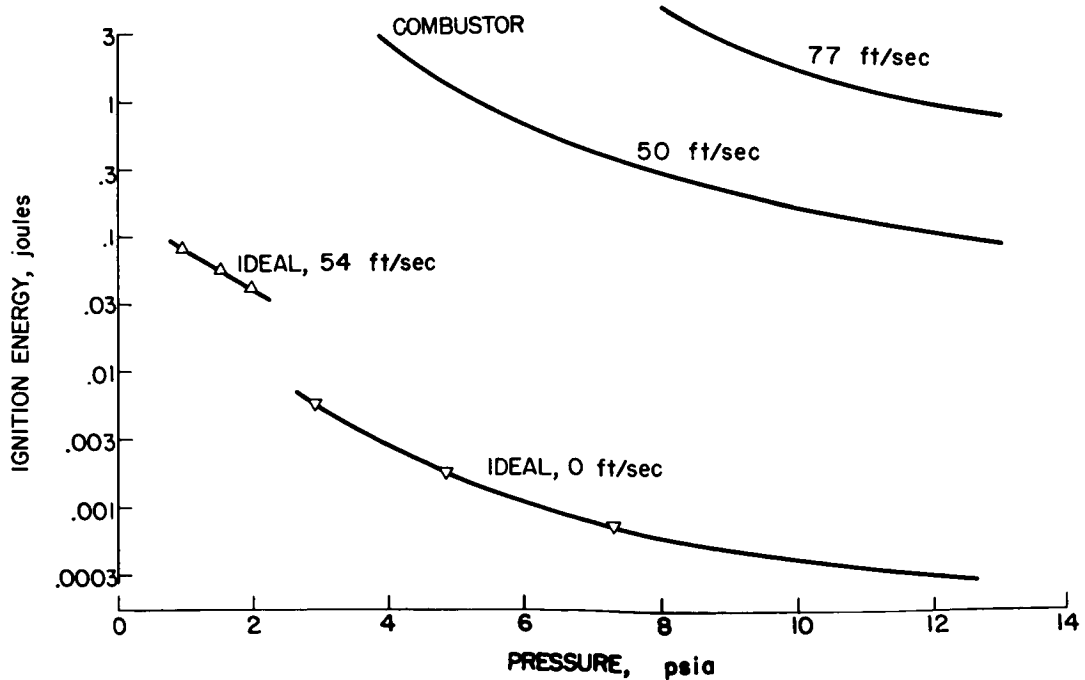
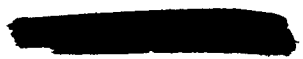


Figure 26



3079-E

## PERFORMANCE OF EXPERIMENTAL TURBOJET COMBUSTORS

By Carl T. Norgren, E. V. Zettle, and J. Howard Childs

## INTRODUCTION

3078 - 2

The preceding papers have indicated the current status and the future requirements of turbojet combustors and have presented the results of recent research on high-speed combustion which indicate design principles required for obtaining high performance in turbojet combustors. The object of this paper is to describe how these design principles have been incorporated into experimental combustor configurations to obtain high performance, to show the performance obtained with these experimental combustors, and to compare this performance with that of a reference combustor which is typical of current production-model turbojet combustors.

Five experimental combustors are described. Each of the combustors represents the product of a research program in which various design features were tailored to achieve high performance. However, none of the combustors necessarily represents an optimum configuration since the investigations were performed for a limited number and range of design variables.

Both tubular and annular combustor configurations are discussed in this paper. The experimental investigations were conducted using single tubular combustors and one-quarter segments of the annular combustors in direct-connect-duct apparatus. For most of the experimental combustors, data are included to show the effect on combustion efficiency of variations in combustor-inlet pressure, temperature rise, velocity, and fuel-air ratio. Data are also included to show the effect of combustor velocity on the total-pressure drop for most of the combustors. Calculated values are included to show the combined effects of combustion efficiency and combustor pressure drop on the specific fuel consumption of a turbojet engine utilizing these combustors.

## TEST CONDITIONS

Four of the experimental combustors were investigated experimentally at the operating conditions shown in the following table:

Combustor-inlet total pressure, lb/sq in. abs	Combustor-inlet total temperature, °F	Combustor-velocity, <sup>a</sup> ft/sec	Combustor-outlet temperature, °F
15	268	78	1448
8	268	78	1448
5	268	78	1448
15	268	102	1448
15	268	132	1448

<sup>a</sup>As defined in the paper by Jonash, Childs, and Olson.

Except for the inlet temperature, these conditions simulate operation of the combustors in a turbojet engine with a compressor pressure ratio of 5 at a Mach number of 0.6 and at altitudes of 61,000 to 84,000 feet. The required inlet-air temperature of 368° F was not obtainable, because the capacity of the inlet-air heaters was insufficient; a temperature at the combustor inlet of 268° F was therefore maintained for most of the experimental investigation. With one combustor, an inlet temperature of only 80° F could be obtained. Another of the combustors was investigated at conditions typical of those encountered in supersonic flight of a turbojet engine. These test conditions are indicated in the following table. The conditions given for a combustor-inlet total pressure of 18.37 pounds per square inch absolute correspond approximately to a flight Mach number of 2.5 at an altitude of 80,000 feet.

Combustor-inlet total pressure, lb/sq in. abs	Combustor-inlet total temperature, °F	Combustor-velocity, <sup>a</sup> ft/sec	Combustor-outlet temperature, °F
18.37	870	204	1800
10.00	870	165	1800
30.00	870	165	1800
18.37	870	125	1800
18.37	870	165	1800
18.37	870	204	2000

<sup>a</sup>As defined in the paper by Jonash, Childs, and Olson.

The fuel used in all the experimental investigations was JP-4.

## GENERAL DESIGN CONSIDERATIONS

All the combustors had some features of design in common, yet each had certain design features which were unique. The design features which were common to all are outlined in the following paragraphs, while the unique features are discussed in the subsequent section dealing with the various combustor configurations.

### Large Combustion Space

In each of the experimental combustors, the upstream end of the combustor liner was made as large as possible consistent with other design features and the requirement of low combustor pressure losses. The large size of the combustion space served to minimize the deleterious wall quenching discussed in the preceding paper.

### Gradual Admission of Primary Air

In each of the five experimental combustors, the primary air was admitted gradually. As shown in the preceding paper, this technique of air admission is required for achieving high combustion efficiency at low-pressure conditions. The ratio of the hole area in the liner upstream of station  $x$  to the total area of the perforations is shown in figure 1 as a function of the distance  $x$  along the length of the combustor liner for each of the five combustors. Only 10 to 18 percent of the liner open area is contained in the upstream 8 inches of the combustor length of combustors A through D. Combustor E had a greater open area in the upstream portion of the combustor liner; this contributed to a low pressure-loss coefficient for the combustor, but as will subsequently be shown, combustor E did not perform well at low pressures.

### Longitudinal Slots for Secondary Air

Each of the experimental combustors had longitudinal slots near the downstream end of the combustor liner for admission of the secondary air. The preceding paper showed that these longitudinal slots provide best penetration of the secondary air into the hot gas stream.

### COMBUSTOR A

The tubular vaporizing combustor (combustor A) is shown in figure 2. In order to provide control of fuel-air mixture composition in the combustion space, the primary air was isolated from the secondary air by means of a snout extending upstream from the combustion space.

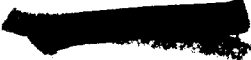
The area at the inlet of this snout was adjusted to determine the area giving best performance; it was fixed at this optimum value. The fuel was delivered through a series of small tubes to the outer walls of the combustor liner. This fuel flowed along the liner walls in a thin annular space between the liner and a sleeve which shielded the fuel from most of the primary air. In this region the fuel received heat from the hot liner and was thereby preheated and partly vaporized. The fuel and the primary air flowed into the combustion space as a mixture through a series of short tubes. The composition of the fuel-air mixture entering through the short tubes is believed to be near stoichiometric and therefore would correspond to mixtures having high flame velocities and good burning properties. An additional fuel injector delivered a small quantity of liquid fuel directly into the combustion space. This fuel injector promoted good ignition characteristics and was operated continuously since it served to improve flame stability. The short tubes which admitted the primary air and the fuel to the combustion space were so oriented that the mixture was directed toward the upstream end of the combustor. This served to increase the circulatory flow which the preceding papers have shown to be necessary for flame stabilization.

#### Effect of Pressure

The effect of the combustor-inlet pressure on the combustion efficiency of combustor A is indicated by the solid curve in figure 3. Included in the figure for comparison is a dashed curve showing the combustion efficiency obtained with a reference combustor at the same test conditions. This reference combustor is a typical current-production-model turbojet combustor. As noted under TEST CONDITIONS, the combustor operating conditions simulate operation of the combustor in a turbojet engine having a compressor pressure ratio of 5, flying at a Mach number of 0.6 over a range of altitudes. Comparison of the curves of figure 3 shows that the combustion efficiency of the experimental combustor was approximately 8 percent above that of the reference combustor throughout the range of pressures investigated.

#### Effect of Temperature Rise

The combustion efficiency of combustor A is shown for a range of values of combustor temperature rise by the solid curve in figure 4. Again, a curve for the reference combustor is included for comparison. The combustion efficiency of the reference combustor decreased markedly at very low and very high values of temperature rise. The decreases in efficiency were not as marked for the experimental combustor.



### Effect of Velocity

The combustion efficiencies and the combustor pressure losses for a range of values of combustor velocity are indicated in figure 5. The combustion efficiency and the pressure losses were higher for the experimental combustor than for the reference combustor. Despite its higher pressure losses, the combustion efficiency was sufficiently higher for the experimental combustor to give a lower specific fuel consumption for the experimental combustor. A comparison of the specific fuel consumption of the experimental combustor with that for the reference combustor is presented in figure 6 for a range of combustor velocities. The specific fuel consumption was computed to allow for combustion efficiencies and pressure losses like those indicated in figure 5 and divided by the specific fuel consumption which would be obtained with an ideal combustor having zero pressure losses and 100 percent combustion efficiency. At a velocity of 78 feet per second, which is typical of current design practice, the specific fuel consumption of the reference combustor is approximately 9 percent above that of the experimental combustor. At this same velocity, the specific fuel consumption of the experimental combustor is 15 percent above the ideal.

3078-E

### COMBUSTOR B

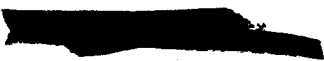
The tubular staged-fuel combustor (combustor B) is shown in figure 7. In addition to those design features previously indicated as being common to all the experimental combustors, fuel staging was incorporated. Approximately 70 percent of the fuel was injected by a single nozzle located at the upstream end of the combustor liner. The remaining 30 percent of the fuel was injected through eight nozzles evenly spaced about the periphery of the combustor as shown in figure 7. The fraction of the total fuel injected through the eight downstream nozzles increased with increase in total flow rate.

### Effect of Pressure

Figure 8 shows the combustion efficiency of combustor B for a range of values of combustor pressure. The efficiency of the experimental combustor was about 12 percent above that of the reference combustor at the lowest pressures investigated.

### Effect of Temperature Rise

Combustion efficiencies for combustor B are shown in figure 9 for a range of values of combustor temperature rise. Perhaps the most important feature of combustor B was the relatively high combustion efficiencies obtained at high values of combustor temperature rise; this is believed to result from the use of fuel staging.





## Effect of Velocity

Figure 10 shows the combustion efficiencies and combustor pressure losses of combustor B at various combustor velocities. The combustion efficiency of the experimental combustor was above that of the reference combustor; however, the pressure losses for the reference combustor were below those for the experimental combustor. Figure 11 compares the specific fuel consumption obtainable with these two combustors at various combustor velocities. The high combustion efficiency of the experimental combustor is sufficient to give a lower specific fuel consumption despite its higher pressure losses.

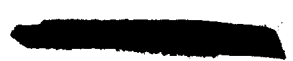
## COMBUSTOR C

The annular staged-fuel combustor (combustor C) is shown in figure 12. The same general design features were used in this combustor as in combustor B. When combustor C was operated without fuel staging, all the fuel was introduced at the upstream end of the liner. During operation with fuel staging, approximately one-third of the fuel was injected at the upstream end of the combustor by means of hollow-cone, pressure-atomizing spray nozzles, and the remaining two-thirds of the fuel was injected farther downstream by means of nozzles producing fan-type sprays of liquid droplets. These fan-spray nozzles injected the fuel radially into the combustion space from the outer wall and from the inner wall of the combustor. For the complete combustor annulus, 40 fuel nozzles were used at the upstream end of the combustor and 24 fan-spray nozzles were located at the downstream fuel-injection stations. Twelve of these fan-spray nozzles were equally spaced around the outer wall and twelve were equally spaced around the inner wall of the combustor liner.

The preceding papers indicated the importance of obtaining a large volume-to-surface ratio in the combustion space. For given over-all combustor dimensions, it is possible to obtain a larger volume-to-surface ratio by using an annular combustor configuration than by using individual tubular combustors. In addition, the combustor velocity is lower in an annular than in a tubular configuration. These considerations would indicate certain advantages in using the annular configuration rather than the tubular configuration.

## Effect of Fuel Staging

The combustion efficiencies obtained with combustor C with and without fuel staging over a range of fuel-air ratios are shown in figure 13. The combustor air-flow rate was typical of current design practice for the low pressures investigated. The curves of figure 13 show that the combustion efficiency was higher without fuel staging at all but the highest



fuel-air ratios investigated. Similar data obtained with combustor C at a higher air-flow rate are presented in figure 14. The air-flow rate was increased above that indicated in figure 13 by approximately 70 percent. At the higher air-flow rate, the combustion efficiency with fuel staging was above that obtained with no staging throughout most of the fuel-air ratio range. Thus, these data indicate that fuel staging is beneficial for obtaining high combustion efficiency at very high fuel-air ratios and that fuel staging is particularly beneficial when operating at high combustor velocity. Fuel staging provides the flexibility necessary to obtain the proper fuel-air ratios in the combustion space over much wider ranges of fuel flow.

#### COMBUSTOR D

The annular vaporizing combustor (combustor D) is shown in figure 15. The low fuel-flow rates required for high-altitude operation were obtained by injecting preheated and partly vaporized fuel through every other one of the injectors located at the upstream end of the combustor. The higher fuel-flow rates required for low-altitude operation were obtained by injecting additional liquid fuel through the other injectors at the same location. In the complete combustor annulus, 20 vapor injectors and 20 liquid-fuel injectors were used. The fuel to be preheated was passed through coils located upstream of the secondary-air slots; in flowing through these coils, the fuel was preheated and partly vaporized and was then passed upstream to the vapor-fuel manifold. The vaporizer coils served not only to vaporize fuel but also to cool the jet shields which were located upstream of the secondary air jets. These jet shields consisted of struts which were semicircular in cross section and which extended radially from the inner to the outer wall of the annular combustor liner. The jet shields served to prevent the blast of hot combustion gases from hitting and bending the cold air jets. With the vaporizer coils located as shown in figure 15, the heat necessary to vaporize the fuel was extracted from the combustion gases after the chemical reaction was substantially complete; the quenching effect on the chemical reaction was minimized by this design principle.

#### Effect of Pressure

The effect of pressure on the combustion efficiency of combustor D is shown in figure 16. At pressures above 4 pounds per square inch absolute, the combustion efficiency of the experimental combustor was substantially 100 percent. At the lowest pressures at which the two combustors could be compared, the efficiency of the experimental combustor was approximately 25 percent above that of the reference combustor.

### Effect of Combustor Temperature Rise

The combustion efficiency of combustor D for a range of values of combustor temperature rise is shown in figure 17. Whereas the combustion efficiency of the reference combustor decreases at low and at high values of temperature rise, the combustion efficiency of the experimental combustor remained at approximately 100 percent throughout the range of temperature rise investigated.

### Effect of Velocity

The combustion efficiency and the pressure losses for combustor D are shown in figure 18 for a range of combustor velocities. Perhaps the most important feature of this experimental combustor is the very high combustion efficiency obtained at high values of combustor velocity. Although the reference combustor encountered blow-out at a velocity of approximately 90 feet per second, the combustion efficiency of the experimental combustor remained near 100 percent to the highest velocities investigated. Velocities up to 140 feet per second were investigated, and this velocity is approximately 80 percent above current design practice in turbojet combustors. The pressure losses for the experimental combustor were also lower than those for the reference combustor at comparable values of combustor velocity. The combined effects of combustion efficiency and pressure loss on the specific fuel consumption are indicated in figure 19. This figure again emphasizes the superior performance of the experimental combustor, particularly at conditions of high combustor velocity.

### COMBUSTOR E

The annular combustor (combustor E) which was especially designed for operation at conditions encountered in supersonic turbojet flight is shown in figure 20. Since the air flow per unit frontal area of the engine is very high in the turbojet for supersonic application, an annular configuration was selected for this combustor in order to take advantage of the lower combustor velocities which result in the annular configuration. In addition, since the air-flow and fuel-flow rates required in this combustor are quite high, provision was made for fuel staging because this technique was indicated to be particularly advantageous at high-flow conditions (figs. 13 and 14). When combustor E was operated without fuel staging, all the fuel was injected through 36 nozzles (complete annulus), at the upstream end of the combustor liner. During operation with fuel staging, two-thirds of the fuel was injected through 32 fan-spray injectors located farther downstream and arranged like those previously described for combustor C.

The preceding paper indicated that combustor pressure losses increase as the square of combustor velocity. Combustor E, which was intended for high-velocity operation, was therefore designed with a somewhat smaller combustion space and hence a lower pressure-loss coefficient than combustors A to D. Making the combustion space smaller, however, adversely affected the combustion efficiency particularly at low pressures. Since the combustor pressure is above 1 atmosphere in the turbojet flying at supersonic speeds, this combustor does not have to meet the requirement of providing high efficiencies at very low pressures; this is fortunate and makes possible a compromise in combustor design to obtain lower pressure losses at the expense of combustion efficiency at low pressures.

#### Effect of Pressure

Figure 21 shows the effect of combustor-inlet total pressure on the combustion efficiency of combustor E operating at a combustor velocity of 165 feet per second. The combustion efficiency falls off markedly below pressures of about 17 pounds per square inch absolute. The range of combustor pressures encountered in high-altitude supersonic flight is indicated in figure 21 to extend from 17 to 30 pounds per square inch absolute. Fortunately, low combustor pressures are not encountered in the range of operation intended for this combustor and its efficiency is quite high in the range of pressures of interest for supersonic flight application. The marked lowering of efficiency at low pressures is partly the result of making the upstream end of the combustor liner small in order to obtain low pressure losses.

#### Effect of Velocity

The effect of combustor velocity on the combustion efficiency of combustor E is indicated in figure 22. The solid curve shows the operation with no fuel staging at a combustor-outlet temperature of 1800° F. The dashed curve is drawn through a single datum point obtained with fuel staging at an outlet temperature of 2000° F. With fuel staging, a combustion efficiency of approximately 98 percent was obtained at a combustor-outlet temperature of 2000° F and a combustor velocity of 205 feet per second. This combustor velocity represents the most severe condition expected in the high-altitude operation of the supersonic turbojet engine discussed in the paper by Gabriel and Hall. The single datum point included in figure 22 shows the efficiency of the reference combustor at test conditions which were identical except for an inlet temperature 500° F below that indicated for combustor E. Because of this lower combustor-inlet temperature, no true comparison of combustion efficiency between the experimental combustor and the reference combustor is possible.

The effect of combustor velocity on the pressure losses attained with combustor E is shown in figure 23. At the highest combustor velocity expected in high-altitude operation of the supersonic turbojet engine, the combustor pressure loss amounts to approximately 15 percent of the combustor-inlet total pressure. The preceding papers have indicated, however, that a combustor pressure loss of this magnitude is permissible at the supersonic flight conditions because the resultant effects on thrust and specific fuel consumption are only slightly greater than those encountered in current turbojet engines. Again, a single datum point for the reference combustor is included on figure 23 for purposes of comparison. The pressure losses for the reference combustor are above those for the experimental combustor.

#### Radial Temperature Profile

The average radial temperature profile at the outlet of combustor E is indicated on figure 24. Each of the points on the figure represents the arithmetic average of six circumferential temperature readings obtained in the one-quarter segment which was investigated. A flat temperature profile of the type shown in the figure is believed to be desirable for cooled turbines of the type which may be used in turbojet engines for supersonic application.

#### CONCLUSIONS

The three reports dealing with the combustion problem have treated, in turn, the present and future requirements of turbojet combustion systems, recent research that has been done or is still going on pertinent to these combustion systems, and the performance of several experimental turbojet combustors intended to indicate the extent to which the research that has been done can be applied. The conclusions here stated take the form of a summary of the state of the combustion art as it has been discussed in this paper together with the preceding two papers.

1. Turbojet combustion efficiencies are low at high altitude but research has demonstrated several ways of keeping efficiencies above 95 percent at altitudes above 60,000 feet for combustor velocities of the order of those in present use.

2. With regard to the problem of the high air flow that is so important to a high performance turbojet, a research combustor has at least demonstrated that combustion efficiencies of 95 to 100 percent can be maintained at combustion velocities of 200 feet per second with a temperature profile and a pressure drop that, at least for supersonic flight conditions, are acceptable.

3078 - E

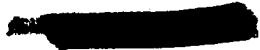
3. A turbine-inlet temperature of over 2000° F could be used with present turbine-cooling techniques and 2500° F will soon be possible. Research toward providing higher temperatures at combustor outlets has demonstrated principles of admitting air and fuel to the combustor which result in high combustion efficiency at these high outlet temperatures. All requirements of a good combustion chamber, particularly the liner durability, have not been incorporated in one design at the present time.

4. Recent research has materially improved the combustion efficiency obtainable with afterburners; in fact, efficiencies of 85 to 95 percent can be achieved at combustor velocities of 400 to 500 feet per second and at pressures down to 1/2 atmosphere at an outlet temperature of 3000° F. Experimental units have demonstrated 3500° F at 625 feet per second. At least one species of screech has been identified and a remedy has been both indicated and demonstrated.

5. Facilities have only recently become available for studying the effects of the high combustor-inlet pressures and temperatures encountered in high-pressure-ratio engines or at very high flight speeds. Data gathered at these conditions indicate that carbon deposits and liner life are the big problems and future research must be directed at them.

6. Finally, there now appears to be enough research information to start development of combustion systems for high performance turbojets for supersonic flight.

308-5



### DISTRIBUTION OF LINER PERFORATIONS

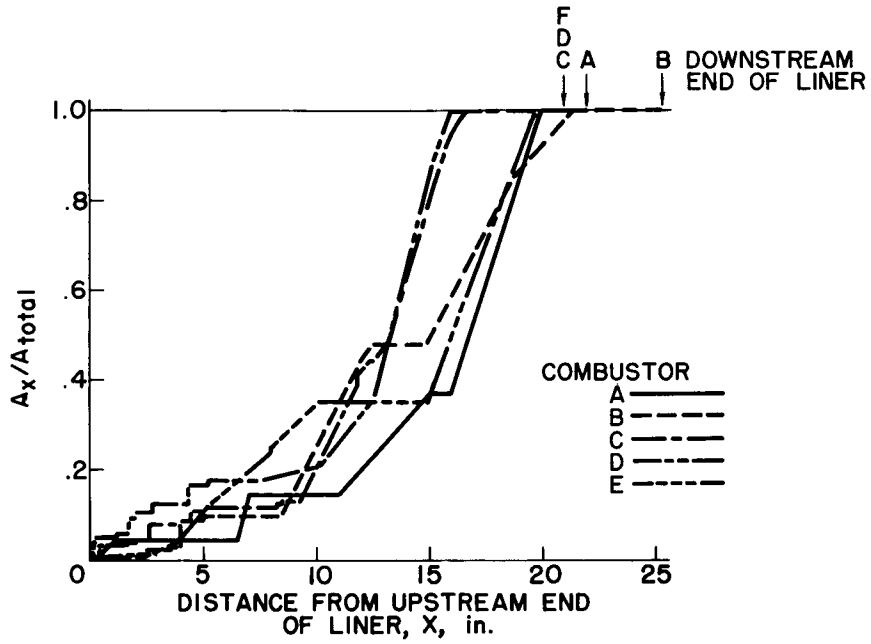


Figure 1

### EXPERIMENTAL TUBULAR VAPORIZING COMBUSTOR

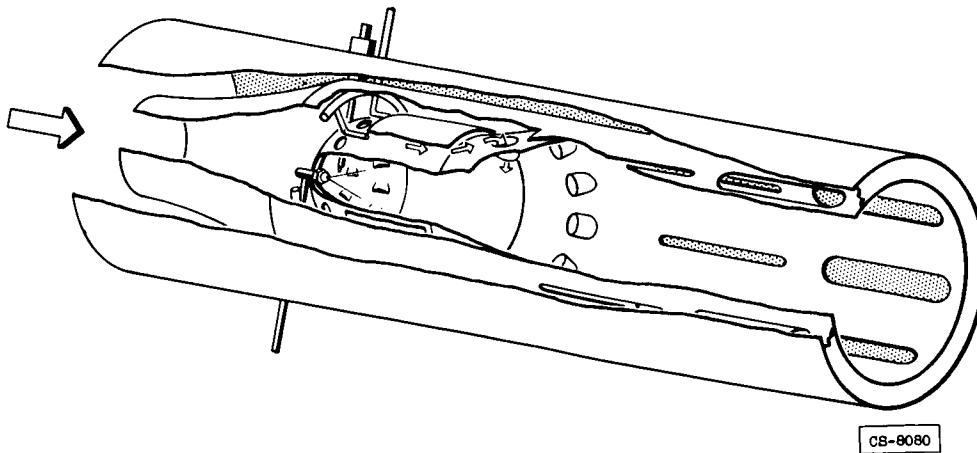


Figure 2



3078-E

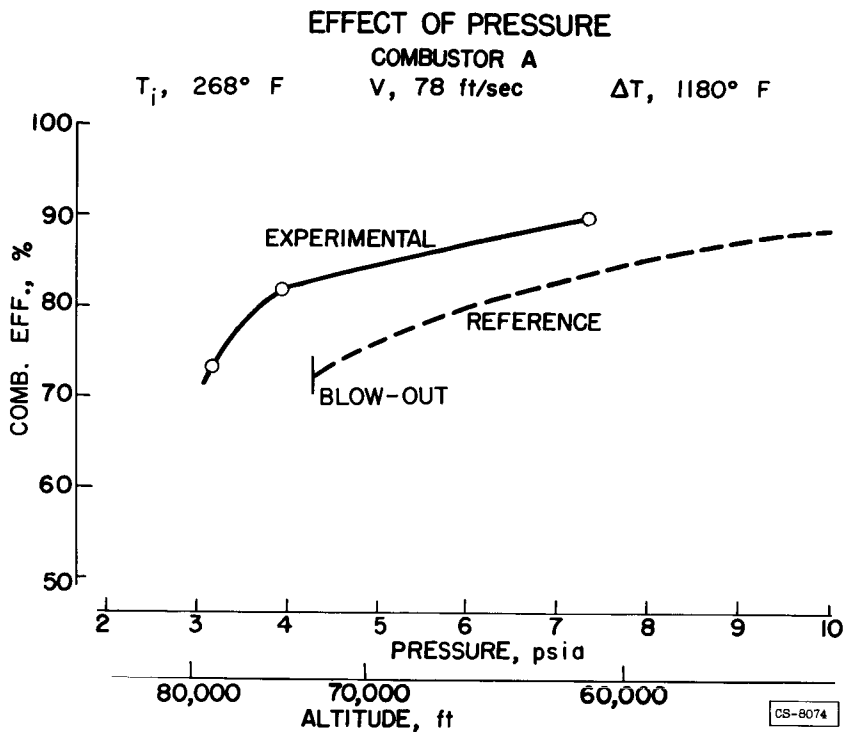


Figure 3

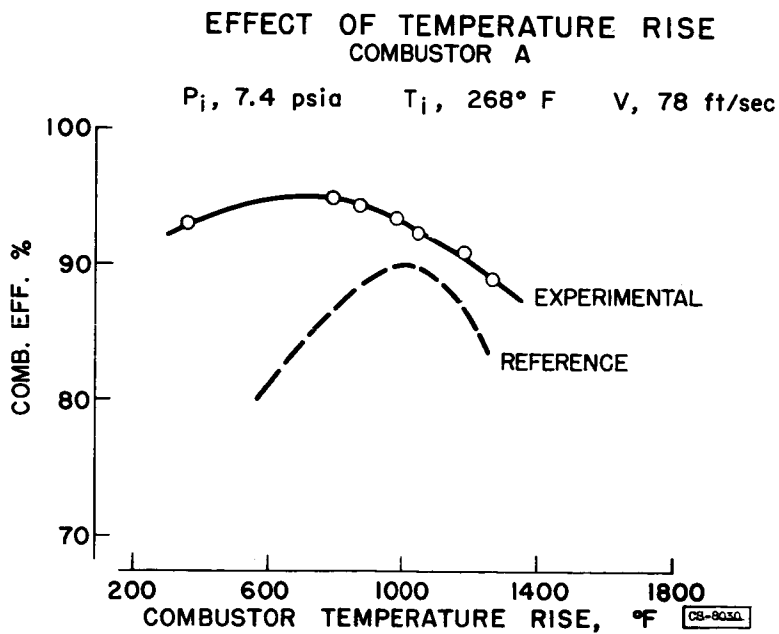


Figure 4

EFFECT OF VELOCITY  
COMBUSTOR A

$P_i, 7.4 \text{ psia}$     $T_i, 268^\circ \text{ F}$     $\Delta T, 1180^\circ \text{ F}$

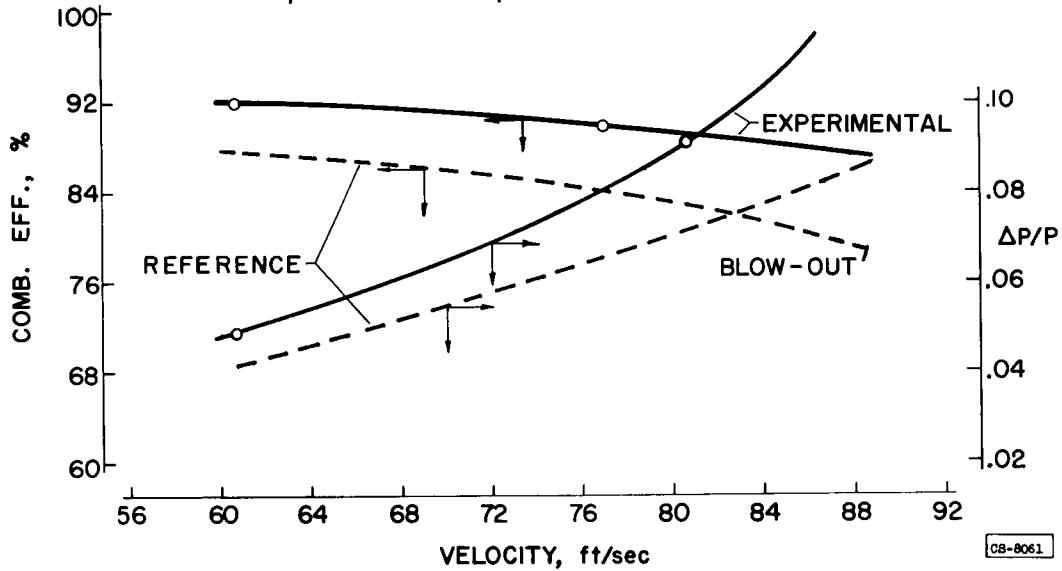


Figure 5

SPECIFIC FUEL CONSUMPTION  
COMBUSTOR A

$P_i, 7.4 \text{ psia}$     $T_i, 268^\circ \text{ F}$     $\Delta T, 1180^\circ \text{ F}$

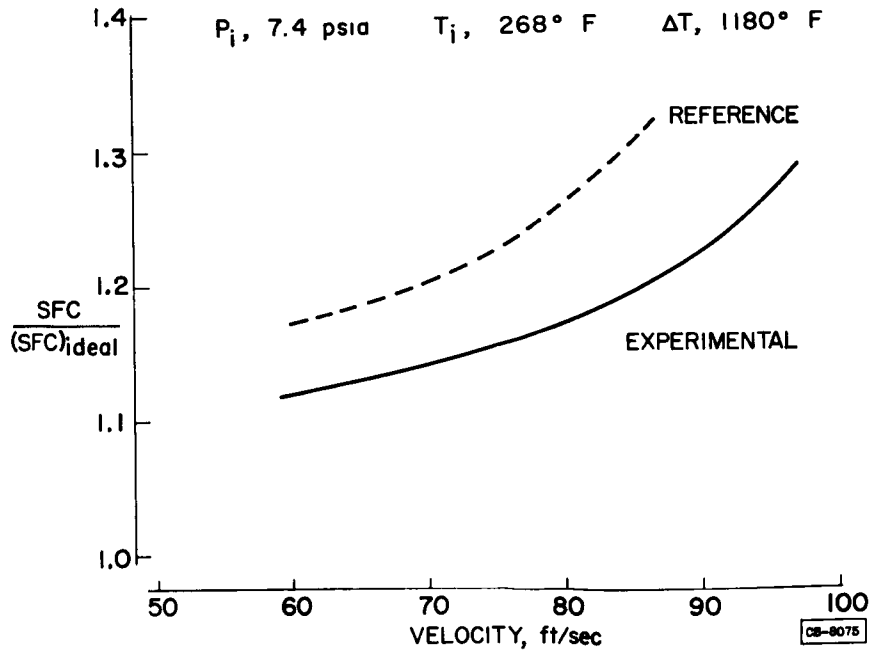


Figure 6

3078-IE

### EXPERIMENTAL TUBULAR STAGED-FUEL COMBUSTOR

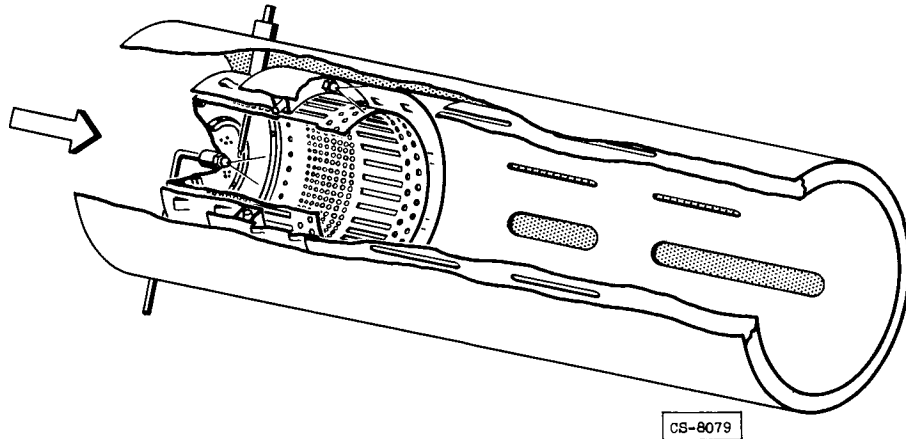


Figure 7

### EFFECT OF PRESSURE COMBUSTOR B

$T_i, 260^\circ \text{ F}$

$V, 78 \text{ ft/sec}$

$\Delta T, 1180^\circ \text{ F}$

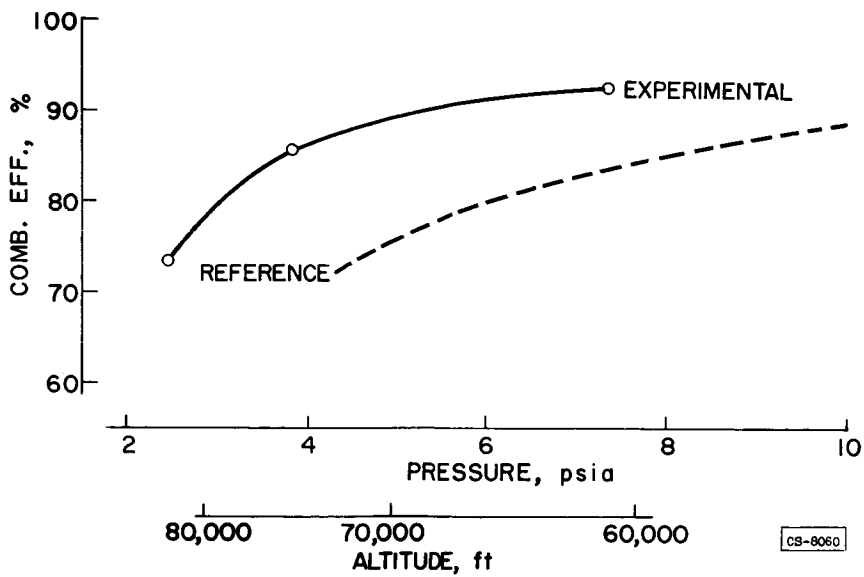


Figure 8

**EFFECT OF TEMPERATURE RISE  
COMBUSTOR B**

$P_i, 7.4 \text{ psia}$      $T_i, 268^\circ \text{ F}$      $V, 78 \text{ ft/sec}$

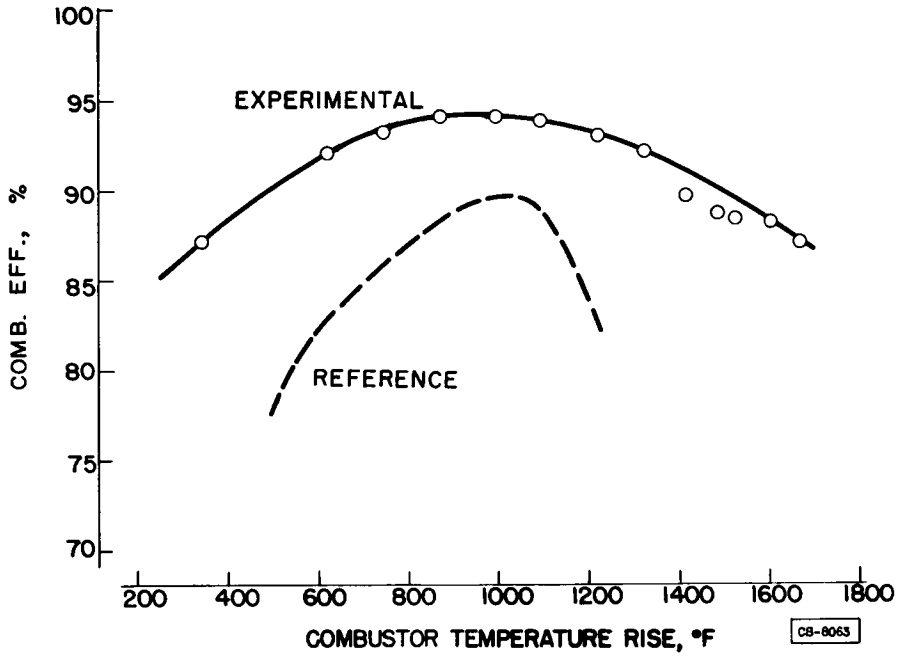


Figure 9

**EFFECT OF VELOCITY  
COMBUSTOR B**

$P_i, 7.4 \text{ psia}$      $T_i, 268^\circ \text{ F}$      $\Delta T, 1180^\circ \text{ F}$

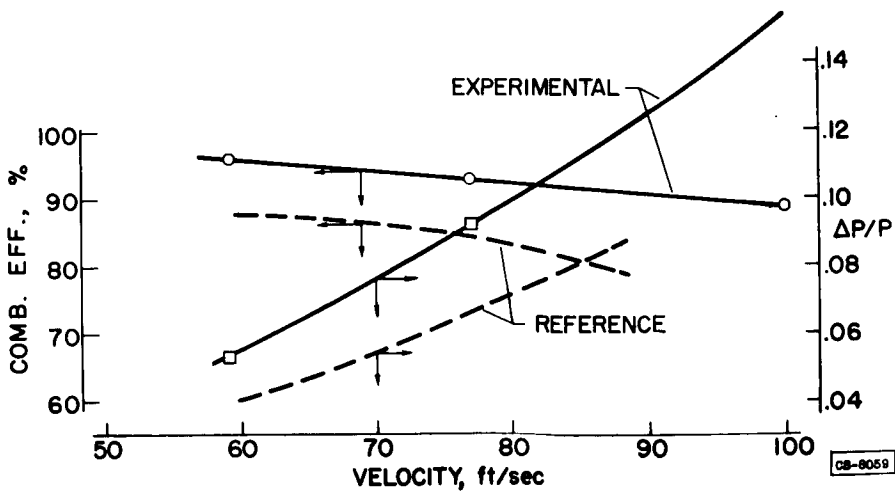


Figure 10

3078-E

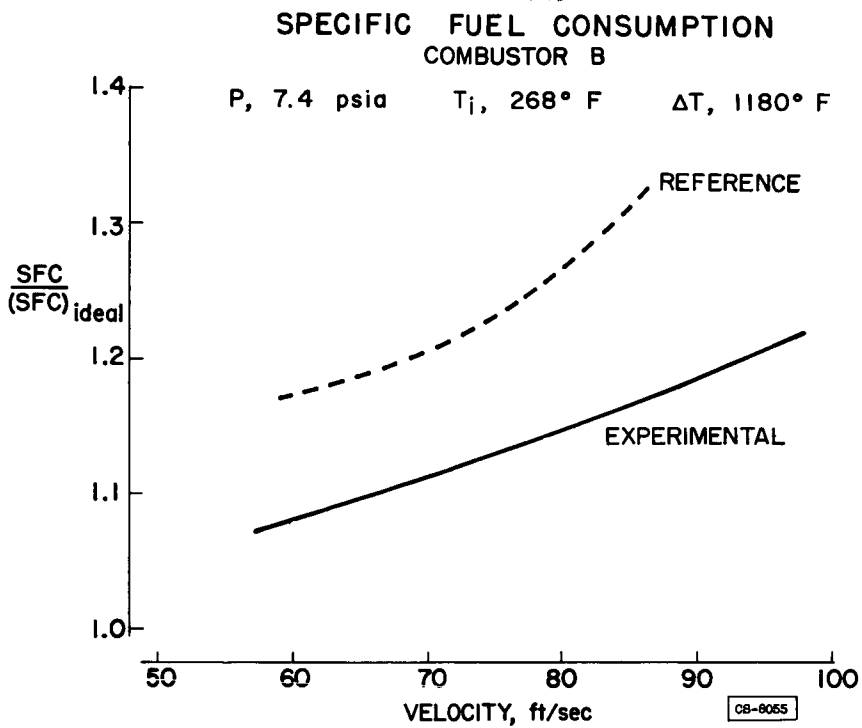


Figure 11

## EXPERIMENTAL ANNULAR STAGED FUEL COMBUSTOR C

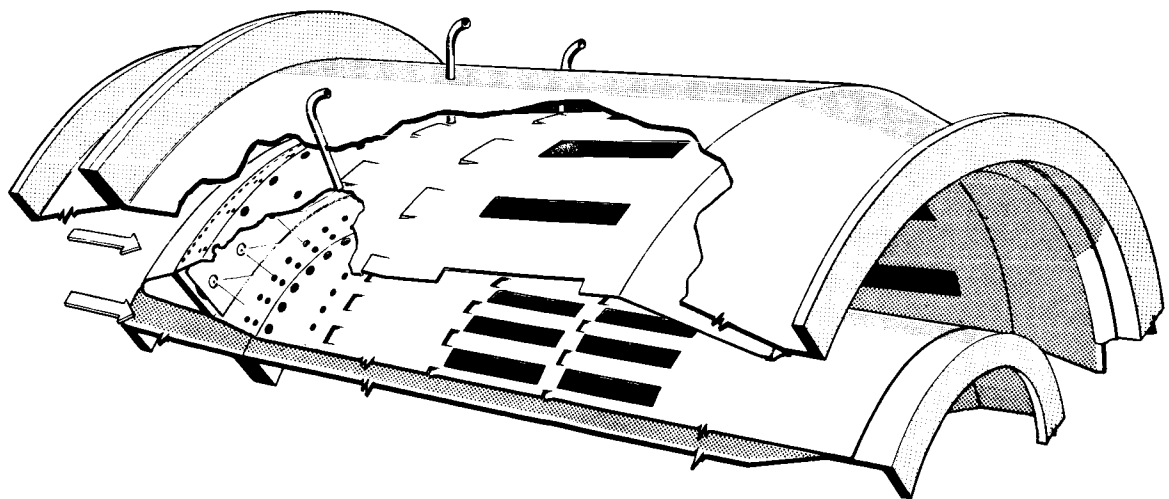
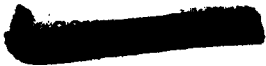


Figure 12



FUEL STAGING AT LOW FLOW RATE  
COMBUSTOR C

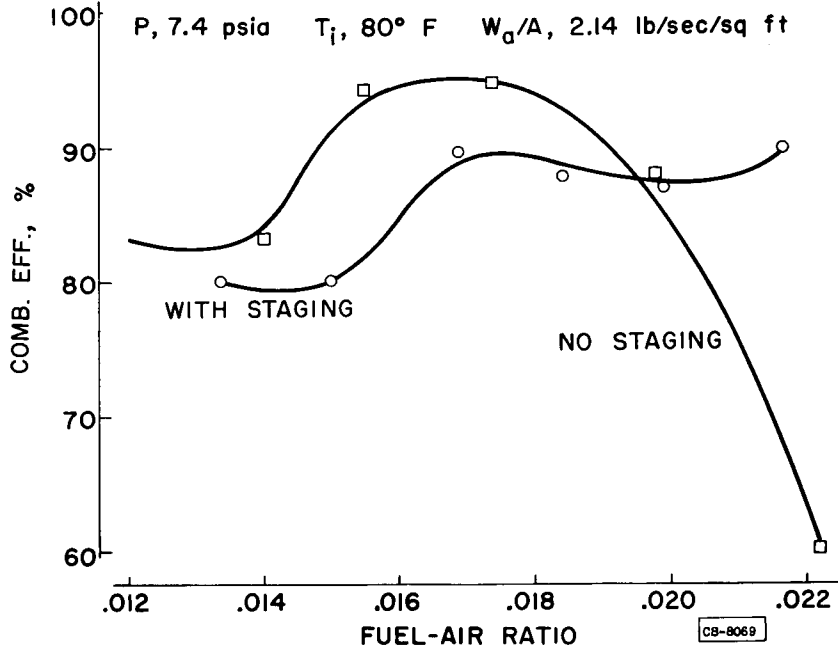


Figure 13

FUEL STAGING AT HIGH FLOW RATE  
COMBUSTOR C

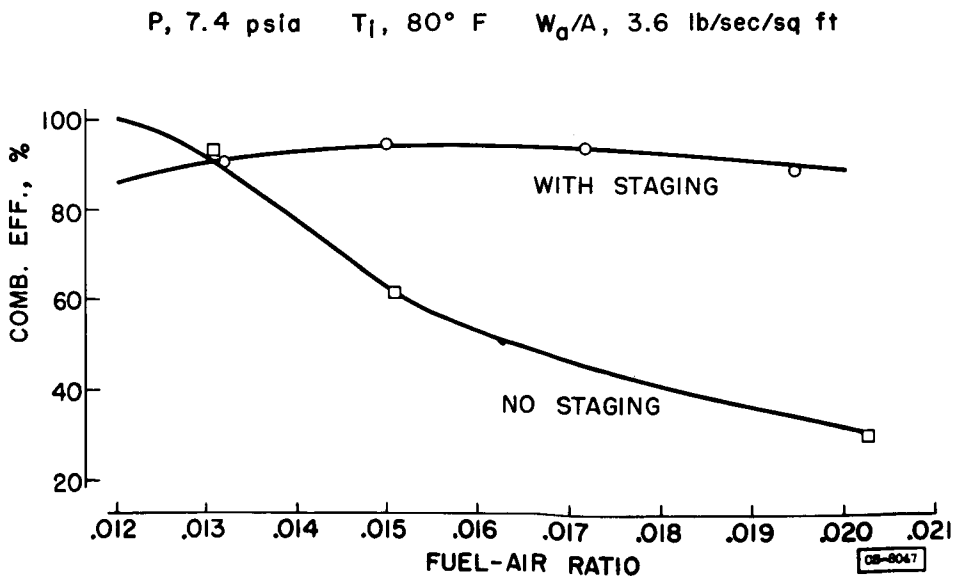


Figure 14



3078-E

# EXPERIMENTAL ANNULAR VAPORIZING COMBUSTOR D

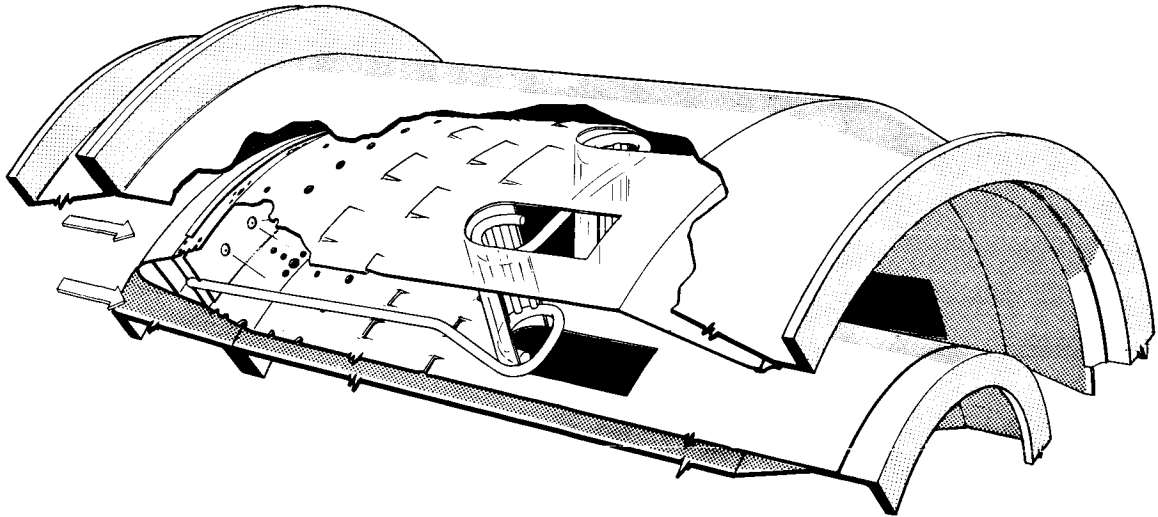


Figure 15

## EFFECT OF PRESSURE COMBUSTOR D

$T_i, 268^\circ T$

$V, 78 \text{ ft/sec}$

$\Delta T, 1180^\circ F$

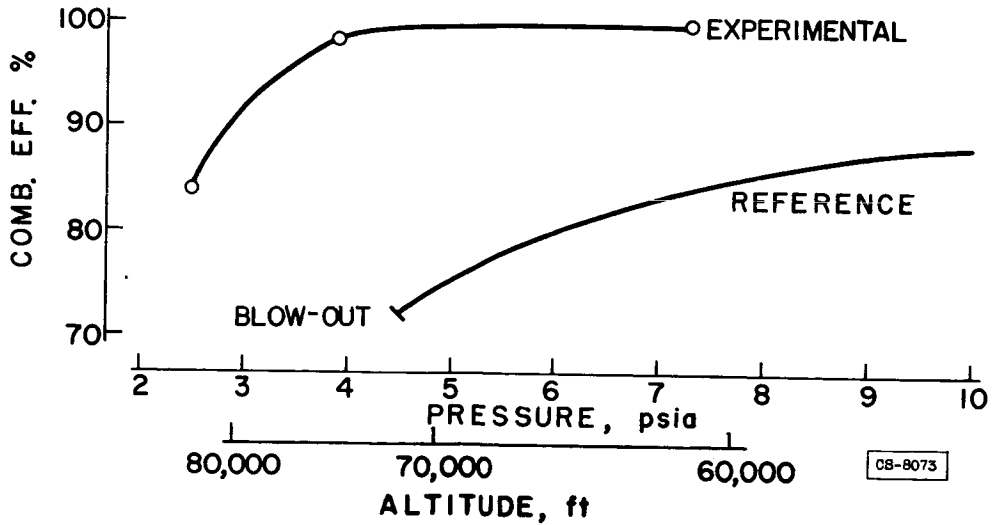


Figure 16

CONFIDENTIAL

### EFFECT OF TEMPERATURE RISE COMBUSTOR D

$P_i, 7.4 \text{ psia}$     $T_i, 268^\circ \text{ F}$     $V, 78 \text{ ft/sec}$

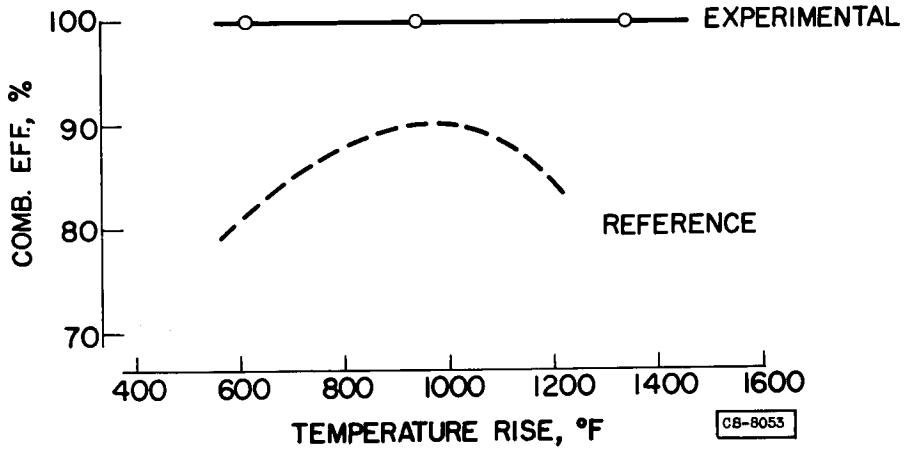


Figure 17

### EFFECT OF VELOCITY COMBUSTOR D

$P_i, 7.4 \text{ psia}$     $T_i, 268^\circ \text{ F}$     $\Delta T, 1180^\circ \text{ F}$

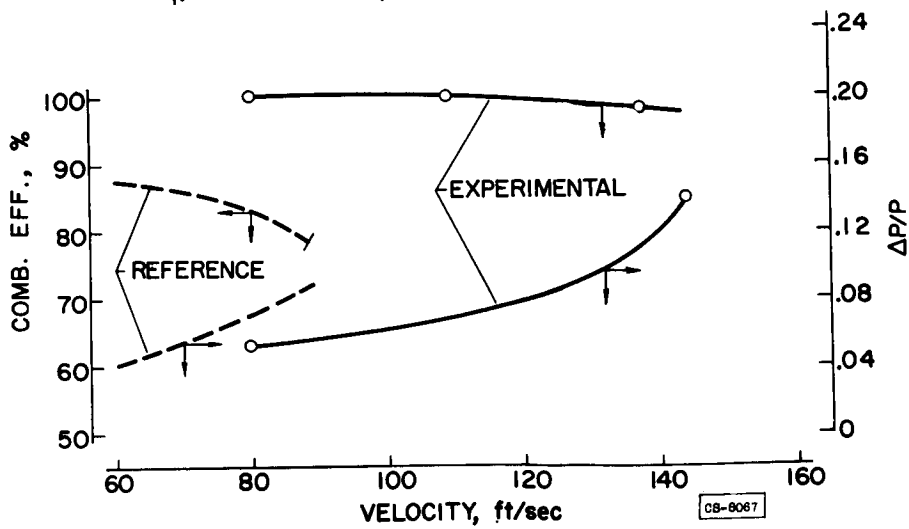


Figure 18

CONFIDENTIAL

3078-E

3078-E

**SPECIFIC FUEL CONSUMPTION  
COMBUSTOR D**

P, 7.4 psia     $T_1$ , 268° F     $\Delta T$ , 1180° F

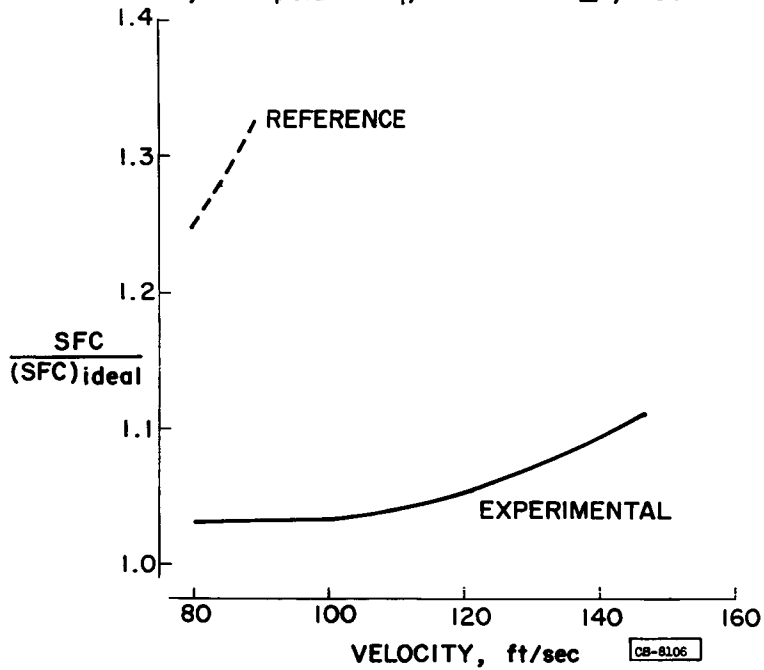


Figure 19

**EXPERIMENTAL ANNULAR COMBUSTOR  
FOR SUPERSONIC FLIGHT**

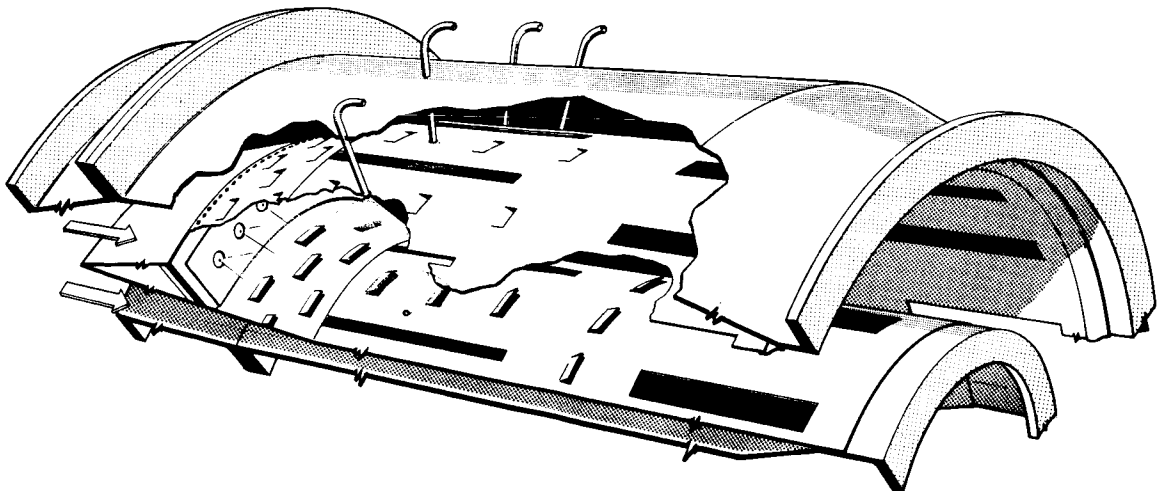


Figure 20

**EFFECT OF PRESSURE ON COMBUSTION EFFICIENCY**

V, 165 ft/sec  $T_i$ , 870° F  $T_o$ , ≈ 1800° F

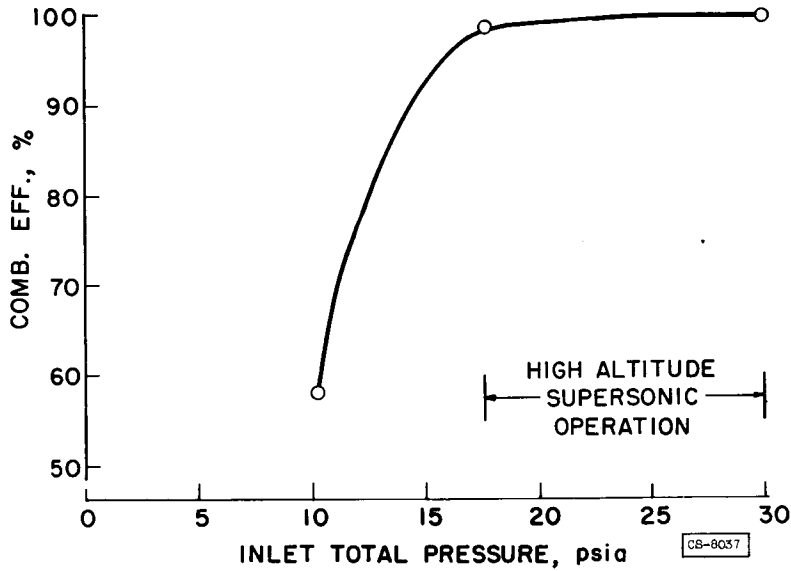


Figure 21

**EFFECT OF VELOCITY ON COMBUSTION EFFICIENCY**

P, 18.4 psia  $T_i$ , 870° F

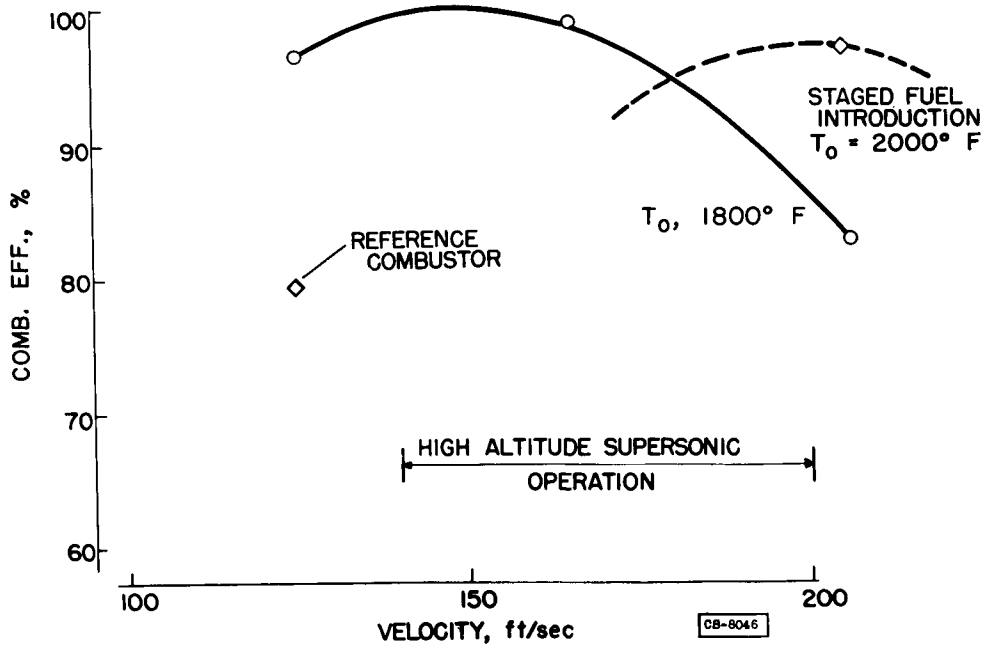


Figure 22

3078-1E

## EFFECT OF VELOCITY ON PRESSURE LOSS

P, 18.4 psia

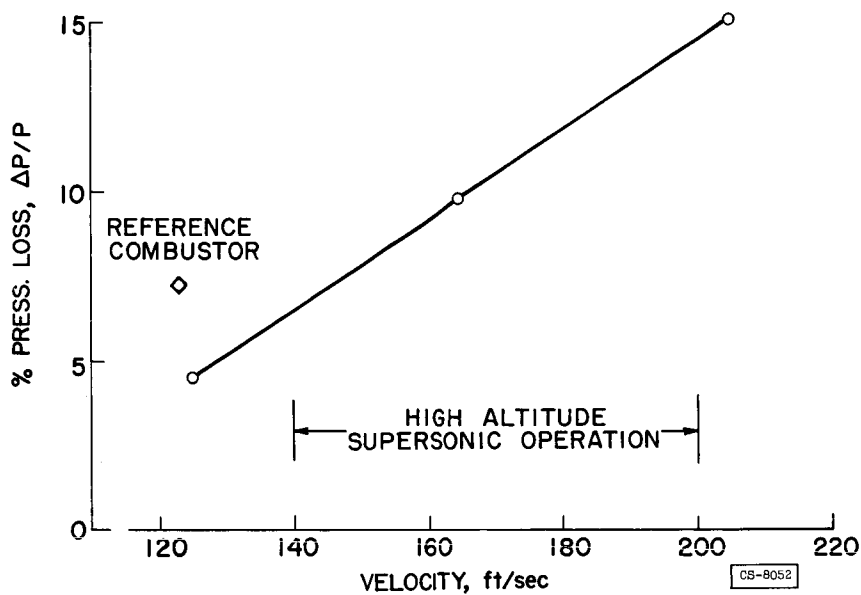


Figure 23

## RADIAL TEMPERATURE PROFILE AT COMBUSTOR OUTLET

V, 165 ft/sec

 $T_i$ , 870° F

P, 18.4 psia

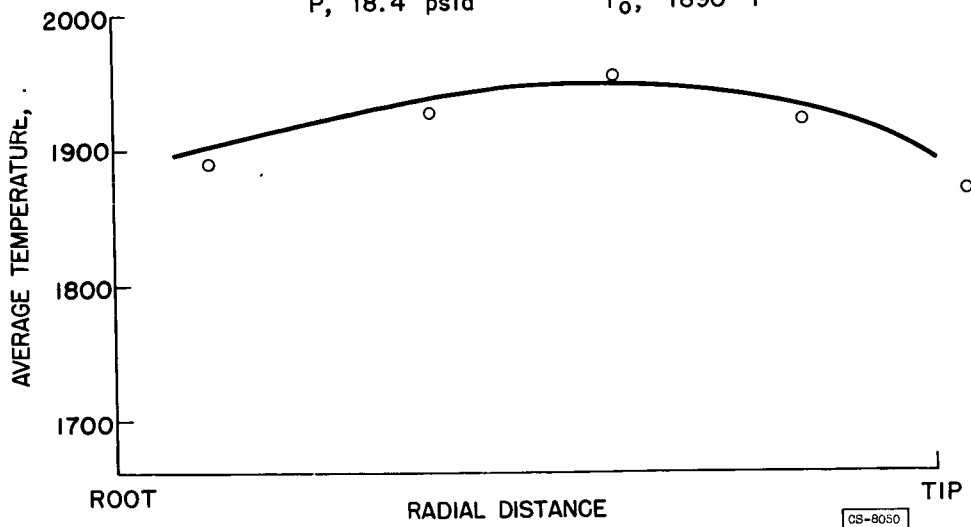
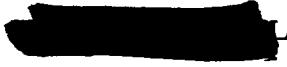
 $T_o$ , 1890° F

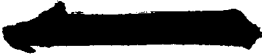
Figure 24



VI - MATERIALS AND STRUCTURES PANEL

- S. S. Manson
- E. E. Bisson
- G. M. Ault
- R. H. Kemp
- G. C. Deutsch





## ALLOYS FOR USE AT INCREASED TEMPERATURES

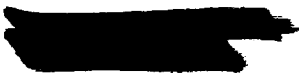
By G. M. Ault

### INTRODUCTION

3078-F

The desire for higher combustion temperatures to permit greater thrust per unit weight of the turbojet engine and thus more efficient supersonic flight has been indicated in other papers of this conference. A limit on temperature for many engine components is imposed by the materials. Current operating temperatures for a typical turbojet engine are shown on figure 1. Under conditions of supersonic flight, all engine components will increase in operating temperature. The parts before the combustor will operate at increased temperatures under supersonic-flight conditions because of increased ram-air temperatures. Speeds approaching Mach 3 will result in compressor-inlet temperatures greater than current compressor-outlet temperatures, shown on figure 1 as 450° F; and compressor-outlet temperatures may be of the order of 1100° F. The combustor and parts downstream of the combustor will be operated at increased temperatures, because the temperature of the entrance air will be much greater and because higher combustor temperatures are used to obtain increased thrust ratios.

The materials problem forward of the combustor will not be too severe, however, since a large number of high-temperature materials with good strength up to 1200° F are available. The major difficulties will be encountered with those parts of the engine already having the highest operating temperature or severest combination of stress and temperature. Thus, attention is focused on the combustion-chamber liner and transition piece, the turbine-inlet guide vanes, and the rotating turbine blades. The combustor liner and transition piece may present a limitation on temperature, but the development history of these parts indicates that alloys of lower temperature limitations are gradually being used as a combustion-chamber design is improved. Sheet materials other than those currently in use will be required for increased temperatures; however, materials are available that will permit substantial temperature increase. The part that generally operates at the highest temperature is the turbine inlet guide vane, but stresses other than thermal stresses are moderate. Probably the component that most limits gas temperatures because of a severe combination of stress and temperature is the rotating turbine blade. In the blade midspan region, where failure is most likely to occur, current operating temperatures are of the order of 1500° F with centrifugal stresses on the order of 13,000 to 22,000 pounds per square inch, depending on engine design. In addition, the blades are subjected to severe vibratory loads, and the combustion gases are, of course, severely oxidizing. These current operating conditions require alloy properties for the turbine blade equivalent to the best of the so-called "super alloys" now commercially available.



It is of interest to consider the status of the development of high-temperature alloys that may be suitable for turbine blades operating at the higher combustion temperatures required for efficient supersonic flight.

### COMMERCIAL HIGH-TEMPERATURE ALLOYS

The strengths of several current commercial high-temperature alloys are shown in figure 2. The data are presented on the basis of the stresses that will result in failure by stress-rupture in 100 hours at various temperatures. The alloys represent three general classes, each of which has been or is currently being used for turbine blades. The classes are the nickel-base wrought alloys, illustrated by Inconel 550, M-252, and Nimonic 90; the cobalt-base wrought alloys, illustrated by S-816 and HS-25; and the cobalt-base cast alloys, illustrated by HS-36 and HS-31. The current nickel-base wrought alloys have very good properties at 1500° F (and below), but the rupture strength decreases rapidly at increased temperatures. The development of the nickel-base alloys has been stimulated by the requirements for alloys of much less critical element content than the cobalt-base types. This need is being fulfilled, and these alloys may be satisfactory up to 1600° F. The cobalt-base cast alloys are superior at increased temperatures; and, at 1600° F and above with stresses below 18,000 pounds per square inch, they will give an 80° or 90° temperature advantage over wrought alloys of either nickel or cobalt base. The allowable stresses at 1600° F are near the minimum that might be allowed for blade design, however. Much more is required in both allowable temperature and stress.

### Developmental Alloys of Cobalt and Nickel Base

Alloys of cobalt and nickel base superior to those described in figure 2 are being developed. For the wrought alloys, most recent effort has been devoted to the development of nickel-base types, because alloys of less critical-material content than the cobalt types are required. The result is that no improvement in the properties of wrought cobalt-base types over those described in figure 2 has been reported. Nickel-base wrought alloys having 100-hour stress-rupture properties equivalent to the cobalt-base cast alloys of figure 2 at 1600° F have been reported (20,000 psi for 100 hr at 1600° F). Considerable study is being continued on wrought nickel-base alloys for improved properties at 1600° F.

In the published literature, the outstanding developmental alloys for possible application at 1600° F and above are cast. The best of these developmental alloys (noncommercial at this time) are shown in

figure 3. Those shown are of both cobalt base (HE-2949, HE-1049, and 73J) and nickel base (Guy alloy, ref. 1). (Alloys HE-2949 and HE-1049 are developments of the Haynes Stellite Co.) The alloys HS-36 and S-816 from figure 2 are included for comparison. The developmental alloys have strengths that represent appreciable gains in allowable stress and temperature over the wrought blade alloy S-816 and the current cast alloy HS-36 for most of the temperature range. As the temperature approaches 1800° F, the alloys tend to become equivalent in strength. As indicated by both figures 2 and 3, the alloys having the better stress-rupture strengths at increased temperatures are cast alloys.

### Cast Alloys

In a general way, it might be said that higher-use temperatures are achieved by adding more of the alloy strengtheners that will give better rupture strength but will also reduce ductility. The reduced ductility or increased brittleness, plus the increased strength at elevated temperatures tends to make these alloys impossible to fabricate by present forging and rolling techniques, so they must be cast. Also, the microstructure of the cast and wrought alloys are inherently different; and, for these cobalt- and nickel-base alloys, better rupture strengths at very high temperatures appear to be associated with this cast structure. It may be expected that the cobalt- and nickel-base alloys that have the best rupture strengths at temperatures above 1600° F will be cast.

Up to the present time, wrought alloys have been used most widely for jet-engine blades. In fact, there has been a strong tendency to avoid the use of cast blade alloys, based on these premises: (1) Their fatigue properties are low; and (2) The scatter in properties of cast blades is very large, and premature failure of one or two blades on a turbine wheel may occur that cannot be prevented by isolation of poor blades through normal inspection techniques.

### Engine Evaluation of Cast Alloys

For some time, turbine blades of cast and wrought alloys have been investigated in full-scale engines at the NACA Lewis laboratory. Figure 4 shows the blade life of several wrought and cast alloys evaluated at full-power conditions at current temperatures in a turbojet engine. The scatter of blade lives for the particular samples is indicated by the length of the bar. Individual blade failures are indicated by the points above the bars. From these data, it is apparent that the scatter in engine life of the cast alloys has been somewhat greater than for the wrought alloys; however, a tendency for a few premature failures has not been generally found with the cast alloys; rather, the first failures are soon followed by subsequent failures in a normal manner. Regardless

of scatter, it is interesting that the best blade life achieved has been with a cast alloy (indicated by alloy I). It has also been apparent that fatigue failures are more common with cast blades than with wrought, and fatigue has been the most important factor in failure of cast blades. The cast alloy (I) that ran best did not show evidence of fatigue failure.

#### Low Ductility of Developmental Alloys

As was mentioned earlier, the alloys that were shown to have good rupture strengths at increased temperatures also have low ductility. Figure 5 illustrates this observation. The ductility, as indicated by elongation in a room-temperature tensile test, generally decreases with increasing allowable operating temperature (measured as the temperature for rupture in 100 hr at 22,000 psi). To date, many alloys have been developed as a compromise between good strength at elevated temperature and good ductility at room temperature. From figure 5, it is apparent that it may be necessary to learn how to use materials of low room-temperature ductility if strength at very high temperatures is to be achieved. The first problem to be solved as a result of low ductility is the fastening of the blade to the disk. The standard fir-tree design of fastening is very strong and quite satisfactory for a ductile alloy but may not be satisfactory for the brittle alloys because of the severe stress-concentration effects of sharp radii. This problem has been encountered with the extremely brittle cermet materials, and fastenings considerably superior to the fir-tree design when applied to brittle materials have been developed. These are described in the paper on cermets. If required, designs similar to the types developed for cermets may be used for the brittle alloys.

A second very important problem, usually implied in low ductility, is low impact strength. The more brittle alloys would be expected to have a much greater tendency toward damage by impact from solid particles in the gas stream, and failure of one blade may cause much more damage to the remaining blades on a wheel than has been experienced with the more ductile alloys in current use. Additional problems usually associated with low ductility are sensitivity to notches under conditions of fatigue and stress-rupture and difficulty in handling and fabrication. More experience is required in the application of these high-strength, low-ductility materials to engines so that a better understanding of the problems and their solutions can be achieved.

#### REFRACTORY ALLOYS

It is apparent that newly developed cast alloys of cobalt and nickel base have rupture properties substantially better than the currently used blade alloys. Even better rupture properties are found for alloys

3078 - F

[REDACTED]

of chromium or molybdenum base. Figure 6 shows the strength of the best molybdenum- and chromium-base alloys compared with several outstanding cobalt-base alloys. On the basis of rupture strength, alloys of molybdenum base have strengths equivalent to the cobalt-base wrought alloy at 500° F higher temperature and strengths equivalent to the best cobalt-base cast alloy at 250° F higher temperature. The strengths of chromium-base alloys are between the best cobalt alloy and the best molybdenum-base alloy.

3078-F

In the case of chromium-base alloys, the better strength alloys have base compositions of about 60-percent chromium, 15-percent iron, and 25-percent molybdenum (ref. 2). The best alloys reported to date have about 2-percent titanium added to this base composition and are cast, usually in vacuum. They have satisfactory oxidation resistance but are extremely brittle, with no ductility at room temperature and negligible impact strength even at high temperatures. On the basis of limited impact data, they are poorer than cermets. Current studies are centered around improving the ductility of these alloys and the development of compositions having somewhat less strength but more ductility. Alloys of chromium-nickel-tungsten demonstrate measureable ductility at room temperature, but 100-hour strengths of only 45,000 to 50,000 pounds per square inch at 1500° F. (ref. 3). Chromium-base alloys are being studied in several laboratories primarily for the purpose of improving ductility. As in the case of the highest-strength cobalt- and nickel-base alloys, it would appear necessary that studies be directed toward possible applications of more brittle materials than have been successfully applied to date.

The data shown in figure 6 for molybdenum-base alloys represent the best strengths obtained in alloys developed by Climax Molybdenum Co. under a research project sponsored by the Office of Naval Research. These alloys have been developed primarily during the last three years. The best molybdenum-base alloys at this time are made by melting in vacuum or neutral-gas atmosphere followed by extrusion or working by other methods. The alloys have maximum strength in the worked condition and lose considerable strength when recrystallized. Molybdenum alloys are malleable and have been forged into experimental blades, but they present ductility problems, primarily in bending. In the tensile test, however, some molybdenum alloys have demonstrated reduction of areas equivalent to current blade alloys at room temperature. Reference 4 reports room-temperature elongations of 30 percent for stress-relieved molybdenum alloys that had been severely worked down to a bar-stock diameter of 5/8. (If worked less, the elongations were 2 to 4 percent.) These alloys showed rupture strengths as high as 37,000 pounds per square inch for 100 hours at 1800° F. Alloys of somewhat higher rupture strength had elongations of the order of 2 to 3 percent. Elongation increases rapidly with temperature, however; and at 1200° F, these latter alloys showed elongations in excess of 10 percent in the tensile test. It is indicated that the best combination of ductility and high-temperature strength might be achieved with molybdenum-base alloys.

[REDACTED]

The primary problem in the application of molybdenum alloys is their extremely poor oxidation resistance. Many types of coatings and alloy additions to prevent oxidation have been attempted, but none has been completely satisfactory. For most alloys, other than molybdenum-base, the addition of chromium generally provides the necessary resistance to oxidation. When added to molybdenum, chromium appreciably reduces the rate of oxidation, but the oxidation resistance is still completely unsatisfactory. Most of the coatings that have been applied have had one or both of the following difficulties: They are brittle and have very low impact strength; or, When large numbers of a part such as a turbine blade have to be coated, the coating cannot be guaranteed to be perfect on all pieces. The oxidation of molybdenum is so rapid that a small pin hole, resulting from an imperfect coating or from impact of small particles in the gas stream, can be expected to result in the loss of a blade in a few minutes under engine operating conditions. The consensus of current opinion is that a coating for molybdenum for a part subjected to impact (such as a turbine blade) must be ductile, as may be expected with diffused metallic coatings as contrasted to ceramic or vitreous coatings. The protection of molybdenum presents one of the most difficult coating problems ever encountered, particularly where the molybdenum part is subjected to direct impingement of high-velocity hot oxidizing gases carrying solid particles that may impact and erode the surfaces. The development of satisfactory strength is well ahead of the coating development, but considerable effort is being expended on the coating problem at this time.

#### MAXIMUM ALLOWABLE BLADE TEMPERATURES

For turbine blades, the primary stresses are determined by centrifugal force and are, therefore, a function of the density of the alloy. For this application, it is necessary to consider the relative strengths of alloys when corrected for density. Figure 7 plots the strengths for rupture in 100 hours at various temperatures corrected to a density of 8.59, the density of a currently used blade alloy S-816. This improves the position of lower-density alloys such as the nickel-base cast alloy and the chromium-base alloy, but the advantage of the molybdenum alloys is lessened because of their high density. The 20-percent increase in density also means heavier blading and greater engine weight and 20-percent increase in loading on the disk. In addition, the thermal conductivity of molybdenum is appreciably higher than that of currently used alloys; thus higher disk rim temperatures result. The combination of higher stress and higher temperature at the rim impose additional problems of disk design and may require disk cooling.

Also shown in figure 7 are lines indicating the centrifugal-stress levels in the blades of two typical current production turbines. One (engine A) is a high-stress engine, and the other (engine B) is a

low-stress engine. For the highly stressed blade, temperatures of around 1700° F are possible through the application of the best cobalt- and nickel-base alloys, while nearly 1950° F is possible with molybdenum-base alloys. At least an additional 100° F is possible if the stress levels of the low-stress engine prevail. Consideration of the 150° to 200° F difference between blade temperature and gas temperature indicates that use of molybdenum-base alloys would permit a gas temperature of about 2250° F.

CRITICAL-MATERIALS PROBLEM

3078-F

The relative criticalness of these alloys can be indicated by comparing them qualitatively on the basis of critical index. Figure 8 outlines the chemical compositions of several of these alloys and their critical indices. The alloy index was calculated from an index for the elements proposed in reference 5. The alloys are tabulated in order of increasing allowable operating temperature for stress-rupture failure in 100 hours at 22,000 pounds per square inch.

Inspection of the table indicates that there is not a definite trend of increasing index with increasing allowable operating temperature. The nickel-base alloys have a very low index, and these alloys should certainly be used to their limit. From the critical-element standpoint, they warrant considerable investigation.

The cobalt-base alloys as a group have similar indices, unless columbium is added (as is the case for S-816). For chromium-base alloys, two indices are shown, depending on whether ferrochromium or pure chromium is used in melting the alloys. Pure chromium is often used in an attempt to avoid embrittling effects that may be due to minor amounts of impurities. Through further development, it may be possible to develop ductility in these alloys even when using ferrochromium. If ferrochromium could be used, availability would be substantially improved. In the case of pure chromium, the limitation on supply is not the lack of ore, but the lack of production capacity to convert the ore to pure chromium. If necessary, this facility could perhaps be expanded. The availability would then approach that of ferrochromium.

The molybdenum-base alloys have an index slightly lower than that of the cobalt-base alloys and about 2 to 4 times that of the nickel-base alloys, which suggests that their usage would be limited in a manner similar to that for the cobalt-base alloys. It is gratifying, however, that the alloys having possible application at higher temperatures do not have greater problems of supply than the cobalt alloys.

As suggested previously, comparison of alloys on the basis of index is qualitative and only partially satisfactory. Such numbers do

not reflect the entire problem, which is, at best, very complex. If used, they should be revised constantly to reflect continuing changes in supply and demand. It is common knowledge that, if full war-time mobilization were necessary, the required number of engines could not be built if all engines were to have turbine blades of cobalt-base alloys. From this knowledge and the fact that molybdenum and cobalt alloy indices are similar, it is indicated that all engines could not use blades of molybdenum-base alloys either. The exclusive use of chromium-base alloys using ferrochromium but containing 25-percent molybdenum may even be marginal. Satisfactory production of high-temperature engines might be achieved by using as much of each critical element as possible rather than concentrating on a particular alloy type. Nickel- and cobalt-base alloys should be used to their limit, and chromium- and molybdenum-base alloys should be applied in those engines that demand the highest temperatures because of the intended mission.

#### CONCLUDING REMARKS

When alloys are considered for turbines operating at increased temperatures, the following are indicated:

1. Although greatly improved wrought alloys of nickel base are being developed, the cobalt- and nickel-base alloys that have the best properties at increased temperatures are cast. At the blade-stress developed in a highly stressed current production engine, the best of these have satisfactory 100-hour stress-rupture properties up to 1700° F. The fact that the very best cast cobalt- and nickel-base alloys have appreciably lower ductility than presently used alloys presents problems of notch sensitivity in fastenings and difficulty in handling and fabrication and usually implies low impact strength.

2. Chromium-base alloys are being studied, and the best of these exhibit stress-rupture strengths considerably superior to the cobalt- or nickel-base types - satisfactory 100-hour stress-rupture strengths up to 1830° F. These alloys are presently so brittle that their use is probably prohibited unless current and future research can improve ductility somewhat.

3. Truly outstanding stress-rupture properties are being developed in alloys of molybdenum base. These have satisfactory 100-hour stress-rupture strengths for operating temperatures up to 1950° F. Although the high density and high conductivity present problems of disk design, the most serious problem in application is the extremely poor oxidation resistance of these alloys. Satisfactory coatings must be developed.

4. Because of the very limited supply of pure chromium cobalt and molybdenum, it is believed that no one alloy using these elements as a

base can meet full mobilization schedules. Nickel-base alloys or ferrochromium-base alloys perhaps could. Production of higher-temperature engines on a schedule approaching the requirements of full mobilization can best be achieved by using progressively each of the alloy classes up to its limitations. It is at least gratifying that none of the alloys for use at increased temperatures presents a more serious problem of raw-material supply than the current cobalt-base alloys.

#### REFERENCES

1. Guy, A. G.: Nickel-Base Alloys for High Temperature Applications. Trans. A.S.M., vol. 41, 1949, pp. 125-140.
2. Havekotte, W. L., and Greenidge, C. T.: Final Report on Chromium-Base Alloys. Battelle Memorial Inst., Mar. 31, 1950. (Contract No. N5ori-111, Task Order I, Proj. Nr 031-003, Office Naval Res., Navy Dept.)
3. Panel of Minerals and Metals Advisory Board: Materials for Use in Gas Turbines. Rep. No. MMAB-41-M, Div. Eng. and Ind. Res., Div. Earth Sci., Nat. Acad. Sci., Nat. Res. Council, Washington (D.C.), Mar. 1, 1953. (Contract DA-49-025-sc-83 between Dept. Defense and Nat. Acad. Sci.)
4. Semchyshen, M., and Hostetter, H. E.: Arc-Cast Molybdenum Base Alloys. Third Annual Rep. NR 034-401, Climax Molybdenum Co. of Michigan, 1952. (Contract N8onr-78700, Task Order N8onr-78701, Proj. NR 034-401, Office Naval Res., Navy Dept.)
5. Herzig, Alvin J., and Meierdirks, J. B., Jr.: The Conservation of High Temperature Materials in Aircraft Gas Turbines. Rep. No. MAB-5-M, Div. Eng. and Ind. Res., Nat. Acad. Sci., Nat. Res. Council, Washington (D.C.), Sept, 15, 1951. (Contract DA-49-025-sc-83 between Dept. Defense and Nat. Acad. Sci.)

3078-7

# TYPICAL OPERATING TEMPERATURES OF A TURBOJET WITH THRUST AUGMENTATION

3078-J

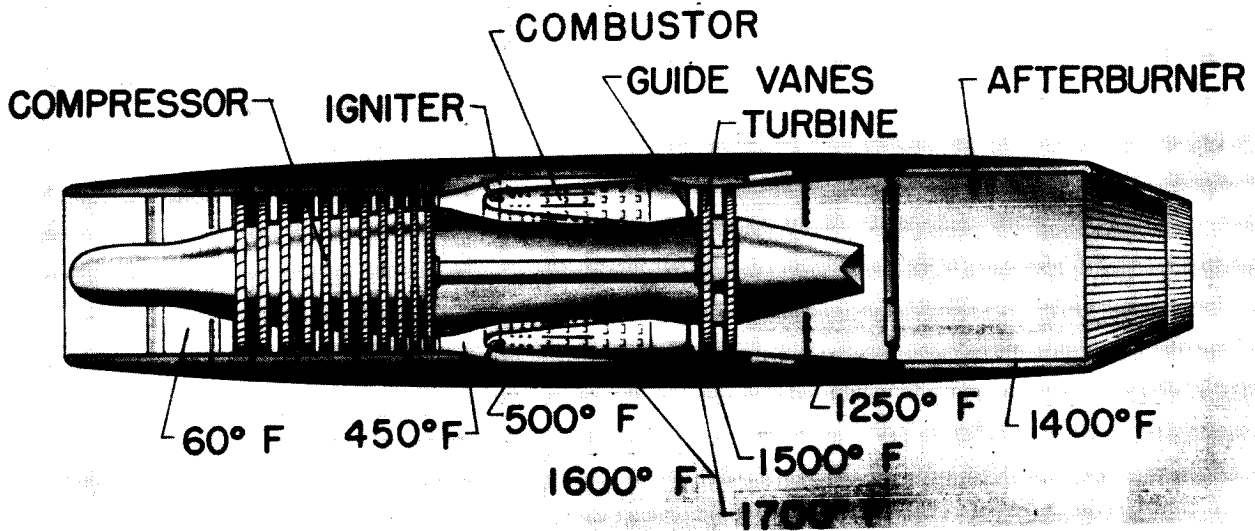


Figure 1

## COMPARISON OF 100-HOUR STRESS-RUPTURE STRENGTHS OF CURRENT BLADE ALLOYS

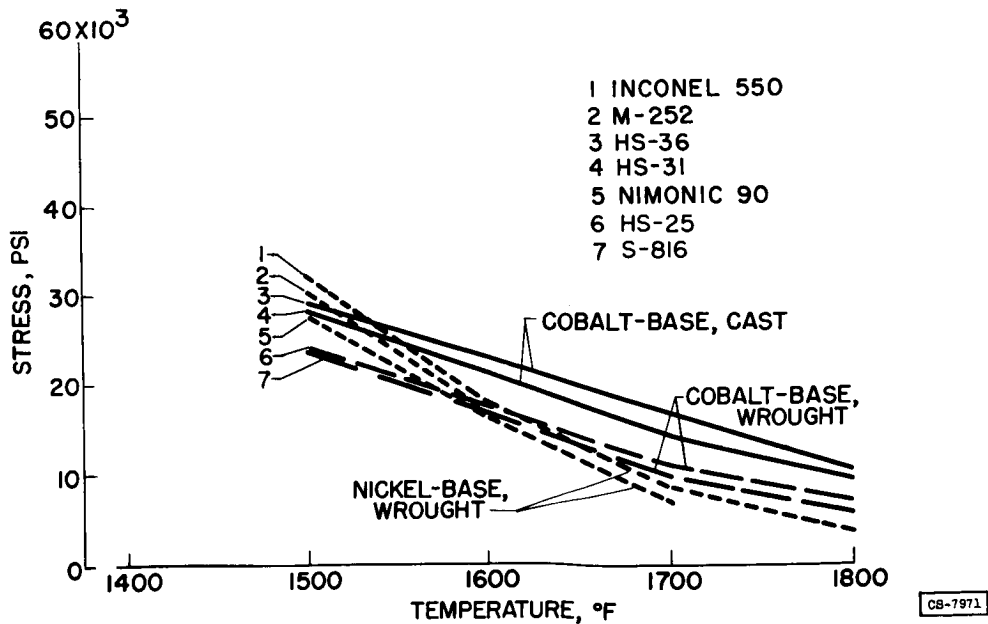


Figure 2

3078-J

### COMPARISON OF 100-HOUR STRESS-RUPTURE STRENGTHS OF NEW CAST ALLOYS WITH CURRENT ALLOYS

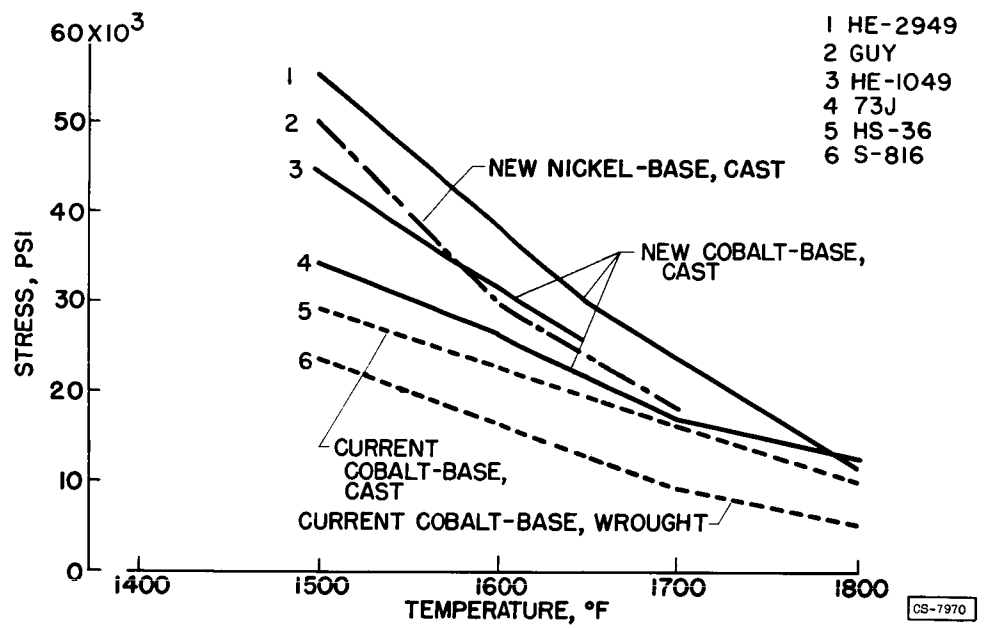


Figure 3

### ENGINE LIFE OF WROUGHT AND CAST ALLOYS AT RATED SPEEDS BLADE STRESS, 22,000 PSI; BLADE TEMPERATURE, 1500° F

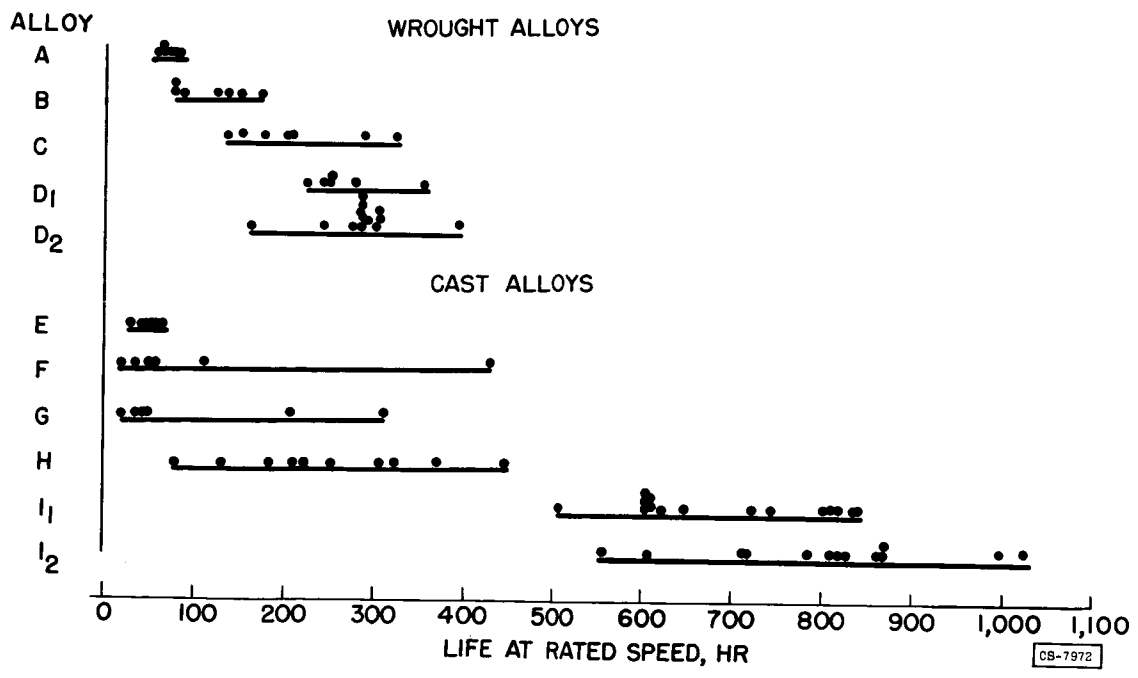
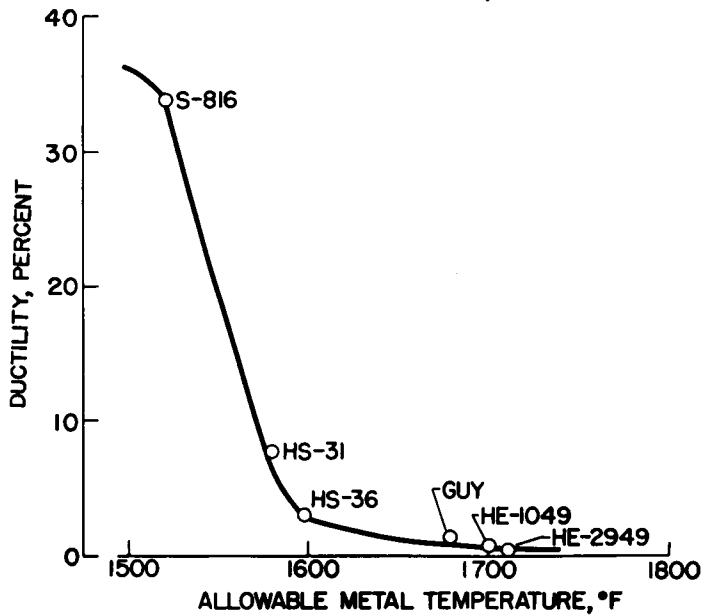


Figure 4

**RELATION BETWEEN ROOM-TEMPERATURE DUCTILITY AND ALLOWABLE BLADE TEMPERATURE FOR RUPTURE IN 100 HOURS AT 22,000 PSI**



**Figure 5**

**MOLYBDENUM AND CHROMIUM ALLOYS COMPARED WITH COBALT AND NICKEL ALLOYS**

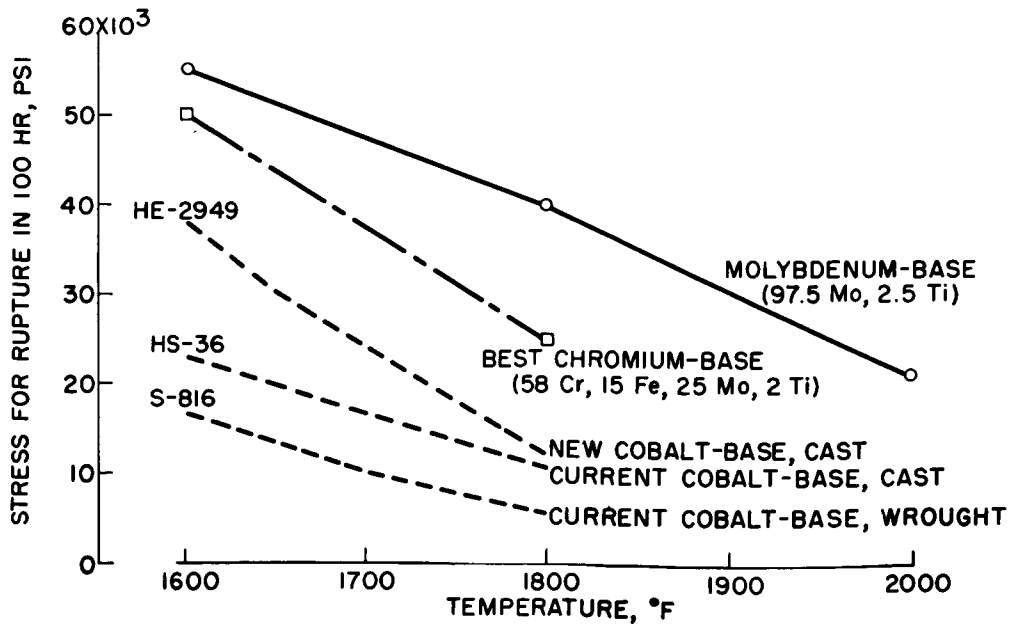


**Figure 6**

3078-F

COMPARISON OF 100-HOUR STRESS-RUPTURE STRENGTHS OF ALLOYS  
ADJUSTED TO DENSITY OF S-816

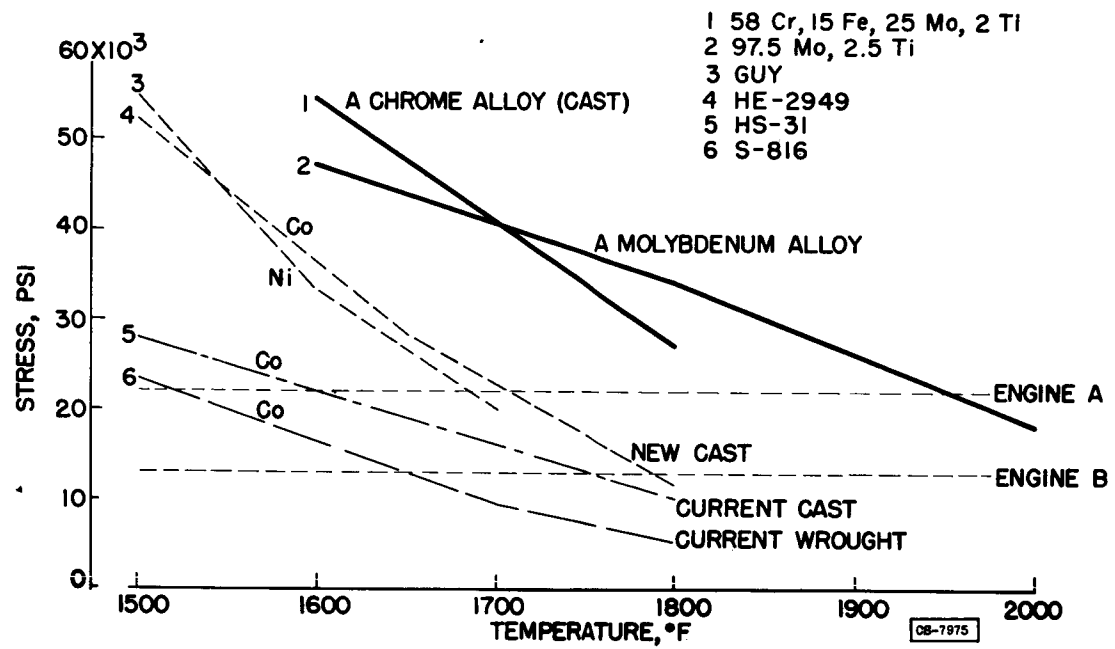


Figure 7

ALLOWABLE OPERATING TEMPERATURE AND CRITICAL INDEX OF BLADE ALLOYS

ALLOWABLE OPERATING TEMPERATURE AT 22,000 PSI, °F	CRITICAL INDEX	ALLOY CLASS	ALLOY DESIGNATION	COMPOSITION (PERCENT BY WEIGHT)												
				Ni	Co	Cr	Mo	Cr in Fe-Cr	W	Cb	Fe	Al	Ti	C	B	Ta
1520	2810	CURRENT WROUGHT COBALT	S-816	20	44	20	4		4	3.75	2.8			0.40		
1560	710	CURRENT WROUGHT NICKEL	M-252	54	10	19	10		2		2	0.75	2.5	.10		
1570	410	CURRENT WROUGHT NICKEL	INC 550	73				15		.9	7	1.2	2.5	.06		
1580	1930	CURRENT CAST COBALT	HS-31	10	55	25			7.4		1			.48		
1600	2070	CURRENT CAST COBALT	HS-36	10	55	18.5			14.5		2			.40	0.01-.05	
1650	1900	NEW CAST COBALT	73J	6	60	23	6							.73		2
1680	850	NEW CAST NICKEL	GUY	66			5	15		2	4.5	6		.5		
1700	1910	NEW CAST COBALT	HE-1049	10	44	26			15		3			.40	.40	
1710	1910	NEW CAST COBALT	HE-2949	10	44	26			15		3			.80	.80	
1830	1150	CAST CHROME				58	25				15		2.0			
1830	460					25	58				25		2.0			
1950	1630	WROUGHT MOLYBDENUM				97.5							2.5			
			CRITICAL INDEX OF ELEMENT	1.25	25	12.5	16.7	1.0	31.3	33.3	0	0	0	0	0	0

Figure 8

## APPLICABILITY OF CERMETS FOR USE AS TURBINE BLADES

By G. C. Deutsch, A. J. Meyer, and W. C. Morgan

## INTRODUCTION

Cermets, combinations of metals and ceramics, were the result of an effort to provide a material of superior high-temperature strength and adequate thermal-shock resistance which could be used for jet-engine turbine blades to be operated at increased temperatures. Thus far only a few combinations of metals and ceramics have been studied, and the results of these studies are promising.

The variation in 100-hour stress-rupture strength with temperature for several cermets is given in figure 1. Several alloys have been included in this figure for comparison purposes. The cermets shown are representative of two categories: The first consists of the titanium carbide plus nickel-molybdenum and the titanium carbide plus nickel-molybdenum-aluminum, which are representative of materials that are well along in development (meaning that their properties have been fairly well defined and techniques for the production of intricate shapes have been developed). The second class of cermets, represented by the titanium carbide-titanium diboride plus cobalt-silicon and the alumina plus chromium, consists of materials which are not so far along in their development but which serve to indicate the future strength potentialities of this class of materials.

The alloys shown on this figure also represent different stages of alloy development. The S-816 is highly developed and is currently the most widely used blade alloy. One of the newer alloys currently being developed with the highest strength is HE-2949; the molybdenum alloy is very promising but is hampered by a very severe oxidation problem. The cermets compare very favorably. For example, if an application requiring the material to withstand a stress of 20,000 pounds per square inch for 100 hours is assumed, the maximum temperature at which S-816 could withstand this combination of stress and temperature is about 1550° F. The best current cermet, on the other hand, could, on the basis of strength, support this load for the required time at about 1850° F or 300° F higher in temperature, while some of the future cermets show promise of being able to withstand these conditions at much higher temperatures. The development alloy HE-2949 comes much nearer to the cermets in strength but is still inferior. Molybdenum alloys exceed the cermets in strength but, as mentioned previously, the utilization of this material is hampered by a severe oxidation problem.

Since the material application with which this paper is concerned is that of turbine blades where the load is centrifugal and is proportional to the material density, the comparison of materials should be

made on a strength-to-weight basis. Such a comparison, again based on 100 hours of life of alloys and cermets, is shown in figure 2. The axes in this figure are the same as those of the previous one except that the strengths have been adjusted on the basis of density. The base line for this adjustment is the density of the alloy S-816. Also on this figure is the range of stresses which the blades of two current jet engines are required to withstand. In the case of the engine in which the blades are highly stressed, the best current cermet would enable the temperature to be raised by about 300° F over the current temperature and about 100° F over that indicated for one of the better alloys under development. The comparison is quite similar in the case of an engine in which the blades are subjected to a low stress. In this case, the cermet offers the possibility of increasing the operating temperatures from about 1650° to 1900° F or about 250° F.

In this comparison, because of density considerations, it can be seen that the future cermets show promise of having strengths equivalent to or superior to that of the molybdenum alloys.

Unfortunately, the strength of cermets is not the entire story and several problems must be solved before these materials can be widely utilized. Perhaps the most difficult problem associated with the use of this material is its brittleness or lack of ductility. A lack of uniformity in strength properties of bodies judged sound by any of the existing inspection techniques is a second current problem. An adequate nondestructive test technique for these new materials is an essential need.

One effect of the brittleness of cermets is their sensitivity to stress concentrations caused by notches and by minor mismatching due to machining tolerances and their susceptibility to damage from thermal or mechanical shocks. Of these, the one most amenable to study and improvement is the sensitivity to stress concentrations.

#### PRELIMINARY ROOT DESIGN

It appeared quite likely that the conventional fir-tree type of root with its small radii and many lands among which the load had to be uniformly distributed was not optimum for cermets, and consequently a design study to yield root forms suitable for use with brittle materials was undertaken. More than 20 different root forms were investigated using plastic models. Figure 3 shows the most promising root configurations. For comparison purposes the conventional fir-tree type root used with alloy blades is included in the figure. The experimental roots have large radii to minimize stress concentrations and the load is carried by only one or two lands with large shear areas. The roots having shaded portions utilized a ductile retaining pin and it was hoped

that these pins would deform and provide some of the ductility lacking in the cermet. The roots which did not utilize a ductile retaining pin were separated from the wheel by a nickel-plated copper screen. This screen was intended to compensate for the small amounts of mismatching between the blade root and the wheel due to machining tolerances.

#### PRELIMINARY ENGINE TESTS

The J33 turbojet engine was chosen for use in evaluating these designs. This engine applies a very high stress to the blades, and it was thought that if the blades performed satisfactorily in this engine, they would probably be satisfactory for most current engines. To minimize the cost of the evaluations, only a few experimental blades were run in a wheel at one time. In most cases, the number of cermet blades was either four or six, with the remaining positions containing conventional alloy blades. Because of this and in order to obtain satisfactory lives from other components in the engine, the tests were run at current engine temperature.

The materials chosen for engine tests were titanium carbide compositions and were produced by cold press and sinter methods by the Kennametal Company. Two compositions were principally used, one containing 30 percent by weight nickel and the other, 25 percent nickel and 5 percent molybdenum. Figure 4 is a photograph of the actual blades used in this study.

In general, the program of initial engine operation for a set of blades consisted of incremental increases in speed from idle to full rated speed. With this cycle it takes about 50 minutes to bring the engine to full rated speed. During subsequent starts with the same blades, the engine was slowly accelerated to rated speed, a procedure that required about 10 minutes. To date there have been 20 runs. A summary of the preliminary operational data is shown in the first four lines of table I.

As a base line for comparison purposes, blades having the fir-tree roots were run. The best run lasted 4 hours, of which 3 hours were at rated speed; and as the design studies predicted, the failure occurred across the top serration of the root.

With the four-pin type root, the operating life at rated speed was increased to 20 hours. The single-land interlock and dovetail roots enabled the improvement of operational time to about 70 hours, but the blades were still failing in the root. Figure 5 shows a typical fracture. The smooth texture of the right half of the fracture surface indicates that bending stress was present and if the airfoil profile is superimposed on this fracture surface, the bending appears to originate

at a point below which the largest mass of the blade was located. This suggested that the load distribution in the root was unfavorable and that the blade should be redesigned to eliminate this condition. This was done in the two designs shown in figure 6.

#### ROOT REDESIGN

In redesigning the blades, the dovetail root form was used. The first redesign of the root involved three changes: First the root was skewed  $14.4^\circ$ , thus minimizing bending moments associated with the overhang of the airfoil; second, the airfoil was translated with respect to the root to bring the center of gravity of the airfoil in line with the center of the root; and third, the radius in the root was enlarged. The root radius was changed to a value indicated to be an improvement by more recent design studies.

The final blade shown in the figure carries this process of minimizing the bending stresses in the root one step further by having the root curve to follow the contour of the airfoil. It should be emphasized that these changes do not alter the number of blades the wheel can hold or the interrelation of the airfoils.

#### ADDITIONAL ENGINE TESTS

Wheels partially bladed with cermets. - The operating data for the skewed dovetail blades is shown in table I. Using the same cermet composition as was used in the earlier tests, the first run lasted for 134.8 hours, of which 129.5 were at rated speed. At this time, the nozzle diaphragm failed (fig. 7) and a fragment damaged the blades. The failed blades are shown in figure 8. A repeat of this run using a composition with higher stress-rupture properties lasted 242 hours at rated engine speed. This test was discontinued, but the blades did not fail.

The first test with the curved root blades is now in progress and thus far the blades have operated for 90 hours without failure. These runs to date indicate that reasonable blade lives can be attained with cermet blades under conditions of slow acceleration and deceleration. To find out how the blades would behave under the mechanical and thermal shock conditions present during rapid changes in speed, runs in which the engine was operated for 15 minutes at take-off speed followed by 5 minutes at idle with rapid acceleration and deceleration between these conditions were tried.

In the first run the blades operated for 50 hours at take-off speed as a proof test after which cyclic operation was attempted. Two of the

[REDACTED]

blades on one side of the wheel failed in the root during the fourteenth cycle.

It was felt that while the displacement and skewing of the airfoil were desirable under all operating conditions, the shallow angle of the enlarged blade root radius might have a progressive wedging action and prove to be detrimental if the operating plan involved frequent changes in speed.

3078 - F

To check this hypothesis, a run was made in which two of the blades having the large radius were run on one side of the wheel while blades having small radii were run on the opposite side. All four of these blades were of the skewed design. Both the large and small radius blades were able to survive 108 cycles of test, at which time one of the large radius blades failed in the root. Thus, while there is an indication that the small-radius root is superior under cyclic operating conditions, both were able to sustain a considerable number of changes in speed.

Wheels completely bladed with cermets. - The encouraging results of steady-state and cyclic operation suggested that wheels containing only cermet turbine blades should be run. Two such runs were made. The first wheel contained blades having the large radius, skewed dove-tail roots. The run lasted for 1 hour and 50 minutes, at which time one blade failed in the root and damaged the remaining blades. The appearance of the failure suggested that the blade may have been defective.

The second run utilized blades having the same type of root except that the radius was reduced to the value which proved to be superior in the cyclic engine runs. This run lasted for 12 hours at full rated speed, which is encouraging in view of the limited experience with wheels fully bladed with cermet blades.

#### INSPECTION PROBLEMS

One problem that must be solved before cermets can be considered practical is that of inspection. Conventional nondestructive methods such as radiographic and penetrant-oil methods are being used, and while these do eliminate some defective blades, some very early failures are still being encountered. Several sonic and magnetic methods are being studied and are promising but as yet have not produced concrete results. Methods involving determinations of the strength of the blade have been attempted but do not appear to be the complete answer to the inspection problem. For example, in selecting blades for the full-wheel evaluations, a group of 136 blades was proof tested by running them in an engine for 1 hour at rated engine speed. This test, which indicated that the blades were able to sustain the required stress, resulted in

[REDACTED]

[REDACTED]

the elimination of only two blades. Yet the operating experience with full wheels indicates that some of the blades which survived this test will fail after only a relatively short additional period of operation. In another test 46 blades were run at continuously increasing speeds until failure occurred. The poorest blade in this group survived 185 percent of rated stress. Yet other blades from the same group when run in the engine at rated speed failed after only a short period of operation. In addition to better methods of inspection, improved methods of production are required. Blades having greater dimensional and physical uniformity are essential to the widespread acceptance of this type of material.

#### IMPACT DAMAGE

Perhaps the biggest problem confronting cermets today is their susceptibility to damage by impact. Figure 8 shows the damage resulting to the turbine blades when a fragment from nozzle diaphragm passed through the turbine. It can be noted that the tips of all four cermet blades were damaged. The alloy blades, on the other hand, were much better able to withstand the impact and were not so severely damaged. However, some of the newer alloys which are being considered for higher temperature operation have impact strengths similar to those of cermets, and were these present in the turbine wheel, the damage to the alloy blades would have been much more extensive.

#### CONCLUDING REMARKS

Cermets are a promising material for raising the operating temperatures of turbine blades by direct material substitution. As in the case of any new material, design procedures and handling experience must be acquired before full utilization can be achieved. The studies to date have shown that the use of more generous radii to minimize stress concentrations, the improvement in the uniformity of load distribution on the lands of the root, and the relocation of the airfoil to minimize the bending stresses in the root have resulted in substantial improvements in operating life. Physical data indicate that the successful use of these materials would enable at least a 300° F increase and possibly greater increases in operating temperature; however, improved inspection procedures and methods to minimize impact damage are required.

[REDACTED]

TABLE I. - SUMMARY OF OPERATION OF CERMET TURBINE  
BLADES IN J33 TURBOJET ENGINE

TYPE ROOT	NUMBER OF RUNS	LONGEST RUN, TIME AT RATED SPEED, HR	REMARKS
FIR TREE	4	3	FAILED ACROSS TOP SERRATION
4-PIN	1	21	FAILED IN ROOT
INTERLOCK	9	68	FAILED IN ROOT
DOVETAIL	2	59	FAILED IN ROOT
SKEWED DOVETAIL	<sup>a</sup> 1	129	NOZZLE DIAPHRAGM FAILED - DAMAGED BLADES
	<sup>a</sup> 1	242	RUN DISCONTINUED - BLADES DID NOT FAIL
SKEWED DOVETAIL	<sup>b</sup> 4	---	COMPLETED 108 CYCLES - LARGE R BLADE FAILED IN ROOT

<sup>a</sup>DIFFERENT COMPOSITIONS USED.

<sup>b</sup>ENGINE OPERATED ON 15 MINUTE CYCLE INVOLVING VERY RAPID ACCELERATION AND DECELERATION.

CS-7968



### COMPARISON OF 100 HOUR STRESS RUPTURE STRENGTHS OF CERMETS AND ALLOYS

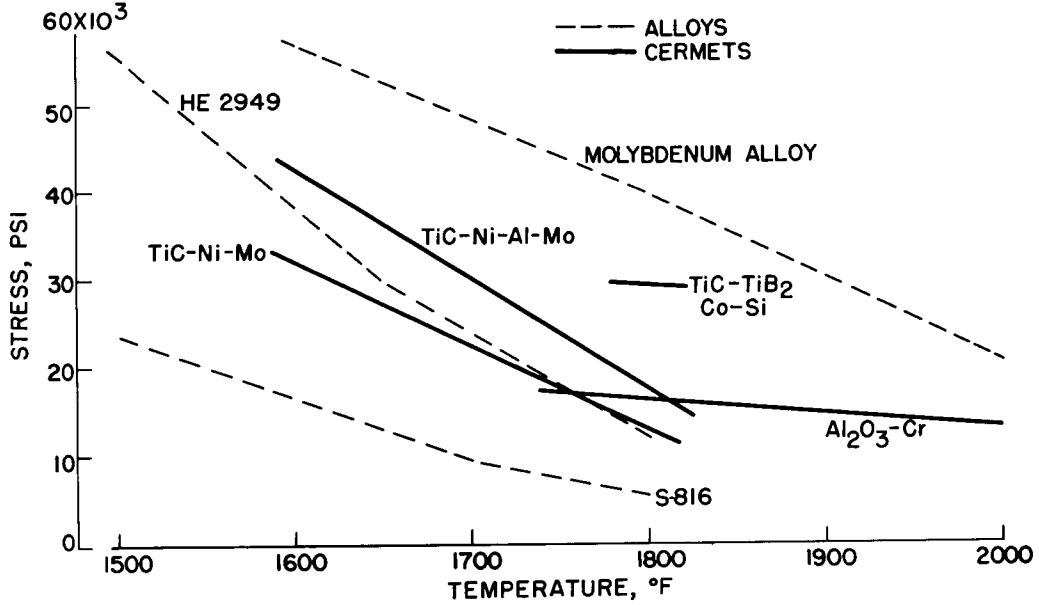


Figure 1

### COMPARISON OF 100 HOUR STRESS RUPTURE STRENGTHS OF CERMETS AND ALLOYS ADJUSTED TO DENSITY OF S-816

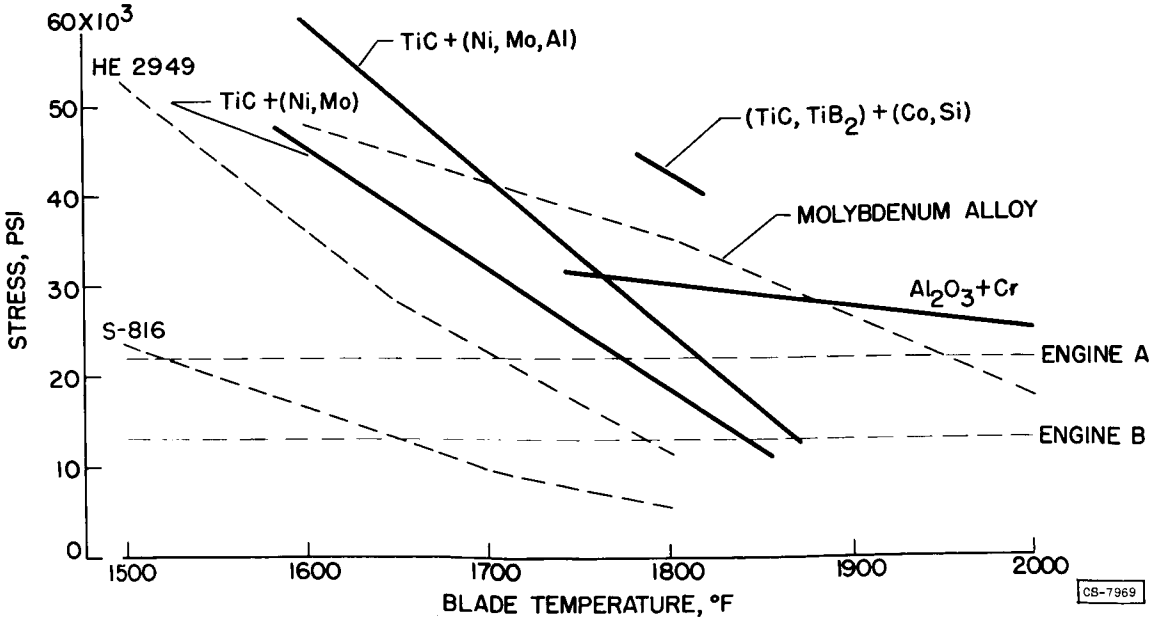
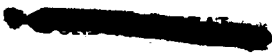


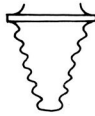
Figure 2



3078-17

CS-7969

CERMET BLADE ROOT DESIGN



STANDARD FIR TREE

DOVETAIL

EXPERIMENTAL CERMET ROOTS

USING SCREEN CUSHION



INTERLOCK

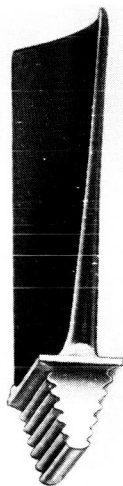
4-PIN

EXPERIMENTAL CERMET ROOTS USING  
DUCTILE RETAINING PINS

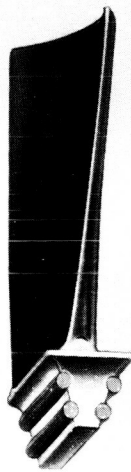
CS-7967

Figure 3

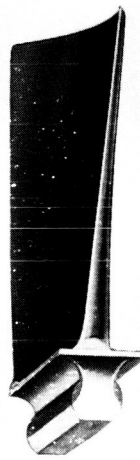
CERMET BLADES HAVING  
VARIOUS ROOT CONTOURS



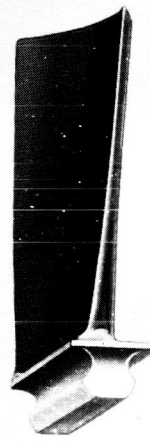
FIR TREE



4-PIN



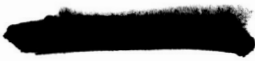
INTERLOCK



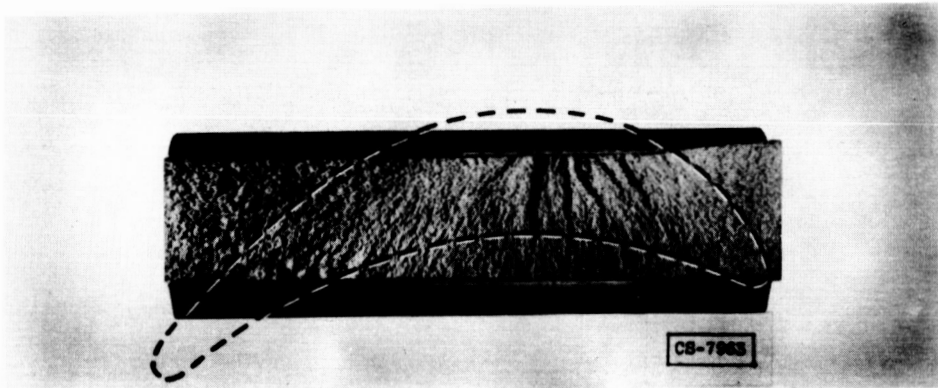
DOVETAIL

CS-7965

Figure 4



### AIRFOIL PROFILE SUPERIMPOSED ON CERMET BLADE ROOT FAILURE SURFACE



3078-F

Figure 5

### REDESIGN OF CERMET BLADES BY RELOCATION OF ROOT WITH RESPECT TO AIRFOIL

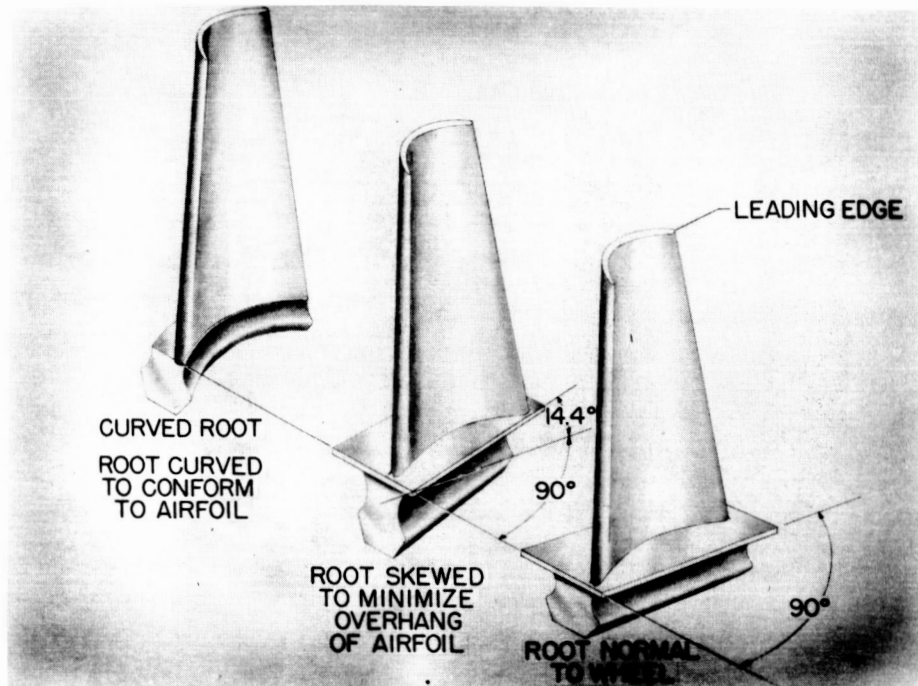


Figure 6



**FAILURE OF NOZZLE DIAPHRAGM  
SHROUD BAND AFTER 129  
HOURS OF OPERATION**

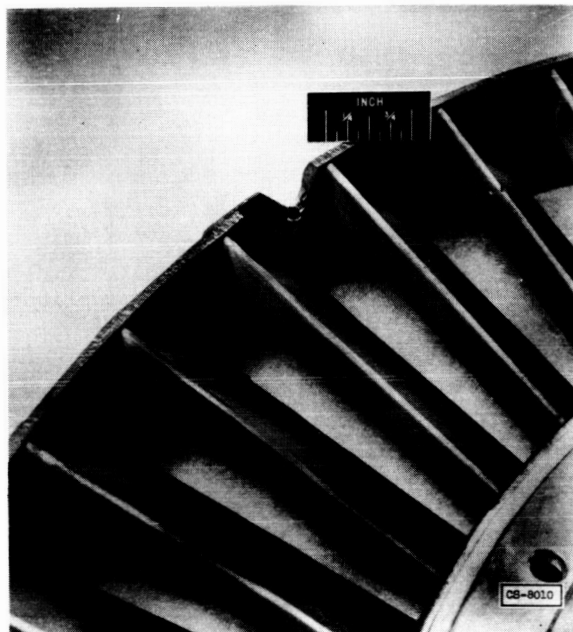


Figure 7

**DAMAGE TO ALLOY AND CERMET BLADES  
RESULTING FROM FOREIGN  
PARTICLE PASSING THROUGH TURBINE**

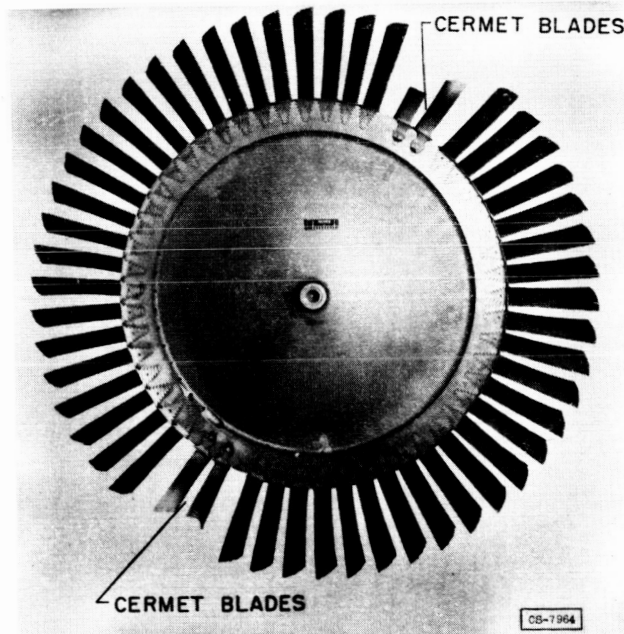


Figure 8

[REDACTED]

EXPERIMENTAL INVESTIGATION OF SEVERAL METHODS OF REDUCING  
THE WEIGHT OF COMPRESSOR AND TURBINE ROTORS OF  
TURBOJET ENGINES

By Richard H. Kemp, Marvin H. Hirschberg, and Merland L. Moseson

INTRODUCTION

Since high thrust per unit engine weight is a requirement for supersonic flight, it is of prime importance to attempt to reduce the structural weight of the engine as much as possible. In particular, certain modifications of the rotating components offer considerable gains in over-all weight savings because the weight of the supporting structure is dependent to a large extent on the weight of the rotating components. It is the purpose of this paper to discuss two such modifications. One is the substitution of plastics for the aluminum and steel components of axial-flow compressors and the second is the reduction in the weight of the turbine wheel through the use of sheet-metal blades and redesigned disks.

UTILIZATION OF PLASTICS IN COMPRESSORS

Plastics have been under consideration for application as axial-flow compressor blades, disks, and casing materials. Their use as blades, for example, would not only reduce the weight of the blading but would also reduce the weight of the disks required to carry the blades. From a vibration damping standpoint, plastics are promising because of their low density and high internal friction (see fig. 1). On the left side of the figure the aerodynamic damping is plotted as a function of the material density for various compressor blade materials. When a blade vibrates freely in an air stream, the air removes energy from the blade, thus decreasing the vibrational energy of the blade. This removal of energy is known as aerodynamic damping. The higher the aerodynamic damping, the less is the tendency for such excitations as rotating stall to induce destructive vibrations. In figure 1 it is seen that the plastic has an aerodynamic damping of 20.8 percent, which is considerably higher than that of the other applicable materials and is 4.5 times that of 403 stainless steel.

On the right side of figure 1 is a comparison of the internal or material damping of the same materials, plastic, aluminum, titanium, and 403 stainless steel. For some materials, the internal damping depends on the stress level; this is the case with the plastic considered, a laminated Fiberglas impregnated with a phenolic resin. For example, an

[REDACTED]

[REDACTED]

internal damping of 9 percent occurs at a vibratory stress level of  $\pm 5000$  pounds per square inch and 20.4 percent damping occurs when the vibratory stress level is at the endurance limit of  $\pm 25,000$  pounds per square inch. For comparison, the material damping for 403 stainless steel is 1.3 percent at  $\pm 5000$  pounds per square inch and 3 percent at the endurance limit of  $\pm 50,000$  pounds per square inch. The high material damping of the plastic is particularly advantageous when the aerodynamic damping cannot be relied upon; this can occur in stall flutter.

Although the damping and strength characteristics of the plastic blades appear favorable, certain unknowns such as fastening methods, erosion, and impact by foreign objects may affect engine life. In order to gain insight into unforeseen problems, the third stage of a J47 compressor was replaced with plastic blades supplied by Thompson Aircraft Products Co. The blades were fabricated from Fiberglas impregnated with a phenolic resin and were fastened in a die-cast aluminum base in the compressor rotor. The engine was operated at full power for over 100 hours without any failures of the plastic blades.

#### LIGHT-WEIGHT TURBINE WHEELS

In the case of the turbine wheel, the use of lighter blades can effect considerable savings in the total weight. Instead of using a substitute material of lower density, however, it is possible to reduce the blade weight by utilizing sheet-metal construction methods. The order of magnitude of the weight savings possible is illustrated in figure 2. The total wheel weight (disk plus blades but without shaft) is plotted on the ordinate as a function of individual blade weight for various arbitrary design stress levels in the center of the disk. For simplicity, the disks were assumed to be parallel-sided; for more efficient use of the disk material, taper would, of course, be incorporated. Two blade weights (including the base) were considered. The one at approximately 0.6 pound represents a conventional solid turbine blade and the one at 0.3 pound represents a hollow sheet-metal blade of comparable aerodynamic design. For example, for an arbitrary stress level in the center of the disk of 70,000 pounds per square inch, the wheel weight could be reduced from 225 pounds to 110 pounds by replacing the solid blade with the sheet-metal blade.

#### SHEET-METAL TURBINE BLADES

Since the use of sheet-metal blades poses a number of problems of design, fabrication, and operation, a study was initiated to learn more about this type of blading. Figure 3 illustrates the method of approach.

[REDACTED]

The two sides of the airfoils were formed independently in soft metal dies and were then welded together along the leading and trailing edges. In the welding process, the two sides were held in a jig and small tack welds were made. The airfoil was then removed from the jig and the welding completed; a helium-shielded electrode and filler rod of the parent metal were used. While the welding was being done, an inert gas was passed through the hollow portion of the airfoil, which substantially improved the quality of the weld by preventing undue oxidation from the inside.

Caps were formed to fit the open tip ends of the airfoils and were welded in place; a helium-shielded electrode and filler rod of the parent metal were again used. The tip caps were felt to be necessary to stiffen the tip region of the blade and reduce the vibrational stresses. The caps were fabricated from the same material as used in the airfoil sides.

To facilitate testing the sheet-metal blades in the turbojet engine, bases were formed by removing the solid airfoil portion from the standard turbine blade. The various sheet-metal airfoils were then attached to the standard bases and operated in the engine. Two methods of attachment were investigated. The first of these was welding as shown on the left side of figure 3. A stub (1/8 to 1/4 in. high) of the original airfoil was retained on the blade-base platform and machined to permit the sheet metal airfoil to slip over it. This stub then functioned as a positioning device. Welding was accomplished with a helium-shielded electrode and filler rod of the parent sheet metal after a preliminary tacking operation in a jig. The second method of attachment investigated was brazing, as shown on the right side of figure 3. The brazing process was tested, however, only on L-605 airfoils. The joint was made between the sides of the stub on the base platform and the inner wall of the airfoil. No attempt was made to obtain a joint between the top of the platform and the end of the airfoil. The entire load of the airfoil was thus transmitted by shear to the blade base.

Three methods of brazing were investigated: hydrogen atmosphere brazing, vacuum brazing, and salt-bath brazing. In each case, the airfoil was positioned on the stub of the base and tack-welded to hold it in place. Microbrazing material was then applied and the blades were heated to approximately 2150° F in the different mediums.

Three high-temperature alloys were selected from which to fabricate test blades. These were N-155, Inconel X, and L-605 and were chosen principally on the basis of availability and high-temperature physical properties of the sheet material. Airfoils were fabricated from 0.020-inch and 0.030-inch sheet N-155, and from 0.030-inch sheet L-605. Of the Inconel X material, airfoils were fabricated from 0.030 and 0.040-inch sheet and also from special taper-rolled sheet, 0.040 inch thick at the base of the blade and varying linearly to 0.020 inch thick at the tip. Particular attention was paid to the rolling direction to utilize the best properties of the sheet.

## ENGINE OPERATION OF SHEET-METAL BLADES

After attachment of the sheet-metal airfoils to the modified bases, they were installed in a conventional turbine wheel. Testing of the blades was accomplished by operation of the engine continuously at military take-off conditions until failure occurred. The turbojet used was the J47-25; the set conditions were an engine speed of 7950 rpm and a tail-pipe temperature of 1260° F.

A summary of the test results on the various sheet-metal blades is given in table I. The 0.020-inch N-155 blades failed very early from cracking of the sheet metal in the vicinity of the tip. Since it was felt that these blades were too weak from a vibration standpoint, the wall thickness of the next blades tested was increased to 0.030 inch. Early failures again occurred but were located in the weld at the base. Examination of the welds showed gross defects to which the premature failures could be attributed. All the Inconel X blades which failed were likewise found to have faulty welds at the base; the time to failure was of the order of 1 hour. Two of the Inconel X blades were not operated to failure, but were also found to have imperfect welds.

Operation of the L-605 sheet-metal blades was considerably more encouraging. It was found that the quality of the welds obtainable was superior to those for the N-155 or Inconel X blades. The thickness of the L-605 sheet used was 0.030 inch. Four methods of attachment were attempted: welding, dry-hydrogen brazing, vacuum brazing, and salt-bath brazing. Table I shows the engine operating times obtained and indicates that, with reasonable control of the attachment processes, lives of at least 30 hours could be expected at military take-off conditions. Five blades which were salt-bath brazed to 1/8-inch stubs were operated for 29 hours and 48 minutes at military take-off conditions without damage occurring to any of the blades. One of these blades is shown in figure 4 after operation. The test was terminated because of unrelated engine operating difficulties.

## INTEGRAL BRAZED ROOT DESIGN

The integral brazed root design was completed first and is shown in figure 6. The two disks were parallel-sided N-155 rolled plates, 5/16 inch thick. Five holes were located near the center for spacers and bolts which attach the wheel to the shaft hub. The blade bases were Microbrazed to the disks in a dry-hydrogen-atmosphere furnace at 2150° F. The airfoils (0.030-in. L-605) were then brazed to the 1/8-inch stubs on the bases in a second pass through the furnace. The ends of the blades were ground to a specified diameter and the tip caps were welded in place.

One of the principal design problems was the support for holding the wheel in the furnace at 2150° F. It was necessary to provide a surface

3078-F

[REDACTED]

approximately the same diameter as the wheel which would remain flat and not warp or buckle. Tests of various fabricated structures indicated that they would not support the wheel without sagging or warping. The solution to the problem was found in tests of small silicon carbide grinding wheels heated to 2150° F. The wheels did not distort or crack if the heating cycle was carried out in the normal manner. A 40-inch silicon carbide wheel was obtained and encased in a thin envelope of Inconel to prevent contamination of the hydrogen atmosphere. A bleed-off tube was run from the envelope to the outside of the furnace to permit the expanding gases to escape on heating. Machined rings were placed on the grinding wheel and the turbine wheel was supported on these rings.

3078-F

The completed wheel was operated in a J47-25 engine for approximately 1/2 hour with about 2 minutes of the time at military take-off conditions. Excessive growth of the wheel occurred, permitting the blades to rub on the shroud band and causing failure of one of the blades. Upon examination, it was found that the disks had flowed plastically, particularly around the bolt holes and it was determined that the failure was associated with the brazing operation as illustrated in figure 7. On the ordinate is plotted the ratio of the disk operating stresses to the yield strength of the material. The smaller this ratio, the greater is the safety factor. The disk radius is plotted on the abscissa. According to published information on the strength of N-155, the design stresses were computed and are shown in the lower curve of figure 7, indicating a substantial margin of safety. However, the yield strength was markedly reduced by the brazing operation and the operating stresses became very close to the yield stress, as shown by the upper curve. The stress concentrations associated with the bolt holes caused the stresses to exceed the yield point and hence accounted for the growth of the wheel.

#### Built-Up Brazed Root Design

The second complete wheel to be fabricated was the built-up brazed root design as shown in figure 8. The problem of reduction of the disk yield strength by the high brazing temperature was solved by cutting out the center of the N-155 disks and welding in SAE 4130 as shown in figure 8. By this means, the yield strength in the center of the disk was substantially increased over that available with N-155. Rated speed was attained in the operation of the wheel in the J47 engine with no plastic flow occurring in the disks. However, cracks developed in several of the blades and one blade was lost. The test was then terminated to permit repair of the wheel.

#### Serrated Root Design

The third complete wheel to be fabricated was the serrated root design as shown in figure 9. Again a composite disk was used with SAE 4340

[REDACTED]

[REDACTED]

in the center welded to a rim of Timken 16-25-6 alloy. In the engine operation of this wheel, rated speed was achieved and held for 15 minutes. Again no plastic flow of the disks occurred, but excessive bowing of the platform of the base resulted as shown in figure 10. This distortion could probably be eliminated by stiffening the platform in one of several methods. A stub on the top of the platform could be integrally cast with the base, and then the airfoil could be brazed instead of welded to the stub. A second method would be to cast an integral web beneath the platform.

#### CONCLUDING REMARKS

Several methods of increasing the thrust per unit engine weight by reducing the weight of the rotating components have been illustrated. It was shown that conventional compressor blading can be replaced with light-weight plastic blades and that the weight of the disks required to carry the blades can thereby be reduced. The possibilities for the reduction of the turbine-wheel weight were demonstrated through the use of hollow sheet-metal blades and complete wheels operated in a J47 engine. The light-weight wheels represented a weight reduction of approximately 40 percent in comparison with the standard wheel. In addition to the many problems of design and fabrication of the components which were considered, other factors such as vibration of the thin disks, creep, gyroscopic loadings, and warpage must all be investigated. Also, cooling systems will be required if less strategic materials are to be used or if turbine-inlet temperatures are to be raised.

TABLE I. - ENGINE OPERATION OF SHEET METAL TURBINE BLADES

Sheet metal alloy	Wall thickness	Method of attachment to base	Stub height	Time of operation at rated conditions		Remarks
				Hr	Min	
N-155	.020	Welded	1/4	0	23	Cracks developed in sheet metal, probably due to vibration. Examination showed Weld at base failed. Cracks in weld at base. } poor quality welds. Crack in weld at base.
N-155	.020			0	23	
N-155	.020			0	23	
N-155	.030			0	6	
N-155	.030			0	6	
N-155	.030			0	6	
Inconel X	.030	Welded	1/4	0	31	Weld at base failed, poor weld. Blade removed - no visible damage. Weld at base failed, poor weld. Blade removed - no visible damage. Weld at base failed, poor weld.
Inconel X	.030			0	31	
Inconel X	.040			1	31	
Inconel X	.040			1	31	
Inconel X	Tapered			1	45	
Inconel X	0.040-0.020			1	45	
Inconel X	Tapered	Vacuum-brazed to stub	1/8	1	45	Blade removed - no visible damage. Weld at base failed, weld defective. Removed due to impact damage. Airfoil failed at midspan. Removed due to impact damage. Failed in braze, gross braze defects. Removed - no damage. Removed - no damage.
L-605	.030			33	3	
L-605	.030			32	17	
L-605	.030			15	39	
L-605	.030			15	39	
L-605	.030			11	2	
L-605	.030	22	58	Failed in braze, gross braze defects. Removed - no damage. Failed in braze joint. Crack in tip cap. Tip section torn off by impact. Failed in braze, gross braze defects. No damage to blades. Test terminated due to engine difficulty.		
L-605	.030	22	58			
L-605	.030	40	2			
L-605	.030	25	50			
L-605	.030	29	48			
L-605	.030	7	46			
L-605	.030	3	58	Test terminated; no damage to blades.		
L-605	.030	3	58			
L-605	.030	29	48			
L-605	.030	29	48			
L-605	.030	29	48			
L-605	.030	29	48			

**DAMPING CHARACTERISTICS OF SEVERAL COMPRESSOR BLADE MATERIALS**

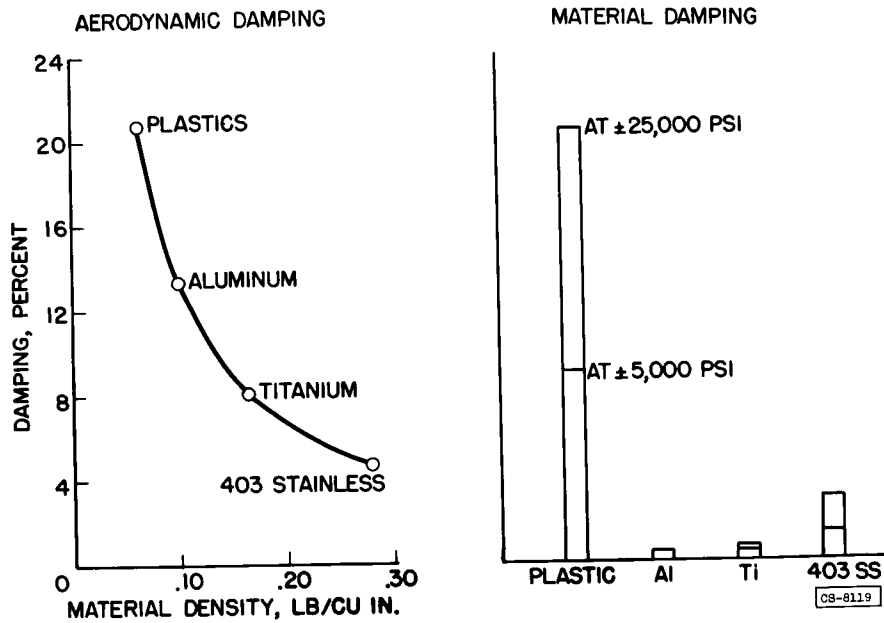


Figure 1

**EFFECT OF BLADE WEIGHT ON TOTAL WHEEL WEIGHT**

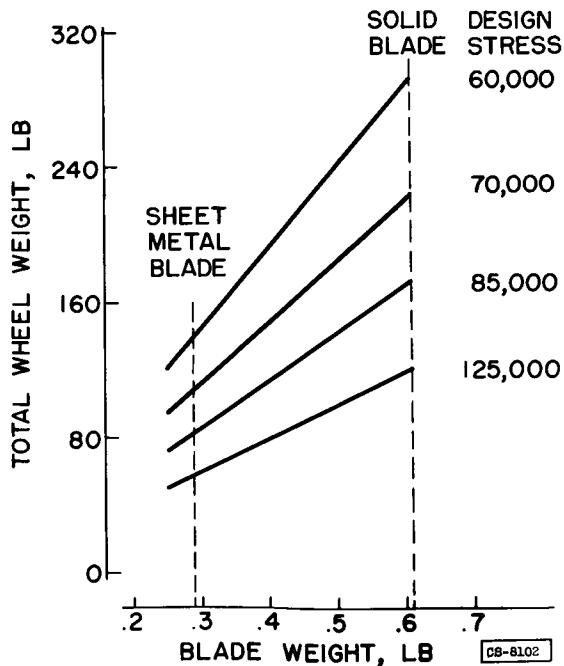
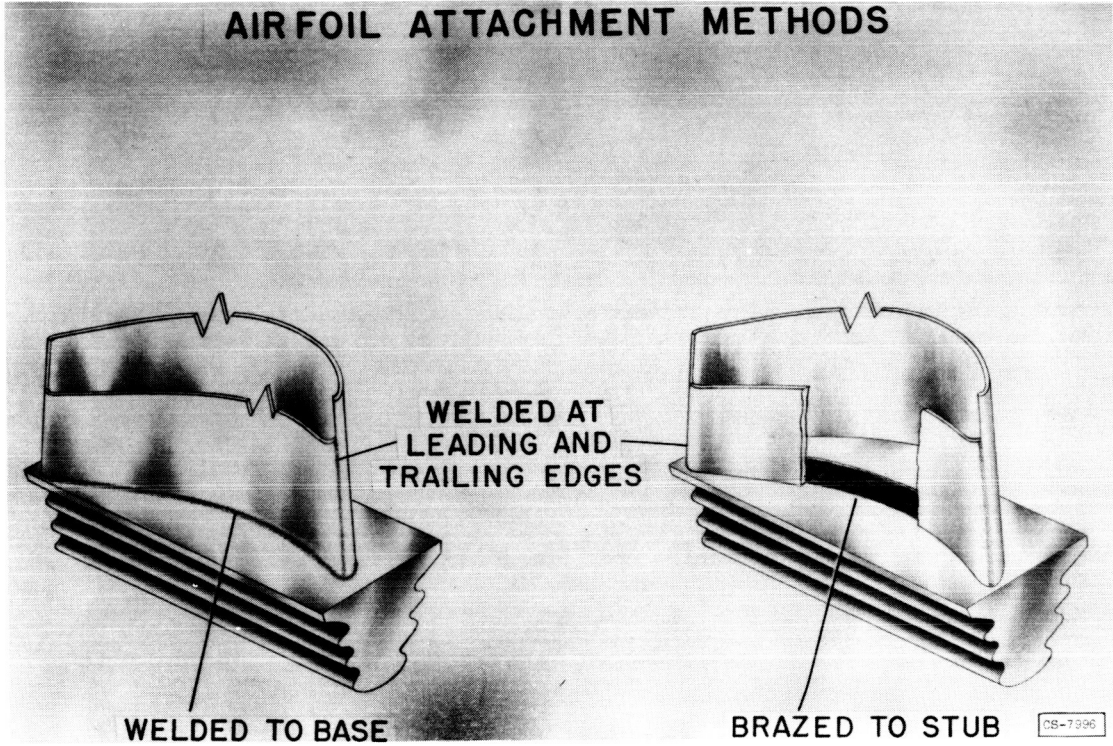


Figure 2

3078-F

**AIRFOIL ATTACHMENT METHODS**



**Figure 3**

**SHEET METAL BLADE AFTER APPROXIMATELY 30 HOURS OPERATION**

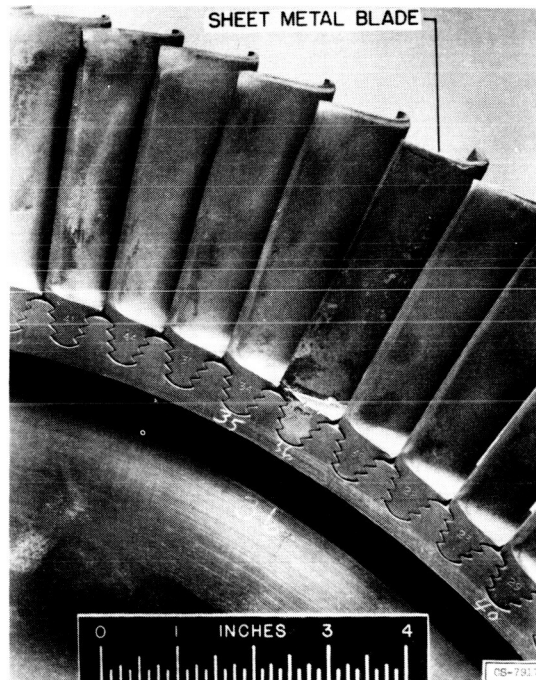


**Figure 4**

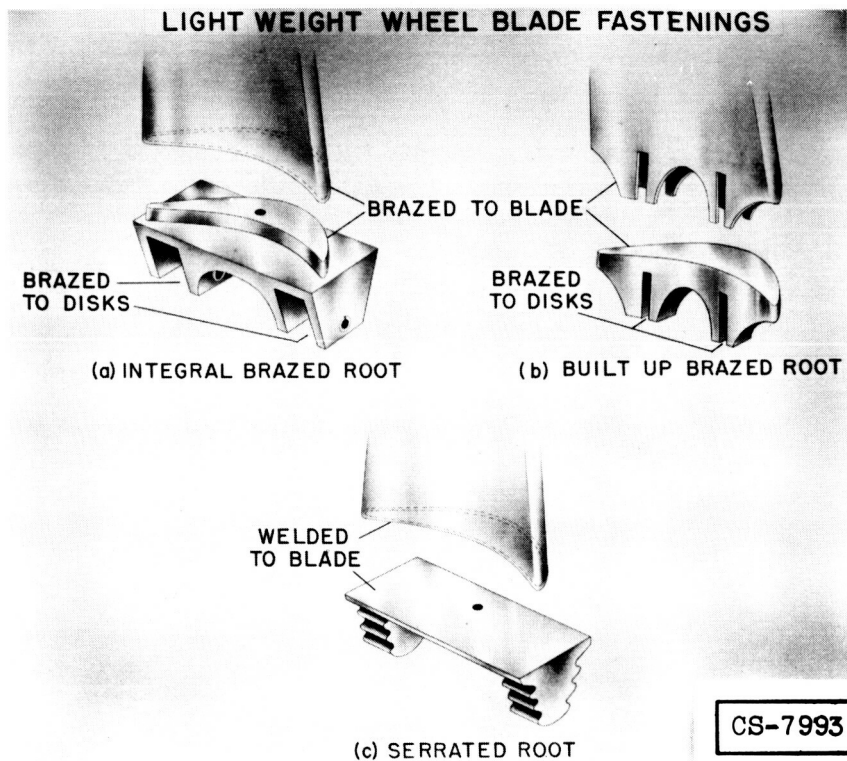


Figure 5

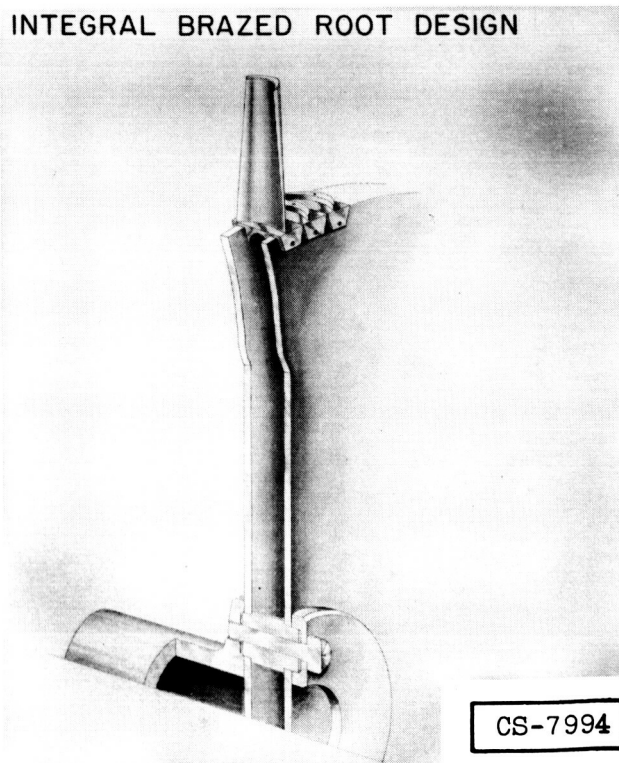


Figure 6

EFFECT OF BRAZING TEMPERATURES ON STRENGTH OF N-155 DISK

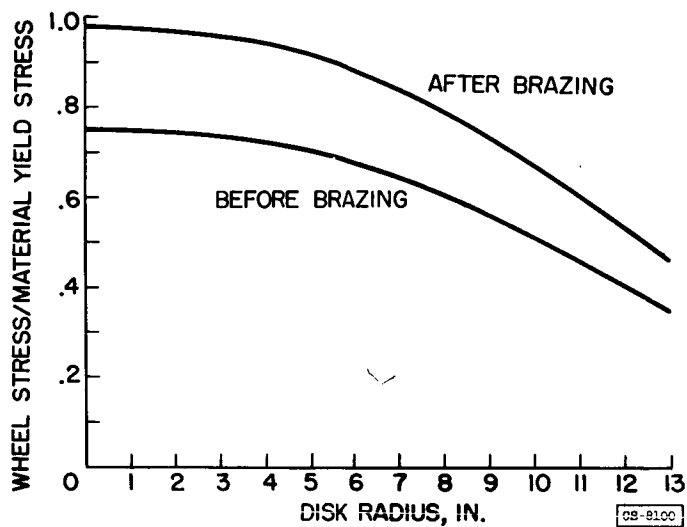


Figure 7

BUILT UP BRAZED ROOT DESIGN

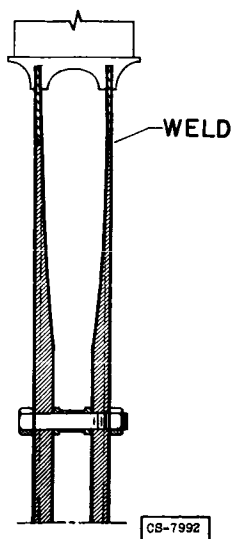
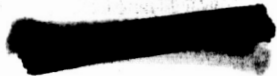


Figure 8



### SERRATED ROOT DESIGN

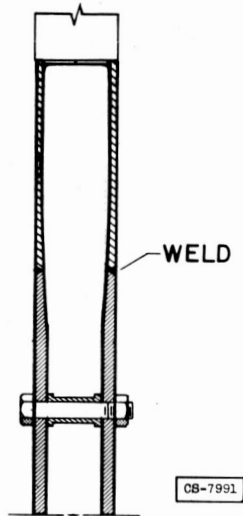


Figure 9

### AFTER OPERATION AT RATED ENGINE SPEED BLADE WITH SERRATED-ROOT DESIGN

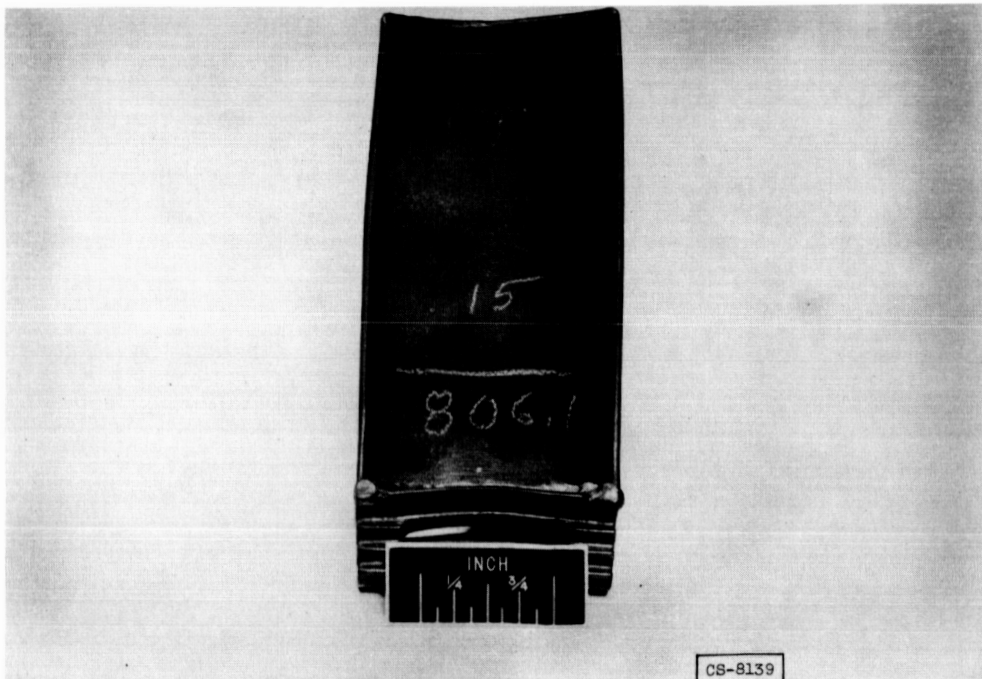


Figure 10



## NACA RESEARCH ON LUBRICANTS AND BEARING MATERIALS

## FOR HIGH-TEMPERATURE TURBINE ENGINES

By R. L. Johnson and E. E. Bisson

## SUMMARY

Studies are reported which have been aimed at increasing the maximum temperatures for lubrication systems of turbojet engines for high-speed flight. Separate studies of lubricants, bearing materials, and improved lubrication methods have been in progress.

Available and new synthetic lubricants are satisfactory for engines now being developed, but their use in future engines may not be satisfactory with bearing temperatures of  $750^{\circ}$  F or higher. For the extremely high bearing temperatures ( $750^{\circ}$  and  $1000^{\circ}$  F), possible lubricants may include future synthetic liquids, solids (e.g.,  $\text{MoS}_2$ ), or gases (e.g., air).

Molybdenum tool steels have promise for races and rolling elements of high-temperature rolling contact bearings. Nickel alloys, nodular iron, and powdered metal compacts containing solid lubricants may be useful as cage materials for the high-temperature ( $750^{\circ}$  and  $1000^{\circ}$  F) bearings.

Bearing designs that provide an easy flow path for the lubricant are promising for high speeds and possibly for high temperatures. Considerable research is required both on new lubricants of all types for high temperatures and on the fatigue properties of potential high-temperature ( $750^{\circ}$  and  $1000^{\circ}$  F) bearing materials.

## INTRODUCTION

Turbine engines for high flight speeds will operate at extreme temperature conditions (refs. 1 to 3). High ambient temperature as well as high heat load (for both bearings and lubricants) will be characteristic of these engines; the high temperatures and high heat loads are a direct result of high ram temperatures, high compressor-discharge temperatures, and high turbine-inlet temperatures. For example, Drabek in reference 2 shows that at approximately 50,000 feet altitude, a Mach number of 2.0, an NACA standard day, ram temperature of  $250^{\circ}$  F, and with compressor pressure ratios of 5 and 15 the compressor-discharge temperatures would be  $680^{\circ}$  F and  $1060^{\circ}$  F, respectively. The bearings are normally cooled by the lubricant which is, in turn, cooled by fuel; a problem is therefore imposed because of the limited heat-absorbing capacity available from the fuel. This limiting of available heat-absorbing capacity is a

result of (1) the increased fuel temperatures (as ambient temperatures and heat load increase), (2) the fact that the fuel is used to cool other airplane components such as hydraulic fluids and aircraft skin surfaces, (3) loss of heat sink as a result of fuel consumption, and (4) the markedly reduced fuel flow without appreciable decrease in heat load at high altitudes when only the fuel flow to the engine is used for cooling. The cumulative effect of the increased ambient temperatures, increased heat loads, and reduced heat-absorbing capacity of the fuel would increase bearing and lubricant temperatures. Thus, unless the complexity, weight, and cost of a refrigeration system for lubricant cooling can be tolerated, there is a definite requirement for bearings and lubricants capable of operation at elevated temperatures.

The discussions of references 1 to 3 and consideration of extreme flight speeds indicate that there are four general temperature ranges of interest, as shown in table I. The tabulation shows that for current and development engines (temperature ranges 1 and 2), maximum bulk lubricant temperatures are 200° and 300° F, maximum bearing operating temperatures are 350° and 500° F, and maximum bearing "soak-back" temperatures are 500° and 700° F. (The "soak-back" temperatures are the temperatures attained by the bearings after the engine is shut down and coolant flow ceases while heat continues to flow into the bearings from hot parts of the rotor, such as the turbine wheel, and from other high-temperature surroundings.) In future engines (for transonic and supersonic flight and particularly in engines for guided missiles), design objectives include maximum bearing operating temperatures of 750° and 1000° F (temperature ranges 3 and 4, table I).

It should be noted that the problems with respect to a "short-time engine" (such as an expendable engine for a guided missile) may be considerably different from the problems for a "long-time engine" (such as an engine designed for long life in aircraft applications).

NACA studies of lubrication and wear problems for high-speed engines have been aimed at increasing the maximum temperatures at which effective operation of lubrication systems and bearings can be obtained. This research involves separate studies of lubricants, bearing materials and designs, and improved lubrication methods.

#### LUBRICANTS

As a consequence of the relatively low temperature levels of most current engine operation (temperature range 1), petroleum lubricants meeting the MIL-O-6081A specification for grades 1010 and 1005 (10 and 5 centistokes viscosity at 100° F, respectively) are generally satisfactory. In temperature ranges 2, 3, and 4, however, where temperatures are

[REDACTED]

appreciably higher, the petroleum lubricants do not have the required combination of properties (among others, low viscosity at  $-65^{\circ}$  F for adequate "pumpability" and low volatility at high temperatures for low oil consumption). As a consequence, synthetic lubricants and other lubricant types are necessary.

One of the very difficult problems with liquids is that of maintaining low volatility at high temperature while meeting the "pumpability" requirement for low viscosity at  $-65^{\circ}$  F since for any one class of lubricant, low viscosity is generally accompanied by high volatility.

At temperatures above those at which liquid lubricants are practical, other lubricant types such as the solids or gases must be investigated.

### Liquids

As indicated in references 1 and 3 and elsewhere, liquid lubricants for use in aircraft turbine engines must meet the following important requirements:

(1) Adequate low-temperature pumpability to permit engine starting at  $-65^{\circ}$  F (the present military specification MIL-L-7808 calls for a maximum viscosity at  $-65^{\circ}$  F of 13,000 centistokes)

(2) Low volatility and adequate resistance to foaming to prevent excessive oil consumption (lubricants having evaporation rates which are in general no greater than 10 percent that of grade 1010 petroleum oil at  $400^{\circ}$  F are desirable)

(3) High-temperature stability with regard to oxidation and decomposition (the lubricant must also be noncorrosive to the various metals of the engine)

(4) Adequate load-carrying capacity to effectively lubricate bearings and gears (a load capacity equivalent to that of a lubricant with the viscosity of grade 1010 (10 centistokes at  $100^{\circ}$  F) has generally been considered marginal in present production turbojet engines; hence, a load capacity equivalent to those of lubricants with the viscosity of grade 1065 (approximately 100 centistokes at  $100^{\circ}$  F) or grade 1100 (approximately 270 centistokes at  $100^{\circ}$  F) is more to be desired)

Other properties, such as toxicity and effect on sealing materials and paints, are also important. Properties of some fluids which partly meet these requirements are listed in table II; these were the fluids included in the NACA high-temperature lubrication investigation.

Lubricating effectiveness at high temperatures. - Studies were made of the lubricating effectiveness at high bulk lubricant temperatures of

[REDACTED]

the various lubricants of table II. These studies are described in detail in reference 4 and were made on an apparatus (fully described in ref. 5) shown schematically in figure 1. The specimens consist of a rotating steel disk (hardness, Rockwell A-50) and a spherical-tipped steel rider (hardness, Rockwell C-60).

Dead weight loading is used to apply the load through the pulley system shown in figure 1. The load used in this investigation was 1000 grams (initial Hertz surface stress, 149,000 psi) and the sliding velocity was 120 feet per minute. Friction force was measured by means of four strain gages mounted on a copper-beryllium dynamometer ring.

The experimental procedure consisted in starting each test with a new set of friction specimens and 440 cubic centimeters of fresh fluid. The apparatus was started simultaneously with the application of heat, and friction readings were taken at 45° F intervals, or more often if necessary. The average time required to raise the temperature of the fluid from 100° to 500° F was 55 minutes. Lubrication failure was easily determined during the experiment as (1) increase in friction force, (2) onset of instability in the friction readings, (3) audible chatter of the sliding specimens, or (4) thermal instability of the bulk lubricant. After the runs in which lubrication failure occurred, visible surface damage was observed. Preliminary wear tests conducted with some of these lubricants showed that either unstable friction values or increases in the coefficient of friction were accompanied by a sharp increase in the rate of wear.

In figure 2 are shown photomicrographs of surfaces which are considered typical of those obtained with three conditions of lubrication: (1) completely effective lubrication, (2) incipient failure in which there was slight evidence of surface welding and metal transfer, and (3) mass failure in which there was violent welding and metal transfer. In all cases there is a large supply of oxygen available in the lubricants, both in these experiments and in actual turbine engines, because of violent agitation of the lubricant.

The results obtained showing the effect of temperature on friction of steel specimens boundary-lubricated by the various synthetic lubricants of table II are shown in figures 3 to 5. As previously indicated, those data were obtained with a load of 1000 grams and at a sliding velocity of 120 feet per minute. In figures 3 to 5 the regions of friction instability (where incipient lubrication failure occurred) are indicated by cross-hatched areas. Effective boundary lubrication was obtained at temperatures lower than those indicated by the cross-hatched areas. The occurrence of high friction coefficients (above 0.3) as the runs were terminated was usually indicative of mass surface failure. The petroleum lubricant, grade 1010 (fig. 3(a)) is included for purposes of comparison. The compounded diester of figure 3(b) is a lubricant of

the MIL-L-7808 specification type. This lubricant does not quite meet these specifications, however, because of slightly excessive viscosity at  $-65^{\circ}\text{F}$  (16,000 centistokes as compared with a maximum specified value of 13,000 centistokes).

The performance of the base stock, di(2-ethylhexyl) sebacate with and without additives, is shown in figure 4. Comparison of figure 3(b) and figure 4(a) shows the compounded diester to have appreciably better high-temperature performance than the base stock alone. The increased lubricating effectiveness of the compounded diester over that of the base stock at higher temperatures is shown in figure 4 to be a function of a partial lubrication contribution by the tricresyl phosphate (fig. 4(c)) and is not dependent on the presence of the oxidation inhibitor (fig 4(b)) or the viscosity index improver (fig. 4(d)). The curves of figure 4 show that instability starts at essentially the same temperature for all except the solution of tricresyl phosphate in di(2-ethylhexyl) sebacate.

Comparison of the results (fig. 3) with the various fluids of this investigation shows that the phosphonate and silicate esters appear to be promising for high-temperature operation. The phosphonate was a completely effective lubricant throughout the entire temperature range to  $572^{\circ}\text{F}$ . At this temperature, however, the fluid refluxed violently, decomposed, and left a reddish brown gel as a residue. The wear track showed no damage and very slight wear, but the surface of the steel specimen appeared to be etched as if by acid wherever contact with the fluid had taken place. Chemical attack of the surfaces to form a lubricating reaction product is a logical explanation for the lubricating effectiveness of this fluid at high temperatures. Visual inspection of the different specimens operated in different phosphonate esters (ref. 4) showed that considerable etching had occurred as a result of the chemical attack. Considerable chemical attack of lubricated parts might be tolerable in a short-time engine (for example, an expendable engine for guided-missile application); therefore, the phosphonate esters might be promising for such short-time operation at relatively high temperatures.

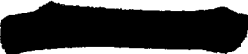
The tetra(2-ethylhexyl) silicate ester (fig. 3(e)) also appears promising for operation at high temperatures. The silicate ester is, however, thermally unstable at bulk temperatures of approximately  $540^{\circ}\text{F}$ . As a consequence, the NACA lubrication studies were limited to a maximum temperature of  $510^{\circ}\text{F}$ . As reported in reference 4, the presence of an oxidation inhibitor (phenyl- $\alpha$ -naphthylamine) appeared to have no effect on the lubricating characteristics of the silicate ester. The oxidation inhibitor also appeared to have no effect on the temperature of thermal instability of the fluids (approximately  $540^{\circ}\text{F}$ ). There was no visible evidence of etching of the steel specimens used in the experiments (ref. 4) with the silicate esters. At this time there is no explanation for the lubricating effectiveness of the silicate esters at high temperatures.

Some improvement in high-temperature lubrication properties of liquids can be obtained provided relaxation of the specifications on low-temperature viscosity is permitted. For example, if it is permitted to use fluids of viscosities higher than the MIL-L-7808 specification value of 13,000 centistokes maximum at  $-65^{\circ}$  F, improved high-temperature stability with respect to volatility and decomposition is usually obtained. This point is illustrated in figure 5, which shows the frictional results for a series of water-soluble polyalkylene glycol fluids having essentially the same structure except for chain length and varying in viscosity from 8.9 to 762 centistokes at  $100^{\circ}$  F. The results obtained at the high temperatures indicate a definite relation to some property commonly associated with viscosity grade, since increasing viscosity is shown to result in an increase in the temperature of incipient failure. For example, incipient surface failure starts at  $290^{\circ}$  F for the 8.9-centistoke fluid, whereas the 762-centistoke fluid shows incipient surface failure starting at  $501^{\circ}$  F. It should be emphasized that increases in temperature with increase of viscosity may be true only within a specific fluid class.

The limiting temperatures at which lubrication failure occurred are not necessarily the bulk lubricant temperatures to which the lubricants can be utilized in practical bearing lubrication. Factors other than lubrication failure may become the limitation; for example, chemical effects such as decomposition, corrosion, and fluid oxidation may limit the use temperature to values lower than those of figures 3 to 5. Since the chemical effects are time-temperature dependent, it may, however, be possible to use these lubricants up to the lubrication failure temperature for short-time applications such as expendable engines for guided missiles. For long-time operation, the use of these fluids will probably be limited to temperatures lower than those for lubrication failure.

The maximum allowable bearing temperatures may be substantially above the bulk oil temperature limits indicated herein. In bearing lubrication, the oil is normally supplied at low "oil-in" temperatures, and the oil residence (dwell) time may not be sufficient so that high bulk oil temperatures are obtained. In some full-scale bearing experiments with low oil-in temperatures, adequate lubrication has been obtained with bearing temperatures approximately  $200^{\circ}$  F higher than the temperature reported herein for incipient surface failure with the same lubricant.

Lubricating effectiveness at high sliding velocities. - Studies reported in reference 6 on the lubricating effectiveness of many of these fluids at high sliding velocities showed that, with some exceptions, there is a general correlation between the maximum temperature of effective boundary lubrication and the limiting sliding velocity for effective boundary lubrication. That is, those fluids which lubricate at high temperatures also, in general, lubricate at high sliding velocities.



## Solids and Gases

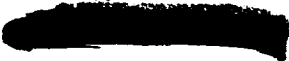
Liquids are inherently temperature-limited because of thermal instability; however, solid or gaseous lubricants may have promise for the extreme high-temperature applications. Solids can be obtained which are either stable at the elevated temperatures or whose instability does not adversely affect the frictional properties of the surfaces to be lubricated. Similarly, gases (such as air) are extremely stable at elevated temperatures.

Solids. - Solids may be used for lubrication in essentially two manners: (a) by including the solid as a minor constituent of the material to be lubricated, and (b) by introducing the solid with an "air-mist" system similar to that described in reference 7 or mixed with a volatile fluid carrier.

Lubrication by a constituent from within the structure of one of two rubbing parts is well known. Common examples of this type of lubrication are found in the use of leaded bronze which forms a lubricating film of extruded lead and also in cast iron which provides graphitic carbon for the lubricating film. Similarly, materials can be made by powder metallurgy techniques which employ, as a minor constituent, solid materials which are excellent lubricants. Results obtained on materials of this type (containing molybdenum disulfide as the solid lubricant) are included in reference 8. As this reference shows, mixtures of silver, copper, and molybdenum disulfide were quite effective in producing low friction and low wear with certain optimum concentrations of molybdenum disulfide. Under the conditions of the experiments of reference 8 this optimum concentration was approximately 7 to 10 percent. These results show that, even under extreme conditions of operating dry, it is possible to obtain moderate wear rates, complete absence of welding, and moderately low friction coefficients.

Lubrication of bearings by the use of solids in an "air-mist" system is discussed in reference 7. The results of reference 7 show that it is possible to operate conventional rolling contact bearings under either high temperatures (to 1000° F) or at high speeds (to DN values of 1,000,000). It was not possible in the preliminary investigation of reference 7 to combine the two variables of high temperature and high speed since the test rigs were limited in either case. Additional research with new apparatus under combined conditions of high speeds and high temperatures is planned.

Gases. - Bearings employing air only as the fluid have been considered as a possible solution to the high-temperature problem, because air bearings would not be subject to fatigue failure or to thermal instability



limitations of the lubricant at high temperatures. In this case, the air serves a different function from the air-mist system. The air-lubrication method provides for the load to be supported by air in an externally pressurized hydrodynamic bearing. The air bearing has the advantage of being generally unaffected by temperature except to show an increase in load-carrying capacity. The disadvantages of the air bearing include the requirement for a high-pressure air source and the necessity for small clearances and careful alignment. Although the studies of reference 9 were limited to a nonrotating bearing, they did show that the air bearing has possibilities for supporting load in a relatively stable manner at temperatures of 1000° F.

#### Temperature Ranges for Various Lubricant Types

A summary of the possible lubricants for operation over the four temperature ranges of table I is shown in table III. As shown, petroleum lubricants of the MIL-O-6081A type are suitable for temperature range 1; synthetic lubricants (presently, diesters of the MIL-L7808 type) are suitable for temperature range 2; solids, gases, or liquids (possible future synthetics) may be suitable for temperature range 3; and, in all probability, only solids and gases will be suitable for the extreme conditions of temperature range 4. Solid lubricants such as MoS<sub>2</sub> may be utilized in an air-mist system where the solid lubricant is suspended in a fluid such as air and continuously supplied to the bearing at a very slow rate (of the order of ounces per hour). As indicated in table III, additional research is required on high-temperature stability and high-temperature lubricating effectiveness of lubricants for temperature ranges 2, 3, and 4.

#### BEARINGS

The problem of operation of bearings at increased temperatures with high load and surface speed will be extremely difficult. In particular, the cage (retainer or separator) problem (specifically, either compatibility of the cage rubbing against the races or cage breakage) is critical at present and is expected to become more severe (Wellons, ref. 2). Provided other limitations can be eliminated, fatigue, while not critical at present, will become the limitation for the thrust bearing operating at high speeds in future engines (Macks, ref. 2).

Figure 6 serves to define the terminology of this discussion with respect to the various parts of a typical high-speed rolling contact bearing design.

## Materials for Races and Rolling Elements

Properties of materials. - The physical properties and requirements of bearing materials for operation at high temperatures have been discussed in reference 2. The most important required properties are as follows:

- (1) Minimum hardness of Rockwell C-58
- (2) Dimensional stability at operating temperature
- (3) Minimum critical alloying elements (particularly tungsten)
- (4) Oxidation resistance at operating temperature and at room temperature
- (5) Reasonable heat-treatment and grinding characteristics
- (6) Ready availability from several sources

Based on these requirements, the molybdenum tool steels appear to show considerable promise as high-temperature bearing materials. Molybdenum tool steels have good hot hardness and dimensional stability at elevated temperature although they are more difficult to grind than SAE 52100 steel (Wellons, ref. 2).

Fatigue properties. - Because of the importance of fatigue and the lack of data on fatigue lives of the tool steels at high loads, high DN values, and high temperatures of future engines, the NACA has initiated fatigue studies in an apparatus described fully in reference 10. The fatigue spin rig is shown in figure 7. Essentially the apparatus consists of a raceway A which is resiliently mounted in the horizontal plane on toothpick springs B, a vertically adjustable nozzle assembly C, and a vertically adjustable bottom plate D. Pressurized air, entering at E, causes two or more balls to rotate within the raceway. The spent air is allowed to escape at F. The speed of ball rotation is controlled by adjusting the pressure of the air entering at E.

Under proper conditions of operation, the balls lift from the bottom plate to ride at an equilibrium position on a vertical raceway wall. Acceleration, gyroscopic, and aerodynamic forces apparently provide the lifting and required stabilization. An analysis of this phenomenon was unsuccessful because of the unknown aerodynamic forces.

Inasmuch as a pair of balls, or a trio of balls of proper mass ratio, rotate in dynamic equilibrium, and since the balls do not touch any surface except the raceway wall, the loads at the respective contact areas between the balls and the cylinder may be accurately calculated.

These loads are caused by the centrifugal forces resulting from the orbital motion of the balls about the raceway axis. Rolling motion under elastic deformation occurs between the surfaces in contact. The stresses produced in the subject apparatus bear the same relation to load as do the stresses in a loaded ball bearing. Surface compressive and tangential stresses and subsurface shear stresses are imposed at the contact area and within the stressed volume, respectively.

Stress frequencies to over 10,000,000 cycles per hour and stress magnitudes to over 700,000 pounds per square inch (calculated Hertz maximum stress) have been obtained. For purposes of comparison, usual fatigue research is carried out at stress frequencies less than 1,000,000 cycles per hour and at stress magnitudes under 200,000 to 300,000 pounds per square inch. In general, turbojet engine thrust bearings of the ball-bearing type operate at stress frequencies of the order of 2,000,000 to 3,000,000 cycles per hour and, under steady-load conditions, at stress magnitudes of 130,000 to 350,000 pounds per square inch (calculated Hertz maximum stress). The stresses in the fatigue spin rig can be varied at a given frequency of application by changing specimen geometry. The apparatus can also be operated with high ambient temperature in order to determine fatigue life at elevated temperatures.

Experiments in progress at the present time are designed to compare the fatigue life of M-1 tool steel to that of 52100 steel at a temperature of 225° F. Additional studies are being made of: (1) the fatigue life of M-1 tool steel at 450° F and (2) the effect of nonhomogeneity of the material (such as grain direction in the ball as a result of the processing methods).

#### Materials for Cages

Properties of materials. - As shown in reference 2 the requirements for cage materials are as follows:

- (1) Adequate strength
- (2) Oxidation resistance
- (3) Compatibility with race materials
- (4) Thermal expansion coefficient approaching that for the race material

Of these requirements, that of compatibility (low friction and wear) is probably the most important and possibly the most difficult to obtain. The friction and wear problem will become more acute at high temperature because, under these conditions, it is much more difficult to obtain effective lubrication; in consequence, compatibility of the solid materials becomes of primary importance.

3078-F

[REDACTED]

An additional factor of importance (to be discussed in the section "Cage and Bearing Designs") is that of friction coefficient. (The studies of ref. 11 indicate that high friction coefficient can be detrimental to bearing performance by inducing cage slip, thus causing excessive wear.) The appearance of cage breakage in high-temperature bearing runs indicates that cage strength can be very important under critical operating conditions.

3078-F

Friction, welding, and wear properties. - As a consequence of the importance of the compatibility problem, an investigation at high temperatures was conducted of the friction, welding, and wear properties of various cage materials sliding against bearing materials of either the molybdenum - tool steel type or the standard 52100 type. The latter material was used only for comparison purposes. In all cases, original selection of the cage materials was based on the three requirements other than compatibility previously listed. These studies provide fundamental information on the friction and wear properties of materials in bench tests only; additional studies are required in full-scale bearings both in test rigs and in actual turbine engines before final conclusions can be made with respect to practical use of these materials. Also, the sliding velocity (120 ft/min) of this investigation is appreciably lower than that encountered in high-speed bearings.

The apparatus used for these studies was essentially similar to that shown in figure 1 and described in reference 5; the apparatus was modified so as to provide temperatures to 1000° F. These studies were conducted either dry (figs. 8 to 10) or lubricated (fig. 11) with a load of 1200 grams, at a sliding velocity of 120 feet per minute for 1-hour periods at controlled temperature levels.

Figure 8 shows the effect of temperature on friction and wear of a conventional (Alcop) bronze, an iron-silicon bronze (Mueller 803), and a cast pearlitic nodular iron. The conventional bronze, which is a presently used cage material for aircraft turbine engine bearings, shows a continual increase in friction with higher temperatures; wear decreases with increasing temperatures to 450° F and then increases with higher temperatures. Experience has indicated that, at sliding velocities greater than that of these experiments, the curves would be displaced to the left. Iron-silicon bronze showed no effect of temperature on friction and wear at temperatures below 600° F; at higher temperatures both friction and wear increased. At temperatures of 450° F and lower, the nodular iron had unstable friction coefficients with occasional increases in the coefficient to values as high as unity; this friction behavior was not, however, accompanied by high wear. Friction of the nodular iron decreased slightly with increase in temperature and, at temperatures above 600° F, the friction was less than that for either of the bronzes. Wear of the nodular iron increased slightly with temperatures of 600° F and above, but the trend of increasing wear was considerably less than for the bronzes.

[REDACTED]

Previous data at high sliding velocities (ref. 12) indicated that nickel alloys can have good resistance to wear and surface failure under conditions where surface oxidation can occur to form protective nickel oxide films. This tendency may become more pronounced at high temperatures. Data obtained from 1-hour runs at a sliding velocity of 120 feet per minute and a load of 1200 grams for modified H monel, cast Inconel, and Nimonic 80 are presented in figure 9. These materials have physical properties that are not affected significantly by temperatures of 1000° F and higher. In general, these materials had high friction coefficients that decreased with increasing temperatures. The materials also showed decreased wear with increasing temperatures. The decrease in wear with increase in temperatures for H monel was quite gradual, but for both the cast Inconel and the Nimonic 80 abrupt changes in wear rates were observed. The low wear rates at high temperature are attributed to the formation on the surface of oxide films such as described in reference 12. As previously stated, it is believed the curves would be shifted to the left by operation at higher sliding velocities.

The importance of surface oxides to the functioning of nickel alloys was demonstrated by making a run with cast Inconel at 1000° F in an atmosphere where the availability of oxygen was reduced by displacing air with argon. The wear was increased by a factor of four, while only a slight increase in friction was observed. Also, as shown in figure 10, when cast Inconel which previously had been run for 1 hour at 1000° F to form an oxide film was run an additional hour at room temperature, the wear at room temperature ( $0.078 \times 10^{-3}$  cu in.) was slightly less than one tenth that obtained with a new specimen at room temperature ( $0.917 \times 10^{-3}$  cu in.). Further, when an unused cast Inconel specimen was heated in molten caustic (NaOH) to preform an oxide film and was then run at room temperature, the wear ( $0.094 \times 10^{-3}$  cu in.) was also approximately one tenth that obtained under identical conditions ( $0.917 \times 10^{-3}$  cu in.) with the untreated specimen of the same material.

The wear experienced with cast Inconel having an oxide film against M-10 steel at room temperature is less than one fourth of that obtained ( $0.447 \times 10^{-3}$  cu in.) under the same conditions with the metal combination (Alcop bronze against SAE 52100 steel) currently being successfully used in bearings of full-scale engines. Wear for the various nickel alloys at 1000° F in air was approximately one tenth that for iron-silicon bronze and was approximately one half that of the iron-silicon bronze at 600° F. It is in the temperature range from 600° to 1000° F that nickel alloys merit particular consideration as cage materials.

It is suggested that it may be possible to obtain low wear both at low and at high temperatures by employing a nodular-type cast iron containing 20 percent nickel (Ni-Resist), which has good strength at temperatures to 1000° F. The combined effect of the free graphitic carbon from the nodules and the possible surface film of nickel oxide could

produce low wear at all temperatures under consideration. An investigation of this material will be made in the near future.

In the unlubricated runs, the high friction of all the materials previously discussed is undesirable because it could cause excessive cage slip. Preliminary experiments conducted with a hot-pressed iron-silicon bronze containing  $\text{MoS}_2$  were unsuccessful because of high wear resulting from low strength of the iron-silicon-bronze powder compacts; however, those experiments did show that significantly reduced friction coefficients could be obtained. This approach appears promising and further research is in progress to obtain reduced wear as well as lower friction for this type of material.

Results of lubricated friction and wear runs of various possible cage materials against M-10 tool steel obtained at  $450^\circ\text{F}$  and at a sliding velocity of 120 feet per minute with a load of 1200 grams are shown in figure 11. The lubricant was di(2-ethylhexyl) sebacate plus 0.5 percent phenothiazine (oxidation inhibitor). Data (from figs. 8 and 9) for these same materials run dry against M-10 tool steel at  $450^\circ\text{F}$  are also included for comparison purposes. The results show that, as expected, the lubricant served to decrease both friction and wear for all except the conventional bronze. The bulk temperature of the lubricant was so high that the specimens were believed to be operating in a range of incipient failure of boundary lubrication where the compatibility of materials is very important. The reduction in wear of the cast Inconel is particularly to be noted since its dry wear was rather high.

Cast Inconel had reasonably good high-temperature friction properties, showed low wear at high temperatures operating against M-10 steel, and had good performance (low wear) at high sliding velocities operating against 52100 steel (ref. 12); and, therefore, it was considered advisable to check the friction and wear properties of cast Inconel against the various tool steels being considered for use in high-temperature bearings. These steels include the molybdenum tool steels previously discussed as well as a high-speed tungsten-chrome-vanadium tool steel (18-4-1). In accordance, friction and wear data were obtained (fig. 12) for cast Inconel operating against these tool steels (M-1, M-2, M-10, and 18-4-1) at  $75^\circ$  and  $1000^\circ\text{F}$  with a sliding velocity of 120 feet per minute and a load of 1200 grams. For comparison purposes, results are included in figure 12 for cast Inconel operating against SAE 52100 (the present, standard rolling contact bearing material); since 52100 becomes soft at elevated temperatures, data for this steel were limited to the  $75^\circ\text{F}$  temperature. The hardness of all the steels was from Rockwell C-60 to C-63 at room temperature. The data of figure 12 show no appreciable difference in either friction or wear properties of the various tool steels, operating against cast Inconel, at either  $75^\circ$  or  $1000^\circ\text{F}$ . Also, at  $75^\circ\text{F}$ , there is no

appreciable difference between the friction and wear values for the tool steels and those for SAE 52100 steel.

### Cage and Bearing Designs

It has been shown (ref. 13) that, for liquid-lubricated bearings, considerable improvement in the operating characteristics and, in particular, in the limiting speeds of a bearing can be obtained by cage design. For example, in reference 13 it is shown that the combination of an outer-race-riding cage with a straight-through outer race and inner-race guided rollers gives the best over-all performance. Figure 13(b) shows this design as compared to conventional inner-race (fig. 13(a)) or outer-race (fig. 13(c)) cage designs. The better performance of this design over both the conventional inner-race-riding cage type and the conventional outer-race-riding cage type with outer-race guided rollers is a result of the relative ease of lubrication and cooling and of the adequate oil flow (inlet and exit) paths which minimize oil churning and friction losses. For example, figure 13(b) shows that a large flow area is provided between cage and inner race for entrance of oil while only a slight obstruction to flow out of the bearing exists at the outer race. In figure 13(b) the surfaces which require lubrication (the cage-locating surface at the outer race) are positively lubricated by oil which is thrown out by centrifugal force to the outer race. To avoid excessive churning of this oil, some relief is provided in the form of cut-outs (fig. 13(b)) to permit oil to flow out of the bearing. The design principle emphasized in these results seems to be that of providing for easy flow of lubricant into, through, and out of the bearing. Under these conditions, both adequate lubrication and adequate cooling are obtained, which tends to extend the limiting speed values. It is possible that application of this design principle will also assist in extending the high-temperature limitations. This concept may be useful only for liquid-lubricated bearings since the data of reference 13 were obtained with a liquid lubricant.

In the studies of reference 11 it was shown that cage slip causes excessive wear in bearings particularly under high-speed conditions. It was also shown that the use of a cage material which has a high friction coefficient might be particularly bad from the standpoint of inducing slip under extreme high speeds. These results would indicate that another extremely important property of a cage material is that of maintaining low friction under the expected conditions of operation. This point was not completely appreciated before the results of reference 11 were obtained, since it was felt that friction coefficient per se was not a particularly important factor as long as the other performance characteristics of the cage material were satisfactory. It should be emphasized, however, that the friction coefficient is of primary importance only insofar as it influences slip within the bearing.

### Temperature Ranges for Various Bearing Materials

A summary of the possible bearing materials (both for rolling contact and for cages) for operation over the four temperature ranges of table I is shown in table III. As shown, the present race and rolling element material (SAE 52100) and the present cage material (silver-plated bronze) are suitable for temperature range 1. Likewise, the present bearing materials may be used in the interim until more information is available on other materials for temperature range 2; this is, however, only an interim measure and the molybdenum tool steels and other cage materials (such as nodular iron and nickel alloys) may be used in the near future. For temperature ranges 3 and 4, the rolling contact bearings will undoubtedly employ tool steels for races and rolling elements, and nickel alloys, nodular iron, or other special materials for the cages. Very little is known about the performance of these materials under these conditions; in consequence, much additional research is required (fatigue as well as friction and wear research) in temperature ranges 2, 3, and 4.

### CONCLUDING REMARKS

In the turbojet engine for high flight speed, the combination of high ram temperatures, minimum available cooling, high compressor-discharge temperatures, and high turbine-inlet temperatures results in a general increase in bearing and lubricant temperatures. Inclusion of current turbojet engines for subsonic flight speeds results in four general temperature ranges of interest:

Temperature range	1	2	3	4
Maximum bearing temperature	350	500	750	1000
Maximum bulk lubricant temperature	200	300	400	----
Minimum temperature	-65			

Table III summarizes the possible lubricants and bearing materials to meet the requirements of the temperature ranges of table I. As shown in table III for temperature range 1, the possible lubricants are the standard petroleum lubricants meeting specification MIL-O-6081A, grades 1010 and 1005; the possible bearing materials include the standard SAE 52100 for the races and rolling elements and the standard silver-plated bronze for the cages.

For temperature range 2, the possible lubricants include the present synthetics (diesters) meeting specification MIL-L-7808; the possible bearing materials include the molybdenum tool steels (and 52100 as an interim

[REDACTED]

material) for the races and rolling elements and nodular iron or the nickel alloys (and silver-plated bronze as an interim material) for the cages.

For temperature range 3, the possible lubricants include future synthetics with high-temperature stability or, if liquid lubricants cannot be developed, solids and gases; the possible bearing materials include the molybdenum tool steels for the races and rolling elements and nickel alloys or nodular iron for the cages.

For temperature range 4, the possible lubricants appear to be limited to solids and gases since there appears little likelihood of obtaining liquids which can adequately lubricate bearings operating at 1000° F; the possible bearing materials include the molybdenum tool steels for the races and rolling elements and the nickel alloys or powdered metals containing solid lubricants for the cages. If future improved liquids or lubrication methods make the use of liquids possible at such high temperatures, it is believed that it will be desirable in the design of future high-temperature engines to allow bearings and lubricants to operate as hot as is practicable in order to minimize the complications of cooling.

Some of the data show that considerable gain (up to 200° F) in high-temperature lubrication limits for liquids can be made by relaxing the low-temperature specification, that is, by use of lubricants of higher viscosity. This relaxation in low-temperature specifications, however, requires a re-evaluation of both low- and high-temperature requirements. Use of high-viscosity fluids might be possible in the the "short-time" engine (e.g., for guided missile application) if some provisions for low-temperature starting and lubricant pumping at low temperature are made. The "short-time" engine could be lubricated by liquids which show corrosive tendencies at high temperatures; because long service life is not important, it may be possible to tolerate some corrosion provided effective lubrication is maintained.

Some gain in the performance characteristics and possible extensions in the limitations of existing rolling contact bearings lubricated by liquids can be obtained by cage designs which are based on the principle of providing an easy flow path of lubricant into and through the bearing.

Considerable research is required on lubricants (particularly stability and lubricating effectiveness) at the high temperatures of temperature ranges 3 and 4. Considerable research is likewise required on the bearing materials (particularly fatigue research on the race and rolling element materials and friction and wear research on the cage materials) at the temperatures of temperature ranges 3 and 4.

[REDACTED]

## REFERENCES

1. Crampton, A. B., and Lifson, W. E.: Jet Engine Lubricants for High Speed Flight. Papers presented at meeting of Inst. Aero. Sci. (Cleveland), Mar. 13, 1953.
2. SAE Panel: Trends of High Speed Rolling Contact Bearings as Applied to Aircraft Gas Turbine Engines. (NACA TN to be pub.)
3. NACA Subcommittee on Lubrication and Wear: Review of Current and Anticipated Lubricant Problems in Turbojet Engines. NACA RM 51D20, 1951.
4. Murray, S. F., Johnson, R. L., and Bisson, Edmond E.: Effect of High Bulk Temperatures on Boundary Lubrication of Steel Surfaces by Synthetic Fluids. NACA TN 2940, 1953.
5. Murray, S. F., and Johnson, Robert L.: Effect of Solvents in Improving Boundary Lubrication of Steel by Silicones. NACA TN 2788, 1952.
6. Johnson, Robert L., Swikert, Max A., and Bisson, Edmond E.: Effective Lubrication Range for Steel Surfaces Boundary Lubricated at High Sliding Velocity by Various Classes of Synthetic Fluids. NACA TN 2846, 1952.
7. Macks, E. F., Nemeth, Z. N., and Anderson, W. J.: Preliminary Investigation of Molybdenum Disulfide-Air-Mist Lubrication for Roller Bearings Operating to DN Values of  $1 \times 10^6$  and Ball Bearings Operating to Temperatures of  $1000^\circ$  F. NACA RM E51G31, 1951.
8. Johnson, Robert L., Swikert, Max A., and Bisson, Edmond E.: Friction and Wear of Hot-Pressed Bearing Materials Containing Molybdenum Disulfide. NACA TN 2027, 1950.
9. Pigott, Joseph D., and Macks, E. Fred: Air Bearing Studies at Normal and Elevated Temperatures. Paper presented at annual meeting Am. Soc. Lubrication Eng., Apr. 14, 1953.
10. Macks, E. F.: The Fatigue Spin Rig - A New Apparatus for Rapidly Evaluating Materials and Lubricants for Rolling Contact. Lubrication Eng., vol. 9, no. 5, Oct. 1953, pp. 254-258.

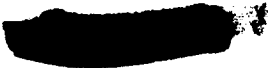
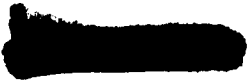
- 
11. Anderson, William J., Macks, E. Fred, and Nemeth, Zolton N.: Effect of Bronze and Nodular Iron Cage Materials on Cage Slip and Other Performance Characteristics of 75-Millimeter-Bore Cylindrical-Roller Bearings at DN Values to  $2 \times 10^6$ . NACA TN 3002, 1953.
  12. Johnson, Robert L., Swikert, Max A., and Bisson, Edmond E.: Wear and Sliding Friction Properties of Nickel Alloys Suited for Cages of High-Temperature Rolling-Contact Bearings. II - Alloys Retaining Mechanical Properties Above 600° F. NACA TN 2759, 1952.
  13. Anderson, William J., Macks, E. Fred, and Nemeth, Zolton N.: Comparison of Operating Characteristics of Four Experimental and Two Conventional 75-Millimeter-Bore Cylindrical-Roller Bearings at High Speeds. NACA TN 3001, 1953.
- 

TABLE I. - BEARING AND LUBRICANT TEMPERATURE TRENDS  
FOR AIRCRAFT TURBOJET ENGINES<sup>a</sup>

Temperature range	1	2	3	4
Engine status	Current	Development plus new production	Future	Future
Maximum operating temperature, °F				
Bearing	< 350	500	750	1000
Bulk lubricant	200	300	400	----
Maximum bearing "soak-back" tem- perature, °F	500	700	1000	----
Minimum tempera- ture for bear- ings and lubri- cant, °F <sup>b</sup>	-65	-65	-65 <sup>c</sup>	-65 <sup>c</sup>

<sup>a</sup>Some of data from references 1 and 3.

<sup>b</sup>Temperatures of -100° F have been encountered in service.

<sup>c</sup>May be necessary to sacrifice on low-temperature prop-  
erties to achieve adequate high-temperature properties.

TABLE II. - PROPERTIES OF EXPERIMENTAL LIQUID LUBRICANTS

Fluid	Viscosity centistokes, at				A.S.T.M. pour point, °F	C.O.C. flash point, °F	C.O.C. fire point, °F
	-65° F	-40° F	100° F	210° F			
MIL-L-7808 Specification	<13,000	-----	-----	> 3.0	< -75	> 385	---
Petroleum: MIL-O-6081A (grade 1010) <sup>a</sup>	40,000	-----	9.95	2.47	< -70	300	---
Diesters: Di(2-ethylhexyl) sebacate <sup>a</sup>	8,297	-----	12.78	3.32	< -70	440	472
Di(2-ethylhexyl) sebacate + additives <sup>b,c,d,e</sup>	16,000	2,700	20.8	5.3	< -75	450	475
Polyalkylene glycols (desig- nated by viscosity at 100° F):							
Water-soluble							
8.9 centistokes <sup>e</sup>	-----	1,800	8.9	2.4	-85	260	285
41 centistokes <sup>e</sup>	-----	30,000	41	8.2	-45	410	480
143 centistokes <sup>e</sup>	-----	<sup>f</sup> 26,000	143	26.2	-30	430	545
762 centistokes <sup>e</sup>	-----	-----	762	120	-20	440	545
Water-insoluble							
7.4 centistokes <sup>e,g</sup>	4,587	905	8	2.52	< -70	270	335
Phosphonates:							
Diocetyl isoctene phosphonate <sup>a</sup>	-----	<sup>h</sup> 9,003	12.22	2.77	-90	---	---
Silicates:							
Tetra(2-ethylhexyl) silicate <sup>e</sup>	1,400	260	6.8	2.4	< -100	395	450

<sup>e</sup>Measured values.<sup>b</sup>4 percent methacrylate polymer.<sup>c</sup>5 percent tricresyl phosphate.<sup>d</sup>0.5 percent phenothiazine.<sup>e</sup>Manufacturer's data.<sup>f</sup>At -20° F.<sup>g</sup>Contains oxidation inhibitor.<sup>h</sup>At -50° F.

TABLE III. - LUBRICANT AND BEARING MATERIAL FOR VARIOUS TEMPERATURE RANGES

Temperature range	1	2	3	4
Maximum operating temperature, °F				
Bearing	< 350	500	750	1000
Bulk lubricant	200	300	400	----
Minimum temperature, °F	-65	-65	-65	-65
Possible lubricants	Liquid-petroleums	Liquid-diesters plus other synthetics	Solids or gases Liquid - possible future synthetics	
Research required on lubricants	None	High-temperature stability	High-temperature stability and lubrication	
Possible rolling contact bearing materials.		Molybdenum tool steels (M-1, M-2+M-10)		
A. For races and rolling elements	52100 (present material)	52100 (interim material)		
B. For cages	Silver-plated bronze (present material)	Nickel alloys		
		Nodular iron		Powdered metals plus solid lubricants
		Silver-plated bronze (interim material)		
Research required on bearing materials				
A. For races and rolling element materials	None	Fatigue research		
B. For cages	None	Friction and wear research		

**SCHEMATIC DIAGRAM OF FRICTION APPARATUS  
FOR STUDYING BOUNDARY LUBRICATION  
BY BULK LUBRICANTS**

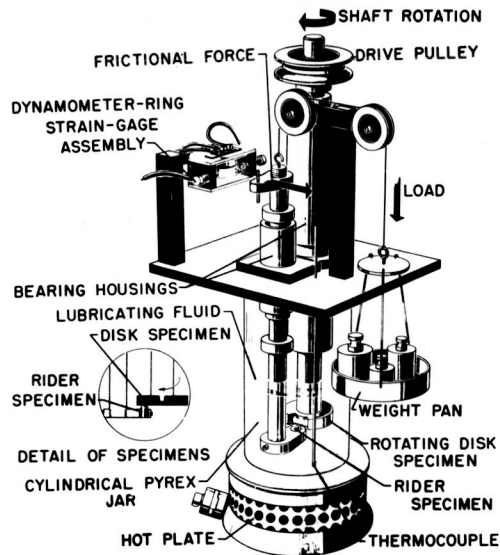
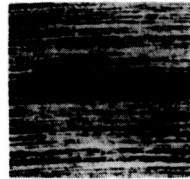


Figure 1

**TYPICAL SURFACE CONDITIONS**

RIDER SPECIMEN

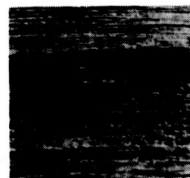
DISK SPECIMEN



(a) EFFECTIVE LUBRICATION.



(b) INCIPIENT FAILURE.



(c) MASS FAILURE.

Figure 2

### FRICION WITH SYNTHETIC LUBRICANTS AT VARIOUS TEMPERATURES

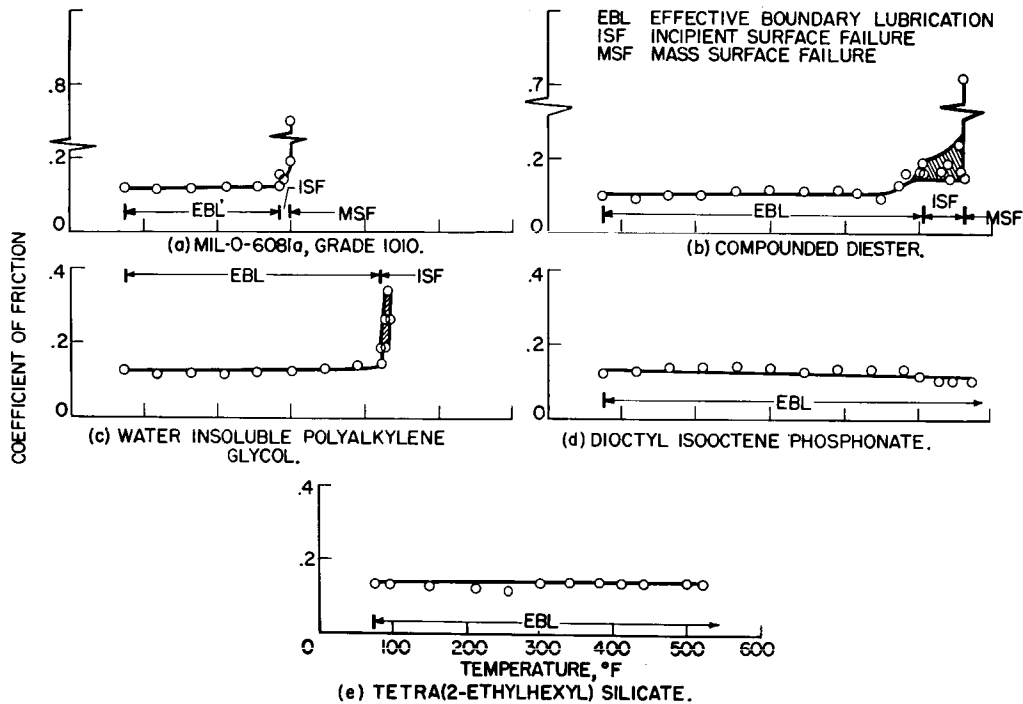


Figure 3

### EFFECT OF ADDITIVES IN DI(2-ETHYLHEXYL) SEBACATE

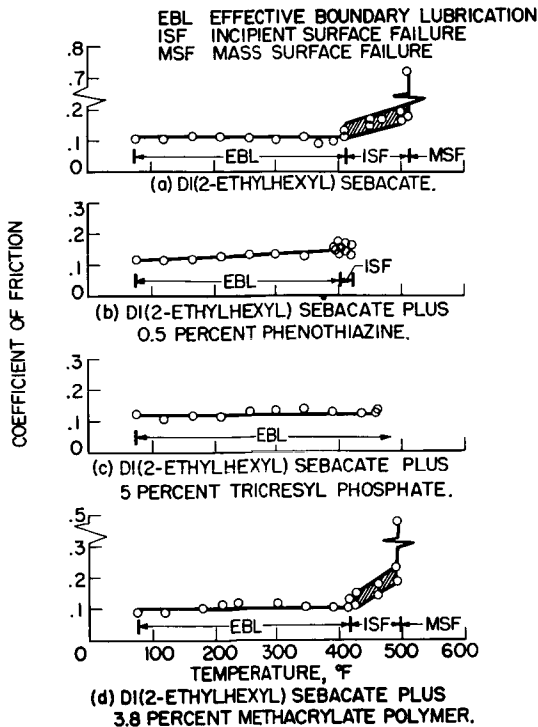


Figure 4

### EFFECT OF VISCOSITY OF GLYCOLS ON CRITICAL TEMPERATURE

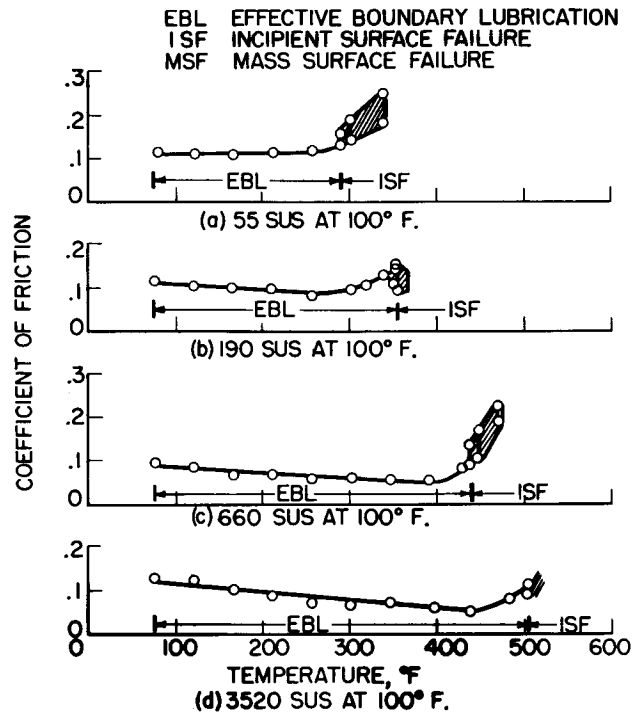


Figure 5

### HIGH-SPEED ROLLER BEARING

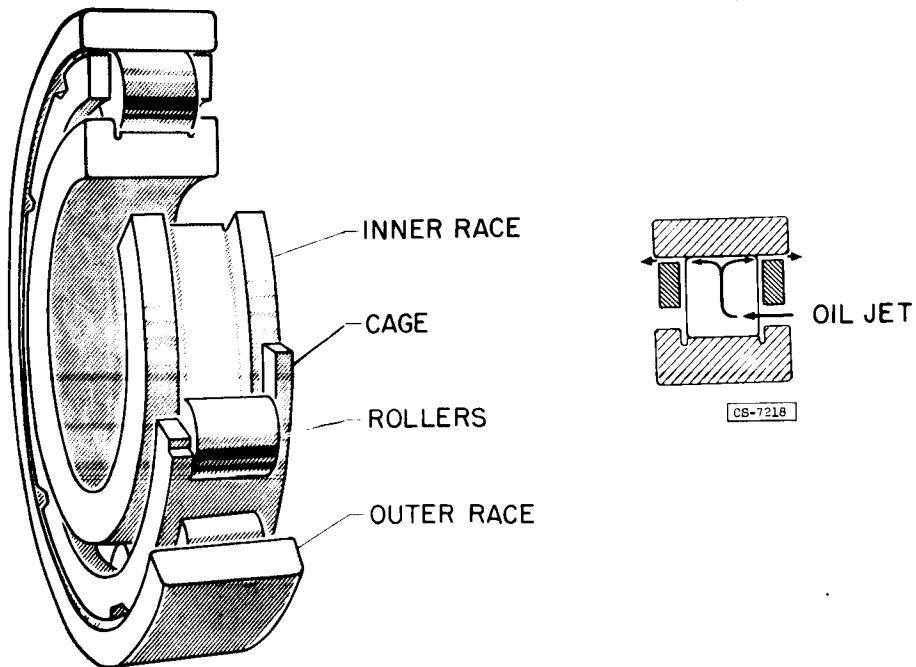


Figure 6

3078-F

3078-F1

[REDACTED]

### FATIGUE SPIN RIG

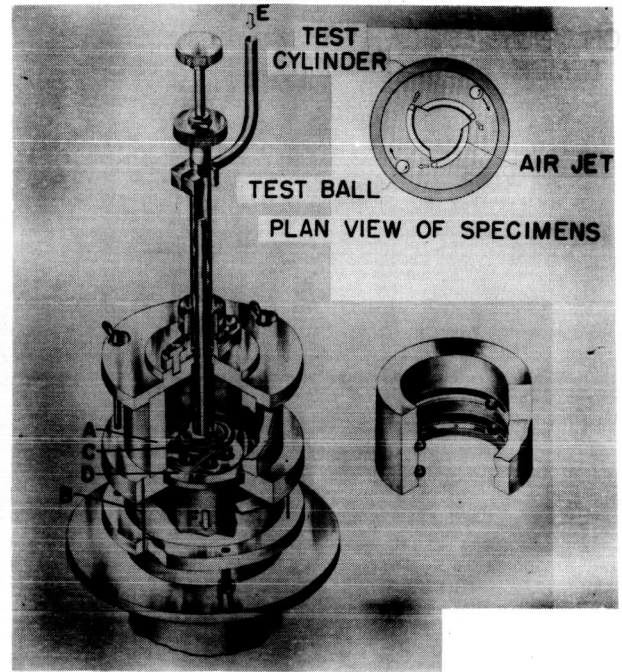


Figure 7

### FRICITION AND WEAR OF VARIOUS MATERIALS AT HIGH TEMPERATURE WITHOUT LUBRICATION

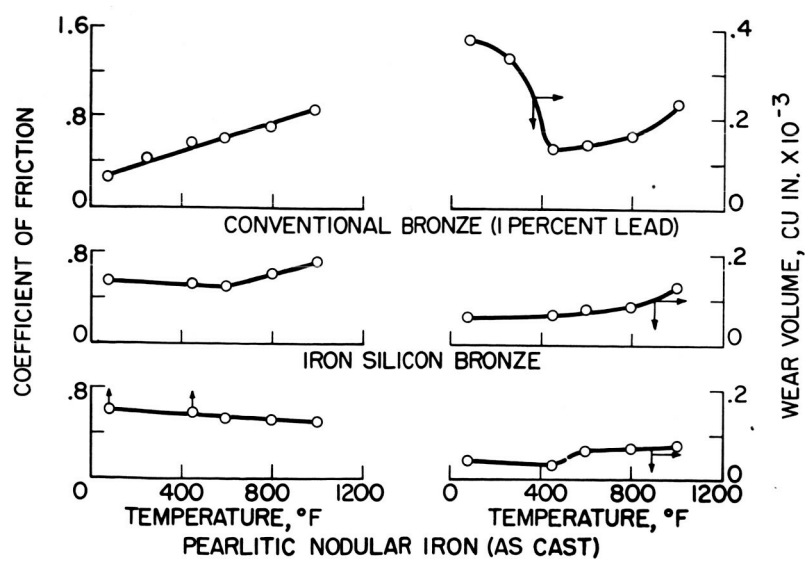


Figure 8

[REDACTED]

FRICITION AND WEAR OF VARIOUS MATERIALS AT HIGH TEMPERATURE WITHOUT LUBRICATION

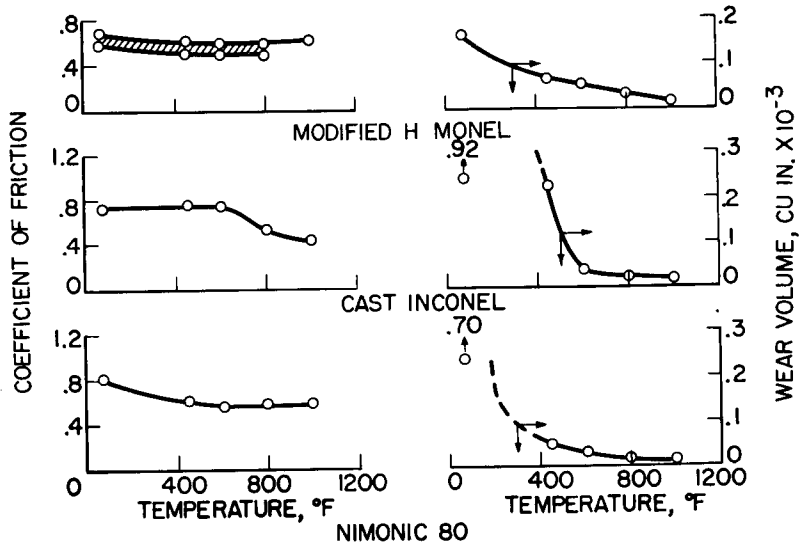


Figure 9

WEAR OF CAST INCONEL AGAINST M-10, DRY

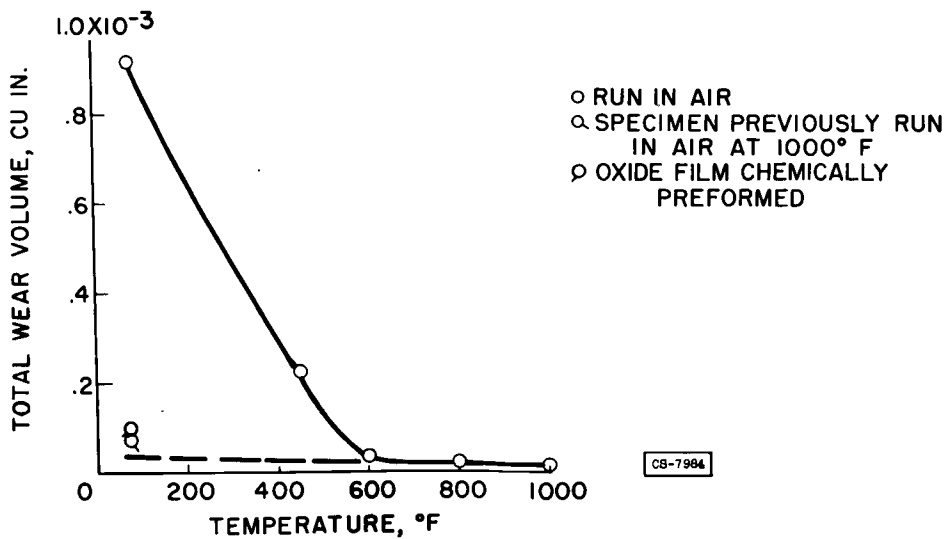


Figure 10

### FRICITION AND WEAR OF POSSIBLE CAGE MATERIALS AGAINST M-10 TOOL STEEL AT 450° F, DRY AND LUBRICATED

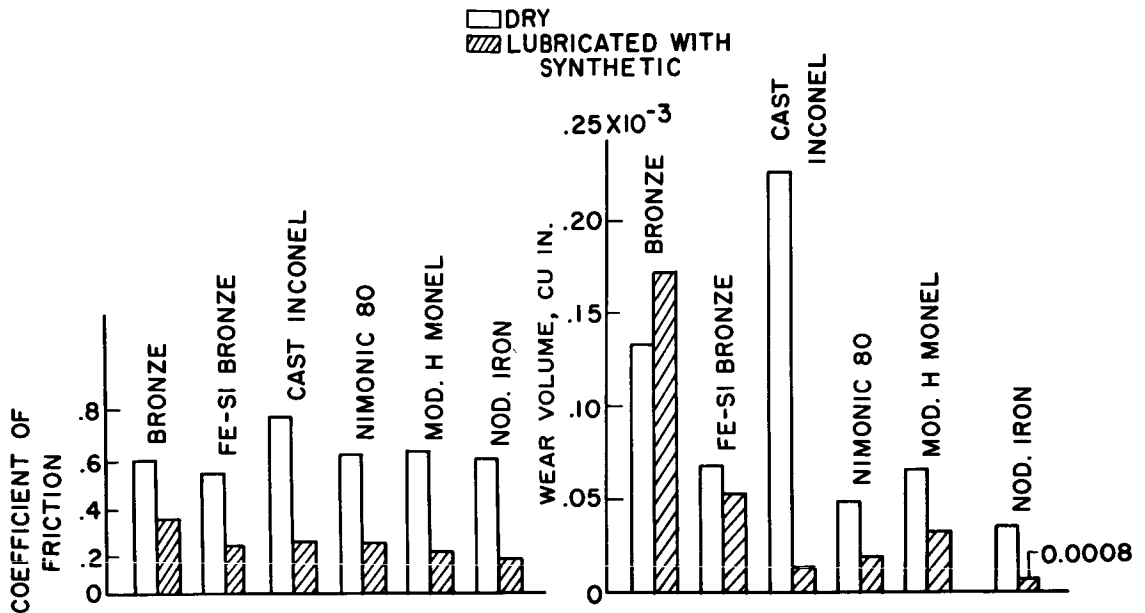


Figure 11

### FRICITION AND WEAR OF POSSIBLE RACE AND ROLLING ELEMENT MATERIALS AGAINST INCONEL, DRY

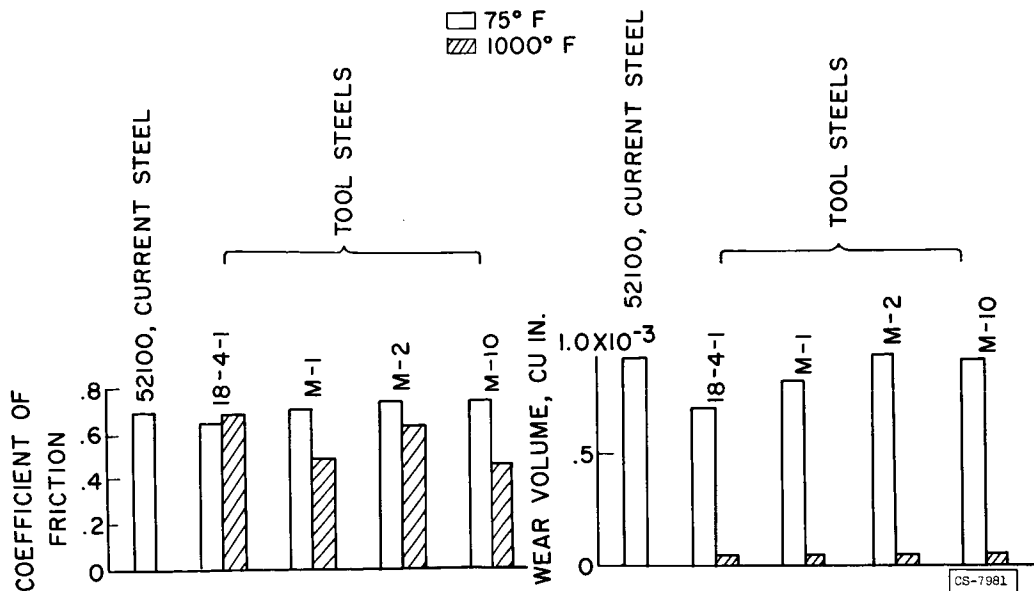


Figure 12

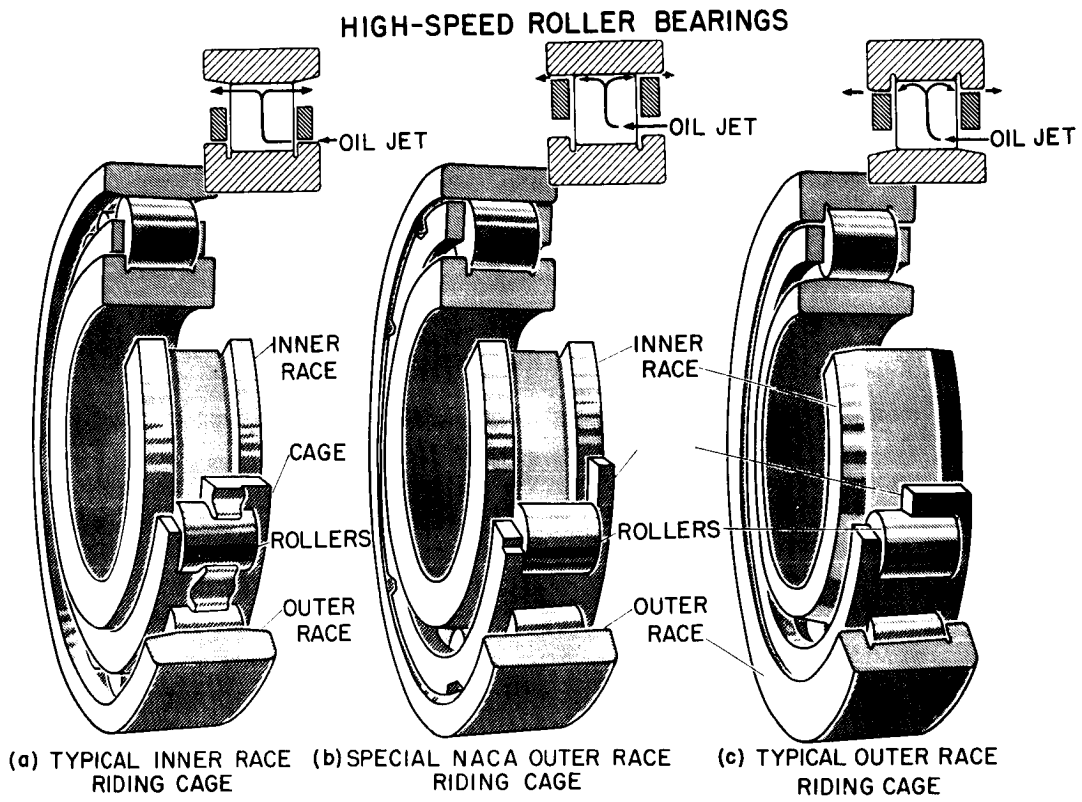
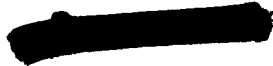
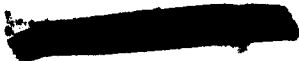
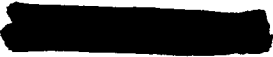


Figure 13



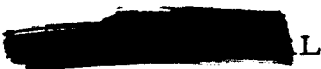
3078-G



VII - INLETS AND OUTLETS PANEL

D. D. Wyatt  
H. D. Wilsted  
E. M. Cortright  
C. F. Schueller  
G. W. Englert

VII - INLETS &  
OUTLETS



L



# FACTORS AFFECTING THE PERFORMANCE OF SIDE INLETS

## AT SUPERSONIC SPEEDS

By Thomas G. Piercy

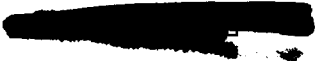
### INTRODUCTION

The location of inlets at fuselage positions other than the nose of a supersonic airplane is sometimes desirable for installational reasons. However, in comparison with nose inlets, the possibilities for obtaining high induction-system performance with side inlets on supersonic aircraft are handicapped by several inherent features of side-inlet installations. In the first place, it is now well known that a side inlet must operate outside of the boundary layer of the body on which it is mounted if high pressure recoveries are to be obtained. An inevitable boundary-layer-removal drag is thereby encountered. Secondly, the supersonic-flow field entering the side inlet may be considerably more complex and therefore less susceptible to accurate analysis than in the case of the nose inlet, inasmuch as this flow field is dependent upon the shape and attitude of the body. Accurate prediction of the required optimum supersonic compression design is therefore complicated. Thirdly, the side inlet is liable for increased subsonic-diffuser losses compared with losses at the nose inlet as a result of generally inherent corner effects in the region of the throat, necessary transitions in the flow-passage shape, and subsonic-diffuser turns required to discharge the air flow at the center of the fuselage. As a consequence of these inherent problems, the application of nose-inlet research results for the prediction or evaluation of side-inlet performance must be undertaken with caution.

It is the purpose of this paper to summarize research on the side inlet and to illustrate the greater complexity in the design of side-inlet systems. Some of the data have been in the published literature for several years and are included herein only for the sake of rounding out the viewpoint of the over-all problem. Much of the information has been obtained only recently, however, and is as yet unpublished. It will be apparent in many areas that further research is necessary for a complete understanding of some of the problems and the best design approach to their solution.

### REVIEW OF SIDE-INLET RESEARCH

The first exploratory tests of fuselage-mounted inlets (refs. 1 to 7) showed that the inlet pressure-recovery performance was severely penalized if the boundary layer generated on the fuselage forebody was



allowed to enter the inlet. This loss of pressure recovery was considerably larger than that which would be caused by the total-pressure decrement of the entering boundary layer and thus may be charged to undesirable boundary-layer - shock-wave interaction. This effect, which occurred because of the inability of the boundary layer to sustain the pressure gradient produced by the shock system of the inlet, caused the boundary layer to thicken ahead of the inlet and to separate in an unsteady manner. The operation of the external compression surfaces and the subsonic diffuser was therefore disrupted when boundary layer was allowed to enter the inlet. However, when suitable control of the boundary layer was provided and attention given to the subsonic-diffuser area variations, it was found that peak pressure recoveries comparable with pressure recoveries of single-shock conical external compression nose inlets could be obtained, at least for Mach numbers up to 2.0; for critical inlet operation, however, the side-inlet pressure recovery fell 0.05 to 0.07 below the pressure recovery of the nose inlet.

The over-all performance of fuselage-mounted side inlets, such as reported in references 1 to 7, is influenced by the body upon which the inlet is mounted since the shape and attitude of the forebody determine the flow conditions at the inlet. These flow conditions are apt to be nonuniform, and therefore it is difficult to isolate the effect of boundary-layer removal. The effect of boundary-layer removal may be isolated, however, by mounting side inlets on flat plates (refs. 8 to 12). With a flat-plate-mounted inlet the boundary-layer thickness can be made uniform across the inlet, and there are no crossflow or angle-of-attack effects. Several systems of boundary-layer removal for single-shock half-conical side inlets have been studied at the NACA Lewis laboratory (refs. 8, 10, and 11). Figure 1 presents most of the boundary-layer-removal systems investigated. Two scoop-type inlets and three simple boundary-layer diverter systems were considered. The relative performance of each is shown in figure 2 for Mach numbers of 1.88 and 2.93. Included is the theoretical inlet pressure recovery, which accounts only for the theoretical shock losses and the total-pressure losses due to the presence of the boundary layer. The indicated losses of total-pressure recovery for incomplete boundary-layer removal (i.e., low values of  $h/\delta$ ) (all symbols are defined in the appendix) are due to the destabilizing effect of the boundary layer on the internal performance of the inlet, as indicated previously.

It is further noted that the system of boundary-layer removal was influential in determining the inlet performance. While the inlet pressure recovery was approximately equivalent for both straight- and swept-leading-edge scoops, the diverter-type systems of boundary-layer removal generally required additional boundary-layer removal over that needed by scoop removal systems to provide comparable inlet pressure recoveries. This requirement arises from the fact that the diverter systems investigated created disturbances in the boundary layer ahead of the inlet, thereby thickening the boundary layer; thus more boundary-layer removal

[REDACTED]

was required for the diverter-type systems. It is of interest to note that the blunt-diverter system at a Mach number of 1.88 provided higher inlet pressure recovery at  $h/\delta$  of 1.0 than was obtained with the  $62^\circ$  included-angle wedge diverter. The blunt diverter, while having a stronger shock disturbance formed ahead of it, was located considerably downstream of the inlet lip station, and as a result a large percentage of the disturbed boundary layer passed around the inlet rather than into the inlet. The  $62^\circ$  wedge diverter, by comparison, was located such that its apex was directly beneath the tip of the compression cone. The bow wave which formed ahead of the wedge then thickened the boundary layer ahead of the inlet, with the indicated results.

The maximum total-pressure recovery obtained at a Mach number of 1.88 is approximately equivalent to the performance of the single-shock conical nose inlet, while at a Mach number of 2.93 the pressure recovery is somewhat below the performance of the nose inlet. While it is possible that the performance of the higher Mach number side inlet could be improved slightly by modifications to the subsonic diffuser, there is considerable evidence to indicate that above Mach numbers of 2.0 the side inlet will be inferior to its companion nose inlet. The majority of the additional pressure losses suffered by the side inlet generally occur in the subsonic diffuser.

#### THRUST AND DRAG PENALTIES OF SIDE-INLET INSTALLATIONS

It has been shown that the performance of the side inlet is improved by removal of the boundary layer ahead of the inlet. However, an inevitable boundary-layer-removal drag is encountered which must be included in the net evaluation of the inlet installation. The drag incurred with boundary-layer removal for side-inlet installations is therefore of interest. The drag of several forebodies utilizing side-inlet installations has been determined in the Lewis 8- by 6-foot supersonic wind tunnel. The bodies investigated are presented in figure 3. The first of these is the RM-10 parabolic body of revolution of forebody fineness ratio of 7.5. Twin inlets utilizing  $16^\circ$  included-angle wedges for boundary-layer removal were located at various circumferential positions at the maximum-thickness station of the body. The second forebody, indicated by configuration A, had a pointed nose which faired into a "quasi-triangular" section, and twin inlets were located in the upper quadrants on each side of the triangle. The forebody fineness ratio at the inlet station was 5.3. The inlets were located in a position to utilize the compression afforded by the canopy and were canted down at  $2^\circ$  to partially account for a cruise angle of  $3^\circ$ .

Configuration B was characterized by a short forebody of fineness ratio of 2.8. Twin inlets were located on the sides of an elliptical-shaped fuselage. Both the forebody and the inlets were canted down at

[REDACTED]

5<sup>0</sup>, the expected cruise angle. Configuration C was again a body of revolution, except that canard-type longitudinal control surfaces were located on the forward upper section of the forebody. The forebody fineness ratio at the inlet station was approximately 5.8. The last configuration investigated, indicated by configuration D, also used canard-type control surfaces. For this model the forebody cross section was elliptical, and a single inlet was located on the bottom of the fuselage, which was flattened out for the installation. The forebody fineness ratio at the inlet station was about 6.1.

In figure 4(a) the percentage increase of forebody drag coefficient for an increase in boundary-layer removal of  $h/\delta$  of 0 to 1.0 is presented for various inlet positions on the body of revolution at angle of attack (ref. 13). The data presented are for critical inlet operation at a free-stream Mach number of 1.99. In general, the largest increase in forebody drag coefficient occurred when the inlet pairs were located in the upper- and lower-quarter quadrants. This phenomenon is believed due to interference effects between the inlets. The 22-percent forebody drag increase at zero angle of attack for inlets diametrically opposed corresponds to about a 6.2-percent increase in the cruise drag coefficient of a complete missile. If with boundary-layer removal this side-inlet configuration would produce inlet performance comparable with nose inlets, the 6-percent drag increase would be representative of the net evaluation of the side-inlet installation compared with the nose inlet. Without boundary-layer removal the side-inlet pressure recovery decreased 27 percent, which corresponds to a propulsive thrust decrease of 32 percent.

In figure 4(b) similar data are presented for the increase of drag coefficient caused by the use of boundary-layer removal on configuration D. Configuration D, however, is a complete missile, and the maximum increase in drag coefficient was approximately 7.2 percent for complete boundary-layer removal ( $h/\delta$  of 0 to 1.0).

Figure 5 presents related performance data for a two-dimensional ramp inlet with a rounded semicircular cowl mounted on supersonic airplane configuration A (ref. 14). The boundary layer was removed with scoops for this application. An increase in  $h/\delta$  from 0 to 1.0 was found to increase the forebody drag coefficient 17 percent and to increase the inlet pressure recovery 25 percent. A net increase in thrust-minus-drag of 43 percent was realized. This corresponds to  $\Delta(F_n - D)/F_{n,i}$  of 0.160.

The performance of other side inlets mounted on configuration A was analyzed in reference 15, and a few of the results at a free-stream Mach number of 2.0 are presented in figure 6. The results are compared at the cruise angle-of-attack condition of 3<sup>0</sup>. The increase in net thrust-minus-drag for several alternate inlets is compared with the

results for the two-dimensional ramp inlet with semicircular rounded-lip cowl. All inlets showed considerable net thrust-minus-drag advantages over the rounded-lip inlet. At Mach number 1.5, however, the advantages over the rounded-lip inlet are considerably reduced.

Theoretical analysis of the possible thrust increases with boundary-layer removal has also been studied for the flat-plate-mounted side-inlet installations mentioned earlier. For this analysis typical turbojet engine data were assumed: The compressor pressure ratio was taken as 5.0; the afterburner temperature was assumed to be 3000° R; and a variable-area convergent-divergent exit nozzle was assumed. The analysis considered flight at altitudes of 35,000 feet. The results of this analysis are presented in figure 7 for free-stream Mach numbers of 1.88 and 2.93. The net thrust is referenced to the ideal thrust, which assumed 100-percent pressure recovery. Three solid curves are presented: The upper curve represents the net-thrust gain if no drag is encountered in boundary-layer removal; the lower curve represents the net-thrust gain with complete loss of boundary-layer momentum; and the intermediate curve assumes that the boundary-layer air is taken into scoops and is discharged through a sonic nozzle. These figures, of course, do not include interference effects of the boundary-layer-removal system.

Also included for comparison is the corresponding thrust performance of well-designed single-shock conical nose inlets (dashed curve). The nose-inlet thrust was obtained with the assumption of 90 and 57.5 percent total-pressure recovery at free-stream Mach numbers 1.88 and 2.93, respectively. It may be observed that side inlets with no penalty for boundary-layer removal realized about 96 percent of nose-inlet thrust at a Mach number of 1.88. With the assumption of sonic discharge of the scoop boundary layer, the side-inlet installation was charged with a drag equal to about 1 percent of the nose-inlet thrust. At a Mach number of 2.93 the side inlet achieved only 77 percent of nose-inlet thrust; 3 percent of this loss was charged to the drag incurred with sonic discharge of the boundary layer.

In general, peak thrust was obtained for  $h/\delta$  values between 0.85 to 0.90. (This compares to  $h/\delta$  of 0.70 for normal-shock side inlets, ref. 12.) The internal drag of the scoop removal system ranged from 12 to 24 percent of the entering boundary-layer momentum at peak thrust-minus-drag for free-stream Mach numbers of 1.88 and 2.93, respectively.

The net increase in thrust-minus-drag  $\frac{\Delta(F_n - D)}{F_{n,i}}$  is about 0.290 at a Mach number of 1.88. This figure compares closely with the half-conical inlet data of figure 6. At a Mach number of 2.93 the net thrust-minus-drag increase is approximately 0.170.

Drag associated with wedge-type boundary-layer removal. - As part of a general study of boundary-layer-removal systems, the drag of various boundary-layer-removal wedges has been studied at the NACA Lewis laboratory. The data are as yet unpublished. Figure 8 presents a schematic diagram of the test setup and the parameters involved. Turbulent boundary layer was generated on a flat plate, and various wedges were immersed in the boundary layer beneath a splitter plate thereby simulating boundary-layer removal ahead of a side-inlet installation. The parameters investigated included the sweep of the splitter plate, the wedge included angle  $\epsilon$ , the wedge thickness ( $h/\delta$ ), the wedge position relative to the fixed leading edge of the splitter  $l/d$ , and the free-stream Mach number. Pressure drag on the wedges has been determined for free-stream Mach numbers of 1.88, 3.16, and 3.83. Friction drag have been estimated only for a free-stream Mach number of 3.16. A few of the characteristic results are presented in figures 9 and 10. The wedge drag coefficient was referenced to the wedge projected area. In figure 9(a) the pressure drag of the  $28^\circ$  included-angle wedge is observed to increase as the wedge thickness is increased. Also, as indicated in figure 9(a), it has been observed that in general the wedge pressure drag is largest for the most forward wedge locations. In figure 9(b) the pressure drag is seen to increase as the included wedge angle is increased. Figure 10 presents the pressure-drag variation with free-stream Mach numbers for several wedges at  $l/d = 0$  and  $h/\delta = 1.0$ . In general, the pressure drag decreases with free-stream Mach number; for wedges further downstream (i.e.,  $l/d > 0$ ) some tendency was noted for the pressure drag to increase slightly at Mach numbers between 1.88 and 3.16. The sweep of the splitter plate was found to have only a small effect on the wedge pressure drag.

An estimate of the friction drag was made at a free-stream Mach number of 3.16 for configurations using a swept splitter plate. A momentum survey was made with movable total-pressure probes of the flow entering and emerging from the volume enclosed by the main plate, the splitter plate, and the wedge. Tunnel limitations restricted probe measurements to the larger-angled wedges in the forward positions. The variation of the friction drag with wedge height is presented in figure 11 for the  $28^\circ$  and  $62^\circ$  included-angle wedges. Also included for comparative purposes are the pressure-drag data. It is observed that the friction drag is about four times the pressure drag of the  $28^\circ$  wedge in figure 11(b). The friction drag is approximately 1.5 times the pressure drag at  $h/\delta = 1.0$  for the  $62^\circ$  wedge.

In terms of the total-drag coefficient at  $h/\delta$  of 1.0, the drag of the  $62^\circ$  included-angle wedge was slightly higher than that of the  $28^\circ$  wedge. Unpublished data for ramp-type inlets with wedge-type removal on the RM-10 body of revolution also show trends of higher drag coefficients for the larger-angled wedges. Figure 12 presents the percentage increase in forebody drag coefficient as a function of boundary-

[REDACTED]

layer diverter wedge included angle. For this figure the drag is referenced to the forebody drag incurred with a  $16^\circ$  included-angle wedge.

The friction drags presented in figure 11 at  $h/\delta$  of 1.0 are approximately 4 and 17 times the theoretical flat-plate friction drag for the  $28^\circ$  and  $62^\circ$  wedges, respectively.

3078-5

Comparison of wedge- and scoop-type removal systems. - The increase in inlet pressure recovery with boundary-layer removal in figure 13 compares scoop-type removal for a flat-plate-mounted inlet (ref. 8), a scoop-type inlet mounted on the fuselage of supersonic configuration A (ref. 14), and a  $16^\circ$  wedge removal system on a body of revolution (ref. 13). The differences in maximum total-pressure recovery are partly due to the differences in local Mach number ahead of the inlet. All these inlets, nevertheless, show approximately the same rate of increase of pressure recovery with boundary-layer removal. The  $62^\circ$  wedge removal system of figure 2(a), by comparison, required more boundary-layer removal to obtain high inlet pressure recovery. The difference between the wedge-removal effectiveness of the  $16^\circ$  and  $62^\circ$  wedges is due to the greater disturbance caused by the  $62^\circ$  wedge in the boundary layer ahead of the inlet. This disturbance may be minimized by the use of smaller-angled wedges or possibly by simply moving the wedges downstream of the leading edge of the splitter plate. Unpublished data for a two-shock-cone side inlet at a free-stream Mach number of 2.96 show considerable gains in inlet pressure recovery when these modifications were incorporated. Some of this data is included in figure 14. Unpublished data for a wedge boundary-layer-removal system on the RM-10 body of revolution also show these trends; in figure 15 the inlet pressure recovery is again seen to increase with reduction in wedge included angle. In addition, inlet performance was considerably improved by moving the wedge downstream (increasing  $l/d$ ).

The penalty of using a poor wedge removal system is indicated in figure 16. The net thrust-minus-drag is compared for scoop and  $62^\circ$  wedge removal at a free-stream Mach number of 2.93. The scoop-removal data assume sonic discharge of the boundary-layer air. The net-thrust gain for wedge removal was considerably less than for scoop-type removal. This loss arises from (1) the loss of inlet total-pressure recovery, as indicated in figure 2, and (2) the higher drag for the wedge operation compared with scoop operation. The latter is shown graphically in figure 17. The wedge drag data presented duplicate the drag data of the  $62^\circ$  wedge presented in figure 11. The scoop internal drag was considerably less than the wedge drag for  $h/\delta$  of 1.0 or less.

The possibility of encountering more drag by the use of wedge removal has been substantiated in force model tests. Unpublished data from the investigations of references 14 and 16, for two-dimensional ramp and half-cone inlets, respectively, show that the forebody drag

[REDACTED]

for critical inlet operation increased by 10 percent or more by the use of  $68^\circ$  wedge removal compared with scoop-type removal at  $h/\delta = 1.0$ . The use of lower-angle boundary-layer-removal wedges would probably reduce the wedge drag, thus making scoop- and wedge-type removal comparable.

The assumption was made that the inlet performance could be made comparable for  $62^\circ$  wedge- and scoop-type removal by, for example, moving the wedge downstream slightly. The 1-percent difference between the net-thrust coefficient of the scoop- and wedge-type removal systems in figure 16 is directly chargeable to the higher drag of the  $62^\circ$  wedge removal system.

### FUSELAGE FLOW-FIELD CHARACTERISTICS AND THEIR EFFECTS ON SIDE-INLET OPERATION

The side inlet, in addition to boundary-layer-removal drag not associated with nose-type inlets, is inherently penalized by its location on the fuselage. The nose inlet at angle of attack experiences an unbalance of static pressure and Mach number across the compression surface; however, for the same angle-of-attack range the side inlet encounters not only an unbalance of static pressure and Mach number but also possible changes of total pressure, local Mach number, boundary-layer thickness, and crossflow. It is apparent that both the shape and altitude of the body upon which the side inlet is mounted influence side-inlet performance. Possible variations of local flow conditions ahead of typical fuselage-mounted side inlets are presented for the forebodies of figure 3 in figures 18 to 20. It is evident from these figures that the flow field entering the side inlet may be considerably more complex and therefore less susceptible to accurate analysis than in the case of the nose inlet. Accurate prediction of the required optimum supersonic compression design is therefore complicated.

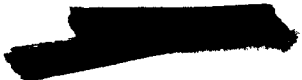
For example, the ratio of the boundary-layer thickness at the inlet at angle of attack to the thickness at zero angle of attack is indicated in figure 18 for several inlet locations on the RM-10 body of revolution and also at the proposed inlet locations on the supersonic aircraft configurations A, B, and D. The boundary layer thickened on the upper quadrants of the body of revolution. In the lower quadrants of the body of revolution and for configurations B and D, the boundary layer either thinned or remained the same. Some thickening of the boundary layer was noted for configuration A at angle of attack. The use of canard-type control surfaces such as used with configurations C and D may severely distort the flow field on the sides and upper quadrants of the body at angle of attack (e.g., ref. 17). Data shown for configuration D were obtained for zero deflection of the canard control surface.

Similarly, the crossflow at the inlet face is indicated in figure 19. The curves shown for the body of revolution are not experimental, but rather are results predicted by linearized potential theory. Along the sides of the body of revolution ( $\phi, 90^\circ$ ) and for the indicated inlet location of configuration B (ref. 20), the rate of crossflow was quite large. Crossflow at the inlet face for configuration A (ref. 14) was reduced somewhat. The curve shown for configuration D, which represents unpublished data from the investigation of reference 18, is not representative of the crossflow at the axis of the inlet, but rather was obtained with a survey wedge off-center of the inlet. Theoretically, the crossflow at the center of the inlet should be zero.

Finally, the local Mach number at the inlet face is shown in figure 20 for a free-stream Mach number of 2.0. Since a low local Mach number is desirable, it is evident that the lower quadrants of a body of revolution are preferable (ref. 19). Configuration A, which utilizes canopy compression, consistently had lower local Mach numbers at angle of attack (ref. 14).

The resultant inlet total-pressure recovery for various inlet locations on bodies of revolution and for proposed inlet locations on supersonic aircraft configurations A, B, and D is shown in figure 21. For a body of revolution of fineness ratio 3.5 (ref. 19) it is seen in figure 21(a) that the bottom of the fuselage is preferable at all angles of attack. For other inlet locations, the local Mach number, the boundary-layer thickness, and the crossflow penalized the inlet performance. In addition, the relative effects of angle of attack on the upper-quadrant body-of-revolution inlets are compared with the upper-quadrant inlet locations on supersonic aircraft configuration A. Generally configuration A was less sensitive to angle of attack. Also, the design of the inlet itself affects the sensitivity to crossflow effects as evidenced by the varying effectiveness of several inlets mounted on configuration A. In figure 21(b)  $9^\circ$  ramp inlets with and without side fairings (ref. 20) are compared on configuration B at a free-stream Mach number of 1.7. These inlets, which were canted down at  $5^\circ$ , enjoyed good angle-of-attack performance, at least for positive angles of attack. The location of the inlet on the bottom of the fuselage for configuration D is also seen to be advantageous in figure 21(c) (ref. 18).

The effectiveness of boundary-layer removal for a body-of-revolution configuration (ref. 19) is presented in figure 22. At zero angle of attack the boundary layer was uniform around the body, and removal of the boundary layer improved the pressure recovery. At angle of attack, the inlet at the bottom of the fuselage showed negligible change in performance, since, as indicated in figure 18, the boundary layer thinned on the bottom of the fuselage. For the upper-quadrant inlet locations, definite benefits to increased boundary-layer removal were noted inasmuch as the boundary layer thickened at angles of attack.

  
Internal Flow Problems of Fuselage-Mounted Side Inlets

When the inlet is satisfactorily located on the fuselage to minimize the external effects previously mentioned, the side inlet is still penalized in comparison with the nose inlet; for the side inlet is liable for increased subsonic-diffuser losses as a result of generally inherent corner effects in the region of the throat, necessary flow-passage-shape transitions, and subsonic-diffuser turns required to discharge the air flow toward the center of the fuselage. Each of these effects is combined into one end result in figure 23. The total-pressure contours following subsonic diffusion are presented for 25° half-angle cone inlets operated (1) as a nose inlet (ref. 21) and (2) as side inlets (refs. 8 and 19). The axes of the subsonic diffusers for the side inlets have been displaced slightly in the direction of the fuselage. The nose inlet (fig. 23(c)) exhibits only a slight variation of total pressure across the diffuser exit, whereas the flat-plate-mounted side inlet (fig. 23(a)) indicates a region of high pressure displaced from the axis and separation on the downstream side of the compression surface. The fuselage-mounted side inlet (ref. 19) had, in general, the same total-pressure variations as the flat-plate-mounted inlet in figure 23(b).

Investigators outside of the NACA have also encountered these subsonic-diffuser problems. For example, the total-pressure contours following subsonic diffusion for a single-shock half-conical side inlet utilizing partial internal compression at a free-stream Mach number of 2.77 is presented in figure 24. These data, which are as yet unpublished, are for critical inlet operation. In figure 24(a) the total-pressure contours exhibit a spread of about 32 percent together with incipient separation on the downstream side of the compression surface. (Additional instrumentation also revealed a spiraling effect as the air passed through the duct.) The use of vortex generators in the subsonic diffuser was found in one application to reduce the spread in total pressure by over 50 percent and also to eliminate the separation, as indicated in figure 24(b). No loss in critical pressure recovery was sustained. While vortex generators may not be a cure-all, it is believed that some internal control may be necessary, especially for free-stream Mach numbers above 2.0. Turning vanes, screens, honeycombs, and internal boundary-layer suction are also examples of possible internal control mechanisms.



## APPENDIX - SYMBOLS

The following symbols are used in this paper:

$C_D$	drag coefficient
$D$	drag
$F_n$	propulsive thrust
$\frac{(F_n - D)}{F_{n,i}}$	thrust parameter
$f$	forebody fineness ratio
$h$	boundary-layer-removal height
$h/\delta$	boundary-layer-removal height parameter
$l/d$	wedge position parameter (fig. 8)
$M$	Mach number
$P/P_0$	total-pressure recovery
$\alpha$	angle of attack, deg
$\beta$	crossflow angle, deg
$\delta$	boundary-layer thickness
$\delta/\delta_{\alpha=0}$	boundary-layer-thickness ratio for angle-of-attack operation
$\epsilon$	wedge included angle, deg
$\phi$	circumferential inlet location, deg
$\psi$	control-surface deflection, deg

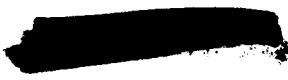
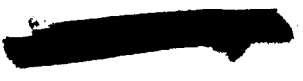
## Subscripts:

$i$	ideal
max	maximum
$p$	pressure
$0$	free stream

## REFERENCES

1. Davis, Wallace F., and Goldstein, David L.: Experimental Investigation at Supersonic Speeds of Twin-Scoop Duct Inlets of Equal Area. I - An Inlet Enclosing 61.5 Percent of the Maximum Circumference of the Forebody. NACA RM A7J27, 1948.
2. Davis, Wallace F., Brajnikoff, George B., Goldstein, David L., and Spiegel, Joseph M.: An Experimental Investigation at Supersonic Speeds of Annular Duct Inlets Situated in a Region of Appreciable Boundary Layer. NACA RM A7G15, 1947.
3. Davis, Wallace F., and Brajnikoff, George B.: Pressure Recovery at Supersonic Speeds Through Annular Duct Inlets Situated in a Region of Appreciable Boundary Layer. I - Addition of Energy to the Boundary Layer. NACA RM A8A13, 1948.
4. Davis, Wallace F., and Edwards, Sherman S.: Experimental Investigation at Supersonic Speeds of Twin-Scoop Duct Inlets of Equal Area. III - Inlets Enclosing 37.2 Percent of the Maximum Circumference of the Forebody. NACA RM A8E04, 1948.
5. Brajnikoff, George B.: Pressure Recovery at Supersonic Speeds Through Annular Duct Inlets Situated in a Region of Appreciable Boundary Layer. II - Effect of an Oblique Shock Wave Immediately Ahead of the Inlet. NACA RM A8F08, 1948.
6. Davis, Wallace F., Edwards, Sherman S., and Brajnikoff, George B.: Experimental Investigation at Supersonic Speeds of Twin-Scoop Duct Inlets of Equal Area. IV - Some Effects of Internal Duct Shape Upon an Inlet Enclosing 37.2 Percent of the Forebody Circumference. NACA RM A9A31, 1949.
7. Edwards, Sherman S.: Experimental Investigation at Supersonic Speeds of Side Scoops Employing Boundary-Layer Suction. NACA RM A9I29, 1949.
8. Goelzer, H. Fred, and Cortright, Edgar M., Jr.: Investigation at Mach Number 1.88 of Half of a Conical-Spike Diffuser Mounted as a Side Inlet with Boundary-Layer Control. NACA RM E51G06, 1951.
9. Wittliff, Charles E., and Byrne, Robert W.: Preliminary Investigation of a Supersonic Scoop Inlet Derived from a Conical-Spike Nose Inlet. NACA RM L51G11, 1951.
10. Piercy, Thomas G., and Johnson, Harry W.: Investigation at Mach Number 2.93 of Half of a Conical-Spike Diffuser Mounted as a Side Inlet with Boundary-Layer Control. NACA RM E52G23, 1952.

11. Piercy, Thomas G., and Johnson, Harry W.: A Comparison of Several Systems of Boundary-Layer Removal Ahead of a Typical Conical External-Compression Side Inlet at Mach Numbers of 1.88 and 2.93. NACA RM E53F16, 1953.
12. Frazer, Alson C., and Anderson, Warren E.: Performance of a Normal-Shock Scoop Inlet with Boundary-Layer Control. NACA RM A53D29, 1953.
13. Valerino, Alfred L., Pennington, Donald B., and Vargo, Donald J.: Effect of Circumferential Location on Angle of Attack Performance of Twin Half-Conical Scoop-Type Inlets Mounted Symmetrically on the RM-10 Body of Revolution. NACA RM E53G09, 1953.
14. Valerino, Alfred S.: Performance Characteristics at Mach Numbers to 2.0 of Various Types of Side Inlets Mounted on Fuselage of Proposed Supersonic Airplane. I - Two-Dimensional Compression-Ramp Inlets with Semicircular Cowls. NACA RM E52E02, 1952.
15. Weinstein, M. I.: Performance of Supersonic Scoop Inlets. NACA RM E52A22, 1952.
16. Allen, J. L., and Simon, P. C.: Performance Characteristics at Mach Numbers to 2.0 of Various Types of Side Inlets Mounted on Fuselage of Proposed Supersonic Airplane. II - Inlets Utilizing Half of a Conical Spike. NACA RM E52G08, 1952.
17. Wise, George A., and Dryer, Murray: Influence of a Canard-Type Control Surface on Flow Field in Vicinity of Symmetrical Fuselage at Mach Numbers 1.8 and 2.0. NACA RM E52E13, 1952.
18. Fradenburgh, Evan A., and Campbell, Robert C.: Characteristics of a Canard-Type Missile Configuration with an Underslung Scoop Inlet at Mach Numbers from 1.5 to 2.0. NACA RM E52J22, 1953.
19. Hasel, Lowell E., Lankford, John L., and Robins, A. W.: Investigation of a Half-Conical Scoop Inlet Mounted at Five Alternate Circumferential Locations Around a Circular Fuselage. Pressure Recovery Results at a Mach Number of 2.01. NACA RM L53D03b, 1953.
20. Obery, Leonard J., and Stitt, Leonard E.: Investigation at Mach Numbers 1.5 and 1.7 of Twin-Duct Side Air-Intake System with 9° Compression Ramp Including Modifications to Boundary-Layer-Removal Wedges and Effects of a Bypass System. NACA RM E53H04, 1953.
21. Moeckel, W. E., Connors, J. F., and Schroeder, A. H.: Investigation of Shock Diffusers at Mach Number 1.85. I - Projecting Single-Shock Cones. NACA RM E6K27, 1946.

- 
22. Esenwein, Fred T.: Performance Characteristics at Mach Numbers to 2.00 of Various Types of Side Inlets Mounted on Fuselage of Proposed Supersonic Airplane. III - Normal-Wedge Inlet with Semi-circular Cowl. NACA RM E52H20, 1952.
  23. Davids, Joseph, and Wise, George A.: Investigation at Mach Numbers 1.5 and 1.7 of Twin-Duct Side Intake System with Two-Dimensional  $6^\circ$  Compression Ramps Mounted on a Supersonic Airplane. NACA RM E53H19, 1953.
  24. Dryer, Murray, and Beke, Andrew: Performance Characteristics of a Normal-Shock Side Inlet Located Downstream of a Canard Control Surface at Mach Numbers of 1.5 and 1.8. NACA RM E52F09, 1952.
- 

BOUNDARY-LAYER REMOVAL SYSTEMS

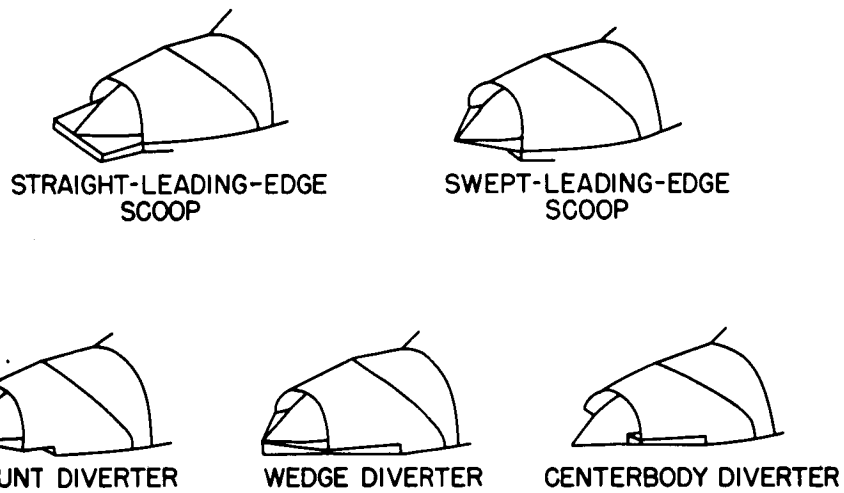


Figure 1

COMPARISON OF SEVERAL SYSTEMS OF BOUNDARY-LAYER REMOVAL

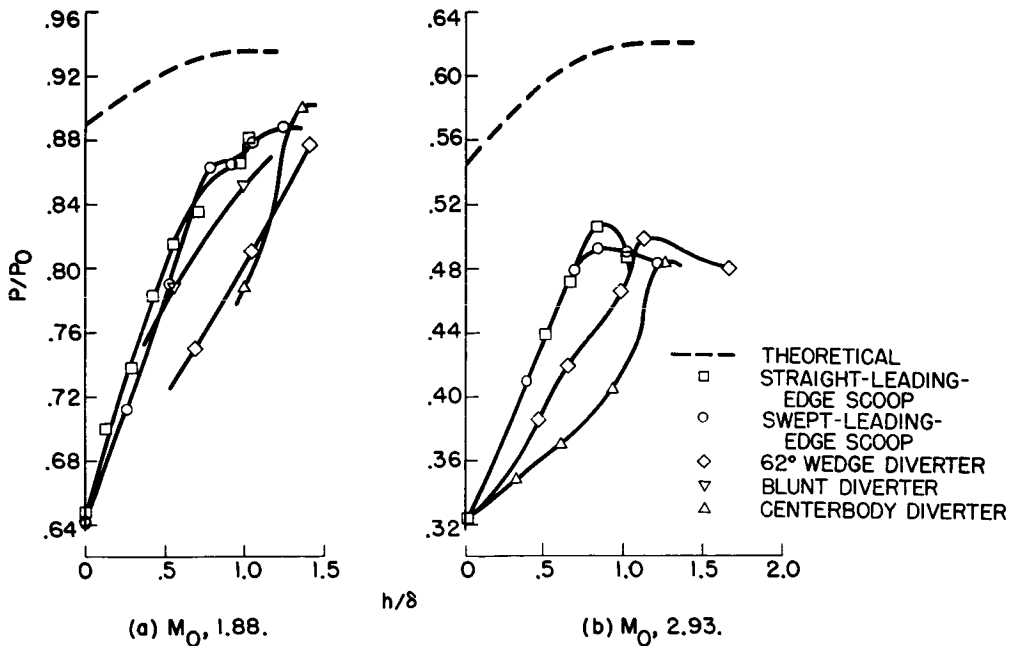
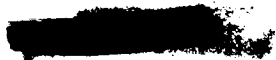
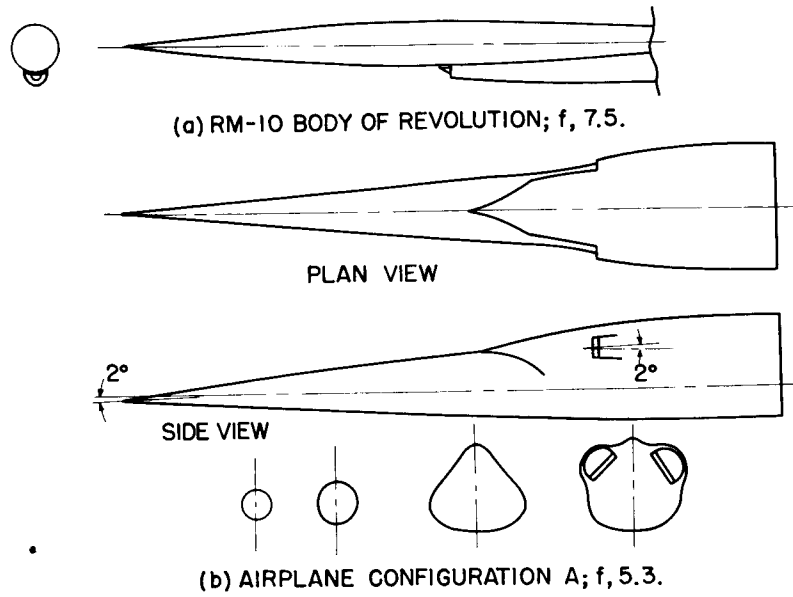


Figure 2

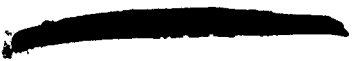


### SUMMARY OF SUPERSONIC AIRCRAFT FOREBODIES

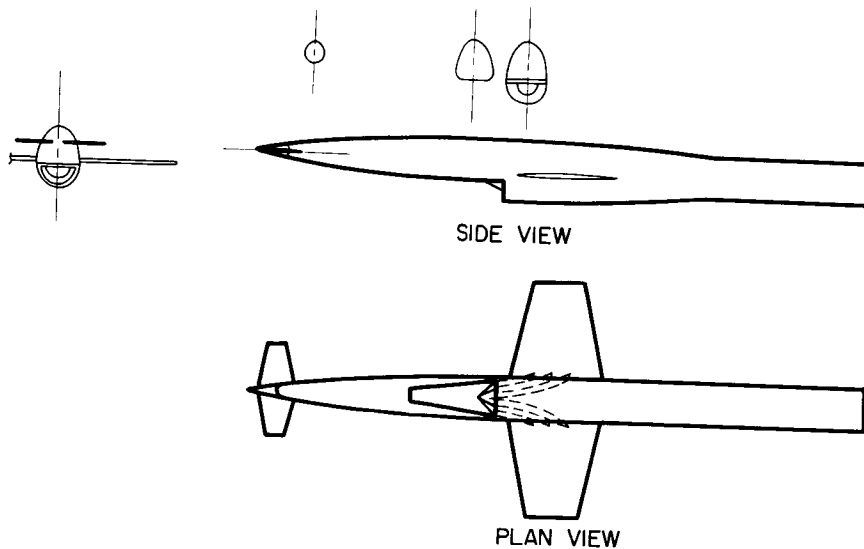


3078-G

Figure 3



SUMMARY OF SUPERSONIC AIRCRAFT FOREBODIES



(e) MISSILE CONFIGURATION D; f, 6.1.

Figure 3

PERCENTAGE INCREASE OF FOREBODY DRAG COEFFICIENT FOR COMPLETE BOUNDARY-LAYER REMOVAL

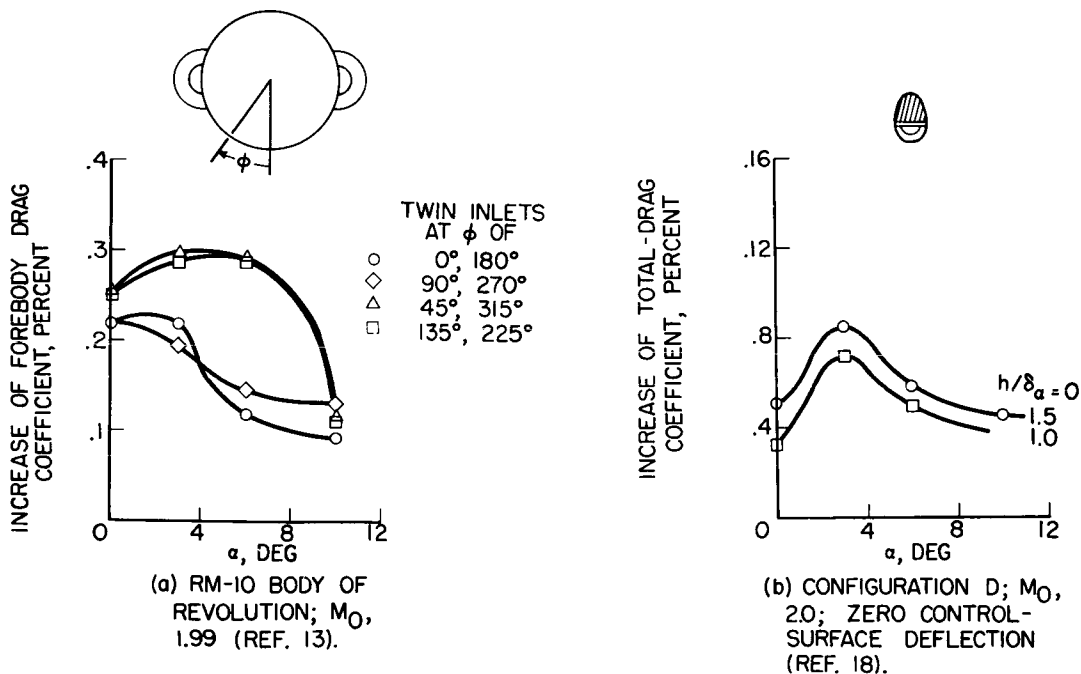


Figure 4

PERFORMANCE OF 14° RAMP INLET WITH  
 ROUNDED SEMICIRCULAR COWLING  
 WITH SCOOP BOUNDARY-LAYER REMOVAL  
 CONFIGURATION A (REF. 14);  $\alpha, 3^\circ$ ;  $M_0, 2.0$

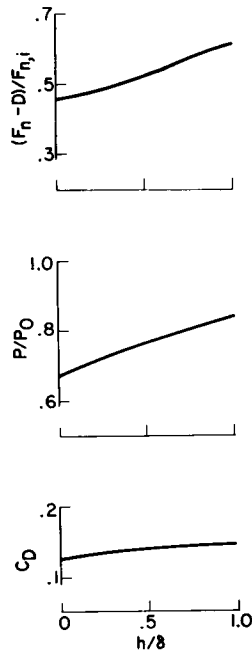


Figure 5

COMPARISON OF INLET PERFORMANCE AT MAXIMUM  
 THRUST-MINUS DRAG  
 CONFIGURATION A (REF. 15);  $h/\delta, 1.0$ ;  $M_0, 2.0$ ;  $\alpha, 3^\circ$

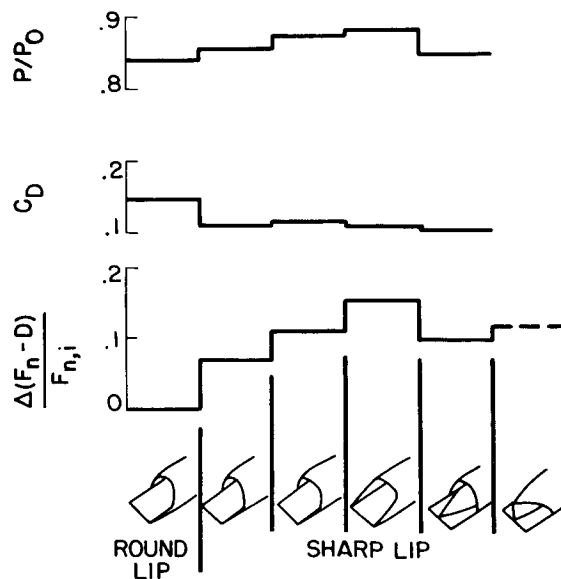


Figure 6

3078-G

THEORETICAL NET-THRUST GAIN WITH SCOOP-TYPE BOUNDARY-LAYER REMOVAL

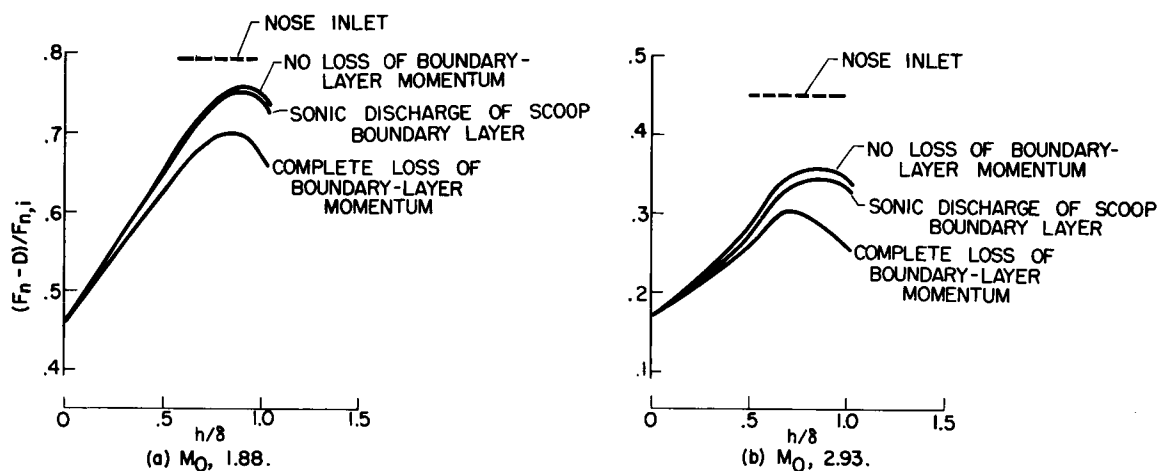


Figure 7

SCHEMATIC REPRESENTATION OF MODEL FOR DETERMINATION OF DRAG OF BOUNDARY-LAYER REMOVAL WEDGES

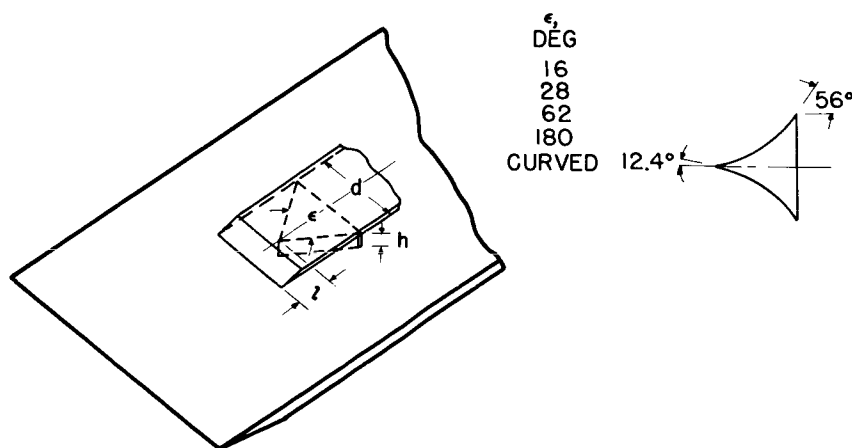


Figure 8

TYPICAL VARIATION OF WEDGE PRESSURE-DRAG COEFFICIENT WITH WEDGE INCLUDED ANGLE AND WEDGE POSITION

$M_0, 1.88$

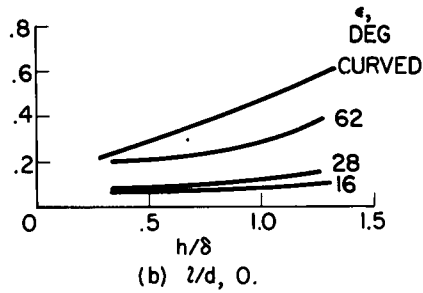
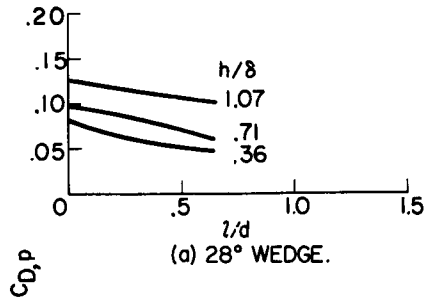


Figure 9

EFFECT OF FREE-STREAM MACH NUMBER ON WEDGE PRESSURE-DRAG COEFFICIENT

$h/8, 1.0; l/d, 0$

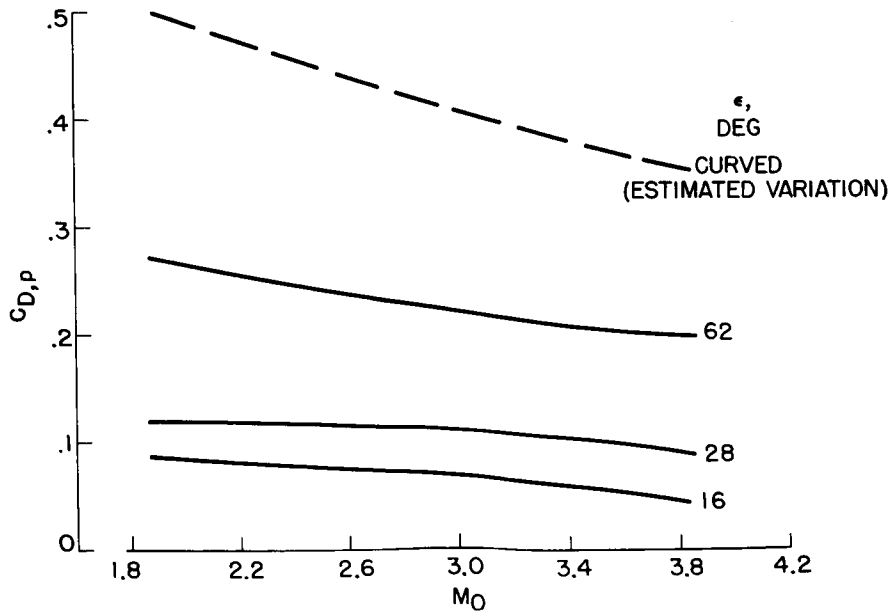


Figure 10

VARIATION OF WEDGE DRAG COEFFICIENT AS FUNCTION OF WEDGE HEIGHT  
 $M_0, 3.16$

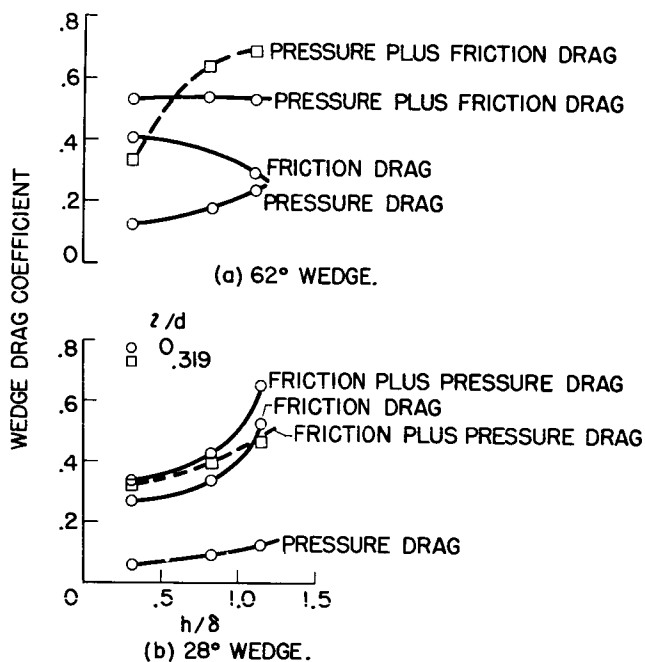


Figure 11

PERCENTAGE INCREASE OF FOREBODY DRAG COEFFICIENT WITH WEDGE INCLUDED ANGLE. RM-10 BODY OF REVOLUTION  
 $\alpha, 0^\circ; M_0, 2.0$

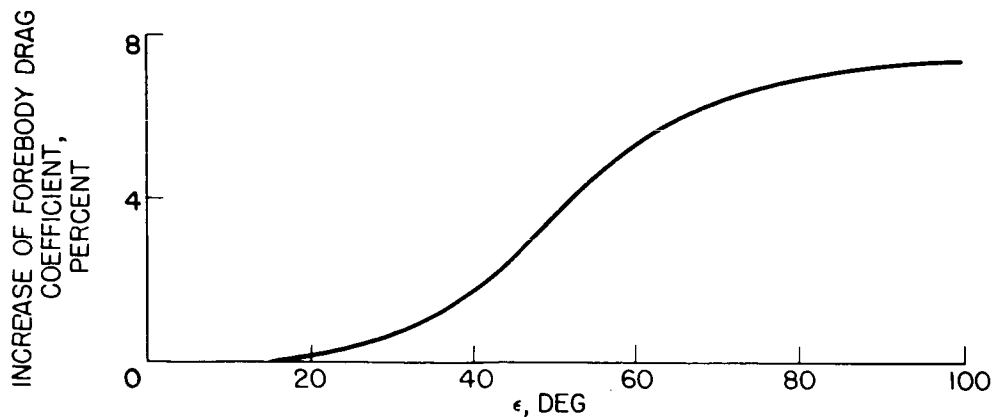


Figure 12

COMPARISON OF SCOOP AND WEDGE BOUNDARY-LAYER REMOVAL SYSTEMS

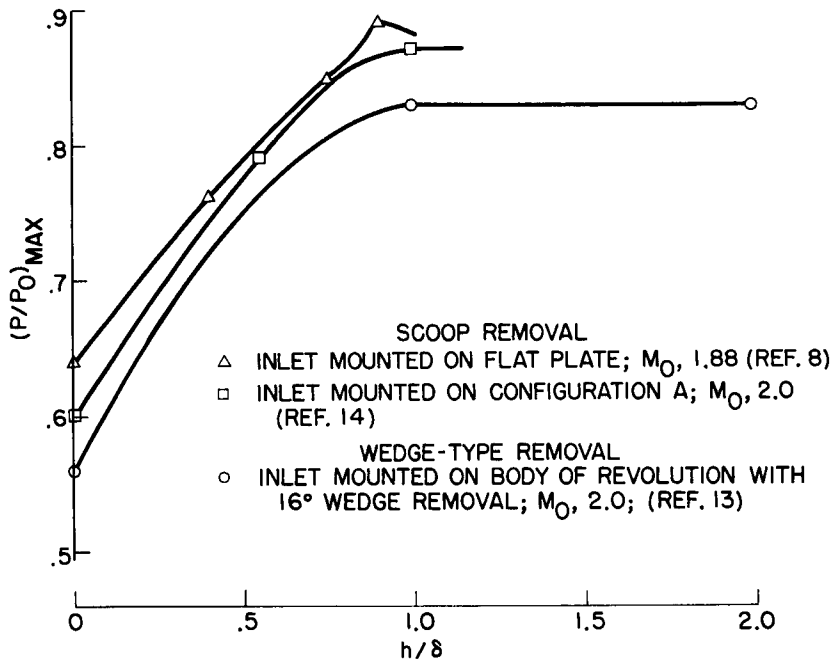


Figure 13

PERFORMANCE OF TWO-SHOCK SEMICIRCULAR INLET  
 $M_0, 2.96$

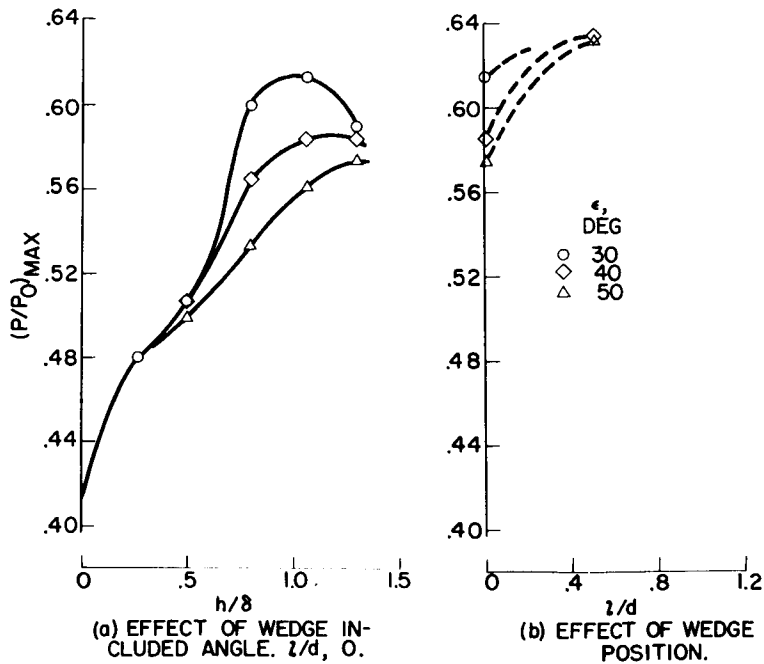


Figure 14

EFFECT OF WEDGE INCLUDED ANGLE AND WEDGE POSITION  
ON INLET PRESSURE RECOVERY

RM-10 BODY OF REVOLUTION;  $\alpha, 0^\circ$ ;  $h/\delta, 1.0$ ;  $M_0, 2.0$

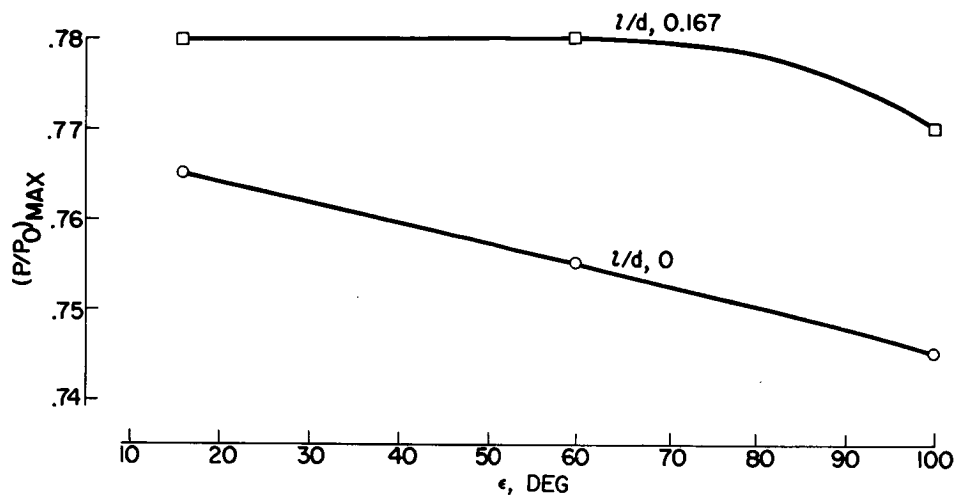


Figure 15

INFLUENCE OF BOUNDARY-LAYER REMOVAL SYSTEM ON  
NET-THRUST PARAMETER

$M_0, 2.93$

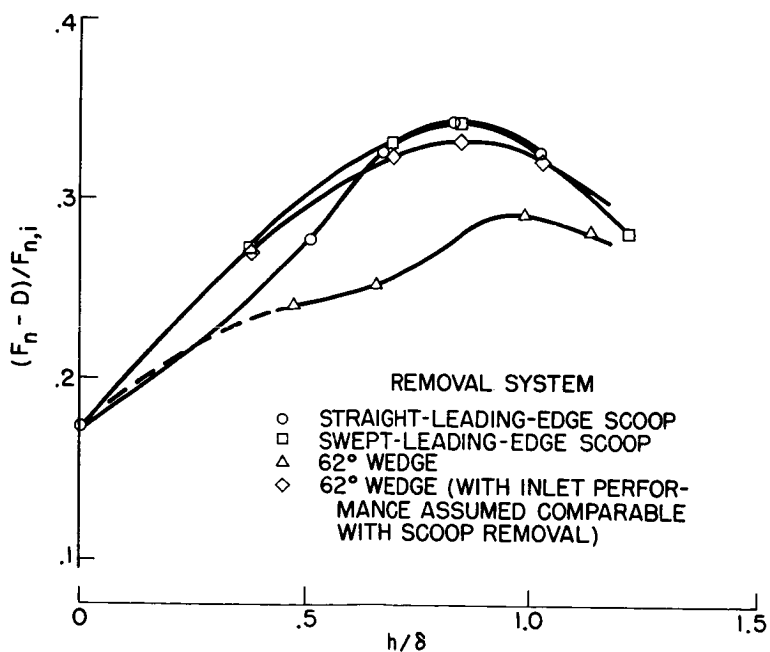
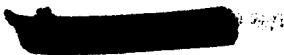


Figure 16



COMPARISON OF SCOOP AND WEDGE BOUNDARY-LAYER REMOVAL DRAG

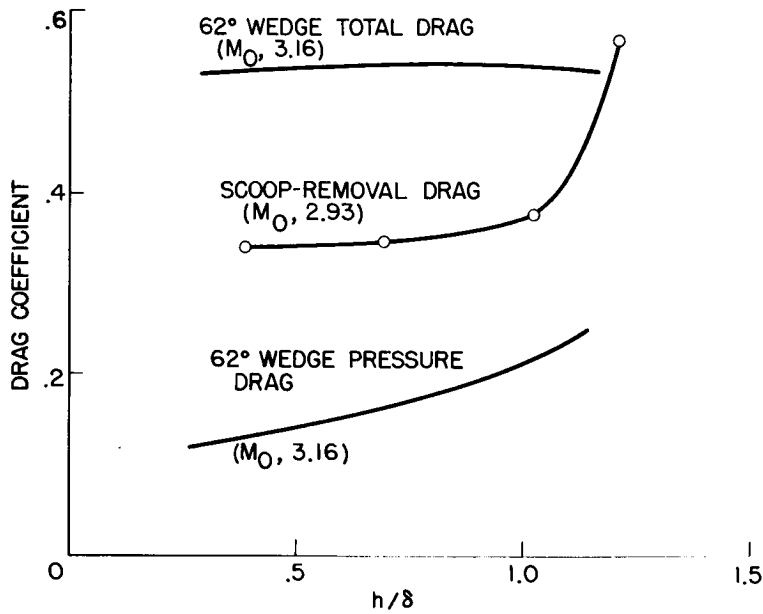


Figure 17

EFFECT OF ANGLE OF ATTACK ON BOUNDARY-LAYER THICKNESS AT INLET STATION  
 $M_0, 2.0$

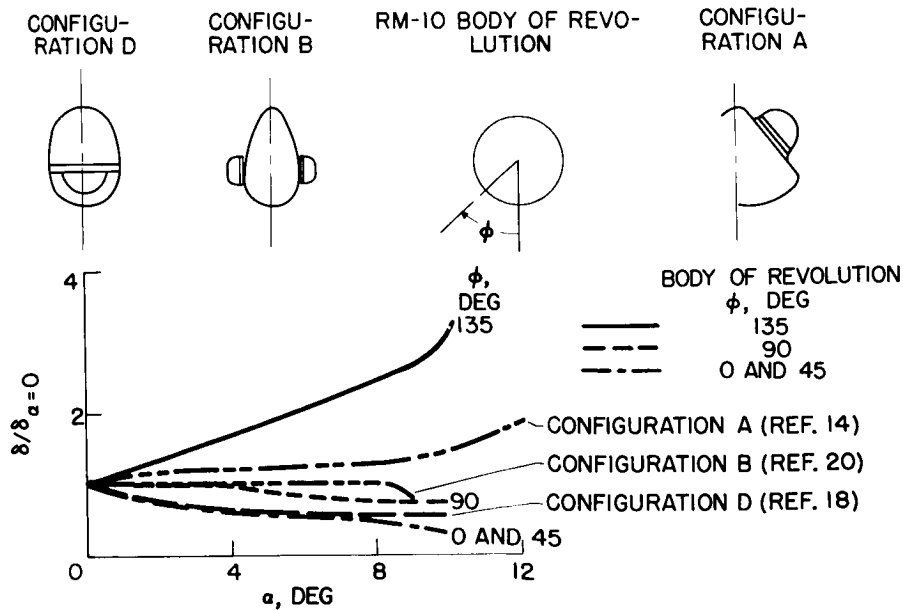
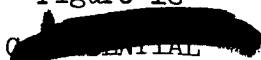


Figure 18



COMPARISON OF CROSSFLOW CHARACTERISTICS AT SELECTED INLET LOCATIONS FOR SEVERAL FOREBODIES  
 $M_0, 2.0$

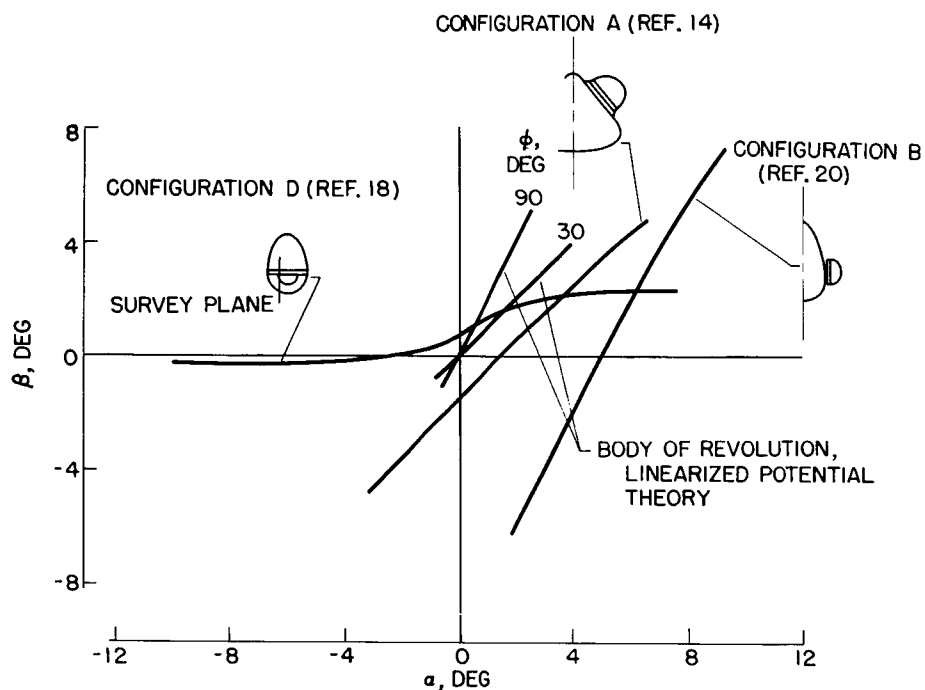


Figure 19

COMPARISON OF LOCAL MACH NUMBER AT SELECTED INLET LOCATIONS FOR SEVERAL FOREBODIES  
 $M_0, 2.0$

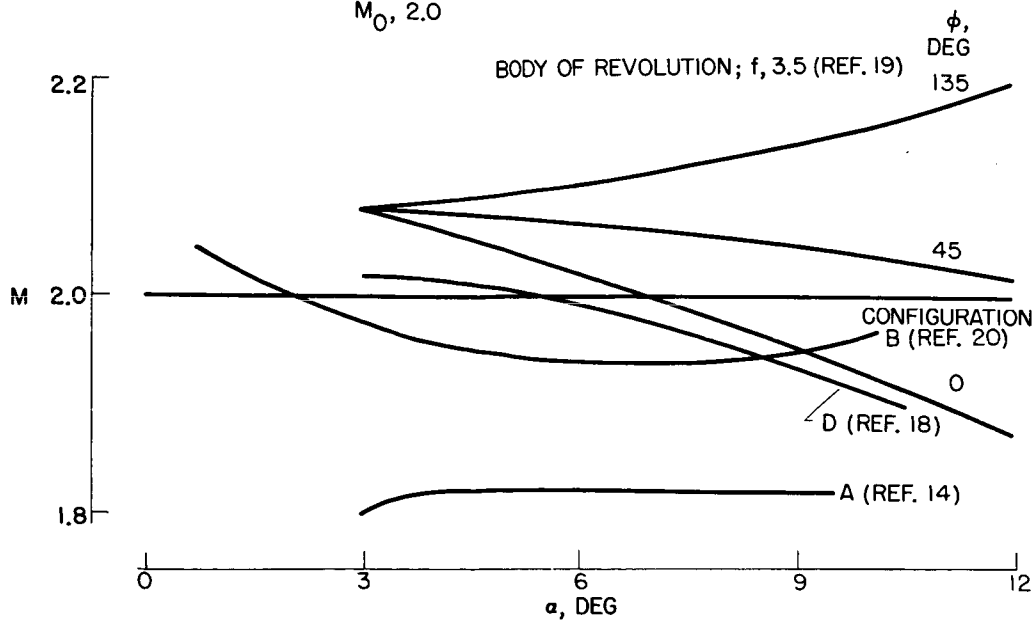


Figure 20

EFFECT OF ANGLE OF ATTACK ON MAXIMUM INLET TOTAL-PRESSURE RECOVERY FOR SELECTED INLET LOCATIONS ON SEVERAL FOREBODIES

- CONFIGURATION A  
 ○ RAMP INLET, ROUNDED LIP (REF. 14)  
 ▽ RAMP INLET, SHARP LIP (REF. 14)  
 ▾ HALF-CONICAL INLET (REF. 16)
- BODY OF REVOLUTION  
 □  $f, 7.5; \phi, 135^\circ$  (REF. 13)  
 ◇  $f, 3.5; \phi, \text{INDICATED}$  (REF. 19)  
 △  $f, 7.5; \phi, \text{INDICATED}$  (UNPUBLISHED DATA FOR  $14^\circ$  RAMP INLET)

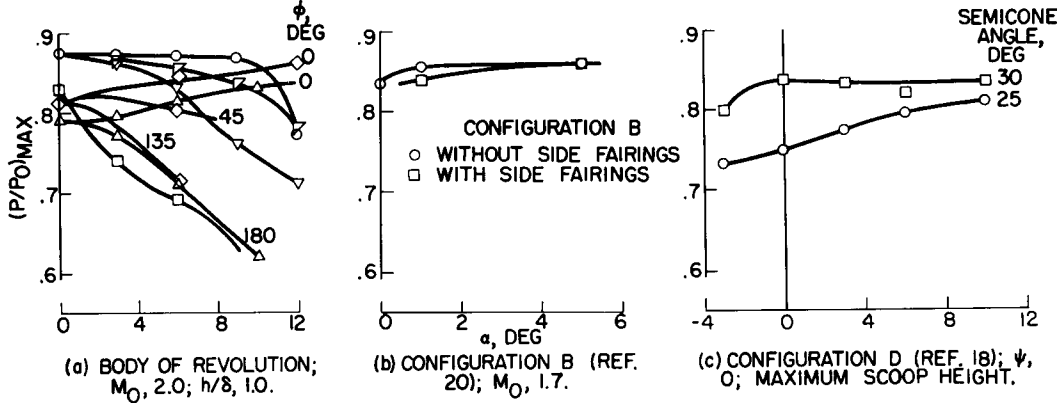


Figure 21

EFFECT OF BLEED HEIGHT ON INLET TOTAL-PRESSURE RECOVERY FOR BODY OF REVOLUTION WITH  $f$  OF 3.5 (REF. 19)  
 $M_0, 2.0$

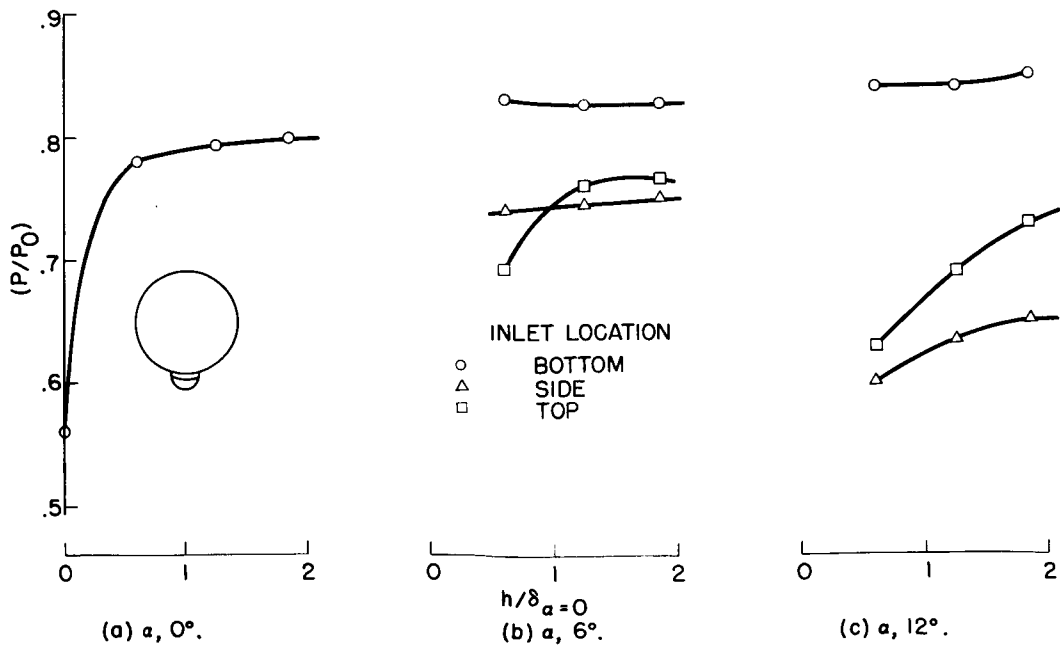


Figure 22

TYPICAL TOTAL-PRESSURE CONTOURS AT EXIT OF SUBSONIC DIFFUSER FOR SIDE AND NOSE INLETS AT PEAK PRESSURE RECOVERY

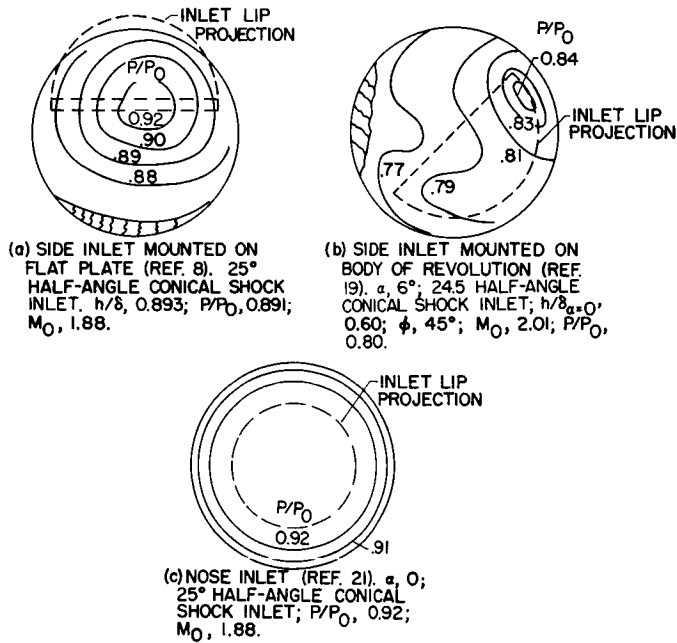


Figure 23

TOTAL-PRESSURE CONTOURS AT EXIT OF SUBSONIC DIFFUSER FOR SIDE-INLET INSTALLATION INCORPORATING DIFFUSER WARPING CONFIGURATION C;  $M_0$ , 2.77

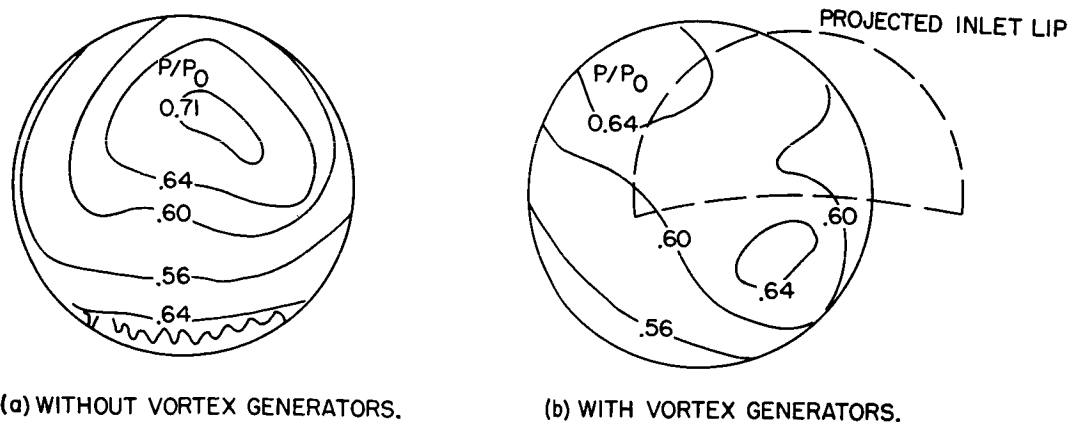


Figure 24

## INLET-ENGINE MATCHING CONSIDERATIONS FOR HIGH-SPEED

## SUPERSONIC AIRPLANES

By Leonard J. Obery and Leonard E. Stitt

## INTRODUCTION

The ultimate performance of a turbojet-powered aircraft is dependent on the individual performances of the components of the internal air-flow system. The engine of present high-speed airplanes cannot be considered separately from the rest of the aircraft; rather it may be regarded as the heat pump in the over-all system of inlet, ducting, engine, and exit nozzle, all of which components except the engine are usually regarded as part of the airframe. The net thrust available to propel the aircraft may be to a large extent controlled by the performance of the inlet and exit nozzle rather than by the physical potentialities of the engine alone. This paper will discuss some of the problems relating to the design of inlets for particular engines, or to what is usually termed inlet-engine matching.

## SYMBOLS

The following symbols are used in this report:

A	area
$C_D$	spillage drag coefficient based on inlet area
$D_A$	additive drag
$F_n$	net thrust
M	Mach number
$m/m_c$	subcritical spillage ratio
$m/m_0$	mass-flow ratio
P	total pressure
T	total temperature, °F
W	actual weight flow, lb/sec
$W\sqrt{\theta}/\delta$	corrected weight flow, lb/sec

- 8 total-pressure correction factor,  $P/2116$   
0 total temperature correction factor,  $T/519$

## Subscripts:

- a available  
c critical  
i ideal  
t throat  
0 free stream  
3 diffuser-exit or compressor-face station

## DISCUSSION AND ANALYSIS

For subsonic flight speeds, few problems exist in designing inlet systems. Provided that the inlet is large enough to deliver air to the engine without internal choking and that reasonably smooth passages, without extremely sharp turns, exist in the internal ducting, reasonably good performance may be expected from most inlet installations. However, at supersonic speeds new problems arise, and phenomena which did not occur subsonically must be considered.

As in the subsonic flight regime, the engine will force the inlet to operate at a particular mass-flow condition for each point in the flight range. Thus, even though the inlet by itself is capable of operating over a large range of mass flow and pressure recovery, when coupled to an engine it will operate only at the condition set by the engine requirements. If the supersonic inlet is made too small, it will be forced to operate supercritically, that is, it will capture a certain maximum mass flow dependent on the inlet geometry, and a normal or terminal shock will be located somewhere in the subsonic diffuser passage. Thus, the air delivered to the engine will be at a lower total-pressure recovery than critical, and a portion of the compression available from ram will be lost to the engine; the thrust output will thus be reduced, as shown in references 1 and 2. Conversely, if the supersonic inlet is made too large, it will be forced to operate subcritically, that is, it will capture less air flow than is possible from its geometry and will produce an attendant additive drag, as discussed, for example, in reference 3, and, perhaps even more serious, possible inlet-shock instability or buzz.

An example of these two conditions is shown in figure 1, where the corrected air flow required by the engine is given by the solid curve.

The dashed curve labeled "supersonic matching" represents the critical corrected weight-flow operating point (highest pressure recovery at maximum mass flow) of an inlet designed to deliver the required air flow to the engine at a Mach number of 2.8. A development of these parameters is presented in reference 4. This particular inlet has a wedge angle of  $20^\circ$  and operates with shock on lip at a Mach number of 2.8. As the free-stream Mach number is reduced, more corrected air flow is required than the inlet can deliver at critical mass-flow conditions, and the inlet is thus forced by the engine to operate supercritically at a low total-pressure recovery. For example, at a Mach number of 0.9, the recovery of the inlet and ducting system is only 55 percent instead of the 95 percent potentially possible from the inlet. If the inlet-engine system had operated at the potential 95-percent pressure recovery, the resulting thrust  $F_{na}$  would have been 93 percent of the ideal engine thrust. However, because of the low total-pressure recovery forced by the engine, the operating engine thrust with this inlet is only 46 percent of the available engine thrust at this Mach number.

The supercritical inlet operation could be eliminated by simply scaling up the inlet to capture the required engine air flow with an inlet velocity ratio of 1 at a Mach number of 0.9. By using the same ramp angle and free-stream Mach number for ramp shock-on-lip operation, the critical operating points for this scaled-up inlet are designated as the subsonic-matching curve of figure 1. As the free-stream Mach number is increased, the inlet can now deliver at critical-flow conditions more air flow than the engine can use, and hence the inlet will be forced to operate subcritically (at a mass flow less than maximum) with attendant additive drag and susceptibility to shock pulsations or buzz. It is estimated that the additive drag of this inlet at a Mach number of 2.8 will be approximately 70 percent of the available engine thrust. This available thrust, with an optimum pressure-recovery ramp but without any additive drag, is approximately 54 percent of the ideal engine thrust at 100-percent pressure recovery.

The problem of inlet-engine matching is thus to design the inlet so that it operates through the range of free-stream Mach number at such conditions that it delivers the required amount of air flow to the engine at a high pressure recovery and with a minimum additive drag which corresponds to near-critical inlet operation. Related analyses on inlet-engine matching are discussed additionally in references 4 to 8.

It is evident that any fixed inlet system will not yield efficient operation over an extended Mach number range, as shown, for example, by the case in figure 1. Generally, for supersonic Mach numbers below 1.5, a fixed-geometry inlet will perform satisfactorily if it is sized and designed properly; however, for Mach numbers much in excess of that value, variable inlet geometry of some sort will be desirable.

Several systems of variable inlet geometry are illustrated in figure 2. These systems will, in general, keep the inlet operating near critical flow in order to obtain the needed engine air flow at a high pressure recovery without incurring subcritical additive drag or pulsing flow. The first example is an annular inlet with a translating conical spike (fig. 2(a)). For this inlet, the spike moves fore and aft to keep the inlet at near-critical operation, coincidentally delivering the proper amount of air flow to the engine. As the spike moves to capture more or less air, the high subcritical or normal-shock additive drag is traded for the lesser supercritical or oblique-shock additive drag. Experimental data are available on this type inlet in reference 9. Several disadvantages are present in this system, however; for example, the cone angle cannot readily be changed to maintain optimum cone angles at each Mach number, and hence maximum ram compression (or total-pressure recovery) may not be attained throughout the range of flight speed. It is also possible that the cone may be translated far enough forward that expansions about the shoulder formed by the transition from the nose cone to a near-cylindrical afterbody may cause poorer pressure recoveries than expected, as illustrated in reference 9. Although good design and proper location on the fuselage may alleviate much of the angle-of-attack flow into the inlet, annular inlets with conical spikes generally suffer considerable performance losses at angle of attack as a result of boundary-layer accumulation on the lee side of the cone caused by body crossflow.

A second general type of variable-geometry inlet is the two-dimensional inlet with a variable-angle wedge used as the external compression surface (fig. 2(b)). The oblique shock generated by the ramp leading edge may be rotated to a desired position by varying the wedge angle. As with the previous example, the variable-wedge inlet may be operated near critical flow, and the high subcritical additive drag is exchanged for the smaller supercritical drag. However, in this case if the inlet is properly designed, near-optimum ramp angles may be selected at each Mach number, and the advantage of higher pressure recovery or external ram compression may be realized. Also, the angle-of-attack characteristics of the ramp inlet are generally superior to those of the conical-spike inlet. Experimental investigations of various fixed ramp inlets are discussed in references 10 to 12.

The object of both types of variable inlets discussed previously was to capture the required amount of air flow through the Mach number range at critical flow conditions. This objective was accomplished by translating or rotating the nose or leading-edge oblique shock ahead of the cowl. If the desired air flow is considerably less than would be possible from the cowl size, the oblique shock will stand far ahead of the cowl and relatively large supercritical additive drags will result. The objective of delivering to the engine smaller amounts of mass flow may also be accomplished by capturing a full free-stream tube of air at the inlet and returning the excess mass flow to the free stream ahead of the turbojet compressor. A configuration of this type is called an air-flow bypass system (fig. 2(c)).

The bypass may be used with any inlet type in the following manner: The inlet shock is kept near the cowl lip to capture the maximum air flow determined by the inlet size or to spill supersonically small amounts of air in order to maintain maximum recovery. The air captured by the inlet in excess of that required by the engine is then discharged in a nearly axial direction at some point in the ducting ahead of the engine compressor, as demonstrated in references 13 to 15. The drag resulting from the capture and discharge of the excess air depends on the momentum lost by that air and is normally quite small. In effect, then, the advantage of the bypass system results from trading supersonic additive drag for a smaller bypass-spillage drag. The bypass may also be used advantageously with the variable-wedge-type inlet, in that the ramp-angle setting is not determined by the engine air-flow requirements and hence may be set for near-optimum pressure recovery.

A comparison of the various types of spillage drag for conical-spike-type annular inlets is shown in figure 3 for a Mach number of 2.0, similar to a development presented in reference 16. Similar comparisons would be expected throughout the Mach number range, with the absolute magnitude of the various spillage drags increasing with increasing Mach number. The trends indicated in the curves would also be expected for two-dimensional inlets (with somewhat different absolute magnitudes however). Theoretical values of normal-shock-spillage (or subcritical spillage) drag for the open-nose inlets of reference 17, oblique-shock-spillage (called supercritical spillage) drag also from reference 17, and bypass-spillage drag based on the momentum loss from free stream to bypass sonic exit are presented in figure 3. The data points shown in the figure are experimental values of the three types of spillage drag obtained from references 13, 14, and 18 to 21 and show quite good agreement with the theoretical values. It should be pointed out that the magnitude of the supercritical additive drag is directly dependent on the type of compression surface used, since it is calculated as the pressure force acting on the limiting entering streamline to the inlet; whereas subcritical additive drag is probably less dependent on the compression surface and more dependent on the pressure existing behind the normal or terminal inlet shock. Bypass drag, of course, is independent of the type of inlet system used to the extent that it depends on the pressure recovery existing at the bypass exit. The drag values presented represent only the additive drag acting ahead of the cowl; therefore, no consideration has been given to the reduction in cowl-pressure drag resulting from spillage. In general, the reduced cowl-pressure drags cancel the additive drag subsonically and are quite important at the lower supersonic Mach numbers (possibly to a Mach number of 2.0) but probably become less important at the higher Mach numbers. This reduction in drag should be considered in any force analysis of the inlet; however, the prediction of cowl-pressure drag, particularly at reduced mass flows, is extremely difficult at the present time and no satisfactory analytical solution is possible. Therefore, since the reduction in cowl-pressure drag is probably small, it will be disregarded in the analysis, thereby tending to make any calculations more conservative.

[REDACTED]

To design and analyze any air-inlet system, it is necessary to estimate both the critical total-pressure recovery and the mass flow that the system will provide the compressor over the flight path of the aircraft. It is possible to determine the critical mass flow from the geometry of the inlet and the attendant shock pattern. However, in order to evaluate the total-pressure recovery, both the supersonic loss through the oblique and normal shocks and the subsonic diffuser loss through the duct must be estimated. The total-pressure recovery across the inlet-shock system may be calculated from two-dimensional or three-dimensional supersonic-flow theory, for example from references 22 and 23. Values of subsonic diffuser recovery are difficult to calculate, and for estimation purposes it has been assumed that the pressure recovery at the diffuser exit will be 95 percent of the supersonic recovery for flight Mach numbers from 1.0 to 2.0. From a survey of the rather meager data available, it has been further assumed that the subsonic recovery will decrease from 95 percent at a Mach number of 2.0 to 90 percent at a Mach number of 2.8. By combining the calculated supersonic recovery with the assumed subsonic diffuser recovery, it is possible to predict an over-all inlet total-pressure recovery consistent with values that have already been obtained experimentally (refs. 10 to 12, 15, 18 to 20, and 24 to 34), as illustrated, in particular, in references 24 and 31.

A theoretical method for determining the total-pressure recovery for sharp-lip inlets operating at subsonic flight Mach numbers has been developed in reference 35. The pressure-recovery curve from this reference has been reproduced in figure 4 together with experimental recoveries from references 34, 36, and 37. The agreement between experiment and theory is quite reasonable; thus, it may be expected that reliable subsonic performance of a particular sharp-lip inlet can be calculated by this method.

#### APPLICATION OF INLET-ENGINE MATCHING TECHNIQUE

Conventional engine. - To demonstrate the technique of inlet-engine matching, three inlets have been designed to supply air to the conventional engine, referred to in a subsequent paper, which powers a proposed supersonic interceptor over a given flight plan. The engine has a compressor area of 1.66 square feet and a constant rotational speed. The proposed flight plan of the interceptor and the resultant corrected air-flow requirements of the engine over this plan are presented in figure 5. The flight plan specified that the airplane take off and accelerate to a Mach number of 0.9 near sea level, climb to 35,000-foot altitude at a Mach number of 0.9 and accelerate to a Mach number of 1.5, accelerate and climb simultaneously to a Mach number of 2.8 and 48,000-foot altitude, and finally climb to 70,000-foot altitude. Because of the large variation in corrected weight-flow requirements over the flight plan, a variable-geometry inlet will be required. All

[REDACTED]

three inlets have been designed for matching at a Mach number of 2.8 in the tropopause and have fixed cowl geometry without internal contraction. Although mechanical details were not studied, it is believed that the inlets presented would be feasible to build.

The aerodynamic characteristics of the three inlets are presented in figure 6 over the range of flight Mach number. The single variable-wedge inlet (dashed curve) was designed to operate with ramp angles from zero to  $22^\circ$ . This inlet operates with the oblique shock on the cowl lip at a Mach number of 2.8 and with the normal shock inside the lip. At Mach numbers less than 2.8, it is possible to match the engine at nearly critical inlet operation by using optimum pressure-recovery wedge angles, since the reduction of air flow with the forward rotation of the oblique shock nearly coincides with the engine operating requirements. In this case the additive drag would result from spillage behind the oblique shock, since the normal shock would stand near the cowl lip. The wedge angle is maintained high enough to cause shock detachment at the low supersonic Mach numbers in order to supply the required air flow without spillage behind the inlet terminal shock. At take-off and subsonic speeds, the wedge angle is reduced to zero to obtain the largest possible inlet area.

Although it is possible in this case to maintain nearly critical inlet flow with close-to-optimum total-pressure-recovery ramp angles, the maximum recovery obtainable from a single wedge is relatively poor in the high Mach number range; at a Mach number of 2.8, for example, the best recovery possible is on the order of 59 percent. The low recovery results in a propulsive efficiency of about 54 percent, as shown in figure 7. Operation in the low supersonic flight range with the detached ramp shock, although somewhat speculative, was indicated from an aerodynamic viewpoint by an efficiency comparison; analysis showed that even though the detached wave resulted in slightly lower pressure recovery, the additive drag behind the detached wave was probably sufficiently smaller than normal-shock spillage to provide an over-all gain. As shown in figure 7, the propulsive efficiency is quite high in the low supersonic range, being above 90 percent at Mach numbers less than 1.6. At take-off and subsonic speeds, the inlet captures less than maximum air flow and should operate at total-pressure recoveries of approximately 81 percent at take-off and 96 percent at a Mach number of 0.9 in the tropopause. An inlet of this type has the advantage of being of relatively simple mechanical design, capable of supplying air to the engine at critical inlet flow with approximately the best total-pressure recovery obtainable from a single variable-wedge system. However, the total-pressure recovery attainable with a single-wedge inlet becomes increasingly poorer than other inlets as the Mach number increases.

In order to increase the total-pressure recovery and thereby increase the performance of the aircraft, a double-wedge inlet was

designed. This inlet had a two-position ( $9^\circ$  and  $0^\circ$ ) precompression wedge followed by a second wedge, variable from zero to  $20^\circ$  with respect to the first ramp. The precompression ramp is used at  $9^\circ$  for supersonic flight and lowered to zero for subsonic operation. This inlet operates with both oblique shocks intersecting the cowl lip at a Mach number of 2.8 and with the normal shock inside the cowl lip at critical inlet flow. For flight Mach numbers less than 2.8, the reduction in weight flow due to the steeper oblique shocks with optimum pressure-recovery wedge angles is not quite enough to satisfy the engine air-flow requirements, so that the stream tube is further reduced by the forward movement of the normal shock out of the inlet; consequently, the inlet will operate slightly subcritical. The maximum subcritical spillage occurs at a Mach number of 1.6, as shown in figure 6 by the corrected weight-flow curve (wherein critical inlet flow is shown to be greater than required) and by the mass-flow-ratio curve, which indicates the subcritical spillage as a percentage of the critical capture mass flow. Shock-wave detachment occurs for the  $9^\circ$  wedge near a Mach number of 1.4; however, additional subcritical spillage is also required, as shown by the curves just mentioned. For subsonic flight Mach numbers with both wedge angles at zero, the inlet will capture less than maximum air flow at both take-off and Mach number of 0.9. The inlet will deliver 87-percent total-pressure recovery at sea level for take-off and 98 percent for Mach number of 0.9 in the tropopause.

In the high supersonic portion of the flight path, the double-wedge inlet increased the total-pressure recovery over that obtained for the single wedge and thus increased the propulsive thrust available to the aircraft (fig. 7); for example, at a Mach number of 2.8, the propulsive thrust was increased from the previous 54 percent to 69 percent, which is maximum for a two-shock configuration. As a result of subcritical spillage, the efficiency was less than maximum for a two-shock inlet throughout the supersonic Mach number range below 2.8.

At supersonic Mach numbers below 1.8, the double-wedge inlet had efficiencies that were lower than those obtained for the single-ramp inlet because of the additive drag caused by subcritical spillage. In the supersonic flight range, the inlet is capable of supplying corrected air flow to the engine at nearly critical flow, with a total-pressure recovery close to the maximum attainable with an optimum two-shock configuration, even though supersonically the inlet had only one variable ramp. This analysis indicates that for engines with air-flow characteristics of the conventional type, a fixed precompression surface may yield sufficiently high propulsion efficiencies to provide adequate performance for the aircraft. To provide sufficient high pressure-recovery air flow to the engine at subsonic speeds, the artifice of lowering both ramps to zero was used. A system of this type would be more complex to build and operate than the single variable wedge (with or without the precompression surface) and, depending on the relative complexities (and also on

[REDACTED]

the necessity for high performance subsonically), other systems, such as blow-in doors or an auxiliary subsonic inlet, could also be used to provide the necessary air flow.

5078-G

A more complex inlet was designed with two variable wedges and a main-duct bypass system to obtain better performance over the entire Mach number range than the inlet with a  $9^\circ$  or  $0^\circ$  precompression wedge plus a variable wedge. Higher efficiencies are effected with this inlet by keeping the intersection of the inlet shock system near the cowl lip at the highest pressure recovery possible and spilling the excess mass flow through the axial discharge bypass. The first wedge angle is variable from zero to  $15^\circ$  and the second from zero to  $18^\circ$  with respect to the first. Critical operation of the inlet at the required engine air flow occurs at a Mach number of 2.8 with the two oblique shocks intersecting at the cowl lip. At flight Mach numbers less than 2.8, the two variable wedges are positioned to obtain nearly maximum total-pressure recovery consistent with the highest possible critical mass-flow ratio, thereby reducing the supercritical or oblique-shock spillage to a minimum. Since the engine requires less air flow than the inlet delivers, the excess mass flow is discharged axially through the main-duct sonic-exit bypass as the flight Mach number decreases. A main-duct bypass capable of discharging up to 30 percent of the inlet mass flow would be required for this installation. With the use of a main-duct bypass, the inlet will supply air to the engine at critical inlet flow at all flight Mach numbers, trading normal-shock-spillage drag for bypass-spillage drag. At subsonic flight speeds, both wedges would be reduced to zero. At take-off and subsonic flight speeds, the inlet would operate at less than maximum air flow, with a total-pressure recovery of 87 percent at take-off and 98 percent at Mach number of 0.9 in the tropopause.

This type of inlet was capable of supplying the required engine air flow with critical inlet operation and maximum pressure recovery for double-wedge design over the entire supersonic flight range, as shown by the curves of figure 6. Since the inlet capture air flow was greater than the engine requirements, the excess air was discharged through the bypass, thereby creating bypass drag. The effect of this drag (which was shown in fig. 3 to be the smallest of the spillage drags) on the propulsive thrust of the engine is shown in figure 7. The highest thrust loss occurs at a Mach number of 2.0 and is of the order of 2 percent of the ideal thrust at this Mach number. Over the entire range, however, this inlet system was calculated to give the best performance of the inlet types, with only small losses in thrust from the maximum attainable with a two-wedge system. As may be expected, this high performance was realized only at the expense of considerable complexity and probable added weight. It is interesting that at Mach numbers above 2.0, the relatively simple inlet with a  $9^\circ$  precompression wedge plus a variable wedge performs nearly as well as the more complex system. This indicates that if high performance is not required in the low supersonic range, the simpler inlet may be more satisfactory.

[REDACTED]

Supersonic engine. - The previous discussion concerned the design of three inlets to match a conventional turbojet engine over the entire Mach number and altitude range of a supersonic interceptor. To provide capabilities for greater thrust per unit frontal area, an engine designated as the supersonic turbojet engine was designed and is described in a subsequent paper. This engine has been selected to point out problems that would arise in the design of an inlet system that matches these particular engine characteristics. The corrected air-flow requirements over the flight plan shown in figure 5 are presented in figure 8. The engine requires a constant corrected air flow to a Mach number of 2.3 and then a decreasing air flow to a Mach number of 2.8. For a schedule of this type, an inlet sized to match the engine at a Mach number of 2.8 would be too large at supersonic Mach numbers less than 2.3, since inlet critical corrected weight flows normally increase with decreasing Mach number. Because of the constant weight-flow requirements, it may also be expected that an inlet sized for a Mach number of 2.8 will have ample air-flow capacity at take-off and subsonic operation. It has been shown previously that double-wedge configurations exhibit total-pressure recoveries substantially higher than single-wedge inlets at Mach numbers over 2.0; therefore, only double-wedge inlets have been considered in this analysis. Furthermore, the engine air requirements indicate the need for a variable-geometry inlet in order to match efficiently throughout the entire flight path.

The first inlet was designed with a fixed cowl and two variable ramps, such that both oblique shocks intersected the cowl lip at a design Mach number of 2.8 without internal contraction. The first wedge varied from zero to  $20^\circ$ , and the second wedge varied from zero to  $18^\circ$  with respect to the first wedge.

The wedge angles at a Mach number of 2.8 were selected to give the maximum pressure recovery possible from a double-wedge configuration, and the cowl was positioned for shock intersection at the lip. At a Mach number of 2.8, then, maximum propulsive efficiency is obtained, as shown in figure 9(a). This inlet has been broken down into three modes of operation, as shown by curves A, B, and C in figures 8 and 9. Method A specifies ramp angles set for nearly maximum pressure recovery throughout the supersonic range without shock detachment. In this case, as the Mach number decreases below 2.8, the inlet is forced to spill increasing amounts of air flow behind the normal shock, since the spillage behind the oblique shocks is insufficient to satisfy the engine requirements. At a Mach number of 1.6, the inlet would be forced to spill 36 percent of the maximum mass flow available at that Mach number behind the normal shock (fig. 8), with a subsequent loss in propulsive efficiency due to subcritical additive drag (fig. 9(a)). At a Mach number of 1.0, the spillage behind the normal shock would be 59 percent of the maximum mass flow available. This method exhibits high pressure recoveries over the supersonic range but large additive drag penalties below a Mach number

of 2.4. Method B consists of selecting a wedge angle to give the required throat area at a Mach number of 1.0 to supply air to the engine at critical inlet operation. This particular wedge angle forces shock detachment from a Mach number of 1.0 to a Mach number of 1.82, with corresponding normal-shock pressure recoveries, as shown in figure 8. This method results in an improvement in propulsive efficiency over that obtained in method A, from a Mach number of 1.0 to a Mach number of approximately 1.6, as shown in figure 9(a). However, at Mach numbers above 1.6, the efficiency decreases rapidly because of the low pressure recoveries attendant with normal-shock recovery. Method C consisted of positioning the wedges for nearly maximum pressure recovery from a Mach number of 2.8 to a Mach number of 1.6 and holding a constant wedge angle below Mach number 1.6 to detach the oblique shock. The inlet characteristics and propulsive efficiency of this system, as shown in figures 8 and 9(a), indicate an improvement over method A below a Mach number of 1.4; however, its efficiency is lower than method B below a Mach number of 1.6. From an efficiency standpoint then, the best schedule for the inlet would be to follow method A from a Mach number of 2.8 to a Mach number of 1.6, raise the ramp angle to obtain the throat area required to match the engine exactly, and apply method B to a Mach number of 1.0. For subsonic flight speeds with both ramps lowered to zero and with the throat area equal to the cowl-plane area, the inlet will capture far more air flow than the engine requires. With the resulting operation, then, at velocity ratios considerably less than 1.0, the pressure recovery at take-off would be of the order of 95 percent and at a Mach number of 0.9 would be approximately 99.5 percent. An inlet of this type would therefore be very efficient subsonically but would be very poor in propulsive efficiency in the Mach number range from 1.2 to 2.3. This result indicates that a bypass configuration would be required in order to eliminate the high subcritical additive drag in the low supersonic flight speed range and to obtain reasonable propulsive efficiencies over the entire flight path of the aircraft.

A second inlet was therefore designed for a Mach number of 2.8, and the resulting configuration at this Mach number was nearly identical to that of the previous inlet. However, a bypass system was incorporated in order to eliminate the subcritical additive drag encountered with the first inlet (method A) at lower supersonic Mach numbers. For this inlet, at Mach numbers less than 2.8 the wedge angles were selected to obtain nearly maximum pressure recoveries consistent with keeping the oblique shocks as near the cowl lip as possible. The reductions in air flow required to match the engine are accomplished by spilling the excess mass flow through the bypass system. As shown in figure 8, the pressure recoveries obtained with this inlet are comparable to the previous inlet (method A), but normal-shock-spillage drag has been traded for bypass-spillage drag, with the inlet operating at critical flow throughout the Mach number range. The resulting increase in propulsive efficiency of this inlet over the previous inlet (shown in figure 9(a)) becomes

considerable in the Mach number range from 1.0 to 2.3. Since this inlet has the same capture area as the previous inlet, the subsonic performance will be identical for both inlets when the ramp angles are reduced to zero.

In the efficiency analysis of these inlets (fig. 9(a)), the reduction in cowl-pressure drag resulting from inlet subcritical operation was not considered. As mentioned previously, this reduction should be accounted for in any force analysis, especially at the lower supersonic Mach numbers. To indicate the possible order of magnitude of this force term, the reduction of cowl-pressure drag has been estimated from reference 38 for subcritical operation and has been included in the efficiency curves of figure 9(b). Although there is an increase in efficiency for curves A and C over those shown in figure 9(a), particularly below a Mach number of 2.0, it is evident that for an engine of this type, a variable-geometry inlet with a main-duct bypass system would be required to match the engine efficiently over the entire flight plan of the supersonic interceptor.

#### CONCLUDING REMARKS

Some of the problems associated with inlet-engine matching in a supersonic airplane have been reviewed and discussed. Primarily, it has been demonstrated that the results of careful and resourceful research leading to high-thrust turbojet engines can be negated simply by the wrong choice of inlet installation. An example has been cited of the variable-angle single-wedge inlet which, although operating at critical (and therefore near-optimum) inlet flow, was unable to produce sufficient total-pressure recovery to maintain more than about half the potential thrust of the engine at a Mach number of 2.8. Thus, even though optimum inlet performance was attained, nearly half of the engine thrust was lost. Efficient aircraft performance over an extended Mach number range therefore requires that extreme care be taken in the inlet selection in order to insure that the fullest possible advantage is taken of the engine potential.

#### REFERENCES

1. Sanders, Newell D., and Behun, Michael: Generalization of Turbojet-Engine Performance in Terms of Pumping Characteristics. NACA TN 1927, 1949.
2. Sanders, Newell D., and Palasics, John: Analysis of Effects of Inlet Pressure Losses on Performance of Axial-Flow Type Turbojet Engine. NACA RM E8J25b, 1948. (Supersedes NACA RM E8CI6a.)

- 3078-G
3. Wyatt, DeMarquis D.: Aerodynamic Forces Associated with Inlets of Turbojet Installations. Aero. Eng. Rev., vol. 10, no. 10, Oct. 1951, pp. 20-23.
  4. Wyatt, DeMarquis D.: An Analysis of Turbojet-Engine-Inlet Matching. NACA TN 3012, 1953.
  5. Schueller, Carl F., and Esenwein, Fred T.: Analytical and Experimental Investigation of Inlet-Engine Matching for Turbojet-Powered Aircraft at Mach Numbers up to 2.0. NACA RM E51K20, 1952.
  6. Luskin, H., and Klein, H.: High Speed Aerodynamic Problems of Turbojet Installations. Douglas Rep. No. SM-13830, Douglas Aircraft Co. (Calif.), Sept. 1, 1950.
  7. Blackaby, James R.: An Analytical Study of the Comparative Performance of Four Air-Induction Systems for Turbojet-Powered Airplanes Designed to Operate at Mach Numbers up to 1.5. NACA RM A52C14, 1952.
  8. Brajnikoff, George B.: Method and Graphs for the Evaluation of Air-Induction Systems. NACA TN 2697, 1952.
  9. Gorton, Gerald C.: Investigation of Translating-Spike Supersonic Inlet as Means of Mass-Flow Control at Mach Numbers of 1.5, 1.8, and 2.0. NACA RM E53G10, 1953.
  10. Valerino, Alfred S.: Performance Characteristics at Mach Numbers to 2.00 of Various Types of Side Inlets Mounted on Fuselage of Proposed Supersonic Airplane. I - Two-Dimensional Compression-Ramp Inlets with Semicircular Cowls. NACA RM E52E02, 1952.
  11. Esenwein, Fred T.: Performance Characteristics at Mach Numbers to 2.0 of Various Types of Side Inlets Mounted on Fuselage of Proposed Supersonic Airplane. III - Normal-Wedge Inlets with Semicircular Cowl. NACA RM E52H20, 1952.
  12. Simon, Paul C.: Performance Characteristics at Mach Numbers to 2.0 of Various Types of Side Inlets Mounted on Fuselage of Proposed Supersonic Airplane. IV - Rectangular-Cowl Inlets with Two-Dimensional Compression Ramps. NACA RM E52H29, 1952.
  13. Allen, J. L., and Beke, Andrew: Force and Pressure Recovery Characteristics at Supersonic Speeds of a Conical Spike Inlet with Bypasses Discharging in an Axial Direction. NACA RM E52K14, 1953.
  14. Allen, J. L., and Beke, Andrew: Force and Pressure Recovery Characteristics at Supersonic Speeds of a Conical Spike Inlet with a Bypass Discharging from the Top or Bottom of the Diffuser in an Axial Direction. NACA RM E53A29, 1953.

- 
15. Obery, Leonard J., and Stitt, Leonard E.: Investigation at Mach Numbers 1.5 and 1.7 of Twin-Duct Side Air-Intake System with 9° Compression Ramp Including Modifications to Boundary-Layer-Removal Wedges and Effects of a Bypass System. NACA RM E53H04, 1953.
  16. Allen, J. L., and Beke, Andrew: Performance Comparison at Supersonic Speeds of Inlets Spilling Excess Flow by Means of Bow Shock, Conical Shock or Bypass. NACA RM E53H11, 1953.
  17. Sibulkin, Merwin: Theoretical and Experimental Investigation of Additive Drag. NACA RM E51B13, 1951.
  18. Nussdorfer, Theodore J., Obery, Leonard J., and Englert, Gerald W.: Pressure Recovery, Drag, and Subcritical Stability Characteristics of Three Conical Supersonic Diffusers at Free Stream Mach Numbers from 1.7 to 2.0. NACA RM E51H27, 1952.
  19. Esenwein, Fred T., and Valerino, Alfred S.: Force and Pressure Characteristics for a Series of Nose Inlets at Mach Numbers from 1.59 to 1.99. I - Conical Spike All-External Compression Inlet with Subsonic Cowl Lip. NACA RM E50J26, 1951.
  20. Obery, L. J., and Englert, G. W.: Force and Pressure Characteristics for a Series of Nose Inlets at Mach Numbers from 1.59 to 1.99. II - Isentropic-Spike All-External Compression Inlet. NACA RM E50J26a, 1951.
  21. Weinstein, Maynard I., and Davids, Joseph: Force and Pressure Characteristics for a Series of Nose Inlets at Mach Numbers from 1.59 to 1.99. III - Conical-Spike All-External-Compression Inlet with Supersonic Cowl Lip. NACA RM E50J30, 1951.
  22. Moeckel, W. E., and Connors, J. F.: Charts for the Determination of Supersonic Air Flow Against Inclined Planes and Axially Symmetric Cones. NACA TN 1373, 1947.
  23. Dailey, C. L., and Wood, F. C.: Computation Curves for Compressible Fluid Problems. John Wiley & Sons, Inc., 1949.
  24. Schaefer, R.: Some Design Considerations for Half-Round Side Inlets. Rep. No. 1692, Supersonic Inlet Symposium, Wright Aero. Div., Curtiss-Wright Corp., Jan. 23, 1953.
  25. Sturtevant, W. C.: Performance Characteristics of a Concentric Wedge Side Inlet. Rep. No. 1692, Supersonic Inlet Symposium, Wright Aero. Div., Curtiss-Wright Corp., Jan. 23, 1953.
  26. Pearce, R. B.: Tests of Multishock Diffusers. Rep. AL-1117, Proj. MX-770, North American Aviation, Inc., Sept. 21, 1950.
- 

27. Clark, Donald B., and Lewis, Robert B.: Development of Wide Range Supersonic Inlets. Wright Aeronautical Corp.
28. Obery, Leonard J., Englert, Gerald W., and Nussdorfer, Theodore J.: Pressure Recovery, Drag, and Subcritical Stability Characteristics of Conical Supersonic Diffusers with Boundary-Layer Removal. NACA RM E51H29, 1952.
29. Moeckel, W. E., Connors, J. F., and Schroeder, A. H.: Investigation of Shock Diffusers at Mach Number 1.85. II - Projecting Double-Shock Cones. NACA RM E6L13, 1947.
30. Dailey, C. L., McFarland, H. W., and Scabee, R.: Development of Ramjet Components. Prog. Rep. 9961-12, Aug., Sept., Oct. 1950, Aero. Lab., Univ. Southern Calif., Nov. 7, 1950. (Navy Res. Contract Noa(s) 9961.)
31. Cortright, Edgar M., Jr., and Connors, James F.: Survey of Some Preliminary Investigations of Supersonic Diffusers at High Mach Numbers. NACA RM E52E20, 1952.
32. Davids, Joseph, and Wise, George A.: Investigation at Mach Numbers 1.5 and 1.7 of Twin-Duct Side Intake System with Two-Dimensional  $6^\circ$  Compression Ramps Mounted on a Supersonic Airplane. NACA RM E53H19, 1953.
33. Allen, J. L., and Simon, P. C.: Performance Characteristics at Mach Numbers to 2.0 of Various Types of Side Inlets Mounted on Fuselage of Proposed Supersonic Airplane. II - Inlets Utilizing Half of a Conical Spike. NACA RM E52G08, 1952.
34. Goelzer, H. Fred, and Cortright, Edgar M., Jr.: Investigation at Mach Number 1.88 of Half of a Conical-Spike Diffuser Mounted as a Side Inlet with Boundary-Layer Control. NACA RM E51G06, 1951.
35. Fradenburgh, Evan A., and Wyatt, DeMarquis D.: Theoretical Performance Characteristics of Sharp-Lip Inlets at Subsonic Speeds. NACA TN 3004, 1953.
36. Brajnikoff, George B., and Stroud, John F.: Experimental Investigation of the Effect of Entrance Width-to-Height Ratio on the Performance of an Auxiliary Scoop-Type Inlet at Mach Numbers from 0 to 1.3. NACA RM A53E28, 1953.
37. Scherrer, Richard, Stroud, John F., and Swift, John T.: Preliminary Investigation of a Variable-Area Auxiliary Air-Intake System at Mach Numbers from 0 to 1.3. NACA RM A53A13, 1953.
38. Graham, E. W.: Notes on the Drag of Scoops and Blunt Bodies. Rep. No. SM-13747, Douglas Aircraft Co., Inc., Apr. 13, 1950.

COMPARISON OF INLET-ENGINE MATCHING WITH FIXED 20°-RAMP INLETS FOR CONVENTIONAL ENGINE IN TROPOPAUSE

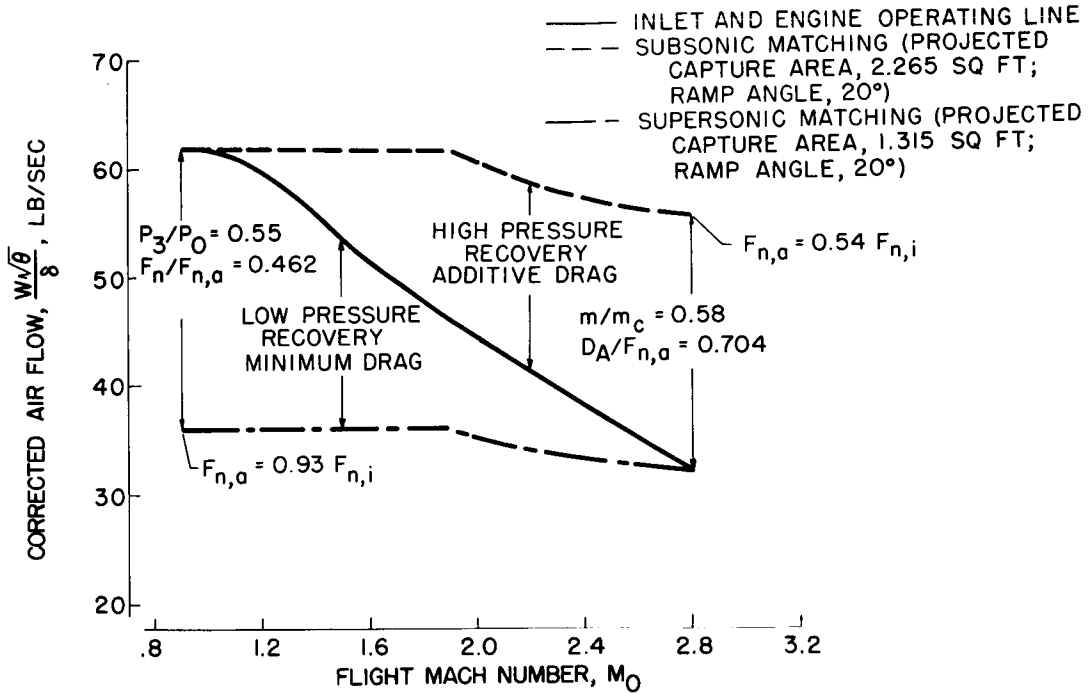


Figure 1

TYPES OF VARIABLE-GEOMETRY INLETS SUITABLE FOR MATCHING TO TURBOJET ENGINES

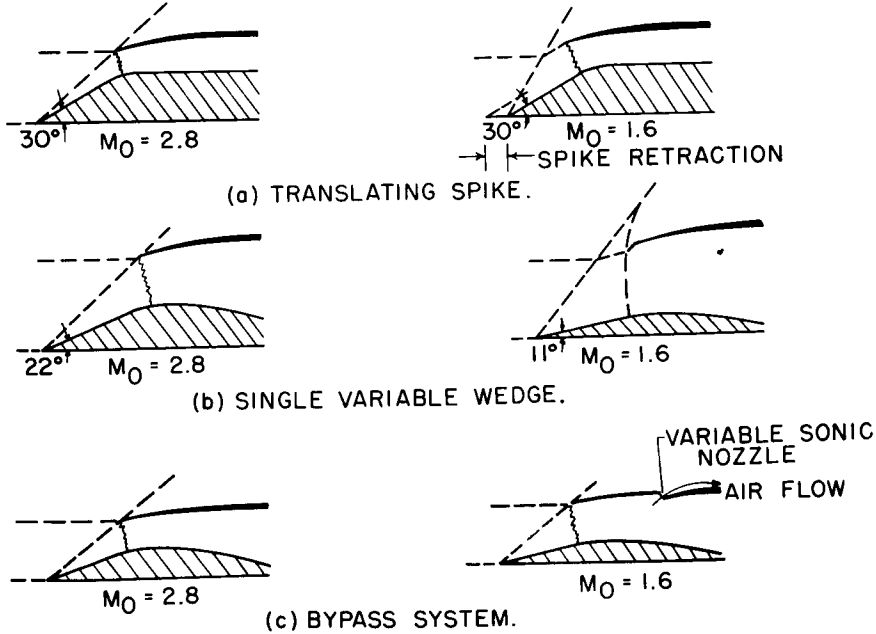


Figure 2

3078-D



FLIGHT PLAN AND WEIGHT FLOW REQUIRED FOR SUPERSONIC INTERCEPTOR POWERED BY CONVENTIONAL TURBOJET ENGINE

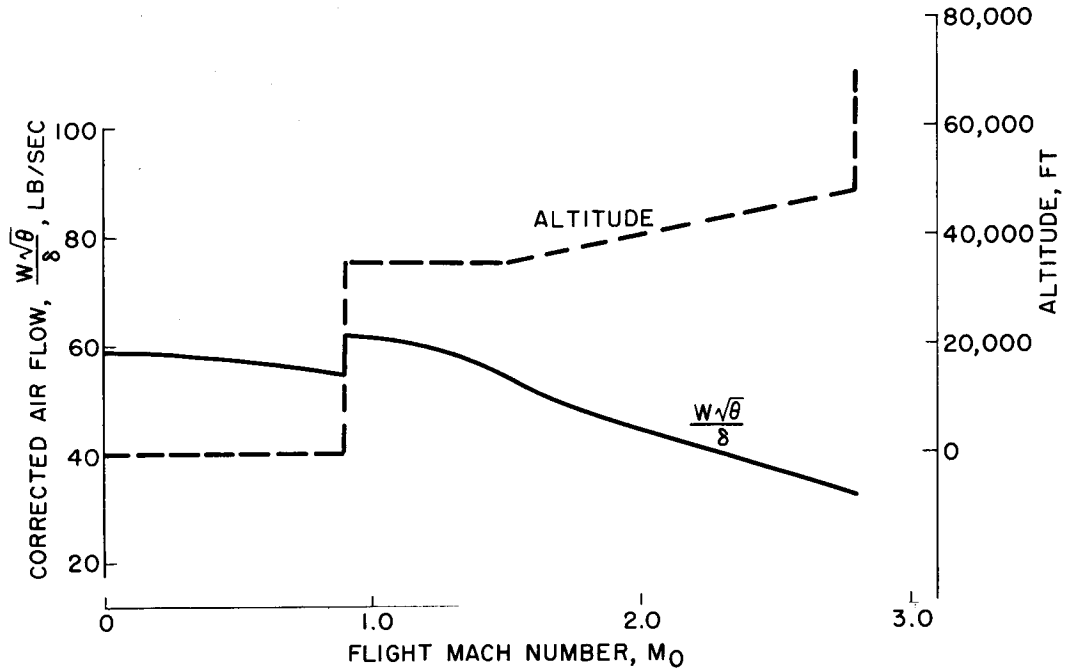


Figure 5

INLET-ENGINE MATCHING CONDITIONS FOR THREE SPECIFIC INLET CONFIGURATIONS DESIGNED FOR CONVENTIONAL ENGINE AT FLIGHT MACH NUMBER OF 2.8

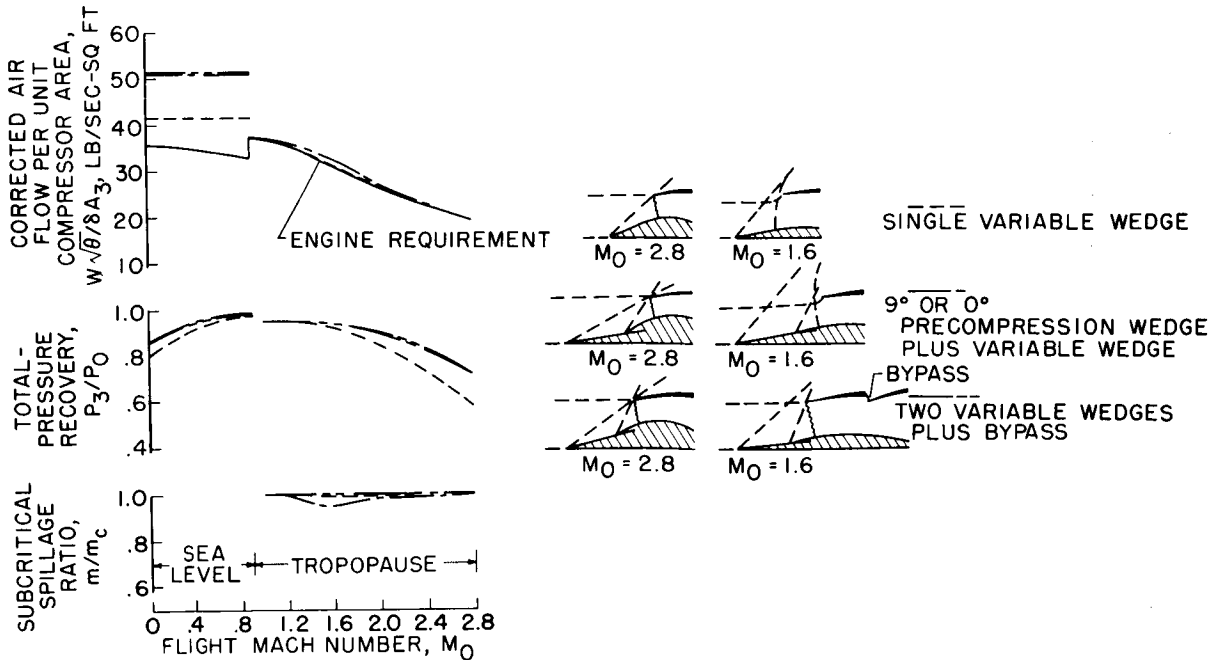


Figure 6

3078-G

PROPULSIVE EFFICIENCY OF THREE SPECIFIC INLET CONFIGURATIONS DESIGNED FOR A CONVENTIONAL ENGINE AT FLIGHT MACH NUMBER OF 2.8

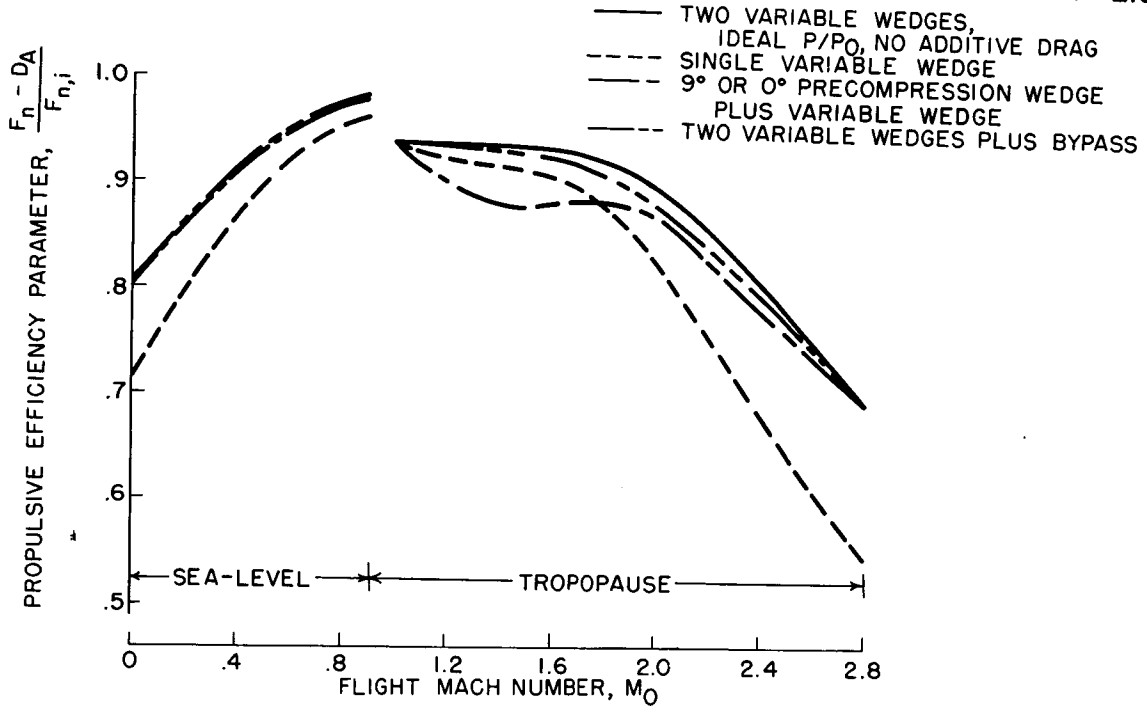


Figure 7

INLET-ENGINE MATCHING CONDITIONS FOR TWO SPECIFIC INLET CONFIGURATIONS DESIGNED FOR SUPERSONIC ENGINE AT FLIGHT MACH NUMBER OF 2.8

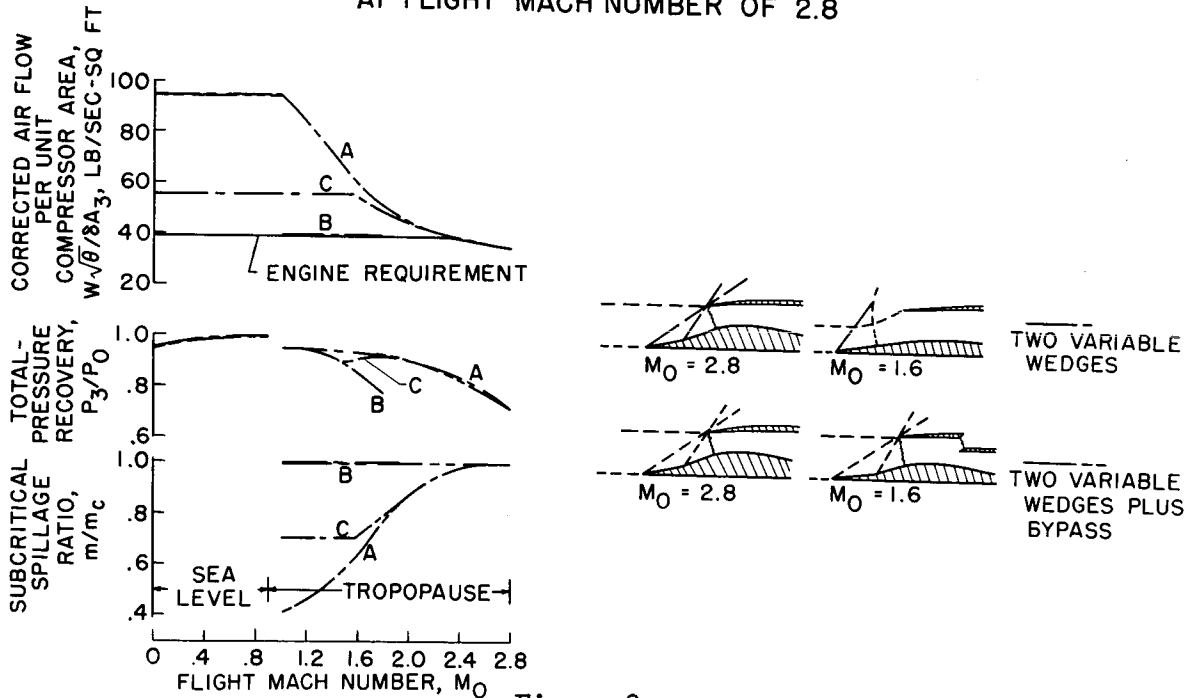


Figure 8

3078-G



PROPULSIVE EFFICIENCY OF TWO SPECIFIC INLET CONFIGURATIONS  
DESIGNED FOR SUPERSONIC ENGINE AT FLIGHT MACH NUMBER OF 2.8

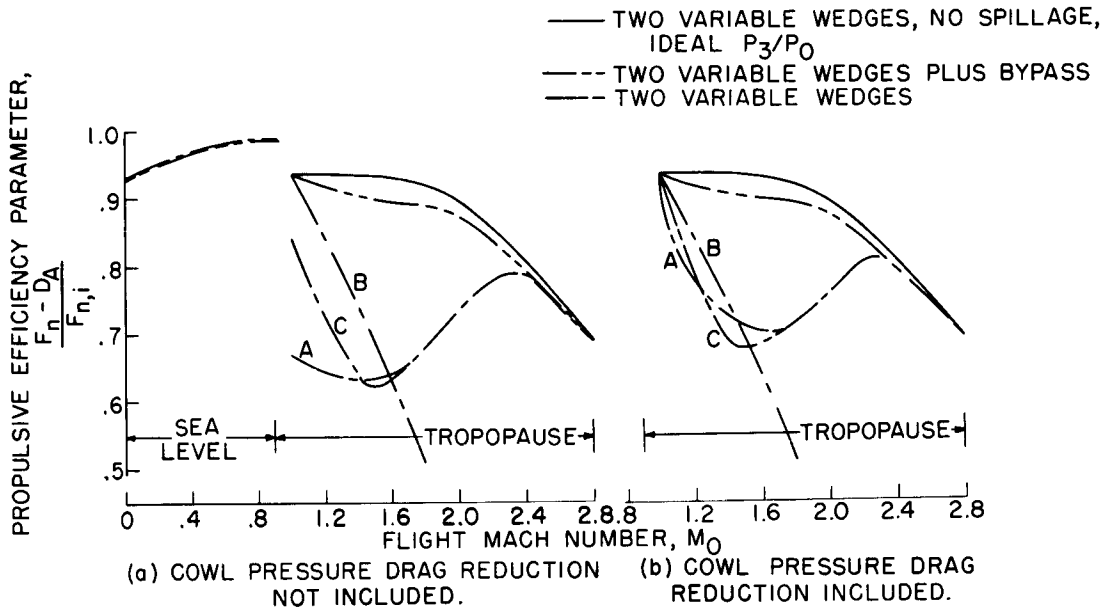
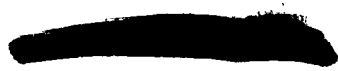


Figure 9



## PERFORMANCE OF SEVERAL PLUG-TYPE NOZZLES

By Gerald W. Englert and Thomas B. Shillito

## NOZZLE REQUIREMENTS

Various modes of operation of engines required to drive aircraft over ranges of flight speed from take-off to high supersonic Mach numbers necessitate the use of exhaust nozzles capable of permitting large throat-area changes. These changes may be required even with the afterburner temperature held constant. Additional throat-area changes imposed upon the nozzle to compensate for afterburner temperature changes may further widen the limits imposed by the basic engine schedule.

Figure 1 presents the nozzle requirements for two engine schedules. The solid lines are for operation of an engine with a constant turbine-inlet temperature ( $2040^{\circ}$  F) and a constant rotative speed over the entire flight path from take-off to a flight Mach number of 2.8. A schedule obtained by permitting the engine to overspeed at a constant turbine-inlet temperature of  $2040^{\circ}$  F is illustrated by the dashed lines. The afterburner temperatures were held constant in both cases and were lowered only at the subsonic and supersonic cruise conditions indicated by the points.

Aside from accommodating the throat-area changes demanded by the engine, the nozzle should be one which can efficiently utilize the thrust potential of the exhaust gases over the available range of pressure ratios. Figure 1 shows that pressure ratios from 2.5 at take-off to 21.0 at a flight Mach number of 2.8 can be supplied by the engines of a Mach 2.8 airplane.

## EXPERIMENTAL RESULTS

The plug-type-nozzle configuration shows promise in satisfying the two foregoing requirements. A throat-area change in this type of nozzle may be obtained by axial translation of the centerbody (or plug) relative to the outer shroud. These nozzles can be so designed that varying amounts of internal (or geometrical) expansion of the flow passages up to the shroud exit station are also obtained as the plug is translated. The expansion or compression processes beyond the shroud trailing-edge stations then appear to be influenced by factors such as the amount the plug extends rearward of the shroud, the plug contour, and the available pressure ratio.

Several plug-type-nozzle configurations have been studied at the NACA Lewis laboratory. Some of the preliminary results are presented in reference 1; however, the bulk of the information most pertinent to turbojet installations is as yet unpublished.

Figure 2 shows the performance of two nozzles which have been experimentally investigated. For both of these designs, the throat area is maximum when the plug is completely retracted. For this plug position, however, the flow passages of the nozzle in the upper part of the sketch are convergent, whereas the flow passages of the nozzle in the lower part of the sketch are convergent-divergent. The upper nozzle has, for reference, been designated nozzle A and the other nozzle B.

As would be expected, nozzle A, when the plug is retracted, has a high thrust ratio at low-pressure ratios (total pressure ahead of nozzle divided by static ambient pressure). Thrust ratio is defined as the measured thrust divided by the jet thrust which would be obtained for a completely expanded isentropic nozzle having the same weight flow as for the measured case. The thrust ratio falls off quite rapidly as pressure ratio is increased; this trend is similar to that of a conventional convergent nozzle. When the plug of nozzle B is retracted, low values of thrust ratio are obtained at low pressure ratios. The thrust ratio increases, however, as the pressure ratio increases to a value corresponding to the geometrical expansion ratio of the internal passages. The performance of nozzle B for this plug position is thus similar to that of a conventional convergent-divergent nozzle.

Consider the opposite extreme of the plug travel, that is, the plug in a greatly extended position as shown by the sketches on the right side of figure 2. For this plug position, both nozzles exhibit a near constant thrust-ratio characteristic over the entire range of pressure ratios (1.5 to 19.0). It is also of interest to note that, for the extended plug, both nozzles have essentially the same value of thrust ratio even though the plug contour of A is that of a double cone and that of B is streamlined. This thrust ratio is lower than that obtained with either plug when fully retracted and operated at the optimum pressure ratio; however, thrust ratios for the extended plug position were never as low as those for the retracted plugs when operated at pressure ratios far from optimum.

A study of nozzle B in the 8- by 6-foot supersonic wind tunnel was conducted to determine whether an external stream flowing about this type of nozzle would influence the nozzle thrust characteristics. In this investigation, the nozzle was attached to a streamlined body (a parabolic nose and boattail, and a cylindrical centerbody) which was supported in the tunnel by means of two hollow struts. These hollow struts served the additional purpose of ducting high-pressure air from a central laboratory supply to the model. Data obtained at free-stream Mach numbers of 0.1, 0.6, 1.6, and 2.0 and at angles of attack of  $0^\circ$  and  $8^\circ$  are presented in figure 3. Here it can be seen that, within the accuracy of these data and over the ranges covered, no effect of the external stream on nozzle performance was encountered. Comparison of measurements obtained from rows of pressure orifices on the top and

[REDACTED]

bottom of the plug surfaces indicated that no significant normal forces or bending moments were present on the plug during these tests even when the model was at an angle of attack of  $8^\circ$ .

Additional flexibility of design of the plug-type nozzle, at the expense of mechanical complexity, would be obtained if the nozzle shroud were replaced by a variable iris as shown on figure 4. Even if the plug were not permitted to move as in the previous examples, this type of configuration affords a means of varying throat area and expansion ratio along some schedule. Data were obtained with the plug left in an extended position, which preserved the flat characteristics of the thrust ratio versus pressure ratio curves. It can be seen that throat-area changes of 86 percent can be made at pressure ratios of 1.5 to 10.0 and that the thrust ratio in most all cases lies within a range of 0.90 to 0.95.

#### NOZZLE MATCHING

Figure 5 presents the results of matching these three nozzles to the throat area and the pressure-ratio characteristics of the two engine schedules of figure 1. The measure of performance of the nozzles for this figure was arbitrarily selected as net-thrust ratio. This ratio is the same as the previously used jet-thrust ratio except that the airplane inlet momentum (mass rate of air flow entering the inlet times free-stream velocity) was subtracted from both the numerator (measured jet thrust) and the denominator (ideal jet thrust for complete expansion) of the jet thrust ratio. All three nozzles were matched to the constant-speed-engine schedule; however, only nozzle A and the iris-type-shroud nozzle were matched to the overspeed-engine schedule because of the limited range of data available for nozzle B.

As would be expected, where a comparison could be made, nozzle A showed better take-off and low-speed net-thrust ratios than nozzle B. The net-thrust ratios of nozzle B exceeded those of nozzle A over most of the supersonic speed range.

The net-thrust ratio of the iris-type nozzle was between that of nozzles A and B over nearly all the range of flight speeds where comparison could be made and when the afterburner was operating at  $3040^\circ$  F. The iris-shroud nozzle had the best cruise performance of the three nozzles.

For comparative purposes, the performance of a clamshell-type nozzle is also included in figure 5. The performance curves are thought to be representative of either a well-designed clamshell or a multiple-leaf converging iris. The curve for the clamshell nozzle was calculated by use of the data in reference 2 and lowered according to the results of reference 3, which compared clamshell to fixed converging nozzles. The

[REDACTED]

clamshell nozzle shows the highest values of net-thrust ratio in the subsonic speed range; however, as the flight Mach number and the nozzle pressure ratio increase, the performance of the clamshell nozzle falls far below that of the others.

## REFERENCES

1. Krull, H. George, Steffen, Fred W., and Ciepluch, Carl C.: Internal Performance Characteristics of Variable-Throat Plug- and Vaned-Type Convergent-Divergent Nozzles. NACA RM E53D09, 1953.
2. Krull, H. George, and Steffen, Fred W.: Performance Characteristics of One Convergent and Three Convergent-Divergent Nozzles. NACA RM E52H12, 1952.
3. Lundin, Bruce T.: Investigation of Several Clamshell Variable-Area Exhaust Nozzles for Turbojet Engines. NACA RM E9B02, 1949.

NOZZLE OPERATING SCHEDULE

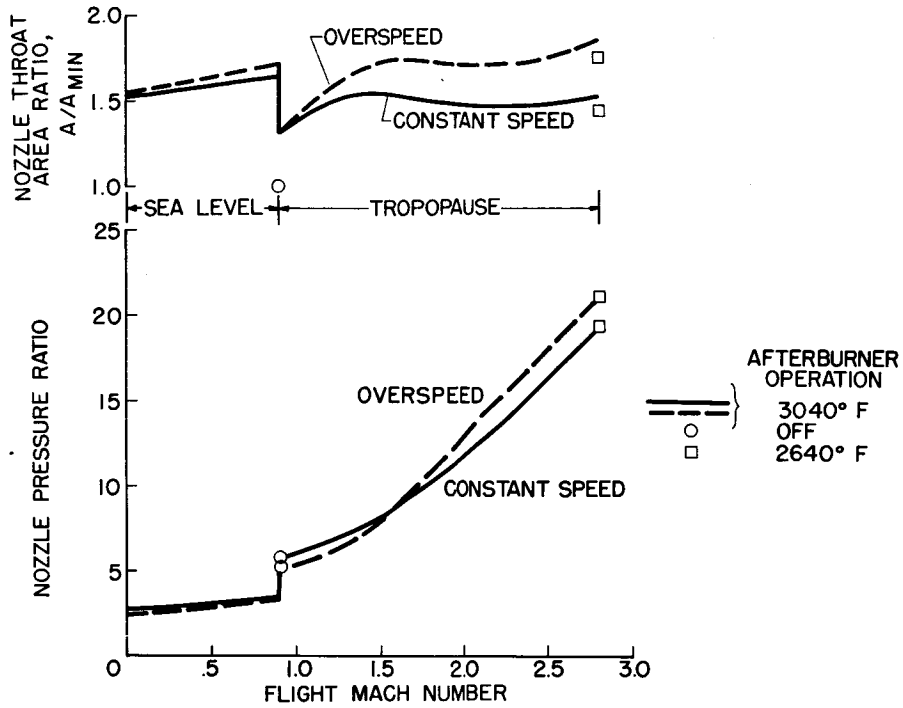


Figure 1

PLUG NOZZLE PERFORMANCE

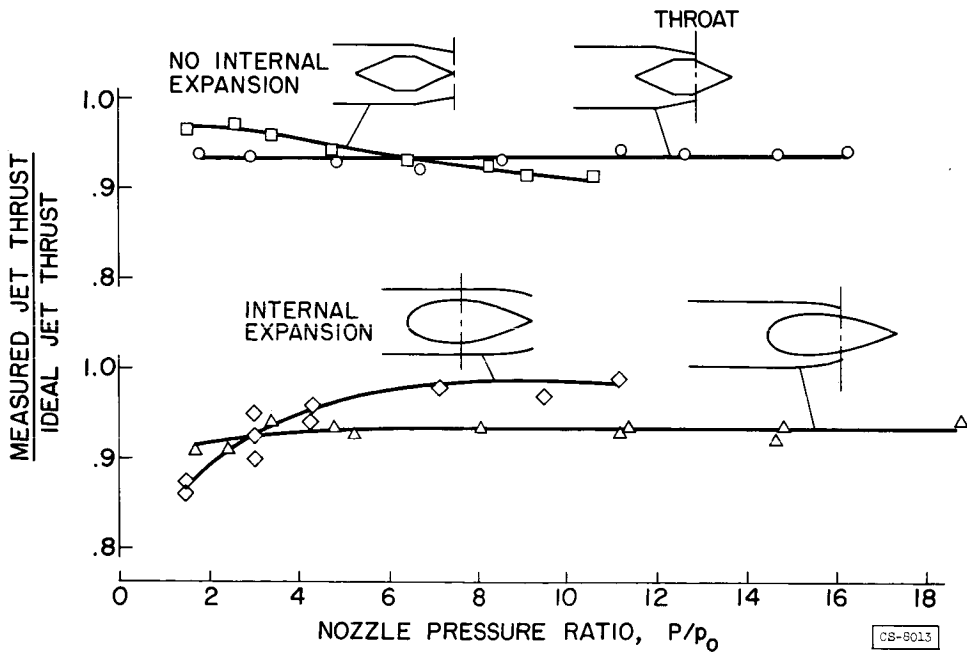


Figure 2

EFFECT OF EXTERNAL FLOW  
STREAMLINED PLUG CONTOUR, EXTENDED POSITION

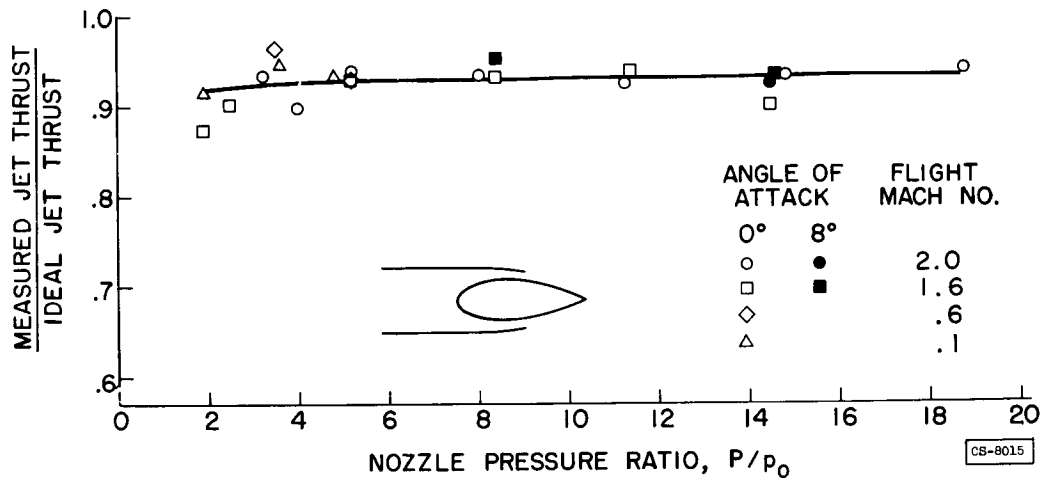


Figure 3

IRIS-SHROUD PLUG-TYPE-NOZZLE PERFORMANCE DATA

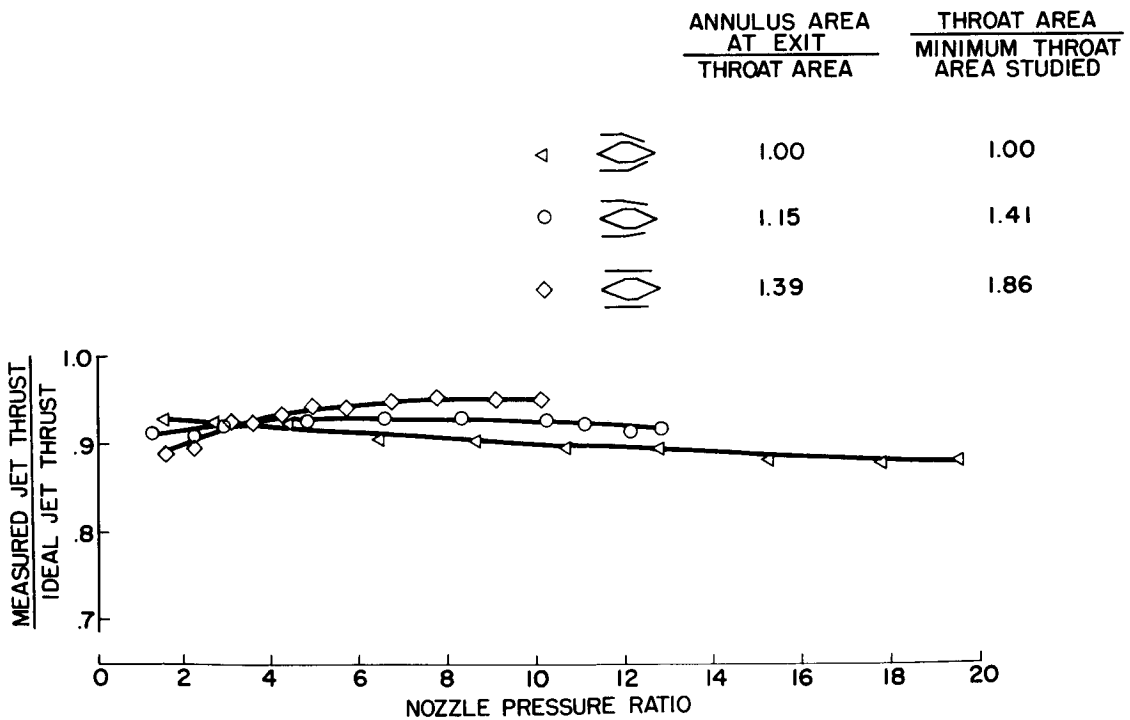


Figure 4

VARIOUS NOZZLES MATCHED TO MACH 2.8 INTERCEPTOR

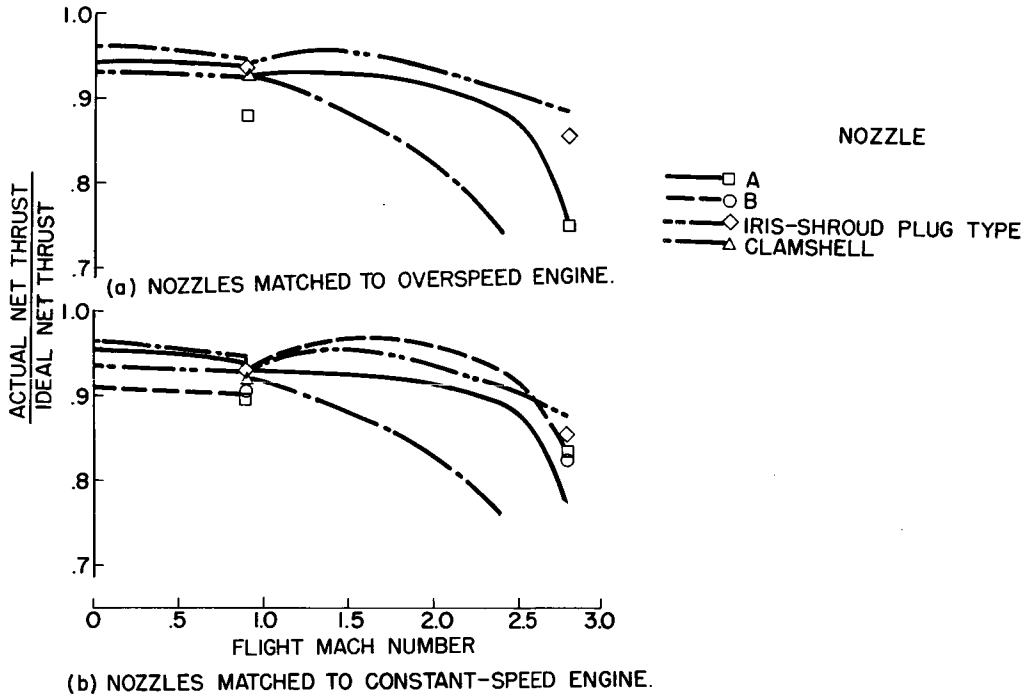


Figure 5

## THE EJECTOR AS A SUPERSONIC NOZZLE AND COOLING DEVICE

By William K. Greathouse, William K. Koffel, and Donald P. Hollister

## INTRODUCTION

3078-2

Supersonic flight requires efficient propulsion nozzles capable of producing thrust near that ideally available. As discussed by Englert and Shillito, a conventional convergent nozzle is incapable of fully expanding gases through a pressure ratio of more than about 2.0. At a pressure ratio of 10 the convergent nozzle loses about 9 percent of the theoretically available thrust because of incomplete expansion, and at a pressure ratio of 20 about 15 percent of theoretical thrust is made unavailable. Such excessive thrust losses as these, accompanied by high aircraft drag at transonic and supersonic flight speeds, make it essential to provide an engine nozzle in which the gases can be fully expanded. The nozzle problem is further complicated for afterburning engines by the requirement of variable nozzle throat area and the inherent need for nozzle cooling. The combination of variable throat area and variable expansion area requires complex designs and ingenious mechanical devices to form nozzles with cooled surfaces and these independent degrees of flexibility.

The ejector with nozzle and shroud being structurally independent lends itself to fully independent control of throat area and expansion ratio. Furthermore, the ejector incorporates a natural cooling system for afterburner shroud, jet nozzle, and adjacent parts of the aircraft structure.

The ejector operation as a supersonic nozzle can be described in connection with figure 1. (The symbols used on this figure and elsewhere in the discussion are defined in appendix A.) Under supersonic flight conditions the primary gas stream  $W_p$  expands supersonically along some boundary such as that shown by the dashed curve, and the secondary stream  $W_s$  will normally have a pressure greater than ambient and will tend to force air through the shroud between the shroud wall and primary jet boundary. The secondary stream expands subsonically to match the falling pressure along the primary stream boundary. With varying operating conditions this pressure equilibrium is maintained by an automatic shifting of the jet boundary. Thrust characteristics of an ejector operating in this manner are very good because both streams are efficiently expanded to ambient pressure.

Although a fixed configuration is indicated in figure 1, variable ejector configurations can be constructed to vary  $D_s$ ,  $D_p$ , and  $L$ , as indicated in figure 2. These configuration changes in any installation

should be aimed at meeting the engine cooling requirements while simultaneously producing a maximum net thrust. The ejector designer generally has to rely on existing small-scale ejector performance (such as refs. 1 to 4) as a guide in establishing the air-handling capacity and thrust characteristics of the ejector. The validity of small-scale ejector performance to predict full-scale engine ejector performance has been seriously questioned. To determine the applicability of small-scale work to design problems, several ejectors were investigated on an afterburning turbojet engine. Exact, 1/5-scale models were also simultaneously investigated on the ejector rig. Partial results of this investigation are presented in the following sections of this paper with a discussion as to the use of air-handling and thrust characteristics of small-scale ejectors in ejector design. These data are then used to analyze the net thrust gains available in a supersonic, area-defense fighter-type mission with various degrees of flexibility and complexity built into the ejector nozzle.

## EJECTOR PERFORMANCE COMPARISONS

### Air-Handling Capacity

The air-handling capacities of a full-scale and a small-scale ejector operating at the same primary gas temperature are compared directly in figure 3. The small ejector was about one-fifth the size of the large ejector and geometric similarity was preserved, except for metal thickness. The comparison indicates good agreement of performance for corrected weight-flow ratios  $W_s/W_p \sqrt{T_s/T_p}$  of 0 and 0.04. The higher secondary pressure ratio required by the full-scale ejector at a corrected weight-flow ratio of 0.08 is in the opposite direction of a Reynolds number or scale effect, but could be attributed to flow disturbances such as whirl and turbulence associated with the engine-afterburner installation used for full-scale ejector testing.

Two small ejectors having different secondary flow passages are compared in figure 4. Diameter ratios of the two ejectors are slightly different (see nomenclature on fig. 4); and, therefore, the performance differences that occurred for corrected weight-flow ratios  $W_s/W_p \sqrt{T_s/T_p}$  of 0 and 0.04 are of no significance. The spread between the corrected weight-flow-ratio curves of 0.08 is partly due to the aforementioned difference in diameter ratio but also results from geometrical dissimilarity of the secondary flow passages. Ejector configuration B (from ref. 1) had a convergent secondary passage with minimum flow area at the plane of the primary nozzle exit and configuration A had a convergent-divergent passage with minimum area located upstream of the primary nozzle exit. The relative passage height was also less for configuration A. The performance decrement of configuration A at  $W_s/W_p \sqrt{T_s/T_p}$  of 0.08

is due to either diffusion losses or shock losses, depending on whether or not the flow at the particular operating condition is subsonic or supersonic in the divergent passage downstream of the minimum secondary passage flow area.

The air-handling capacity of two full-scale ejectors operating at various primary gas temperatures is shown in figure 5. The effect of temperature on performance is indicated to be small for either ejector at the corrected weight-flow ratio  $W_s/W_p \sqrt{T_s/T_p}$  of 0.04. At  $W_s/W_p \sqrt{T_s/T_p}$  of 0.08 there is little effect of temperature indicated for the short ejector (fig. 5(a)), but the long ejector (fig. 5(b)) required a higher secondary pressure ratio for gas temperatures of 3000° and 3700° R than for the gas temperature of 1120° R. Ejector air-handling capacity at different temperatures is reasonably well generalized by the corrected weight-flow parameter  $W_s/W_p \sqrt{T_s/T_p}$  for corrected weight-flow ratios up to about 0.04. Fortunately this is about the range of weight-flow ratios of general interest, as will be shown. For the very short shroud ejector, the air flow generalized even at the higher corrected weight-flow ratios. This effect has been previously reported in reference 5.

Air-handling capacity of full-scale hot-gas ejectors can thus be predicted reasonably well from cold model ejector tests for corrected weight-flow ratios up to at least 0.04, especially for short length ejectors. At corrected weight-flow ratios much above 0.04, the combined effects of ejector size, secondary passage geometry, gas temperature, and flow disturbances make the use of model data uncertain. Also, it appears that flow disturbances peculiar to every turbojet engine (such as whirl, nonplanar velocity profiles, and burning through the ejector) could have a major effect.

#### Thrust

A comparison of ejector thrust for full-scale and small-scale ejectors is shown in figure 6. The thrust parameter is the ratio of measured ejector thrust to the sum of the calculated isentropic thrust available from the primary and secondary systems using measured pressure ratios, temperatures, and mass flows. This plot indicates, as a general trend, a decrease in thrust parameter as temperature was increased from 1120° R for the full-scale ejector. For the same temperature of 1120° R the thrust parameter was generally higher for the full-scale ejector than for the small-scale ejector. These apparent trends cannot be considered conclusive because the magnitude of their variation is less than the accuracy of the thrust data presented, which is about  $\pm 1\frac{1}{2}$  percent. From the limited amount of data examined, it appears that small-scale

[REDACTED]

ejector test data can be utilized to determine full-scale hot-gas ejector thrust performance if thrust results within about  $1\frac{1}{2}$  percent accuracy are sufficient. Exact scale models may, however, be required to obtain data for this purpose.

#### APPLICATION OF EJECTOR AS A SUPERSONIC NOZZLE

Several ejector configurations that can serve as supersonic nozzles have been shown in figure 2. The ejector, of course, must be matched to the operating schedule of a particular flight plan, aircraft, and engine. In addition, the type of engine-afterburner installation will determine cooling requirements and consequently the pressure losses and temperature rise of cooling air flowing through the ducting systems.

The net thrust performance of ejector configurations can be evaluated only by application to a particular set of flight requirements. For this purpose a single-engine area-defense type fighter flight plan has been assumed. An analysis of the obtainable exhaust-gas temperatures (as limited by cooling of the nozzle) was made, and the required nozzle-throat areas were determined and are presented in figure 7 as a function of flight Mach number. These operating schedules specify non-afterburning cruise at 0.8 Mach number, acceleration with the afterburner in operation to design Mach number of 2.0 and exhaust-gas temperature of  $3500^{\circ}$  R, and then operation at the design Mach number with reduced afterburner-gas temperature of  $2500^{\circ}$  R. This schedule requires increases in nozzle-throat area as great as 78 percent of the throat area at nonafterburning cruise.

#### Cooling Requirements

An afterburner configuration (fig. 8) was selected that simplifies the cooling requirements by use of a perforated liner. Use of the liner also insures screech-free operation of the afterburner as discussed in the paper by Childs. The perforated liner installation requires about 12 percent of the gases from the turbine outlet for cooling purposes. Use of this liner essentially eliminates the need for external cooling of the afterburner shell, but some cooling air is necessary for aircraft structure and nozzle cooling. These cooling requirements are shown in figure 7, and the method of computing the necessary cooling-air flow is described in appendix B.

#### Matching Duct and Ejector

The data used in this analysis are based on small-scale ejector tests using  $80^{\circ}$  F ( $540^{\circ}$  R) air for both primary and secondary air.

[REDACTED]

Since the cooling requirements are less than 0.05 corrected weight-flow ratio, these model data will give a fair estimate (previously discussed) of full-scale hot-gas ejector performance. Cooling-air duct characteristics were computed for each flight condition, and the ejector operating conditions were determined by a graphical matching method. The method of computing duct characteristics and graphical matching to an ejector is described in appendix B.

#### NET THRUST OF EJECTOR PERFORMING AS A SUPERSONIC NOZZLE

Net thrust ratio was calculated for the various ejector configurations shown in figure 2. The net thrust parameter used herein is the ratio of net ejector thrust to the ideal net thrust available from the engine. The ideal net thrust is based on actual engine mass flow and velocity of complete isentropic expansion.

Only the ejector configurations that supplied enough air to cool the primary nozzle over the range of flight conditions are considered herein. For other flight plans and engine conditions, the values of net thrust ratio could be raised or lowered depending on cooling requirements and consequent inlet momentum losses due to cooling-air flow.

#### Fixed Shroud Ejector

Net thrust ratio of the fixed-shroud ejector shown in figure 9(a) indicated rather poor thrust performance at the two cruise conditions but good thrust performance during acceleration. This characteristic is typical of the fixed-shroud ejector because a relatively large diameter ratio results when the primary nozzle throat area is decreased to the cruise condition. These excessive losses with the large diameter ratio ejectors may result from any one of the following causes: (1) The primary stream is overexpanded if secondary flow is choked and cannot increase, (2) if secondary flow is not choked and is free to

increase, the inlet momentum term  $\frac{W_p}{g} \left( 1 + \frac{W_s}{W_p} - \frac{W_f}{W_p} \right) V_0$  goes up (and

hence decreases net thrust), or (3) the shroud may be too large to act as the divergent portion of the nozzle such that two streams are discharged as from simple convergent nozzles with the associated under-expansion losses. The fixed-shroud ejector thus cannot give good thrust performance over the complete range of flight conditions for an afterburning engine because of the large necessary changes in primary nozzle size. As a matter of interest, the fixed-shroud ejector could perform very well with regard to thrust when used with a nonafterburning fixed-nozzle engine.

### Variable Shroud Length

Performance of a variable-shroud-length ejector is presented in figure 9(b). Net ejector thrust for a specific diameter ratio and set of operating pressure ratios does not change appreciably with changes in shroud length. Thus, net thrust of the variable-shroud-length ejector in figure 9(b) is only slightly higher than net thrust of the fixed-shroud ejector in figure 9(a). The variable-shroud-length ejector has poor thrust characteristics at both cruise conditions for the reasons previously discussed in connection with the fixed-shroud ejector when the primary nozzle throat is reduced in size.

### Variable Shroud Diameter

An ejector of variable shroud diameter is a very practical configuration because both the primary and ejector nozzles can be iris-type nozzles in use at the present time. The net thrust ratio of such an ejector is shown in figure 9(c) to be relatively high at 0.8 Mach number cruise and during acceleration. The drop in net thrust ratio to 93 percent at Mach number of 2.0 cruise condition is not desirable but such a drop occurred (even with a convergent nozzle) because gross thrust was reduced by the decreased afterburning temperature while inlet momentum remained almost constant.

### Variable Shroud Diameter and Variable Shroud Length

A variable shroud diameter and variable shroud length permit control of both expansion area and ejector air-handling capacity. Such a configuration (which should certainly be expected to have good net thrust performance) is shown in figure 9(d) to maintain a net thrust ratio between 0.96 and 0.98 over the entire flight plan. The excellent performance of this type ejector, however, will be compromised by the complexity of the control problems and weight of the control mechanism.

### PERFORMANCE COMPARISON OF COOLED AND UNCOOLED PLUG NOZZLE

The paper by Englert and Shillito discussed the thrust characteristics of an uncooled plug-type variable-area nozzle, whereas the net thrust ratios presented for the ejector acting as a supersonic nozzle included the losses due to nozzle cooling. The surface of the plug and its conical shroud will require cooling during afterburning. One of the most effective methods is transpiration cooling, in which a quantity of compressor-discharge air is forced through the porous metal surfaces that are to be cooled (fig. 10). Calculations were made of the coolant

requirements at each flight condition, for a transpiration-cooled plug-type nozzle. The nozzle was geometrically similar to the plug nozzle discussed by Englert and Shillito but with the slenderness ratio of the plug reduced from 3 to 2.1 in order to decrease the surface areas of the porous metal. The axial distributions of permeability in the porous metal of the plug and shroud were assumed to be variable for each flight condition so that the porous metal surface exposed to the combustion gas could be maintained at a strength-limited temperature of 1860° R (1400° F). The resulting flow ratios of compressor-discharge bleed air to the compressor-inlet air  $W_c/W_a$  shown in figure 11(a) therefore represent the minimum cooling-air requirements for compressor discharge air at each of the flight conditions with the assumed limiting temperature of 1860° R. The flow ratios with afterburning ranged from about 0.012 to 0.029, respectively, for combustion-gas temperatures of 2500° and 3500° R at a flight Mach number of 2.0. Nozzle cooling is unnecessary during nonafterburning, but the flow ratio of 0.0066 at a flight Mach number of 0.8 represents a small purging air flow to prevent gradual plugging of the porous metal surface by soot or fuel residues over extended periods of nonafterburning. In actual practice, the flow ratios shown might become 50 to 100 percent greater because the distribution of permeability would be fixed for some design point or compromised for a range of flight conditions so as to minimize extravagant use of compressor bleed air at off-design conditions. However, these considerations were beyond the scope of this preliminary analysis.

The net thrust ratio of the plug nozzle with cooling takes into account the decrease in jet velocity due to the mass addition of cooling air, with no axial momentum, to the combustion gas flow. Air bled from the compressor discharge lowers the compressor pressure ratio and increases the work per unit of mass flow through the turbine. Because the turbine-inlet temperature is limited, the increased work per unit of mass flow through the turbine requires an increase in pressure ratio across the turbine which is obtained by an increase in exhaust-nozzle area which lowers the total pressures at the nozzle inlet and at the turbine discharge. Therefore, the jet velocity is further reduced by compressor air bleed because of the accompanying decrease in nozzle-inlet total pressure. With cooling, the net thrust ratio (fig. 11(b)) was about 5 to 7 percent lower than for the uncooled plug nozzle at flight Mach number of 0.8 to 2.0, respectively, and 3500° R exhaust-gas temperature. The percent loss in net thrust ratio per percent of compressor bleed air at the Mach 2.0 condition was about 1.3 at a gas temperature of 3500° R and about 2.4 at a gas temperature of 2500° R.

A direct comparison of the net thrust ratio for the transpiration-cooled plug nozzle and the net thrust ratio of the ejector is not intended here because the plug nozzle design was not optimum for the flight plan investigated. Design data were incomplete for plug nozzles

having better performance characteristics. Other methods for cooling plug nozzles may possibly result in higher net thrust ratios. Several methods for improving the performance of a transpiration-cooled plug nozzle suggest themselves by the approach in net thrust performance for the cooled and uncooled plug nozzle at cruise conditions for flight Mach numbers of 0.8 and 2.0 (fig. 11(b)). The losses decrease as the cooling-air requirements decrease. Primary reductions in cooling-air requirements would result if the plug surface area could be reduced by shortening without adversely affecting the jet velocity coefficient  $C_v$ , or if the shroud could be adequately cooled by a nonperforated extension of the perforated combustion-chamber liner. The cooling-air requirements would also decrease if the strength of porous metals were improved so as to permit a higher limiting porous surface temperature. Cooling-air requirements and the decrease in turbine discharge pressure due to compressor bleed can be reduced to a limited extent by using cooler compressor air bled from an inner stage at just sufficient pressure to force the cooling air through porous metal surfaces. Unfortunately, data are lacking at present on the feasibility of these alternative cooling methods.

#### SUMMARY

Performance of the ejector as a supersonic nozzle and cooling device was evaluated for several ejector configurations at typical flight conditions experienced by an area-defense fighter aircraft equipped with a turbojet engine and afterburner assembly. The analysis was based on experimental data obtained from model ejector tests and in order to indicate the validity of this assumption, full-scale hot-gas ejector performance was compared with model ejector performance. From the limited data examined it appears that model ejector tests can be utilized to predict thrust of geometrically similar full-scale ejectors within about  $1\frac{1}{2}$  percent. Air-handling capacity of full-scale ejectors can be predicted with reasonable accuracy for corrected weight-flow ratios up to at least 0.04, but much above 0.04 the combined effect of ejector size, secondary passage geometry, gas temperature, and flow disturbances make the use of model data uncertain, except for very short shroud-length ejectors.

Net thrust performance of the fixed shroud ejector was good during acceleration with afterburning (0.94 to 0.97 percent of ideal thrust), but was rather low at nonafterburning cruise (0.90 percent) and at reduced-afterburning cruise (0.91 percent). Performance of the variable-shroud-length ejector was only slightly higher than that of the fixed-shroud ejector and thus indicates no pronounced advantage in designing an ejector of variable length. Both of these configurations experienced

[REDACTED]

low net thrust at cruise because of the excessive expansion-area ratio that existed when the primary nozzle throat area was reduced. The fixed-shroud ejector could perform very well with regard to thrust when used with a nonafterburning fixed-nozzle engine.

3078 - G

An ejector of variable shroud diameter is a very practical configuration because both the engine and ejector nozzles can be designed similar to nozzles being used at the present time, such as the iris-type nozzle. Net thrust of the variable-shroud-diameter ejector was relatively high (above 93 percent of ideal thrust) over the entire flight plan.

The variable-shroud-diameter and variable-shroud-length ejector, which permits control of both expansion ratio and ejector air-handling capacity, maintained a net thrust between 96 percent and 98 percent of ideal thrust over the entire flight plan. The excellent performance of this type ejector, however, will be compromised by complexity and weight of the control mechanism.

The brief analysis of a transpiration-cooled plug-type nozzle indicated that cooling this nozzle to a constant porous wall temperature of  $1860^{\circ}$  R ( $1400^{\circ}$  F) at an exhaust-gas temperature of  $3500^{\circ}$  R, can produce net thrust losses of about 5 and 7 percent over that of the uncooled plug nozzle at flight Mach numbers of 0.8 and 2.0, respectively. However, other plug nozzle designs and cooling methods can probably be devised that will impose smaller losses in net thrust.

[REDACTED]

## APPENDIX A

## SYMBOLS

The following symbols are used:

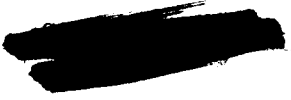
A	flow area, sq ft
$C_v$	jet velocity coefficient, measured jet thrust divided by isentropic jet thrust for measured mass flow
$C_1, C_2$	empirical constants
D	diameter, ft
F	thrust, lb
g	acceleration due to gravity, ft/sec <sup>2</sup>
h	heat-transfer coefficient, Btu/(hr)(sq ft)(°R)
L	axial distance between exit planes of primary nozzle and ejector shroud, ft
M	Mach number
P	total pressure, lb/sq ft abs
p	static pressure, lb/sq ft abs
q	dynamic pressure, lb/sq ft
R	gas constant, ft-lb/(lb)(°R)
S	surface area, sq ft
T	total temperature, °R
V	velocity, ft/sec
W	weight flow, lb/sec
$\gamma_p$	ratio of specific heats of primary gas
$\delta_2$	ratio of compressor inlet total pressure to NACA standard pressure at sea level

$\theta_2$  ratio of compressor inlet total temperature to NACA standard temperature at sea level

$\rho$  density, lb/cu ft

Subscripts:

a compressor inlet air  
b conditions existing with compressor bleed  
c coolant or compressor bleed air  
e ejector  
f fuel to engine and afterburner  
g combustion gas  
i corresponding to isentropic expansion to ambient pressure  
j jet  
k a general incremental segment  
n net  
p primary fluid  
r rated engine conditions  
s secondary fluid  
w nozzle wall  
0 ambient free-stream conditions  
2 compressor inlet  
5 turbine discharge


  
 APPENDIX B

## ANALYSIS OF FORCED-CONVECTION-COOLED IRIS NOZZLE WITH EJECTOR

The dimensions of the afterburner combustion chamber assumed in this analysis are typical of current afterburners for turbojet engines having a corrected air flow  $W_a \sqrt{\theta_2}/\delta_2$  at sea level of about 104 pounds per second. The combustion chamber had a mean diameter of 32 inches and a length of 55 inches from flame holder to exhaust-nozzle inlet. An annular passage 3/4-inch in height conducts the cooling air, hereinafter called secondary fluid, from boundary-layer scoop inlets to the exhaust-nozzle inlet. The secondary fluid then flows over the nozzle segments, cooling them by forced convection, and is discharged to the ejector. A perforated liner upstream of the nozzle forms an annular flow passage for turbine discharge gas so that the temperature of the structural wall of the afterburner combustion chamber is practically equal to the turbine discharge gas temperature. Temperatures, pressures, and flow areas within the engine and afterburner were computed by means of standard cycle analysis using one-dimensional-flow equations. Typical values were assumed for component efficiencies and the turbine-inlet temperature was held at 2000° R.

3078-G

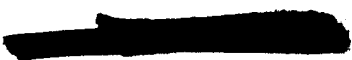
## CALCULATIONS

## Calculation of Temperatures

The maximum temperature of the iris nozzle segments corresponding to various assumed ratios of secondary to primary (combustion gas) flows was computed from a heat balance (eq. (B1)) across the segment at the exhaust nozzle exit:

$$T_w = \frac{C_1 h_g T_g + C_2 h_c T_s}{C_1 h_g + C_2 h_c} \quad (B1)$$

The empirical factors  $C_1$  and  $C_2$ , respectively, modified the conventional convective heat-transfer coefficients for fully developed turbulent boundary-layer flow on the combustion gas and coolant sides of the nozzle segments to account for radiant heat transfer and for fin effectiveness of the nozzle segments. The values of  $C_1$  and  $C_2$  used were:



Flight Mach number, $M_0$	Primary gas temperature, $T_p$ , °R	$C_1$	$C_2$
0.8	1654	1.03	1.155
.8	3100	1.20	1.155
1.5	3500	1.20	1.155
2.0	3500	1.20	1.155
2.0	2500	1.20	1.155

The total temperature of the secondary fluid  $T_s$  at the exhaust-nozzle exit was computed from the free-stream total temperature and the rise in secondary fluid temperature up to the exhaust-nozzle exit. This temperature rise was computed in two steps with the assumption of no external heat losses. The temperature rise of the secondary fluid up to the nozzle inlet was computed for flow through a constant-area duct having a constant wall temperature equal to the turbine-discharge gas temperature. The rise in secondary fluid temperature along the iris nozzle segments was computed for a constant rate of heat flux.

The total temperature of the combustion gas  $T_g$  in equation (B1) was taken as  $100^\circ$  R less than the bulk total temperature of the primary jet  $T_p$  in order to account for the gas-temperature profile near the nozzle wall.

#### Calculation of Pressures

The total pressure of the secondary fluid at the inlet to the 3/4-inch-high annular passage was taken as one passage inlet dynamic pressure  $q$  less than the total pressure derived from the pressure-recovery ratio for a boundary-layer scoop inlet in reference 6. The total pressures at the inlet and at the exit  $P_s$  of the iris nozzle corresponding to the assumed values of secondary to primary flow ratios and the calculated temperatures of the secondary fluid at the respective stations were computed by the method of reference 7.

#### Matching Procedure

The matching point of the pumping characteristics of each ejector configuration with the flow characteristics of the secondary passage at each flight condition was found by graphical solution. The values of the secondary fluid temperature  $T_s$  and total pressure  $P_s$  computed

for a range of secondary to primary flows  $W_s/W_p$  up to choking for each flight condition were used in constructing the plot (fig. 12(a)) of secondary passage flow characteristics.

Pumping data for each type ejector and for all combinations of diameter ratio  $D_s/D_p$  and spacing ratio  $L/D_p$  or  $S/D_p$  from references 1 to 4 were cross-plotted to obtain pumping characteristics (fig. 12(b)) for primary pressure ratios  $P_p/p_0$  corresponding to those at each flight condition.

Because the ordinates and abscissas of figures 12(a) and (b) were chosen identical, the superposition of one figure upon the other will yield a simultaneous solution or matching point for each intersection of a secondary passage flow characteristic curve with a curve of constant primary pressure ratio  $P_p/p_0$  (see fig. 12(c)) corresponding to the flight condition of the respective flow characteristic curve.

Having found the matching points, the matching values of  $W_s/W_p \sqrt{T_s/T_p}$  and  $P_s/p_0$  for each ejector configuration and flight condition can be read and tabulated. The nozzle temperature  $T_w$  corresponding to each matching point is then read from a plot (fig. 12(d)) of the previously calculated nozzle temperatures against the corrected weight-flow ratio  $W_s/W_p \sqrt{T_s/T_p}$ .

#### Calculation of Net Thrust Ratio

The procedure for calculating the net thrust for each ejector configuration that would cool to or below the limiting nozzle temperature of 2260° R (1800° F) is given in the following paragraphs.

The matching point values of the ratio of jet thrust with the ejector  $F_{ej}$  to the jet thrust  $F_{pj}$  of the same primary nozzle without an ejector were read from plots (fig. 12(e)) of ejector thrust data of references 1 to 4, corresponding to the matching point values of primary and secondary pressure ratios  $P_p/p_0$  and  $P_s/p_0$ , respectively.

The experimentally determined ratio of the actual jet velocity to the ideal jet velocity for complete isentropic expansion  $C_v$  or  $F_{pj}/F_{pi}$  for the same primary mass flow were read from figure 12(f) for the same primary nozzle as used in the model ejector investigations.

The net thrust ratio for the ejector as a supersonic nozzle  $(F_{ej}/F_{ip})_n$  is defined as the ratio of the net thrust of the iris nozzle

and ejector combination to the net thrust that would be obtained if the same primary gas flow were expanded isentropically to free-stream ambient pressure. The net thrust ratio is given in equation (B2):

$$\left(\frac{F_{ej}}{F_{ip}}\right)_n = \frac{C_v \left(\frac{F_{ej}}{F_{pj}}\right) \frac{V_{ip}}{V_0} - \frac{W_a}{W_p} \left(1 + \frac{W_s}{W_a}\right)}{\frac{V_{ip}}{V_0} - \frac{W_a}{W_p}} \quad (B2)$$

where

$$V_{ip} = \sqrt{\frac{2\gamma_p}{\gamma_p - 1} gRT_p \left[1 - \left(\frac{P_0}{P_p}\right)^{\frac{\gamma_p - 1}{\gamma_p}}\right]}$$

## APPENDIX C

## ANALYSIS OF TRANSPIRATION-COOLED PLUG NOZZLE

The same afterburner assumed in the analysis of a forced-convection-cooled iris nozzle with an ejector was also assumed to be fitted with a sliding plug-type variable-area exhaust nozzle (fig. 10). The profiles of the plug and its conical shroud were the same as those of reference 8 only modified to a plug slenderness ratio of 2.1. The surfaces of the plug and of the aft end of the conical shroud, from 1 inch upstream of the most forward position of the minimum projected flow area, were assumed to be transpiration cooled by the flow of compressor-discharge air through their porous walls. The plug had a length of 49.6 inches and the porous wall of the shroud had a length of 24.7 inches. Their respective surface areas were 18 and 17.5 square feet.

## Calculation of Cooling-Air-Flow Requirements

The experimentally determined correlation of the parameter  $\frac{T_w - T_c}{T_p - T_c}$  with the parameter  $\frac{(\rho V)_c}{(\rho V)_p}$  for an experimental transpiration-cooled afterburner (ref. 9) was used in obtaining the axial distribution of  $\frac{(\rho V)_c}{(\rho V)_p}$  along the plug and shroud surfaces. The parameter  $\frac{T_w - T_c}{T_p - T_c}$  was evaluated from known values of the primary fluid total temperature  $T_p$  (assumed to be constant through the nozzle), the compressor-discharge temperature  $T_c$ , and the limiting temperature of the porous metal  $T_w$ . The axial distribution of the compressor bleed air normal to the porous surfaces  $(\rho V)_c$  was obtained from the parameter  $\frac{(\rho V)_c}{(\rho V)_p}$  and the known distribution of primary flow area and from the relation

$$(\rho V)_p = \left( \frac{W}{A} \right)_p$$

The cooling-air flows through the porous surfaces of the plug and shroud were obtained from

$$W_c = \sum_{k=1}^n (\rho V)_{ck} \Delta S_k \quad (C1)$$

[REDACTED]

### Calculation of Net Thrust Ratio

The net thrust ratio without cooling was computed from the equation

$$\left(\frac{F}{F_1}\right)_n = \frac{C_v \left(1 + \frac{W_f}{W_a}\right) \frac{V_1}{V_0} - 1}{\left(1 + \frac{W_f}{W_a}\right) \frac{V_1}{V_0} - 1} \quad (C2)$$

and with cooling, from the equation

$$\left(\frac{F}{F_1}\right)_{n,c} = \frac{C_v \left(1 + \frac{W_f}{W_a} - \frac{W_c}{W_a}\right) \frac{V_{1b}}{V_0} - 1}{\left(1 + \frac{W_f}{W_a}\right) \frac{V_1}{V_0} - 1} \quad (C3)$$

The experimental values of  $C_v$  for the uncooled plug nozzle of reference 8 were used in both equations for net thrust ratio. The values of jet velocity for isentropic expansion to ambient pressure without cooling  $V_1$  and with compressor bleedoff  $V_{1b}$  were computed from equation (B3) corresponding to the pressure ratios  $p_0/p_p$  and  $p_0/p_{pb}$ . The pressure ratio  $p_0/p_{pb}$  was determined in the following manner:

$$\frac{p_0}{p_{pb}} = \frac{p_0}{p_p} \frac{p_p}{p_{pb}} \quad (C4)$$

With the assumption that the total-pressure ratio across the afterburner combustion chamber is the same with and without compressor bleed,

$$\left(\frac{p_p}{p_5}\right)_b = \frac{p_p}{p_5}$$

or

$$\frac{p_p}{p_{pb}} = \frac{p_5}{p_{5b}} = \frac{\frac{(p_5/p_2)}{(p_5/p_2)_r}}{\frac{(p_5/p_2)_b}{(p_5/p_2)_r}} \quad (C5)$$

and combining equations (C4) and (C5) gives

[REDACTED]

$$\frac{P_0}{P_{pb}} = \frac{P_0 \frac{(P_5/P_2)_r}{(P_5/P_2)_b}}{\frac{(P_5/P_2)_r}{(P_5/P_2)_b}} \quad (C6)$$

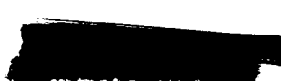
The values of

$$\frac{P_5/P_2}{(P_5/P_2)_r}$$

with and without compressor bleed were read from pumping characteristic curves of reference 10 for the appropriate values of air-bleed ratio  $W_c/W_a$ .

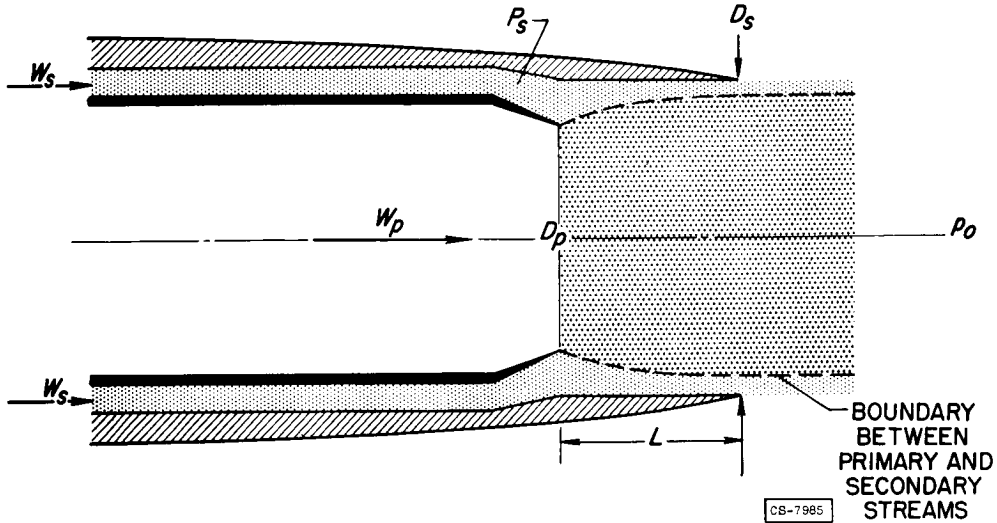
#### REFERENCES

1. Greathouse, W. K., and Hollister, D. P.: Air-Flow and Thrust Characteristics of Several Cylindrical Cooling-Air Ejectors with a Primary to Secondary Temperature Ratio of 1.0. NACA RM E52L24, 1953.
2. Greathouse, W. K., and Hollister, D. P.: Preliminary Air-Flow and Thrust Calibrations of Several Conical Cooling-Air Ejectors with a Primary to Secondary Temperature Ratio of 1.0. I - Diameter Ratios of 1.21 and 1.10. NACA RM E52E21, 1952.
3. Greathouse, W. K., and Hollister, D. P.: Preliminary Air-Flow and Thrust Calibrations of Several Conical Cooling-Air Ejectors with a Primary to Secondary Temperature Ratio of 1.0. II - Diameter Ratios of 1.06 and 1.40. NACA RM E52F26, 1952.
4. Kochendorfer, Fred D., and Rousso, Morris D.: Performance Characteristics of Aircraft Cooling Ejectors Having Short Cylindrical Shrouds. NACA RM E51E01, 1951.
5. Wilsted, H. D., Huddleston, S. C., and Ellis, C. W.: Effect of Temperature on Performance of Several Ejector Configurations. NACA RM E9E16, 1949.
6. Samuels, John C., and Yanowitz, Herbert: Analysis of Several Methods of Pumping Cooling Air for Turbojet-Engine Afterburners. NACA RM E52K26, 1953.

- 
7. Sibulkin, Merwin, and Koffel, William K.: Chart for Simplifying Calculations of Pressure Drop of a High-Speed Compressible Fluid under Simultaneous Action of Friction and Heat Transfer - Application to Combustion-Chamber Cooling Passages. NACA TN 2067, 1950.
  8. Hearth, Donald P., and Gorton, Gerald C.: Investigation of the Thrust and Drag Characteristics of a Plug-Type Exhaust Nozzle. (NACA RM to be pub.)
  9. Koffel, William K.: Preliminary Experimental Investigation of Transpiration Cooling for an Afterburner with a Sintered, Porous Stainless-Steel Combustion-Chamber Wall. NACA RM E53D08, 1953.
  10. Hensley, Reece V., Rom, Frank E., and Koutz, Stanley L.: Effect of Heat and Power Extraction on Turbojet-Engine Performance. I - Analytical Method of Performance Evaluation with Compressor-Outlet Air Bleed. NACA TN 2053, 1950.
- 



EJECTOR SHOWING BOUNDARY BETWEEN  
PRIMARY AND SECONDARY STREAMS



3078-G

Figure 1

EJECTOR CONFIGURATIONS WITH VARIABLE GEOMETRY

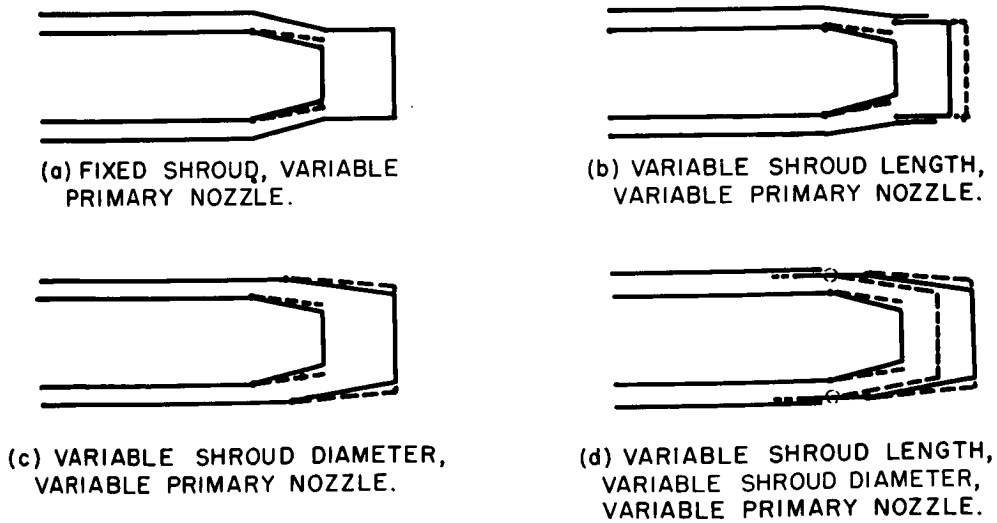


Figure 2



COMPARISON OF AIR-HANDLING CHARACTERISTICS OF SMALL AND FULL-SCALE EJECTORS

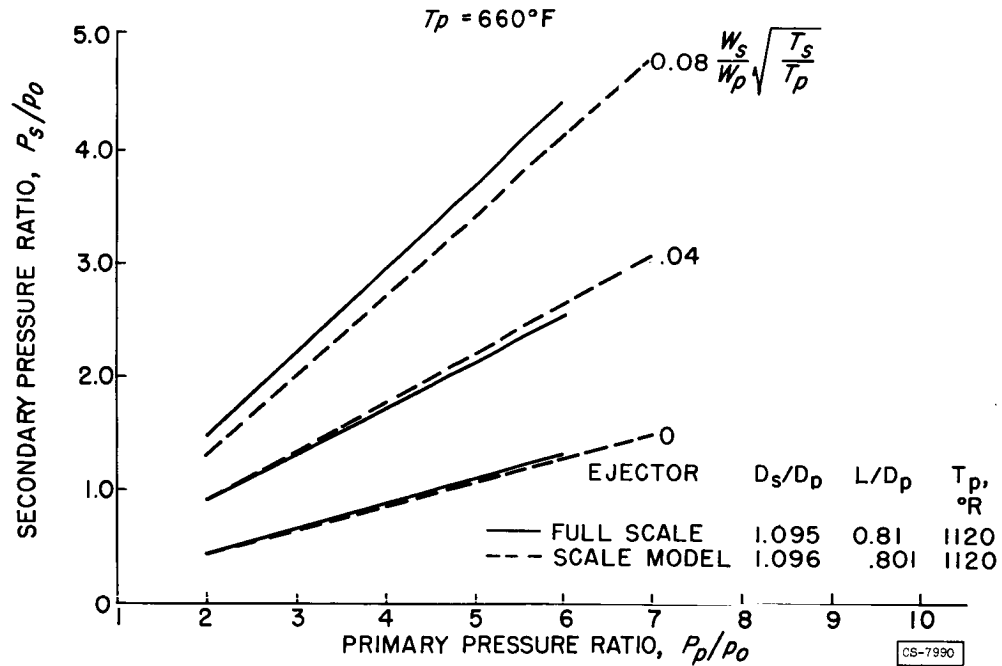


Figure 3

EFFECT OF SECONDARY PASSAGE CONFIGURATIONS

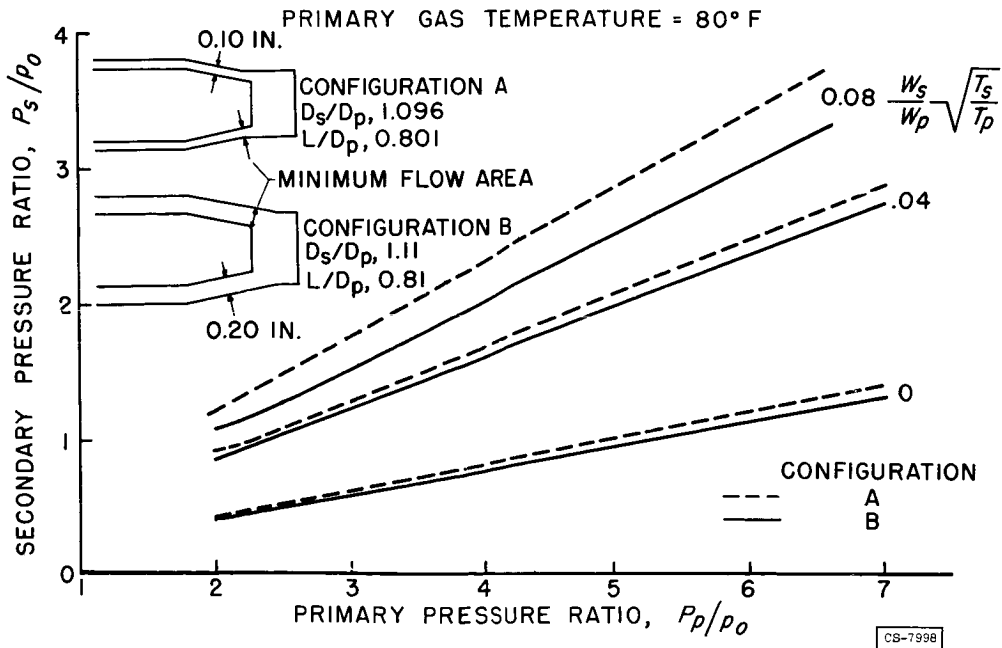


Figure 4

AIR-HANDLING CAPACITY OF FULL-SCALE EJECTORS

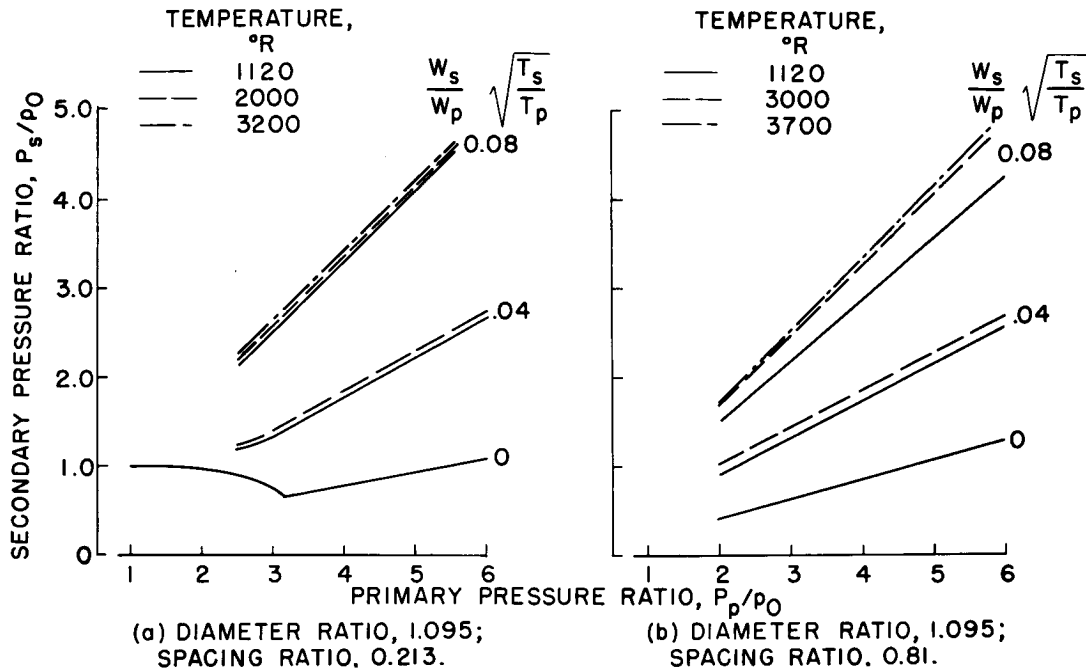


Figure 5

COMPARISON OF THRUST CHARACTERISTICS

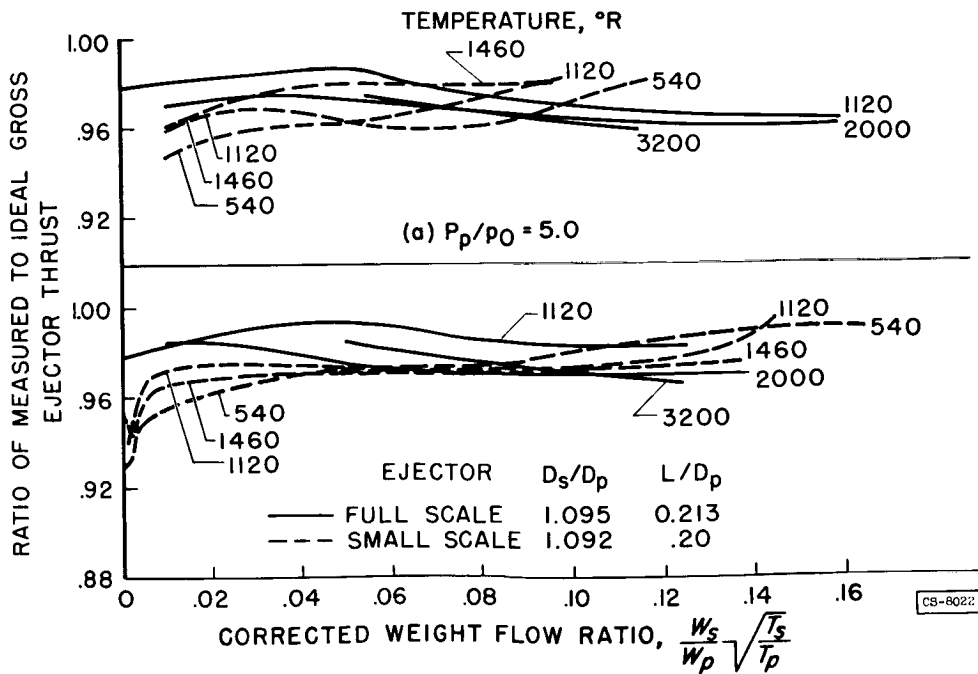


Figure 6

3078-G

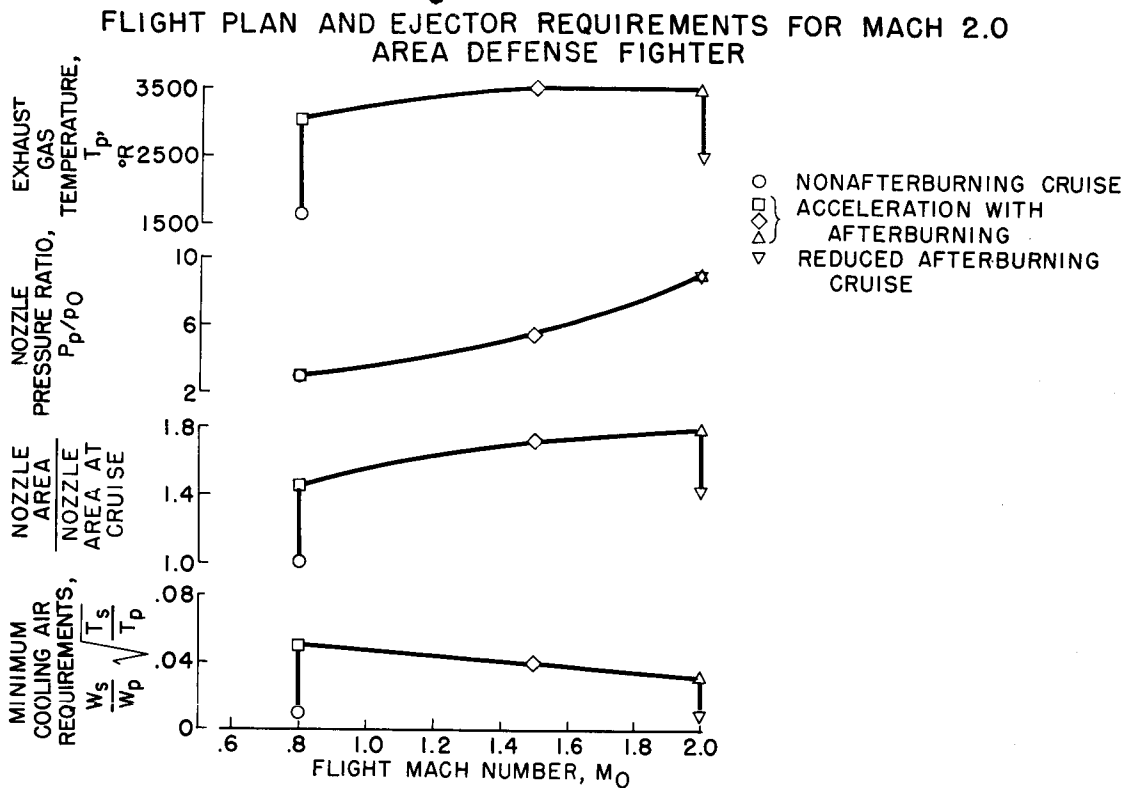


Figure 7

**SCHEMATIC SKETCH OF AFTERBURNER  
SHOWING INSTALLATION OF PERFORATED LINER**

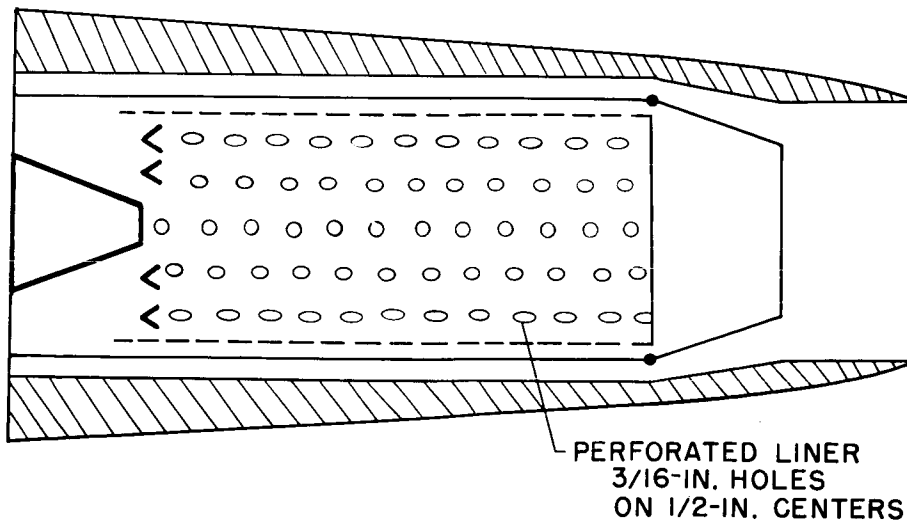
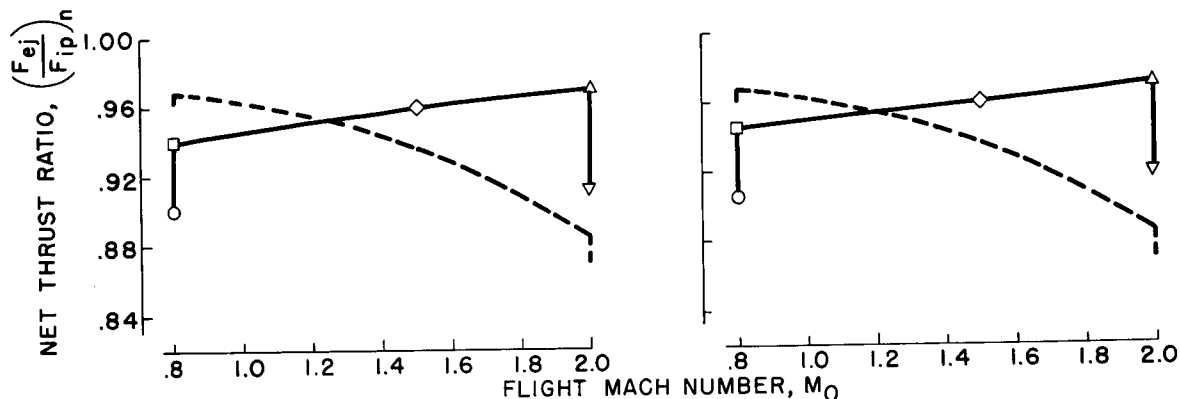


Figure 8

PERFORMANCE OF EJECTOR AS A SUPERSONIC NOZZLE

	$M_0$	$D_s/D_p$	$L/D_p$	
			FIXED SHROUD	VARIABLE SHROUD
○ CRUISE	0.8	1.62	1.13	1.00
□ ACCELERATION	.8	1.29	.86	.60
◇ ACCELERATION	1.5	1.24	.82	.80
△ ACCELERATION	2.0	1.21	.80	.80
▽ CRUISE	2.0	1.37	.91	.80

--- UNCOOLED CONVERGENT NOZZLE

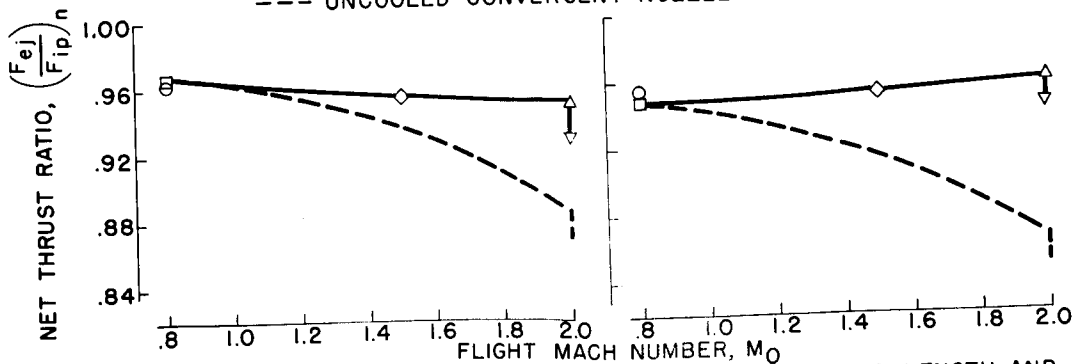


(a) FIXED-SHROUD CYLINDER EJECTOR. (b) VARIABLE-SHROUD-LENGTH CYLINDER EJECTOR. DIAMETER, 30.4 INCHES; LENGTH, 20 INCHES.

PERFORMANCE OF EJECTOR AS A SUPERSONIC NOZZLE

	$M_0$	$D_s/D_p$		$L/D_p$	
		VARIABLE SHROUD DIAMETER	VARIABLE SHROUD LENGTH AND DIAMETER	VARIABLE SHROUD DIAMETER	VARIABLE SHROUD LENGTH AND DIAMETER
○ CRUISE	0.8	1.10	1.06	0.84	0.2-0.4
□ ACCELERATION	.8	1.10	1.10	.63	.7-.8
◇ ACCELERATION	1.5	1.21	1.21	.61	.7-.8
△ ACCELERATION	2.0	1.21	1.10	.59	.8-1.2
▽ CRUISE	2.0	1.21	1.10	.67	.8-1.2

--- UNCOOLED CONVERGENT NOZZLE



(c) VARIABLE-SHROUD-DIAMETER EJECTOR. LENGTH, 1.5 INCHES. (d) VARIABLE-SHROUD-LENGTH AND VARIABLE-SHROUD-DIAMETER

Figure 9

3078-G

PLUG NOZZLE CONFIGURATION

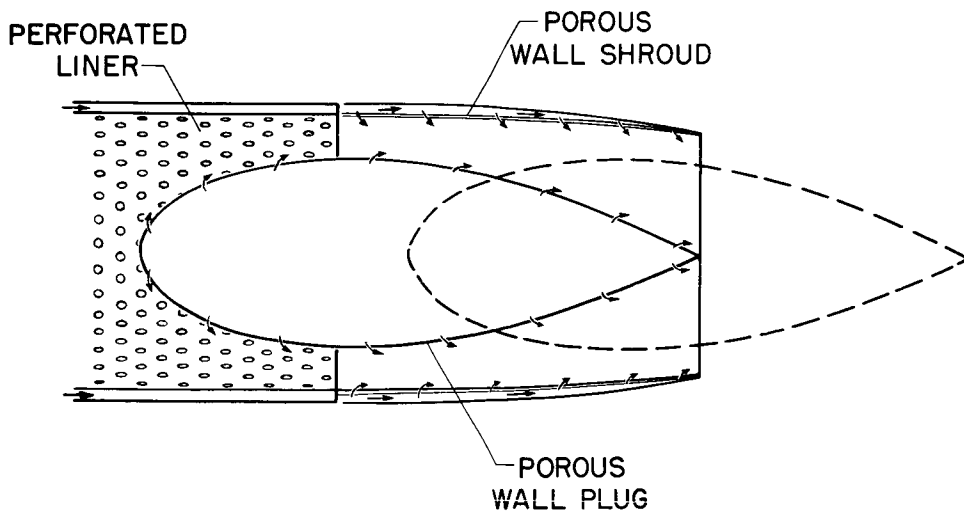


Figure 10

PERFORMANCE CHARACTERISTICS AND MINIMUM COOLING-AIR REQUIREMENTS OF A PLUG NOZZLE

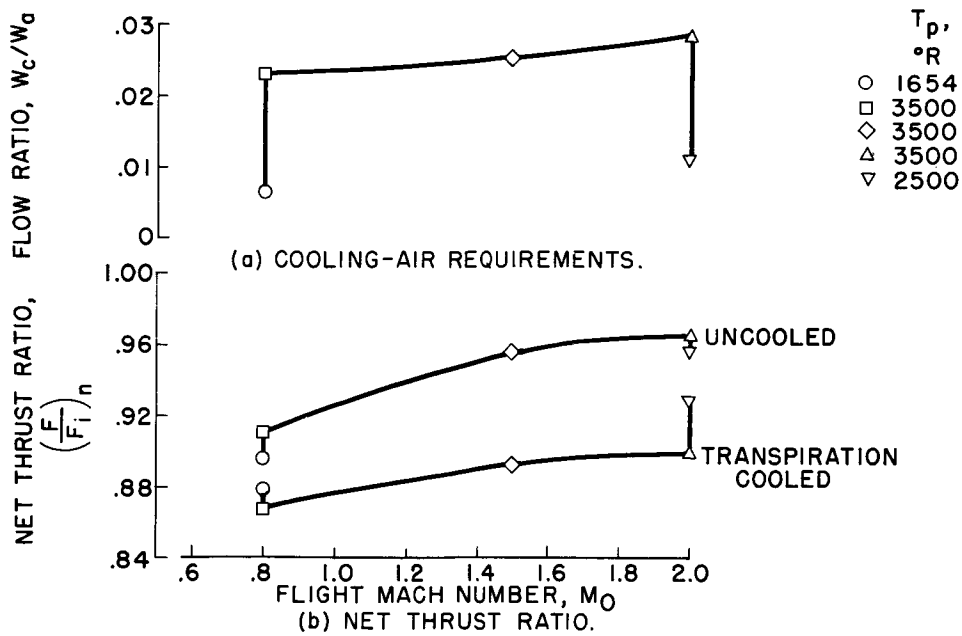


Figure 11

AUXILIARY PLOTS FOR GRAPHICAL SOLUTION OF MATCHING POINT AND CALCULATION OF NET THRUST RATIO

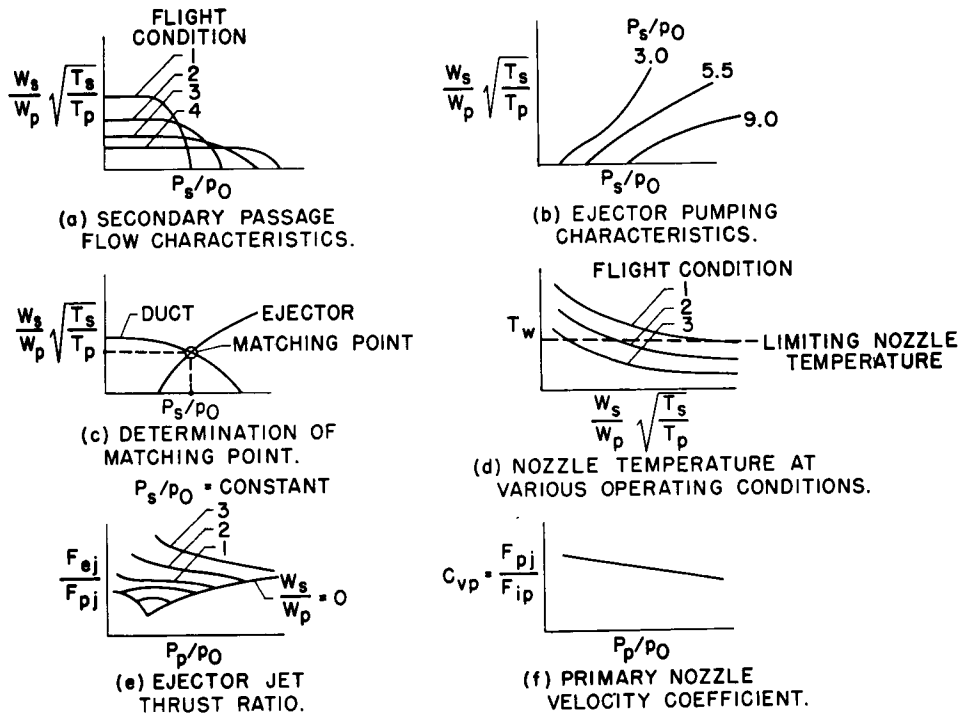


Figure 12

[REDACTED]

SOME AERODYNAMIC CONSIDERATIONS OF AFTERBODY DESIGN

AT SUPERSONIC SPEEDS

By E. M. Cortright, Jr.

INTRODUCTION

When a propulsive jet discharges from the base of a fuselage, it is usually necessary to boattail the fuselage from the maximum cross-sectional area to that required for the nozzle exit. The present paper is concerned with the prediction of the drag forces associated with boattailing and the possibility of jet interference effects on the drag for the case of turbojet-powered aircraft.

All boattails are subjected to an initial boundary layer as well as some degree of interference from other parts of the aircraft such as the forebody, wings, and tail surfaces. Generalization of the problem is made even more difficult by the many geometric configurations encountered in practice as a result of such basic design considerations as whether a single or side-by-side engine installation is utilized and whether the jets discharge from the base of the body or from the underside at some forward station. In addition, nacelle and pod installations present somewhat different boattail problems.

Insufficient data exist to permit detailed discussion of the many possible afterbody cases. Only the most simple class of afterbodies composed of bodies of revolution with single jets issuing from the base will be discussed herein. No interference effects other than those arising from the jet itself will be considered. Fortunately, many of the conclusions derived from such simple considerations apply in the case of more complicated installations.

SYMBOLS

The following symbols are used in this paper:

- A      cross-sectional area
  - $C_D$     pressure-drag coefficient,  $D/q_0 A_B$
  - $C_p$     pressure coefficient,  $(p-p_0)/q_0$
  - D      drag force
  - d      diameter
- [REDACTED]



M	Mach number
P	total pressure
p	static pressure
q	dynamic pressure, $\frac{\gamma p M^2}{2}$
x	axial distance downstream from start of boattail
$\beta$	angle of boattail at rearmost station, deg
$\epsilon$	angle of nozzle at exit station, deg

## Subscripts:

B	body maximum
b	annular base
des	design
j	jet conditions at nozzle exit
n	nozzle exit
O	free stream

## DISCUSSION

Nozzle installations. - The amount of boattailing required and the resulting contour of the boattail depend to some extent on the type of nozzle utilized. In addition, the degree of jet interference is very much a function of the nozzle type. As has been discussed in earlier papers, the ejector nozzle and the plug nozzle are two of the more promising nozzles for providing variation of throat area and expansion area ratio over a wide range of operating conditions. Possible installations of these nozzles are therefore shown schematically in figure 1. Figure 1(a) depicts the installation of double-iris ejector nozzle in the fuselage of a hypothetical Mach 2.8 interceptor airplane and in a typical nacelle. The iris flap lengths have been arbitrarily chosen but are typical, at least of some "hardware" under development. In general, for the case of fuselage installations the afterbody must be boattailed to the secondary iris hinge line; additional boattailing may then result from the iris flaps themselves, which vary their angle with flight speed and afterburner temperature. The iris angle can become quite large at reduced flight speeds and may exceed  $30^\circ$  in the subsonic cruise condition



[REDACTED]

with afterburning off. In the case of nacelle installations, no boattailing is generally required except that which arises from the iris flaps. If the nacelle proper were kept to a minimum diameter for the hypothetical case under consideration (fig. 1(a)), it would be necessary to either flare the iris at Mach 2.8 or restrict the expansion slightly (alternate nacelle 1). An alternate approach (alternate nacelle 2) would be to increase the nacelle diameter so as to eliminate the flare while providing complete expansion in the ejector.

3078-G

Among other ejector variations are the single-step ejector with fixed shroud (fig. 1(b)) and with retractable shroud (fig. 1(c)). The fixed shroud results in a compromise expansion ratio at all but one flight speed. If such an ejector is to be effective at flight speeds as high as Mach 2.8, it will generally result in considerable thrust loss at the Mach 0.9 cruise condition with the afterburner off. If the shroud is retracted for the cruise condition, the overexpanded ejector problem is replaced by the drag problem of a large blunt base with secondary flow through it. At very high flight speeds, a two-step ejector (fig. 1(d)) may prove superior to the single-step ejectors just discussed (ref. 1). The problem of inefficient cruise operation remains, however.

The last nozzle installation to be considered is the plug-type nozzle. Previous discussion has concentrated primarily on plug types requiring appreciable axial movement primarily in order to provide internal expansion at high speeds. Illustrated in figure 1(e) is a plug-type nozzle designed for primarily external expansion with afterburner on at high speeds. The type of flow from such a nozzle is easily visualized if it is remembered that a so-called isentropic spike inlet can ideally be operated in reverse as a nozzle to yield axial jet flow at the design pressure ratio. The effectiveness of such a plug in the cruise condition when compared with the "streamlined" plugs of a previous paper by G. W. Englert and T. B. Shillito is a matter of conjecture. Cooling of this nozzle is not illustrated.

The purpose of discussing nozzle types at such length is so that certain general observations can be made for conventional aircraft designed for flight to Mach 2.8. These observations are as follows:

- (1) All the nozzle types require boattailing in a fuselage installation.
  - (2) No boattailing is required in a nacelle installation except that associated with iris flaps or that required to permit throat area variation of the plug nozzle. In fact, with isentropic expansion ratios the question may arise as to whether to flare the nacelle.
  - (3) None of the nozzle types are apt to operate in the highly overpressure condition, that is, with a static pressure at the nozzle exit greatly in excess of the ambient static pressure.
- [REDACTED]

(4) The subsonic cruise condition with afterburner off imposes severe internal or external flow conditions depending on the nozzle configuration.

(5) Optimum afterbody-nozzle design may require compromises in which afterbody drag changes are weighed against nozzle thrust changes.

The significance of these observations will become more apparent as the discussion proceeds.

Prediction of boattail drags. - Since boattailing is a problem common to many nozzle installations, it will be discussed first. In the case of axially symmetric potential flow, the method of characteristics (ref. 2) as well as the theory of second-order linearized potential flow (refs. 3 and 4) provide reasonably good predictions of the pressure distributions and drag forces acting on boattails provided the flow is unseparated. The second-order theory is less laborious for hand computation. Unfortunately, the first-order linearized theory is inadequate for prediction of pressures except for small boattail angles. In figure 2 experimental and second-order theoretical pressure distributions for conical boattails of various half-angles  $\beta$  and at various Mach numbers are compared. The theoretical curves neglect the small amount of forebody interference which was present. The Mach 1.5 data were obtained from reference 5; the Mach 1.9 data were obtained from reference 6, and the Mach 3.1 data are unpublished. In all cases agreement is relatively good as the experimental pressures fall only slightly higher than those predicted by theory, which is in part caused by boundary-layer displacement thickness. The single large discrepancy at Mach 1.5 and  $\beta = 12^\circ$  may have arisen from separation at the rear of the boattail as a result of a reflected shock from the nose of the model combined with a trailing shock resulting for the high base pressure to be expected from such a configuration.

In reference 7, the theory of reference 4 was used to calculate the pressure distributions and drags of conical boattails for a range of boattail angles and Mach numbers. This reference was used in obtaining the theoretical curves of figure 2 as well as those of figure 3. Figure 3 illustrates the variation of boattail pressure drag with boattail angle, base area, and Mach number. It is evident that large afterbody drags can result from the use of large boattail angles, a fact which is most pronounced in the low supersonic speed range. Although the theory may not be applied at sonic velocity, it is clear that large boattail angles are apt to contribute to large transonic drag rises. Additional discussion of the transonic case may be found in reference 8. Experimental pressure drags indicated on the figure average approximately 90 percent of the theoretical values.

In actual installations, of course, the drags of the isolated boattails will be modified by forebody, wing, and tail interference effects. If the forebody is nearly axisymmetric, its effect may be readily estimated by the theory of reference 4 with the solution started from the beginning of the body. This interference effect will generally tend to increase the boattail drag but will be small if a length of cylindrical section precedes the boattail. The interference of forebodies on afterbodies is discussed in reference 9. Wing and tail interference effects are more difficult to estimate and little experimental aid exists. In general, if the interfering surface superimposes a compression flow field on the boattail, the boattail drag will be reduced and conversely in the case of an expansion flow field. Unfortunately, the usual case involves both positive and negative pressure disturbances.

In order to gain some appreciation of the magnitude of afterbody pressure drag, it is plotted in figure 4 as a fraction of engine thrust for the case of a hypothetical Mach 2.8 interceptor airplane with the engine in the fuselage. This interceptor utilizes an engine with a compressor pressure ratio of 7, constant engine rotative speed, turbine-inlet temperature of 2040° F, afterburning as indicated on the figure, and a double-iris ejector nozzle. Again the high drag associated with large boattail angles is evident. At the lower supersonic flight speeds, the drag of the ejector shroud iris contributes appreciably to the large afterbody drag. For a flight plan in which Mach 2.8 cruise consumes the predominant portion of the flight, the use of an 11° boattail with twice the pressure drag of a 5° boattail results in a 7-percent increase in the interceptor weight to accomplish the identical mission. Although structural and storage considerations play a large part in the determination of boattail angle or fineness ratio, it is apparent that appreciable drag reductions will reward the application of design ingenuity to the use of slender afterbodies.

Although the preceding discussion has concentrated on conical afterbodies, the same points generally hold true for other than conical profiles. In figure 5 the method of reference 4 is applied to the predictions of the pressure distributions of tangent-parabolic boattails. Again the experimental pressures are slightly higher than predicted and the drags correspondingly lower. Some separation is indicated at the rear of the boattails at the lower Mach numbers. The data at Mach 1.6 and 2.0 were obtained in the Lewis 8- by 6-foot supersonic wind tunnel with a model having a side strut support which may have introduced some interference. The Mach 3.1 data were obtained with a sting-supported model. For comparison, the theoretical drags of conical boattails having the same base area and fineness ratio are presented. With allowance made for the variation between experiment and theory for conical boattails, it is evident that tangent-parabolic boattails will generally have slightly higher drags than the equivalent inscribed conical boattails at supersonic speeds. If this fact is recognized it should be possible to

make quick engineering estimates of the drags of boattails other than conical by the use of reference 7. If slender afterbodies are slightly asymmetric, they may be represented by their equivalent bodies of revolution for the purpose of drag estimates.

Jet interference effects on boattail drags. - In some cases boattail drags may be modified by interference effects from the jet exit flow. Current research on this problem is summarized in reference 10, which also presents a comprehensive bibliography on the subject. When the afterbody is boattailed to a sharp trailing edge at the nozzle exit, the jet may affect the boattail pressures in the following manner: If the static pressure in the plane of the nozzle exit exceeds the rearmost static pressure on the boattail, the jet will expand on leaving the nozzle and deflect the external stream so as to equalize the pressures along the common mixing boundary of the two streams. The deflection of the external stream results in a trailing shock wave and since the pressure rise across this shock wave cannot be discontinuous in the body boundary layer, it begins forward on the boattail. Sufficient overpressure of the jet will create a trailing shock wave of enough strength to separate the flow from a portion of the boattail. Such phenomena are illustrated in figure 6 for a parabolic boattail at Mach numbers of 1.6 and 2.0. Three nozzle types are considered: a convergent nozzle for reference purposes, a convergent-divergent nozzle with angular exit flow, and a convergent-divergent nozzle with axial exit flow. In all cases there was evidence of some separation with no jet flow. Increasing the jet total-pressure ratio in the case of the convergent nozzle rapidly increased the nozzle-exit static pressure, which was equal to 0.528 times the total pressure for this nozzle type. The resulting external expansion or billowing out of the jet appreciably increased the boattail pressures by the mechanism already discussed. With convergent-divergent nozzles designed for a total-pressure ratio  $P_j/p_0$  of 5.6, an overpressure condition with attendant jet interference did not occur until the jet pressure ratio exceeded 5.6. Above design pressure, however, the boattail pressures did increase as a result of jet interference. The increase was most pronounced in the case of the large nozzle-exit angle, which resulted in a relatively stronger trailing shock wave and pressure feedback. As can be seen, the extent of the jet interference was somewhat reduced with increasing Mach number.

The magnitude of these effects is illustrated in figure 7, where boattail pressure drag is shown as a function of jet total-pressure ratio for the parabolic boattails of figure 6 and for several conical boattails of reference 6. A slight difference from the convergent-nozzle configuration of figure 6 arises since convergent nozzles having a zero exit angle  $\epsilon$  were used to obtain these data. As previously illustrated by the boattail pressure distributions (fig. 6), the boattail drag decreases from the value with no jet as the jet pressure ratio is increased into the practical operating range (fig. 7(a)). The amount of drag decrease is greatly

dependent on the boattail shape. In general, boattails having the steepest slope at their rearmost station experience the greatest drag reduction because of jet interference since they result in relatively strong trailing shock waves. For example, the parabolic boattail which has an equivalent inscribed conical boattail of  $\beta = 8.8^\circ$  actually has a pressure drag less than a conical boattail of  $\beta = 7^\circ$  at jet pressure ratios above 8. In the case of convergent-divergent nozzles, figure 7(b) again illustrates the small interference effect until the design pressure ratio is exceeded as well as the fact that the interference effect increases with nozzle exit angle. These observations for a convergent-divergent nozzle should apply equally well to an ejector nozzle.

As has already been observed, the convergent nozzle is not competitive from a thrust standpoint with convergent-divergent nozzles at Mach numbers appreciably greater than unity. The increased drag reduction due to jet interference in the case of the convergent nozzle generally is not sufficient to alter this viewpoint. For example, at the design pressure ratio of slightly less than 6, the increased exit area of the convergent-divergent nozzle had eliminated sufficient boattail area to reduce the drag as much as the favorable jet effect of the convergent nozzle. Although not shown, the same was found to be true at a more realistic pressure ratio of 9 when the convergent-divergent nozzle was designed for the higher pressure ratio. Thus with nearly equal afterbody drags, the convergent-divergent nozzle remained superior on the basis of its superior thrust.

Jet interference effects on blunt annular base drags. - If a blunt annular base surrounds the nozzle exit, the jet interference is confined primarily to the base pressure except for very small annuli. Some data from reference 10 are reproduced in figure 8 to illustrate the range of annular base pressures to be expected with various nozzle types at a Mach number of 1.9. Base pressure coefficient is plotted as a function of jet static-pressure ratio for  $5.6^\circ$  conical boattails having various ratios of base-to-nozzle exit diameter. The clarity of this figure is enhanced if a single characteristic variation is first studied. For the case of a convergent nozzle with  $d_b/d_n$  of 1.11, a slight amount of jet flow produces an appreciable increase in base pressure; further increases in jet pressure and thus jet flow result in the jet stream tending to aspirate the annulus to a lower pressure. However, as the jet pressure is increased still further, the jet expands more and increases the strength of the trailing shock wave where the internal and external streams meet. Since the mixing boundaries of the two streams are limited in the pressure rise which they can undergo from the base to the wake region, an increase in the wake pressure as the jet pressure ratio increases results in an increase in the base pressure as indicated. As the base diameter becomes larger relative to the nozzle-exit diameter, the expanding jet curves increasingly toward the axis before meeting the external stream; the net effect is to lower the base pressure as indicated. The portions of these curves corresponding to very low jet total pressures are not included except in the single illustration case.

Compressed into the lower end of the pressure-ratio range are the variations of base pressure coefficient obtained with a convergent-divergent nozzle having an expansion ratio corresponding to a design total-pressure ratio of 10.5. A nozzle of this type has a design static-pressure ratio of 1 and requires a total-pressure ratio of 21 to operate at a static-pressure ratio of 2. It can be seen that the variations are essentially parallel to the corresponding variations with convergent nozzles (if the portions of the curves below pressure ratios producing minimum base pressures are neglected) but are displaced slightly in the positive direction. The agreement between the jet effects of convergent and convergent-divergent nozzles when plotted as a function of jet static-pressure ratio is even more pronounced at Mach 3.1, as shown in reference 10. A single variation obtained with an ejector nozzle designed for the same total-pressure ratio is included, and it is seen that this nozzle resulted in slightly higher base pressures than did the equivalent convergent-divergent nozzle.

For a practical comparison of the effects of jets from convergent and convergent-divergent nozzles, the case of a jet total-pressure ratio of 10.5 corresponding to a typical turbojet engine at the subject Mach number will be considered. The convergent nozzle with its static-pressure ratio near 5.5 generally increases the base pressure above its no-flow value, except for extremely large annuli, and may generate appreciably positive base pressures. The convergent-divergent nozzle ( $\epsilon = 0$ ), however, with its jet static-pressure ratio of 1 decreases the base pressures below the jet-off values with the resulting tendency to create relatively large base drags. A point of interest is that replacing the blunt base with a  $45^\circ$  bevel did not greatly alter the base pressures with either nozzle type.

The significance of the base pressures just discussed is illustrated in figure 9 (ref. 10, fig. 13), where afterbody drag coefficient including jet interference effects is presented as a function of the ratio of base diameter to nozzle-exit diameter for both convergent and convergent-divergent nozzles with the same throat areas and with axial exit flow. The case of a relatively small boattail angle at a Mach number of 1.9 and with a jet total-pressure ratio of 10 is considered. In the case of the convergent nozzle, the total afterbody drag at first decreases somewhat as an annular base is added and does not increase until the base diameter attained a relatively large value. In the case of the convergent-divergent nozzle designed for a pressure ratio of 10, however, the drag is indicated to increase immediately as an annulus is added. Thus, although the two nozzle installations result in nearly equal afterbody drags with no blunt annulus, the afterbody drag with a convergent-divergent nozzle surrounded by a blunt annulus may consume an appreciable quantity of the basic thrust advantage of that nozzle type if the annulus size is not kept to a minimum.

In aircraft engineering practice it appears that blunt annuli need not be present in most designs unless as an annular opening through which

[REDACTED]

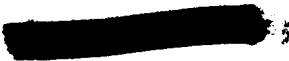
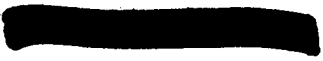
to discharge cooling or air-conditioning air. This discharge of air rapidly increases the base pressure and completely modifies the above discussion. With secondary flow, the net drag of the system is dependent on the source and quantity of the secondary air, as discussed in reference 10.

#### CONCLUDING REMARKS

In conclusion it would appear that the pressure drags of axially symmetric boattails may be predicted at supersonic speeds with a fair degree of accuracy if wing and tail interference effects are small. Jet interference effects on boattail pressures and drags are generally small at supersonic speeds if the nozzles are designed to expand the flow internally in order to realize the maximum jet thrust. With such nozzle types, blunt annular bases are to be avoided except, possibly, as a region to discharge auxiliary air. The subsonic cruise condition imposes severe flow requirements on either or both the internal and external streams as a result of the large reductions required in nozzle throat area and expansion ratio; additional research is required to clarify the seriousness of this problem.

#### REFERENCES

1. Reshotko, Eli: Performance Characteristics of a Double-Cylindrical-Shroud Ejector Nozzle. NACA RM E53H28, 1953.
  2. Ferri, Antonio: Application of the Method of Characteristics to Supersonic Rotational Flow. NACA Rep. 841, 1946. (Supersedes NACA TN 1135.)
  3. Van Dyke, Milton D.: First- and Second-Order Theory of Supersonic Flow Past Bodies of Revolution. Jour. Aero. Sci., vol. 18, no. 3, Mar. 1951, pp. 161-178.
  4. Van Dyke, Milton D.: Practical Calculation of Second- Order Supersonic Flow Past Nonlifting Bodies of Revolution. NACA TN 2744, 1952.
  5. Maxwell, N. E.: Results of Experimental Studies of Boattail Effects at Supersonic Velocities. NAVORD Rep. 1651, Proc. Bur. Ord. Symposium on Aeroballistics, pp. 93-119.
  6. Cortright, Edgar M., Jr., and Schroeder, Albert H.: Investigation at Mach Number 1.91 of Side and Base Pressure Distributions Over Conical Boattails Without and With Jet Flow Issuing from Base. NACA RM E51F26, 1951.
- [REDACTED]

- 
7. Jack, John R.: Theoretical Pressure Distributions and Wave Drags for Conical Boattails. NACA TN 2972, 1953.
  8. Stoney, William E., Jr.: Some Experimental Effects of Afterbody Shape on the Zero-Lift Drag of Bodies for Mach Numbers Between 0.8 and 1.3. NACA RM L53I01, 1953.
  9. Fraenkel, L. E.: The Theoretical Wave Drag of Some Bodies of Revolution. Rep. Aero. 2420, British R.A.E., May 1951.
  10. Cortright, Edgar M., Jr., and Kochendorfer, Fred D.: Jet Effects on Flow over Afterbodies in Supersonic Stream. NACA RM E53H25, 1953.
- 

### NOZZLE INSTALLATIONS

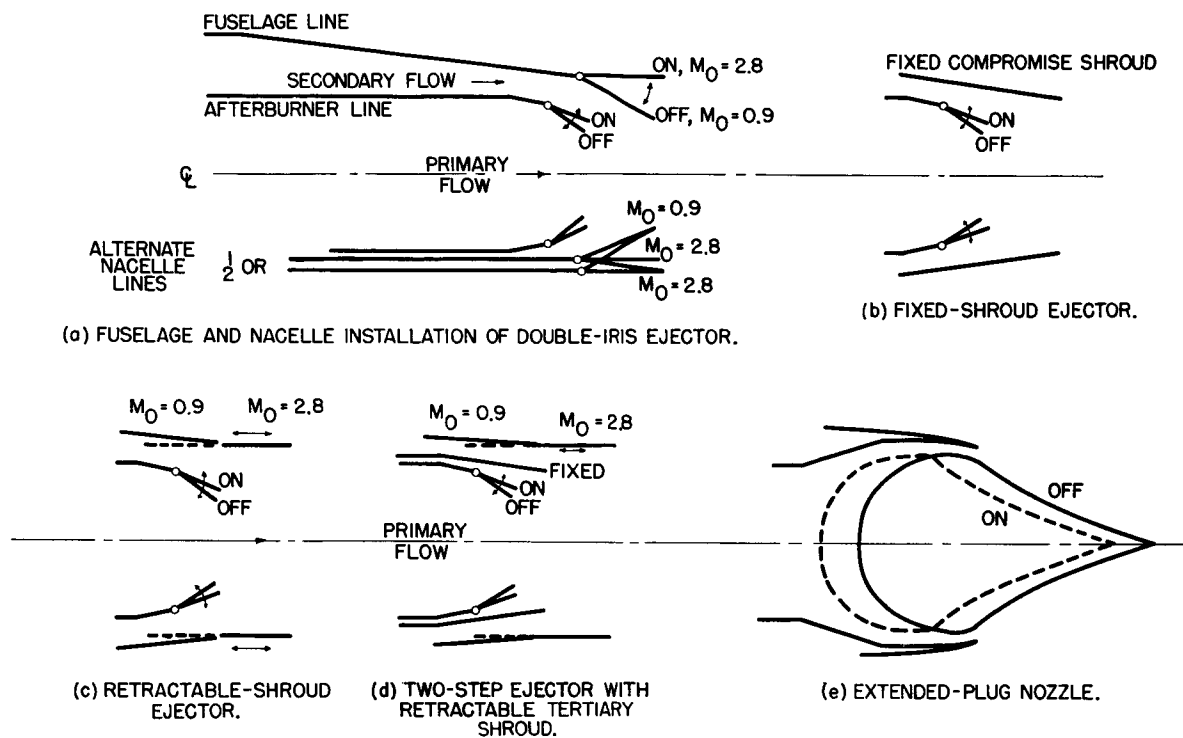


Figure 1

### CONICAL BOATTAIL PRESSURE DISTRIBUTIONS

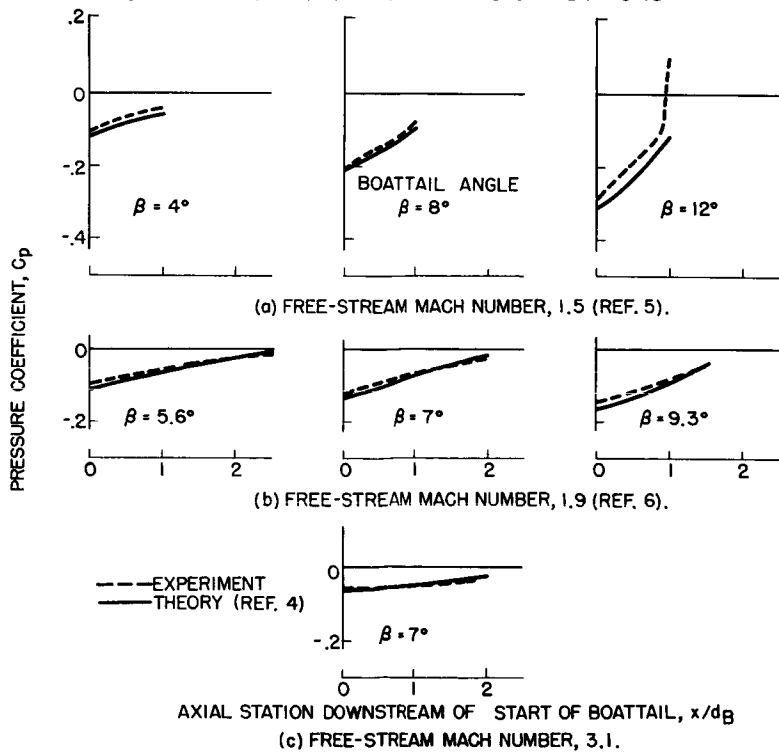


Figure 2

CONICAL BOATTAIL PRESSURE DRAGS

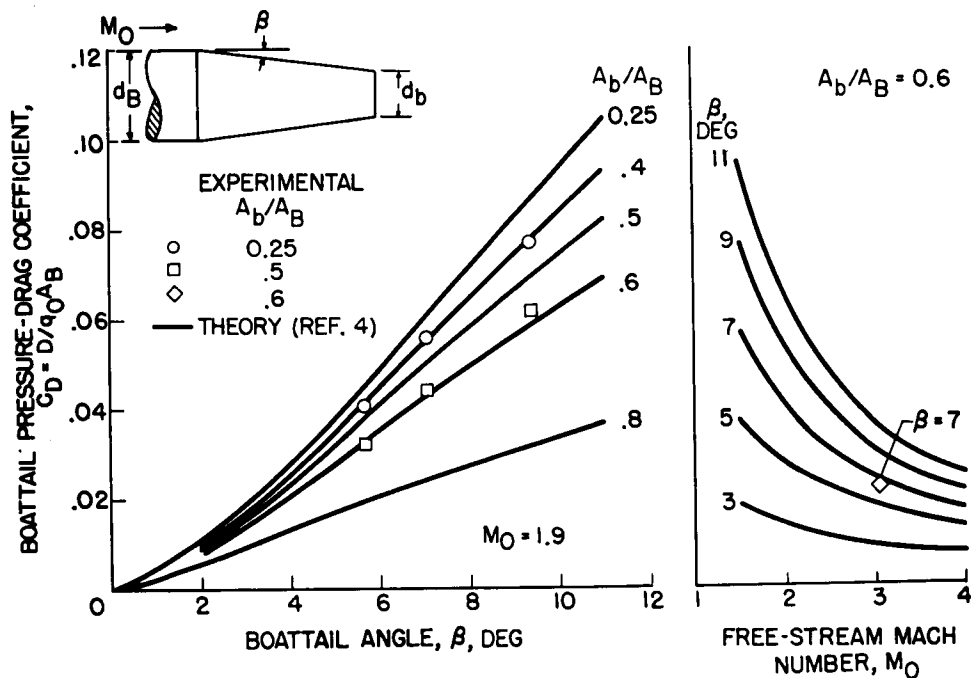


Figure 3  
AFTERBODY DRAG OF MACH 2.8 INTERCEPTOR

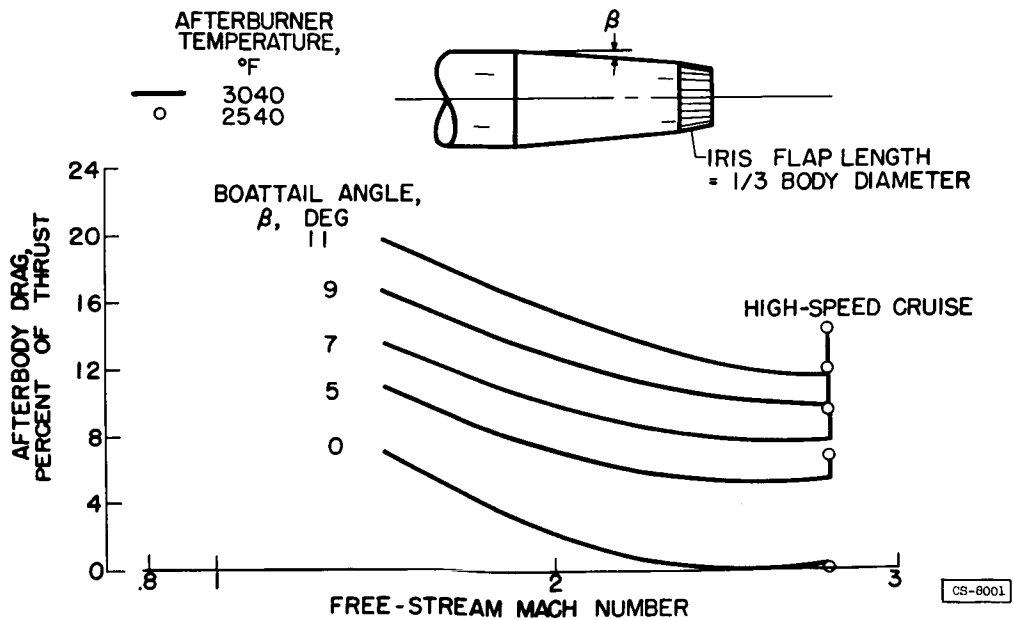


Figure 4

PARABOLIC BOATTAIL PRESSURE DISTRIBUTIONS

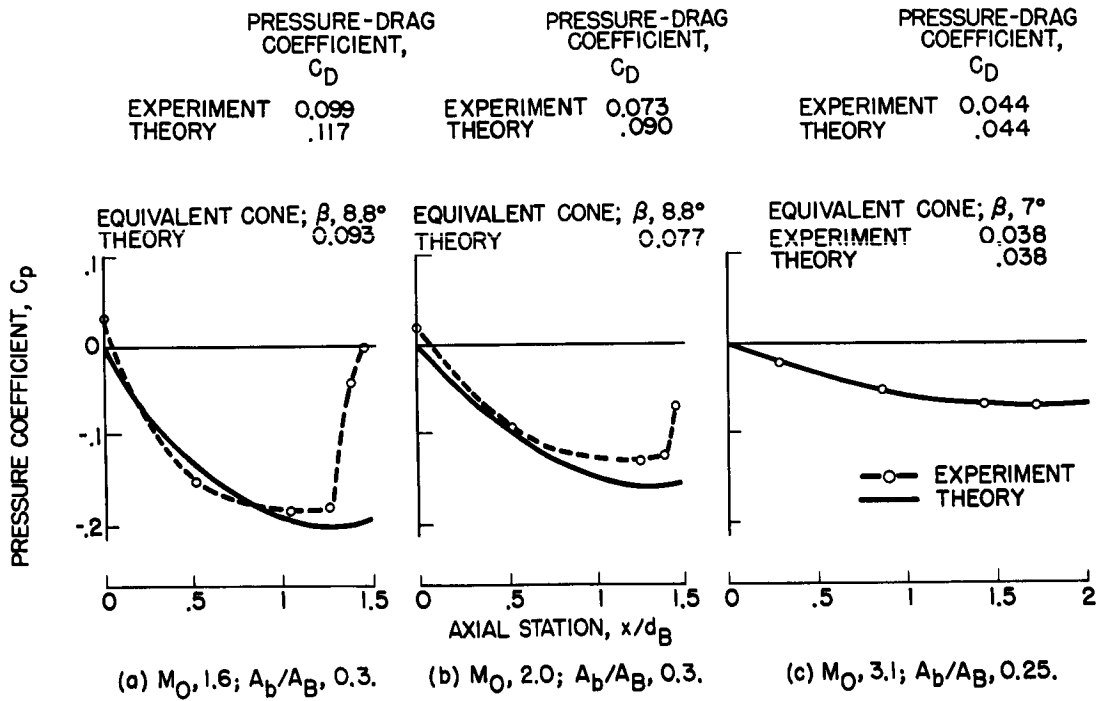


Figure 5

JET EFFECTS ON PRESSURES OVER PARABOLIC BOATTAILS

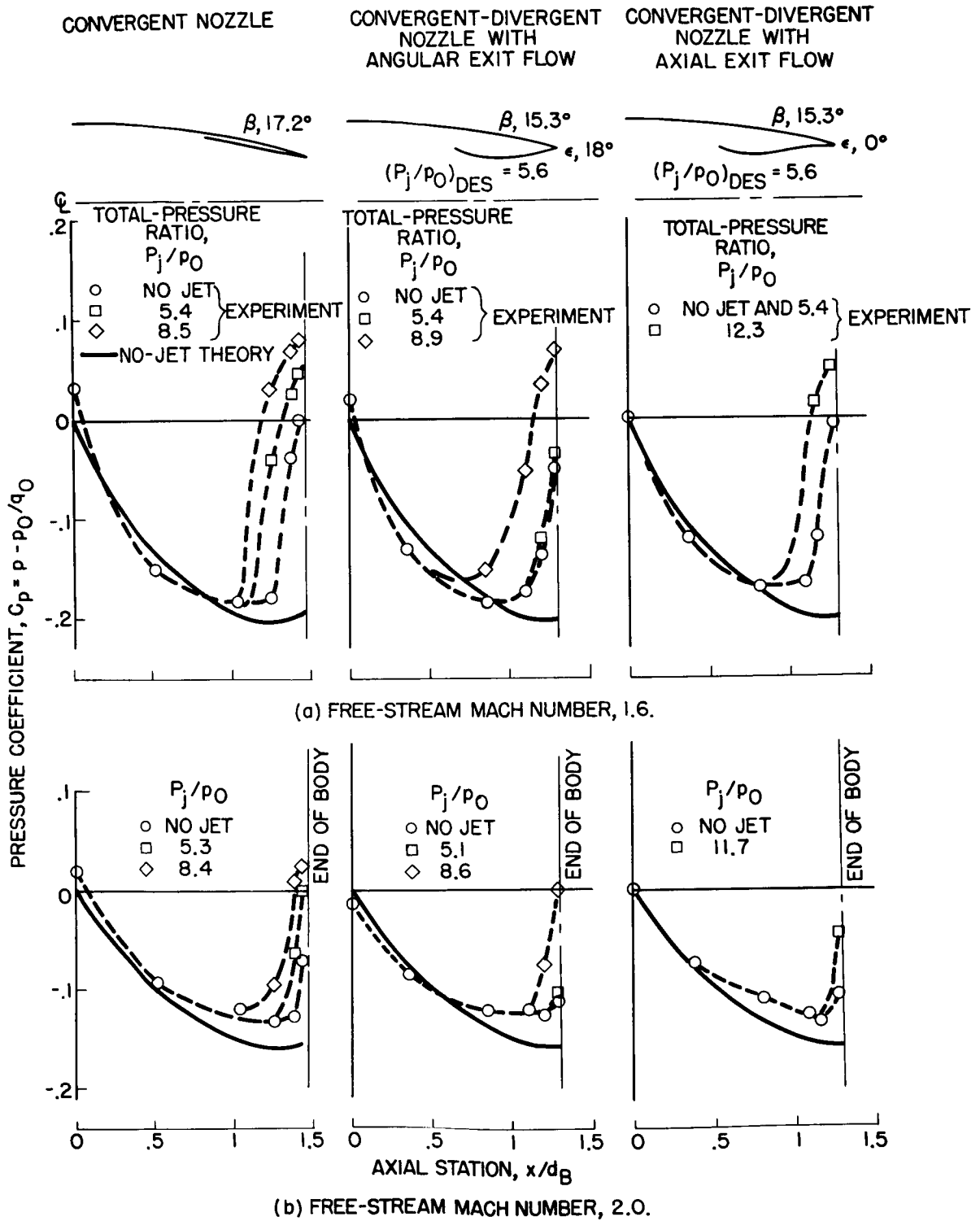


Figure 6

JET EFFECTS ON BOATTAIL PRESSURE DRAG  
 $M_0 = 1.9$  TO  $2.0$

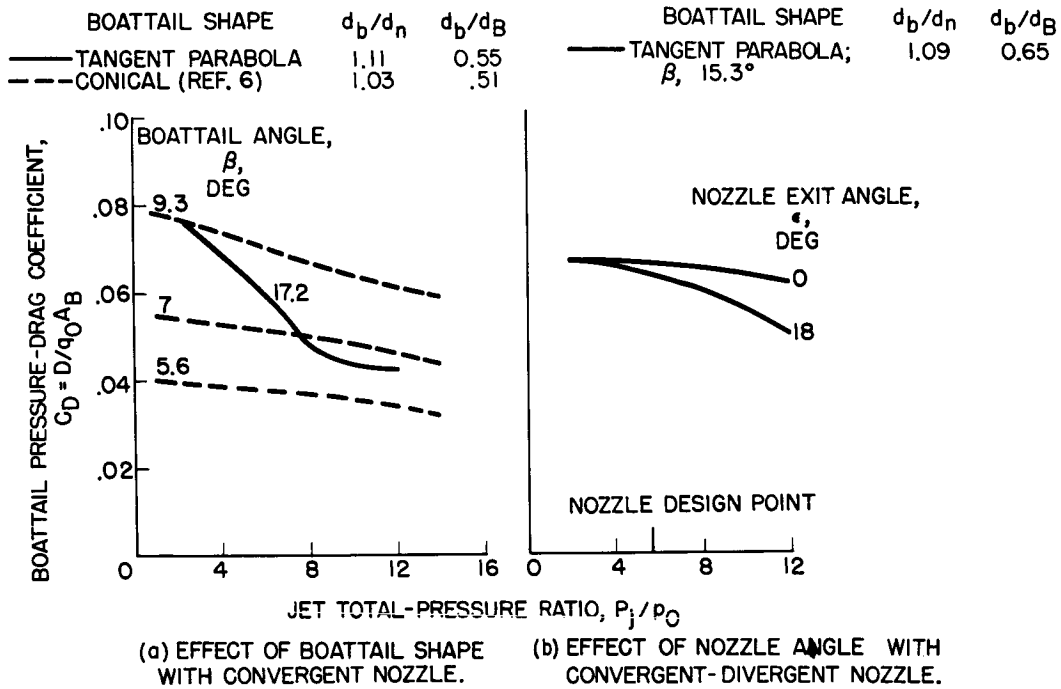


Figure 7

JET EFFECTS ON BASE PRESSURE  
 $M_0, 1.9$

(NO JET VALUES ON ORDINATE)  
 (REF. 10, FIG. 6)

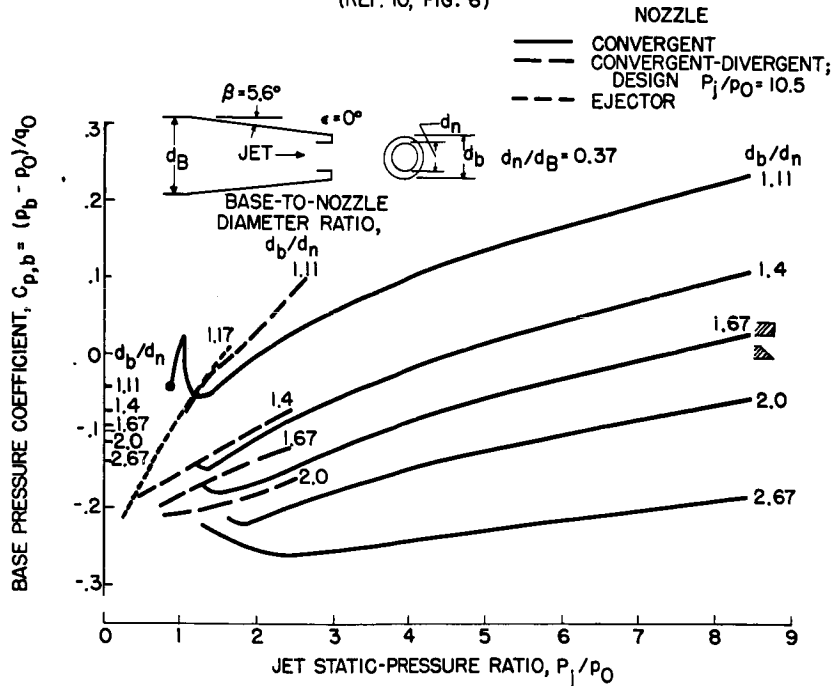


Figure 8

3078-G

DRAG OF BLUNT ANNULAR BASE

$M_0 = 1.9; P_j / P_0 = 10; A_t / A_B = 0.25$

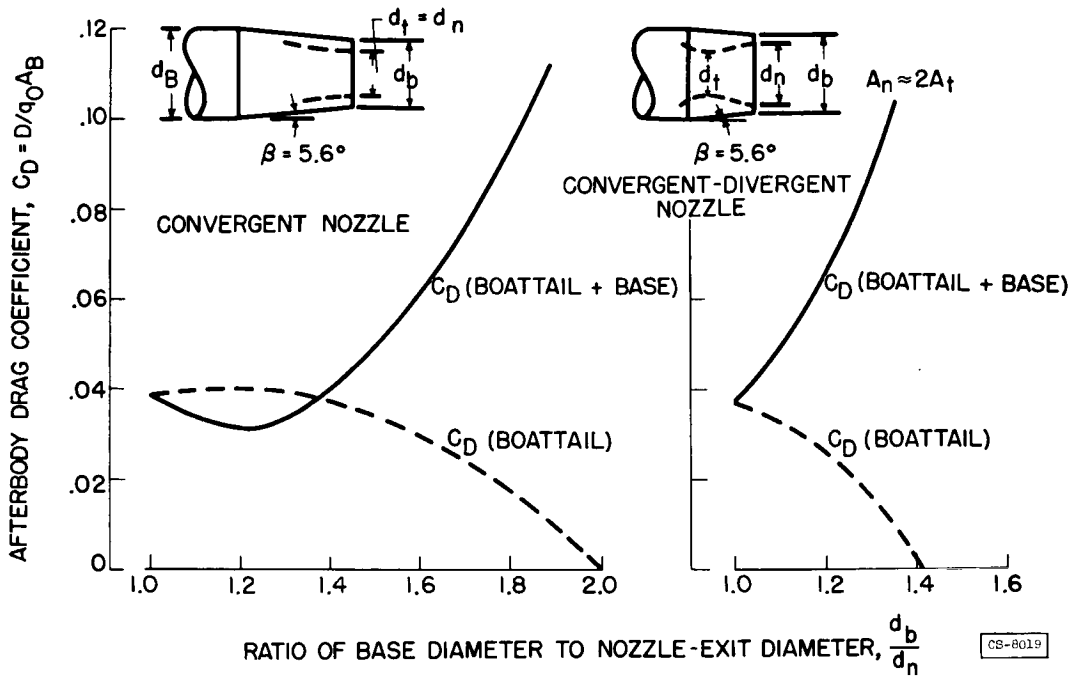
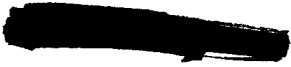


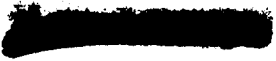
Figure 9



VIII - ENGINE AND AIRPLANE PERFORMANCE PANEL

- B. T. Lundin
- E. W. Hall
- R. W. Luidens
- H. M. Henneberry
- R. O. Bullock





## INTRODUCTION TO ENGINE AND AIRPLANE PERFORMANCE STUDIES

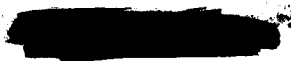
By Bruce T. Lundin

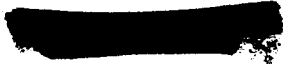
3078 - H

In the preceding series of papers, various research projects being conducted at the NACA Lewis laboratory were reviewed. These projects, which are aimed at the general problems of supersonic flight propulsion, have produced improvements in either the performance or the operating characteristics of all of the principal components of the turbojet engine. A consideration of the utilization of the advanced components in engines reveals that they offer possibilities of better engine performance from two important aspects. The first of these is, of course, the better thermodynamic or aerodynamic performance of the component itself; the second source of better engine performance arises from the better off-design performance of the components or from the characteristics that they possess that are more intimately associated with the method of operation of the engine and of the integration of the components into a complete engine. The over-all improvements in airplane performance afforded by both of these advantages are considered in the succeeding papers, which present the performance of several different types of engine or engine design that incorporate various advancements of component design and engine operation.

Typical items of better component performance are the higher air-flow capacity of the transonic compressor and the possibility of operating at higher turbine-gas temperatures because of turbine cooling. These two features are evaluated by comparing the performance of what might be considered a current engine, typical of present development types, with an advanced engine having the higher air-flow capacity of the transonic compressor and a maximum turbine-inlet temperature of 2040° F.

Further improvements in engine performance by virtue of better component off-design characteristics and integration are not obvious on the basis of component performance alone, although several features present themselves as offering promise. The transonic compressor has, for example, in addition to a higher air-flow capacity, a good efficiency over a large plateau of operating conditions. Also, turbine cooling, in addition to permitting increases in gas temperature, will enable higher stress levels to be reached in the blading and, consequently, will permit the use of higher tip speeds and longer blades that become particularly useful for engines of high mass-flow capacity. Other component improvements that become important in over-all engine design and operation are the higher velocity levels that may be used in both the primary combustor and the afterburner of the engine as well as the possible use of a variable-area turbine-nozzle assembly to provide the engine with an additional degree of freedom. It is

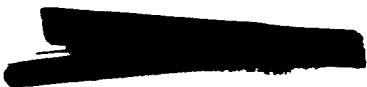




the utilization of these features of component performance and capabilities that forms the basis for the following studies of advanced engines. Improvements in engine performance in this connection are not made by further increases in maximum flow capacity or gas temperature but, instead, by using nonconventional methods of operation and design of the engine in order to keep the engine and its components operating at their maximum aerodynamic capacity at supersonic flight speeds.

In the following papers, proposal of definite types of engines or specific engine designs is not intended; such matters obviously involve many considerations beyond the scope of the present study. The engine designs chosen are intended primarily to illustrate the various problems and compromises involved and to evaluate the performance potentialities associated with the use of the advanced components.

The effectiveness of any of the advanced engines depends not only on its performance but also upon the flight requirements and the type of airplane in which it is installed. It is, therefore, necessary to integrate the studies of engine performance with airplane type and flight plan in order to obtain useful and significant results. Although this requires the selection of certain cases for study, an objective viewpoint of general applicability is pursued, to a certain degree, by study of various types of airplanes and missions. The airplanes studied include both supersonic interceptors and supersonic bombers. The range of flight Mach numbers considered is from about 1.5 to 2.8 for both types of airplanes.



## GENERAL CONSIDERATIONS OF COMPONENT SELECTION AND INTEGRATION

By Robert O. Bullock and Harold B. Finger

30784

Because of the inherently low values of the lift-drag ratios associated with supersonic flight, as well as the corresponding large nacelle drags, it is imperative that the diameter, length, and weight of the engine be as small as possible. For the same reasons, low specific fuel consumptions are also required. At subsonic and low supersonic flight speeds, the diameter of the engine is determined by the flow capacity of the compressor, primary combustor, turbine, or afterburner. For this flight regime, the flow capacities of these units therefore should be as high as possible. At higher flight speeds, the diameter of the inlet or outlet may theoretically determine the diameter of the engine. Even for this condition, however, there is a strong incentive to maintain high flow capacity in the other components; not only is engine weight a relevant consideration, but low component diameters permit the arranging of accessories in such a manner that the length and complexity of the engine is not adversely affected. Throughout the entire airplane and engine analysis, particular attention was therefore paid to maintaining a high flow capacity through the components.

High efficiency or low pressure drop is also required of the components in order to minimize both the size of the engine and the specific fuel consumption. Excessive pressure losses reduce the specific thrust and, hence, larger engines are required to develop a given thrust. Again, these losses reduce the density of the air in the components downstream of them; the frontal area of these downstream components must therefore be increased in proportion to the upstream losses. In selecting the components no sacrifice was made in efficiency in order to obtain other desirable characteristics. In fact, the distinguishing feature of most of the results presented in the preceding papers is that the size of the components can be measurably reduced without paying a penalty in efficiency.

Two other factors influencing engine size and specific fuel consumption are the total temperature of the exhaust gases and the turbine-inlet temperature. Specific thrust is directly proportional to the total temperature of the exhaust gases; hence, the mass flow or the diameter of the components required for a given thrust is reduced when this temperature is increased. When this increase in temperature is provided by an afterburner, these favorable trends are opposed by increases in specific fuel consumption, and the net effect must be evaluated by an analysis of airplane performance. Increasing the turbine-inlet temperature also increases the total temperature of the exhaust gases. In this case, the size of the turbine may be even further reduced. Moreover, the pressure drop across the turbine is reduced; this

VII - 2

not only provides an additional increase in thrust but tends to reduce the specific fuel consumption at high flight Mach numbers. On these bases, high turbine-inlet temperatures as well as afterburning were investigated.

#### Components Selected for Analyses

The papers on inlets and outlets indicate that the selection of these components will be primarily determined by the pumping characteristics of the engine and the design of the airplane; these are discussed by Luidens, Zimmerman, Henneberry, and Evans.

Transonic compressors were utilized throughout the analysis of the advanced engines. Both the maximum blade Mach numbers and the diffusion factors were below the limiting values indicated in the papers by Lieblein and Klapproth. This type of design was assumed because available experimental data indicate that the resulting compressors will have high flow capacity, a minimum number of stages, high efficiency over a wide range of flows and pressure ratios, and good stall-line characteristics.

In order to utilize the highest turbine-inlet temperatures deemed practical from available data, air-cooled turbines were assumed throughout the analysis. Another factor involved in this decision is the fact that the strength-to-weight ratio of cooled blades is more than 50 percent greater than that of uncooled blades. Longer turbine blades and higher rotative speeds could then be employed to increase the air-flow capacity and to reduce the number of stages, respectively, of both the compressor and turbine. The aerodynamic design of the turbines was reasonably conservative because the problem of cooling high Mach number turbine rotor blades has not been explored.

The diameter, the pressure loss, and the combustion efficiency of both the primary combustor and the afterburner have a critical effect on engine size and performance. The primary combustor was assumed to have characteristics similar to the experimental annular combustor for supersonic flight, described in the paper by Norgren, Zettle, and Childs. The use of staged fuel introduction together with the other features described permit the attainment of the desired turbine-inlet temperatures. At the same time, a reasonable compromise among efficiency, pressure drop, and diameter is offered. The afterburner sizes and performance were consistent with existing experimental data.

#### Factors Influencing Integration of Compressor and Turbine

The optimum integration of the compressor and turbine of the engine depends, to a large degree, on the general propulsive requirement that

[REDACTED]

must be satisfied for supersonic airplanes, that is, on the particular flight requirements that impose the greatest demand on the engine. The final results of a general study of the size of engine that must be installed in an airplane to satisfy certain prescribed performance objectives are summarized in figure 1. The relative size of engine that must be installed in the airplane is indicated by the bar graph and the various portions of a flight plan or mission are represented by the Mach number scale in the abscissa. The requirements are shown for both an interceptor airplane and a bomber. The engine size that is required to permit take-off over a 50-foot obstacle in 5000 feet is indicated by unity. In order to satisfy an acceleration requirement for the interceptor from a Mach number of 0.9 to a Mach number of 2.0 in 5 minutes would require an engine 2.3 times as large as that required for take-off alone. Similarly, the combat condition which is specified to consist of a 1.3 g maneuver without loss in speed or altitude at an altitude of 65,000 feet would require an engine size of over 2.5 times that for take-off, depending somewhat on the combat Mach number. A similar situation exists for the bomber airplane, although to a less pronounced degree. The supersonic cruise portions of the flight plan again set the requirement on engine size; in this case, engines 40 to 50 percent greater than those necessary for take-off are required. These requirements, moreover, were computed for the advanced engine that has a high air-flow capacity and a turbine-inlet temperature of 2040° F. If more conventional types of engine had been used, an even greater difference between low-speed and high-speed flight would have resulted.

In view of this requirement for greatest thrust output at relatively high supersonic speeds, present methods of engine design and operation, while entirely adequate and proper for subsonic or transonic flight applications, possess some serious disadvantages for supersonic applications. Principal among these disadvantages is the loss in air-flow capacity at high inlet-air temperatures as a result of the reduction in the aerodynamic speed of the compressor as outlined by the papers on turbine and compressor aerodynamics. Better integration and utilization of the engine components is attained if the air-flow capacity of the engine is maintained at its maximum value at supersonic flight speeds instead of only at take-off or low-speed conditions. This may, of course, be accomplished by simply increasing the rotative speed of the engine as the inlet temperature is increased in order to maintain a constant aerodynamic speed and at the same time increasing the exhaust area to maintain limiting turbine-inlet gas temperature. This method of operation results in a reduction in compressor pressure ratio which, while not harmful in itself, may involve operation at conditions of low compressor efficiency; the wide plateau of good efficiency of the transonic compressor is of considerable benefit in this regard. Of greater importance is the increase in centrifugal loads imposed by operation at the increased tip speeds at the higher flight speeds. Staying within prescribed stress limits requires that, at low flight speeds, the tip speeds be reduced

[REDACTED]

3078-H

to below those currently employed and, in turn, that a greater number of stages be used to develop a given pressure ratio. Although this method of operation would result in engines that are impractically heavy if conventional stress limits are used, the higher stress limits that may be used in cooled turbine blades afford a practical realization of this method. In the engines studied in the following papers, the stress at the rotor blade roots of the turbines was limited to 45,000 pounds per square inch and the maximum air-flow capacity was taken as 39 pounds per second per square foot of compressor-tip frontal area.

The limitations imposed on engine operation and design by both structural and aerodynamic considerations may be further relieved by using a variable-area turbine nozzle in the engine because of the extra degree of freedom it provides in engine operation. The compressor pressure ratio, for example, need not follow the variation uniquely prescribed by air flow, pressures, and temperatures but may, with proper adjustment of the turbine flow area, be set at values representing a better compromise of the various design and operating limitations.

In the following paper, engines with both fixed and variable-area turbines are considered. In both types of engine, maximum aerodynamic performance is maintained over a range of inlet temperatures, or flight Mach numbers, up to some given flight speed that is considered the primary design point of the engine. The resulting engines are somewhat heavier per unit of thrust output at take-off conditions because of the stronger structure or larger number of stages required, but they provide a greater thrust output at supersonic speeds, where the need for thrust is greatest. In essence, then, the study concerns engines that have a supersonic flight condition for their design point rather than a more conventional low-speed design point, and that operate at reduced mechanical speed at take-off rather than at reduced aerodynamic speeds during supersonic flight.

### ENGINE SIZES REQUIRED FOR SUPERSONIC AIRPLANES ADVANCED TAKE-OFF ENGINE

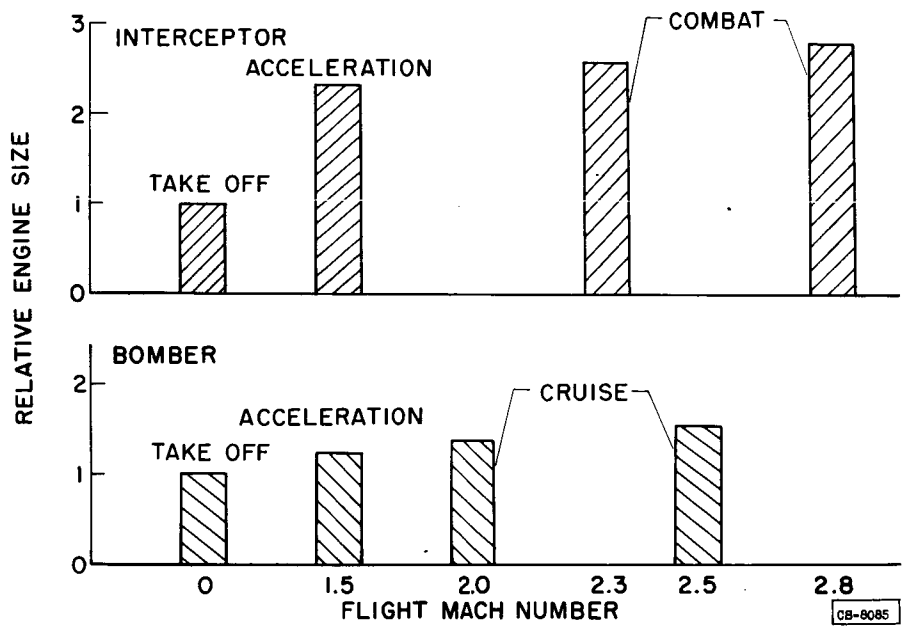


Figure 1

# ONE-SPOOL TURBOJET ENGINES FOR PROPULSION OF SUPERSONIC AIRCRAFT

By Robert E. English, E. Clinton Wilcox, and Henry W. Plohr

## INTRODUCTION

3078 - H

The relatively low airplane lift-drag ratios available at supersonic velocities lend greatly increased importance to attaining a power plant having high thrust per unit engine weight in order to keep the total power-plant weight to a reasonable value. Conventional turbojet engines with current material limitations in turbine-inlet temperature suffer serious losses in engine thrust at high flight speeds because of the decreased engine temperature ratio. For example, for a turbine-inlet temperature of 1640° F, the ratio of turbine-inlet absolute temperature to compressor-inlet absolute temperature varies from about 4 during static operation at sea level to approximately 2 during flight at a Mach number of 2.8 and altitudes greater than the tropopause. An additional decrease in thrust is incurred in conventional turbojet engines because of the large decreases in air flow resulting from operation at decreased engine equivalent, or aerodynamic, rotational speed at high flight speeds. This effect results from the conventional practice of operating the engine at a constant rotational speed. For flight at a Mach number of 2.8 in the stratosphere, the engine equivalent rotational speed is about 30 percent less than that during static operation at sea level.

Recent advancements in design techniques for the various components comprising the turbojet engine have led to the possibility of incorporating in the engine design factors that greatly improve the engine performance at supersonic speeds. If the air flow per unit frontal area is increased, the engine thrust per unit frontal area and thrust per unit engine weight are increased. Through the use of turbine cooling, the material limitations previously mentioned are circumvented, thus allowing greater thrust output for a given engine size. For conventional turbine-inlet temperatures, the thrust output of the engine can be increased markedly, especially at the higher flight speeds, by the addition of an afterburner. On the other hand, the addition of an afterburner has a more adverse effect on specific fuel consumption than the combustion of the same amount of additional fuel in the engine primary combustion chamber. The decrease in engine air flow at high flight Mach numbers which results from operation of the engine at constant rotational speed can be at least partially eliminated by allowing the engine rotational speed to rise somewhat with flight Mach number, that is, by the method of operating the engine off design.

Available turbojet-engine design techniques generally involve the design of the components for a particular flight condition with

restrictions imposed on the tolerable component design characteristics in order that the range of engine operating requirements be fulfilled. Inasmuch as the turbojet engine for supersonic propulsion must operate satisfactorily over a wide range of flight speeds from take-off to maximum speed, the off-design operation becomes increasingly important as flight speeds are increased. The value of design flight Mach number and the method of off-design engine operation would therefore be expected to have important effects on the over-all performance of engines intended for use at flight Mach numbers above 2.

The purpose of the analysis presented herein is to investigate the ways in which engine thrust per unit frontal area can be increased for flight at high Mach numbers, for example, from 2 to 2.8. For flight conditions varying from take-off to a Mach number of 2.8 in the stratosphere, engine performance was investigated in order to determine the effects of the following variables on engine over-all performance: engine air-flow capacity per unit frontal area, turbine-inlet temperature, afterburner-exit temperature, design value of flight Mach number, and method of operating the engine off design. Design flight Mach number as used herein can be defined as the Mach number for flight in the stratosphere for which, during maximum-thrust operation, the engine is operating at the maximum equivalent rotational speed which the aerodynamic characteristics of the compressor will permit and simultaneously operating at the maximum mechanical rotational speed which the structure of the engine will permit. In investigating the effects of the variation in design flight Mach number, three design flight Mach numbers are considered: 0.6, 1.5, and 2.3. Two engines are analyzed for a design flight Mach number of 0.6 and one for each of the design flight Mach numbers of 1.5 and 2.3. The designations and characteristics of these engines are given in the following table:

Engine designation	Design flight Mach number	Maximum air-flow capacity, (lb/sec)/sq ft of compressor-tip frontal area	Maximum turbine-inlet temperature, °F
Current take-off	0.6	30	1640
Advanced take-off	0.6	39	2040
Advanced Mach 1.5	1.5	39	2040
Advanced Mach 2.3	2.3	39	2040

Engine performance is expressed as thrust per unit compressor-tip frontal area and specific fuel consumption. The investigation was limited to one-spool turbojet engines. For all calculations a double-wedge, variable-ramp inlet was assumed. A compressor with characteristics similar to a recent research transonic compressor was incorporated in all the engines considered, and the characteristics for the remaining components of the engine were commensurate with those obtained in laboratory investigations.

## RESULTS AND DISCUSSION

### Effect of Flow Capacity and Temperature

The effects of varying the compressor air-flow capacity per unit frontal area, the turbine-inlet temperature, and the afterburner-exit temperature were investigated for the conventional method of engine operation, that is, constant rotational speed during maximum-thrust operation. The manner in which this type of engine operation affects engine off-design performance will therefore be described first.

The compressor map for the advanced take-off engine is shown in figure 1, wherein compressor pressure ratio is shown as a function of compressor specific air flow for lines of constant engine equivalent, or aerodynamic, rotational speed. Also included are compressor-efficiency contours. From a consideration of the continuity of flow through the engine, it is possible to relate compressor pressure ratio, compressor air flow, and ratio of turbine-inlet temperature to compressor-inlet temperature. For engine operation at constant rotational speed and constant turbine-inlet temperature, the engine operating line shown in figure 1 can then be constructed.

Take-off occurs at an equivalent rotational speed which is 90 percent of the maximum. For engines operated in this manner, take-off is typically the design condition. Recent compressor research shows that a value of specific air flow of 35 pounds per second for each square foot of compressor-tip frontal area can be achieved at the design point of the compressor (see paper by Finger and Robbins). The design equivalent rotational speed for such a compressor is usually about 90 percent of the maximum tolerable equivalent rotational speed. At the maximum equivalent rotational speed, a specific air flow of about 39 pounds per second per square foot would then be obtained. For maximum-thrust operation at constant rotational speed, maximum equivalent rotational speed is reached during flight in the stratosphere at a Mach number of 0.6. As the flight Mach number is increased, the equivalent rotational speed for a given mechanical rotational speed decreases because of the increase in compressor-inlet temperature. At a flight Mach number of 2.8, the equivalent rotational speed is 64 percent of

[REDACTED]

the maximum with corresponding decreases in compressor air flow. Compressor pressure ratio decreases as the flight Mach number is increased, varying from about 9 at a flight Mach number of 0.6 to about 3 at a flight Mach number of 2.8. By means of thermodynamic cycle calculations, this decrease in compressor pressure ratio can be shown to have a desirable effect on specific fuel consumption at high flight Mach number. On the other hand, the large decrease in specific air flow results in a proportionately large decrease in engine thrust at high flight Mach number.

For flight in the stratosphere, the variation in compressor air flow with flight Mach number along the operating line shown in figure 1 is presented in figure 2. The compressor air flow decreases approximately 50 percent as the flight Mach number is increased from 0.6 to 2.8. This decrease in air flow results in a 50-percent decrease in thrust. The introductory paper by Benser shows that, in addition to this decrease in specific air flow, operation at such low equivalent rotational speeds may introduce a severe blade-vibration problem.

One reason for operating the engine at constant rotational speed is that under these circumstances the mechanical and stress-limited rotational speeds are identical; this results in a light engine for any given take-off thrust. Another reason is that over a wide range of engine operation the turbine operates under conditions closely approximating its design conditions. At constant afterburner-exit temperature, these engine operating conditions also require only a small adjustment of the exhaust-nozzle throat area.

Effect of increasing compressor specific air flow. - The effect of changing the maximum specific air-flow capacity of the compressor from 30 to 39 pounds per second per square foot was investigated. The values of maximum flow were obtained at maximum equivalent rotational speed and correspond to values of design flow of 27 and 35 pounds per second per square foot, respectively. Within the limits of current laboratory investigations, the primary burner, turbine, and afterburner could all pass this increased flow within a frontal area no greater than 133 percent of the compressor-tip frontal area.

The thrust of turbojet engines having maximum compressor specific air flows of 30 and 39 pounds per second per square foot is shown as a function of flight Mach number in figure 3. The thrust per unit compressor-tip area divided by the ambient static pressure is presented as a function of flight Mach number. Engine thrust is presented in this form in order that the results will be independent of engine size and altitude in the stratosphere. Engine frontal area is important because of its effect on engine weight and nacelle drag. In order to avoid circumlocution, the term  $F/p_0A_c$  will hereinafter be called "thrust

[REDACTED]

per unit area;" the term  $F/p_0 A_c$ , where  $F$  is engine thrust,  $p_0$  is ambient static pressure, and  $A_c$  is compressor-tip frontal area, is directly proportional to  $C_T M_0^2$ , where  $C_T$  is thrust coefficient and  $M_0$  is the flight Mach number.

The data of figure 3 are for a turbine-inlet temperature of 1640° F. Performance is presented for flight at Mach numbers from 0 to 0.9 at sea level and from 0.9 to 2.8 in the stratosphere.

3078-H  
Increasing the maximum compressor specific air flow from 30 to 39 pounds per second per square foot, a 30-percent increase, is shown in figure 3 to result in a 30-percent increase in thrust per unit area over the entire range of flight Mach number. For the assumed component characteristics, the specific fuel consumptions were unaltered by this change in flow capacity. The reduction in frontal area which accompanies such a rise in specific air flow would result in a reduction in nacelle drag. In terms of engine thrust minus nacelle drag, the thrust would rise more than 30 percent and the specific fuel consumption would decrease as a result of the rise in flow capacity.

Effect of turbine-inlet temperature. - Because of the temperature limitations of turbine materials, the thrust output at high flight speeds in figure 3 is rather low due to the low engine temperature ratio across the engine. By the use of turbine cooling, it appears possible to increase the turbine-inlet temperature and hence the engine thrust. In order to cool the rotor blades of the two-stage turbine required for this service, 7.6 percent of the compressor-inlet air flow was bled for operation with a turbine-inlet temperature of 2540° F. The flow of cooling air was kept this low even at a flight Mach number of 2.8 by cooling the bled air to 400° F in an air-to-fuel heat exchanger.

The thrust per unit area and specific fuel consumption are shown as functions of flight Mach number for various turbine-inlet temperatures in figures 4(a) and (b), respectively. It can be seen that increasing the turbine-inlet temperature greatly increases thrust, especially at the high flight Mach numbers. For an increase in turbine-inlet temperature from 1640° to 2540° F, the thrust is increased 66 percent at a flight Mach number of 1.5 and 162 percent at a flight Mach number of 2.8. This rise in turbine-inlet temperature increases the specific fuel consumption for flight Mach numbers up to 2.5 and decreases the specific fuel consumption for higher Mach numbers.

If the effects of nacelle drag were accounted for, these results would change somewhat. The low nacelle drag which accompanies the high values of turbine-inlet temperature increases the advantage of high turbine-inlet temperature at high flight Mach numbers. On the

basis of engine thrust minus nacelle drag, the flight Mach number at which a rise in turbine-inlet temperature has no effect on specific fuel consumption is reduced from the value of 2.5 shown in figure 4(b) to 1.8. If the rise in thrust per unit frontal area is also considered, it clearly becomes advantageous to go to higher turbine-inlet temperatures at some flight Mach number less than 1.8 in spite of the losses associated with turbine-blade cooling.

Effect of afterburner temperature. - Additional thrust can be obtained from a turbojet engine by the use of an afterburner. The thrust increases are obtained, however, only at the expense of an increase in specific fuel consumption. In figure 5, the thrust and the specific fuel consumption for an engine having a turbine-inlet temperature of 2540° F and a compressor specific air flow of 39 pounds per second per square foot are shown as a function of flight Mach number for both the nonafterburning configuration and for a configuration having an afterburner temperature of 3040° F. It is seen that the thrust rise available from the use of an afterburner increases as the flight Mach number is increased. For a flight Mach number of 1.5, the thrust is increased 28 percent by the use of an afterburner. At a flight Mach number of 2.8, the thrust increase is 49 percent. At a flight Mach number of 1.5, the specific fuel consumption is increased from 1.46 to 1.77 by the use of an afterburner. For a flight Mach number of 2.8, the specific fuel consumption increases from 1.47 to 1.79.

The thrust increases indicated for the afterburner presented in figure 5 are much less than those that would be obtained for engines utilizing lower turbine-inlet temperatures.

#### Effect of Design Flight Mach Number and Mode of Operation

All the previous discussion is concerned with the engine improvements that result from aerodynamic and thermodynamic improvements in the engine components when the engine is operated in the conventional manner. In the following discussion, some insight will be given into the performance improvements that result from changing the design flight Mach number and mode of operation.

Constant-equivalent-rotational-speed operation. - In order to alleviate the loss in air flow occurring at high flight Mach numbers, it would be desirable to operate at constant equivalent rotational speed throughout the entire Mach number range. Such a mode of operation is indicated on the compressor map of figure 6. The turbine-inlet temperature is maintained at the desired constant value by adjusting the exhaust-nozzle area. This method of operation, although it alleviates the loss in air flow occurring at high flight Mach numbers, has several rather serious problems involved in its operation. Because of the

large change in compressor-inlet temperature, the actual rotational speed at a flight Mach number of 2.8 must be 55 percent greater than the rotational speed at a flight Mach number of 0.6 in order to maintain a constant equivalent speed. For a given maximum equivalent rotational speed, this would involve designing an engine capable of withstanding approximately 2.4 times the stress of an engine operating at constant rotational speed. One way to avoid this increase in stress is to maintain the same maximum value of rotational speed. This would result in low equivalent rotational speeds at the higher flight Mach numbers and necessitate the addition of compressor and, very likely, turbine stages. Rather than analyze engine operation at constant equivalent, or aerodynamic, rotational speed, two cases between the extremes of constant-rotational-speed and constant-equivalent-rotational-speed operation were considered; the performance of these engines is presented subsequently.

Engine designed for Mach number of 1.5. - It was assumed that the advanced take-off engine was redesigned in order to permit operation at limiting values of both rotational and equivalent rotational speeds at a flight Mach number of 1.5. These conditions correspond to operation at a maximum rotational speed which is 17 percent higher than for the current and advanced take-off engines. The operating line for this method of operation is shown on the compressor map of figure 7. Also shown in figure 7 is the operating line for constant-rotational-speed operation. The advanced Mach 1.5 engine operating line has been shifted away from the compressor surge line toward the region of lower compressor efficiency. For all flight Mach numbers above 0.6, the compressor air flow is greater for this engine than for the engine operated at constant rotational speed. The thrust per unit area for an engine operated in this manner, and with a turbine-inlet temperature of 2040° F, a compressor maximum specific air flow of 39 pounds per second per square foot, and an afterburner temperature of 3040° F, is shown in figure 8(a). Included for comparison is the performance of the current and advanced take-off engines having afterburner temperatures of 3040° F. For the advanced Mach 1.5 engine, the thrust per unit area is greater than for the advanced take-off engine for all operating conditions except flight in the stratosphere at Mach numbers less than 0.6. At a flight Mach number of 2.8, the thrust per unit area of the advanced Mach 1.5 engine is approximately 30 percent greater than the thrust per unit area of the advanced take-off engine. The specific fuel consumption for the three engines is compared in figure 8(b). It can be seen that the specific fuel consumption for the advanced Mach 1.5 engine is very nearly equal to that for the advanced take-off engine over the entire range of flight Mach numbers. If the effects of nacelle drag are taken into account, the high thrust per unit area of the advanced Mach 1.5 engine reduces its specific fuel consumption below that of the advanced take-off engine over the range of flight Mach numbers from 0.9 to 2.8.

Inasmuch as high air flow is obtained at high flight Mach numbers with the advanced Mach 1.5 engine, the velocities through the engine combustion chamber and afterburner were investigated. These velocities are shown in figure 9 as functions of flight Mach number. It can be seen that the velocity in the primary combustor approaches 200 feet per second while that in the afterburner approaches 600 feet per second, approximately the maximum values obtained in laboratory investigations for satisfactory operation.

In changing from the advanced take-off engine to the advanced Mach 1.5 engine, some turbine problems are aggravated. At any given flight Mach number, increasing the engine rotational speed at constant turbine-inlet temperature requires that the exhaust-nozzle throat area be increased. This increase in exhaust-nozzle throat area shifts the turbine toward limiting blade loading, a condition limiting turbine design and operation. For the purpose of driving the specified compressor under static sea-level operating conditions for the advanced take-off engine, a two-stage turbine having conservative aerodynamic characteristics can be designed to fit within a cylindrical nacelle suitable for the compressor. Such a turbine would have sufficient operating latitude to permit increasing the engine maximum rotational speed by 17 percent over that of the advanced take-off engine. A significantly greater increase in maximum rotational speed would necessitate that the turbine be redesigned for the higher turbine pressure ratio required for such operation; both turbine-tip frontal area and centrifugal stress of the turbine would increase.

In changing from the advanced take-off engine to the advanced Mach 1.5 engine, the compressor and turbine were considered to have no change in aerodynamic characteristics, but the structural characteristics were changed so that the rotational speed was increased 17 percent for a given engine frontal area. This rise in rotational speed results in a rise in centrifugal stress and, concomitantly, a rise in engine weight. Whether the evaluation of the combination of higher thrust and higher weight results in an improvement in engine specific weight is beyond the scope of this investigation. The centrifugal stress in the turbine-rotor blades would rise from 31,000 to 42,000 pounds per square inch. If a value of centrifugal stress of 50,000 pounds per square inch were accepted as the limiting value for cooled turbine blades, the extent to which the rotational speed of this engine can be further raised is rather small, not only because of the rise in centrifugal stress with centrifugal acceleration but also because of the increased turbine-rotor blade length required to permit such operation within limiting blade loading.

In order to alleviate this problem created by centrifugal stress, a different approach could be employed in redesigning the advanced take-off engine in order to convert it into the advanced Mach 1.5 engine.

The compressor and turbine could be designed for lower equivalent rotational speed and stages added to each to compensate for the lower equivalent rotational speed. The effect of such a change is that at a flight Mach number of 1.5 the same rotational speed for both the advanced take-off and advanced Mach 1.5 engines would then correspond to a higher fraction of maximum equivalent rotational speed and thus to a higher specific air flow for the advanced Mach 1.5 engine.

The advanced Mach 1.5 engine has two limits on its rotational speed, one mechanical and the other aerodynamic. For a given engine, higher thrust is obtained by operating the engine at the highest rotational speed which the more conservative of these two limits will permit. For take-off and for flight in the stratosphere at Mach numbers no greater than 1.5, the engine is thus operated at the maximum equivalent rotational speed. For flight at higher Mach numbers, the mechanical rotational speed is the limiting value and the equivalent rotational speed is less than the maximum allowable.

The addition of turbine-stator adjustment to this engine was considered. For maximum thrust operation, the compressor pressure ratio was varied by means of stator adjustment in order to maximize the engine thrust at any given flight Mach number. No significant improvement in thrust was obtained. For flight at a Mach number of 0.9 in the stratosphere, turbine-stator adjustment was analyzed as a means of providing reduced specific fuel consumption for a range of engine thrust values. In general, the specific fuel consumption was reduced only a very small amount; the greatest reduction was 4 percent of that obtainable without turbine-stator adjustment.

Engine designed for Mach number of 2.3. - If the engine structure is designed so that the engine can operate at the maximum value of equivalent rotational speed during flight at a Mach number of 2.3, even higher values of thrust per unit frontal area can be obtained. The methods presented in the paper by English and Rebeske were employed in order to explore the range of specific air flow and compressor pressure ratio for which a high-output, two-stage turbine could be designed. The turbine-rotor-inlet Mach number was set equal to 0.8 and the turbine-exit axial Mach number, to 0.7. The following conditions were selected for engine operation at a flight Mach number of 2.3: compressor pressure ratio, 5.5; turbine blade-tip speed, 1254 feet per second; and turbine hub-tip radius ratio, 0.5. These conditions correspond to a specific air flow of 34 pounds per second for each square foot of turbine-tip frontal area and a turbine blade stress of 44,000 pounds per square inch.

The compressor pressure ratio at a Mach number of 2.3 was chosen as high as 5.5 in order to keep the primary-burner inlet velocity at a practicable value, in this case 220 feet per second if nacelle

proportions permit a primary-burner frontal area 23 percent greater than for the compressor. The compressor pressure ratio at a Mach number of 2.3 was kept as low as 5.5 in order to restrict the compressor-exit temperature to a value not requiring use of critical blade materials, in this case 1620° R at a Mach number of 2.8.

The manner in which this engine was operated in order to obtain maximum engine thrust over a wide range of flight Mach numbers is as follows: The equivalent rotational speed was kept constant at the limiting or maximum value for flight Mach numbers less than 2.3, and the rotational speed was maintained constant for flight Mach numbers between 2.3 and 2.8. In order that the turbine-inlet temperature need not be decreased below the design value for flight Mach numbers less than 2.3, the engine was considered to be equipped with turbine-stator adjustment.

The range of turbine-rotor-inlet relative flow directions (comparable to angle of attack on the turbine-rotor blades) was found to be 77°, a value so large that it is doubtful that satisfactory low Mach number performance can actually be achieved. One way to circumvent this wide range of turbine-rotor-inlet flow direction is to operate the engine at a constant engine temperature ratio (ratio of turbine-inlet to compressor-inlet temperature) over a portion of the range of Mach numbers. Such a change has an undesirable effect on engine thrust at low flight speeds.

An alternative way is to redesign the compressor so that the compressor is capable of operating over a range of pressure ratios at constant equivalent rotational speed. Such an engine operating line is shown on the compressor map in figure 10. The rise in compressor pressure ratio from 5.5 to 6.2 as the flight Mach number decreases from 2.3 to 0.6 is sufficient to reduce the variation in turbine-rotor-inlet relative flow direction from 77° to 30°. The incorporation of this reserve capacity for pressure ratio requires that stages be added to the compressor with a resulting increase in engine weight. Turbine-stator adjustment is then used only at flight Mach numbers less than 1.9.

The performance of this advanced Mach 2.3 engine is compared in figure 11 with that of other engines. At a flight Mach number of 2.8, the advanced Mach 2.3 engine has a thrust which is 55 percent greater than that of the advanced Mach 1.5 engine and 145 percent greater than that of the current take-off engine; the specific fuel consumption is approximately midway between that of the advanced Mach 1.5 engine and that of the current engine. If the effects of nacelle drag are considered in determining the specific fuel consumption, the advanced Mach 2.3 and advanced Mach 1.5 engines have essentially identical specific fuel consumptions. At low flight Mach numbers, the advanced Mach 2.3

[REDACTED]

engine has little or no advantage in thrust and the specific fuel consumption is somewhat increased because of the low compressor pressure ratio for this engine.

#### CONCLUDING REMARKS

3078-H

In addition to the gains in engine performance which result from advances in component design techniques, large increases in engine thrust per unit frontal area at high flight Mach numbers are obtainable by raising the maximum rotational speed of the engine above the rotational speed during take-off; this rise in thrust at high flight Mach numbers results from increased engine flow capacity at high flight Mach numbers. Designing the engine for such increased rotational speeds requires that the engine weight be increased.

The paper by Dugan, Bernatowicz, and Schoeberle shows that, relative to the design-point performance, the off-design performance of two-spool turbojet engines designed for take-off is about the same as the off-design performance of one-spool turbojet engines for operation of both engine types under conditions which vary from take-off to flight at a Mach number of 2.8 in the stratosphere. For this reason, the performances of the advanced take-off engine and the advanced Mach 1.5 engine are essentially those that would be obtained from comparable two-spool engines. In raising the maximum rotational speed of the advanced take-off engine to that of the advanced Mach 1.5 engine in order to increase the specific air flow of the engine at high flight Mach numbers, only the low-pressure spool of the two-spool engine need be redesigned for the higher-speed operation, whereas for the one-spool engine the entire compressor must be redesigned.

[REDACTED]

OPERATION OF ADVANCED TAKE-OFF ENGINE

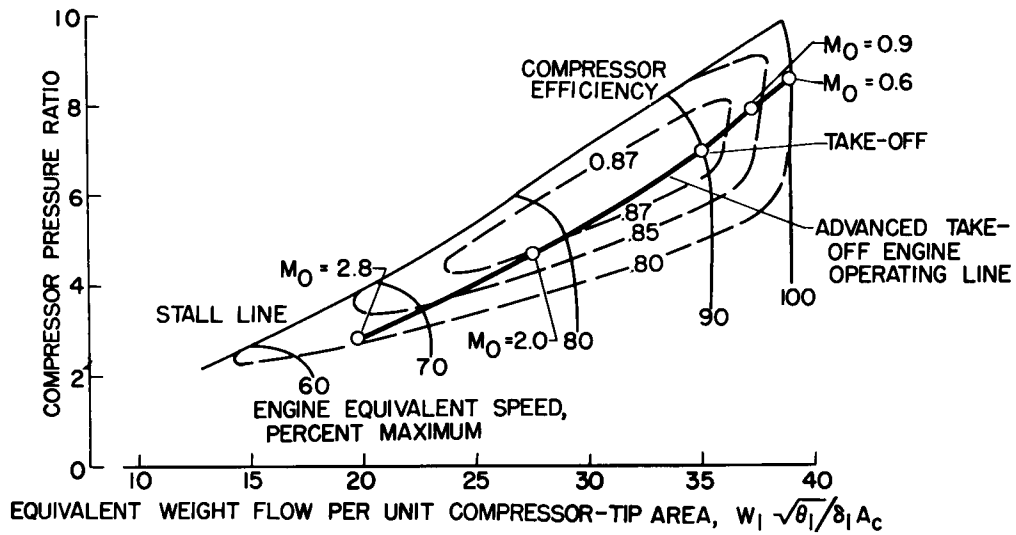


Figure 1

EFFECT OF FLIGHT MACH NUMBER ON ENGINE AIR-FLOW CAPACITY

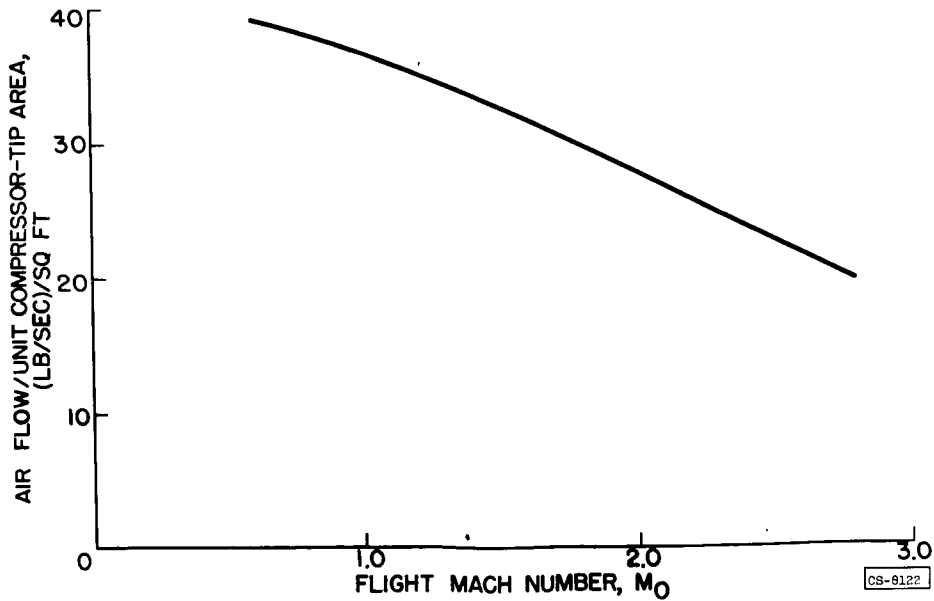


Figure 2

3078-H

CS-9122

EFFECT OF COMPRESSOR MAXIMUM AIR FLOW ON  
TURBOJET-ENGINE PERFORMANCE  
NO AFTERBURNER

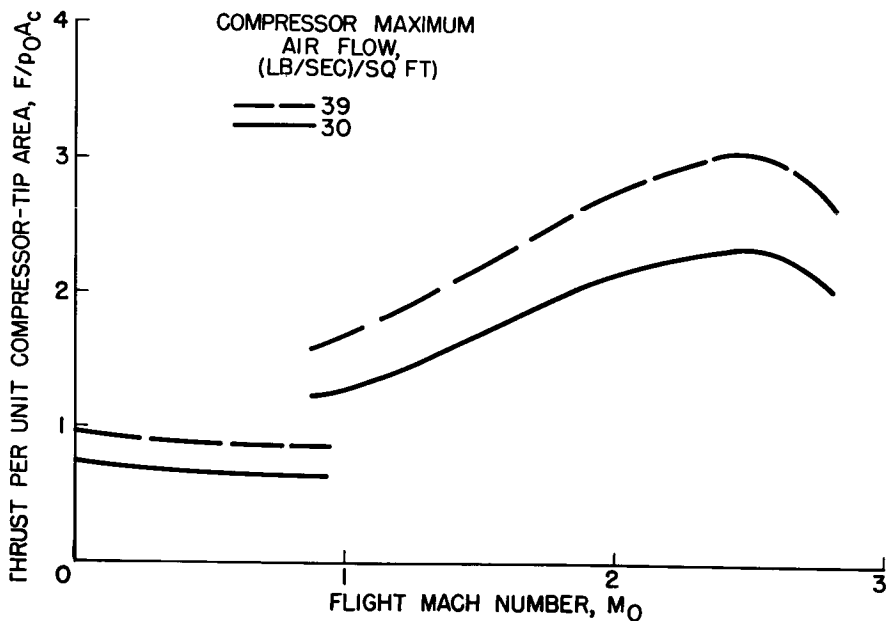
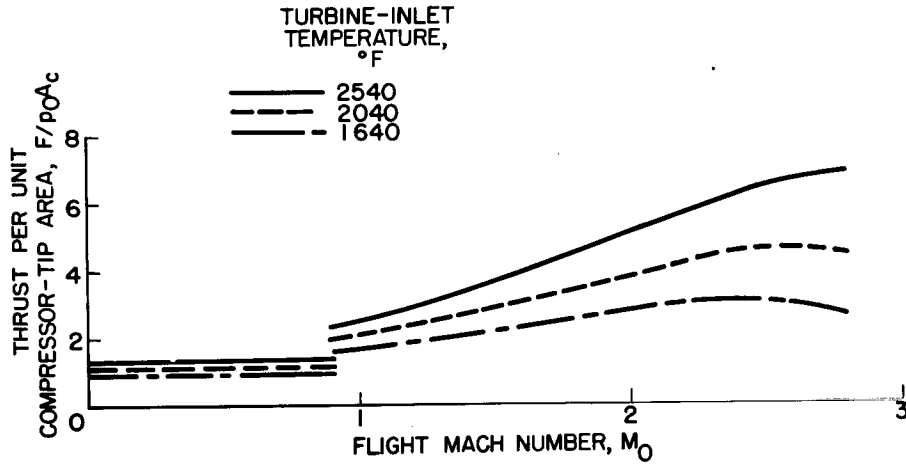


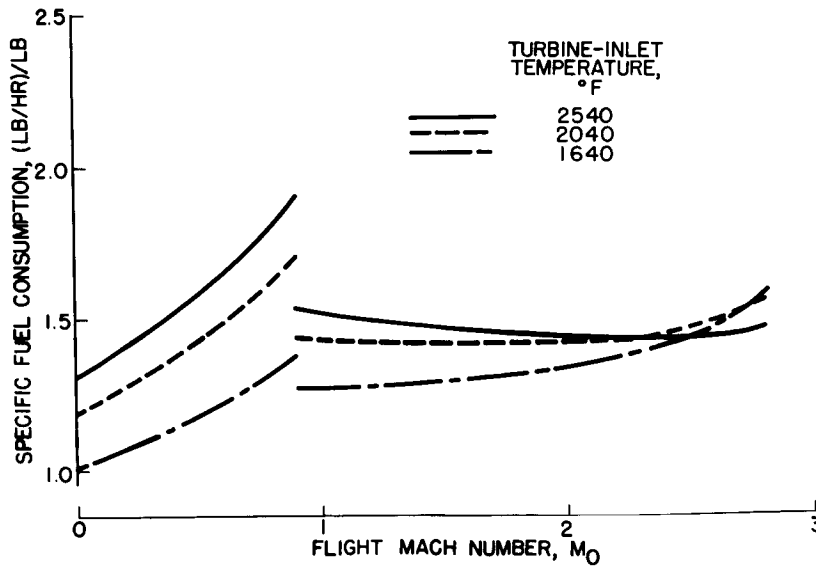
Figure 3

EFFECT OF TURBINE-INLET TEMPERATURE ON  
TURBOJET-ENGINE PERFORMANCE  
NO AFTERBURNER

3078-H



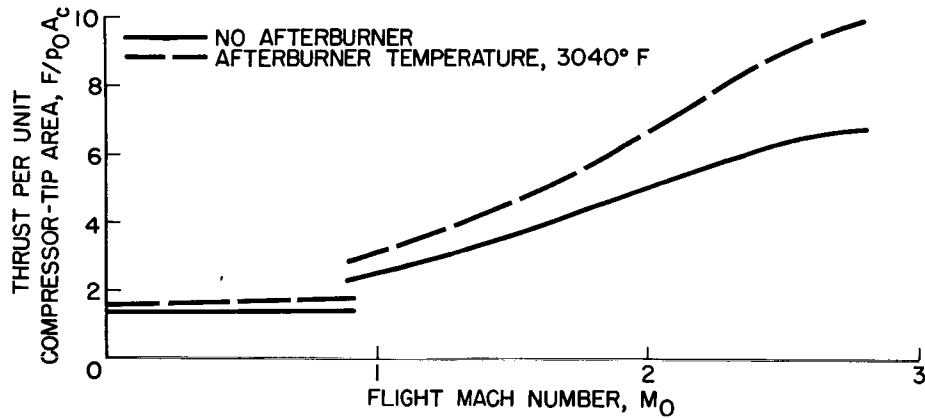
(a) THRUST.



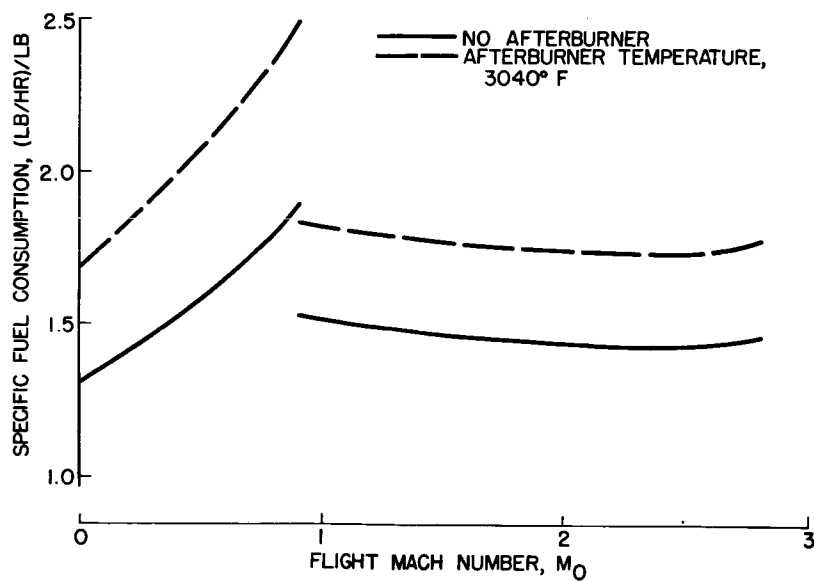
(b) SPECIFIC FUEL CONSUMPTION.

Figure 4

EFFECT OF AFTERBURNING ON TURBOJET-ENGINE PERFORMANCE  
TURBINE -INLET TEMPERATURE, 2540° F

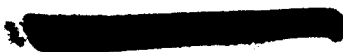


(a) THRUST.



(b) SPECIFIC FUEL CONSUMPTION.

Figure 5



OPERATION OF CONSTANT-EQUIVALENT-ROTATIONAL-SPEED ENGINE

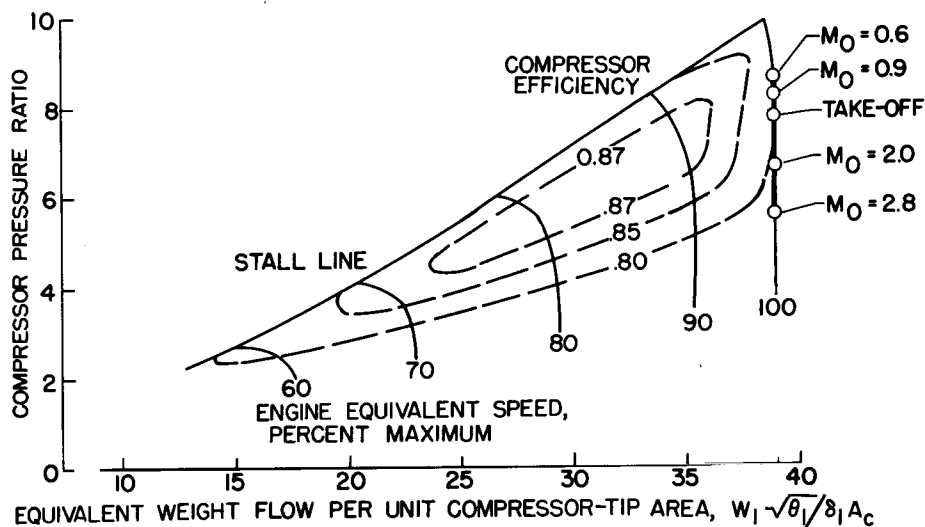


Figure 6

OPERATION OF ADVANCED MACH 1.5 ENGINE

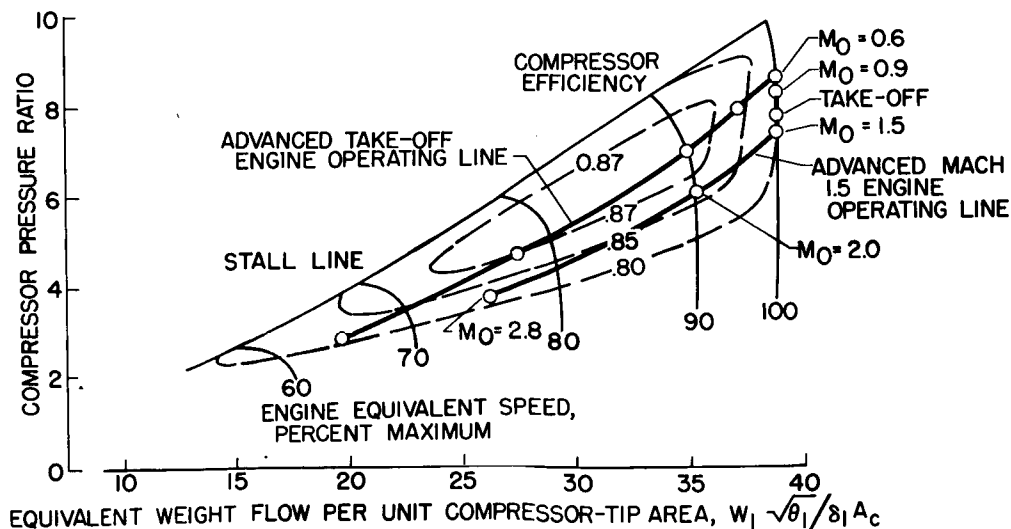
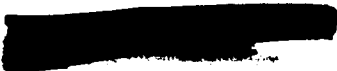


Figure 7



EFFECT OF ENGINE DESIGN POINT ON TURBOJET-ENGINE PERFORMANCE  
AFTERBURNER TEMPERATURE, 3040° F

3076-H

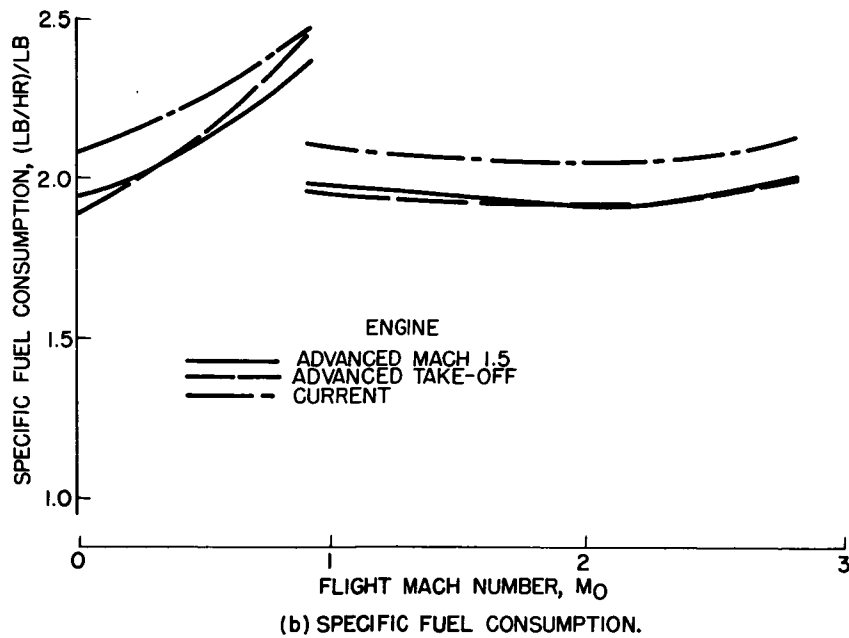
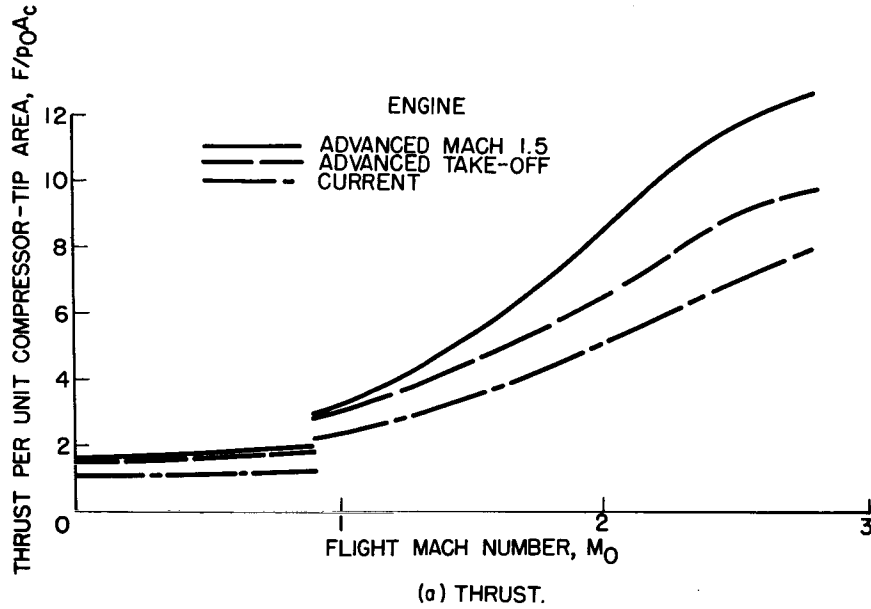


Figure 8

COMBUSTOR VELOCITIES OF ADVANCED MACH 1.5 ENGINE

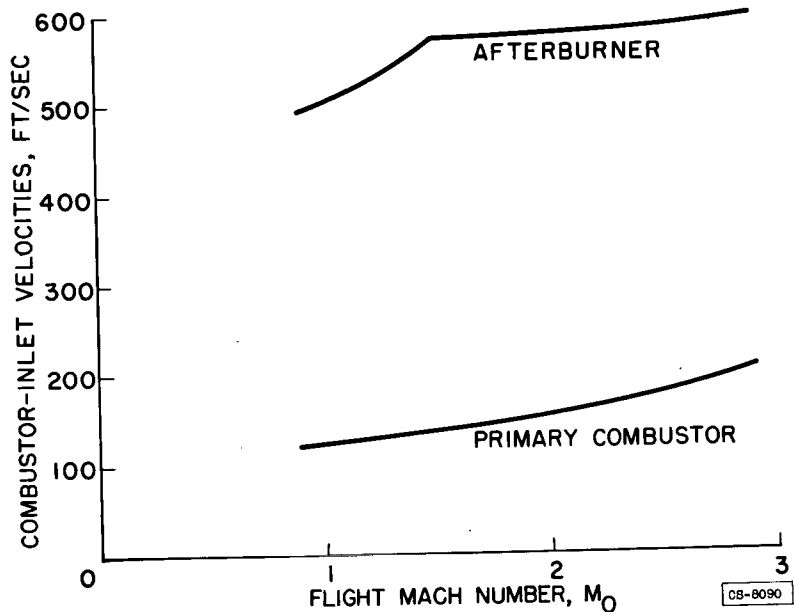


Figure 9

OPERATION OF ADVANCED MACH 2.3 ENGINE

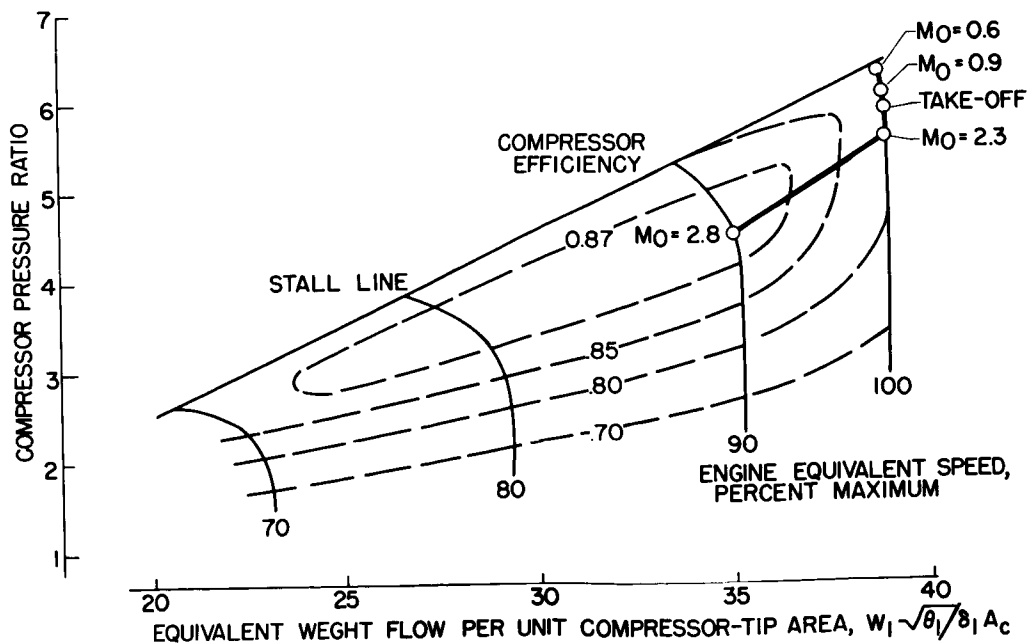
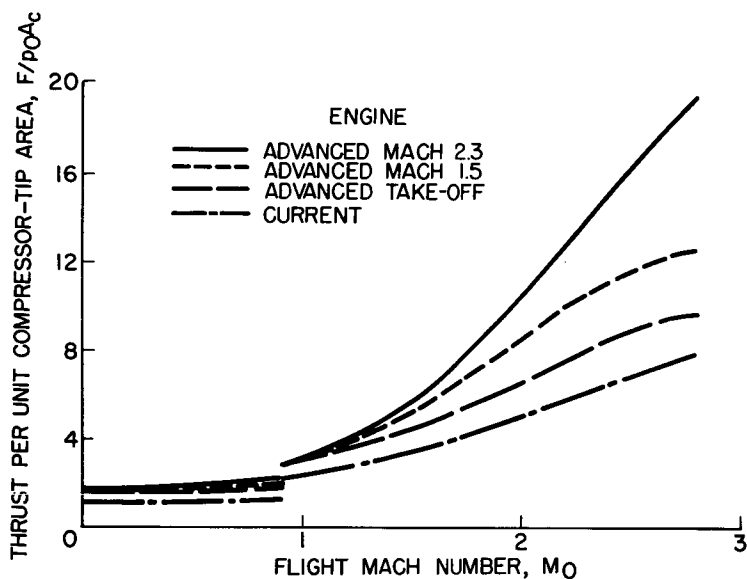


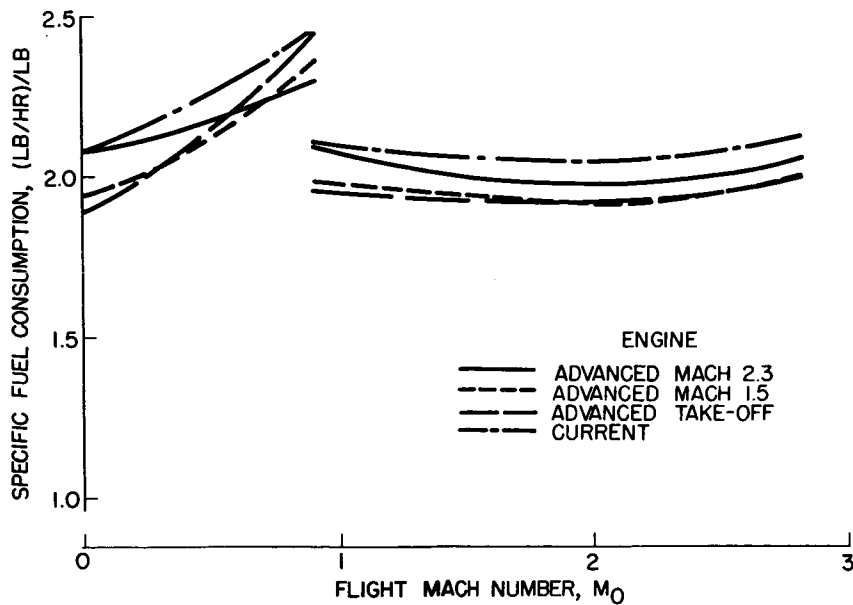
Figure 10

EFFECT OF ENGINE DESIGN POINT ON TURBOJET - ENGINE PERFORMANCE  
AFTERBURNER TEMPERATURE, 3040° F

3078-II



(a) THRUST.



(b) SPECIFIC FUEL CONSUMPTION.

Figure 11

[REDACTED]

## TWO-SPOOL ENGINES FOR SUPERSONIC FLIGHT

By James F. Dugan, Jr., Daniel T. Bernatowicz,  
and Daniel F. Schoeberle

### INTRODUCTION

3078-H

The advantages of two-spool engines to obtain high pressure ratios are well recognized. Although the two-spool engine is intrinsically more complex than the one-spool engine, the use of two spools to achieve high pressure ratios helps the stage-matching and stall problems. In addition, considerable freedom can be exercised in the design of the two-spool engine, in that different pressure-ratio splits and speed relations can be used to favor various flight conditions.

Accordingly, the use of the two-spool engine as a power plant for supersonic propulsion is investigated herein. The performance characteristics of the two-spool engine are examined to determine the effect of compressor-pressure-ratio split on performance. Operation with the inner-spool speed held constant is also compared with constant outer-spool speed operation. The effect of design Mach number on two-spool-engine performance is investigated. The performance of various two-spool engines is compared with that of the single-spool types of the preceding paper by English, Wilcox, and Plohr for similar methods of operation. The effect of over-all design compressor pressure ratio on performance is also investigated.

The performance of the two-spool engines presented in this paper was calculated by matching compressor and turbine components. The compressor and turbine performance was estimated from actual research and commercial compressor and turbine component data. The compressors are of the transonic type discussed in the papers of the first section. The outer compressor of each engine is characterized by a tip speed of 1100 feet per second, an inlet hub-tip ratio of 0.39, and a relative Mach number at the first rotor tip of 1.18. The inner compressors are characterized by tip speeds from 1240 to 1300 feet per second, inlet hub-tip ratios from 0.48 to 0.66, and relative Mach numbers at the first rotor tip from 1.05 to 1.14. Exit axial Mach numbers from the inner compressor were of the order of 0.3. Primary and afterburner velocities were of the same order of magnitude as for the single-spool engines discussed in the single-spool paper. For each two-spool engine, two conservatively designed turbine stages were required to drive the compressors. The design value of rotor hub relative Mach number was either 0.6 or 0.7, while the design value of exit axial velocity ratio  $\left(\frac{V_x}{a_{cr}}\right)_d$  (all symbols are defined in the appendix) was 0.50. Rotor-blade-hub stress of the inner turbines ranged from 37,000 to 47,000

[REDACTED]

[REDACTED]

pounds per square inch, while that for the outer turbines ranged from 24,000 to 30,000 pounds per square inch. The stage-loading parameter  $\frac{-gJ\Delta h}{U_h^2}$  varied from 1.3 to 2.2. The inlets and exhaust nozzles were the same as those for the single-spool engines.

## RESULTS AND DISCUSSION

The components of a two-spool engine may be matched to obtain engine performance just as they can for a single-spool engine. For each operating point of any component, the operating points of the other components are uniquely determined. Thus, lines of constant temperature ratio or pressure ratio across any part of the engine may be plotted on any component performance map. Analogous to the compressor performance map of a single-spool engine is the combined compressor performance map of a two-spool engine.

The combined compressor performance of a two-spool engine is presented in figure 1 as a plot of over-all compressor pressure-ratio against equivalent weight flow for constant values of outer-spool aerodynamic speed. Also shown are lines of constant turbine-inlet to compressor-inlet temperature ratio and the surge lines of the outer and inner compressor. For operation along a line of constant outer-spool aerodynamic speed, increasing turbine-inlet temperature is accompanied by increasing over-all compressor pressure ratio, weight flow, and inner-spool speed and decreasing exhaust-nozzle area. Turbine-inlet temperature may be increased until surge of the inner compressor or a limiting turbine temperature is encountered and decreased until outer-compressor surge is encountered (unless operation is limited by turbine limiting loading or maximum nozzle size).

For full-throttle performance, the two-spool engine might be operated at constant values of outer-spool speed and turbine-inlet temperature. At high flight Mach numbers at altitude, the compressor-inlet temperature rises above its sea-level static value. Operation therefore is at turbine-inlet to compressor-inlet temperature ratios and aerodynamic speeds below design. This simultaneous reduction in engine temperature ratio and aerodynamic speed causes the engine operating point to approach the surge limit of its outer compressor. Consequently, when a two-spool engine is operated at high flight Mach numbers, surge of the outer compressor may be encountered. Compressor design points must be selected to avoid this and, if necessary, low-speed performance should be compromised.

Comparison of two-spool engines with one-spool engines. - The performance of a single-spool engine and a two-spool engine is presented in figure 2. Both engines have a sea-level-static over-all compressor

[REDACTED]

pressure ratio of 7 at the maximum compressor efficiency point and operate at maximum aerodynamic speed at a subsonic flight Mach number. Operation is with a turbine inlet temperature of 2040° F and an afterburner temperature of 3040° F.

The one-spool engine, designated A, is the advanced take-off engine of the single-spool paper. This engine operates at a constant mechanical speed corresponding to sea-level-static conditions. The two-spool engine, designated B, operates at a constant mechanical speed of the outer spool corresponding to sea-level-static conditions.

3078 - H

Figure 2(a) shows the full-throttle performance of engines A and B as a plot of specific fuel consumption and equivalent thrust per rated air flow against flight Mach number in the stratosphere. Engine A exhibits a 3-percent lower specific fuel consumption at a flight Mach number of 0.9 and a 1.5 percent higher specific fuel consumption at a flight Mach number of 2.8. The thrust values are the same at lower Mach numbers, but engine B has a 7 percent higher thrust value at a flight Mach number of 2.8. These differences are small and well within design variations of either type engine. The cruise performance at a flight Mach number of 0.9 in the stratosphere for engines A and B is presented in figure 2(b) as a plot of specific fuel consumption against thrust per rated air flow. Again, the differences are small; the minimum specific fuel consumption of engine A is only 1.5 percent lower than that of engine B.

The full-throttle performance of two Mach 1.5 engines is shown in figure 2(c). Engine AA is the advanced, Mach 1.5 engine of the single-spool paper. Engine BB is a two-spool, advanced, Mach 1.5 engine. For flight Mach numbers up to 1.52, the outer spool is operated at a maximum aerodynamic speed. Above this Mach number, operation is at a constant mechanical speed of the outer spool. The maximum specific-fuel-consumption difference is only 3 percent. At a flight Mach number of 0.9, engine BB has a 12 percent higher thrust value than engine AA; at a flight Mach number of 2.8, engine AA has a 3.5 percent higher thrust value than engine BB. These differences depend on the component characteristics of the engine. The component performance maps used herein are considered typical so that the conclusion that may be drawn from the preceding comparisons is that the one- and two-spool engines give about the same full-throttle and cruise performance.

Effect of design Mach number. - Figure 3(a) shows the effect of design Mach number on two-spool engine performance. Engine BB, the advanced, Mach 1.5, two-spool engine, has about the same specific-fuel-consumption values as engine B, the advanced, take-off, two-spool engine, but from 12 to 30 percent greater values of thrust per rated air flow. These results are comparable with those shown in the one-spool paper for the comparison of the one-spool, advanced, take-off engine with the one-spool, advanced, Mach 1.5 engine.

[REDACTED]

If both engines B and BB have the same value of design aerodynamic compressor tip speed, the outer-compressor mechanical speed of engine BB is appreciably greater than that of engine B but the inner-compressor mechanical speed is only slightly greater than that of engine B. The speed variations of engines B and BB with flight Mach number are shown in figure 3(b). The mechanical speed of engine B is plotted as a ratio of mechanical speed to the sea-level-static mechanical speed. The maximum value of inner-spool speed is for a flight Mach number of 2.8 so that the inner spool would be designed for this speed. The mechanical speed of engine BB is plotted as a ratio of mechanical speed to the design speed of engine B. The outer-compressor mechanical speed of engine BB is 17 percent greater than that of engine B, while the inner-compressor mechanical speed is 0.5 percent greater than that of engine B. The outer-spool turbine-rotor stress of engine BB would be 36 percent greater than that of engine B, while the inner-spool turbine-rotor stress of engine BB would be only 1 percent greater than that of engine B because of the increases in mechanical speed. If the outer-compressor design aerodynamic tip speed of engine BB is lowered to avoid the increased outer-turbine-rotor stress, it is likely that additional outer-compressor stages and perhaps another outer-turbine stage would be required to maintain the design compressor pressure ratio.

Effect of work split. - The effect of work split on two-spool-engine performance is shown in figure 4. The full-throttle performance of three two-spool engines is presented in figure 4(a) as a plot of specific fuel consumption and thrust per rated air flow against flight Mach number in the stratosphere. All three engines are designed to operate at maximum compressor efficiency at sea-level-static conditions at an over-all compressor pressure ratio of 12 and a turbine-inlet temperature of 2040° F. All three engines operate at maximum aerodynamic speed at a flight Mach number of 0.59. Full-throttle operation is for a turbine-inlet temperature of 2040° F, an afterburner temperature of 3040° F, and an outer-spool mechanical speed corresponding to sea-level-static conditions. Engine C has a work split of 2:6; that is, the sea-level-static outer-compressor pressure ratio is 2 and the inner-compressor pressure ratio is 6. Engine D has a work split of 3:4 and engine E has a work split of 4:3. Figure 4(a) shows that the maximum difference in specific consumption is 5.5 percent and the maximum difference in thrust per rated air flow is 5.5 percent. The cruise performance at a flight Mach number of 0.9 in the stratosphere of engines C, D, and E is presented in figure 4(b) as a plot of specific fuel consumption against equivalent thrust per rated air flow. The difference in minimum specific fuel consumption is less than 2.5 percent. The differences in full-throttle and cruise performance that result from work split are small and within the variation that may be obtained by varying the match point for a given set of components.

Effect of operating mode. - The effect of operating mode on two-spool engine performance is shown in figure 5. Figure 5(a) presents the full-

[REDACTED]

3078 - H

[REDACTED]

throttle performance of engine E for two modes of operation. One mode is with constant outer-spool speed and the other with constant inner-spool speed. Both modes are for operation with a primary burner temperature of 2040° F and an afterburner temperature of 3040° F. Constant outer-spool speed operation (fig. 5(a)) results in higher thrust per rated air flow and specific fuel consumption above a flight Mach number of about 1.3. At a flight Mach number of 2.8, constant outer-spool speed operation gives 39 percent more thrust and 3 percent greater specific fuel consumption than constant inner-spool speed operation. The large increase in thrust for constant outer-spool speed operation results from the larger air flow that accompanies the higher outer-spool speed. Figure 5(b) is a plot of mechanical speed to sea-level-static mechanical-speed ratio against flight Mach number for the two modes of operation. For constant inner-spool speed operation, above a flight Mach number of about 1.3, the outer-spool speed is less than its sea-level-static value; below this Mach number, the outer-spool speed is greater than its sea-level-static value. Therefore, above a flight Mach number of 1.3, constant outer-spool speed operation yields higher air flows and hence higher thrust values while below a flight Mach number of 1.3, constant inner-spool speed operation yields higher air flows and hence higher thrust values.

Effect of pressure ratio. - The effect of pressure ratio on the full-throttle performance of two-spool engines is shown in figure 6(a) and the effect on cruise performance at a flight Mach number of 0.9 in the stratosphere in figure 6(b). Engine B (sea-level-static over-all compressor pressure ratio of 7) and engine D (sea-level-static over-all compressor pressure ratio of 12) are compared. Figure 6(a) is a plot of specific fuel consumption and thrust per rated air flow against flight Mach number in the stratosphere. Engine D has a 5.5 percent lower specific fuel consumption value at a flight Mach number of 0.9 and a 2.5 percent higher value at a Mach number of 2.8. Engine D has a 1 percent higher thrust value at a flight Mach number of 0.9 and an 8 percent lower thrust value at a flight Mach number of 2.8. Figure 6(b) is a plot of specific fuel consumption against thrust per rated air flow for cruise performance at a flight Mach number of 0.9 in the stratosphere. The minimum specific fuel consumption for engine D is 11.5 percent lower than that for engine B. Increasing the design pressure ratio of the two-spool engine resulted in a sacrifice of full-throttle thrust at the high flight Mach numbers and an improvement in cruise performance.

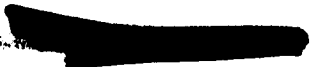
#### CONCLUSIONS

On the basis of thermodynamic and aerodynamic considerations, both the one-spool and the two-spool engines are equally suited as power plants for supersonic propulsion. The small differences in full-throttle and cruise performance are largely due to detailed assumptions of

[REDACTED]



component characteristics and are within design variations of either type engine. The effect of work split on both the full-throttle performance and the cruise performance is slight, although consideration must be given to the fact that a stall limit is approached at high flight Mach numbers. For operation at flight Mach numbers above about 1.3, the two-spool engine should be operated at constant outer-spool speed rather than constant inner-spool speed. As for single-spool engines, the full-throttle performance of the two-spool engine can be improved by operating at maximum aerodynamic speed up to a supersonic flight Mach number. The necessary increase in outer-spool mechanical speed with increasing design Mach number to achieve this improved performance can, moreover, be obtained with a very slight increase in inner-spool mechanical speed.



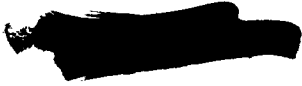
## APPENDIX - SYMBOLS

The following symbols are used in this paper:

$a_{cr}$	critical velocity
$F_n$	net thrust
$g$	standard gravitational acceleration
$\Delta h$	change in total enthalpy
$J$	mechanical equivalent of heat
$K$	constant
$M_0$	flight Mach number
$N$	mechanical speed
$P$	total pressure
$sfc$	specific fuel consumption
$T$	total temperature
$U_h$	turbine-blade-hub speed
$V$	velocity
$W$	weight flow of air
$\delta$	ratio of total pressure to standard sea-level-static pressure
$\theta$	ratio of total temperature to standard sea-level-static temperature

## Subscripts:

$d$	design
$i$	inner spool
$o$	outer spool



r        rated

sl        sea-level-static conditions

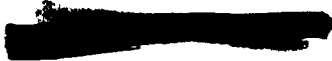
x        axial component

0        ambient conditions

1        compressor inlet of one-spool engine  
         outer-compressor inlet of two-spool engine

3        compressor exit of one-spool engine  
         inner-compressor exit of two-spool engine

4        turbine inlet of one-spool engine  
         inner-turbine inlet of two-spool engine



COMBINED COMPRESSOR PERFORMANCE OF TWO-SPOOL ENGINE

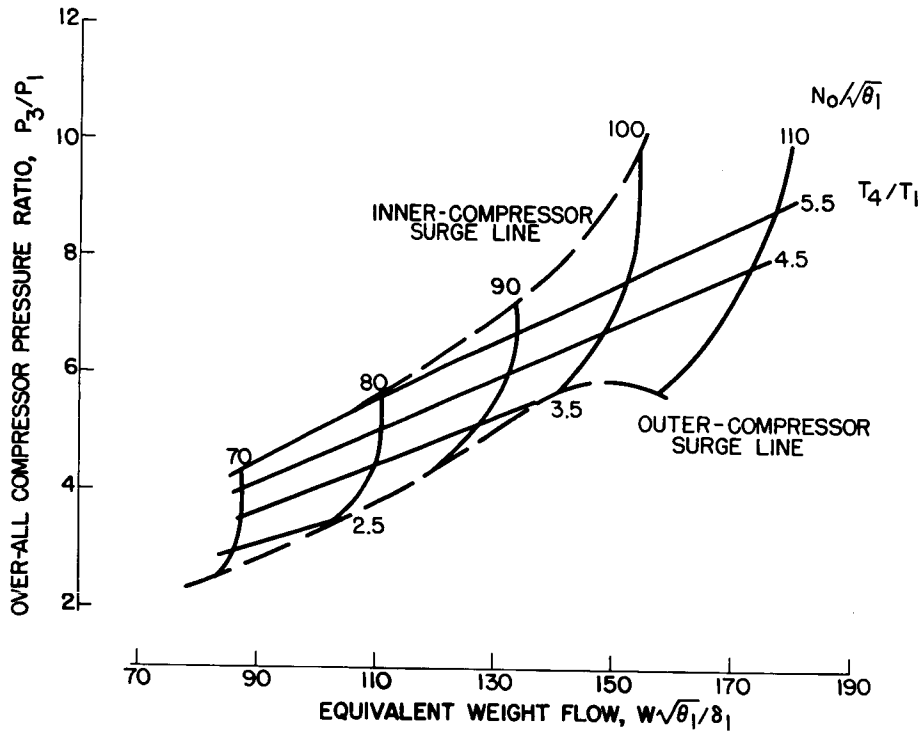
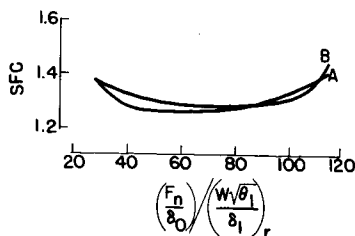
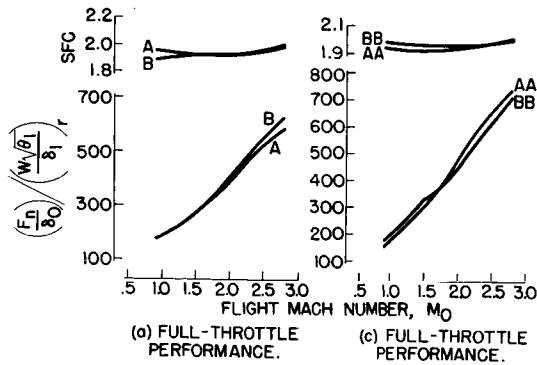


Figure 1

COMPARISON OF ONE- AND TWO-SPOOL ENGINE PERFORMANCE



- ENGINE
- A ONE-SPOOL ADVANCED TAKE-OFF
  - AA ONE-SPOOL ADVANCED MACH 1.5
  - B TWO-SPOOL ADVANCED TAKE-OFF
  - BB TWO-SPOOL ADVANCED MACH 1.5

(b) CRUISE PERFORMANCE AT FLIGHT MACH NUMBER OF 0.9 IN STRATOSPHERE.

Figure 2

EFFECT OF DESIGN MACH NUMBER ON PERFORMANCE OF TWO-SPOOL ENGINE

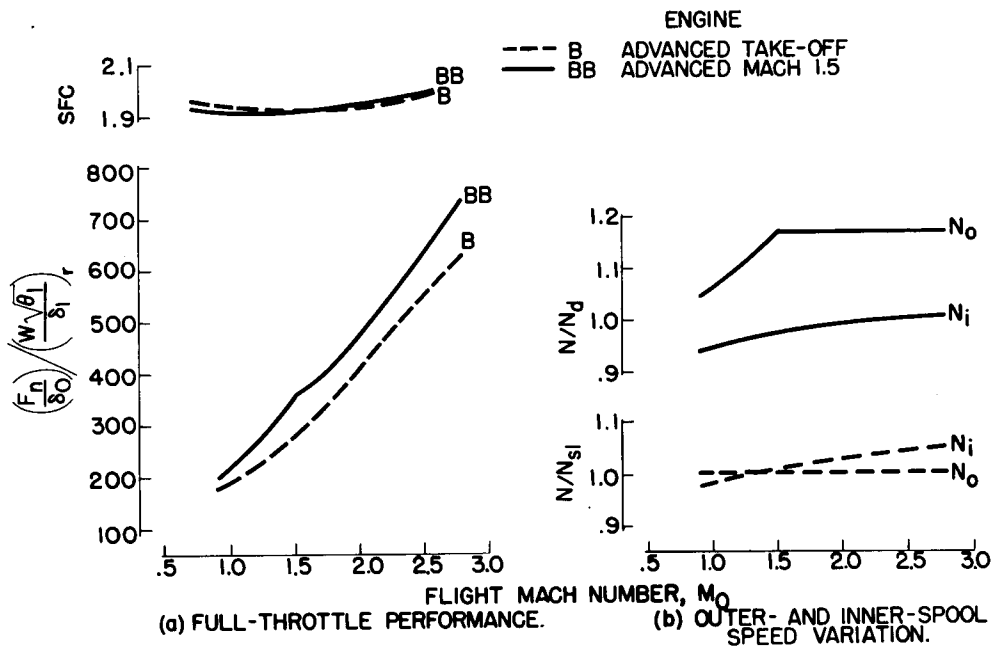


Figure 3

EFFECT OF WORK SPLIT ON TWO-SPOOL-ENGINE PERFORMANCE

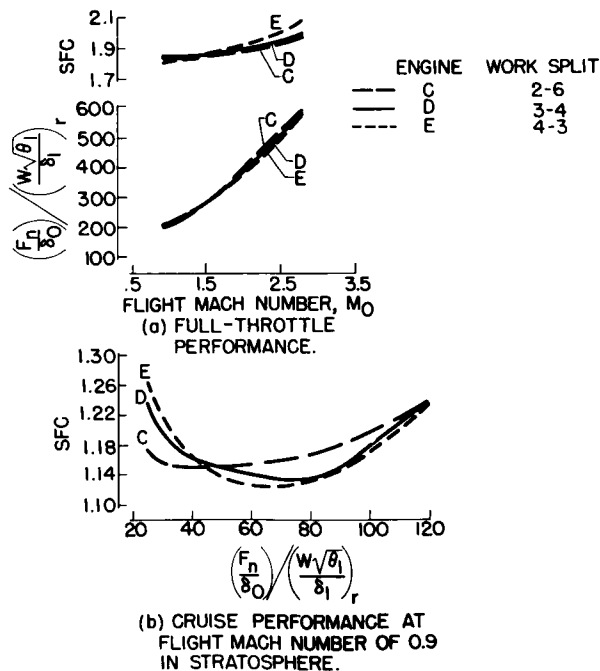


Figure 4

EFFECT OF OPERATING MODE ON PERFORMANCE OF TWO-SPOOL ENGINE E

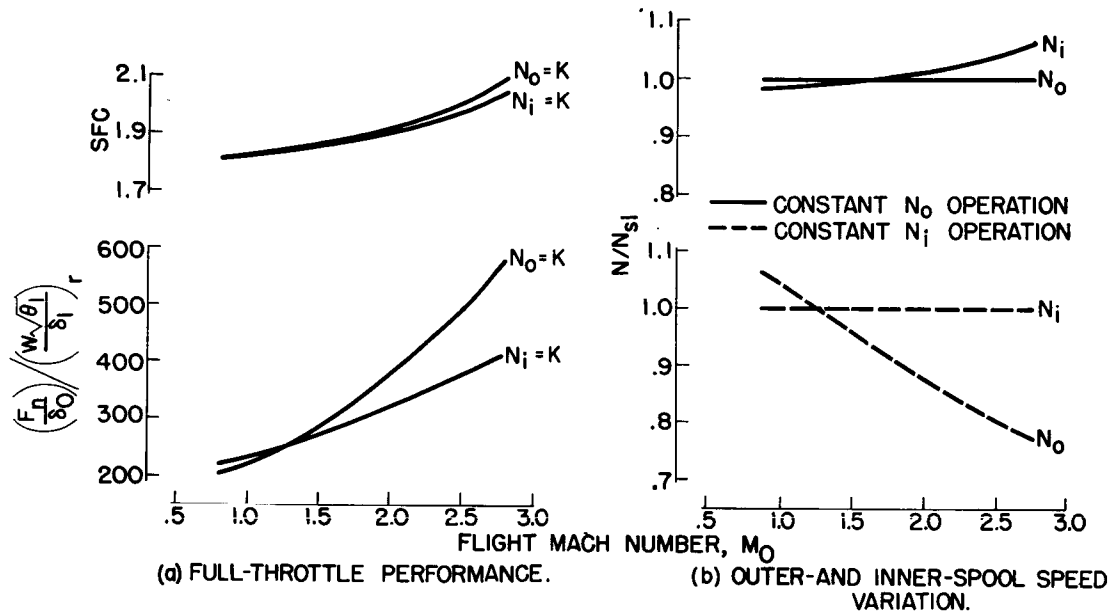


Figure 5

EFFECT OF PRESSURE RATIO ON PERFORMANCE OF TWO-SPOOL ENGINES

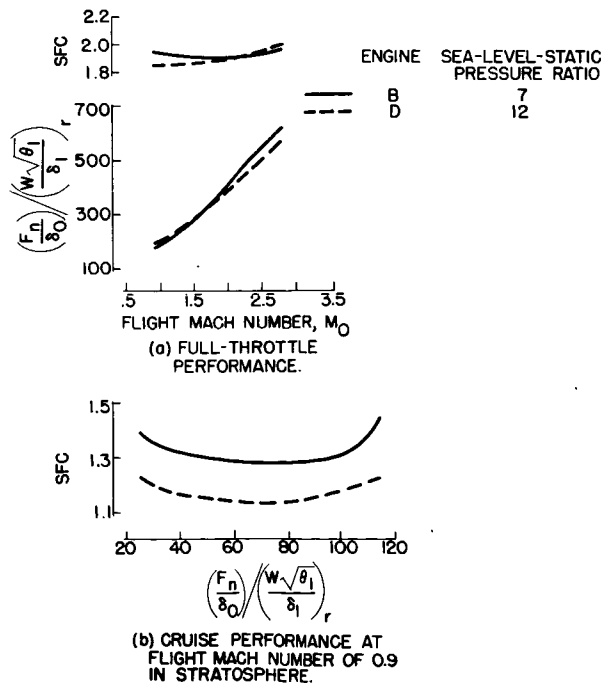


Figure 6

## AIRPLANE PERFORMANCE

By Roger W. Luidens, Hugh M. Henneberry,  
Arthur V. Zimmerman, and Philip J. Evans, Jr.

## INTRODUCTION

3078 - H

Previous papers have discussed variations in engine performance resulting from the use of advanced components and from changes in engine design and operating techniques. The purpose of the airplane performance paper is to evaluate these variations in engine performance in terms of bomber and interceptor airplane parameters. For the bomber, this evaluation was accomplished by fixing gross weight and studying airplane total cruise radius as a figure of merit. In the case of the interceptor, the mission was fixed and the airplane gross weight necessary to perform this mission was selected as the figure of merit for comparing the various engines.

The changes in engine performance resulting from increases in air-flow handling capacity and turbine-inlet temperature and the changes resulting from advanced modes of operation were evaluated. Also discussed is the desirability of the afterburner in relation to possible increases in turbine-inlet temperature.

The bomber analysis included missions having subsonic cruise with a brief supersonic dash over the target as well as missions conducted entirely at supersonic velocities. Cruise altitudes and engine size were optimized for all bomber missions except when the effects of engine size were specifically analyzed.

The interceptor gross weight evaluations were made for two missions: one which had supersonic cruise to and returning from combat as well as supersonic combat, and a second which had subsonic cruise to and from combat and combat at supersonic speeds. A range of flight Mach numbers from 1.5 to 2.8 and several values of power loading or maneuverability were studied. The results of the investigation are presented in plots of gross weight against flight Mach number or against the parameter being investigated.

## AIRPLANES AND MISSIONS

For both interceptor and bomber a straight wing with a taper ratio of 0.4 and an aspect ratio of 3 was assumed, together with a thin bi-convex profile.

Maximum take-off lift coefficients can be obtained with a straight wing at angles of attack near  $12^\circ$ , whereas maximum lift occurs near  $30^\circ$  for a delta wing. The straight wing therefore appears attractive for take-off because it simplifies the landing gear problem. However, many of the flight plans investigated called for cruise at a subsonic Mach number of 0.9 - a region in which drag rise on a straight wing might normally be encountered. Recent wind-tunnel results on small scale models indicate that fuselage indentation according to the area rule for Mach number 1.0 may provide transonic drag characteristics for a straight-wing configuration only slightly inferior to the characteristics for a delta-wing configuration. If this can be successfully applied to airplanes such as those assumed herein, the advantages of a straight wing at take-off may be obtained without a large sacrifice in transonic drag performance. For these reasons, a straight wing was assumed in the analysis, although similar results could be obtained with a delta wing provided the take-off problem does not severely compromise the airplane design.

Empennage drag was taken as 25 percent of wing zero lift drag, and no lift was attributed to the horizontal tail or body.

#### Bomber

Airplane. - The bomber assumed for the analysis was a representative supersonic configuration with a take-off gross weight of 100,000 pounds, a pay-load weight of 5000 pounds, and fixed-equipment weight of 3000 pounds. The fuselage was a body of revolution, having a fineness ratio of 12, with drag allowances for a canopy and other irregularities. A straight wing with a thickness ratio of  $3\frac{1}{2}$  percent was used.

Take-off wing loading was 100 pounds per square foot. To allow for sufficient volume in the fuselage for pay load, fixed equipment, fuel, controls, and retracted landing gear, the ratio of wing area to maximum body cross-sectional area was fixed at 20. Engines were assumed to be mounted in two nacelles beneath the wings. The foregoing assumptions resulted in maximum bomber lift-drag ratios (without nacelles) near 6 for supersonic Mach numbers and lift-drag ratios near 12 for a Mach number of 0.9.

Trailing-edge flaps should provide lift coefficients up to 1.2 for landing and take-off. Fully loaded take-off speed was 162 knots at a lift coefficient of 1.1, and landing speed empty was about 115 knots for the airplanes studied. In most cases, optimum engine size for climb and cruise resulted in take-off distances to clear a 50-foot obstacle of less than 5000 feet. In all cases the 5000-foot take-off distance was satisfied even when it required installing slightly larger engines than would have been optimum for best cruise operation.

[REDACTED]

Structural weight, which includes all items except pay load, fixed equipment, fuel, fuel tanks, and engines, was varied with the supersonic Mach number for which the airplane was designed. Structure-to-gross weight ratio was 0.23 for a Mach 2 airplane and 0.25 for a Mach 2.5 airplane. A fuel reserve of 5 percent of total fuel load was specified for all missions.

3078-H

Missions. - The bomber was assumed to rely mainly on high speed for its defense over defended areas. Consequently, no defensive armaments were provided and only 3000 pounds of fixed equipment were included. All flight plans therefore included supersonic flight over the target area. Two cases were investigated: the first called for subsonic cruise to and from the target along a Breguet path with only a brief supersonic dash over the target; the second case investigated was an all-supersonic mission consisting of cruise along a Breguet path to and from the target at constant supersonic Mach number. Results will be presented for both subsonic and supersonic cruise missions.

For all flight plans, both subsonic and supersonic cruise were conducted at optimum altitude for best range; also, an optimum size engine was installed in the airplane for each mission in order to maximize range, except in a few instances where take-off requirements demanded engine sizes slightly larger than the optimum for best range.

#### Interceptor

Airplane. - The interceptor assumed for the analysis had a take-off wing loading of 100 pounds per square foot and a wing thickness ratio of 4 percent. Fixed load was 3000 pounds, of which 1000 pounds was assumed to be air-to-air missiles. Typical airplane characteristics for a Mach 2.8 interceptor were a structure-to-gross-weight ratio of 0.31 and airplane lift-drag ratio (including engine drag) of 3.3.

Missions. - In order to bracket realistic interceptor missions with supersonic combat, two widely different interceptor flight plans were considered. These flight plans are illustrated in figure 1. For the supersonic mission, the interceptor takes off in less than 5000 feet, climbs and accelerates to supersonic speed, and cruises out at this speed 350 nautical miles. Combat occurs at the end of cruise-out and consists of  $220^\circ$  of turning without loss of speed or altitude. Return to base is also at the supersonic velocity, and the airplane holds for 15 minutes at subsonic speed over the base and lands with a fuel reserve of 5 percent of original fuel weight.

The subsonic mission was similar except that the cruise to and from combat was at a Mach number of 0.9, and the radius of the mission was 550 nautical miles.

[REDACTED]

[REDACTED]

The airplane power loading was determined by specifying the required interceptor maneuverability at the altitudes shown in figure 2. Maneuverability is defined as the normal g's that can be sustained by the airplane without loss of speed or altitude (1 g corresponds to level flight). This curve is consistent with the bomber calculations and corresponds to the target ceiling for a bomber with advanced take-off engines flying an all-supersonic mission. In all cases the interceptor is required to have a speed advantage over the bomber of 0.3 Mach number in addition to its advantage in maneuverability.

A typical result for a Mach 2.8 interceptor attacking a Mach 2.5 bomber is shown in figure 3. In most of the calculations, a maneuverability of 1.3 g's was required. In general, as illustrated in figure 3, a 1.3 g maneuverability results in an interceptor gross weight considerably above the minimum gross weight necessary to fly the mission if the airplane maneuverability were unspecified. Airplanes with maneuverabilities less than 1.0 in figure 3 have ceilings lower than 70,000 feet.

#### Engines

Engine data were obtained from the engine-performance papers already presented. Nacelle drags including friction, additive, cowl pressure, and boattail drags were subtracted from the engine data to obtain the installed engine performance.

Inlet recovery and inlet off-design performance were identical for interceptor and bomber. For the bomber, this could be obtained by a two-wedge variable-angle ramp two-dimensional inlet adapted to the nacelle installation; or, as additional calculations showed, similar performance could be obtained with a three-dimensional inlet using a two-cone translating spike.

Basic engine weight was taken as 577 pounds per square foot of compressor frontal area for the engines with maximum pressure ratio near 7. An additional 15 percent was added to this when an afterburner was employed, and some additional weight was also added for inlet, outlet, and nacelle. For engines with a maximum pressure ratio near 12, an additional 17 percent was also added to the basic engine weight. For the advanced Mach 1.5 and the advanced Mach 2.3 designs, an estimated maximum basic weight increase of 22 percent was considered.

All missions considered for both interceptor and bomber involved at least some operation at supersonic Mach numbers. For the missions involving some subsonic cruise, considerable engine throttling was necessary for the subsonic flight. This is a consequence of the high lift-drag ratios obtained at subsonic conditions; in fact, subsonic lift-drag ratios for the airplanes considered were about twice the supersonic

[REDACTED]

3078-H

[REDACTED]

lift-drag ratios. For engines with afterburners, some thrust reduction for subsonic cruise can be obtained by simply turning off the afterburner. Further thrust reductions are necessary, however, for efficient subsonic operation. These thrust reductions were obtained for engines with and without afterburners by operating the engines at the most favorable combination of exhaust area and engine speed in order to obtain minimum specific fuel consumption for any given thrust level.

### EFFECT OF ENGINE COMPONENTS

The advanced components discussed in previous papers offer improvements in engine thrust, specific fuel consumption, and flexibility; these improvements can be reflected in improved airplane performance when properly exploited in the airplane and mission.

Some of the components discussed are transonic compressors, cooled turbines, high-velocity burners, high-recovery inlets, and efficient variable-area convergent-divergent nozzles. The improvement in airplane performance resulting from the use of some of these advanced components will be treated briefly in this section.

#### Effect of Turbine-Inlet Temperature

Bomber. - Bomber radius as a function of turbine-inlet temperature is presented for two missions in figures 4 and 5 for engines with a design compressor pressure ratio of 7 both with and without afterburners. Both figures demonstrate the advantages of high turbine-inlet temperatures regardless of whether an afterburner is used. The increases in range are a consequence of the high cycle efficiency associated with high turbine-inlet temperature, especially at supersonic Mach numbers.

Figure 4 shows the results for an all-supersonic mission conducted at a Mach number of 2. Because of the higher thrust capabilities of the afterburning engine, smaller engines can be installed in the airplane and larger fuel loads can be carried. This is offset to a large extent by the increased specific fuel consumption characteristic of afterburning operation. At each point on the curves, engine size was optimized for best range. For the afterburning engine, this resulted in cruising afterburner temperatures considerably below maximum attainable in order to secure more efficient cruising operation. Figure 4 shows comparable performance for engines with and without afterburners over the range of turbine-inlet temperatures investigated.

One important advantage of an afterburner is the increased flexibility which it can provide for various engine operating requirements. This is especially important for a mission involving both subsonic and

[REDACTED]

[REDACTED]

supersonic flight, such as the subsonic cruising mission which requires only a brief supersonic dash over the target. Figure 5 shows the results for such a mission consisting of cruise at a Mach number of 0.9 and a brief dash over the target at a Mach number of 2. For this mission, flexibility in the afterburning engine is provided by turning off the afterburner during the subsonic portion of the flight and operating the engine with the afterburner ignited only for the brief supersonic dash. The high specific fuel consumption accompanying afterburning operation is then of little consequence because this portion of the flight is of short duration. Because of its flexibility, the afterburning engine is well suited to this type of mission; and in figure 5, the afterburning engine has a radius advantage of 20 percent at a turbine-inlet temperature of 2000° F. At higher turbine-inlet temperatures this advantage is somewhat reduced.

Interceptor. - Because the interceptor must have a greater maneuverability than the bomber, it must have relatively more thrust; consequently a greater need for the afterburner exists in an interceptor. This is illustrated in figure 6 where interceptor gross weight is plotted against turbine-inlet temperature for airplanes with and without an afterburner. For the particular case illustrated, the airplane flies a supersonic combat mission of 350 nautical miles radius at Mach 2.3. The all-supersonic case is illustrated because, as with the bombers just discussed, if the afterburner appears desirable for the all-supersonic mission, it will further improve the mission which is part supersonic and part subsonic.

It can be seen in figure 6 that interceptors with afterburners always have lower gross weights than those without afterburners. In fact, for turbine-inlet temperatures less than 2200° F, it is doubtful that this mission can be performed without an afterburner. As with the bomber there are large advantages to be gained by increasing turbine-inlet temperature even when an afterburner is assumed. For example, as shown in figure 6, the gross weight of an airplane having a turbine-inlet temperature of 2540° F is about one-half the gross weight of an airplane with a 1640° turbine-inlet temperature.

It should be pointed out that, in this example, the interceptor was required to have a 1.3-g maneuverability at 65,000 feet. (A maneuverability of 1.3 g's at 65,000 ft is equivalent to a maneuverability of 2.6 g's at 50,000 ft.) This requirement results in a fairly high-powered airplane and, as would be expected, an afterburner shows distinct advantages. The results of figure 6 were calculated for a flight Mach number of 2.3, but similar results were found at higher Mach numbers.

#### Effect of Afterburner Temperature

The total radius of a bomber having engines with advanced components is shown in figure 7 as a function of the afterburner temperature required

[REDACTED]

3078 -H

for the supersonic portion of the flight. Missions calling for both subsonic and supersonic cruise are included, and target Mach number in both cases was 2. For the mission using subsonic cruise, compressor design pressure ratio was 12 and for the mission with supersonic cruise, design pressure ratio was 7. All engines were operated along a conventional operating line; that is, engine mechanical speed was maintained constant as flight Mach number increased, resulting in reductions in compressor aerodynamic speed. Best afterburner temperature for these engines for supersonic cruise was near 2300° F; for subsonic cruise, best afterburner temperature for the supersonic dash was the maximum investigated, 3040° F. Increases in afterburner temperature allow the use of smaller engines. This effect was mitigated somewhat by adjusting cruise altitude to obtain maximum range in all cases; so that bomber radius is seen to be somewhat insensitive to changes in afterburner temperature, especially for the case of supersonic cruise. Take-off requirements were satisfied by an engine size corresponding to a Mach 2.0 afterburner temperature of approximately 3000° F; afterburner temperatures below this value would result in larger engine sizes and, therefore, more than adequate take-off performance. The take-off requirement is therefore not limiting for the conditions of figure 7.

#### Advanced Take-Off Engine

The combined effects of utilizing advanced compressor and turbine designs were investigated by comparing the advanced take-off engine with the current engine.

The advanced engine had a maximum compressor air flow of 39 pounds per second per square foot of compressor frontal area compared with 30 for the current engine. Turbine-inlet temperature was 2040° F for the advanced engine compared with 1640° F for the current engine. In all other respects, the two engines were similar, and both were operated along a conventional operating line using fixed turbine area and variable exhaust area, holding engine mechanical speed fixed so that compressor aerodynamic speed decreased as flight Mach number increased. Both engines were assumed to have equal weight per unit of compressor area.

Bomber. - The advanced take-off engine is compared with the current engine in a bomber in figures 8 and 9. The all-supersonic mission is illustrated in figure 8 in which both engines have design compressor pressure ratios of 7. Both engines were assumed to have afterburners; but for this mission, at Mach numbers below 2, similar performance could have been obtained without afterburners, as can be seen from figure 4. The results shown in figure 8 demonstrate a 30-percent improvement in range by going from the current engine to the advanced take-off engine. This improvement in range is, of course, the result of the better thrust and specific fuel consumption provided by the advanced components.

Figure 9 shows the comparison for the mission employing subsonic cruise with a supersonic dash over the target at the Mach numbers plotted on the abscissa. For this case, the engine design compressor pressure ratio was 7 for the current engine and 12 for the advanced take-off engine. Both engines had afterburners, and again the advanced take-off engine gave superior range performance, about 15 percent better than the current engine for this mission.

Interceptor. - The two engines in an interceptor flying an all-supersonic mission at various Mach numbers from 1.5 to 2.8 are compared in figure 10. Required maneuverability was 1.3 g's at the altitude specified in figure 2. Figure 10 shows that over the range of Mach numbers considered, the gross weight of the interceptor having the advanced take-off engine is about 50 percent less than the weight of an interceptor having the current engine. The improvements shown are a direct result of the improved air flow and increased turbine-inlet temperature.

#### EFFECT OF ENGINE OPERATION AND DESIGN

Large gains in engine and airplane performance have been shown to be derived from the use of advanced components; that is, from high-flow compressors and cooled turbines. In addition, further improvements in engine performance may be expected from unconventional engine design and operating techniques. These improvements have been described in the previous papers, and have led to the advanced Mach 1.5 and the advanced Mach 2.3 designs. In the following discussion, the performance of these engines will be integrated into the airplanes of this study to find the improvements they may offer in airplane performance. The advanced Mach 1.5 and the advanced Mach 2.3 designs provide better supersonic performance than the advanced take-off engine but have equal or inferior subsonic performance. The following discussion will therefore be concerned mainly with supersonic missions. All engines, whatever their design Mach number, were studied in missions covering a range of Mach numbers, and results are presented as a function of flight Mach number.

#### Advanced Mach 1.5 Engine

Bomber. - The advanced Mach 1.5 engine is compared with the advanced take-off and current engines in a bomber in figure 11 for all supersonic cruise at the Mach numbers plotted on the abscissa. Compressor maximum pressure ratio was near 7 for all three engines and afterburners were assumed for all engines, although again this is not significant for the lower cruise Mach numbers. The performance of the advanced Mach 1.5 design is presented as a band. The lower limit of the band represents the results for an engine design with the same number of compressor and

3078 -H

[REDACTED]

turbine stages as were used in the advanced take-off engine. Tip speeds for such a design were considerably higher than the tip speeds used in the advanced take-off engine, and engine weight was correspondingly higher. The upper limit of the band represents the results for an advanced Mach 1.5 engine having the same weight per square foot of compressor area as the advanced take-off engine. Thus the lower limit of the band represents a conservative weight estimate for the advanced Mach 1.5 design, and the upper limit of the band represents an optimistic estimate. A judicious compromise between tip speed and number of compressor and turbine stages should result in performance somewhere within the band.

3078-H

The advantages of the advanced Mach 1.5 design are less apparent in the bomber than in the interceptor, as will be shown subsequently. Because the bomber is a lower powered airplane than the interceptor, the thrust increases at high Mach number which the advanced Mach 1.5 design provide are less important to the bomber. Bomber performance is more sensitive to changes in specific fuel consumption, and in this respect the advanced take-off and advanced Mach 1.5 designs are similar. Figure 11 therefore shows that an average increase in radius of only 10 percent is obtained by going from the advanced take-off to the advanced Mach 1.5 engine.

Interceptor. - Figure 12 compares the advanced Mach 1.5 engine with the advanced take-off and current engines for all supersonic interceptor missions conducted at the Mach numbers plotted on the abscissa. The performance of the advanced Mach 1.5 engine is shown as a band, as was done for the bomber, to allow for engine weight uncertainties. A practical design should fall somewhere within the band.

Figure 12 shows that in addition to the 50-percent reduction in gross weight which was realized by going from the current to the advanced take-off engine, a further reduction of about 15 percent is possible with the advanced Mach 1.5 design over the Mach number range investigated. With the advanced Mach 1.5 engine the interceptor can fly the 350-nautical-mile supersonic mission with a gross weight of 17,000 pounds at Mach 2.0 and with a gross weight of 25,000 pounds at Mach 2.8.

Figure 13 shows similar results for the interceptor mission which specified 550-nautical-miles subsonic cruising radius. The advanced Mach 1.5 engine again shows gross weight reductions of 15 to 20 percent when compared with the advanced take-off engine.

#### Advanced Mach 2.3 Engine

Bomber. - The advanced Mach 2.3 engine is compared with the other three engines for the all-supersonic bomber mission in figure 14.

[REDACTED]

[REDACTED]

Results for the Mach 1.5 and Mach 2.3 designs were obtained in the form of a band to allow for weight uncertainties, but for simplicity only the middle of the band is shown in figure 14 as a single line. The current, advanced take-off, and advanced Mach 1.5 performance is the same as that shown in figure 11.

Although the advanced Mach 2.3 engine showed thrust increases at high Mach number over the advanced Mach 1.5 design, this is of little benefit to the bomber because thrust margins with the Mach 1.5 design were already adequate. Furthermore, specific fuel consumption for the Mach 2.3 and Mach 1.5 designs was similar at the supersonic Mach numbers so that, as might be expected, figure 14 shows little difference in range for the two engines, a maximum advantage of about 5 percent being obtained with the Mach 2.3 design at a Mach number of 2.5.

Interceptor. - Although the calculations showed little gain to be achieved by using the advanced Mach 2.3 engine in the bomber, this engine can improve interceptor performance, especially at high Mach numbers when good maneuverability is required. This is illustrated in figures 15 and 16 by considering an all-supersonic mission with two values of maneuverability. Figure 15 is similar to figure 12 except that only the center line of the advanced Mach 1.5 band is shown, and, in addition, a line representing the middle of the band for the advanced Mach 2.3 engine is shown. For the 1.3 g maneuverability specified in figure 15, the advanced Mach 2.3 engine is superior to the advanced Mach 1.5 engine at Mach numbers above 2, and the differences are greatest at the highest Mach numbers. At Mach 2.8, for example, interceptor gross weight was reduced about 20 percent beyond the weight reductions achieved by the advanced Mach 1.5 engine.

At the highest Mach numbers included in figure 15, minimum engine size for the advanced Mach 2.3 engine was specified by the transonic acceleration requirements, resulting in engines larger than necessary for supersonic combat at 1.3 g. The advanced Mach 2.3 design is therefore better suited to combat missions specifying higher maneuverability than the 1.3 g illustrated in figure 15.

The results for such a mission are presented in figure 16, which shows interceptor gross weight as a function of Mach number for an all-supersonic mission with 1.6 g combat maneuverability. To meet the increased maneuverability, the gross weight of an interceptor with advanced Mach 2.3 engines was only slightly increased at the Mach 2.8 condition, because the thrust potential of the engines which satisfied the transonic acceleration requirement was nearly adequate for a 1.6-g combat. In contrast, gross weight for the other engines increased considerably when the higher maneuverability was required. At a mission Mach number of 2.8, the interceptor with the advanced Mach 2.3 engine is 45 percent lighter than the interceptor with the advanced take-off

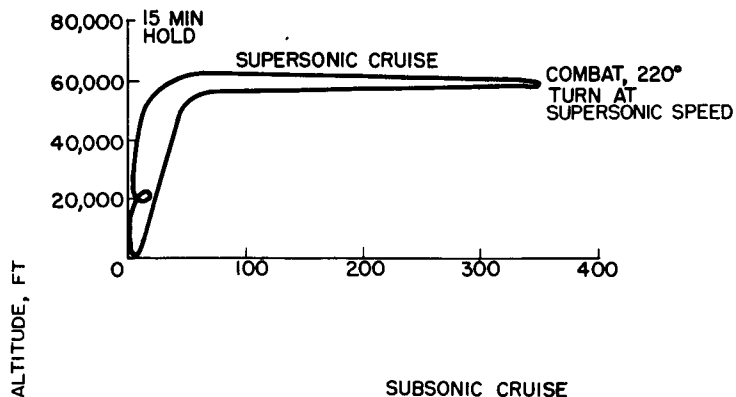
[REDACTED]

engine and 35 percent lighter than an interceptor with advanced Mach 1.5 engines. Figures 15 and 16 demonstrate that the advanced Mach 2.3 engine has outstanding advantages for high-performance interceptors flying supersonic missions at Mach numbers above 2.0.

3078-H

INTERCEPTOR FLIGHT PLANS

SUPERSONIC CRUISE



SUBSONIC CRUISE

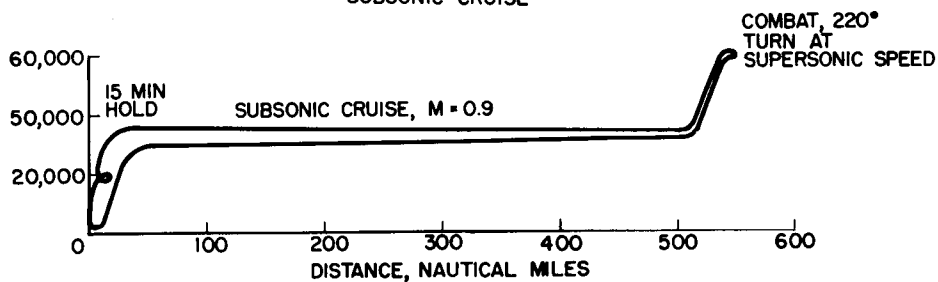


Figure 1

ASSUMED INTERCEPTOR COMBAT ALTITUDE

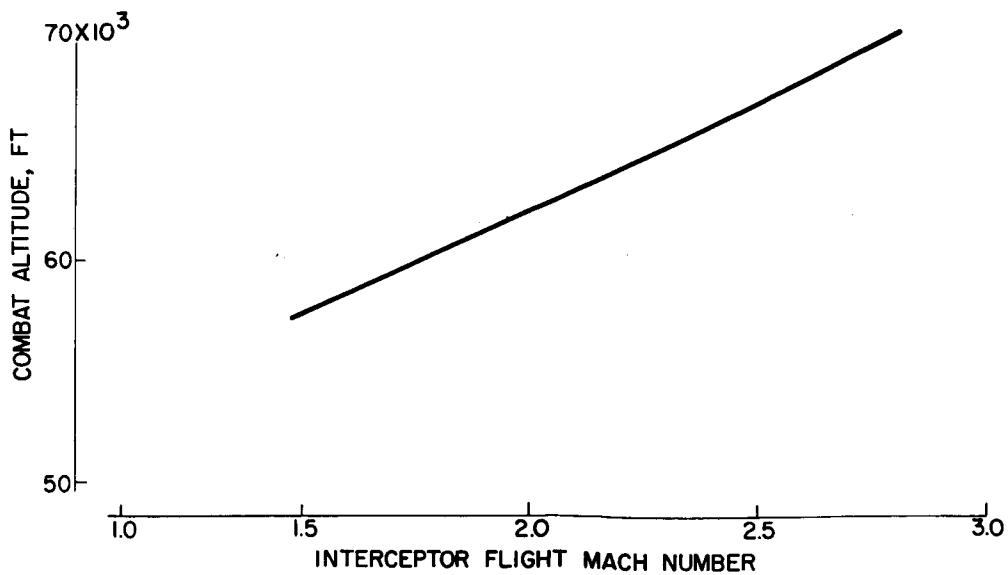


Figure 2

3078-H

**EFFECT OF MANEUVERABILITY REQUIREMENT ON INTERCEPTOR GROSS WEIGHT**  
SUPERSONIC MISSION; MACH NUMBER, 2.8

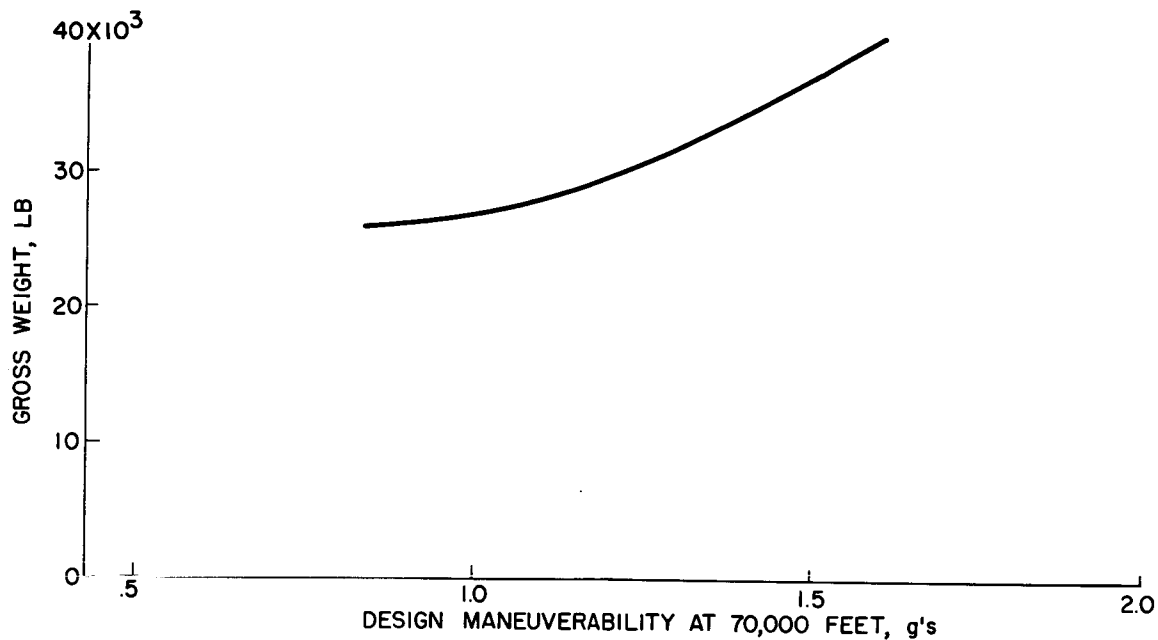


Figure 3

**EFFECT OF ENGINE TEMPERATURES ON BOMBER RANGE FOR SUPERSONIC CRUISE**  
CRUISE MACH NUMBER, 2.0

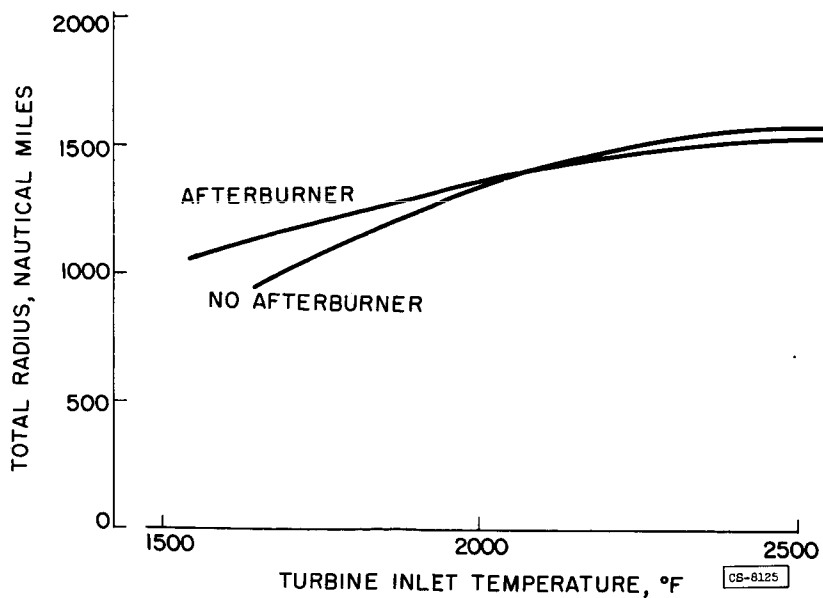


Figure 4

**EFFECT OF ENGINE TEMPERATURES ON BOMBER RANGE**  
**FOR SUBSONIC CRUISE**  
**TARGET MACH NUMER, 2.0**

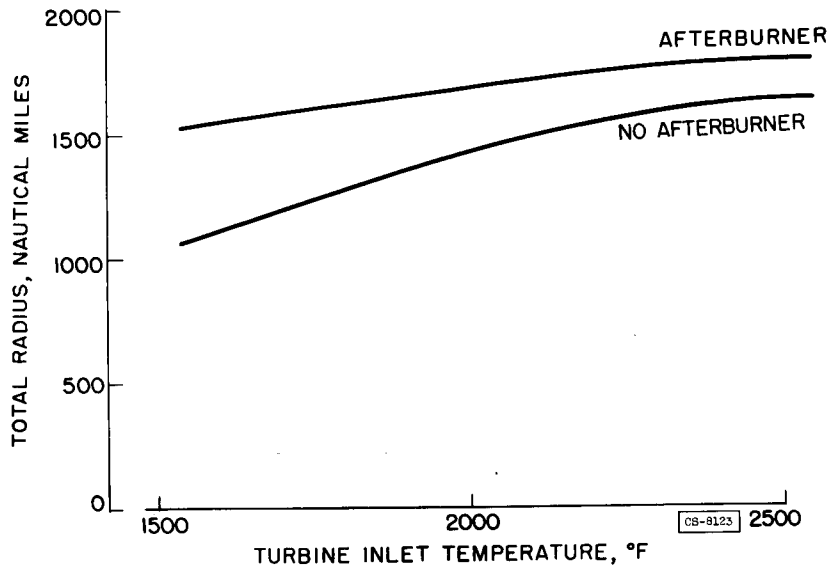


Figure 5

**EFFECT OF ENGINE TEMPERATURES ON**  
**INTERCEPTOR GROSS WEIGHT**

**SUPERSONIC MISSION; MACH NUMBER, 2.3;**  
**MANEUVERABILITY, 1.3 g's**

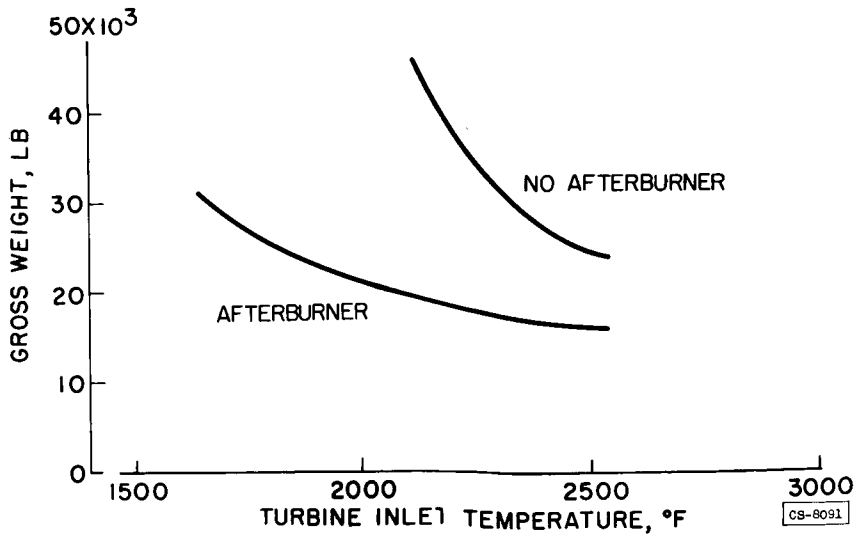


Figure 6

EFFECT OF AFTERBURNER TEMPERATURE ON BOMBER RANGE

TARGET MACH NUMBER, 2.0

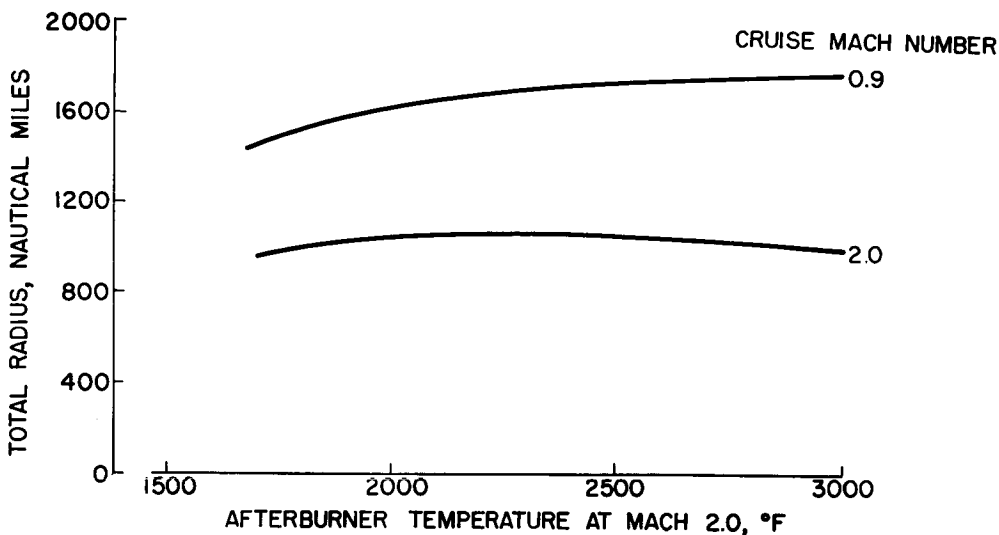


Figure 7

EFFECT OF TWO ENGINE DESIGNS ON BOMBER RANGE FOR SUPERSONIC CRUISE

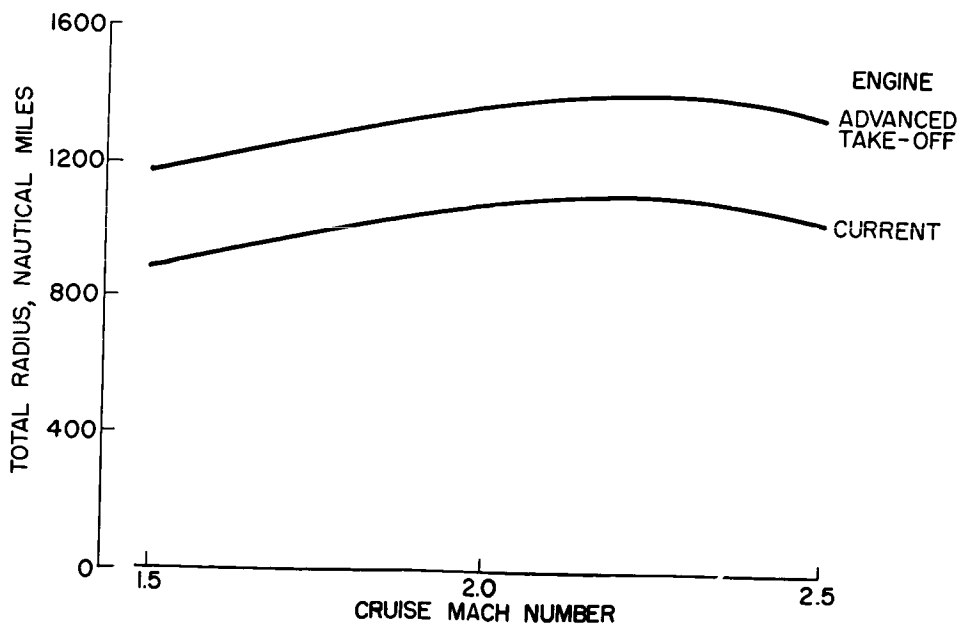


Figure 8



### EFFECT OF ENGINE DESIGN ON BOMBER RANGE FOR SUBSONIC CRUISE

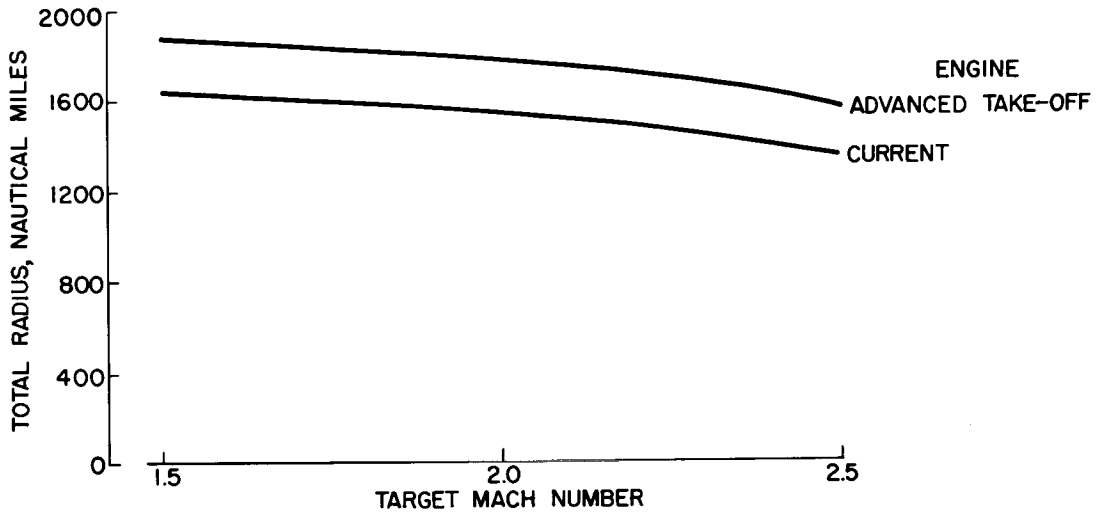


Figure 9

### EFFECT OF ENGINE DESIGN ON INTERCEPTOR GROSS WEIGHT SUPERSONIC CRUISE

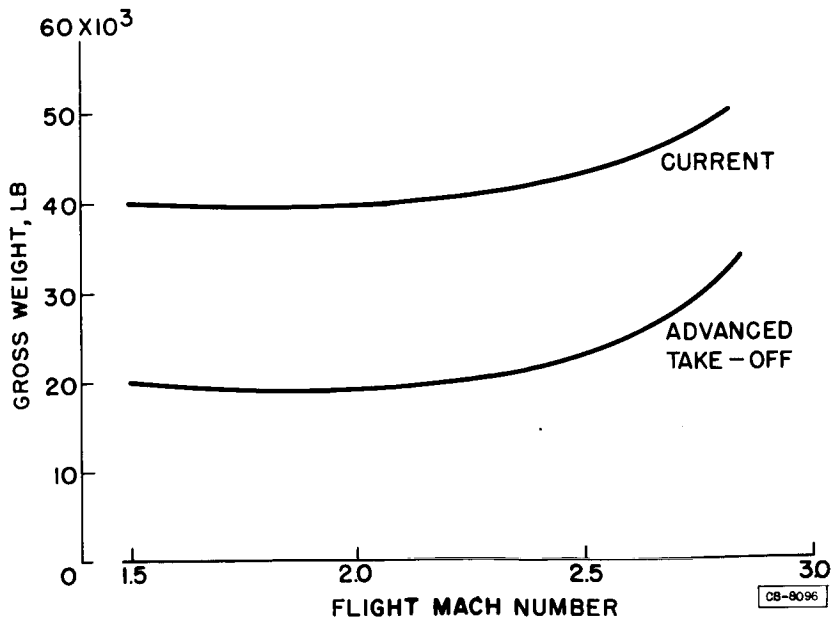
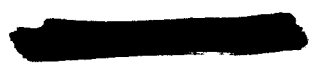


Figure 10



3078-H

CB-8096

### EFFECT OF THREE ENGINE DESIGNS ON BOMBER RANGE FOR SUPERSONIC CRUISE

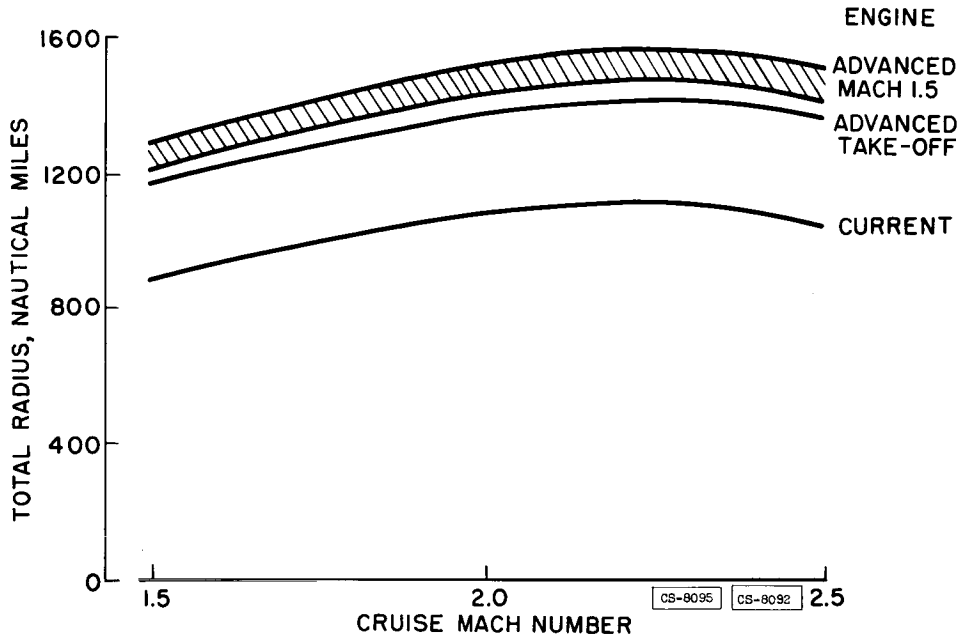


Figure 11

### EFFECT OF ENGINE DESIGN ON INTERCEPTOR GROSS WEIGHT FOR SUPERSONIC CRUISE

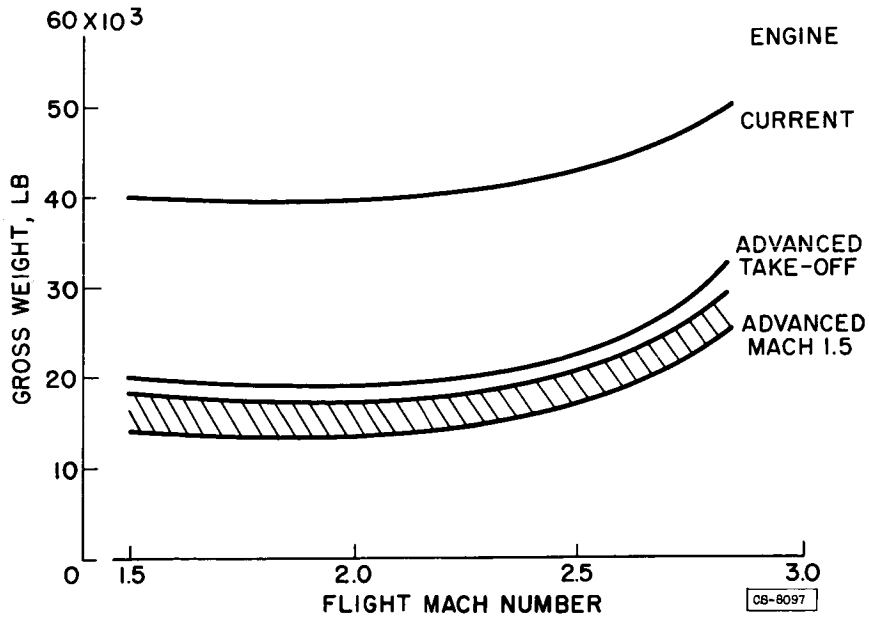


Figure 12



### EFFECT OF ENGINE DESIGN ON INTERCEPTOR GROSS WEIGHT FOR SUBSONIC CRUISE

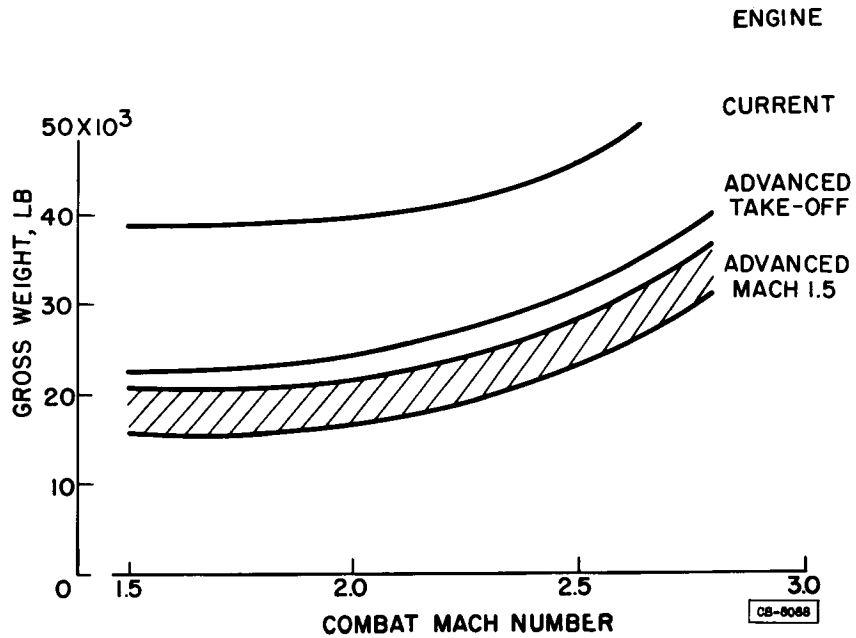


Figure 13

### EFFECT OF FOUR ENGINE DESIGNS ON Bomber Range FOR SUPERSONIC CRUISE

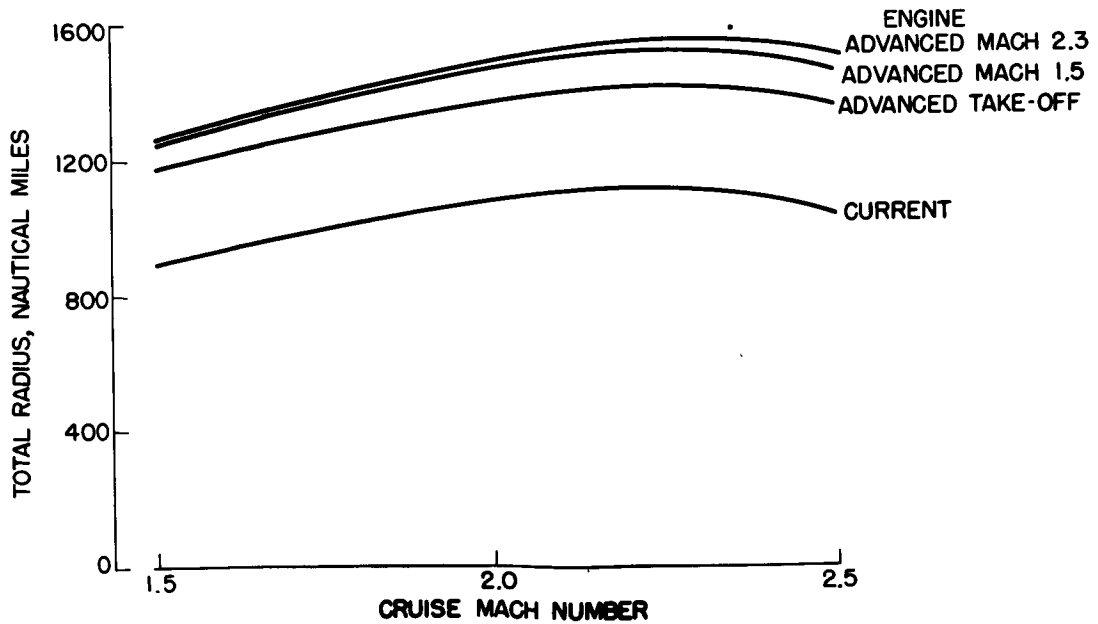


Figure 14



EFFECT OF ENGINE DESIGN ON INTERCEPTOR GROSS WEIGHT FOR SUPERSONIC CRUISE AND MANEUVERABILITY OF 1.3 g's

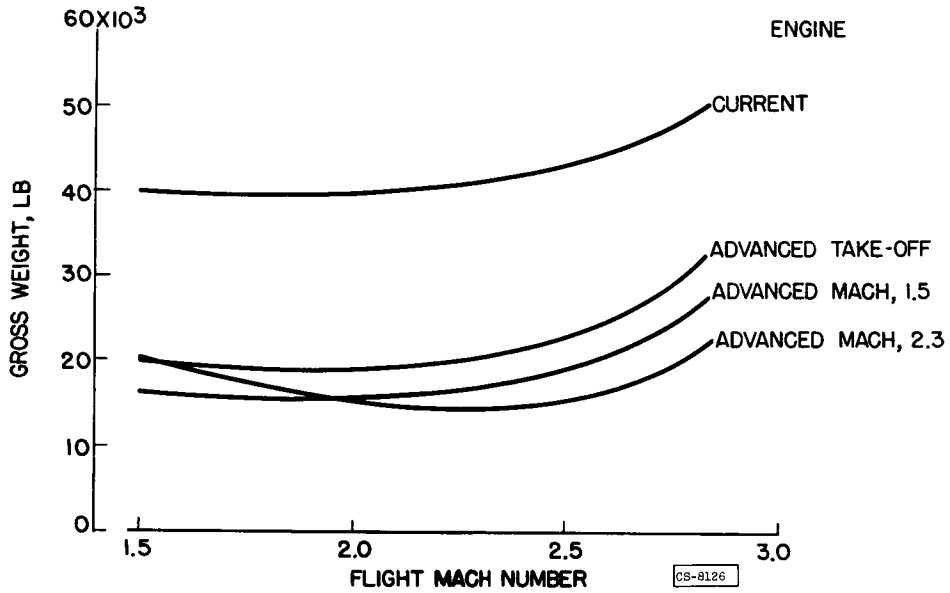


Figure 15

EFFECT OF ENGINE DESIGN ON INTERCEPTOR GROSS WEIGHT FOR SUPERSONIC CRUISE AND MANEUVERABILITY OF 1.6 g's

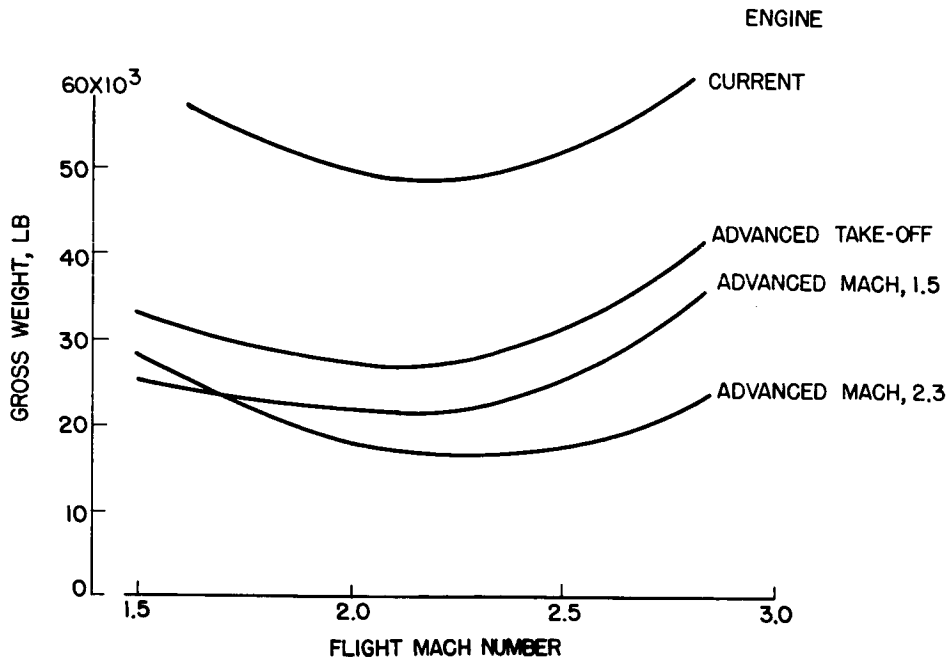


Figure 16

## SUMMARY OF ENGINE AND AIRPLANE ANALYSIS

By David S. Gabriel and Eldon W. Hall

3078-H

Research on components for turbojet engines has resulted in significant advancements in component performance. It has been shown that the transonic compressor is capable of delivering high air flow with efficiencies comparable to those of the best subsonic designs and with a smaller number of stages than subsonic compressors. In addition, these high efficiencies are maintained over a wide range of rotative speeds and pressure ratios. Primary combustors have been developed which operate efficiently with moderate pressure drop at velocities up to 200 feet per second. Developments in methods of fabrication, support, and attachment of cooled turbine blades show promise of culminating in turbine-gas temperatures of 2000° to 2500° F with blade metal temperatures as low as 1100° F and, therefore, with allowable blade stresses of 40,000 to 50,000 pounds per square inch. It has been shown that variable-area turbines may be designed that operate with little change in turbine efficiency over a range of rotor-blade incidence angles of about 30°. In order to keep pace with these developments, afterburners with high combustion efficiencies at velocities over 600 feet per second have been developed, along with engine inlets and exhaust nozzles suitable for very high flight speeds.

These advanced components were shown to be useful in improving the thrust and fuel consumption of turbojet engines at high flight speeds in two ways. First, the transonic compressor and cooled fixed-area turbines may be incorporated in engines operating at constant rotative speed at all flight Mach numbers. Such an engine would have air-handling capacities and turbine-inlet temperatures higher than for current engines. Second, these advanced components either with or without the variable-area turbine may be incorporated in engines operating at varying mechanical speed as flight Mach number is varied. This second type of engine would be capable of maintaining higher air-handling capacity at the very high flight speeds than either the current engines or the engines with advanced components operating at constant rotative speed.

Although a final judgment of the relative merit of the numerous engine designs which could be evolved around these components would entail complete engine designs which are beyond the scope of this analysis, four possible engine designs were discussed as examples of the advantages offered by these components and the order of magnitude of the performance gains available were described.

The first engine, which was designated the advanced, take-off design, incorporated the transonic compressor and cooled turbine and operated at constant rotative speed. When compared with a hypothetical current

VII-6

development engine, the differences in performance were therefore the result of improved component performance only. The important design characteristics of the advanced take-off engine were: maximum air flow, 39 pounds per second per square foot of compressor frontal area; turbine-inlet temperature, 2040° F; turbine blade tip speed, 1100 feet per second; six compressor stages; two turbine stages; and maximum turbine stress at blade roots, 35,000 pounds per square inch. The hypothetical current development engine had a maximum air flow of 30 pounds per second per square foot of compressor frontal area and a turbine-inlet temperature of 1640° F. Primarily because of the higher air flow and turbine-inlet temperature, the advanced take-off engine had higher thrust at all flight speeds and lower specific fuel consumption at flight Mach numbers greater than 1.8 than the current development engine. For example, at a flight Mach number of 2.5, the advanced take-off engine had 50 percent greater thrust than the current development engine. It was also shown that higher turbine-inlet temperatures are beneficial for both afterburning and nonafterburning engines.

In both the advanced take-off engine and the current development engine which operated at constant mechanical rotative speed, the increase in compressor-inlet temperature as flight Mach number increased resulted in a reduction in compressor corrected air flow. To eliminate this decrease in air flow in the advanced take-off engine by increasing the rotative speed sufficiently to maintain a constant aerodynamic speed at flight Mach numbers up to 2.8 would have required excessive blade stresses.

The advantages of increasing rotative speed and thereby maintaining high compressor air flow as flight Mach number is increased could, however, be utilized in an engine which was designed for a lower stress level at low flight speeds than the advanced take-off engine. An engine capable of delivering the same compressor pressure ratio and air flow at take-off conditions as the advanced take-off engine but at a lower stress level must have a lower rotative speed to satisfy the stress requirement and hence a larger number of stages in the compressor to satisfy the pressure ratio requirement. Whereas the number of stages required is inversely proportional to the tip speed, the engine weight must increase as either the number of stages or the tip speed increases. A compromise design in which rotative speed or tip speed and the associated stresses are allowed to increase and thereby maintain constant compressor aerodynamic speed up to the intermediate flight Mach number of 1.5 at the sacrifice of a small increase in the number of stages required was shown to result in improved performance over the advanced take-off design.

This engine, designated the advanced Mach 1.5 engine, would require a seven-stage compressor, tip speeds from 1070 feet per second at take-off to 1285 feet per second at Mach numbers of 1.5 and higher, a 2040° F turbine-inlet temperature, and a two-stage turbine with a maximum root

[REDACTED]

stress of 45,000 pounds per square inch. The air flow as a result of these changes in operating mode (increased rotative speed) and component design would be the same as the advanced take-off design at the conditions of low flight Mach number corresponding to minimum compressor-inlet temperature, but would be greater at high Mach numbers. For example, the advanced Mach 1.5 design would have an air flow over 30 percent higher than the advanced take-off design at a flight Mach number of 2.8 and correspondingly higher thrust. Because of the higher stress levels and larger number of stages, the advanced Mach 1.5 design engine would, however, be heavier than the advanced take-off design engine. A quantitative measure of the increase in weight was not possible from these preliminary calculations.

A study of the twin-spool engine showed that insofar as thrust and fuel consumption were concerned approximately the same performance could be realized at all flight speeds as for the single-spool engine if proper design practices were followed. In the twin-spool engine, for example, operation of the outer spool at constant aerodynamic speed up to a flight Mach number of 1.5 resulted in performance equivalent to the single-spool advanced Mach 1.5 engine.

In the advanced Mach 1.5 design, the compressor pressure ratio decreased as flight Mach number increased. For example, the pressure ratio decreased from 7.0 at take-off to approximately 3.0 at a Mach number of 2.8. If a variable-area turbine had been used in the engine, independent control of pressure ratio and engine temperature ratio would have been possible. With independent control of pressure ratio, a mode of operation may be chosen such that rotative speed may be increased as flight Mach number increases to maintain high engine air flow, and compressor pressure ratio may be maintained at higher values than if a fixed-area turbine is used; the air-handling capacity of the turbine is thereby increased for the same turbine rotative speed and flow area. As an example of the application of these principles to engine design, the performance of an engine designated the advanced Mach 2.3 design was calculated. In this engine a variable-area turbine was used together with an increase in rotative speed with increase in flight Mach number to maintain the engine air flow constant up to a flight Mach number of 2.3, and to limit the decrease in compressor pressure ratio from 6.1 to 5.5 over the flight speed range up to a flight Mach number of 2.3. Above a Mach number of 2.3 both turbine area and rotative speed were constant. In this engine about eight compressor stages, tip speeds from 850 to 1182 feet per second, turbine-inlet temperature of 2042° F, and a two-stage turbine with a maximum root stress of 45,000 were required. As compared to the advanced Mach 1.5 design, the advanced Mach 2.3 design had over 20 percent higher air flow at a Mach number of 2.3 and comparable increases at other flight speeds. Although the advanced Mach 2.3 engine would probably be heavier than the advanced Mach 1.5 engine, the thrust at Mach numbers above 2.0 was considerably increased.

[REDACTED]

At a Mach number of 2.8 the engine thrust was over 40 percent greater than the advanced Mach 1.5 engine. This thrust gain at high speeds was obtained, however, with some sacrifice in specific fuel consumption at subsonic speed.

The advanced take-off, Mach 1.5 and Mach 2.3 engines, although of no particular intrinsic significance, demonstrate the advantages in improved thrust at high flight speeds which may be realized by the use of advanced components and by designs which permit the use of unconventional methods of engine operation. In addition, the nature of the design compromises between blade stresses or rotative speed and number of stages or engine length was apparent. It was further observed that in successively increasing the high-speed thrust, some increase in engine weight was unavoidable even with a considered choice of the design compromises, and in some cases increases in thrust at high speeds were obtained at a sacrifice in low-speed specific fuel consumption. Because these unfavorable engine-weight and fuel-consumption effects accompany high-thrust designs, the merit of the various engine types for propulsion of airplanes could not be judged from the engine performance alone. The performance of interceptor and bomber airplanes powered by each of the advanced engines and by a hypothetical current development engine and flying at Mach numbers up to 2.8 was therefore computed. In these calculations the weight of the advanced engines was bracketed by assuming for a minimum weight the weight of a comparable current development engine and for a maximum weight the full weight change due to changes in centrifugal stresses.

The airplane performance calculations showed that the advanced take-off design engine was superior in all flight plans for supersonic flight to the current development engine. Increases in bomber range of 30 percent up to flight Mach numbers of 2.5 and decreases in interceptor gross weight of about 40 percent at flight Mach numbers up to 2.8 were possible. Even though additional gains in airplane performance are difficult to realize because improvements are being made in a situation which is already good, the achievement of increased thrust at high flight Mach number over the advanced take-off design by the advanced Mach 1.5 engine resulted in further improvements in airplane performance. The Mach 2.5 bomber range, for example, was increased 10 percent and the Mach 2.8 interceptor gross weight was reduced an additional 15 to 20 percent. The further increases in thrust obtainable with the advanced Mach 2.3 engine were beneficial in applications to very high-powered airplanes. The range of the bomber airplanes was not appreciably different with either the advanced Mach 1.5 or advanced Mach 2.3 engines. In the interceptor airplanes, reductions in gross weight of over 35 percent at a flight Mach number of 2.8 were obtained if a maneuverability of 1.6 g's at 65,000 feet was required and the reduction in gross weight was about 20 percent if maneuverability was reduced to 1.3 g's.

~~CONFIDENTIAL~~

These results show that large performance gains in supersonic airplanes powered by turbojet engines may be made by incorporating the advanced components that have been developed in the last few years. In addition, the high permissible stress levels in the cooled rotating turbine blades and the wide range of efficient operating conditions of the advanced components make it possible to incorporate these advancements in engines which are designed to operate at varying rotative speed and with varying turbine flow area. By proper design, this additional flexibility in the engine may be used to greatly increase the thrust of turbojet engines at high flight speeds with resultant large improvements in airplane performance.

3078-M

~~CONFIDENTIAL~~